PROCEEDINGS OF THE

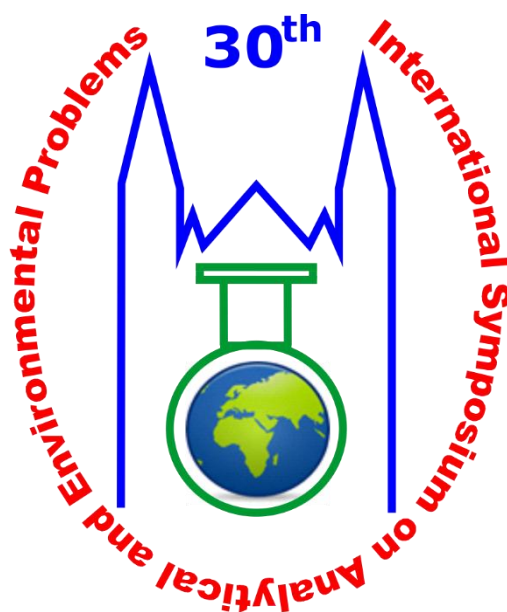# *30th International Symposium on Analytical and Environmental Problems*

Szeged, Hungary
October 7-8, 2024

University of Szeged

Edited by:
Tünde Alapi
Róbert Berkecz
István Ilisz

Publisher:
University of Szeged, H-6720 Szeged, Dugonics tér 13, Hungary

2024.
Szeged, Hungary

The 30ᵗʰ International Symposium on Analytical and Environmental Problems

Organized by:
SZAB Kémiai Szakbizottság Analitikai és Környezetvédelmi Munkabizottsága

Supporting Organizations
Institute of Pharmaceutical Analysis, University of Szeged
Department of Molecular and Analytical Chemistry, University of Szeged
Hungarian Academy of Sciences
Hungarian Chemical Society Group of Csongrád County

Symposium Chairman:
István Ilisz, DSc

Honorary Chairman:
Zoltán Galbács, PhD

Organizing Committee:
István Ilisz, DSc
professor of chemistry
University of Szeged, Institute of Pharmaceutical Analysis
Tünde Alapi, PhD
assistant professor
University of Szeged, Department of Molecular and Analytical Chemistry
Róbert Berkecz, PhD
associate professor
University of Szeged, Institute of Pharmaceutical Analysis

Scientific Committee:
István Ilisz, DSc
Tünde Alapi, PhD
Róbert Berkecz, PhD
Daniela Sojic Merkulov, PhD
full professor
University of Novi Sad, Faculty of Sciences, Department of Chemistry, Biochemistry and Environmental Protection

Lecture Proceedings

12 YEARS OF A CITY – NOISE AND OTHER ENVIRONMENTAL MEASUREMENTS IN THE CITY OF SZEGED

Zsolt I. Benkő

Department of Technology, University of Szeged, H-6725 Szeged, Boldogasszony sgt. 6, Hungary
e-mail: benko.zsolt.istvan@szte.hu

Abstract
On selected locations of Szeged measurements were carried out to achieve an approximate noise distribution of the city. The aim was to obtain the noise load values caused by traffic mostly. The first measurements were carried out in 2012 and they were repeated on the same spots in 2015, 2018, 2021 and 2024.

Introduction
Almost all the information achieved by a person is acquired through sight and hearing (about 83% percent through sight and 11% through the hearing). Presently more and more people live in crowded, large cities. This artificial environment – compared to the natural environment – is usually noisy. It can be even harmful to the hearing. It is a good initiative to check at regular intervals wether our environment is still within the healthy limits.
The normal human hearing ranges from 20 Hz frequency to 20000 Hz.[1]
The hearing process itself is logarithmic. The usual industrial tools for noise measurements are based on sound pressure level (SPL) and the data are given in decibel (dB) scale.[2] Eq.1 shows the correct formula:

$$L_p = 20 log_{10} \left(\frac{\Delta p}{p_0} \right) \ dB \tag{1}$$

where Δp is the sound pressure fluctuation, and p_0 is the reference pressure fluctuation value (audition threshold); $p_0 = 20$ µPa. For example 40 dB is living area at night or stillness of nature; 60 dB is a busy office room.
Over a long-term exposure the 85 dB or higher sound pressure level can cause permanent damage to the hearing. It is important because this damage is cumulative throughout the whole life.

The auditory sensation depends on the frequency of the sound very strongly: at the same sound pressure level a 200 Hz sound feels much weaker than a 1000 Hz sound. It can be visualized by the equal loudness curves which are measured first by Harvey Fletcher and Wilden A. Munson in 1933. The measurement was repeated between the years 2000 and 2003.[3][4][5][6]

Professional noise meter tools use weighting curves to show similar responses to the human hearing. The A-weighting is used for auditory purposes. The C-weighting is almost flat; that can be used to measure the real physical sound pressure values.[7] Though +6 dB means twice the power, the human perception works in different way. If a sound is observed two times louder than the previous one – it means about +10 dB higher level.[8][9]

beginning by 2018, the measurements were completed to acquire samples of the CO_2 and CO gas concentrations of the air. CO measurements were barely detectable.

The atmospheric level of CO_2 is 423 ppm by Mauna Loa Observatory, Hawaii (NOAA-ESRL) [10]; the normal value of CO_2-concentration at sea level is 250-350 ppm by industrial

recommendations. [11]

Experimental

The different locations in Szeged where the measurements were carried out are shown by Figure 1. Locations 1, 3 and 5 are close to main roads in Szeged with heavy traffic. Locations 2 and 6 are near to less important roads, but sometimes they have heavy traffic, too. Location 4 is chosen to be far away from any traffic; it is among housing blocks (sleeping area – no heavy daytime activity). The measurements contain morning, mid-day and evening data.
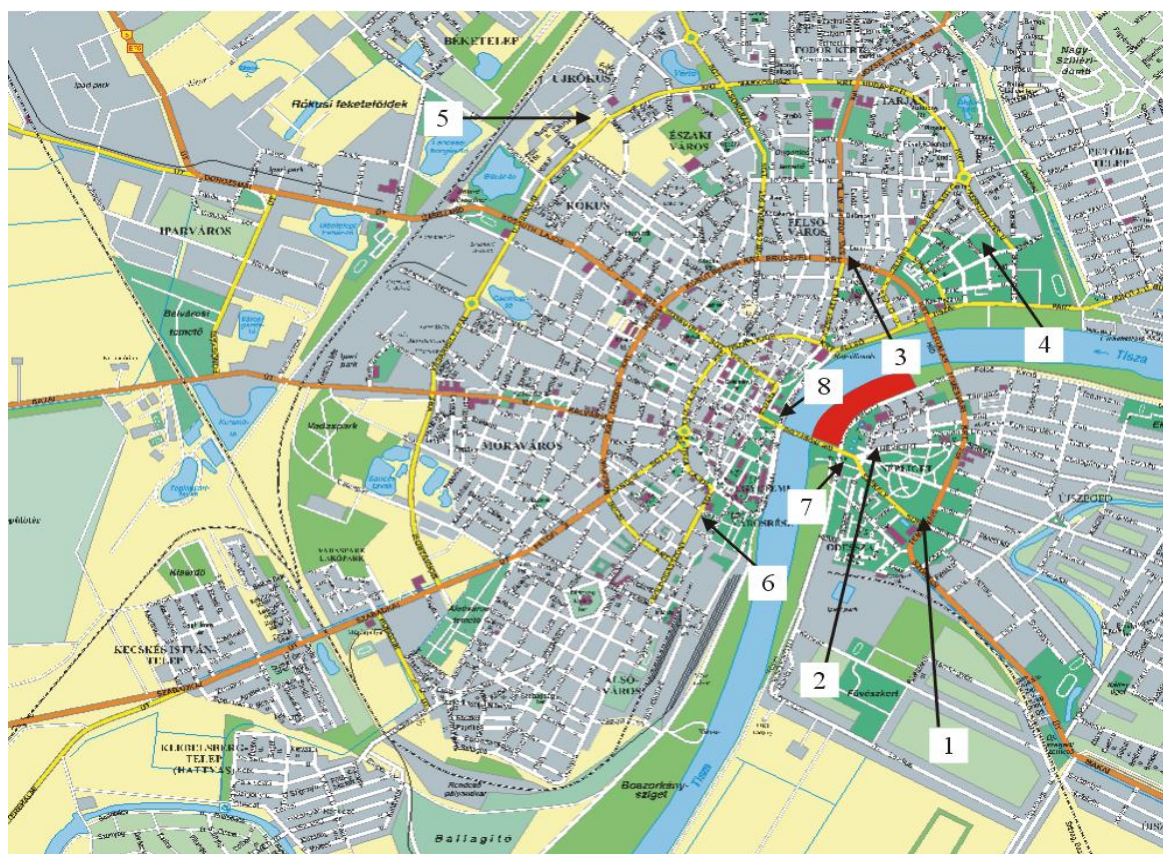

Figure 1. Locations of the measurements in Szeged

The noise levels around the area of the Youth Days of Szeged (red area) were measured, too. This festival is held in each August. Locations 7 and 8 are used only for these measurements.

location	description (and GPS coordinates)
1	intersection of "Székely sor" and "Temesvári krt." (46º 14.728' N ; 020º 09.842' E)
2	close to the inner city bridge (46º 14.991' N ; 020º 09.605' E)
3	intersection of roads "Római krt." and "József Attila sgt." (46º 15.696' N ; 020º 09.479' E)
4	near a housing block, "Csaba u. 43" (46º 15.732' N ; 020º 10.116' E)
5	school at "Rókusi krt." near Tesco (46º 16.253' N ; 020º 08.290' E)
6	school at "Boldogasszony sgt. 8" (46º 14.759' N ; 020º 09.738' E)
7	parking area at the bridge (46º 14.933' N ; 020º 09.410' E) – *only for YDS*
8	museum garden (46º 15.124' N ; 020º 09.162' E) – *only for YDS*

Table 2. Measurement locations and descriptions.

Results and discussion

The following tables show all the measured data for each location.[12]

location 1	Year	*workday morning (7:00-8:00)*	*workday daytime (12:00-15:00)*	*workday evening (20:00-22:00)*
Sound level (dB)	2012	61.9 ± 5.2	55.5 ± 7.1	52.9 ± 6.8
Sound level (dB)	2015	64.6 ± 6.0	58.0 ± 8.0	52.2 ± 7.7
Sound level (dB)		58.6 ± 7.6	56.1 ± 7.3	50.7 ± 7.0
CO_2 (ppm)	2018	286 ± 3	189 ± 9	268 ± 6
CO (ppm)		0	0	0
Sound level (dB)		61.7 ± 6.3	60.0 ± 6.8	56.6 ± 8.1
CO_2 (ppm)	2021	385 ± 5	255 ± 6	391 ± 10
CO (ppm)		0	0	0
Sound level (dB)		59.9 ± 5.8	57.6 ± 6.9	55.7 ± 5.9
CO_2 (ppm)	2024	288 ± 7	232 ± 13	274 ± 6
CO (ppm)		0	0	0

Table 3. Measurements on location 1.

location 2	Year	*workday morning (7:00-8:00)*	*workday daytime (12:00-15:00)*	*workday evening (20:00-22:00)*
Sound level (dB)	2012	59.2 ± 7.3	57.4 ± 7.8	54.9 ± 8.1
Sound level (dB)	2015	60.7 ± 8.5	56.9 ± 9.9	55.6 ± 7.1
Sound level (dB)		59.3 ± 7.7	60.1 ± 6.0	50.1 ± 6.4
CO_2 (ppm)	2018	293 ± 17	193 ± 2	273 ± 20
CO (ppm)		0	0	0
Sound level (dB)		57.9 ± 5.6	61.6 ± 8.1	54.3 ± 6.2
CO_2 (ppm)	2021	390 ± 19	301 ± 6	330 ± 6
CO (ppm)		0	0	0
Sound level (dB)		58.3 ± 5.0	55.3 ± 8.8	53.2 ± 8.9
CO_2 (ppm)	2024	286 ± 7	211 ± 2	288 ± 9
CO (ppm)		0	0	0

Table 4. Measurements on location 2.

location 3	Year	*workday morning (7:00-8:00)*	*workday daytime (12:00-15:00)*	*workday evening (20:00-22:00)*
Sound level (dB)	2012	64.4 ± 3.4	63.4 ± 4.3	60.0 ± 4.9
Sound level (dB)	2015	67.5 ± 2.7	65.1 ± 4.0	60.1 ± 5.0
Sound level (dB)		66.0 ± 3.7	64.9 ± 4.1	61.5 ± 4.7
CO_2 (ppm)	2018	282 ± 15	174 ± 4	258 ± 5
CO (ppm)		0	0	0
Sound level (dB)		67.8 ± 2.8	66.9 ± 2.7	65.9 ± 3.7
CO_2 (ppm)	2021	416 ± 9	263 ± 18	291 ± 3
CO (ppm)		0	0	0
Sound level (dB)		64.3 ± 3.1	62.8 ± 3.6	58.6 ± 4.3
CO_2 (ppm)	2024	262 ± 12	210 ± 26	307 ± 19
CO (ppm)		0	0	0

Table 5. Measurements on location 3.

location 4	Year	*workday morning (7:00-8:00)*	*workday daytime (12:00-15:00)*	*workday evening (20:00-22:00)*
Sound level (dB)	2012	43.4 ± 2.1	50.0 ± 3.5	42.9 ± 2.9
Sound level (dB)	2015	44.6 ± 2.1	35.3 ± 2.7	42.1 ± 4.1
Sound level (dB)		41.4 ± 2.5	42.5 ± 2.9	41.9 ± 0.9
CO_2 (ppm)	2018	270 ± 7	169 ± 20	262 ± 8
CO (ppm)		0	0	0
Sound level (dB)		52.1 ± 1.3	52.0 ± 2.8	50.4 ± 1.1
CO_2 (ppm)	2021	429 ± 5	287 ± 10	309 ± 11
CO (ppm)		0	0	0
Sound level (dB)		42.0 ± 1.9	47.9 ± 1.4	38.3 ± 1.1
CO_2 (ppm)	2024	270 ± 3	182 ± 5	278 ± 17
CO (ppm)		0	0	0

Table 6. Measurements on location 4.

location 5	Year	*workday morning (7:00-8:00)*	*workday daytime (12:00-15:00)*	*workday evening (20:00-22:00)*
Sound level (dB)	2012	57.5 ± 2.9	49.3 ± 2.5	51.4 ± 3.2
Sound level (dB)	2015	52.1 ± 3.3	51.0 ± 3.3	49.0 ± 3.2
Sound level (dB)		51.2 ± 2.9	52.4 ± 3.0	49.9 ± 3.1
CO_2 (ppm)	2018	285 ± 12	189 ± 12	266 ± 6
CO (ppm)		0	0	0
Sound level (dB)		62.8 ± 1.8	55.2 ± 2.2	52.3 ± 4.4
CO_2 (ppm)	2021	428 ± 4	301 ± 10	311 ± 2
CO (ppm)		0	0	0
Sound level (dB)		54.7 ± 2.3	51.3 ± 2.9	49.7 ± 4.3
CO_2 (ppm)	2024	277 ± 9	210 ± 25	267 ± 9
CO (ppm)		0	0	0

Table 7. Measurements on location 5.

location 6	Year	*workday morning (7:00-8:00)*	*workday daytime (12:00-15:00)*	*workday evening (20:00-22:00)*
Sound level (dB)	2012	64.0 ± 3.4	59.6 ± 6.2	51.9 ± 8.3
Sound level (dB)	2015	62.9 ± 4.7	63.8 ± 4.6	60.2 ± 4.0
Sound level (dB)		57.4 ± 7.6	60.3 ± 6.7	60.1 ± 3.9
CO_2 (ppm)	2018	279 ± 7	218 ± 14	237 ± 3
CO (ppm)		0	0	0
Sound level (dB)		64.4 ± 6.0	63.8 ± 5.9	57.1 ± 7.4
CO_2 (ppm)	2021	349 ± 23	306 ± 11	323 ± 16
CO (ppm)		0	0	0
Sound level (dB)		63.7 ± 4.1	64.9 ± 4.9	58.1 ± 5.7
CO_2 (ppm)	2024	242 ± 5	229 ± 13	258 ± 21
CO (ppm)		0	4 ± 1	0

Table 8. Measurements on location 6.

The measurements to check the noise levels of the Youth Days of Szeged are shown in table 9. The samples were taken in the time period of 22:00-24:00. No CO could be detected.

Youth Days of Szeged	Year	*location 1*	*location 2*	*location 7*	*location 8*
Sound level (dB)	2012	54.2 ± 6.1	59.0 ± 4.1	59.7 ± 2.4	64.9 ± 2.5
Sound level (dB)	2015	53.8 ± 7.2	60.6 ± 4.4	64.2 ± 2.3	61.3 ± 2.3
Sound level (dB)	2018	49.4 ± 4.3	58.8 ± 5.8	62.5 ± 1.6	64.4 ± 2.0
CO_2 (ppm)		254 ± 2	256 ± 11	247 ± 4	255 ± 3
Sound level (dB)	2021	56.2 ± 6.5	59.5 ± 6.3	65.0 ± 2.7	70.4 ± 2.1
CO_2 (ppm)		333 ± 10	279 ± 4	276 ± 7	269 ± 4
Sound level (dB)	2024	49.0 ± 6.4	56.4 ± 5.1	63.5 ± 2.4	71.4 ± 1.4
CO_2 (ppm)		251 ± 9	238 ± 4	241 ± 4	241 ± 9

Table 9. Measurements during Youth Days of Szeged.

Conclusion

The results show that Szeged is an exceptional city to live in. It has a somewhat silent acoustical environment. Even during summer festivals.

The structure of the city is very good for the air ventilation, too. The CO_2 values are quite low, despite the fact that sometimes the measurements were carried out in *1 m* distance only from the traffic (location 2 and 6). CO could hardly be measured at all.

This work aims to measure the environmental load created mainly by traffic. Currently there is no real trend in the data. If electric vehicles will be more common a change may arise.

References

[1] Rossing, T., Springer Handbook of Acoustics, Springer (2007), ISBN 978-0387304465, pp. 747-748

[2] Thompson, A. and Taylor, B. N. sec 8.7, "Logarithmic quantities and units: level, neper, bel", Guide for the Use of the International System of Units (SI) 2008 Edition, NIST Special Publication 811, 2nd printing (November 2008)

[3] Suzuki, Yôiti, et al. "Precise and full-range determination of two-dimensional equal loudness contours." Tohoku University, Japan (2003)

[4] http://www.mp3-tech.org/programmer/docs/IS-01Y-E.pdf

[5] ISO 226:2003

[6] http://en.flossmanuals.net/csound/ch008_c-intensities/_booki/csound/static/Fletcher-Munson.png

[7] http://en.wikipedia.org/wiki/A-weighting

[8] Stanley Smith Stevens: A scale for the measurement of the psychological magnitude: loudness. See: Psychological Review. 43, Nr. 5,APA Journals, 1936, pp. 405-416

[9] https://en.wikipedia.org/wiki/Sone

[10] https://www.co2.earth/ (accessed: Sep.19.2024)

[11] Bonino, S., "Carbon Dioxide Detection and Indoor Air Quality Control", Occupational Health & Safety (April 2016) {*https://ohsonline.com/articles/2016/04/01/carbon-dioxide-detection-and-indoor-air-quality-control.aspx*}

[12] Benkő, Zsolt I.," NOISE AND EXTRA ENVIRONMENTAL MEASUREMENTS IN THE CITY OF SZEGED – A 9 YEAR SURVEY", Proceedings of the 27th International Symposium on Analytical and Environmental Problems (November 22-23, 2021), ISBN 978-963-306-835-9, pp. 91-95

PERCEPTION OF GLOBAL PROBLEMS AMONG STUDENTS: AN 8-YEAR RETROSPECTIVE

László Berényi

Institute of Management Science, University of Miskolc, H-3515 Miskolc-Egyetemváros, Hungary
e-mail: laszlo.berenyi@uni-miskolc.hu

Abstract

Global social and environmental problems frame the development actions for sustainability. UN conferences and other sources display a long list of problems, which enhances the evaluation of the relative importance of the items. The paper presents the results of empirical data collection among higher education students about their preferences between 2016 and 2024. The results show that the perception of the most critical global problems is differently assessed in their local environment and worldwide. Some changes in the orders were found, especially before and after 2020, but there was no fundamental change in the opinions.

Introduction

Solving global social and environmental problems has been in focus for decades. However, it is not easy to even define the scope and the content of global problems. The international conferences organized by the United Nations (UN) [1] [2] emphasized and covered the progress.

The United Nations Conference on the Human Environment, 5-16 June 1972, Stockholm [3], already showed that global problems mean a complex phenomenon. 26 principles and 109 recommendations are difficult to manage without making preference orders. Further conferences [2] tried to focus the efforts and change the approach from exploring to solving the problems more or less successfully. Local differences and competing interests made the prioritization confused. The 'Limits to Growth' report by the Club of Rome in 1972 [4] suggested zero growth, and moving towards a catastrophe was confirmed in more recent analyses of the authors [5]. Both the Club of Rome world models and the concept of sustainable development in the Brundtland Report [6] emphasized the economic aspects of the problems. Recently, the Millenium Goals [7] followed by the 17 Sustainable Development Goals [8] by the UN, offer a comprehensive but still complex briefing to the development of mankind. We are at the peak of ESG [9], which is about the evaluation of environmental, social, and governance issues of corporations.

Although the solutions for global problems are unequivocally based on the achievements of engineering sciences, material sciences, medical sciences, and others, social aspects have been appreciated. For example, a priority task of education can be highlighted through spreading knowledge and raising awareness. Learning the perception of global problems at the people level seems to be a soft approach, but understanding their preferences and sensitivity gives a relevant source of information at higher levels. Corporations can use the results for targeted marketing actions, and governments can adjust their strategies and communication for better acceptance and social support. Schools and higher education institutions can explore characteristic patterns of opinions and lead back the results to support engineering work. Due to the complexity of humans, a comprehensive survey is not feasible, but any contributions to the body of knowledge are essential.

The study aims to show the relative assessment of global problems based on a survey among Hungarian higher education students. A historical database between 2016 and 2024 that allows for the monitoring of changes was available.

Experimental

I developed a comprehensive online questionnaire for higher education students to support management education in sustainability. The questionnaire includes a list of global problems and asks the respondents two questions to mark a maximum of three items that they consider the most important problems in the closer environment and worldwide. The frequencies of markings show the relative importance of the items. The research sample in this study is based on the responses of Hungarian business, engineering, and public administration students, and the year of data collection was used as a grouping factor. The data collection covered 2016, 2018, 2020, 2022 and 2024. The results are presented in the percentage of the number of respondents in each subsample. Sample characteristics are summarized in Table 1.

Table 1. Sample characteristics

Year	Female	Female (%)	Male	Male (%)	Total
2016	886	64.5	488	35.5	1374
2018	277	65.5	146	34.5	423
2020	162	56.8	123	43.2	285
2022	138	52.9	123	47.1	261
2024	46	48.9	48	51.1	94

The research questions are as follows:
- Which social and environmental problems are considered the most important by the respondents?
- Do the samples by year show a change in preferences?

Results and discussion

The results confirm that the perception of the highlighted global problems differs in the closer environment and worldwide. The most argued topic is household waste in the local environment, and climate change worldwide. Table 2 summarizes the ratios of the markings for the total sample with a bold highlight of the highest values.

Table 2. Marking of the items by sub-samples (%)

	2016 Local	2016 World	2018 Local	2018 World	2020 Local	2020 World	2022 Local	2022 World	2024 Local	2024 World
Crime	22.3	*35.7*	15.4	*27.2*	15.1	*20.7*	10.7	*9.6*	13.8	*16.0*
Starvation	5.5	***52.0***	5.9	*48.5*	2.8	*44.9*	4.6	*35.6*	2.1	*39.4*
Healthy foods	14.6	*7.4*	13.5	*5.2*	10.2	*8.1*	20.7	*9.6*	16.0	*12.8*
Depletion of energy resources	4.1	*23.4*	4.5	*16.8*	3.2	*22.5*	9.2	*26.4*	7.4	*21.3*

Degradation of built environment	16.4	*1.8*	18.7	*2.1*	18.2	*1.8*	14.2	*2.3*	18.1	*0.0*
Extinction of species	1.0	*17.0*	1.9	*18.7*	1.8	*23.2*	0.4	*22.6*	1.1	*18.1*
Household waste	**39.0**	*3.3*	**43.7**	*4.3*	**50.2**	*5.3*	**45.2**	*5.0*	33.0	*1.1*
Industrial waste	10.0	*11.9*	10.2	*13.0*	13.7	*12.6*	14.6	*15.7*	14.9	*11.7*
Climate change	10.9	*49.6*	18.0	***60.3***	21.1	***66.3***	28.7	***66.3***	21.3	***53.2***
Public safety	34.4	*11.9*	29.3	*9.0*	29.5	*5.6*	24.9	*2.7*	23.4	*5.3*
Cultural changes	15.4	*7.1*	15.6	*4.7*	13.7	*5.6*	13.4	*7.3*	25.5	*5.3*
Air pollution	35.2	*19.1*	39.0	*23.2*	43.9	*26.3*	41.0	*31.0*	**34.0**	*40.4*
Soil degradation	10.6	*6.0*	14.2	*6.4*	10.2	*6.7*	13.0	*8.8*	19.1	*10.6*
Destruction of natural values	23.6	*22.7*	22.2	*27.4*	21.4	*24.6*	30.3	*22.6*	33.0	*23.4*
Emission to water	9.9	*19.9*	8.7	*23.6*	17.5	*23.2*	13.4	*30.7*	19.1	*36.2*

Figure 1 represents the changes in preferences in the closer environment, and Figure 2 shows them in the case of worldwide assessment. The main local concerns include household waste and air pollution, which had an increasing importance until 2020 (the COVID-19 lockdown) and a decrease after that. Depreciation of natural values shows an increasing value. Although climate change is not among the top issues, it is increasingly important.
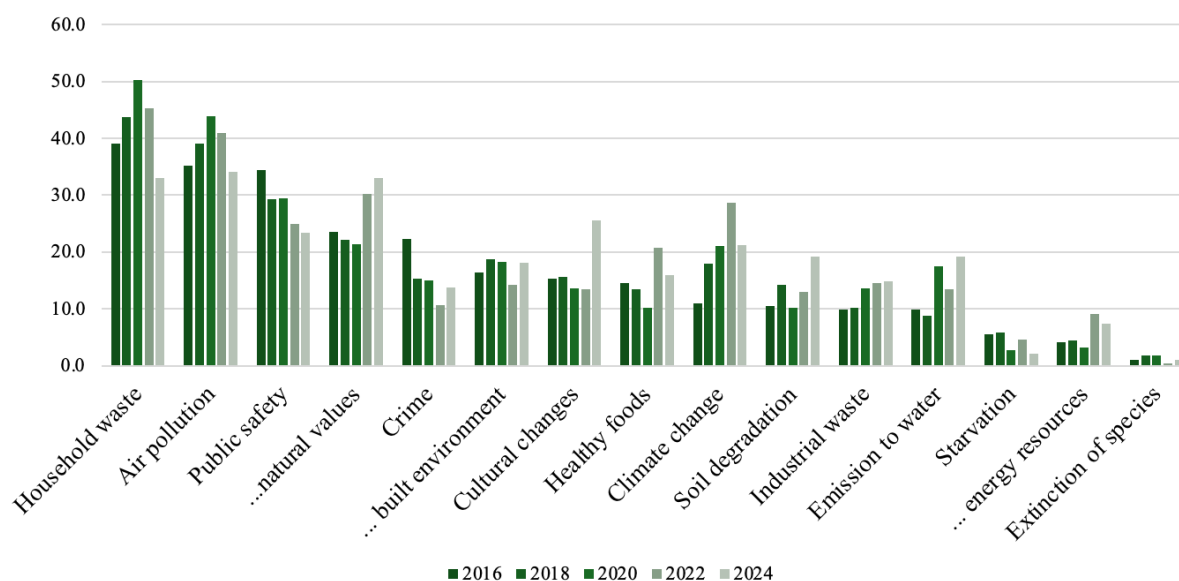
Figure 1. Frequencies of marking the problem items in the closer environment (%)

The worldwide assessment results emphasize starvation and climate change among the most important problems. Crime is an item that has a decreasing importance on both levels. Emissions to water and air pollution have been appreciated as a worldwide problem (Figure 2).
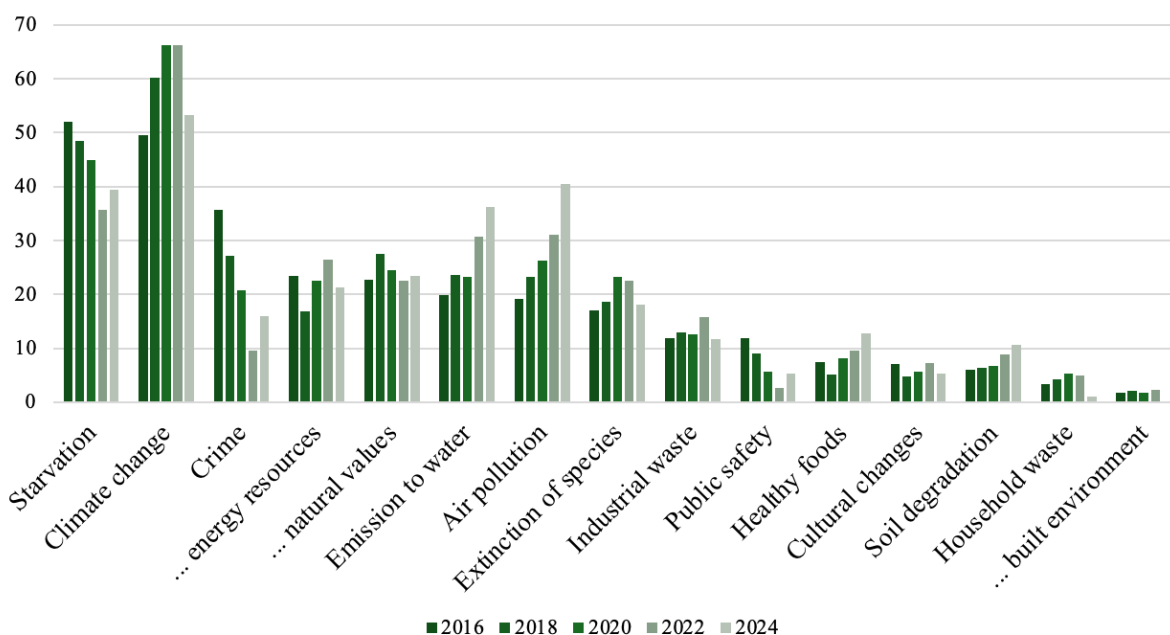
Figure 2. Frequencies of marking the problem items worldwide (%)

The rankings presented in Table 2 were tested by non-parametric correlation (Spearman Rho) analysis. The test shows non-significant low correlations between the ranking orders between the assessment of local and worldwide assessments in each year (Spearman's Rho values are -0.346 in 2016, -0.239 in 2018, -0.150 in 2020, -0.132 in 2022, and -0.084 in 2024), while each value is high and significant between the years (Table 3). That suggests that the perception of global social and environmental problems has not essentially changed during the research period.

Table 3. Correlation analysis results by years, total sample (Spearman's Rho)

Local:	2016	2018	2020	2022	2024
2016	1	.957**	.866**	.788**	.789**
2018	.957**	1	.918**	.849**	.866**
2020	.866**	.918**	1	.876**	.845**
2022	.788**	.849**	.876**	1	.844**
2024	.789**	.866**	.845**	.844**	1
Worldwide:	2016	2018	2020	2022	2024
2016	1	.943**	.873**	.832**	.858**
2018	.943**	1	.928**	.844**	.895**
2020	.873**	.928**	1	.963**	.981**
2022	.832**	.844**	.963**	1	.972**
2024	.858**	.895**	.981**	.972**	1
**: significant at 0.001 level					

Conclusion

Ranking the perception of global social and environmental problems may not be the fundamental question about sustainability. Still, the complexity of the topic and the high

number of factors considered make navigation difficult. Since the challenges are common, education and training programs can greatly benefit from learning the individual value systems. The crisis events in recent years raise the question of whether those have an impact on these values. The study presented in this paper has serious limitations. The data collection was performed among students, and the representativeness of the data could not be assured. At the same time, the methodology can serve as an example, and the results of the large sample highlight the critical problems. The main conclusions of the study can be summarized as follows:

- There are spatial differences in the perception of global problems in the sense that students' preferences are fundamentally different for their closer environment and worldwide.
- Issues of social and natural environment are mixed in the top rankings. That is in line with the concept of the SDG's tailored approach [8]. Managing household waste as an integrative topic can be an initial point for developing management actions.
- There are changes in the preference orders, and in some cases, the 'COVID-19 year' represents a breaking point. At the same time, the statistical analysis does not show fundamental differences.

The question of how to change the value system on an international or national level goes beyond the limits of the study and the author. On the corporate level and in education, understanding preferences can help shape the mind.

References
[1] I. Láng, Lesz-e új a nap alatt a környezetvédelemben?, Magyar Tudomány, 48/12 (2001) 1415-1422.
[2] K.A. Hite, J.L. Seitz, Global Issues. An Introduction. 5th edition, Wiley Blackwell, Chichester, 2016.
[3] United Nations, Report of the United Nations Conference on Human Environment, Stockholm, 5-16 June 1972, 1972, A/CONF.48/14/Rev.1.
[4] D.H Meadows, Limits to Growth, Signet, Exeter, 1972.
[5] D.H Meadows, J. Randers, D. Meadows, Limits to Growth: The 30-Year Update, Chelsea Green Publishing, Vermont, 2004.
[6] World Commission On Environment and Development, Our Common Future, Oxford University Press, Oxford, 1987.
[7] United Nations 55/2. United Nations Millennium Declaration, 2000, General Assembly resolution 55/2.
[8] United Nations Environmental Programme, Transforming our World: The 2030 Agenda for Sustainable Development, 2015, A/RES/70/1.
[9] A. Edmans, The end of ESG, Financial Management, 52/1 (2023) 3-17.

GROWTH OF TmF₃ DOPED CaF₂ CRYSTALS AND INVESTIGATION OF THEIR OPTICAL PROPERTIES

<u>Gabriel Buşe</u>[1], Maria Poienar[1], Marius Ştef[2], Carla Zeicu[2], Daniel Vizman[2], Vincent Motto-Ros[3], Frédéric Pelascini[4] and Philippe Veber [1,2]

[1]ICAM, West University of Timisoara, Bvd. Vasile Parvan, No.4, Timisoara, ROMANIA
[2]Physics Faculty, West University of Timisoara, Bvd. Vasile Parvan, No.4, Timisoara, ROMANIA
[3]Université Lyon, Université Claude Bernard Lyon 1, CNRS, Institut Lumière Matière, UMR 5306, F-69100, Villeurbanne, FRANCE
[4]CETIM, Grand Est, 67305 Schiltigheim, FRANCE
gabriel.buse@e-uvt.ro

Abstract

Rare-earth (Tm, Er, Yb etc.) ions-doped calcium fluoride (CaF₂) crystals have been extensively investigated due to the possible use in applications as for example: optical windows, lenses, optical communications, laser host materials or scintillators[1]. Among the rare earths, thulium-doped crystals are very interesting in the field of high-power lasers and for wavelength-tunable solid-state lasers in medical treatments[2].

Introduction

CaF₂ crystalline matrix is formed into a fluorite cubic structure (Fm-3m space group), with the Ca^{2+} cations surrounded by eight F⁻ ions, while F- atoms are enclosed by four Ca^{2+} ions[3]. The Tm^{3+} doping into the host lattice is made without change in the symmetry and the excess of charge is compensated by interstitial F- ions in different positions leading to isolated site symmetry centers at low Tm^{3+} content like tetragonal (C4v), trigonal (C3v), cubic (Oh)[4,5]or more complex clusters for higher Tm^{3+} doping[6]. These differences in site symmetries influence the optical characteristics. Optical investigations by absorption and emission spectroscopy were carried out at room temperature in order to point out the influence of Tm content. Moreover, the Judd-Ofelt theory was used to determine the intensity parameters Ω_2, Ω_4, and Ω_6 from the optical absorption spectra using various groups of transitions of Tm^{3+}. As crystalline imperfections may influence the laser performance, the study of the dislocations density was performed in order to characterize the crystal quality. Finally segregation behavior of thulium was studied through LIBS, ICP measurements and optical spectroscopy.

Experimental

The different concentrations of Tm-doped fluoride CaF₂ crystals (0.1, 1 and 5 mol%) where grown by using an in-house vertical Bridgman configuration[7-9]. Thulium elemental content measurements were performed by using Inductively Coupled Plasma - Atomic Emission Spectroscopy (ICP-AES) using the Vista MPX (Varian) and a specific LIBS set-up[10]. The influence of the Tm dopant concentration on the dislocation density has been investigated using the chemical etching method by in immersing a cleaved sample in 2N HCl at 60^0C for 2 minutes. The room temperature optical absorption spectra in the UV-VIS-NIR spectral range were recorded using a Shimadzu 1650PC and Nexus 470 FTIR spectrophotometer. To measure the room temperature luminescence spectra, in the UV- VIS domain a PerkinElmer LS55 spectrofluorimeter was used.

Results and discussion

Performing ICP-AES and LIBS measurements we observed that as the concentration of the TmF_3 in the initial melt increases, the effective segregation coefficient, k_{eff} of both Tm^{3+} and Tm^{2+} ions decreases. The study of the dislocations density showed an increase with the TmF_3 content and is at an order of 10^3 cm^{-2}. Analyzing the absorption spectra of CaF_2 :x mol% TmF_3 (where x = 0.1, 1, and 5mol%) revealed multiple absorption bands corresponding to both trivalent and divalent thulium ions. The UV emission spectra of Tm^{2+}-doped CaF_2 crystals under 305 nm excitation show a pronounced peak at 353 nm for CaF_2:0.1 mol% TmF_3. Room temperature emission spectra under excitation at (a) 260 nm, corresponding to the $^3H_6 \rightarrow ^3P_2$ transition, and (b) 353 nm, corresponding to the $^3H_6 \rightarrow ^1D_2$ transition revealed emission peaks at 343, 358, 378, 449, 482, 510 nm, and 690 nm. By analyzing six absorption bands corresponding to specific transitions of Tm^{3+} ions from the ground state $^3H_6$ to excited states: $^3F_4$, $^3H_5$, $^3H_4$, $^2F_{2,3}$, $^1G_4$, and $^1D_2$, the JO parameters were determined.

Figure 1. CIE chromaticity diagram of CaF_2:Tm^{3+} crystal under excitation at 260 and 356 nm.
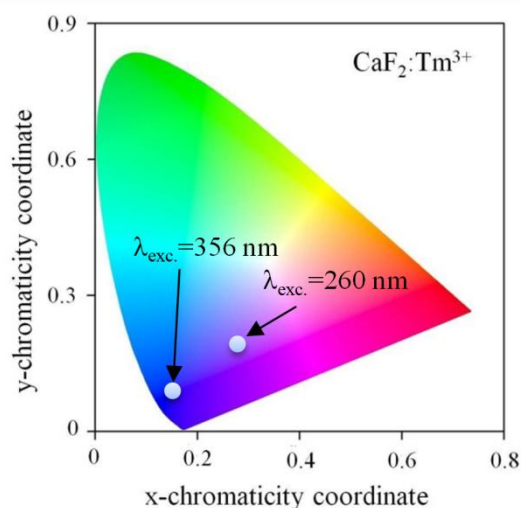
Conclusion

Different concentration of optical quality TmF_3-doped CaF_2 crystals were grown using vertical Bridgman method. The dislocations density is at an order of 10^3 cm^{-2} which demonstrate good to very good quality (and appropriate growth conditions) of the obtained crystals for optical and laser measurements. The segregation coefficient of Tm decreases with the increase of the TmF_3 concentration in the melt. The absorption peaks intensities strongly depend on the TmF_3 concentration and we observed the presence of Tm^{2+} ions. The PL spectra (under excitation in 260 and 356 nm) reveal two emission bands in UV and VIS spectral region with the one from UV being higher. Judd-Ofelt analysis revealed that the calculated radiative transition probability is in good agreement with the emission spectra.

References

[1] D.Hahn., Opt. Photonik. 9 (2014) 45–48.

[2] C. Gaida, M. Gebhardt, T. Heuermann, F. Stutzki, C. Jauregui, and J. Limpert Opt. Lett. 43 (2018) 5853-5856.

[3] W.P. Davey, Phys. Rev. 19 (1922) 248.

[4] R.A. Catlow, J. Phys. C Solid State Phys. 9 (1976) 1845–1856.

[5] J.-P.R. Wells, T. Dean, R.J. Reeves, J. Lumin. 96 (2002) 239–248.

[6] V. Petit, P. Camy, J.-L. Doualan, X. Portier, R. Moncorge, Phys. Rev. B. 78 (2008) 085131.

[7] I. Nicoară and M. Stef, Growth and Characterization of Doped CaF_2 Crystals, in Modern Aspects of Bulk Crystal and Thin Film Preparation, edited by N. Kolesnikov and E. Borisenko, Vol. chapter 4, 2012, pp. 71–96.

[8] D. Nicoară and I. Nicoară, Mater. Sci. Eng. 102 (1988) L1-L4.

[9] I. Nicoară, M. Stef, G. Buse, and A. Racu, J. Cryst. Growth. 547 (2020) 125817.

[10] V Motto-Ros. S. Moncayo, C. Fabre, B Busser, Chapter 14 - LIBS Imaging Applications. In Laser-Induced Breakdown Spectroscopy (Second Edition); Singh, J. P., Thakur, S. N., Eds.; Elsevier: Amsterdam, 2020, pp 329–346

VISIBLE-LIGHT PHOTOCATALYSIS OF AZO DYES USING COPPER(II) COORDINATION POLYMERS

Ildiko Buta, Maria Andreea Nistor, Simona Gabriela Muntean[*]

"Coriolan Drăgulescu"Institute of Chemistry, Bdul Mihai Viteazu no. 24, Timişoara, Romania
E-mail: sgmuntean@acad-icht.tm.edu.ro

The growing awareness of water pollution problems has been the main cause for the development of new technologies and methods of wastewater treatment with the main purpose to reduce the negative impact on the environment [1]. Photocatalysis proved to be a promising tool for the production of hydrogen fuel, generating electricity from solar cell systems but also for the degradation of pollutants like dyes, phenols, pesticides and antibiotics [2]. Three copper(II) coordination polymers, namely $^1_\infty[Cu_3L_2(N_3)]CH_3COO$ (**1**), $^1_\infty[Cu_3L_2(NO_3)]NO_3 \cdot 2MeOH \cdot 2H_2O$ (**2**), and $^1_\infty[Cu_3L_2(H_2O)](ClO_4)_2$ (**3**), (H_2L = N,N'-bis[(2-hydroxybenzilideneamino)propyl]-piperazine) [3] were investigated for the degradation of Acid Orange 7 (AO7) and Methyl Orange (MO) dyes, under irradiation with visible light. Dye concentrations before and after irradiation were determined by UV/vis spectrophotometry, by measuring the absorbance at the maximum wavelength of the dyes, and with these data the photodegradation efficiency was calculated. The influence of the hydrogen peroxide presence, reaction time, and dye concentration on the photodegradation efficiency of AO7 and MO was investigated. The obtained results with and without H_2O_2 under visible light irradiation, highlights the fact that the removal efficiency of AO7 and MO increased slightly in the presence of hydrogen peroxide.

The photodegradation efficiency decreases and the necessary time for the degradation process increases with increasing concentration of the dye solutions. The kinetic of dyes photodegradation was investigated using the Langmuir-Hinshelwood model and the obtained results showed that the degradation process followed a pseudo-first-order kinetic. The excellent stability of the copper(II) coordination polymer after the photodegradation process of dyes was demonstrated by the consistency of the initial and final structure of the complex. A photocatalytic oxidation mechanism was proposed, for the AO7 and MO photodegradation.

References
[1] P.H.M. Andrade, H. Palhares, C. Volkringer, T. Loiseau, M. Hureau, E. Nunes, A. Moissette, J. Photochem. Photobiology, C: Photochem. Rev. 57 (2023) 100635;
[2] M. Saeed, M. Muneer, A. Haq, N. Akram, Environm. Sci.Poll. Res. 29 (2022) 293;
[3] I. Buta, A. Ardelean, P. Lönnecke, G. Novitch, E. Hey-Hawkins, M. Andruh, O. Costisor, Polyhedron 190 (2020) 114766.

SYNTHESIS AND MESOMORPHIC PROPERTIES OF NOVEL THERMOTROPIC LIQUID CRYSTALS

Livia Deveseleanu-Corici[1], Daniela Haidu[1], Angela Maria Spirache[1], Milenca Vorga[1], Xiangbing Zeng[2], Goran Ungar[3], Liliana CSEH[1]

[1] *"Coriolan Dragulescu" Institute of Chemistry, Timisoara 300223, Romania*
[2] *Department of Materials Science and Engineering, University of Sheffield, Sheffield S1 3JD, U.K*
[3] *State Key Laboratory for Mechanical Behaviour of Materials, Xi'an Jiaotong University, Xi'an 710049, P.R. China*
e-mail: liviacorici@yahoo.com

The design and development of polycatenar molecules carrying chromophoric aromatic groups has gained an increased interest due to their optoelectronic applications such as OLED devices [1], memory devices [2], nonlinear optical materials [3], as well as solar cells [4], sensors and imaging agents [5]. Fluorenone is an interesting and widely studied rigid core unit which promotes the formation of higher order liquid crystalline phases such as SmC and SmC* in thermotropic and lyotropic systems [6]. Another interesting chromophore is benzothiophene where the polarizability of the mesogenic group is changed due to the polarity changes of the local bonds. It was reported that thiophene-based heterocyclic systems can be successfully used for design of various mesogens with ferroelectric properties [7]. Moreover, the presence of fluorinated benzothiophene rings in the core of liquid crystal molecules creates a favorable effect on the properties, in particular chiral smectic mixtures [8].

This study presents the synthesis and mesomorphic properties of a series of biphenyl-benzothieno-thiophene and fluorenone liquid crystals carrying peripheral flexible alkoxy side chains of different numbers and lengths. The purity and structural characterization of the intermediates and target compounds were carried out using 1D and 2D-NMR spectroscopy. The mesomorphic properties were investigated by differential scanning calorimetry (DSC), polarizing optical microscopy (POM) and Small and Wide Angle X-ray Scattering (SAXS/WAXS). The results showed the formation of different liquid crystalline phases depending on the nature and the ratio of rigid/soft parts. Smectic phases were found when the number and the length of the side chains were small, while the cubic phase was found for the compound carrying biphenyl-benzothieno-thiophene rigid core with three long end chains.

References
[1]. S.L. Ta., Z.K. Peng, X.H. Zhang, Adv. Funct. Mater., 15(10) 2005 1716–1721.
[2]. T. Mulia, M. Mumtaz, E. Ercan, C.L. Liu, Y.C. Lin, Y.Y. Yu, W.C. Chen, ACS Appl. Polym. Mater. 5(6) (2023) 3898–3911.
[3]. S. Semin, X. Li, Y. Duan, T. Rasing, Adv. Optical Mater. 9 (2021) 2100327.
[4]. X.J. Wang, E. Perzon, J.L. Delgado, P.D.L. Cruz, F.L. Zhang, F. Langa, M. Andersson, O. Inganas, Appl. Phys. Lett. 85 (2004) 5081-5083.
[5]. S.W. Thomas, G.D. Joly, T.M. Swager, Chem. Rev. 107 2007 1339-1386.
[6]. C. Schilling, A. Zens, S. Laschat, Liq. Cryst. 51(4) (2024) 641-655.

[7]. K. Cernovska, B. Kosata, J. Svoboda, V. Novotna, M. Glogarova. Liq. Cryst. 33 (2006) 987.

[8]. R. Wingen, A. Ogawa, B. Hornung, W. Schmidt. Ger. Offen. DE 19913349 (2000); Chem. Abstr. 133, 274346 (2001).

DETECTION OF MICROPLASTICS IN GANGA RIVER WATER IN UTTARAKHAND STATE OF INDIA

Manisha Dhiman[1], Prashant Pandey[2], Amit Pokhriyal[3], Rimpi Upadhyay[1], Anupama Lakhera[4]

[1]Uttaranchal Institute of Management, Uttaranchal University, Prem Nagar, Dehradun-248001, Uttarakhand, India
[2]Department of Applied Bioeconomy, Wroclaw University of Environmental and Life Sciences, 51-630 Wrocław, Poland
[3]Uttarakhand Pollution Control Board, IT Park, Dehradun- 248001, Uttarakhand, India
[4]Dev Bhoomi University Uttarakhand, Chakrata Road, Naugaon, Dehradun- 248007, Uttarakhand, India
e-mail: dmanisha518@gmail.com

Abstract

Plastics are sweet poision in now a days. Wherein Microplastic (MP) pollution are considered as a serious threat to aquatic ecosystem because of their lower amount and detection limit. The River Ganga is the life line in India by travelling 2525 KM which supports an enormous species diversity and economy of the country. The cities situated on its bank discharge untreated domestic waste and plastic related materilas by tourists or locals in River Ganga which are largely responsible for generating MPs. Every day millions of people use the river recreationally, for bathing and for drinking water. This study is the first to elucidate the distribution of MPs according to their shape, size and type in River Ganga in Haridwar which is one of the important place in India. Surface water samples of the river were obtained at 10 locations of the city Haridwar. Microplastic particles were identified using binocular microscope and categorized by shape, size and type. MPs were present at all the sampling sites in Hardwar along the River Ganga and highest concentrations of MPs was at Har Ki Paudi with an average concentration of 167.6 ± 21 particles m^{-3}). The average MPs concentration was 101.8 ± 36.12 (SD) particles m^{-3} (-0.1 particle L^{-1}) of surface water. Polyesters and nylon fibres were the dominated filamental particles in the river. The MPs concentration was positively correlated with population density in the vicinity ($r=0.71$; $p<0.001$) and sewage volume discharged ($r=0.6$; $p<0.01$) in the river. The MPs in Ganga water may pose potential risk to the local population and tourists because of the direct consumption of Ganga water on the occasions of ritualistic bathing. The present work adds new knowledge and understanding of MPs pollution in the Ganga River and the effects of highly urbanized cities on MPs pollution, which may be used as baseline data to evaluate precise mitigation.

Acknowledgements

References

[1] R. Kumar, A. Faiyaz, R. Kumar, J. Hazard. Mater. Adv. 11 (2023) 100342.
[2] D. J. Sarkar, S. D. Sarkar, R. K. Manna, S. Samanta, B. K. Das, J. Inland. Fish. Soc. India 52, no. 1 (2020) 05-15.
[3] S. P. Subuddhi, A. Kansal, P. Pandey, T. Ghoshal, N. Singhal, Environ. Eng. Res. 28, no. 5 (2023).

INVESTIGATION OF THE DEGRADATION OF A BIODEGRADEABLE PBAT-BIOPOLYMER USING A GC-MS METHOD

**Mária Mörtl[1], Damak Mariem[1], Zsolt Varga[2], György Fekete[2], András Székács[1]
László Alexa[2]**

[1]*Institute of Environmental Sciences, Hungarian University of Agriculture and Life Sciences,
H-2100 Gödöllő, Páter Károly u. 1, Hungary*
[2]*Profikomp Environmental Technologies Inc, H-2100 Gödöllő, Kühne Ede u. 7.
e-mail: mortl.maria@uni-mate.hu*

The decomposition of biopolymers is much more rapid process than that of traditional plastics, typically a few months [1]. To follow this, infrared spectroscopy is only of limited utility, because the FT-IR spectra of the polymer and the degradation products overlap significantly. For determination of decomposition products, we developed a method using gas chromatography coupled with mass spectrometry (GC-MS) applied after chemical derivatization of the target compounds.

Degradation of the polybutylene adipate co-terephthalate (PBAT) biopolymer was investigated under composting conditions on an industrial scale. Three parallel samples have been taken after 2, 6 and 12 weeks and 1 year. PBAT is a copolymer [2] made of monomers of 1,4-butanediol, adipic acid and terephthalic acid, which is used together with thermoplastic starch (TPS) and other additives to produce for example a biodegradable shopping bags.

PBAT
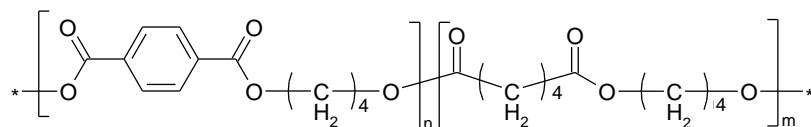
The composted plastic samples were fractionated (to >2 mm and <2 mm fraction), and the components were also extracted from the shopping bag product with organic solvents (acetonitrile and dichloromethane). The extracts were finally converted into silyl derivatives with N,O-bis(trimethylsilyl)trifluoroacetamide and analyzed by GC-MS. Some of the extracted compounds were identified, and we also performed quantitative determination of three substances (silylated 1,4-butanediol, adipic acid and terephthalic acid). Based on the mass spectra, we have found three futher molecules with structures containing the corresponding acid and one or two butanediol units. In addition, silylated sugars and glycerol were also detected in the extract.

Based on the results, it can be concluded that the concentration of terephthalic acid among the decomposition products is typically low (<35 µg/ml) and shows no significant changes over time. The concentration of adipic acid is higher (<152 µg/ml) and usually shows an increasing level. 1,4-Butanediol showed maximal levels in two samples taken on the 6th week, while a further increase was observed for a 3rd sample with the maximum average concentration of 535 mg/ml. The composition of the samples taken in parallel from the compost shows a vaste variability, the degree of decomposition largely depends on the local conditions (temperature). We observed no significant differences according to the size of the fractions.

It can be established that the decomposition products, including the complex (acid + butanediol) molecules, are still present in the compost even after one year, although their concentration has decreased (<35 µg/ml). Despite the incomplete degradation of the biopolymer, however, the sugars were no longer detectable in the sample. Although the main decomposition products cannot be classified as substances that pose a threat to the aquatic environment in terms of

toxicity, the presence of microplastics in our environment is of concern from several aspects [e.g., 3].

Acknowledgements

References
[1] Z. Üveges, M. Damak, S. Klátyik, M.W. Ramay, G. Fekete, Z. Varga, C. Gyuricza, A. Székács, L. Aleksza, Fermentation 9(3) (2023) 261.
[2] M. Dammak, Y. Fourati, Q. Tarrés, M. Delgado-Aguilar, P. Mutjé, Industrial Crops & Products 144 (2020) 112061.
[3] C. Campanale, G. Dierkes, C. Massarelli, G. Bagnuolo, V.F. Uricchio, Toxics 8 (2020) 100.

THE EFFICIENCY OF COBALT BASED MOFs IN THE ADSORPTION AND PHOTODEGRADATION OF DYES FROM AQUEOUS SOLUTIONS

<u>Simona Gabriela Muntean</u>, Maria Andreea Nistor, Ildiko Buta, Aurelia Visa

"Coriolan Dragulescu" Institute of Chemistry, Bdul Mihai Viteazu, 300223, Timişoara, Romania
e-mail: sgmuntean@yahoo.com

Abstract

In the last decades, there has been an increased interest in the removal of pollutants, such as organic dyes from industrial wastewater, mainly resulting from the textile industry [1]. The characteristics of metal–organic frameworks (MOFs), such as large specific surface area, variable pore structure, well-controlled pore size distribution, and tunable surface properties have made these materials used in various applications [2]. A series of cobalt based MOFs [3, 4] were applied as potential adsorbents and catalysts, respectively, for the removal of two anionic dyes: Acid Orange 7 (AO7) and Congo Red (CR), and two cationic dyes: Methylene Blue (MB) and Basic Fuchsine (FB) from aqueous solution. UV-Vis spectrophotometry was used to follow the decrease in absorbance over time and implicitly the discoloration of the dye solutions due to adsorption and degradation of the dyes, respectively. The experimental results showed that, in the case of anionic dyes (AO7, CR), the maximum adsorption capacity was obtained using the CoVP compound, and for cationic dyes (MB and FB) maximum yields were obtained using the CoPA compound. The obtained results indicated that the experimental adsorption data fitted well with the pseudo-second order kinetic model and the Langmuir isotherm model. The results obtained fron photodegradation studies shows that under irradiation at 546 nm, the discoloration (decrease in the concentration of the dye solution) does not occur in the absence of MOFs and is significant, and rapid in the presence of the investigated MOFs, occurring in just 30 minutes. The dyes degradation were found to follow pseudo-first-order kinetics.

The obtained experimental results demonstrated that the investigated MOFs can be used both as adsorbents and as photocatalysts, for the effective removal of dyes from model (laboratory) wastewater. Depending on the structure and nature of the dye, as well as the working conditions, the most effective method for removing dyes from aqueous solutions can be selected.

References

[1] M. Beydaghdari, F. Hooriabad Saboor, A. Babapoor, V.V. Karve, M. Asgari, Energies, 15 (2022) 2023.
[2] M.J. Uddin, R.E. Ampiaw, W. Lee, Chemosphere, 284 (2021) 131314.
[3] L. Lupa, N.S. Tolea, M. Iosivoni, B. Maranescu, N. Plesu, A. Visa, RSC Adv. 14 (2024) 4759.
[4] B. Maranescu, L. Lupa, A. Visa, Pure Appl. Chem. 88(10-11) (2016) 979.

FACTORIAL DESIGN AND RSM FOR OPTIMIZATION OF DYES ADSORPTION FROM WASTEWATER BY MAGNETIC NANOCOMPOSITE

Maria Andreea Nistor, Simona Gabriela Muntean*, Liliana Halip*

"Coriolan Dragulescu" Institute of Chemistry, 24 Mihai Viteazul Bvd., 300223, Timisoara, Romania,
e-mail: sgmuntean@acad-icht.tm.edu.ro, lili.ostopovici@gmail.com

Abstract

The textile industry consumes large amounts of water during technological processes, thus generating large amounts of wastewater, which contain polluting dyes [1]. The treatment of textile wastewaters has become a worldwide concern in order to protect the aquatic environment [2]. Factorial design and Response Surface Methodology (RSM) are powerful tools in optimizing conditions for dyes removal by adsorption [3]. The paper presents a factorial design experiment carried out in order to establish the optimal conditions for removal of dyes by adsorption with maximum yields and reduced resources. A magnetic nanocomposite based on activated carbon and iron oxide (magnetite) was synthesized by the combustion method [4], characterized, and applied as adsorbent material for the removal of dyes from wastewater by adsorption. The adsorption experiments of dyes were design based on three factors: solution pH, initial dye concentrations (C_{AO7}, C_{MB} and C_{ChS}), and adsorbent dosage (D_S). Using the experimental design matrix, a regression analysis was performed in order to find the best empirical model that evidences the maximum removal efficiency for investigated dyes. Optimal working conditions were established using the contour maps and 3D representations for each pair of factors present in the model. High removal efficiencies of over 92% for AO7, 99% for MB and 60% for Ch-S were obtained, even working under normal conditions: natural solution pH, and room temperature (25°C).

The study was extended to the simultaneous adsorption of dyes from bicomponent systems. Very good removal efficiencies, up to 98%, were obtained for the removal of the investigated dyes from bicomponent systems.

The kinetic studies indicated that the model that best describes the adsorption process for the investigated dyes was the pseudo-second order kinetic model. The equilibrium data were best fitted by the Sips isotherm model and a maximum adsorption capacity of 136.36 mg/g, 132.59 mg/g and 146.26 mg/g was obtained for AO7, MB and Ch-S respectively.

Six consecutive adsorption-desorption cycles were performed, and the high regeneration and reusability of the nanocomposite was demonstrated by the high removal efficiency of over 75% for AO7 and MB dyes and over 59% for Ch-S dye after the sixth use as adsorbent.

The obtained results demonstrate that the synthesized magnetic nanocomposite is a promising adsorbent material for the removal of dyes from single and binary systems. Optimization of the adsorption process using Factorial design and RSM proved to be an efficient method to determine the optimal working conditions that predict the highest dye removal yields.

References

[1] B.M. Adesanmi, Y.T. Hung, et al, GSCARR. 0 (2022) 126.
[2] J. Fito, M. Abewaa, et al, Sci. Rep. 13 (2023) 5427.

[3] M.A. Nistor, L. Halip, S.G. Muntean, L. Kurunczi, O. Costişor, Sustain. Chem. Pharm. 29 (2022) 1-20.

[4] R. Ianoş, C.,Păcurariu, G. Mihoc, Ceram. Int. 40 (2014) 13649.

NATURAL SOURCE BASED CARBON ADSORBENTS FOR SELECTIVE REMOVAL OF BETA LACTAM ANTIBIOTICS FROM WASTEWATER

<u>Prashant Pandey</u>[1*], Chinenye Adaobi Igwegbe[1], Andrzej Białowiec[1], Amit Pokhriyal[2]

[1]*Department of Applied Bioeconomy, Wroclaw University of Environmental and Life Sciences, 51-630 Wrocław, Poland;*
[2]*Amit Pokhriyal, Uttarakhand Pollution Control Board, Dehradun- 248001, India*
prashant.pandey@upwr.edu.pl

Abstract

Antibiotics can act as a hidden poison when overused or misused that can contaminate water quality even at low concentrations. The situation has become a severe problem in the world because of the accumulation of certain beta lactam froups in the living organisms posing risks to human and ecological health. In this context, natural source-based carbon adsorbents materials have been proven to be capable adsorbents for the removal of such bulky beta lactam antibiotics. In reference their high surface area and porosity, low cost, and significant physical & chemical properties plays vital role in adsorptive removal. In the present study, low-cost carbon adsorbent was synthesized from the local available Saw Dust material collected from the local market at Pasaż Grunwaldzki, Wrocław, Poland. N_2 adsorption-desorption isotherm, X-Ray Diffraction, and point of zero charge (pH_{ZPC}) characterization were used to confirm the successful synthesis of the material and changes in surface chemistry. The batch adsorption experiment revealed the higher efficiency of the prepared natural source-based carbon adsorbents as compared with the unprocessed saw dust, with maximum adsorption capacities of 22.2 mg/g for ampicillin and 9.16 mg/g for amoxicillin. Kinetic studies showed that the adsorption of both antibiotics followed a pseudo-second-order model indicating chemisorption, while the Langmuir isotherm provided a strong fit for the experimental data with correlation coefficients (R^2) > 0.90 implying adsorption occurred on monolayer surfaces, The adsorption on natural source-based carbon adsorbents was pH and temperature dependent, with lower adsorption observed at higher temperatures. Additionally, the adsorbent was easily regenerated using HNO_3 solution. The results of present study suggest that such adsorbents prepared from natural based carbon materials can be potentially used for the removal of beta lactam antibiotics group especially in waste water treatment offering a sustainable solution.

Keywords: Carbon adsorbents, Amoxicillin, Ampicillin, Adsorption, Wastewater treatment

Introduction

The widespread use of Beta lactam antibiotics is ascribed to its ability to treat some common diseases. However, their incomplete metabolism in bodies, high amount of such chemicals is released to the surrounding environment. Their presence in water system become a challenge for their removal because of low concentration [1]. Nevertheless, natural based carbon materials are considered as suitable candidates because of its structure, high surface area, low cost, regeneration and reusability [2]. Many documents reveal that carbon adsorbents can be prepared from natural sources which may include biomass waste, fruits, flowers, seeds, agricultural waste, and vegetable waste for the removal of various contaminants [3]. In this context, carbon adsorbents prepared from saw dust has been used for removal of contaminants from waste water but are not much explored and studied especially for the adsorptive removal of Beta lactam antibiotics.

Hence, the main shove of the present study is to develop and characterize the low-cost carbon adsorbents from natural based carbon material (Saw Dust) for the adsorptive removal of Beta lactam antibiotics mainly Amoxicillin (AMX) and Ampicillin (AMP).

Experimental

Saw Dust material collected from Pasaż Grunwaldzki, Wrocław, Poland. Hydrogen Chloride-38 wt.% (HCl), Zinc Chloride (ZnCl$_2$), were purchased from Sigma-Aldrich. In the study double distilled water and Helium gas was used for experimental work whenever is required. Amoxicillin of 500 mg of Cipmox 500mg Strip by CIPLA GX were purchased. Ampicillin of 500 mg- Cipla Ltd. were purchased. Brunauer–Emmett–Teller (BET) was used for the analysis of surface area and pore size distribution of the developed NCA and SDR materials through N$_2$ adsorption–desorption isotherms (Bet Surface Area Analyzer Micromeritices-ASAP2020). Whereas, XRD powdered technique (Bruker-D8-Advance) was used to confirm their crystalline structure before and after the development of the material.

Result and Discussion

In the study carbon adsorbents were prepared using the earlier study [4] with some modifications. In brief, 50 g ground saw dust was infused with ZnCl$_2$ solution (1.5 impregnation ratio) which was then placed for overnight at 90 °C for dehydration keeping at slow ramp. These dehydrated samples were carbonized at 550°C for 2h in absence of oxygen which was further treated with 0.1N HCl. The treatment with acid is to remove unexploited ZnCl$_2$ from the developed carbon adsorbent (Alslaibi, Abustan, Ahmad, Foul, & Biotechnology, 2013). Moreover, the obtained material was repeatedly washed with double distilled water until its pH reach to neutral. The washed material was then filtered using Whatman filter paper, dried, named as NBC and stored in desiccator for further utility. Wherein the starting material was named as SDR.

The developed materials were characterized with N$_2$ adsorption-desorption isotherm and pore size distribution are presented in Figure 1. The resultant isotherms show high adsorption of N$_2$ at low relative pressure that reflect the nature of pores as microporous for the samples. A high N$_2$ adsorption at a low relative pressure (under 0.1 p/p^0) labels high volume of the micropores with a thin pore size distribution.
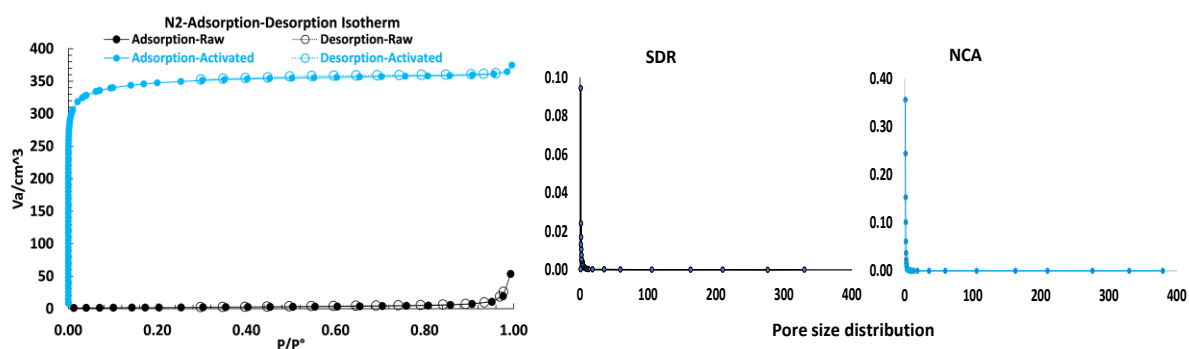

Figure 1: N$_2$ adsorption/desorption isotherm of the saw dust and developed carbon adsorbent

According, International Union of Pure and Applied Chemistry (IUPAC) classification, the nitrogen adsorption isotherms correspond to the Type I isotherm shape [5]. This reflects the prepared activated carbon has majority of micropores with the average pore size diameter of 1.5 nm, presented in Table 1. Further, isotherm also reveals that after impregnation of functional group and activating at higher temperature, surface area of the activated carbon increased from 72 m^2/g to 559.3 m^2/g (6).

Table 1: Surface area and pore size distribution of the starting material and prepared activated carbon

Sample	Surface area, m² g⁻¹	Vp, cm³ g⁻¹	Avg. pore diameter, nm
SDR	72	0.00729	2.9
NCA	559.3	0.2181	1.5

Where in powder XRD pattern of the materials displayed the characteristic diffraction peaks at 2theta = 14.9° (amorphous phase) and 2 theta = 22° (crystalline phase), shown in Figure 2a. The presence of the strong peak at 2theta which is 14.9° indicates the presence of a high proportion of compositions of noncellulose particles which is also confirmed by the previous study [7].
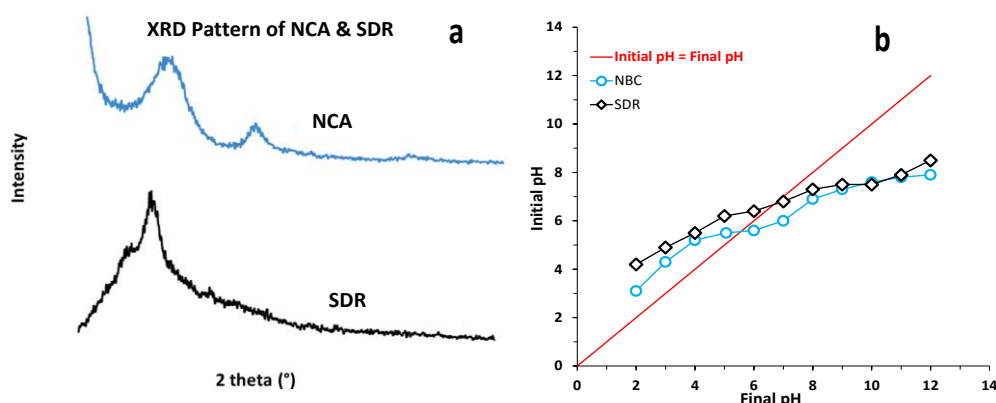

Figure 2: XRD pattern (a) and pHzpc (b) of the saw dust and prepared carbon adsorbent representing the stability of crystalline structure

Meanwhile pH$_{ZPC}$ analysis shown in Figure 2b displays the pH$_{ZPC}$ is approximately 5.8-6.0 for the prepared carbon adsorbent and 6.8-7.0 for the saw dust. This signify that the pH < 5.8, activated carbon would be dominated by positive charges and for pH > 5.8, surface will be dominated by the negative charges. The positive surface charge of the activated carbon is the result of acid treatment. In preparation, $ZnCl_2$ and HCl was used for the activation which are acidic in nature and has changed the surface properties of the activated carbon.

The solid-liquid interaction of antibiotics and adsorbents are evaluated by varying the contact time from 1 to 120 min. The result shows that the adsorption of antibiotics increases with the increase of reaction time. It was observed that > 50% adsorption was achieved within 15 min and shows quick adsorption rate due to availability of maximum active sites and same result was also observed in the previous study [8]. The higher amount of adsorption capacity can be observed for NCA because of presence of functional groups and increased surface area 559.3 m²/g. In the present study, the influence of pH can be observed on the surface adsorption characteristic of the NCA and SDR materials. The adsorption capacity of the NCA increases with increase in pH for both the antibiotics either AMX or AMP and shows higher amount of adsorption at pH 5-6.

The effect of variation in temperature on adsorption efficiency of the adsorbents for AMX and AMP was evaluated. Both the adsorbents show higher adsorption capacity at 25° C which decreases with the increase in temperature and follows the order 25° C > 35° C > 45° C. The increased temperature may affect the intermolecular interaction between heavy metals and adsorbents as a result of increased entropy. Moreover, the correlation coefficient R² values were used to obtain the best-fit linear equation which suggest the well-fitting of the experimental

data to Langmuir isotherm for both the antibiotics. Wherein, the correlation coefficient (R^2) for different antibiotics against NCA are > 0.9 and the obtained values of 1/n are < 1.0 indicates the favourable adsorption [9]. Among the various desorbing agents HNO_3 shows maximum desorption of Amoxicillin and Ampicillin in both the materials NCA and SDR which is followed by NaOH > NaCl > H_2O. The H^+ released from HNO_3 from an acidic medium may actively displace the other ions adsorbed on the materials.

Conclusion

The present study shows the successful synthesis and characterization of $ZnCl_2$ impregnated carbon adsorbents from saw dust using impregnation method. The prepared activated carbon shows > 50% of adsorption within 15 min in acidic condition at 25° C. The maximum removal on developed adsorbents was observed for AMP followed by AMX for both the materials. The result further explains the Freundlich model was well fitted with the experimental data indicates the favourable adsorption. Correlation coefficient (R^2) for different heavy metals on activated carbon was evaluated > 0.9. It was further observed that the adsorption capacity of both the materials decrease with increase in temperature. The activated carbon can be easily regenerated with HNO_3 solution and can be used up to 4 cycles with exhaustion of adsorption capacity < 50%. Hence, the result of present study suggests that carbon adsorbents prepared from saw dust can be potentially used for the removal of Beta lactam antibiotics especially in waste water treatment.

References

1. N. Jendrzejewska & Karwowska. E, Microorganisms. 10(12) (2022) 2323.
2. H. O. Orugba, C. Osagie, D. Ukpenusiowho, C. A. Igwegbe, G. O. Odigie, Desalin. Water. Treat. (2024) 100534.
3. P. Pandey, A. Kansal, M. Dhiman, S. P. Subudhi, A. S. Gautam, S. Gautam, Environ. Dev. Sustain. (2023) 1-13.
4. P. Pandey, A. Kansal, M. Dhiman, S. P. Subudhi, A. S. Gautam, S. Gautam, Environ. Dev. Sustain. (2023) 1-13.
5. K. Kiełbasa, A. Kamińska, O. Niedoba, B. Michalkiewicz, Materials. 14 (2021) 7458.
6. S. Suhdi, S. C. Wang, Nanomaterials. 11 (2021) 2038.
7. Y. O. Al-Ghamdi, M. Jabli, R. Soury, S. Ali Khan, Polym. 12 (2020) 2539.
8. V. K. Saini, S. Suthar, C. Karmveer, K. Kumar, J. Chem. 2017.
9. P. Pandey, A. Shankar, M. Biney, V. K. Saini, Colloids. Interface Sci. Commun. 43 (2021) 100432.

ELECTROCHEMICAL REGENERATION OF PHENOL- IMPREGNATED IONIC LIQUID/METAL PHOSPHONATES

Nicoleta Plesu[1], Lavinia Macarie[1], Bianca Maranescu[1,2], Adriana Popa[1], Aurelia Visa[1]

[1]*"Coriolan Dragulescu" Institute of Chemistry, 24 M. Viteazul Ave, Timisoara, Romania;*
[2]*Department of Biology-Chemistry, Faculty of Chemistry, Biology, Geography, West University Timisoara,16 Pestalozzi Street, 300115 Timisoara, Romania*
plesu_nicole@yahoo.com

Abstract

Over the past few decades, there has been a tremendous improvement in the efficiency and cost of using adsorbents to remove hazardous organic chemicals from water.

However, there has been little focus on recycling used adsorbents and recovering hazardous organic compounds from them. Researchers have extensively studied the regeneration and reuse of adsorbents. Metal-organic frameworks (MOFs), compounds made up of metal ions and organic linkers, are an appropriate adsorbent for dangerous pollutants from water. Effluents from the food and chemical industries contain phenolic compounds, a potentially hazardous organic molecule [1]. Electrochemical oxidation is a promising technique to remove the phenol from spent adsorbents. There are a few benefits to this strategy over the traditional ones: an easy reaction operated at room temperature and pressure in situ with minimal energy consumption and a short time. Using electrons as the only reagent and adjusting the applied current (or electrode potential) and other operational variables (like electrolysis time) can help recover organic pollutants, change them into less harmful compounds, or even turn them into minerals [2]. Therefore, the adsorbed contaminants do not require further oxidants for remediation. Numerous studies have been conducted on phenol electrooxidation. More investigation into this process is required. The electrooxidation process produces phenoxy radicals. These radicals can react with more phenol molecules to form dimeric radicals, or they can combine with other species already present in the solution to form products. Depending on the circumstances, we can oxidize this radical in one of two ways to generate either quinones or polymers. Basic media and moderate phenol concentrations favor quinone formation, while high phenol concentrations and basic media favor polymerization [3]. The quinone oxidation process produces carboxylic acids. Electrochemical oxidation can also regenerate MOF-type adsorbents impregnated with ionic liquids, used to extract phenols from waste water. We examined the electrochemical performance of Pt, glassy carbon electrodes in an acidic, basic, or 3% NaCl solution.

References

[1] H. Dong, H. Su, Z. Chen, H. Yu, H. Yu, Electrochim. Acta, 222 (2016) 1501.
[2] P. Canizares P, J. Lobato, J . Garcıa-Gomez J, M.A. Rodrigo. J Appl Electrochem. 34(1) (2004) 111.
[3] G. Mengoli, S. Daolio, M.M. Musiani, J. Appl. Electrochem. 10 (1980) 459.

SYNTHESIS OF IRON(II)-COMPLEXES WITH GLYOXIMES AND BORIC ACID DERIVATIVES, AND THEIR PHYSICAL-CHEMICAL AND BIOLOGICAL STUDIES

Csaba Várhelyi jr.[1], Ernő Kuzmann[2], Zoltán Homonnay[2], Roland Szalay[2], János Madarász[3], Raluca-Anca Mereu[1], Judit Papp[4], Melinda Simon-Várhelyi[1], Róbert Tőtős[1], Judith Mihály[5]

[1] *Faculty of Chemistry and Chemical Engineering, "Babeş-Bolyai" University, RO-400 028 Cluj-N., Arany János str. 11, Romania*
[2] *Institute of Chemistry, "Eötvös Loránd" University, H-1117 Budapest, Pázmány Péter str. 1/a, Hungary*
[3] *Faculty of Chemical Technology and Biotechnology, Budapest University of Technology and Economics, H-1111 Budapest, Műegyetem rkp. 3, Hungary*
[4] *Faculty of Biology and Geology, "Babeş-Bolyai" University, RO-400 015 Cluj-Napoca, Gheorghe Bilaşcu str. 44, Romania*
[5] *Institute of Materials and Environmental Chemistry, HUN-REN Research Centre for Natural Sciences, H-1117 Budapest, Magyar tudósok körútja 2, Hungary*
e-mail: ifj.varhelyi.cs@gmail.com

Abstract

Iron(II) complexes obtained with glyoximes are macrobicyclic ligand systems, which are formed under mild conditions with high yields [1]. The biological activity of these compounds is of particular importance. Some boric acid derivatives have been proposed as new radiopharmaceuticals for boron neutron capture therapy of cancer [2].

In our research work new iron(II) complexes were synthesized with α-dioximes, amines, boric acid derivatives, such as [Fe(Ph-Me-DioxH)$_2$L$_2$], [Fe(Me-i-Pr-DioxH)$_2$L$_2$] [Fe(Ph-Me-Diox)$_3$(BO–R)$_2$], [Fe(Bu-Me-Diox)$_3$(BO–R)$_2$], [Fe(i-Pr-Me-Diox)$_3$(BO–R)$_2$], where DioxH, Diox = mono- or bi-deprotonated dioxime, L = 1-naphthylamine, 2-methyl-imidazole, 2-amino-4-methyl-pyridine, lepidine, m-toluidine, dicyclohexylamine, 2-amino-5-picoline, R = H, methyl, ethyl, isopropyl, n-propyl, isobutyl, n-butyl. For preparation iron^{II}-sulfate was dissolved in water and mixed with alcoholic solution of the glyoxime, then the corresponding amines or the other complexing agents were added. The mixture so obtained was refluxed under an inert atmosphere.

The molecular structures of our products were studied using a range of techniques, including IR, Raman, Mössbauer and UV–VIS spectroscopies, mass spectrometry (MS) and thermoanalytical measurements (TG-DTG-DTA). In addition, their biological activity, including the antimicrobial effect against certain bacterial strains, was also investigated.

Introduction

Iron compounds are widely used, especially in pharmaceutics and nanotechnology. The use of nanoparticles in medicine in the fight against bacteria can be beneficial because their size is much smaller than that of bacteria (they are micrometres in size), or more precisely, the right size nanoparticles are able to penetrate the pores of their cell membrane [3]. The use of iron complexes as antibacterial agents which contain N- and O-donor ligands are also advantageous because they show more pronounced antibacterial effect against both Gram-positive and Gram-negative bacteria than the free ligands themselves [4].

[M(Dioximate)$_3$(BOR)$_2$] type complexes were discovered by Schrauzer, who noted that the classic [Ni(Me$_2$DioxH)$_2$] complex easily reacts with BF$_3$ and alkylboranes in ethereal

media. Voloshin et al. prepared a series of [Fe(Dioximate)$_3$(BOR)$_2$]-type complexes and characterized them using different physicochemical methods. Clathrochelates containing transition metals are used in HIV infections treatment [5].

In this paper we report the synthesis, characterization and biological evaluation of novel iron complexes with glyoximes and boric acid derivatives.

Experimental

Used materials: FeSO$_4$·7H$_2$O, Ph-Me-DioxH$_2$, Me-i-Pr-DioxH$_2$, Bu-Me-DioxH$_2$, 1-naphthylamine, 2-methyl-imidazole, 2-amino-4-methyl-pyridine, lepidine, m-toluidine, dicyclohexylamine, 2-amino-5-picoline, boric acid, borax, ascorbic acid, MeOH, EtOH, *i*-PrOH, *n*-PrOH, i-BuOH, *n*-BuOH.

Methods:

- Synthesis of [Fe(DioxH)$_2$L$_2$] type complexes

0.002 mol phenyl-methyl-DioxH$_2$, methyl-isopropyl-DioxH$_2$ or butyl-methyl-DioxH$_2$ was dissolved in 20 ml EtOH and this solution was added to the aqueous solution of 0.001 mol (0.3 g) FeSO$_4$ and 0.4 g ascorbic acid dissolved in 10 ml water. Then 0.002 mol amine (1-naphthylamine, 2-methyl-imidazole, 2-amino-4-methyl-pyridine, lepidine, m-toluidine, dicyclohexylamine, 2-amino-5-picoline) dissolved in 5 ml EtOH was added. The obtained solution was heated for 2–3 hours on a water bath under inert atmosphere. The filtered crystalline complexes were washed with EtOH–water mixture (1:1) and diethyl ether. A typical reaction as an example:
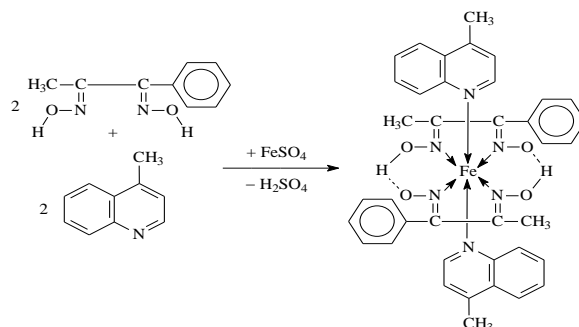
- Synthesis of [Fe(Diox)$_3$(BO-R)$_2$] type complexes

0.0075 mol phenyl-methyl-DioxH$_2$, methyl-isopropyl-DioxH$_2$ or butyl-methyl-DioxH$_2$ was dissolved in 20 ml MeOH, EtOH, i-PrOH, n-PrOH, i-BuOH or *n*-BuOH, then this solution was added to an aqueous solution of 0.0025 mol (0.7 g) FeSO$_4$ and 0.4 g ascorbic acid dissolved in 25 ml water. The role of ascorbic acid is to prevent the oxidation of Fe^{II} to Fe^{III}. Afterwards 0.0075 mol (0.46 g) boric acid dissolved in 15 ml H$_2$O was added. The mixture was refluxed for 15 min under inert atmosphere, and then 0.00375 mol (1.4 g) borax dissolved in 15 ml distilled water and 55 ml of the corresponding alcohol were added. The obtained solution was heated for 2–3 hours on a water bath, under inert atmosphere. After cooling the crystalline complexes were filtered off, washed with the used alcohol and diethyl ether, then dried in air. A representative reaction is illustrated below:
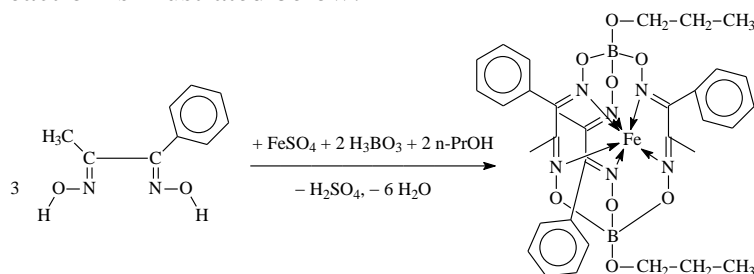
Microscopic characterization and yields of the prepared complexes are presented in Table 1.

Table 1. Microscopic characterization, calculated molecular weights and yields of the prepared complexes.

Nr.	Compound	Calc. mol. weight	Yield (%)	Microscopic characterization
1.	[Fe(Ph-Me-DioxH)$_2$ (1-naphthylamine)$_2$]	696.58	51	Reddish-brown triangle-based prisms
2.	[Fe(Ph-Me-DioxH)$_2$ (2-methyl-imidazole)$_2$]	574.42	74	Reddish-brown triangle-based prisms
3.	[Fe(Ph-Me-DioxH)$_2$ (2-amino-4-methyl-pyridine)$_2$]	626.49	56	Reddish-brown triangle-based prisms
4.	[Fe(Ph-Me-DioxH)$_2$(lepidine)$_2$]	696.58	99	Dark reddish-brown triangle-based prisms (microcrystals)
5.	[Fe(Ph-Me-DioxH)$_2$ (m-toluidine)$_2$]	624.52	98	Reddish-brown triangle-based prisms (microcrystals)
6.	[Fe(Ph-Me-DioxH)$_2$ (dicyclohexylamine)$_2$]	772.85	59	Reddish-brown triangle-based prisms (microcrystals)
7.	[Fe(Bu-Me-DioxH)$_2$ (m-toluidine)$_2$]	584.54	20	Brown triangle-based prisms
8.	[Fe(Bu-Me-DioxH)$_2$ (dicyclohexylamine)$_2$]	732.87	23	Brown triangle-based prisms (microcrystals)
9.	[Fe(Me-i-Pr-DioxH)$_2$ (1-naphthylamine)$_2$]	628.55	52	Dark reddish-brown triangle-based prisms (microcrystals)
10.	[Fe(Me-i-Pr-DioxH)$_2$ (2-amino-5-picoline)$_2$]	558.46	33	Purple-brown small triangle-based prisms (microcrystals)
11.	[Fe(Ph-Me-Diox)$_3$(BO-i-Bu)$_2$]	752.22	96	Greenish-brown triangle-based prisms (microcrystals)
12.	[Fe(Ph-Me-Diox)$_3$ (BO-2-propil)$_2$]	724.16	79	Red triangle-based prisms
13.	[Fe(Ph-Me-Diox)$_3$(BO-n-Bu)$_2$]	752.22	53	Brown triangle-based prisms
14.	[Fe(Ph-Me-Diox)$_3$(BO-n-Pr)$_2$]	724.16	90	Reddish-brown triangle-based prisms
15.	[Fe(Bu-Me-Diox)$_3$(BO-2-Pr)$_2$]	664.19	99	Reddish-brown triangle-based prisms (microcrystals)
16.	[Fe(Bu-Me-Diox)$_3$(BO-Et)$_2$]	636.14	83	Reddish-brown irregular microcrystals
17.	[Fe(Me-i-Pr-Diox)$_3$(BOH)$_2$]	537.95	57	Reddish-brown triangle-based prisms
18.	[Fe(Me-i-Pr-Diox)$_3$(BO-Et)$_2$]	594.06	64	Brown irregular microcrystals
19.	[Fe(Me-i-Pr-Diox)$_3$(BO-Me)$_2$]	566,00	16	Dark brown triangle-based prisms
20.	[Fe(Me-i-Pr-Diox)$_3$(BO-i-Pr)$_2$]	622.11	75	Reddish-brown irregular microcrystals
21.	[Fe(Me-i-Pr-Diox)$_3$(BO-i-Bu)$_2$]	650.16	94	Brown triangle-based prisms (microcrystals)
22.	[Fe(Me-i-Pr-Diox)$_3$(BO-n-Pr)$_2$]	622.11	90	Brown triangle-based prisms

Infrared spectroscopic study

The mid-IR spectra were recorded with a Bruker Alpha FTIR spectrometer (Platinum single reflection diamond ATR), at room temperature, in the wavenumber range of 4000–400 cm^{-1}, and the far-IR range of 500–50 cm^{-1}, respectively, on a Bio Rad – FTS 60A, PIKE Gladi ATR spectrometer, with a resolution of 4 cm^{-1}. The samples were measured in solid state (in powder

form). The data of the most characteristic IR bands for some selected complexes are presented in Table 2.

Table 2. IR data of the selected complexes.

Comp. cm^{-1}	1	4	5	6	7	8	11	14	15	17
$\nu_{O–H}$	3648 w	-	-	3592 w	-	-	-	-	-	3648 w
$\nu_{N–H}$	3217 w	3237 m	3237 m	3219 m	3220 w	3246 m	3206 m	3231 m	3201 s	3254 m
$\nu_{C–H}$	3058 w 2930 w	3085 w 3066 w	3065 w 2927 w	3054 m 2931 m	2955 m 2928 m	2956 m 2929 m	2952 m 2869 m	3067 w 2887 w	2959 m 2872 m	2964 s 2873 s
$\nu_{C=C}$	1653 vs	1637 s	1651 m	1645 vs	1649 vs	1646 vs	1651 w	1735 w	1634 w	1682 s
$\nu_{C=N}$	1577 s	1604 vs	1611 s 1593 m	1578 m	1558 s	1557 s	1507 m	1578 m 1495 s	1574 m	1558 m
δ_{CH2}	1445 s	1413 m	1418 s	1424 s	1456 s	1455 m	1449 s	1405 m	1393 vs	1456 vs
δ_{CH3}	1315 s	1356 s	1369 m	1354 s	1379 s	1379 s	1361 vs	1370 m	1378 vs	1363 s
$\nu_{N–O}$	1239 vs	1230 m	1198 m	1200 s	1182 vs	1181 s	1192 vs	1200 m	1175 vs	1189 vs
$\nu_{N–OH}$	1110 vs	1100 vs	1109 m	1107 s	1106 vs	1104 vs	-	-	-	-
$\nu_{B–O}$	-	-	-	-	-	-	1114 vs	1016 s	1109 vs	1092 vs
$\tau_{O–H}$	955 vs	1020 vs	976 vs	975 vs	1023 vs	1023 vs	971 vs	975 vs	978 s	968 vs
$\gamma_{C–H}$	695 vs	696 vs	695 vs	697 vs	746 s	743 s	695 vs	709 vs	703 vs	676 m
$\nu_{Fe–N}$	556 s 422 vs	560 s 507 s	505 m 498 m	484 s 418 s	533 vs 424 s	528 s 419 s	511 m 492 s	492 vs	544 vs	566 vs
$\delta_{N–Fe–N}$	376 s	363 m	361 m	357 s	380 vs	376 s	359 s	359 s	378 w	372 w

(Abbreviations: vs = very strong, s = strong, m = medium, w = weak)

The most important bands for the characterization of complexes are $\nu_{C=N}$ (1495 – 1611 cm^{-1}) and $\nu_{Fe–N}$ (418 – 566 cm^{-1}) [6]. In the far IR region appears the $\delta_{N–Fe–N}$ deformation bands, which demonstrate the stability of complexes. In case of [Fe(Diox)$_3$(BO-R)$_2$] type complexes $\nu_{B–O}$ valence band appear with high intensity.

Mass spectrometry

Mass spectra of the samples were recorded on an Agilent 1200/6410B Triple Quad LC-MS/MS system using electrospray ionization (ESI). In the spectra we could detect the molecular ions and some decomposition fragments.

Mössbauer spectroscopy

The Mössbauer spectra were recorded at room temperature (295 K) and liquid nitrogen temperature (78 K) with Wissel type Mössbauer spectrometer in constant acceleration mode and in transmission geometry.
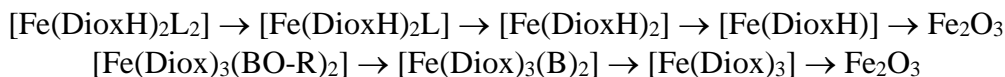
The Mössbauer spectroscopic measurements indicate the oxidation and spin state of Fe, and also the purity of the complexes. In case of aromatic ligands the high spin Fe[III] oxidation state is observed due to the electron attraction of the ligand, however, in case of aliphatic ligands we obtain low spin Fe[II].

Thermoanalytical measurements (TG-DTG-DTA)

Thermal measurements were performed with a 951 TG and 910 DSC calorimeter (TA Instruments), in Ar or N$_2$ at a heating rate of 10 K·min^{-1} (sample mass of 4–10 mg).

The thermal stability of complexes in the case of *[Fe(DioxH)$_2$L$_2$]* type is limited within the temperature range of 74–141 °C. The first step of the decomposition is the loss of the amino

group until 300 °C, then the dioxime units leave. The end of the process is between 379–650 °C. The decomposition of the dioxime unit is accompanied by big exothermic peaks. In the case of *[Fe(Diox)₃(BO-R)₂]* type complexes the thermal stability is limited between 96–98 °C. The first decomposition step belongs to leaving RO group, until 140 °C, then the BO_x part is lost until 250 °C. Subsequently, the decomposition of the glyoxime unit takes place, which is accompanied by big exothermic peaks. This behavior can be explained with the presence of oxygen in the molecule. The process ends at 700 °C. The general mechanism for decomposition is as follows:

$$[Fe(DioxH)_2L_2] \rightarrow [Fe(DioxH)_2L] \rightarrow [Fe(DioxH)_2] \rightarrow [Fe(DioxH)] \rightarrow Fe_2O_3$$

$$[Fe(Diox)_3(BO\text{-}R)_2] \rightarrow [Fe(Diox)_3(B)_2] \rightarrow [Fe(Diox)_3] \rightarrow Fe_2O_3$$

UV–VIS spectroscopy

The electronic spectra were recorded with a Jasco V-670 Spectrophotometer in 10% EtOH/water solutions containing the substance in 10^{-4} mol/dm³ concentration. Using Sörensen buffer solutions the electronic spectra were also recorded as a function of pH, and then the acidity constants were calculated, too. The obtained values were between $9.1 \cdot 10^{-13} – 1.1 \cdot 10^{-10}$.

Biological study

The antimicrobial effects of three complexes: [Fe(Ph-Me-Diox)₃(BO-i-Bu)₂], [Fe(Ph-Me-Diox)₃(BO-n-Pr)₂] and [Fe(Ph-Me-Diox)₃(BO-i-Pr)₂] were studied against *Staphylococcus aureus*, *Bacillus cereus* Gram-positive and *Escherichia coli*, *Serratia marcescens* Gram-negative bacteria, respectively. The investigations were carried out by Kirby-Bauer disk diffusion method. The complexes were dissolved in DMSO at 10 mmol/l concentration, and 30 μl was applied on sterile paper discs. Antibacterial effect was observed only in case of [Fe(Ph-Me-Diox)₃(BO-i-Bu)₂] against *Staphylococcus aureus*. The inhibition zone was 15.33 mm, which is a good value in comparation with the literature data.

Conclusion

New iron(II) complexes were synthesized and characterized using a range of physicochemical methods. The thermal decomposition mechanism was monitored by thermoanalytical measurements. The antibacterial activity of the compounds was also investigated.

Acknowledgement

References

[1] Y.Z. Voloshin, N.A. Kostromina, A.Y. Nazarenko, *Inorganica Chimica Acta* 170 (1990) 181

[2] S.Y. Erdyakov, Y.Z. Voloshin, I.G. Makarenko, E.G. Lebed, T.V. Potapova, A.V. Ignatenko, A.V. Vologzhanina, M.E. Gurskii, Y.N. Bubnov, *Inorganic Chemistry Communications* 12 (2009) 135

[3] A. Azam, A.S. Ahmed, M. Oves, M.S. Khan, S.S. Habib, A. Memic, *International Journal of Nanomedicine*, 7 (2012) 6003–6009

[4] A.N. Srivastva, S.C. Pahwa, P.C. Jain, N.P. Singh, *Research on Chemical Intermediates*, 42 (2016) 8023–8037

[5] Y.Z. Voloshin, N.A. Kostromina, A.Y. Nazarenko, *Inorganica Chimica Acta* 110 (1990) 181–190

[6] K. Nakamoto, Infrared and Raman Spectra of Inorganic and Coordination Compounds. Part B: Applications in Coordination, Organometallic and Bioinorganic Chemistry, Wiley J., 38, NY 1997

ANALYZING FLOW DYNAMICS WITH 3D PRINTED TURBULENCE PROMOTERS IN ULTRAFILTRATION UNIT TO MITIGATE MEMBRANE FOULING

Aws N. Al-Tayawi[1*], Hajnalka Csott[2], József Richárd Lennert[3], Zsuzsanna Horváth Hovorka[4], Zsuzsanna László[2], Cecilia Hodúr[2], Tamás Szabó[5], Szabolcs Kertész[2]

[1] *Doctoral School of Environmental Sciences, University of Szeged, Szeged H-6725, Hungary*
[2] *Department of Biosystems Engineering, Faculty of Engineering, University of Szeged, Szeged H-6725, Hungary*
[3] *Department of Power Electronics and E-Drives, Audi Hungaria Faculty of Automotive Engineering, Széchenyi István University, Győr H-9026, Hungary*
[4] *Department of Mechanical Engineering, Faculty of Engineering, University of Szeged, Szeged H-6725, Hungary*
[5] *Department of Physical Chemistry and Materials Science, University of Szeged, Rerrich Béla tér. 1, H-6720 Szeged, Hungary*
e-mail: awsaltayawi@uomosul.edu.iq

Abstract

This study investigates the impact of various *3D* printed turbulence promoters (*3DPTP*) in a lab-scale low-pressure ultrafiltration membrane separation stirring unit using dairy model wastewater effluent. The research focuses on evaluating the performance of different *3DPTP* shapes; and identifying the optimal *3DPTP* material for the unit based on the best-performing shape. Multiple *3DPTP* designs were developed, fabricated, and tested using various materials to assess key membrane separation parameters, such as permeate flux, membrane retention, and total, reversible, and irreversible resistances. Specific *3DPTP* designs, particularly *PLA-UE* and *PLA-S*, significantly enhanced average permeates flux and reduced the total resistance. Among the tested materials, the resin material demonstrated superior performance by notably increasing permeate flux and reducing total resistance. Statistical analysis was employed to confirming the influence of *3DPTP* designs and materials on the separation performance.

Introduction

The escalating environmental challenges, driven by rapid population growth, have highlighted the importance of protecting natural water resources [1]. Within the food industry, particularly in dairy operations, substantial water use and wastewater management present significant issues [2]. The need for advanced technologies, such as hybrid/combined processes, for managing high-organic-content wastewater has become critical. Ultrafiltration, a membrane-based process, is increasingly utilized in industrial and wastewater treatment applications due to its effectiveness. However, membrane fouling and concentration polarization are persistent challenges in these processes [3]. Mitigating membrane fouling requires optimizing membrane parameters, including transmembrane pressure, stirring speed, and membrane cut-off values, as well as enhancing hydrophilicity to reduce fouling [4]. Additive manufacturing (*3D* printing) has emerged as a solution, enabling the fabrication of complex geometries and addressing various industrial challenges. The use of *3D* printed turbulence promoters (*3DPTP*) into the membrane filtration units has shown significant potential in reducing membrane fouling. Studies have demonstrated the effectiveness of *3DPTP* in improving energy efficiency and reducing fouling in membrane distillation processes. Optimizing the geometry of *3DPTP* has enhanced mixing and membrane performance. Moreover, the integration of *3DPTP* as led to superior fouling resistance and increased output flux compared to traditional spacers [5].

This study aims to examine the operational parameters of ultrafiltration membranes in a laboratory-scale dairy wastewater treatment model. After determining optimal parameters, the impact of *3DPTP* shapes on filtration efficiency and the effect of various materials on filtration performance were evaluated through comprehensive statistical analyses. The study uniquely addresses the shape and material analysis of *3DPTP* in small-scale membrane separation units.

Experimental

Model Wastewater Preparation

Model effluent simulating dairy wastewater was prepared using skimmed milk powder and anionic detergent dissolved in tap water at 25°C, achieving concentrations of 5 g/L and 0.5 g/L, respectively. Parameters such as chemical oxygen demand (*COD*) (5200 mg/L), turbidity (1150 NTU), conductivity (0.89 mS), and pH (8.7) were recorded.

Membrane Filtration Equipment

A static, stirred ultrafiltration system (Merck Millipore, Germany) was used in the laboratory. The apparatus utilized *PES* (polyethersulfone) membranes with various cut-off values, providing a total effective filtration area of 0.0036 m². Transmembrane pressure was controlled by nitrogen gas from a cylinder, regulated via a pressure valve. Filtrate was discharged through a tube at the base, maintaining a volume reduction ratio (*VRR*) of 2, reducing volumes from 100 mL to 50 mL. The mass of the permeate was continuously monitored using an electric balance (Kern EW, Germany).

Measurements for Shape and Material of 3DPTP

After selecting the optimal parameters, all variable settings associated with the equipment were documented. Measurements were then conducted using four different designs for shape testing (polylactic acid -unrestricted endstarting (*PLA-UE*), Polylactic acid-slim (*PLA-S*), polylactic acid thin barrier (*PLA-TB*) polyamide dual barrier (*PA-DB*)), and simultaneously, four identical designs were used for material testing (*PLA*, Resin, Metal, and thermoplastic polyurethane (*TPU*)), with *3DPTP* of various materials inserted along with control measurements, which were then repeated. The ultrafiltration measurements were carried out similarly to the initial series of experiments, except that the selected *3DPTP* was also directly placed on the membrane surface inside the device.

Results and discussion

The evaluations of various *3DPTP* designs showed differences in average flux. Figure 1 shows that the *PLA-UE* and *PLA-S* designs provide significant improvements in flux values compared to the control and the other designs. Additional testing with alternative printing materials demonstrated notable gains in average flux, particularly with resin material, which also contributed to decreased total resistance. Overall, the findings underscore the critical role of *3DPTP* in enhancing ultrafiltration performance.
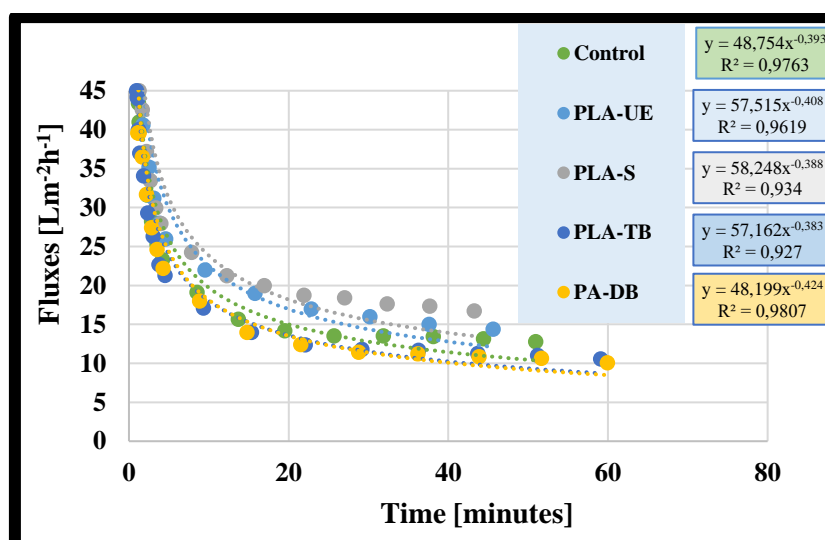
Figure 1. Variation of permeate fluxes as a function of time with different *3DPTP*
(20 kDa *UF* membrane, T = 25°C, *TMP* = 3 bar, n = 400 rpm).

Conclusion

This study investigates the effects of 3D printed turbulence promoters (*3DPTP*) in a laboratory-scale ultrafiltration membrane separation unit using dairy model effluent. Various designs of *3DPTP* were tested, along with different materials, to evaluate key ultrafiltration parameters: permeate flux, membrane retention, and total resistance. The experiment with different 3D printed promoter designs revealed variations in average flux, with the *PLA-UE* and *PLA-S* designs showing notable improvements. Further assessments with alternative printing materials highlighted substantial gains in average flux, especially with resin material, which also decreased total resistance. The findings demonstrate the significant impact of *3DPTP* on ultrafiltration efficiency, with the *PLA-UE* design and resin material showing the most promising results in improving flow dynamics and overall performance.

Acknowledgements

References

[1]   W. Musie, G. Gonfa, Fresh water resource, scarcity, water salinity challenges and possible remedies: A review, Heliyon. (2023).

[2]   L.K.S. Lima, L.N.L. Santana, H.L. Lira, M.A. Rodríguez, M.Y.M. Souza, M.G.S. Júnior, B.S. Lira, Development of asymmetric ceramic membranes for dairy wastewater treatment–A comparison between co-sintering and conventional firing process, J. Water Process Eng. 57 (2024) 104611.

[3]   L.N. Nthunya, M.F. Bopape, O.T. Mahlangu, B.B. Mamba, B. Van der Bruggen, C.A. Quist-Jensen, H. Richards, Fouling, performance and cost analysis of membrane-based water desalination technologies: A critical review, J. Environ. Manage. 301 (2022) 113922.

[4]   S. Elhady, M. Bassyouni, R.A. Mansour, M.H. Elzahar, S. Abdel-Hamid, Y. Elhenawy, M.Y. Saleh, Oily wastewater treatment using polyamide thin film composite membrane technology, Membranes (Basel). 10 (2020) 84.

[5]   N. Thomas, N. Sreedhar, O. Al-Ketan, R. Rowshan, R.K.A. Al-Rub, H. Arafat, 3D printed spacers based on TPMS architectures for scaling control in membrane distillation, J. Memb. Sci. 581 (2019) 38–49.

COMBINING PHOTOACOUSTIC SPECTROSCOPY AND SCANNING MOBILITY PARTICLE SIZER INSTRUMENTS FOR CHARACTERIZATION OF DIESEL EMISSIONS

Rana Khawar Ashfaq, Abdul Rahman, Tibor Ajtai, Zoltán Bozóki

Department of Optics and Quantum Electronics, University of Szeged, H-6720 Szeged, Dóm tér 9, Hungary
e-mail: khawarashfaq499@gmail.com

Abstract
In this study, we explored the use of Multi-Wavelength Photoacoustic Spectroscopy (4λ-PAS) in combination with a Scanning Mobility Particle Sizer (SMPS) to analyze diesel particulate matter (DPM). The goal was to provide a comprehensive, real-time analysis of diesel emissions across three engine modes using two different fuel types. Additionally, we investigated the thermal evolution of emissions at three different temperatures. The total number concentration (TNC) and total volume concentration (TVC) showed a retrograde tendency with increasing torque and RPM. The Optical Absorption Coefficient (OAC), measured using the 4λ-PAS instrument, also decreased with rising torque and RPM. The qualitative analysis quantified using the Aerosol Ångström Exponent (AAE) showed a decline at higher engine RPM and torque, indicating an increase in the proportion of inorganic carbon in the emissions.

Introduction
Diesel-emitted aerosols are the primary source of light-absorbing carbonaceous (LAC) particulate matter, one of the most harmful air pollutants [1]. Diesel emissions are also a major contributor to black carbon, which is the second most important climate-relevant atmospheric component [2]. Emission-based fuel development offers a promising approach for reducing emissions and developing eco-friendly fuels. Precise and accurate measurement of exhaust particles is essential to emission-based fuel development. While regulated parameters such as number concentration and mass concentration are commonly measured, they have limited usefulness when we explain DPM air quality and climate relevance. For complete characterization of DPM, it is critical to assess size distribution, volatility classification, and the spectral response of diesel soot. Thermally Pretreating DPM emissions with a Thermodenuder (TD) have proven to be an effective method for volatility classification. The SMPS can be used to measure size distribution and number concentration, while the 4λ-PAS is well-suited for analyzing the spectral response of DPM.

DPM is a complex mixture of volatile organic and non-volatile inorganic substances, with their ratio changing based on temperature. The optical properties of DPM can shift during processes like condensation and evaporation of volatile organic compounds. Additionally, the physicochemical properties of DPM depend on engine operational conditions, such as speed and torque, and the fuel being used [3]. The AAE is the only real-time measurable quantity with relevance to both combustion processes and air quality [4][5]. Light absorption by aerosols is one of the most challenging quantities to measure accurately [6]. Photoacoustic Spectroscopy (PAS) is the most suitable method for in-situ, filter-free, precise, and accurate measurement of light-absorbing aerosols. Using a combination of SMPS and 4λ-PAS, we monitored DPM that had been preheated by the TD. This setup allows us to observe all parameters in real time as we adjust the different diesel engine modes and TD temperatures.

Experimental

The experiment was conducted using a four-cylinder diesel engine to generate diesel particulate matter (DPM). The exhaust gas was diluted by a factor of 10 using an ejector diluter in an isokinetic manner. The exhaust was then thermally treated with a Thermodenuder (TD) at temperatures of 40°C, 150°C, and 300°C. The Scanning Mobility Particle Sizer (SMPS) was used to measure the number concentration and size distribution of the exhaust particles. The SMPS consists of two components: the Long Differential Mobility Analyzer (LDMA), which classifies particles based on their electrical mobility, and the Condensation Particle Counter (CPC), which counts the size-selected particles.
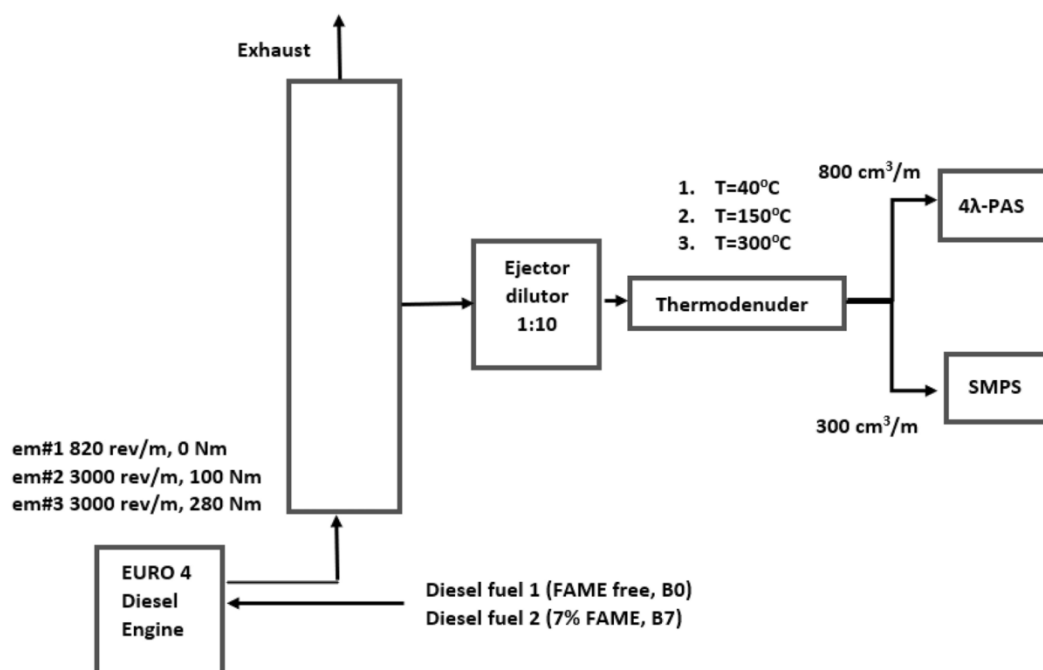

Figure 1 . The experimental set-up of the sampling system. Operatory conditions of engine, type of fuels, posterior temperature treatment conditions.

The OAC and its wavelength dependency were measured using the 4λ-PAS instrument. In brief, the system operates by detecting sound waves generated when modulated light is absorbed by light-absorbing carbonaceous (LAC) particles. The absorbed energy is released as heat, which causes gas expansion and contraction, producing sound waves. These sound waves are amplified by a resonator and measured by a microphone. The 4λ-PAS instrument uses four wavelengths: 266 nm, 355 nm, 532 nm, and 1064 nm, each in identical cells.

Two fuels were used in the experiment: B0 (Biofree), used as a reference, and B7, which is a blend of B0 with 7% FAME (fatty acid methyl ester). The engine was operated in three modes: idle mode (0 Nm, 820 rpm) (em#1), low load mode (100 Nm, 3000 rpm) (em#2), and high load mode (280 Nm, 3000 rpm) (em#3).

Results and discussion

B0 and B7 have more than a 10% difference in TNC at em#1 and 40°C, but in all other modes and temperatures, the TNC and TVC trends for both fuels remain similar. From em#1 to em#2, there is an increase in TNC, with little change in TVC. However, from em#2 to em#3, TNC remains relatively unchanged, but TVC increases.
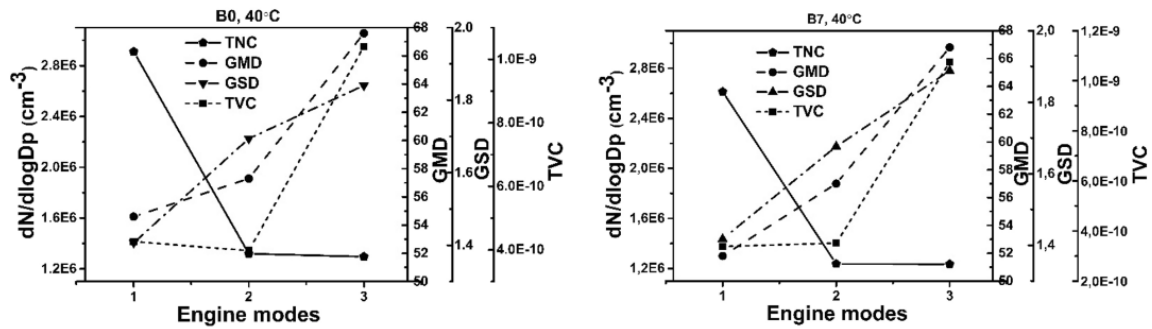
Figure 2. DPM characteristic parameters using B0 and B7 fuels at three different operatory parameters of the test engine. The TNC, GMD, GSD and TVC.

Using the 4λ-PAS instrument, the OAC of the particles was measured, and from this, the AAE was deduced, providing more insight into the physicochemical content of the exhaust. OAC values increase across all wavelengths when transitioning from em#1 to em#2 and from em#2 to em#3. However, AAE shows a decreasing trend from em#1 to em#2 and further from em#2 to em#3, indicating a higher ratio of inorganic carbon as engine speed increases.
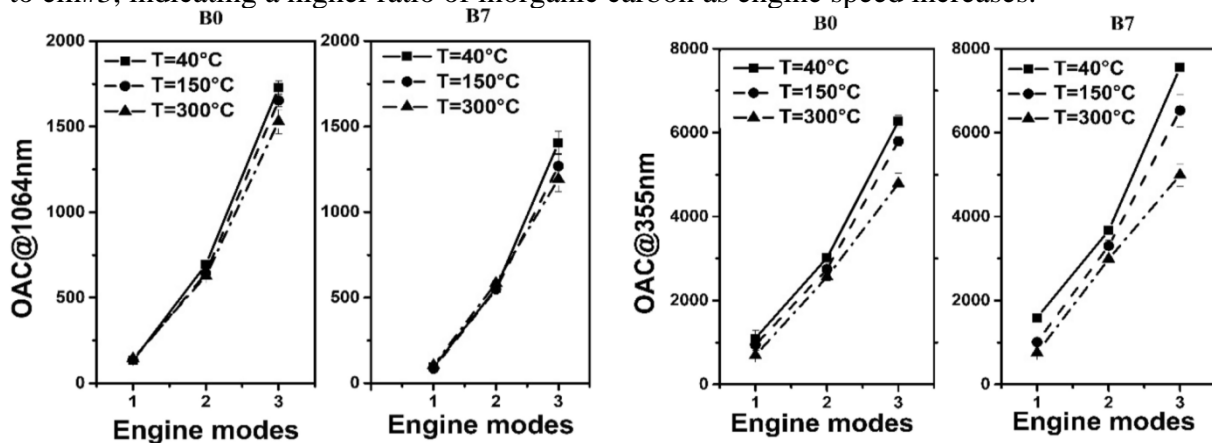

Figure 3 . OAC measured at 1064 nm and 355 nm in the function of em's at three different temperatures using two types of fuels.

B7 consistently exhibits a higher AAE value than B0, suggesting that B7 exhaust contains a higher concentration of organic particles. As temperature increases, AAE decreases across all engine modes and for both fuel types. This reduction in AAE with rising temperature indicates that volatile organic components evaporate, leading to a mixture with a higher concentration of inorganic carbon.
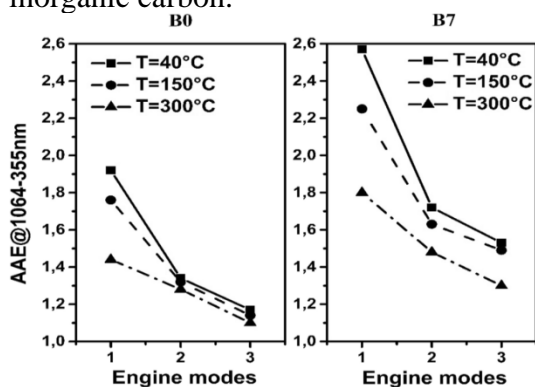

Figure 4 . AAE of diesel emission in the function of engine modes using different type of fuels and sampling temperature.

Conclusion

The primary goal of the study was to demonstrate the applicability of multi-wavelength photoacoustic spectroscopy for the qualitative investigation of diesel emissions and thermal particle evolution using a combination of a multi-wavelength photoacoustic instrument and a thermodenuder (PA-TD) unit. Experimental observations revealed a retrograde tendency in both TNC and TVC. The OAC measured and AAE were deduced, and the results were analyzed accordingly. This system provides a powerful method for gaining a deeper understanding of the environmental impact of DPM aerosols, as well as investigating the volatility and thermal evolution of diesel emissions, thereby a promasing candidate for supporting the development of emmission based fuel development.

References

[1] Lloyd, A. C. & Cackette, T. A. Diesel engines: Environmental impact and control. J. Air Waste Manag. Assoc. 51(6), (2001) 809–847

[2] Bond, T. C. et al. Bounding the role of black carbon in the climate system: A scientific assessment. J. Geophys. Res. Atmos. 118, (2013) 1–173.

[3] Gangwar, J. N., Gupta, T. & Agarwal, A. K. Composition and comparative toxicity of particulate matter emitted from a diesel and biodiesel fuelled CRDI engine. Atmos. Environ. 46, (2012) 472–481.

[4] Utry, N. et al. Correlations between absorption Angström exponent (AAE) of wintertime ambient urban aerosol and its physical and chemical properties. Atmos. Environ. 91, (2014) 52–59.

[5] Ajtai, T. et al. A method for segregating the optical absorption properties and the mass concentration of winter time urban aerosol. Atmos. Environ. 122, (2015) 313–320.

[6] Lack, D. A., Lovejoy, E. R., Baynard, T., Pettersson, A. & Ravishankara, A. R. Aerosol absorption measurement using photoacoustic spectroscopy: Sensitivity, calibration, and uncertainty developments. Aerosol Sci. Technol. 40(9), (2006) 697–708.

DEVELOPMENT OF NOVEL PHOTOCATALYTIC MATERIALS FOR WASTEWATER TREATMENT

Dániel Berkesi[1], Nikita Sharma[1] Szilvia Szabó[2], Klára Hernádi[1]

*[1]Institute of Physical Metallurgy, Metal Forming and Nanotechnology
University of Miskolc, H-3515 Miskolc-Egyetemváros, Egyetem út 1 C/2, Hungary
[2]Kis Analitika LTD, H-3792 Sajóbábony, Gyártelep Pf. 4., Hungary
e-mail: daniel.simon.berkesi@uni-miskolc.hu*

Abstract

The growing concern over environmental pollution, particularly from pharmaceutical wastewater, has driven the need for advanced treatment methods[1]. Photocatalysis, an eco-friendly and efficient approach, holds significant promise for the degradation of persistent organic pollutants[2]. This study focuses on the development and characterization of novel photocatalytic materials, including basic bismuth nitrate (BBN)[3], ilmenite (FeTiO$_3$)[4], and bismuth-decorated titanium dioxide (TiO$_2$) nanoparticles. The primary goal is to synthesize these semiconductor materials using grind-assisted and hydrothermal methods, optimize their structural properties, and test their photocatalytic efficiency in degrading pharmaceutical pollutants[5]. The research also includes the design of a photocatalytic reactor with multiple light sources and temperature control to ensure reliable performance testing under various conditions[2], [6]. The outcomes of this work will contribute to bridging gaps in the literature, offering insights into the synthesis of effective photocatalysts and their application in wastewater treatment.

Introduction

The increasing industrialization and urbanization over the last few decades have significantly contributed to environmental pollution, particularly in wastewater systems. Among the various types of pollutants, those stemming from pharmaceutical industries present a unique challenge due to their toxicity, non-biodegradability, and potential impact on human health[7]. Traditional wastewater treatment methods often fail to adequately degrade pharmaceutical pollutants[8]. Therefore, advanced technologies like photocatalysis have emerged as a promising solution. Photocatalysis leverages semiconductor materials that, when activated by light, generate reactive species capable of breaking down organic contaminants[9]. The current research focuses on synthesizing and characterizing novel photocatalytic materials to enhance the degradation of pharmaceutical pollutants in wastewater[10].

Experimental

This research involves a multi-phase approach, which includes:

1. Synthesis of Photocatalytically Active Materials: We synthesized BBN, FeTiO$_3$, and bismuth-decorated TiO$_2$ nanoparticles using two primary methods: grind-assisted synthesis and hydrothermal methods[11], [12], [13]. Grind-assisted synthesis is a relatively simple and cost-effective technique, whereas the hydrothermal method allows for more controlled particle size and morphology. Both approaches were explored to determine the most effective process for producing photocatalysts with desirable structural properties.

2. Characterization of Synthesized Materials: Advanced characterization techniques such as X-ray diffraction (XRD), transmission electron microscopy (TEM), and scanning electron microscopy (SEM) were applied to determine the structural, morphological, and compositional properties of the synthesized materials. XRD was used to identify the crystal phases and verify

the successful synthesis of the targeted compounds. TEM and SEM provided detailed insights into particle size, distribution, and surface morphology.

3. Design of Photocatalytic Reactor[14]: A custom-built photocatalytic reactor was fabricated for the evaluation of the photocatalytic efficiency of the materials. The reactor includes three LED light sources with different color temperatures (3000K, 4000K, and 6000K) to simulate different light conditions. The reactor is also equipped with a temperature control system to maintain consistent experimental conditions.

4. Photocatalytic Activity Testing: The synthesized photocatalysts were tested for their ability to degrade model dye molecule pollutants in aqueous solutions. The experiments were conducted under different light conditions to determine the effect of light wavelengths on the degradation efficiency. The extent of degradation was monitored through spectroscopic techniques, and the results were analyzed to determine the optimal material and synthesis approach for photocatalytic activity.

Results and discussion
1. Synthesis and Characterization of BBN and FeTiO$_3$: The XRD results confirmed the successful synthesis of basic bismuth nitrate (BBN) and ilmenite (FeTiO$_3$) using both synthesis methods. The grind-assisted method produced materials with a broader size distribution, while the hydrothermal method yielded more uniform and smaller particles, which are advantageous for photocatalysis due to the higher surface area.

The central aim of this project is to develop and characterize a range of semiconductor-based photocatalytic materials, such as basic bismuth nitrate (BBN), ilmenite (FeTiO$_3$), and bismuth-decorated titanium dioxide (TiO$_2$) nanoparticles. Our goal is to determine their efficiency in degrading pharmaceutical pollutants under various light conditions. Additionally, we seek to optimize the morphology and structural properties of these materials to enhance their photocatalytic performance. This research will contribute to filling critical gaps in the literature regarding the optimal synthesis and application of photocatalytic materials for environmental remediation.

2. Bismuth-Decorated TiO$_2$ Nanoparticles: TEM images revealed that the bismuth compounds were uniformly distributed on the surface of the TiO$_2$ nanoparticles. This decoration plays a critical role in enhancing the photocatalytic performance of TiO$_2$, as the bismuth compounds can promote efficient charge separation, reducing recombination rates and increasing the number of reactive species generated.

3. Photocatalytic Activity: The photocatalytic activity tests demonstrated that the bismuth-decorated TiO$_2$ nanoparticles exhibited superior performance compared to pure TiO$_2$. This is attributed to the enhanced charge separation provided by the bismuth compounds. Additionally, FeTiO$_3$, with its tunable electronic properties, showed promising photocatalytic activity under visible light, making it a potential candidate for practical applications in wastewater treatment. However, the BBN samples demonstrated moderate photocatalytic performance, suggesting further optimization is needed.

4. Light Source Effects: The experiments conducted under different LED light conditions revealed that the photocatalysts' performance varied with the wavelength of light. Photocatalytic efficiency was the highest under the 6000K LED light source, which emits a

higher proportion of blue light, indicating that the synthesized materials are particularly responsive to shorter wavelengths. This finding is crucial for optimizing the light conditions in real-world photocatalytic systems.

5. Future Plans: Building on these results, future research will focus on further optimizing the synthesis parameters to enhance the photocatalytic efficiency of the materials. This will include fine-tuning the hydrothermal synthesis conditions and experimenting with different doping elements to modify the electronic properties of the photocatalysts. We also plan to expand the scope of our photocatalytic tests by using real pharmaceutical wastewater samples. Additionally, the development of nanocomposites involving other semiconductor materials will be explored, providing an avenue for enhanced performance through synergistic effects.

Conclusion

This research demonstrates the successful synthesis and characterization of novel photocatalytic materials, including basic bismuth nitrate, ilmenite, and bismuth-decorated TiO_2 nanoparticles. These materials have shown potential for application in the degradation of pharmaceutical pollutants in wastewater. Our findings highlight the critical role of synthesis techniques and material morphology in determining photocatalytic efficiency. By addressing gaps in the literature and verifying the importance of this research field, this work paves the way for more efficient and sustainable wastewater treatment technologies. The next steps involve optimizing the photocatalytic materials and reactors, expanding pollutant testing, and exploring real-world applications in wastewater treatment plants.

Acknowledgements

References
[1] M. N. Chong, B. Jin, C. W. K. Chow, and C. Saint, "Recent developments in photocatalytic water treatment technology: A review," 2010, *Elsevier Ltd*. doi: 10.1016/j.watres.2010.02.039.
[2] D. Chen *et al.*, "Photocatalytic degradation of organic pollutants using TiO2-based photocatalysts: A review," Sep. 20, 2020, *Elsevier Ltd*. doi: 10.1016/j.jclepro.2020.121725.
[3] A. N. Christensen, M.-A. Chevallier, J. Skibsted, and B. B. Iversen, "Synthesis and characterization of basic bismuth(III) nitrates," 2000.
[4] R. Bin Lee, K. M. Lee, C. W. Lai, G. T. Pan, T. C. K. Yang, and J. C. Juan, "The relationship between iron and Ilmenite for photocatalyst degradation," *Advanced Powder Technology*, vol. 29, no. 8, pp. 1779–1786, Aug. 2018, doi: 10.1016/j.apt.2018.04.013.
[5] F. Franceschini, P. Jagdale, M. Bartoli, and A. Tagliaferro, "Perspectives on the use of bismuth-based materials for sensing and removal of water pollutants," Apr. 01, 2022, *Elsevier B.V.* doi: 10.1016/j.coesh.2022.100345.
[6] Q. Xu, L. Zhang, J. Yu, S. Wageh, A. A. Al-Ghamdi, and M. Jaroniec, "Direct Z-scheme photocatalysts: Principles, synthesis, and applications," Dec. 01, 2018, *Elsevier B.V.* doi: 10.1016/j.mattod.2018.04.008.
[7] R. P. Schwarzenbach, T. Egli, T. B. Hofstetter, U. Von Gunten, and B. Wehrli, "Global water pollution and human health," *Annu Rev Environ Resour*, vol. 35, pp. 109–136, Nov. 2010, doi: 10.1146/annurev-environ-100809-125342.

[8] Y. Guo, P. S. Qi, and Y. Z. Liu, "A Review on Advanced Treatment of Pharmaceutical Wastewater," in *IOP Conference Series: Earth and Environmental Science*, Institute of Physics Publishing, May 2017. doi: 10.1088/1755-1315/63/1/012025.

[9] R. Ameta, M. S. Solanki, S. Benjamin, and S. C. Ameta, "Photocatalysis," in *Advanced Oxidation Processes for Wastewater Treatment: Emerging Green Chemical Technology*, Elsevier Inc., 2018, pp. 135–175. doi: 10.1016/B978-0-12-810499-6.00006-1.

[10] M. R. Hoffmann, S. T. Martin, W. Choi, and D. W. Bahnemannt, "Environmental Applications of Semiconductor Photocatalysis," 1995.

[11] M. Zheng, Q. Han, X. Jia, and J. Zhu, "Grinding-assistant synthesis to basic bismuth nitrates and their photocatalytic properties," *Mater Sci Semicond Process*, vol. 101, pp. 183–190, Oct. 2019, doi: 10.1016/j.mssp.2019.06.009.

[12] L. Miersch, T. Rüffer, M. Schlesinger, H. Lang, and M. Mehring, "Hydrolysis studies on bismuth nitrate: Synthesis and crystallization of four novel polynuclear basic bismuth nitrates," *Inorg Chem*, vol. 51, no. 17, pp. 9376–9384, Sep. 2012, doi: 10.1021/ic301148p.

[13] A. T. Raghavender *et al.*, "Nano-ilmenite FeTiO3: Synthesis and characterization," *J Magn Magn Mater*, vol. 331, pp. 129–132, Apr. 2013, doi: 10.1016/j.jmmm.2012.11.028.

[14] Y. Serhane, A. Bouzaza, D. Wolbert, and A. Amin Assadi, "New UV-LED frontal flow photocatalytic reactor for VOCs treatment: Compactness, intensification and optimization studies," *Chemical Engineering Journal*, vol. 451, p. 138784, 2023, doi: 10.1016/j.cej.2022.138784ï.

APPLICATION OF NANOPOROUS GLASS SUBSTRATES TO FACILITATE THE DIRECT TRACE ANALYSIS OF LIQUIDS BY LASER-INDUCED BREAKDOWN SPECTROSCOPY

<u>Gyula Kajner</u>[1], Ádám Bélteki[1], Judit Kopniczky[2], Gábor Galbács[1]

[1]*Department of Molecular and Analytical Chemistry, University of Szeged, H-6720 Szeged, Dóm tér 7, Hungary*
[2]*Department of Optics and Quantum Electronics, University of Szeged, H-6720 Szeged, Dóm tér 9, Hungary*
e-mail: galbx@chem.u-szeged.hu

Abstract
Laser-induced breakdown spectroscopy (LIBS) is a powerful and flourishing analytical technique in atomic spectroscopy. Although LIBS is compatible with gaseous, aerosol and liquid samples too, it is mainly utilized for the analysis of solid samples. This is because all other samples types pose multiple challenges in terms of sensitivity and practicality. The analysis of (bulk) liquid samples are especially challenging because they are prone to focusing difficulties, splashing, plasma quenching, etc., leading to decreased limits of detection and reproducibility as well as substantially increased laser energy requirements [1]. To tackle these challenges, multiple approaches has been reported in the literature. Most of them rely on liquid-solid conversion, while others use specialized equipment to present the liquid as jets, films or droplets, etc. [2, 3]. Nevertheless, while eliminating some of the drawbacks of bulk liquid analysis, the approaches presented so far still fall short in either sensitivity, reproducibility or practicality compared to solid analysis.

In this study we present an alternative methodology for the analysis of liquid microsamples via LIBS by utilizing strongly hydrophilic, nanoporous glass as a substrate. The premise of this approach is that the capillary forces will drive any aqueous sample that comes in contact with the glass into the nanopores, creating a fine, two-phase structure with a solid glass frame that actually serves as the laser target. This structure has multiple advantages in practice: a.) a very small volume of liquid sample (5-10 μL) is needed for the analysis, b.) usual problems with bulk liquid samples don't apply, c.) the nano-scale structure ensures efficient laser coupling and the homogeneous distribution of the liquid sample, facilitating reproducibility.

A thorough investigation of this approach for direct liquid analysis was done, examining the analytical benefits and capabilities as well as the detection limits and reproducibility achievable.

References
[1] G. Galbács, Anal. Bioanal. Chem. 407 (2015) 7537.
[2] K. Keerthi, S.D. George, S.D. Kulkarni, S. Chidangli, V.K. Unnikrishnan, Opt. Laser Technol. 147, (2022) 107622.
[3] I. Goncharova, D. Guichaoua, S. Taboukhat, A. Tarbi, et al., Spectrochim. Acta B 217 (2024) 106943.

DEPOSITION TECHNIQUES OF HIGH ENTROPY ALLOY CATALYST THIN FILM FOR CARBON NANOTUBE FORESTS GROWTH BY CCVD

Bugumba John Majondo[1], Lilla Nánai[1], Eszter Baradács[2,3], Zoltán Erdélyi[2], Klára Hernádi[1]

[1]*Institute of Physical Metallurgy, Metal forming and Nanotechnology, University of Miskolc, 3515 Miskolc-Egyetemváros, Hungary*
[2]*Department of Solid State Physics, Faculty of Sciences and Technology, University of Debrecen, H-4002 Debrecen, Hungary*
[3]*Department of Environmental Physics, Faculty of Sciences and Technology, University of Debrecen, H-4002 Debrecen, Hungary*
e-mail: bugumba.john.majondo@student.uni-miskolc.hu, klara.hernadi@uni-miskolc.hu

Abstract

Catalytic chemical vapor deposition (CCVD) for the growth of vertical aligned carbon nanotubes (VACNT) requires not only a suitable substrate but also a thin catalyst layer to facilitate the deposition and alignment of carbon nanotube forests [1]. The choice of technique for constructing a thin catalyst layer is influenced by the specific needs of the application. Atomic Layer Deposition (ALD) is frequently preferred for its precision and uniformity over complex geometries, making it ideal for high-tech applications [1]. In contrast, Chemical Vapor Deposition (CVD) is well-suited for a broad spectrum of materials and large-scale production [2]. Magnetron sputtering-PVD is advantageous for producing high-purity, dense coatings [3]. For certain applications, solution-based methods and sol-gel techniques present more cost-effective options. In this study, ALD and magnetron sputtering were employed for the deposition of the support layer and catalyst layer, respectively.

In the preliminary experiments, nine (9) titanium substrate samples have been prepared, each with a 10 nm support layer deposited *via* the ALD technique, and Fe:Co catalyst layers of varying thicknesses applied using magnetron sputtering. These samples can be cut into smaller pieces for parallel synthesis. Specifically, three samples have a TiO_2 support layer, three have ZnO, and three have Al_2O_3, all coated with a 1:1 Fe:Co catalyst in thicknesses of 2 nm, 5 nm, and 10 nm. The primary goal is to evaluate how different metal oxide support layers and catalyst thicknesses affect CNT forest growth. The experiments will start with bimetallic catalysts to determine the best support layer and optimal catalyst deposition technique, with the goal of using HEA catalysts to promote CNT forest growth.

In green chemistry, CNTs forests are sightseen for contaminant filtration, water decontamination, and carbon capture, serving cut greenhouse gas emissions and sanitary polluted water [4]. Moreover, CNT-built materials can supplant risky chemicals or energy-severe processes in manufacturing, supporting with the principles of green chemistry by reducing waste, by means of harmless solvents, and decreasing energy consumption [5].

Acknowledgements

References

[1] R. L. Puurunen, 'Surface chemistry of atomic layer deposition: A case study for the trimethylaluminum/water process', 2005. doi: 10.1063/1.1940727.

[2] K. F. Jensen, 'Chemical Vapor Deposition', 1989, pp. 199–263. doi: 10.1021/ba-1989-0221.ch005.

[3] G. D. Nessim, 'Properties, synthesis, and growth mechanisms of carbon nanotubes with special focus on thermal chemical vapor deposition', *Nanoscale*, vol. 2, no. 8, pp. 1306–1323, Aug. 2010, doi: 10.1039/b9nr00427k.

[4] V. N. Popov, 'Carbon nanotubes: Properties and application', Jan. 15, 2004, *Elsevier Ltd*. doi: 10.1016/j.mser.2003.10.001.

[5] P. M. Ajayan and O. Z. Zhou, 'Applications of Carbon Nanotubes'.

INVESTIGATING THE EFFECT OF SIC ON THERMAL MECHANICAL PROPERTIES OF MULLITE-CORDIERITE CERAMIC COMPOSITES

John. W. Makokha[1, 2], Imre Szenti[1], Tamás Boldizsár[2], Gábor Kozma[1], András Sápi[1], Zoltán Kónya[1]

[1]*Department of Applied and Environmental Chemistry, University of Szeged, H-6720 Szeged, Rerrich Bela ter 1, Hungary.*
[2]*H, K Ceramic Limited, Bese Laszlo Utican, Szentes 6600, Hungary.*
email: sapia@chem.u-szeged.hu

Abstract

This work investigated the effects of SiC particle size on the microstructure and physical, thermal, and mechanical properties of cordierite-mullite composites. SiC milled for 3 hours at 200 rpm (MPS~2.99µm/ microparticles), and 600 rpm (MPS~0.140µm/ nanoparticles) was incorporated in ceramic composites to investigate the size effect. XRD analysis of ceramic composites revealed cordierite, mullite, chamotte, and SiC peaks in ceramic composites. SEM results illustrated that the composites formed acicular microstructure attributed to mullite, with cordierite-mullite-chamotte-SiC nanoparticle ceramic composites exhibiting refined grains. At 7.5% SiC, nanoparticles reduced porosity by 24.15% and enhanced thermal conductivity and flexural strength by 40.72% and 12.12%, compared to microparticles at 23.11%, 34.20%, and 8.98%, respectively. SiC nanoparticles were observed to outperform SiC microparticles.

Keywords: SiC nanoparticles, Flexural Strength, Thermal Conductivity

References

[1] K. Wang, H. Jiang, Q. Wang, Y. Wang, Grain Refinement Mechanisms of TiC0.5N0.5 Nanoparticles in Aluminum, Materials 16 (2023) 1214. https://doi.org/10.3390/ma16031214.
[2] Brezan, I, B. Zelenak, F, Microstructure Characterization of Advanced Ceramics, in Improving the Effectivity of Work with Rosin-Rammler Diagram by Using MATLAB GUI Tool, Elsevier, 2014: pp. 151–172. https://doi.org/10.1016/B978-0-12-394619-5.00008-0.
[3] J. Chen, H. Javaheri, B. Al-Chikh Sulaiman, Y. Dahman, Synthesis, characterization and applications of nanoparticles, in Fabrication and Self-Assembly of Nanobiomaterials, Elsevier, 2016: pp. 1–27. https://doi.org/10.1016/B978-0-323-41533-0.00001-5.
[4] Z. Sun, Y. Zhou, J. Wang, M. Li, Thermal Properties and Thermal Shock Resistance of γ-Y 2 Si 2 O 7, Journal of the American Ceramic Society 91 (2008) 2623–2629. https://doi.org/10.1111/j.1551-2916.2008.02470.x.
[5] W.D. Kingery, M.C. McQUARRIE, Thermal Conductivity: I, Concepts of Measurement and Factors Affecting Thermal Conductivity of Ceramic Materials, Journal of the American Ceramic Society 37 (1954) 67–72. https://doi.org/10.1111/j.1551-2916.1954.tb20100.x.

CRITICAL IMPORTANCE AND APPLICATIONS OF PROCESS INTENSIFICATION FOR TACKLING ENVIRONMENTAL CHALLENGES

<u>Masoud Shirzadi</u>, András Sápi

Department of Applied and Environmental Chemistry, University of Szeged, Hungary
shirzadi@chem.u-szeged.hu
Corresponding author: <u>sapia@chem.u-szeged.hu</u>

Abstract

Environmental problems such as global warming, pollution and resource depletion continue to pose important challenges that require a rethink of traditional industrial processes. Process intensification (PI) is a solution that enables the efficiency and environmentally friendly process to meet the principles of sustainability. The focus of the PI is to reduce the physical size of the equipment, minimize energy consumption and optimize resource use, thereby reducing the impact of industrial operations on the environment. The aim of the paper is to highlight the role of PI in addressing these environmental challenges and to demonstrate its growing significance in the global effort for sustainable development.

Introduction

Industries have long been recognized as a major source of environmental degradation, contributing to carbon emissions, resource depletion, and waste generation. Traditional processes, while efficient in production, are often energy-intensive and produce large amounts of waste. In response, Process Intensification (PI) has gained traction as a powerful tool to transform these processes. PI can lead to more compact systems, higher efficiency, and reduced material and energy requirements. These benefits directly translate into a lower environmental footprint.

Process Intensification and Its Role in Environmental Protection

PI techniques are diverse, ranging from the use of novel reactor designs to advanced separation techniques that optimize energy and resource use. For example, membrane reactors and microreactors have shown potential in reducing both the size of the equipment and the amount of energy required for reactions. Furthermore, PI can improve heat and mass transfer efficiency, ensuring that industrial processes consume less energy and release fewer pollutants into the atmosphere [1].

The application of PI has proven particularly effective in chemical industries, where equilibrium-limited reactions and energy-intensive separations are common [3]. By integrating innovative PI methods, such as reactive distillation and intensified heat exchangers, industries have managed to cut down both operational costs and environmental impact.

Case Studies in Process Intensification

Several industries have already begun integrating PI techniques to address environmental challenges. For instance, petrochemical plants have employed PI to develop smaller, more energy-efficient equipment, reducing emissions and minimizing the consumption of non-renewable resources. Similarly, the pharmaceutical industry has embraced PI for improving reaction selectivity, thus reducing waste production and hazardous by-products [2].

One notable example is the use of microreactors, which allow for precise control over reaction conditions. This leads to better yields, less energy consumption, and a reduction in the formation of by-products. Moreover, PI strategies have been instrumental in minimizing the

environmental impact of industrial waste by promoting efficient recycling processes and reducing the overall amount of waste generated.

Future Outlook

As the global demand for sustainable processes increases, PI is expected to play an even more significant role in industries worldwide. The integration of PI into environmental policy frameworks can help guide industries toward greener, more sustainable operations. By continuously innovating and improving PI techniques, industries can meet both economic and environmental objectives. The need for further research in PI remains high, particularly in addressing the rising concerns about climate change, atmospheric CO_2 levels, and the growing demand for energy-efficient technologies.

Conclusion

Process Intensification offers a promising pathway to reduce the environmental footprint of industrial processes. By focusing on efficiency and sustainability, PI is becoming a key strategy in addressing some of the world's most pressing environmental challenges. With continued research and innovation, PI can help industries achieve greener, more sustainable processes while maintaining economic growth.

References

1. S. Srivastava, et al., "A literature review on process intensification," *Industrial & Engineering Chemistry Research*, 2023.
2. C. S. Pereira, et al., "The role of process intensification in addressing dual challenges," *Chemical Engineering Research and Design*, 2019.
3. J. G. Segovia-Hernández, "Challenges and opportunities in process intensification," *Journal of Chemical Engineering*, 2023.
4. L. J. R. Nunes, "The Rising Threat of Atmospheric CO_2: A Review on Process Intensification," *MDPI*, 2023.

EXPERIMENTAL AND THEORETICAL ASPECTS OF CCVD SYNTHESIS OF VERTICALLY ALIGNED CARBON NANOTUBES ON AZO SUBSTRATE

Lilla Nánai[1], George Kaptay[1,2], Klára Hernádi[1]

[1]Institute of Physical Metallurgy, Metal Forming and Nanotechnology
University of Miskolc, H-3515 Miskolc-Egyetemváros, Egyetem út 1 C/2, Hungary
[2]HUN-REN-ME Materials Science Research Group, H-3515 Miskolc-Egyetemváros, Egyetem út 1, Hungary
e-mail: lilla.nanai@uni-miskolc.hu

Abstract

During catalytic chemical vapor deposition (CCVD), the synthesis parameters and the quality of the catalyst thin film both have to be precisely tuned to synthesize VACNTs in an efficient and reproducible way. In this work, CNT forests were grown on AZO (aluminum doped zinc oxide) glass substrate which was coated *via* dip coating method with few nanometers thick Al_2O_3 support layer and bimetallic iron-cobalt catalyst layer. The study of the effect of catalyst composition and synthesis parameters during CCVD growth has revealed the optimal conditions to synthetize CNT forests on AZO. The samples were analyzed *via* SEM, TEM and Raman spectroscopy to verify the structure and quality of the carbon deposition. Theoretical aspects have confirmed the role of the support layer for conducting substrates during CCVD synthesis; the transformation of the catalyst layer in the presence of hydrogen gas and the growing mechanism of CNTs.

Introduction

Carbon nanotubes (CNTs) have been a prominent part of nanotechnology research for more than three decades [1,2]. CNTs can play an essential role in solving the growing energy and environmental crises [3,4] A unique type of CNTs, vertically aligned CNTs (VACNTs), have the exceptional nanoscale properties (mechanical, surface area, electrical and thermal conductivity) of individual CNTs, combined with a hierarchical and anisotropic morphology, which provides great potential for a wide range of practical environmental applications, from water filtration to energy storage [4–8]. Catalytic Chemical Vapor Deposition (CCVD) is the preferred method for the mass production of CNTs because it is cost-effective and easy to set up, moreover it is the only suitable technique for the synthesis of VACNTs [9]. In comparison to the possibilities for the synthesis of VACNTs, there are various methods to fabricate thin catalyst layers (e.g. atomic layer deposition (ALD), physical vapor deposition (PVD), pulsed laser deposition (PLD), magnetron sputtering (MS), dip coating, etc. [10,11]), which are able to control the layer thickness and morphology but require rather expensive instruments. Dip coating can be an exception to the above-mentioned methods, as it requires less complicated instruments, scalable and cost-effective, and therefore is widely used for catalyst deposition.

Transparent conductive oxides (TCOs) are drawing more and more attention in various research due to the infrastructural evolution of renewable energy exploitation [12,13]. The best known TCOs are indium tin oxide (ITO), fluorine tin oxide (FTO) and aluminum doped zinc oxide (AZO). ITO has been extensively used for various TCO applications (opto-, microelectronic devices, photovoltaic devices, such as sensors, solar cells, LEDs, display panels etc.) due to its suitable properties[14,15]. However, the lack of the rare earth indium, the natural brittleness of ITO and its high production costs have limited the mass production of flexible and low-cost devices [12,16,17]. ITO and FTO glass substrates are the most used and well known among TCO substrates, but their applications are limited for VACNT growth due to their temperature

sensitive properties [13]. In the literature, the suitability of AZO-coated glass substrates for VACNT growth was not found. Few studies have focused on thermodynamic analysis of aligned carbon nanotubes. The growth rate of CNT forests is affected by various parameters: the growth rate can be limited by the synthesis temperature, the quality and concentration of the catalyst, the type of gas precursor, the surface reactions on the catalyst particle, the diffusion of carbon through the bulk phase of the catalyst particle or on the surface of the catalyst particle [18].

In this work, the growth of vertically aligned carbon nanotubes on AZO glass substrate is demonstrated with and without Al_2O_3 support layer and Fe-Co bimetallic catalyst layer arrangement, which have not been used in previous research. Beyond the experimental approach, our aim was to have better understanding of the behavior of the support (alumina) and the catalyst layer under the applied reaction conditions.

Experimental

A simple and cost-effective thin layer deposition technique, dip coating method was used, firstly to build the support oxide layer with 0,11 mol/dm^3 absolute ethanol solution of aluminum nitrate and then to build bimetallic iron-cobalt catalyst layer at different molar ratios (0:1, 1:3, 2:3, 1:1, 3:2, 3:1, 1:0) with 0,11 mol/dm^3 mixture of absolute ethanol solution of cobalt(II) nitrate hexahydrate and iron(III) nitrate nonahydrate. Precursor solutions were freshly prepared to avoid undesirable components formation and degradation. The substrates with support and catalyst layers were annealed in a static oven at 400 °C for 1 h to stabilize the nitrate-based precursor layers on the surface.

The CCVD synthesis was performed in a horizontal quartz tube reactor (diameter 20 mm, length 80 mm) at 600, 650 and 700 °C. During the growth of VACNTs, the reaction time was 30 min, the gas inlet contained ethylene (70 cm^3/min) as carbon source, nitrogen (50 cm^3/min) as carrier gas, hydrogen (50 cm^3/min) for the reducing environment and water vapor (25 cm^3/min) to prolong the activity of the catalyst particles.

Results and discussion

Due to the lack of information in the literature on VACNT synthesis on AZO substrate, experiments were conducted at three different synthesis temperatures, with seven different Fe:Co catalyst ratios, in the absence and presence of Al_2O_3 support layer, to study the effect of synthesis parameters on the properties of VACNTs.

During the first set of experiments, the development of carbon deposition was studied as a function of reaction temperature and catalyst composition in the absence of Al_2O_3 support layer. The following conclusions can be drawn from the results: no carbon deposition was observed on the AZO substrate surface in case of using only pure cobalt as a catalyst at 600, 650 and 700 °C; similar results were achieved at 700 °C for the pure iron catalyst in the absence of the support layer, and neither carbon deposition nor CNT growth was significant for the pure iron catalyst at other temperatures, at 600 °C, mainly amorphous carbon, carbon fibres and coiled CNTs were identified, at higher temperatures CNTs were formed randomly in larger bundles on the AZO surface. The series of experiments were repeated in the presence of Al_2O_3 support layer and the following results were obtained: all three synthesis temperatures resulted in significant evolution in the presence of support layer, and carbon nanotubes were apparently formed, however, at 600 °C the carbon nanotubes were still not aligned, at 650 °C, obviously vertically aligned carbon nanotubes were observed on the surface of AZO substrate surface at all catalyst ratios, and at 700 °C, besides the pure iron catalyst, also VACNTs were formed. In this work, short carbon nanotubes were grown, with the highest average height of VACNTs (9.0 μm and 8.7 μm) achieved at 650 °C for Fe:Co 2:3 and at 700 °C for Fe:Co 1:3, which is

an additional difference from previous studies that the highest carbon nanotubes were not formed at the 1:1 catalyst composition [19]. Application of the support layer was beneficial during the synthesis as it was assumed to inhibit the aggregation and diffusion of catalyst particles, which ensured a homogeneous distribution of catalyst nanoparticles on the surface. This claim was verified by performing blank syntheses in which hydrogen gas was circulated in the system for 5 minutes without the carbon source. In order to confirm the graphitic properties, the samples synthesised in the second experimental series were analysed by TEM and Raman spectroscopy. Based on the results, the following conclusions were drawn: multi-walled CNTs were grown during the CCVD process, with the number of walls varying between 7 and 10, with irregularities in the walls, suggesting that the CNTs contain numerous defect sites in the structure, which indirectly predicts that the graphitic and conductive properties of the CNTs might be average.

Theoretical considerations have confirmed that the nitrate compounds used to prepare support and catalyst layers were unstable thus annealing the nitrate precursors at 400 °C for 1 h indeed ensures the formation of the desired oxides, which was our goal. Based on the results, it was found that at all three synthesis temperatures (600, 650, 700°C), Fe_2O_3 and CoO layers were reduced to metallic iron and cobalt under the influence of hydrogen gas, and even the ZnO in the AZO layer was reduced to metallic zinc under the influence of hydrogen gas, whereas the support layer was stable, not reduced to elemental aluminum. The reduction of the surface ZnO layer of AZO to elemental zinc at the synthesis temperature under the influence of hydrogen gas resulted in both melting and the reaction with the reduced cobalt and iron nanoparticles, which led to the formation of intermetallic compounds, and therefore the iron and cobalt nanoparticles lost their catalytic properties. Presumably this was the case in the first series of experiments in the absence of support layer. Under the synthesis conditions used, iron-cobalt bimetallic catalysts formed bcc phase iron-cobalt solid solutions on the AZO surface in the presence of the support layer, which, due to interface effects, formed a core-shell structure, where iron formed the shell and cobalt the core. The solubility and diffusion rates of carbon atoms in iron are higher than in cobalt, resulting in the hollow structure characteristic of CNTs.

Conclusion

The conclusion is that Al_2O_3 support layer and iron-cobalt bimetallic catalyst layer are essential to synthetize VACNTs on AZO substrate. Based on experimental and theoretical results, it has been confirmed that a multi-walled CNT forest can be grown on AZO substrate by dip coating a bimetallic catalyst layer and an alumina support layer at 650 and 700 °C. It is confirmed that at CCVD synthesis temperature, in the presence of hydrogen gas, the initial iron and cobalt oxides were reduced to iron and cobalt metals, while Al_2O_3 remained stable and therefore able to fulfill the role of the support layer. On the basis of thermodynamic considerations, the bcc crystalline structured biphasic iron-cobalt nanoparticles formed core/shell structures in the presence of a support layer on AZO substrate.

Acknowledgements

References

[1] Li Y. Carbon Nanotube Research in Its 30th Year. ACS Nano 2021;15:9197–200. https://doi.org/10.1021/acsnano.1c04972.

[2] Iijima S. Helical microtubules of graphitic carbon. Nature 1991;354:56–8. https://doi.org/10.1038/354056a0.

[3] Chufa BM, Murthy HCA, Gonfa BA, Anshebo TY. Carbon nanotubes: a review on green synthesis, growth mechanism and application as a membrane filter for fluoride remediation. Green Chem Lett Rev 2021;14:640–57. https://doi.org/10.1080/17518253.2021.1991484.

[4] Huang S, Du X, Ma M, Xiong L. Recent progress in the synthesis and applications of vertically aligned carbon nanotube materials. Nanotechnol Rev 2021;10:1592–623. https://doi.org/10.1515/ntrev-2021-0102.

[5] Shi W, Plata DL. Vertically aligned carbon nanotubes: production and applications for environmental sustainability. Green Chemistry 2018;20:5245–60. https://doi.org/10.1039/C8GC02195C.

[6] Bodzek M, Konieczny K, Kwiecińska-Mydlak A. New generation of semipermeable membranes with carbon nanotubes for water and wastewater treatment: Critical review. Archives of Environmental Protection 2023. https://doi.org/10.24425/aep.2021.138460.

[7] Liu D, Shi L, Dai Q, Lin X, Mehmood R, Gu Z, Dai L. Functionalization of carbon nanotubes for multifunctional applications. Trends Chem 2024;6:186–210. https://doi.org/10.1016/j.trechm.2024.02.002.

[8] Makgabutlane B, Nthunya LN, Maubane-Nkadimeng MS, Mhlanga SD. Green synthesis of carbon nanotubes to address the water-energy-food nexus: A critical review. J Environ Chem Eng 2021;9:104736. https://doi.org/10.1016/j.jece.2020.104736.

[9] Nessim GD. Properties, synthesis, and growth mechanisms of carbon nanotubes with special focus on thermal chemical vapor deposition. Nanoscale 2010;2:1306. https://doi.org/10.1039/b9nr00427k.

[10] Fejes D, Pápa Z, Kecsenovity E, Réti B, Toth Z, Hernadi K. Super growth of vertically aligned carbon nanotubes on pulsed laser deposited catalytic thin films. Applied Physics A 2015;118:855–61. https://doi.org/10.1007/s00339-014-8965-3.

[11] Guo Y, Zhai G, Ru Y, Wu C, Jia X, Sun Y, Yu J, Kang Z, Sun B. Effect of different catalyst preparation methods on the synthesis of carbon nanotubes with the flame pyrolysis method. AIP Adv 2018;8. https://doi.org/10.1063/1.5020936.

[12] Stadler A. Transparent Conducting Oxides—An Up-To-Date Overview. Materials 2012;5:661–83. https://doi.org/10.3390/ma5040661.

[13] Ferguson V, Li B, Tas MO, Webb T, Sajjad MT, Thomson SAJ, Wu Z, Shen Y, Shao G, Anguita J V., Silva SRP, Zhang W. Direct Growth of Vertically Aligned Carbon Nanotubes onto Transparent Conductive Oxide Glass for Enhanced Charge Extraction in Perovskite Solar Cells. Adv Mater Interfaces 2020;7. https://doi.org/10.1002/admi.202001121.

[14] Wang Z, Chen C, Wu K, Chong H, Ye H. Transparent Conductive Oxides and Their Applications in Near Infrared Plasmonics. Physica Status Solidi (a) 2019;216. https://doi.org/10.1002/pssa.201700794.

[15] Minami T. Transparent conducting oxide semiconductors for transparent electrodes. Semicond Sci Technol 2005;20:S35–44. https://doi.org/10.1088/0268-1242/20/4/004.

[16] Trejo-Cruz C, Mendoza-Galván A, López-Beltrán AM, Gracia-Jiménez M. Effects of air annealing on the optical, electrical, and structural properties of indium-tin oxide thin films. Thin Solid Films 2009;517:4615–20. https://doi.org/10.1016/j.tsf.2009.02.134.

[17] Kiruthiga G, Rajni KS, Geethanjali N, Raguram T, Nandhakumar E, Senthilkumar N. SnO2: Investigation of optical, structural, and electrical properties of transparent conductive oxide thin films prepared by nebulized spray pyrolysis for photovoltaic applications. Inorg Chem Commun 2022;145:109968. https://doi.org/10.1016/j.inoche.2022.109968.

[18] Wirth CT, Zhang C, Zhong G, Hofmann S, Robertson J. Diffusion- and Reaction-Limited Growth of Carbon Nanotube Forests. ACS Nano 2009;3:3560–6. https://doi.org/10.1021/nn900613e.

[19] Magrez A, Smajda R, Seo JW, Horváth E, Ribič PR, Andresen JC, Acquaviva D, Olariu A, Laurenczy G, Forró L. Striking Influence of the Catalyst Support and Its Acid–Base Properties: New Insight into the Growth Mechanism of Carbon Nanotubes. ACS Nano 2011;5:3428–37. https://doi.org/10.1021/nn200012z.

ANIONIC SURFACTANT ADSORPTION ON ROCKS COVERED WITH ASPHALTENE

<u>Tibor István Ördög</u>[1], Lilla Balassa[2], Sándor Puskás[1], Imre Dékány[2]

[1]MOL PLC. Group Oilfield Business Development, Budapest 1117 Dombóvári street 28.
[2]University of Szeged, Physical-Chemistry and Material Science Department, Szeged,6720,
Rerrich Béla Square.1.
E-mail: tordog@mol.hu

In addition to natural surfactants, in certain processes of crude oil production, artificial surfactants are injected into the reservoir layer in order to extract more crude oil and to extract less amount of brine in the case of tertiary crude oil production processes [1]. With these processes, the production of crude oil has a smaller CO_2 footprint compared to traditional production processes.

In this work, we provide information how the amount of asphaltene adsorbed on the core samples affects the adsorption of surfactants on core samples or asphaltene-modified core sample. It is important to know the crude oil displacement technologies using surfactants especially in chemical EOR (Enhanced Oil Recovery), the adsorption processes of injected surfactant solutions in the rock pores of the reservoir layer could influence these processes.

Surfactant adsorption processes occurring at the solid-liquid interface were studied and, in order to study it quantitatively, surfactant adsorption isotherms were determined using the anionic surfactant sodium dodecylbenzenesulfonate (hereinafter referred to as NaDBS). The zeta potential values of the grounded reservoir core samples were measured in DI water with different NaDBS concentrations.

It was found that preliminarely asphaltene adsorbed on the surface of the particles, and in increasing amounts increases the adsorption capacity of the surface, and thereby the demand for the amount of surfactant necessary for the displacement of crude oil. During industrial scale application, the knowledge of surfactant adsorption is important because it affects the costs of crude oil production [2]. The adsorption mechanism was also proven, as based on the measured values of the zeta potential, the asphaltene coating reduces the value of the zeta potential, thus confirming that the anionic functional groups of NaDBS turn towards the aqueous phase, thereby forming an additional possible adsorption active surface for the injected NaDBS.

[1]   Ahmadi, M., & Chen, Z. (2020). Challenges and future of chemical assisted heavy oil recovery processes. Advances in colloid and interface science, 275, 102081
[2]   Druetta, P., Raffa, P., & Picchioni, F. (2019). Chemical enhanced oil recovery and the role of chemical product design. Applied Energy, 252, 113480.

IMPACT OF THE FEEDSTOCK, PYROLYSIS TEMPERATURE AND MODIFICATIONS IN THE PHYSICAL, CHEMICAL AND ADSORPTIVE PROPERTIES OF BIOCHARS. CASE STUDY: AMMONIUM IONS ADSORPTION

Fernanda Pantoja[1], Sándor Beszédes [2], Tamás Gyulavári [3], Erzsébet Illés[4], Gábor Kozma[3], and Zsuzsanna László [2].

[1] *Doctoral School of Environmental Sciences, University of Szeged, H-6720 Szeged, Hungary*
[2] *Department of Process Engineering, University of Szeged, H-6725 Szeged, Hungary*
[3] *Department of Applied and Environmental Chemistry, Institute of Chemistry, University of Szeged, Rerrich Béla Sqr. 1, H-6720 Szeged, Hungary.*
[4] *Department of Food Engineering, University of Szeged, H-6725 Szeged, Hungary*
e-mail: fernanda.pantoja@mk.u-szeged.hu

Abstract

Adsorption on biochar is becoming an increasingly promising technology in water treatment; thus research on physical and chemical characteristics of biochar is an important task in order to forecast how the adsorbent will behave when it comes into contact with the adsorbates. In the present research, the physical and chemical characteristics of thirteen types of biochar derived from poplar chop and banana leaves were investigated, those raw materials are considered as agricultural wastes. The different pyrolysis temperatures to which the feedstocks were subjected were 300, 400, and 500 °C. The characterization of biochars samples was carried out through scanning electron microscopy, energy dispersive X-ray spectroscopy, Fourier transform infrared spectroscopy and specific surface area measurements. The adsorption properties of biochars were evaluated by ammonium ion adsorption experiments. The results demonstrated that the pyrolysis temperature has a large impact on the yield, structure, elemental composition, and surface chemistry of the biochar. Banana leaves-derived biochar prepared at 300 °C is the most efficient for NH_4^+ adsorption, achieving a capacity of 7.0 mg of adsorbed NH_4^+ on each gram of banana leaves-derived biochar used, while biochar samples prepared at 400 and 500 °C show lower values of 6.1 and 5.6 mg/g, respectively. In the case of poplar chop derived biochar the alkaline modified sample pyrolyzed at 400 °C, showed the best maximum adsorption capacity determined by Langmuir isotherm model, reaching 47 mg of NH_4^+on each gram of biochar. The lower ammonium ions adsorption capacity 9mg/g was obtained for the acidic modified poplar chop-derived biochar pyrolyzed at 400 °C.
The Harkins-Jura isotherm model fits the experimental data best for banana leaves derived biochar, pointing out that multilayer adsorption occurs. On the other hand, Temkin isotherm model fits better the experimental data for poplar chop biochars, indicating that monolayer adsorption occurs with this raw material.

Keywords: biochar, pyrolysis temperature, physico-chemical properties, water treatment, adsorption, ammonium removal.

AMBIENT AIR POLLUTION AS A CAUSAL FACTOR FOR GESTATIONAL DIABETES MELLITUS IN MINING COMMUNITIES: A ROADMAP TO REAL-TIME PHOTOACOUSTIC SPECTROSCOPY APPLICATION

Naomi Tracey Tsebe-Sibiya

Department of Optics and Quantum Electronics, University of Szeged, H-6720 Szeged, Aradi Vértanúk tér 1, Hungary
Email: naomitraceysibiya@gmail.com

Abstract

Air pollution has been implicated as an emerging risk factor to gestational diabetes mellitus (GDM). There is a growing prevalence of GDM in South Africa. This study aims to investigate, using photoacoustic spectroscopy (PAS); the potential correlation of long-term exposure to enhanced levels of air pollutants with the prevalence of GDM in women living near coal mining operations.

Introduction

Long-term exposure to elevated concentrations of air pollutants is increasingly recognised as one the most important contributors to social vulnerability and human health risks, particularly in communities near industrial activities [1] [2] [3]. Mining host communities are vulnerable to mining-induced air pollution due to their spatial proximity and exposure to gaseous emissions, suspended aerosols and particulates [4]. Various studies have implicated air pollution in different acute and chronic respiratory and cardiovascular diseases, cancers, mortality and cognitive disorders [5] [6] [7] [8] [9] [10]. Recent epidemiological studies, as shown in Table 1 below, have revealed air pollution as being one of the environmental health threats which is associated with the pathogenesis of various pregnancy-related disorders, including GDM.

Table 1: Epidemiological studies associating air pollution to GDM

Author	Outcome	Exposure	Model used	Exposure estimates
[11]	GDM	PM2.5, traffic exposure	spatiotemporal models	1st trimester $PM_{2.5}$: 10.4±1.7 µg/m3; 2nd trimester $PM_{2.5}$: 10.4±1.7 µg/m3
[12]	GDM	PM2.5, O_3	USEPA models	1st trimester: PM2.5: 9.73±2.07 µg/m3; O3: 37.20±6.04 ppb 2nd trimester: PM2.5: 9.88±2.06 µg/m3; O3: 37.54±6.10 ppb Full term: PM2.5: 9.93±1.67 µg/m3; O3: 37.40±4.10 ppb
[13]	GDM	PM2.5, SO_2, NOx, CO, O_3	Singe fixed monitoring station	3 months pre-pregnancy: PM2.5: 44.38±12.09 µg/m3 1st trimester: PM2.5: 43.52±12.87 µg/m3; 2nd trimester: PM2.5: 41.20±13.43 µg/m3

Commonly, these studies indicate that GDM presents higher risks of progressing into type 2 diabetes (postpartum) as well as risks of other short and long-term health outcomes in both the women and their young. Further studies have asserted that pre-conception exposure to air pollution may cause elevated blood glucose levels, which is associated with insulin resistance and the development of GDM [14] [15]. Air pollution is a major concern in developing countries [16]. However, scientific inquiries of the health effects of air pollution, particularly on the development of GDM, in developing countries are still scarce.

South Africa is a developing country, that is heavily dependent on its mining sector as a key contributor to its gross development product. The coal mining industry is said to account for 73% of the country's primary energy supply and is a significant source of SO_2, NO_2, CO_2, O_3 and sulfate particulates [17]. There is also a growing recognition that other perilous socio-economic living conditions contribute to the state of air quality in the country. Approximately 5million South Africans live in informal settlements, and they largely use of coal and wood as a source of domestic heating and energy [18]. This choice of energy source is largely owing to the affordability of coal and firewood; and to the lack of energy supply infrastructure in informal settlements. There are 84 communities in close proximity of mining operations in South Africa, most of which are categorised as informal settlements, poor, low income and/or marginalized communities [19]. South Africa's coal mining industry is centred in the Mpumalanga Province, where an estimated 45% of the provincial population still use coal and wood (Figure 1):
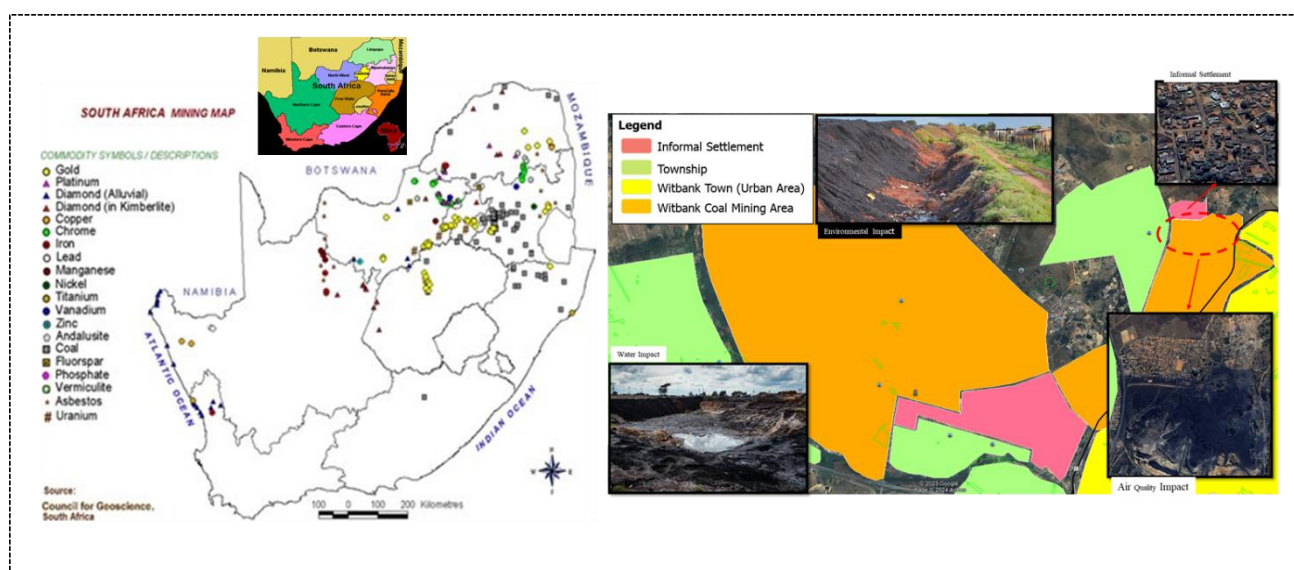

Figure 1: Active mines in South Africa
Source: Adapted from Cole and Broadhurst, 2022

Studies conducted in South Africa indicate a sharp rise in GDM, with the prevalence ranging from 1.6% to 25.8% between 1969 and 2018 [20] [21]. However, these studies do not expound and/or establish the relationship between atmospheric pollutants and the prevalence of GDM in mining communities. In addition, available studies were undertaken in varying geographical areas, with different risk variables. This research will seek to close the gap in existing body of knowledge by investigating, specifically, the correlation of long-term exposure to air pollution on GDM in women living near mining operations.

Discussion

Real-time spatial concentrations of ambient air pollutants will be collected through the PAS. PAS will be used for concentration measurements, volatility classification and spectral response to gain a better understanding of the potential contribution of air pollutants within Mpumalanga Province, to GDM. PAS is the most suitable method for in-situ (filter free), precise and accurate measurement of light absorption. Furthermore, the PAS is a direct, fast and easily calibrated method, which does not contain the fundamental difficulties associated with filter-based measurements or in-situ measurement using the difference of extinction and scattering [22] [23].

Triangulation and correlation of data collected through the PAS will be done through a cross-sectional investigation of GDM diagnosis at primary obstetrics health care facilities in the mining communities. Additionally, data access clearance will be sought to gain access to the Department of Forestry, Fisheries and Environment (South Africa) National Atmospheric Emissions Information System (NAEIS). The NAEIS is a government-owned and regulated emission reporting and data management system.

Research Objectives and Questions

Table 2 below provides an outline of the research objectives and questions to be answered by the study:

Research Objective- Question Alignment	Data Source	Analysis Technique
Research Objective 1: To assess concentration patterns of mining-induced ambient air pollutants within mining host communities		
(i) What are the spatial and temporal concentration patterns of ambient air pollutants within mining host communities? (ii) What is the relationship between pollutant concentration patterns and the incidences of GDM among women living in mining host communities	Existing literature review industry data NAEIS PAS existing literature	Statistical and thematic analysis Arc GIS
Research Objective 2: To attribute specific contribution of ambient air pollution to mining operations, differentiating them from other sources		
(iii) What are the point and non-point sources of atmospheric pollutants in mining host communities? (iv) What are the relative contributions of point and non-point sources to pollutant concentration patterns in mining host communities?	Existing literature, Questionnaire Air Quality Emissions Licences Emissions Inventory (NAEIS) Site Observations	Photoacoustic spectroscopy analysis Arc GIS
Research Objective 3: To evaluate the extent to which the character of air pollutants from mining operations contribute to the rate of GDM in women living near mining operations.		
(v) What is the prevalence of GDM among women living in mining host communities? (vi) How does the rate of GDM in mining host communities compare to national averages? (vii) What is the statistical correlation between the recorded GDM incidences and mining-induced air pollution? (viii) Which exposure levels are harmful to maternal health?	Questionnaires and semi-structured interviews Survey	Regression analysis Thematic analysis Photoacoustic spectroscopy analysis

Conclusions

The study applies an integrated approach of scientific methodologies, which means it is reliable and relevant in providing evidence-based and data driven critical insight on environmental pollution, public health and epidemiology. Growing evidence shows that the biophysical environment plays a crucial role in human health, thus making a compelling rationale for interdisciplinary research and collaboration such as one proposed in the study. It is envisaged that the outcomes of the research will provide insight into the potential relationship between mining-induced atmospheric pollutants and the prevalence of GDM in surrounding communities. The findings of the study will be useful to policymakers, mining industry stakeholders, community development and spatial planning practitioners in South Africa and other developing countries. The study may generate new theoretical insights and empirical evidence that could inform future research in sustainable development, community health, mining, and socio-economic development.

REFERENCE LIST

[1]. Jacobson, T.A, Kler, J.S, Hernke, M.T, Braun, R.K, Meyer, K.C, & Funk, W.E. Direct human health risks of increased atmospheric carbon dioxide. *Nature Sustainability* **2**, 691-701 (2019)

[2] Bierwirth, P., Long-term carbon dioxide toxicity and climate change: a critical apprehended risk for human health. 2024

[3] Cutter, S.L, Boruff, B.J, & Shirley, W.L. Social vulnerability to environmental hazards. *Social Science Quarterly* **84(2)**, 242-261 (2003)

[4] Sununianti, V.V. Social vulnerability of oil miners in rural areas. *Advances in Social Science, Education and Humanities* **(129)**, 137-140 (2018)

[5] Brunekreef, B. Health effects of air pollution observed in cohort studies in Europe. *Journal of Exposure Science and Environmental Epidemiology* **(17)**, 61-65 (2007).

[6] Todovoric, M.N. et al. Evaluation of mortality attributed to air pollution in the three most populatd cities in Serbia. International journal of Environmental Science and Technology (2019)

[7] Turner, M.C. et al. Outdoor air pollution and cancer: An overview of the current evidence and public health recommendations. *CA Cancer Journal (70), 460–479, 2020*

[7] Beelen, R. et al. Effects of long-term exposure to air pollution on natural-cause mortality: an analysis of 22 European cohorts within the multicentre ESCAPE project. *Lancet* **1(383)**, 785-795 (2014)

[8] Tang, X. et al. Air pollution and gestational diabetes mellitus: evidence from cohort studies. *BMJ Open Diabetes Research Care* **8(1),** 2020

[9] Taniyama, Y., & Griendling, K. K. Reactive oxygen species in the vasculature: molecular and cellular mechanisms. *Hypertension* **42(6)**, 1075-1081 (2003)

[10] Caturano, A. et al. Oxidative stress in type 2 diabetes: Impacts from pathogenesis to lifestyle modifications. *Current Issues In Molecular Biology* **45**, 6651–6666 (2023)

[11] Fleisch, A.F. et al. Air pollution exposure and gestational diabetes mellitus among pregnant women in Massachusetts: A cohort study. *Environmental Health* **15(40),** 121-124 (2016)

[12] Hu, H. et al. Association of atmospheric particulate matter and ozone with gestational diabetes mellitus. *Environmental Health Perspectives* **(123)**, 853–859 (2015)

[13] Lu, M.C. et al. Association of temporal distribution of fine particulate matter with glucose homeostasis during pregnancy in women of Chiayi City, Taiwan. *Environmental Research* **(152)**, 81–87 (2017)

[14] Preston, E.V. et al. Climate factors and gestational diabetes mellitus risk- a systematic review. *Environmental Health* **19(112)**, 1-19 (2020)

[15] da Silva, C.M. et al. Behaviour of pregnant women regarding physical activity in gestational diabetes mellitus: Secondary analysis of a descriptive cross-sectional study. *The Journal of Maternal-Fetal & Neonatal Medicine* **35(25)**, 7216-7221 (2021)

[16] Altieri, K.E. and Keen, S.L. Public health benefits of reducing exposure to ambient fine particulate matter in south Africa. *Science of The Total Environment* **(684)**, 610-620 (2019).

[17] Mirzania, P. et al., Barriers to powering past coal: Implications for just energy transition in South Africa. *Energy Research & Social Science* **(101),** 2023

[18] Phogole, B., Kelso, K., and Langerman, K.E. The effectiveness of household energy transition interventions in a coal-using community on the South African Highveld. *Energy for Sustainable Development* **(71)**, 1-12 (2022)

[19] Cole, M.J. & Broadhurst, J.L. Sustainable development in mining: A case of South Africa's west Wits Goldfield. Frontiers in Sustainable Cities (4), (2022)

[20] Dias, S., Pheiffer, C., & Adam, S. Screening and diagnosis of gestational diabetes mellitus in South Africa: what we know so far. South African Medical Journal **(109)7**, 457-462 (2019)

[21] Dias, S. et al. Prevalence of and risk factors for gestational diabetes mellitus in South Africa. South African Medical Journal **(109)7**, 463-467 (2019)

[22] Ajtai, T.et al. Absorption based size characterisation of aerosol by using photoacoustic spectroscopy. *Atmospheric Environment* **(304)**, (2022)

[23] Sigrist, M.W. Photoacoustic spectroscopy, applications. *Encyclopaedia of Spectroscopy and Spectrometry* **(3),** 589-597 (2017)

PREDICTION OF MONTHLY PM$_{10}$ CONCENTRATION IN URBAN LANDSCAPES USING RANDOM FOREST MODELLING

Seyedehmehrmanzar Sohrab[1], Péter Szilassi[1], Nándor Csikos[2,3]

[1]Department of Geoinformatics, Physical and Environmental Geography, University of Szeged, Egyetem u. 2-6, H-6722 Szeged, Hungary
[2]HUN-REN Department of Soil Mapping and Environmental Informatics, Institute of Soil Sciences, Centre for Agricultural Research, Budapest, Herman Ottó út 15, 1022, Budapest, Hungary
[3]MTA-SZTE Lendület Applied Ecology Research Group, Közép fasor 52, Szeged, 6726, Hungary
e-mail: mehrmanzar_sohrab@geo.u-szeged.hu

Air quality is a major public health concern, particularly in cities where various human activities contribute to the dispersion of particulate matter (PM). Even at low concentrations, PM$_{10}$ is linked to adverse health effects. Previous studies have explored the correlations between influential factors such as land use structures, climatological variables, and soil properties with PM$_{10}$ or PM$_{2.5}$ individually, typically on a local or regional scale. However, advanced modeling methods are essential due to the complex relationship between air pollution and environmental factors. This study aims to predict monthly average PM$_{10}$ concentrations using Conditional Inference Forest (CRF), considering environmental variables around air quality (AQ) measurement station points. The significance of each variable is evaluated to predict the average monthly concentration of PM$_{10}$ during the heating and cooling periods in European urban landscapes. We analyzed the relationship of PM$_{10}$ with variables such as land use proportion, road and rail density, soil texture, and meteorological variables, including temperature, total precipitation, wind speed, and mean sea level pressure within the 1000 m and 3000 m buffer zones under the heating and non-heating (cooling) period. We performed a grid search on the data set using cross-validation to select the optimal 'ntrees' and 'mtry' parameters, and then we trained the model using k-fold cross-validation and identified the best model as a final step, we retrained the final model on the entire training dataset using the best hyperparameters. Within a 1000 m circle radius of the AQ monitoring stations during the cooling period, soil texture emerges as the most influential factor, accounting for 20.75% of the importance in predicting PM$_{10}$ concentration. At a 3000 m radius during the same period, forests become the most significant variable (15.44%), underscoring the beneficial role of green spaces in reducing PM$_{10}$ levels, especially during the vegetation period. During the heating period within a radius of 1000 m, the monthly average temperature is the dominant factor (26.33%). When extended to a radius of 3000 m around the AQ monitoring stations, temperature (24.02%) and wind speed (21.28%) remain crucial. These findings emphasize the importance of considering geographical factors in air quality management strategies to promote healthier urban environments in Europe. Furthermore, the moderate precision indicated by R-squared values between 0.36 and 0.61 is comparable to those reported in some prior studies. However, these values underscore the need to improve our models in future research.

Keywords: Random forest, land use, soil texture, air temperature, air pollution, particular matter

INNOVATIVE AND NOVEL APPROACHES TO REDUCING MANURE EMISSIONS: ADVANCING SUSTAINABLE AGRICULTURE

Vineet Srivastava[1,4], Edit Mikó[2], George Wanjala[2], László Horváth[3], Anna Szabó[3,4], Zoltán Bozóki[3,4]

[1]*Doctoral School of Environmental Science, University of Szeged, Dugonics tér 13, 6720, Szeged, Hungary.*
[2]*Institute of Animal Sciences and Wildlife Management, Faculty of Agriculture, University of Szeged, Andrássy út 15., 6800, Hódmezővásárhely, Hungary.*
[3]*HUN-REN-SZTE Research Group for Photoacoustic Monitoring of Environmental Processes, Szeged, Hungary.*
[4]*Department of Optics and Quantum Electronics, University of Szeged, Dugonics tér 13, 6720 Szeged, Hungary.*
e-mail: srivastava.vineet@stud.u-szeged.hu

Abstract

According to Food and Agriculture Organization (FAO), the increasing global demand for animal products is projected to rise by over 70% by 2050. This has intensified the need for sustainable manure management practices. With the livestock sector responsible for approximately 14.5% of global greenhouse gas emissions, effective manure management is essential to mitigate environmental impacts. Poorly managed manure contributes to emissions of methane (CH_4) and nitrous oxide (N_2O), both potent greenhouse gases, while ammonia (NH_3) emissions degrade air quality and harm ecosystems. This study explores a range of advanced manure management techniques, including chemical, plant-based, and microbial additives, as well as emerging technologies like seaweed, larvae, and nanoparticles. Each approach offers unique mechanisms for reducing emissions and improving nutrient retention in manure. Chemical additives modify pH and suppress microbial activity, while plant-based additives such as tannins bind nitrogen compounds. Biological solutions, including microbial additives, seaweed, and larvae, help reshape microbial communities and reduce emissions naturally. Nanoparticles, as a separate category, offer cutting-edge potential due to their high reactivity and unique properties for emission mitigation. This review examines the effectiveness of these methods, highlights recent advancements, and proposes future directions for innovation. By adopting these novel strategies, this study aims to enhance sustainable agricultural practices and minimize environmental impacts.

pH DEPENDENCE OF PARACETAMOL REMOVAL BY NANOFILTRATION IN AQUEOUS SOLUTIONS

Máté Sütő, Tamás Szabó, Gábor Peintler

Department of Physical Chemistry and Materials Science, 6720, Szeged, Rerrich Béla tér 1.
e-mail: matesuto17@gmail.com

Abstract

I was removed one of the most consumed active pharmaceutical compounds, paracetamol, from aqueous solutions using nanofiltration membranes. I was measured the filtration efficiency by varying the pH and ionic composition of the solution. I used NF270 wide pore size and NF90 narrow pore size membranes for filtration. I was found that increasing the pH of the pure aqueous paracetamol solution also significantly increased the retention. I wqs observed a nearly 30-fold increase in membrane retention in the alkaline (pH 8-12) range for NF270 and a 1.3-fold increase for NF90. I was also investigated the effect of the ionic strength of the NaCl solution and the pH dependence at different ionic strengths. Increasing the concentration of salt significantly reduces retention. In addition to pure aqueous and saline media, I was also investigated membrane separation in a synthetic model wastewater containing salts of Mg, K, Ca, Na and ammonium salts, which resulted in higher retention for paracetamol than for saline or pure aqueous solutions. While NaCl reduces membrane retention by charge screening, magnesium increases it due to the formation of bonds with the membrane. To explain the pH dependence, it was also necessary to determine the pKa of paracetamol, which was obtained as 9.62 at the ionic strength used. Using this, I was determined the degree of dissociation of paracetamol at each pH value and found that membrane retention correlated strongly with the degree of dissociation.

Finally, I was also determined the fluxes characterizing the filtration rate under different conditions, which decreased almost linearly with increasing pH. I was found that the added NaCl further reduced the flux, but overall the NF270 membrane showed the lowest values for the model aqueous paracetamol solution. The variation of the volumetric fluxes measured for NF90 showed a similar trend as for NF270 membrane, but only lower fluxes could be achieved due to the narrower nominal pore size. The results presented in this thesis can be directly used to develop drinking water purification and pharmaceutical separation operations for the efficient recovery of paracetamol.

ASSESSMENT OF THE DISTRIBUTION OF GOLD NANOPARTICLES IN THIN POLYMER FILMS BY LASER-INDUCED BREAKDOWN SPECTROSCOPY ELEMENTAL MAPPING

Orsolya Urbán[1,2], Fernando Casian Plaza[1,2], Ádám Bélteki[1,2], Márk Aladi[2], Miklós Kedves[2], Attila Bonyár[2,3], Miklós Veres[2], Gábor Galbács[1,2]*

[1]*Department of Molecular and Analytical Chemistry, University of Szeged, H-6720 Szeged, Dóm tér 7-8, Hungary*
[2]*Nanoplasmonic Laser Fusion Research Laboratory (NAPLIFE), HUN-REN Wigner Research Centre for Physics, 1121 Budapest, Konkoly-Thege Miklós út 29-33, Hungary*
[3]*Department of Electronics Technology, Budapest University of Technology and Economics, Hungary*
e-mail: galbx@chem.u-szeged.hu

Our research group is also contributing to the Nanoplasmonic Laser Fusion Research Laboratory (NAPLIFE) project that aims at using nanoplasmonic effects generated by a femtosecond laser impulse to initiate fusion reactions. This project requires gold nanorods (nano antennae) to be distributed in a special way in thin polymer films, which serve as laser targets and also contains the hydrogen that is the fuel for the reactions [1,2]. The preparation of these polymer targets require some method that allows for the assessment of the distribution of the nanoparticles (NPs). While UV-Vis absorption spectroscopy is also capable of measuring the NP concentration, but it has practically no spatial resolution. SEM-EDX or TEM-EDX is also capable of such measurements, however the thickness of the polymer film might pose a problem and it is difficult to cover a macroscopic area with such high resolution techniques. At the same time, LIBS elemental mapping can provide micrometer-range spatial resolution and can ablate thin polymer layers [3]. This is the direction in which our method development project has advanced.

We prepared a range of test samples for the experiments. In these experiments we used magnetron sputtering followed by thermal treatment to produce a series of depositions of spherical Au nanoparticles on silicon substrates. By changing the sputtering parameters (pressure, time, current) we were able to change the surface concentration of nanoparticles in a 3.46-743.8 ng/mm^2 range. The exact surface concentrations were measured by ICP-MS. The nanoparticles were then covered by a polymer thin layer prepared by spin coating. PLA, MMA and PS polymers were tested and the thickness of the layers (0.07 to 4 microns) determined by contact profilometry. By calibrating the LIBS signal using these test samples, we could construct a method which uses LIBS elemental mapping and can be used to determine the surface mass or number concentration distribution of the NPs in the polymer. We demonstrated that patterned distributions can be also mapped and analyzed this way, in these demonstrations we used metal masks cut out by a fiber laser.

References

[1] N. Kroó, M. Aladi, M. Kedves, B. Ráczkevi, A. Kumari, P. Rácz, M. Veres, G. Galbács, L.P. Csernai, T.S. Biró, Sci. Rep. 14 (2024) 18288.
[2] T. S. Biró, N. Kroó, L. P. Csernai, M. Veres, M. Aladi, I. Papp, M.Á. Kedves, et al.; Universe, 2023, 9, 233.
[3] D.J. Palásti, O. Urbán, F.A. Casian-Plaza, J. Kámán, I. Rigó, et al.; Polymer Testing, 2024, 139, 108565.

INTACT PROTEIN ANALYSIS OF SNAKE VENOMS WITH CZE-MS

Gayatri Vishwakarma[1], Melinda Andrási[1], Ruben Szabó[1], Péter Hajdú[2], Vladimir Petrilla[3,4] Monika Petrillová[5], Jaroslav Legath[6,7], Attila Gáspár[1]

[1]Department of Inorganic and Analytical Chemistry, University of Debrecen, Egyetem ter 1., Debrecen 4032, Hungary
[2]Department of Dental Biochemistry and Department of Biophysics and Cell Biology, University of Debrecen, Egyetem tér 1., Debrecen 4032, Hungary
[3]Department of Biology and Physiology, University of Veterinary Medicine and Pharmacy, Košice, Slovakia
[4]Zoological Department, Zoological Garden Košice, Košice-Kavečany, Slovakia
[5]Department of General Competencies, University of Veterinary Medicine and Pharmacy, Košice, Slovakia
[6]Department of Pharmacology and Toxicology, University of Veterinary Medicine and Pharmacy, Košice, Slovakia
[7]Department of Biotechnology and Bioinformatics, Faculty of Chemistry, Rzeszow University of Technology, Rzeszow, Poland.
e-mail: gayatri.vishwakarma@science.unideb.hu

Abstract

In this research work we demonstrated the potential analytical performance of capillary zone electrophoresis coupled with mass spectrometry (CZE-MS) for the intact protein analysis of similar venom samples. Using 1 M formic acid (pH=1.9) as BGE, minimal adsorption and narrow peaks shapes - thus good separation efficiencies - were obtained for the protein components of the venom samples.

Introduction

Venoms consist of several biologically active components, primarily peptides and proteins. these toxin components have the potential to cause lethal effects [1,2]. Top-down mass spectrometric technique when combined with capillary zone electrophoresis, becomes highly effective in studying the structural characteristics of intact proteins. This methodology can be utilized for the analysis of complex protein molecules such as snake venom [3].

Experimental

Analyses were conducted using a 7100 model CE instrument (Agilent) with UV and MS (maXis II UHR ESI-QTOF MS instrument, Bruker) detection. Fused silica capillaries of 85 cm x 50 μm I.D. and 370 μm O.D. was used. UV detection was carried out by on-capillary photometric measurement (detection wavelength: 200 nm). Background electrolytes were 1 M formic acid (pH=1.8), sheath liquid: 0.1% formic acid in 1:1 isopropyl alcohol.

Results and discussion

The precision of migration times and peak areas were 1.9-2.8 RSD% and 0.8-7.2 RSD%, respectively and the theoretical plate numbers were 32000-238000 for peaks having signal-to-noise ratio (S/N) larger than 50. More than 250 different toxin components (7-10 kDa) were detected in the venoms obtained from snakes of 9 different subspecies (belonging either to Naja or Dendroaspis species). The protein contents of the venoms of the same subspecies collected from different geographical regions are similar and differ only in a few (less than 10%)

components. However, the venom samples collected from different organisms (within the same species) exhibit very different protein patterns.

Conclusion

Our study utilizes fused silica capillaries for their simplicity and cost-effectiveness, employing background electrolytes with extremely low pH conditions to separate and characterize various components in snake venom samples. Notably, our findings revealed discrete protein patterns among venoms from different subspecies, highlighting the unique fingerprinting potential of venom in various snake populations.

Acknowledgements

References

[1] J. J Calvete, P. Juárez, L. Sanz, J Mass Spectrom. 42 (2007) 1405.
[2] G. Vishwakarma, M. Andrasi, R. Szabo, P. Hajdu, V. Petrilla, M. Petrillová, J. Legath, Attila Gaspar, Microchem. J. 200 (2024) 110290
[3] N. Hamidli, M. Andrasi, C. Nagy, A. Gaspar, J. Chromatogr. A 1654 (2021) 462448.

Poster Proceedings

THE AGRICULTURAL SYSTEM AND THE VARIETY OF CROPS FROM CIACOVA

Okros Adalbert[1], Mihuț Casiana[1], Cozma Antonela[1], Mircov Vlad Dragoslav[2], Eremi Ovidiu[1]

[1]*Department of Soil Sciences, University of Life Sciences "King Mihai I" from Timişoara, Calea Aradului nr.119, 300645 Timişoara, country Timiş, România*
[2]*Department of Agricultural Tehnologies University of Life Sciences "King Mihai I" from Timişoara, Calea Aradului nr.119, 300645 Timişoara, country Timiş, România*
e-mail:casiana_mihut@usvt.ro

Abstract

The development of human society was possible and directly conditioned by the provision of an appropriate and stable trophic base, this being possible through the creation and improvement of agroecosystems, in other words through the modernization of agriculture over time. [9] From the point of view of the main form of relief, the commune of Ciacova falls into the Plain category: low plain with alluvial-proluvial deposits in the Timiş - Bega - Bârzava sector. The general slope of the plain is from E to W from 180m to 90m (Făget-Timişoara). In this paper, data on the agricultural system and the composition of the crops in the locality were analyzed in order to gain a better understanding of the agricultural development and the assortment of crops.[2,1] Within the range of crops present in the locality, there is a varied range of both plants intended for large crops and plants intended for vegetable cultivation. The year 2023 presented the highest production of the autumn wheat crop with 7615 tons, while from the point of view of the harvested areas, the year 2023 is in the first position with 1523 hectares.

Introduction

Human food resources are provided mainly from agricultural ecosystems and to a lesser extent from natural or other sources (modern food industries, biotechnologies)

For a long period of time in which the human species was formed and evolved, natural ecosystems constituted the basis of food, but with the emergence and progressive transition, in the last 10-15 millennia, one of the most profound revolutions of humanity was realized in the practice of agriculture. [8]

Since ancient times, mankind has developed a strategy to cultivate plants and transform the environment in such a way as to obtain the maximum possible conversion of solar energy into food, fodder or other agricultural products.

The development of human society was possible and directly conditioned by the provision of an appropriate and stable trophic base, this being possible through the creation and improvement of agroecosystems, in other words through the modernization of agriculture over time. [3,5]

The activities of design, organization and management of the created agroecosystems, of their management, activities that can be found in the term agriculture, faithfully reflect the level of development of human society.

From the point of view of the main form of relief, the commune of Ciacova falls into the Plain category: low plain with alluvial-proluvial deposits in the Timiş - Bega - Bârzava sector.[10,12] The low plains in this meadow sector are relatively recent, drained by rivers with a permanent regime: Bega, Timiş, Bârzava, Moraviţa and represent a typical region of Holocene drift in which both local and general subsidence in the lower course of the Tisa river determined the coverage loessoid deposits and older alluvium with more recent alluvial-proluvial materials, on

the surface of which the soils are found in reduced stages of evolution. The general slope of the plain is from E to W from 180m to 90m (Făget-Timişoara). [4,5,7]

The banat plain is at the interference of continental air masses, of western and eastern origin, suffering in addition the invasion of warm, southern air masses. The frequency with which these types of air masses influence the thermal and pluviometric regime gives the area a temperate climate, with a moderate degree of continentality, with sub-mediterranean influences, more or less accentuated. [6]

Experiment

In this paper, data on the agricultural system and the composition of the crops in the locality were analyzed in order to gain a better understanding of the agricultural development and the assortment of crops.

Results and discussion

Crops	Production (t)	Surface (he)
Autumn wheat	5800	1500
Rye	1200	300
Barley	200	55
Autumn oats	250	60
Maize	5500	1500
Sunflower	900	500
Rape	1748	92

Figure 1. Harvested area and production of the main crops in year 2021

As can be seen from the table above, the main crops in Ciacova are wheat with an area of 1500 ha and a total production of 5800 t, which means an average production of 3860 kg/ha, followed by maize with an area of 1500 ha with a total production of 5500 tons representing an average production of 3600kg/ha. The next crops are Sunflower with 500 ha and Rye with 300 ha.

Crops	Surface (he)	Production (t)
Potatoes	120	1200
Tomato	20	80
Cabbage	6	75
Pepper	4	25
Cucumbers	4	40
Peas	4	50
Beans	2	2
Eggplant	2	6
Cauliflower	1	28

Figure 2. Harvested area and production of vegetable crops in year 2021

Related to the vegetable crops present in the locality, as can be seen from the table above, the main crop is potatoes with 120 ha and on smaller areas tomatoes, cabbage, peppers, cauliflower, eggplant are grown, which completes the cultural palette of the locality.

Crops	Surface (he)	Production (t)
Autumn wheat	1600	7200
Barley	200	800
Autumn oats	10	30
Maize	1680	3360
Sunflower	250	375
Rape	250	375

Figure 3. Harvested area and production of the main crops in year 2022
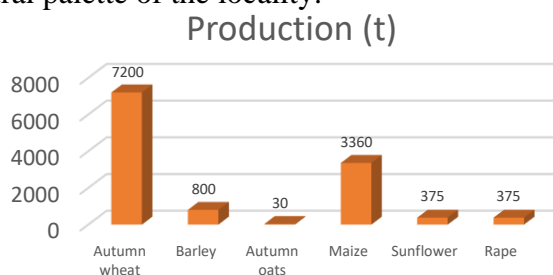

Table 1. Harvested production of the main crops in 2022

As can be seen from the table and figures above, the main crops in Ciacova in 2022 are wheat with an area of 1600 ha and a total production of 7200 t, which represents an average production of 4500 kg/ ha, followed by grain maize with an area of 1680 ha with a total production of 3360 tonnes representing an average production of 2000kg/ha. The next crops are Sunflower with 375 ha and Barley with 200 ha.

Crops	Surface (he)	Production (t)
Potatoes	90	1000
Tomato	6	42
Onion	5	70
Garlic	5	30
Cabbage	12	120
Pepper	2	12
Peas	20	30
Eggplant	2	10

Figure 4. Harvested area and production of vegetable crops in year 2022
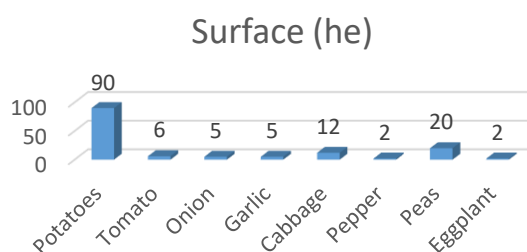
Table 2. Harvested area of vegetable crops in year 2022

Related to the vegetable crops present within the locality in 2022, as can be seen from the table and figures above, the main crop is potatoes with 90 ha from 120 ha in 2021 and on smaller areas cabbage, peppers, onion, garlic, cauliflower, eggplant that complete the locality's crop palette.

Crops	Surface (he)	Production (t)
Autumn wheat	1523	7615
Autumn rye	1	
Barley	259	
Spring oats	88	
Maize	956	6692
Sunflower	548	1918
Rape	444	1332

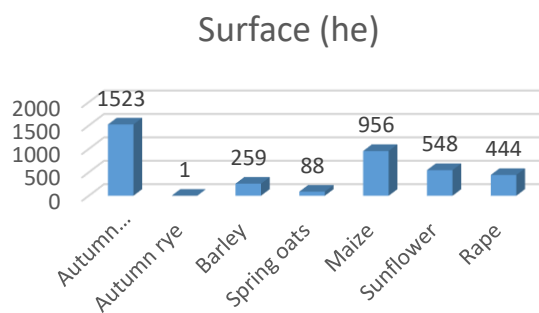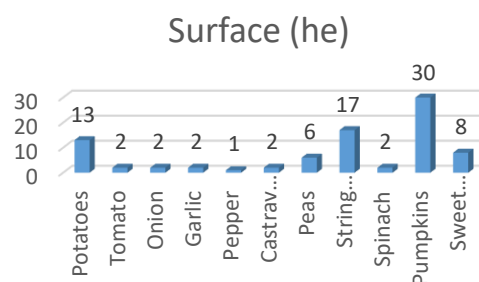Figure 5. Harvested area and production of the main crops in year 2023

Table 3. Harvested area of main crops in year 2023

As can be seen from the table and figures above, the main crops in Ciacova in 2023 are wheat with an area of 1523 ha and a total production of 7615 t, which represents an average production of 5000 kg/ ha, followed by grain maize with an area of 956 ha with a total production of 6692 tonnes representing an average production of 7000kg/ha. The next crops are barley with 259 ha and spring oats with 88 ha.

Crops	Surface (he)	Production (t)
Potatoes	13	24
Tomato	2	12
Onion	2	28
Garlic	2	12
Pepper	1	
Castraveți	2	
Peas	6	21
String beans	17	
Spinach	2	
Pumpkins	30	360
Sweet corn	8	64

Figure 6. Harvested area and production of vegetable crops in year 2023

Table 4. Harvested area of vegetable crops in year 2023

Related to the vegetable crops present in the locality in 2023, as can be seen from the table and figures above, the main crop is pumpkin with 30 ha, green beans with 17 ha, tomato with 2 ha and on more areas cabbage, peppers, and cucumbers are grown on small farms, which complete the locality's crop palette.

Conclusion

1. Wheat is the main crop in Ciacova, followed by maize. The next crops are sunflowers, rapeseed, barley and oats.

2. Within the range of crops present in the locality, there is a varied range of both plants intended for large crops and plants intended for vegetable cultivation.

3. The year 2023 presented the highest production of the autumn wheat crop with 7615 tons, while from the point of view of the harvested areas, the year 2023 is in the first position with 1523 hectares.

4. The potato crop represents in 2021 and 2022 the crop with the largest harvested areas and the highest productions of the three years analyzed.

5. In 2023, the pumpkin crop represented the main vegetable crop with a production of 360 tons harvested from an area of 30 hectares.

References

[1]. Berbecel O., Cusursuz B., 1979 – *Resursele agroclimatice ale judeţului Timiş*, Studiu monografic, I.M.H., Bucureşti;

[2]. Borcean I., Tabără V., David G., Borcean Eugenia, Ţărău D., Borcean A., 1996 - *Zonarea, cultivarea şi protecţia plantelor de câmp în Banat*, Ed. Mirton, Timişoara;

[3]. Imbrea F. - Tehnologii integrate - 2014 – Eurobit

[4]. Ianoş G., Puşcă I., Goian M., 1997 - *Solurile Banatului II – Condiţii naturale şi fertilitate*, Ed. Mirton, Timişoara;

[5]. Mihuţ, C., Niţă L., 2018, Atmospheric Factors used to characterize soil resources https://www.rjas.ro/issue_detail/44, Timișoara, pag. 114-120.

[6]. Niţă L. - Pedologie, Ed. Eurobit, Timișoara, 2007;

[7]. POSEA G., 1995 – *Câmpia de Vest a României (C. Banato-Crişană)*, Ed. Fundaţiei „România Mare", Bucureşti;

[8]. Puşcă I., 2002 - *Câmpia Banatului*, Fundaţia Naţională „Satul românesc", Bucureşti;

[9]. Sala Florin – Sisteme de Agricultura, Editura SOLNESS Timişoara 2002

[10].   Toncea I., Alecu I.N., *Ingineria sistemelor agricole*, Ed. Ceres, Bucureşti, 1999.
[11].   Ţărău D., Luca M., 2002 - *Panoptic al comunelor bănăţene din perspectivă pedologică*, Ed. Marineasa, Timişoara;
[12].   xxx. Date furnizate de Primăria Ciacova;

ENHANCING THE SURFACE REACTIVITY OF SEASHELLS BY THERMO-CHEMICAL METHODS

Alexandra Ioana Bucur[1], Mihai-Cosmin Pascariu[1,2], Raul Alin Bucur[1], Cristina Mosoarca[1], Bogdan-Ovidiu Taranu[1], Radu Banica[1]

[1]National Institute of R&D for Electrochemistry and Condensed Matter,
144 Dr. Aurel Păunescu-Podeanu, RO-300569 Timisoara, Romania
[2]„Vasile Goldiş" Western University of Arad, 86 Liviu Rebreanu, RO-310414 Arad, Romania
e-mail: alexandra.i.bucur@gmail.com

Abstract

Phosphorus removal from wastewaters is a subject of intense scientific research. The present study proposes a new material with pollutants adsorbing properties, obtained by a combination of thermal and chemical approaches, applied to Black Sea shells' exoskeletons, which are considered to be a hazardous material in some situations. For the presented case, the XRD results revealed the fact that the chemical reaction was incomplete, the reagent being present in the sample investigated after the burning process.

Introduction

Phosphorus is an essential element for agriculture, being applied as fertilizer on a large scale. Its discharge limits in urban wastewater are set by the European law to 1-2 mg/L as total phosphorus, with the proposal to lower these values to 0.5 mg/L and also to include the nutrient recovery in the coming decades [1]. A large amount of phosphate in water is the result of human industrial and household activities, therefore the excess needs to be removed in order to protect the living organisms. The phosphate recovery has a positive impact on the preservation of the natural resources such as phosphate rocks or bodies of water [2]. Its extraction from wastewater by using renewable materials, ideally cheap and abundant, is intensively studied. One of the most promising such materials is the seashells exoskeletons, consisting mainly in calcium carbonate, which has proven its good adsorption properties [3]. Shells are mostly considered a waste which is produced in large amounts all over the world. The surface of seashells' exoskeletons can be modified by various chemical or thermal approaches, in order to increase their superficial reactivity and specific surface area. The improvement of these characteristics affect the properties of shells, and could lead to an increase in their adsorption potential and thus the efficiency regarding the processing of residual waters [4, 5].

In this paper, we present some preliminary work regarding an adsorbent material for water phosphate, obtained by using a combination of chemical and thermal treatments, both of them beneficial for surface modification. The efficiency regarding the removal of pollutants is expected to increase following this working hypothesis.

Experimental

Shells were collected from the Black Sea shore (the city of Mangalia, Romania) and were washed repeatedly with tap water, then with bidistilled water and were finally dried at 110 °C. Next, they were broken to pieces of various sizes and sieved, separating the different dimensional fractions.

Larger size shell fragments were tested in order to create a material with good adsorption properties on its surface, increased by a combination of thermal and chemical treatment. A high temperature was tested (> 800 °C) for a short time period, obtained by using a chemical reaction which generated a high amount of heat, i.e. the reaction between $KClO_3$ and sugars. Larger size

shell fragments were chosen because, when being used as a reactor bed, the larger size will facilitate the circulation of water to be treated and will reduce the equipment's clogging.

The shells were weighed and mixed with various amounts of oxidizer ($KClO_3$) and fuel (sugar), then the mixture was directly ignited. Depending on the reagent type (specific sugar) and the stoichiometry, the reaction took place with different intensities, in some cases with a flame and the intended strong exothermic effect.

X-ray diffraction (XRD) and scanning electron microscopy (SEM) were used in analyzing the modified exoskeleton's surface and structure.

Results and discussion

The XRD pattern of one sample of shells modified by using the sugar/$KClO_3$ chemical reaction is presented in Figure 1:

Figure 1. XRD pattern of a sample of shells and sugar/$KClO_3$ mixture after combustion

From the diffraction pattern it was noticed that KCl is present in the sample after the combustion, confirming that the assumed redox reaction took place. Calcium carbonate polymorphs aragonite and calcite are also present, meaning that the shells have at least partially retained their chemical identity and were not completely decomposed during the process. $KClO_3$ is also present in the diffraction pattern, suggesting an incomplete reaction, possibly due to the heterogeneity of the chemical system involved. The lack of calcium oxide in the pattern is probably due to its carbonation soon after air exposure.

The SEM investigation has shown that, post-combustion, the surface morphology resembles a sponge-like surface, with a number of pores of various dimensions, compared to the raw shells that have a different surface morphology. This means that the strong exothermal effect, which accompanied the chemical reaction, led to the partial decomposition of the seashell fragments, and that the method could be promising in tailoring the superficial properties of these materials, including the capability of removing the pollutants from waters.

Conclusion

Multiple tests were performed in order to transform a waste, i.e. shells exoskeletons, into an adsorption material for pollutants in wastewaters. Shells were mixed with various oxidant/fuel combinations, which were tested for combustion. Our results showed that a combination of thermal and chemical treatment has the potential to offer a useful material,

considering the partial decomposition of calcium carbonate and the morphology of the shells fragments' surfaces after the decomposition chemical process.

Acknowledgements

References

[1] https://www.phosphorusplatform.eu/scope-in-print/news/2244-draft-revision-of-eu-urban-waste-water-treatment-directive, accessed September 12, 2024;

[2] Oladoja N. A., Adelagun R. O. A., Ahmad A. L., Ololade I. A., Process Saf. Environ. 98 (2015);

[3] Pap S., Gaffney Paul P.J., Bremner B., Turk Sekulic M., Maletic S., Gibb S. W., Taggart M. A., Sci Total Environ 814 (2022): 152794;

[4] Bucur A. I., Poienar M., Bucur R. A., Mosoarca C., Banica R., *Braz J Chem Eng* 40 (2023), 1067-1076;

[5] Lee J.-I., Kang J.-K., Hong S.-H., Lee C.-G., Jeong S., Park S.-J., Chemosphere 263 (2021), 128328.

GANGLIOSIDOMICS OF CEPHALIC DISORDERS BY ION MOBILITY MASS SPECTROMETRY

Maria-Roxana Biricioiu[1,2], Mirela Sarbu[1], Raluca Ica[1], Željka Vukelić[3], David E. Clemmer[4], Alina D. Zamfir[1,5]

[1]National Institute for Research and Development in Electrochemistry and Condensed Matter, Plautius Andronescu Str. 1, 300224, Timisoara, Romania;
[2]West University of Timisoara, Faculty of Physics, Vasile Parvan, 4, 300223, Timisoara, Romania;
[3]University of Zagreb, Faculty of Medicine, Šalata 2, 10000, Zagreb, Croatia;
[4]Indiana University, Faculty of Chemistry, 800 E. Kirkwood Ave., IN 47405, Bloomington, USA;
[5]Institute for Research, Development and Innovation in Natural and Technical Sciences, Aurel Vlaicu University of Arad, B-dul Revoluţiei 77, 310130, Arad, Romania
e-mail: maria.biricioiu99@e-uvt.ro

Abstract
In this study we report on the determination of anencephaly gangliosidome by ion mobility separation (IMS) mass spectrometry (MS), introduced here for the first time in the research of cephalic disorders. Ganglioside (GG) extracts from residual brains of anencephalic fetuses in various gestational weeks were comparatively profiled by IMS MS, structurally analyzed by IMS tandem MS (MS/MS), and, finally, assessed against a native ganglioside mixture from normal fetal brain. The comparative assay disclosed variations in GG expression with fetal age and a correlation of the pattern with the developmental stage. In contrast to the normal fetal brain, the neural tissue in anencephaly was found to contain an elevated number of polysialogangliosides and a lower expression of *O*-Ac- and GalNAc-modified glycoforms.

Introduction
Cephalic disorders are congenital malformations caused by damage or abnormal fetal development of the nervous system. They are mainly caused by a defective closure of the neural tube. These disorders include acephaly, acrania, encephalocele, spina bifida, however, the most severe is anencephaly, as it can lead to death before or within a week after birth [1] due to the total or partial absence of the brain [2]. The most common detection technique is ultrasound screening, usually in the first trimester of pregnancy [3], yet an early antenatal diagnosis is crucial. Over the years, various techniques have been developed for biomarker identification, including mass spectrometric techniques for mapping and characterization of gangliosides, due to their high abundance in the central nervous system and the biomarker role played at this level. In this context, we have optimized nanoelectrospray (nanoESI) IMS MS and collision induced dissociations (CID) MS/MS and introduced this analytical platform in the investigation of gangliosides expressed in human anencephaly.

Experimental
The native GG extracts from histopathologically-defined residual cerebra originating from anencephalic fetuses in the 28th (denoted 28GW), 35th (35GW) and 37th (35GW) gestational week were extracted, purified and submitted to IMS MS separation and under identical conditions. For all MS experiments a Synapt G2-S mass spectrometer (Waters, Manchester, UK) encompassing IMS, a quadrupole time of flight (QTOF) mass analyzer, equipped with nanoESI source, tuned in the negative ion mode and operated under identical conditions was

employed. All samples were infused by nanoESI at 10 µL·min⁻¹ flow rate, 1.5 kV applied to the capillary and 45V potential applied to the cone. After the electrospray ionization, packets of ions were release through the quadrupole and entered the traveling wave separation region of IMS, where ions are travelling under an electric field, through a buffer gas and separated base on their mobility. Since IMS allows the separation of molecules by size, charge, shape and apparent surface area, to attain the best separation, the IMS parameters were optimized as follows: IMS gas flow 90 mL/min, IMS wave velocity 650 m/s and IMS wave height 40 V. Ganglioside structural characterization was performed in the transfer cell, after mobility separation, by MS/MS at low energies CID of 40-55 eV, to generate the highest number of diagnostic ions and prevent the exhaustive fragmentation of the labile residues.

Results and discussion
The comparative assignment of all major ions detected in the 28GW, 35GW and 37GW samples together with the experimental and theoretical *m/z* values and the mass accuracies, indicated that, overall, by IMS MS a remarkable number of anencephaly-related GGs were discovered. IMS MS provided data on 343 anencephaly-associated gangliosides *vs.* only 157 known before and revealed a correlation of their expression pattern with the developmental stage. The detected species showed evidence of a high heterogeneity in the composition of their glycan core and a complementary molecular diversity conferred by their ceramide moieties, which vary not only in the length of the sphingosines and fatty acyl chains, but in their hydroxylation and degree of saturation as well. Due to the excellent separation of ions according to their mobility in a drift gas, the IMS MS platform was able to discover for the first time anencephaly-associated GGs of higher sialylation degree than 4, *i.e.* penta-, hexa-, hepta- and octasialylated structures. Additionally, the comparative screening of the extracts indicated substantial variations in ganglioside composition and a correlation of their expression and structure with the intrauterine developmental stage. Hence, the gangliosidomes of the residual brain of older fetuses encompass a higher number of complex species in the G1 class, *O*-Ac- and GalNAc-modified structures as well as an important number of components characterized by ceramides of long fatty acyl chains. Moreover, as compared to the normal fetal brain, the residual neural tissue in anencephaly was found to contain an elevated number of polysialogangliosides and a lower expression of *O*-Ac- and GalNAc-modified glycoforms. The overexpression of polysialylated species appears associated to brain development stagnation occurring in anencephaly. On the other side, the lower expression of *O*-acetylated GGs is seemingly an effect of neural tissue degradation and underdevelopment. As a result, *O*-Ac-gangliosides together with the other biologically interesting species, which were discovered and characterized structurally by CID MS/MS, among which the polysialogangliosides GH2, the structures in the GQ, GP, GS, and GO classes, the GalNAc-modified GGs and those with unusual ceramide composition worth further detailed investigation as new potential anencephaly markers.

Conclusion
Considering the role played by gangliosides in brain development and the previous achievements of IMS MS and MS/MS in biomarker discovery, here, we introduced this advanced analytical technique in the research of cephalic disorders, and optimized the approach for decoding the anencephaly gangliosidome. The IMS MS and CID MS/MS allowed: a) the detection 2.2 times more species associated to this disorder than any other method used before; b) the discovery of fucosylated, acetylated, and GalNAc-modified GG structures associated to anencephaly; c) establishing of a correlation between the GG pattern and the intrauterine developmental stage of anencephalic fetuses and d) the discrimination of isomers and the detailed structural characterization of species with potential biomarker role.

Acknowledgements

References

[1] M. Ishida, T. Cullup, C. Boustred, C. James, J. Docker, C. English, GOSgene, N. Lench, A.J. Copp, G.E. Moore, N.D.E. Greene, P. Stanier, Clin. Genet. 93 (2018) 870-879.
[2] N. Salari, B. Fatahi, R. Fatahian, P. Mohammadi, A. Rahmani, N. Darvishi, M. Keivan, S. Shohaimi, M. Mohammadi, Reprod. Health. 19 (2022) 1-18.
[3] N. Obeidi, N. Russell, J.R. Higgins, K. O'Donoghue, Prenat. Diagn. 30 (2010) 357-360.

AMARANTHUS VIRIDIS AND *ATRIPLEX HORTENSIS*: PIONEERING SUSTAINABLE FOOD SOLUTIONS FOR ADDRESSING ENVIRONMENTAL PROBLEMS

Mihaela Lacatus[1], Ioan Ladislau Caba[2,*], Patricia Tarkanyi[1], Mariana-Atena Poiana[1], Georgeta-Sofia Popescu[1], Liana-Maria Alda[1], Diana Moigradean[1], Laura, Radulescu[1], Simion Alda[3], Despina-Maria Bordean[1]

[1]Faculty of Food Engineering, University of Life Sciences "King Michael I" from Timisoara, 300645, Timisoara, Romania;
[2]National Institute of Research - Development for Machines and Installations designed to Agriculture and Food Industry - INMA, Bucharest 013813, Romania;
[3]Faculty of Engineering and Applied Technologies, University of Life Sciences "King Michael I" from Timisoara, 300645, Timisoara, Romania
*Corresponding author, e-mail: cabaioan@yahoo.com

Food is crucial for our survival and a major requirement of life, but our relationship with food is dangerously imbalanced. We produce enough food, still billions of people cannot afford a healthy diet or don't have sufficient to eat. At the same time we waste potential food when we cultivate crops or during producing food, ignoring potential nutritious foods, treating some plants, practically ignoring major environmental problems, global food security and global health.

Amaranthus viridis and *Atriplex hortensis* are very common plant and can be a serious weed in nearly any crop usually occurring with numerous other weeds. Even both are considered serious troubling weeds both plant species are non-toxic and nutritious staples for centuries. The use of *Amaranthus* and *Atriplex* as food is known since at least Mesolithic.

Salinity is one of the most important environmental factors limiting crop production in many parts of the world. Salt stress affects many aspects of plant metabolism and, as a result, growth and yields are reduced. According to multiple studies low levels of salinity (5 g/l NaCl) did not cause considerable inhibition of growth for *Amaranthus viridis* and *Atriplex hortensis* but increasing concentrations of salt induced an advanced decline in development and weight of the plants.

The aim of this study is to evaluate the nutritional potential of two common weeds to reduce environmental problems and to reinvent innovative foods.

Keywords: food security, food safety, innovative food products, mathematical models

IMPROVED FERROELECTRIC PROPERTIES IN BaTiO₃ CERAMICS

Bucur Raul Alin, Badea Iuliana, Bucur Alexandra Ioana

National Institute for Research and Development in Electrochemistry and Condensed Matter, Condensed Matter Department, No. 1 Plautius Andronescu, 300224 Timisoara, Romania. e-mail: raul_alin_bucur@yahoo.com

Abstract

$BaTiO_3$ is the best known member of the ferroelectric perovskite family, with applications ranging from tunable dielectrics [1], piezoelectric sensors [2] to elasto-optic elements [3]. Its piezoelectric properties, the nonlinearity of its dielectric properties, a very low production (cheap precursors) and also a high dielectric constant value at room temperature, makes $BaTiO_3$ the ideal candidate for obtaining cost efficient high power capacitors. Since its discovery [4], interesting characteristics useful for different applications were obtained, by adding different perovskite dopants: $BaSnO_3$ [5], $NaNbO_3$ [6], $(Bi_{0.5}Na_{0.5})TiO_3$ [7] or $Pb(Sn,Ti)O_3$ [8]. The transitional metal perovskite oxide $SmCoO_3$, is a potential candidate for applications in electromechanical devices, such as solid oxide fuel cells [9], gas sensor for O_2 and CO_2 [10] or electrolyte-gated thin-film transistors [11]. Recent reports related to $(Bi_{0.5}Na_{0.5})_{0.94}Ba_{0.06}TiO_3$ lead-free ceramics shows that Sm_2O_3 doped ceramics exhibit a typical relaxor behavior with diffuse phase transition, while enhancing the degree of ferroelectric relaxation behavior as Sm_2O_3 concentration increases [12], with a maximum piezoelectric constant of $d_{33} = 202$ pC·N^{-1} and a quality factor of 101. $SmCoO_3$ doping [13] will contribute to an increase of the quality factor (219) and a good value of the piezoelectric constant $d_{33} = 144$ pC·N^{-1}.

In this study, we focused on improving the dielectric and ferroelectric properties of $BaTiO_3$ ceramics, by means of doping with different amounts of $SmCoO_3$ and using an intermediate dry ball milling ceramic processing. $SmCoO_3$ doped $BaTiO_3$ ceramics ($BaTiO_3$-x mol% $SmCoO_3$, x=0, 0.5, 1, 1.5, 3, 5, 7) were obtained by solid state method at 1250ºC in air, subsequent a dry ball precursors milling for 20 minutes. As the doping percentage increases, the crystalline structure distorts towards the cubic system, but maintaining in the compositional range studied ($0 \leq x \leq 5$ mol%) a tetragonal symmetry. The effects of the temperature (room temperature $\rightarrow$ 350ºC, at 10 kHz) and of the frequency (50 Hz $\rightarrow$ 500 kHz, at room temperature), on the variation of the real part of the complex permittivity and dielectric loss are investigated with an RLC-meter (Tegam 3550). $SmCoO_3$ doping decrease the value of the dielectric constant at room temperature and at Curie temperature, and also lead to a gentle decrease of the Curie temperature. The polarization versus electric field hysteresis loop of the ceramics was observed at 100 Hz, using a Sawyer-Thomson capacitive voltage divider [14], and an Atten ADS 1152CML digital storage oscilloscope. The remnant polarization reach a maximum value simultaneous with the minimum value of the coercive field in the case of 1 mol% doping. Exponential loss of ferroelectricity was observed for the end members of the studied doping percentages. Our research show that a short dry milling precursor grinding process can effectively decrease the sintering temperature and increase the ferroelectric properties of the $SmCoO_3$ doped $BaTiO_3$ ceramics.

References

[1] K. Uchino, Ferroelectrics 151 (1994), 321–333;
[2] J. Cieminski, H. Beige, J. Phys. D: Appl. Phys. 24 (1991), 1182–1186;

[3] W. Kleemann, J. Mater. Sci. 41 (2006), 129–136;

[4] G.A. Smolensky, J. Phys. Soc. Jpn. 28 (1970), 26;

[5] Y. Liua, R.L. Withersa, X. Weib, J.D.F. Geraldc, J. Solid State Chem. 180 (2007), 858–865;

[6] W. Sakamoto, Y. Hamazaki, H. Maiwa, M. Moriya, T. Yogo, Thin Solid Films 518 (2010), 4256–4260;

[7] H.D. Li, C. Feng, W.L. Yao, Mater. Lett. 58 (2004), 1194– 1198;

[8] S. Gao, S. Wu, Y. Zhang, H. Yang, X. Wang, Mat. Sci. Eng. B 176 (2011), 68–71;

[9] E. Chinarro, J.R. Jurado, Apple Academic Press, Key Engineering Materials 1227 (2001), 206-213;

[10] C.R. Michel, E. Delgado, G. Santillán, A.H. Martínez, A.C. Chávez, Mater. Res. Bull. 42 (2007), 84–93;

[11] P.H. Xiang, S. Asanuma, H. Yamada, H. Sato, I.H. Inoue, H. Akoh, A. Sawa, M. Kawasaki, Y. Iwasa, Adv. Mater. 25 (2013), 2158-61;

[12] P. Fu, Z. Xu, R. Chu, W. Li, G. Zang, J. Hao, Mater. Chem. Phys. 12 (2010), 1065-1070;

[13] L. Shao, R. Chu, Z. Xu, Y. Liu, M. Chen, J. Zhao, G. Li, Physica B. 1 (2013), 164-168;

[14] S.C. Das, A. Majumdar, A. Shahee, N.P. Lalla, T. Shripathi, R. Hippler, Ferroelectr. Lett. 28 (2011) 78–86.

DETERMINATION OF PHYSICAL PARAMETERS FOR DIFFERENT EDIBLE OILS

Cozma Antoanela[1], Velciov Ariana[2], Mihuț Casiana[1], Anisoara Duma-Copcea[1], Mircov Vlad[1], Popescu Sofia[2], Radu Florina[2], Rotariu Lia[2], Stoin Daniela[2], Alexa Ersilia[2], Maria Rada[3]

[1]*Department of Soil Sciences, University of Life Sciences "King Michael I" from Timisoara, 300645, Timisoara, Romania e-mail: antoanelacozma@yahoo.com*
[2]*Department of Food Science, University of Life Sciences "King Michael I" from Timisoara, 300645, Timisoara, Romania ariana.velciov@yahoo.com*
[3]*University of Medicine and Pharmacy "Victor Babes" – Faculty of Medicine, 2 Eftimie Murgu Sq., 300041, Timisoara, Romania; e-mail: mariaradam@gmail.com*

Abstract

Edible oils are vegetable fats, which are used in food in various forms: for frying, in salads, in batters, in cakes, etc. Among the many characteristics that are standardized for oils, some are especially important to traders and especially for the consumers namely: color, smell, density, viscosity, melting point, smoke point, boiling point, flame behavior, light resistance, rancidity resistance, etc. This paper presents the results obtained from the analysis of five types of local edible oils: sunflower, soybean, rapeseed, corn and pumpkin oil. The following physico-chemical parameters have been determined: refractive index, density, viscosity, surface tension and acidity (as oleic acid). The physico-chemical analyzed parameters shows different values, depending on the nature of the analyzed oil: 1.4704 (sunflower oil) – 1.4742 (soybean oil), for refractive index ; 0.9050 (rapessed oil) - 0.2023 (pumpkin oil) g/cm ^{3}– for density ; 32.5428 (soybean oil) – 37.6482 (rapessed oil) cp – for viscosity ; 21.12 (soybean oil) -35.02 (pumpkin oil) dyn/cm - for surface tension ; 0.06 (soybean) - 0.88 (pumpkin oil) % oleic acid – for acidity. The values of the physico-chemical parameters of the analyzed vegetable oils show that they are suitable for use in human consumption.

Introduction

It is a well-known the fact that different cooking oils have been known since ancient times. Vegetable oils, together with fats, are indispensable components of a healthy diet and perform a series of vital functions in maintaining the human body. Choosing cooking oils it does not only influence the taste of food but also our health. Therefore it is useful to know what we choose and why. Because oil is an important ingredient in our diet, it is important to consume a healthy oil [1]. Along with carbohydrates and proteins, the basic nutrients for the body, they provide energy, protect against cold, ensure absorption of fat-soluble vitamins and serve as flavor carriers. Oils and fats are important parts of the human diet, constituting a rich source of dietary energy. Edible oils play an important role in the body through their content of essential fatty acids (EFA). The types of fatty acids in oils decide choosing the best oil. In general, healthy oils have more polyunsaturated and monounsaturated fatty acids and less saturated fat. Due to their high energy potential, vegetable oils and fats are used both in the food industry and for industrial, medical and fuel purposes. Due to its nutritional content (vitamins A, B1, B2, B6 C, E, D, carotenes, minerals: selenium, zinc, potassium) and the beneficial intake of saturated fats, it helps to reduce inflammatory processes and health problems such as diabetes, cholesterol, blood pressure [2, 3]. Edible oils become unhealthy when they are consumed in excess or when the quality of the cooking oil is questionable. Among the appropriate parameters for establishing the food quality of oils, a series of organoleptic and physicochemical parameters

can be mentioned, such as: color, smell, density, viscosity, melting point, smoke point, boiling point, flame behavior, light resistance , resistance to rancidity, etc. [4]. Therefore, we need to consider the physico-chemical properties for selecting a good type of edible oil. Considering the above presented, this experiment aims to determine some physico-chemical parameters of five varieties of autochthonous vegetable oil sold in local specialty stores.

Experimental

The analyzed edible oil samples were made up of local, autochthonous oils (sunflower, soybean, rapeseed, corn and pumpkin oil) sold in local markets in Timisoara (Romania).

Three sets of samples corresponding to each type of oil were formed for each of them, determining: refractive index, density, viscosity, surface tension and acidity (as oleic acid). Experimental determinations were carried out in accordance with the recommendations of Cozma et al., 2019 [5]. The refractive index were obtained using the refractometry method, with the Abbe refractometer corrected to the equivalent reading at 25°C (AOAC, 1995). The oils density was measured using the pycnometer by weighing on the analytical balance and for the dynamic viscosity was used the Ostwald type viscometer. The surface tension was determined using the stalagmometer [7].The free oils acidity is an important indicator due to the free fatty acids present in the product. The oils acidity was determined by titration with a 0.1 n KOH solution.

Results and discussion

The obtained results of the physico-chemical characteristics of alimentary (edible) oils taken in the experiment are presented in table 1 and figures 1-2.
For the utilised oils, it can be observed that their values are different from one category to another.

Table 1. The physico-chemical characteristics of some food edible oils sold in local markets

Parameters	Values	Sunflower	Soybean	Rapeseed	Corn	Pumpkin
Refractive index	Limits	1.4704 - 1.4718	1.4734- 1.4742	1.4713- 1.4725	1.4723- 1.4732	1.4716- 1.4724
	Mean value	*1.4710± 5.7x10⁻⁴*	*1.4738± 3.3x10⁻⁴*	*1.4719± 4.9x10⁻⁴*	*1.4728± 3.7x10⁻⁴*	*1.4721± 3.5x10⁻⁴*
Density, g/cm³	Limits	0.9127- 0.9132	0.9121- 0.9133	0.9050- 0.9149	0.9111- 0.9122	0.1959- 0.2023
	Mean value	*0.9130± 2.2x10⁻⁴*	*0.9127± 4.9x10⁻⁴*	*0.9100± 4.0x10⁻³*	*0.9116± 4.4x10⁻⁴*	*0.1991± 3.5x10⁻⁴*
Viscosity, cp	Limits	34.1242- 34.8756	32.5428- 33.5162	33.2175- 34.2316	36.5672- 37.6482	34.3541- 35.3152
	Mean value	*34,4953± 0.31*	*33,0349± 0.40*	*33,7066± 0.41*	*37,0761± 0.44*	*34,8484± 031*
Surface tension, dyn/cm	Limits	23.45- 24.95	21.12- 27.87	23.58- 25.06	25.69- 26.67	33.56- 35.02
	Mean value	*24.24± 0.62*	*27,91± 0.66*	*24,29± 0.61*	*26,13± 0.41*	*34,24± 0.60*
Acidity, (%) oleic acid	Limits	0.08- 0.15	0.06- 0.09	0.18- 0.25	0.11- 0.22	0.61- 0.88
	Mean value	*0,12± 0.02*	*0,08± 0.01*	*0,21± 0.03*	*0,20± 0.02*	*0,74± 0.11*
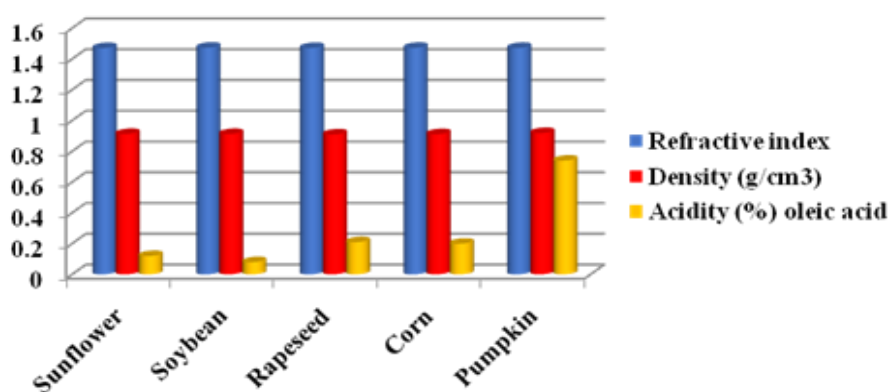
Figure 1. The refractive index, density and acidity of some edible oils

Measuring the refractive index can provide insight into the quality of the oils because any change in their optimal composition will also affect the refractive index value. The evaluation of the refractive index as a quality parameter helps to differentiate between types of vegetable oils or fats [5,6]. Refractive index values for oil samples at 25 ° C are included in the interval 1.4704 (sunflower oil) – 1.4742 (soybean oil). Many studies show that oils with lower density values are highly appreciated by consumers.The oils density varies with the type of analyzed oil and also with the temperature [7]. The results presented in table 1 show that, at room temperature of 25°C, the highest and lowest values of the densities are (0.9050) and (0.2023 g/ml) for the rapessed and pumpkin oil, respectively. Compared to water, which has a density of 1.00 g /ml, oils are less dense. Acidity is a measure of the free fatty acid content of the oil. Is defined as the number of milligrams of potassium hydroxide required to neutralize the free acids present in one gram of oil.The free acidity oils studied was determined according to STAS 145-67. Acidity is determined by direct titration of the oil sample in an alcoholic medium, against a standard solution of potassium hydroxide, in the presence of phenolphthalein as an indicator [8]. The values of free acidity values for the analyzed oils are between 0.06 (soybean) - 0.88 (pumpkin oil) % oleic acid [9].
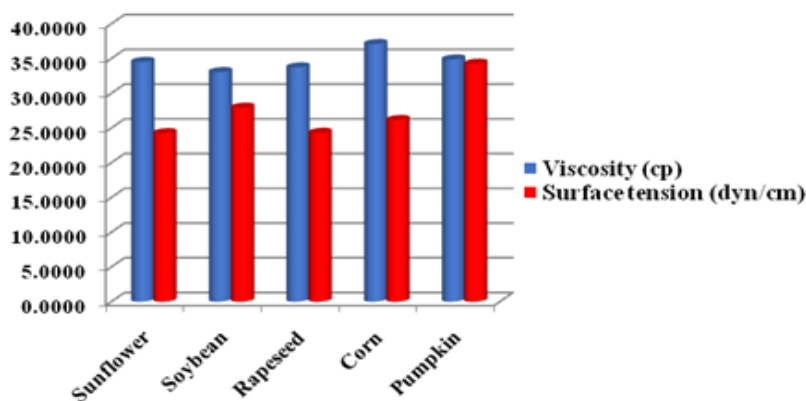
Figure 2. The viscosity and surface tension of some edible oils

Viscosity is considered an important physical property which offers indications regarding the oils fluidity. The viscosity of edible oils depends on the composition of saturated fatty acids in

different oils. From table 1, the obtained data showed that the viscosity of corn oil (37.6482 cP) is highest and is lowes for soybean oil (32.5428 cP). This highlight the fact that the sample of corn oil contains more fat than soybean oil. The ratio between the surface force and the length of the contour on which it acts is called the coefficient of surface tension (or surface tension) [7]. The surface tension values of the oil types, analyzed at 25°C , are in the range of 21.12 (soybean oil) -35.02 (pumpkin oil) dyn/cm. It is shown that, pumpkin oil contains more fat compared to soybean oil. The high surface tension of the oil means less spreading of the oil on the surfaces and consequently more energy loss. With an increase in temperature, the surface tension within the limits of a specific concentration, decreases. As can be seen from table 1 and from figures 1-2, the physico-chemical parameters present values within concentration limits depending on the assortment of edible oil analyzed: 1.4704 (sunflower oil) – 1.4742 (soybean oil), for refractive index ; 0.9050 (rapessd oil) - 0.2023 (pumpkin oil) g/cm ^{3}– for density ; 32.5428 (soybean oil) – 37.6482 (rapessd oil) cp – for viscosity ; 21.12 (soybean oil) -35.02 (pumpkin oil) dyn/cm - for surface tension ; 0.06 (soybean) - 0.88 (pumpkin oil) % oleic acid – for acidity. The average values of the refractive index, density, viscosity, surface tension and acidity: 1.4710 - 1.4738, 0.9100 - 0.1991 g/cm^3, 33.0349 – 37.0761 cp, 24.24 – 34.24 dyn/cm, and 0.08 – 0.74 % acid oleic, shows that the analyzed oils are comparable to the edible oils used in consumption. Therefore, these oils can be used for cooking or in other food formulas. It is desired that these parameters can be used to identify the varieties of food oils from oil mixtures.

Conclusion

The physico-chemical parameters: refractive index, density, viscosity, surface tension and acidity of the analyzed oils are important criteria for establishing the quality and choosing the appropriate oil for consumption. Therefore, it is necessary to monitor oil quality parameters. The results obtained (average values) for the determination of the physico-chemical parameters refractive index, density, viscosity, surface tension and acidity of the analyzed food oils show specific values depending on the oil assortment. The values of the physico-chemical parameters of the food oils analyzed: sunflower, soybean, rapeseed, corn and pumpkin are comparable with the data from the specialized literature and can find applications in different food formulas.

References

[1] Calugar, L., Grozea, I., Butnariu, M., 2024, Vegetable Oils in Maintaining Health. J Med Clin Nurs Stud, 2(2), 1-7 .
[2] Stoin Daniela, 2008, Food chemistry, Ed. Solness, Timisoara
[3] Frank D.Gunstone, 2000, Vegetable Oils in Food Technology Composition, Properties and Uses, Second Edition
[4] Bhukya PB, Wakulkar AP and Shah SA., 2020, To determine physical parameters of different edible oils, *Int. Res. Journal of Science & Engineering,* Special Issue A7: 81-84.
[5] Cozma A., Velciov A., Stoin D, Moigrădean D., Lalescu D., Petcu M., Crețescu I., Mihuț C., 2019, Cluster analysis for some different types of vegetable oils by the physicochemical characteristics, Journal of Agroalimentary Processes and Technologies, 25.3: 121-126.
[6] Ramon Aparicio, Garcia-Gonzalez, 2009, Chemical Analysis of Food: Techniques and Applications, First Edition, USA
[7] Cozma Antoanela, 2019, Practical guide of Physics, Eurobit, Timisoara
[8] Neagu Anișoara, Niță Irina, Botez Elisabeta, Geacai S., 2013, A physico-chemical study for some edible oils properties, Ovidius University Annals of Chemistry, Vol 24, Nr 2, pp.121-126

[9] Jiang, X., Li, S., Xiang, G., Li, Q., Fan, L., He, L., & Gu, K., 2016, Determination of the acid values of edible oils via FTIR spectroscopy based on the OH stretching band. *Food chemistry*, *212*, 585-589

H₂O₂ ELECTROANALYTICAL DETECTION AT MODIFIED ELECTRODE BASED ON MELDOLA BLUE AND CARBON AEROGEL MATRIX

Carmen Ioana Fort, Graziella Liana Turdean

"Babes-Bolyai" University, Faculty of Chemistry and Chemical Engineering, Department of Chemical Engineering, Laboratory of Electrochemical Research and Nonconventional Materials, Arany Janos 11, RO-400028 Cluj-Napoca, Romania
*ioana.fort@ubbcluj.ro

Frequently, porous materials such as carbon [1,2], clays [3] or metal oxide (TiO_2) [4] were used in electrochemistry research for example in electrode construction, especially as modifiers. The essential properties of Meldola's Blue (M), a redox dye with electrocatalytic abilities [5], combined with that of carbon aerogel matrix (C), with great surface area, good catalytic support, mechanical stability, good conductivity and low cost [1,2], make of the new nanocomposite (MC) a competitive modifier for electrode developments. While there are many reports on the usage of C nanocomposite for the construction of C-based electrodes, the application of MC has significant importance for the development of competitive electrochemical electrodes.

Thus, the new developed glassy carbon electrodes (GCE) based on MC nanomaterial used for the electroanalytical detection of H_2O_2 lead to promising electroanalytic performances. MC-based modified GCEs were prepared by a drop-casting method. The electrochemical behaviour of the obtained modified electrodes and their ability to detect H_2O_2 has been investigated by electrochemical techniques.

The electroanalytical parameters of the investigated modified GCE recommend it as a stable, sensitive and reproducible electrode for H_2O_2 detection. The results obtained by testing pharmaceutical products proved the new electrode's performance.

References
[1] C. I. Fort, L. C. Cotet, A. Vulpoi, G. L. Turdean, V. Danciu, L. Baia, I. C. Popescu, Sensors and Actuators B: Chemical 220 (2015) 712-719. http://dx.doi.org/10.1016/j.snb.2015.05.124
[2] C. I. Fort, L. C. Cotet, V. Danciu, G. L. Turdean, I. C. Popescu, Materials Chemistry and Physics 138 (2013) 893-898. http://dx.doi.org/10.1016/j.matchemphys.2012.12.079
[3] C. I. Fort; A. Sanou, M. Coulibaly, K. B. Yao, G. L. Turdean, Green modified electrode for sensitive simultaneous heavy metal ions electrodetection, Sensors and Actuators B: Chemical, 418 (2024) 136326. https://doi.org/10.1016/J.SNB.2024.136326
[4] J. S. Hidalgo, É. Tóth, H. Jankovics, C. I. Fort, G. L. Turdean, E. Tombacz, I. Galambos, Bioengineered Flagellin–TiO2 Nanoparticle-Based Modified Glassy Carbon Electrodes as a Highly Selective Platform for the Determination of Diclofenac Sodium. Chemosensors, 11 (2023) 576. https://doi.org/10.3390/chemosensors11120576
[5] I. C. Ladiu, I. C. Popescu, Lo Gorton, NADH Electrocatalytic Oxidation at Carbon Paste modified Electrodes with Meldola Blue Adsorbed on Zirconium Phosphate, J. Solid State Electrochem., 9 (2005) 296-303. https://doi.org/10.1007/S10008-004-0618-6

SOME ASPECTS REGARDING THE TRACEABILITY OF FOOD PRODUCTS

Zeno Gârban[1,6], Florin Muselin[2,6], Cristina Szabo[3,6], Robert Ujhelyi[4,6], Sorin Marinescu[5]

[1]*Department of Biochemistry and Molecular Biology (former), Faculty of Food Products Technology, University of Life Sciences "King Michael I of Romania" Timişoara, Romania*
[2]*Department of Toxicology, Faculty of Veterinary Medicine, University of Life Sciences "King Michael I of Romania" Timişoara, Calea Aradului No. 119, Romania;*
[3] *National Institute of Public Health-Branch Timişoara, Bd. Dr. V. Babeş, No.16, Timişoara, Romania;*
[4]*Medical Department, S.C. CaliVita International, Timişoara, Romania;*
[5]*Institute of Chemistry of the Romanian Academy, Bd. M. Viteazu Nr.24, Timişoara, Romania*
[6]*Working Group for Xenobiochemistry, Romanian Academy-Branch Timişoara, Bd. M. Viteazu No. 24, Romania*
e-mail: zeno.garban@yahoo.com

Abstract
The traceability of food products is of major interest for ensuring the composition quality and protecting the consumers. The improvement of traceability control methods is based on preliminary stages of checking the purity of the component ingredients, technologies / biotechnologies for which analytical, bioanalytical and biophysical methods are used. A brief presentation of the specific methods for traceability control is presented in this paper.

Key words: foods, traceability, control methods

Introduction
The issue of traceability of food products has acquired a major importance with the globalization of agriculture and industries. In the food industries there are data on the origin of the raw material, its processing, distribution and location. Knowledge of traceability is of importance also in case of pharmaceutics and cosmetics which use substances obtained by extraction (phyto- and zoochemical) and/or obtained by chemical synthesis. The implementation of traceability systems to improve the ability to verify the safety and quality of products is aimed primarily at food products (e.g. raw materials and processed foods).

1. Traceability systems
Traceability can be approached in two distinct ways:

a) *Traceability in an integrated system.* This system involves tracking a particular product in the chain: raw material-transport-processing-storage-distribution-marketing-consumer
b) *Traceability in a differentiated system.* This system covers more limited areas of logistics management in the food chain. Within this system, internal traceability and external traceability are distinguished.
The specifics of the integrated systems will be briefly discussed below.

2. Systems of product identification
Different systems of identification can be used to know the food traceability data. Among these more important proved to be: a) *barcodes*; b) *landmarks based on radio frequency*; c) *biological*

and biochemical tests; d) *biodegradable markings;* e) *markings based on geospatial technology*. A brief description of them is of theoretical and applied interest (some in the perspective of expanding use).

2.1.Barcodes

This means of identification encodes the information on the basis of figures represented by a sequence of black and white bars of various sizes. Barcode decryption is done with a scanner.

In practice, the introduction of this system has been made in the USA and Canada since 1973 and has been called the "Uniform Product Code" - UPC. Subsequently in Europe, since 1979, the code has been used at the suggestion of the European Article Numbering Association (EAN). It has gradually spread to all continents. Representative figures for a particular code are integrated based on the "labeling program" entered into the scanner and can be used as a verification tool.

In practice, depending on the importance of the marketed product, 8 -14 digit codes are used for identification (indicating the country, manufacturer, product, other details).

Bar codes also allow the integration of a particular item in global trade. These codes can be used online. Mobile phone scanning is also possible.

2.2. Landmarks based on radio frequencies

In this case, the so-called "identification by radio frequency devices" - RFIDs (*Radio Frequency Identification Devices*) are used. For this purpose, food data are stored in "electronic circuits" or in "microchips" embedded in plastic material, constituting the so-called "*electronic label*".

Various devices that operate at various radio frequencies, in the ranges: 100 kHz - 2 GHz, are used for identification. These "tags" allow remote data reading. The data can also be entered in "menus" that are suitable for input on the touch screen.

2.3.Biological and biochemical tests

Biological and biochemical tests used for identification draw attention to the performance of histology, biochemistry, and molecular biology (Alford and Caskey, 1994; Cunningham and Meghen, 2001; Cutroneo et al., 2014; Gârban, 2018).

Among the specific methods of this system are mentioned: a) identification of the *retinal image*; b) identification of the *genetic imprint* - also known as "*DNA imprint*" (deoxyribonucleic acid) or simply "DNA test". The application of these methods, although accurate, is limited due to high costs. One can mention their specificity.

a) Identification of the retinal image. The method is specific to biology (histology), being based on recording with special digital cameras the "retinal vascular aspect". This is an attribute of individuality (especially in animals), which is maintained throughout life. This method can be applied to live animals transported for slaughter (elsewhere in the world).
The method is also suitable for use in "modern zooculture" for the surveillance of live animals as well as animals intended for use in breeding to breed improvements (sent to various locations around the world). One of the applications of the method - given the rigor of the information - concerns zoo parks and nature reservations for animals protected by law.

b) Identification of the DNA imprint. The method is specific to biochemistry and molecular biology. It is suitable for application to live animals, by taking samples from blood, hair, saliva,

etc., but also from animal products (animal carcasses). This method is based on specific analyses to molecular biology applied in genetics. In the case of meat and meat products, for example, analyzes based on "DNA imprints" can be compared with data on animals in slaughtered lots. Details on these applications (Cunningham and Meghen, 2001) reveal the importance of using biomarkers / markers in this field.

In general, there is a great ability to discriminate methods based on molecular biology (Gârban and Ilia, 2024). It is reiterated that the method has been very useful in forensic medicine, pathology and animal and plant identification studies (Alford and Caskey, 1994).

From the above data it is noted that tests based on biology (histology) and molecular biology are in fact specific biomarkers / markers that provide accurate information on the traceability of animals / products of animal origin.

2.4. Biodegradable markings

These markings are also known as "*edible markings*" because they are placed directly on the food. They are invisible and made of an edible substance, e.g. cellulose derivatives.

The compound used for labeling is mixed with a certain food ingredient (usually additives). They are "fixed" due to the physico-chemical effects of food constituents (electrostatic forces, non-destructive interactions with protein compounds, lipids, etc.). The size of such markings is about 200 $\square$m^2 readable area for a barcode.

2.5. Markings based on geospatial technology

These markings include: a) *Geographic Information System* - GIS; b) *Global Positioning System* - GPS . The latter is a satellite-based radio positioning system - which contains information and the GPS receiver indicates the location in the field (IUFoST, 2012; FAO, 2017).

For information, it is mentioned that for agricultural activities it is possible to collect, analyze and present data. It even becomes possible to "*mapping information*" to certain regions of the Earth. Marks that use geospatial technology may include the "Quick Response Code", commonly known as the QR Code.

QR codes arranged in squares (so two-dimensional) were initially used only in Japan (1995). The two-dimensional specificity originates from the barcode system. Such codes are printed on packaging, posters, billboards, online advertisements, various types of advertising, labels and even business cards. Usually, the QR code is a means of storing information in a visual tag, which can be read by a device (even a smartphone).

Such a code integrates black dot and white space templates, arranged in a square grid. QR codes have an extremely wide use, e.g.: postal addresses, telephone numbers, email addresses, websites or web pages, company inventory labels, etc.

In current practice there are online applications that allow the generation of QR codes. Consumers can access accurate information and valid traceability as well as food safety information only by accessing the QR code printed on the product label. A general observation regarding geospatial technologies draws attention to the difficulties related to the high economic costs of implementing the system.

All the above described systems can provide safe and qualitative products to consumers (Vermeer et al., 2013; Klein and Stolk, 2018).

Concluding remarks

Application of the traceability system is important not only for food products but also for biologically active substances which could be ingredients of food and/or medicine. It is recommended to know details on the: a) *natural sources*; b) *manufacturing procedures*; c) *control methods* (chemical and microbiological); d) *distribution chain.* In case of biologically active substances, the measures regarding nutrivigilance, respectively pharmacovigilance are also important.

References

Alford R.L., Caskey C.T. – DNA analysis in forensics, disease and animal/plant identification, *Curr. Opin. Biotechnol.*, 1994, 5(1), 29-33.

Cunningham E.P., Meghen C.M. – Biological identification systems: genetic markers, *Rev. sci. tech. Off. int. Epiz.*, 2001, 20(2), 491-499.

Cutroneo M. Paola, Isgrò Valentina, Russo Alessandra, Ientile Valentina, Sottosanti Laura, Pimpinella G., Conforti Anita, Moretti U., Caputi P.A., Trifirò G. - Safety Profile of Biological Medicines as Compared with Non-Biologicals: An Analysis of the Italian Spontaneous Reporting System Database, *Drug Safety*, 2014, 37, 961-970.

Gârban Z. - *Quo vadis food xenobiochemistry*, 3rd edition, Publishing House of the Romanian Academy, Bucharest, 2018.

Gârban Z., Ilia G. – *Biologically active substances usable in food, pharmaceutical and agrobiological fields*, CRC Press, Boca Raton, 2024.

Klein K., Stolk P. - Challenges and Opportunities for the Traceability of (Biological) Medicinal Products, *Drug Safety*, 2018, 41, 911-918.

Vermeer N.S., Straus S.M.J.M., Mantel-Teeuwisse A.K., Domergue F., Egberts T. C. G., Leufkens H. G. M., De Bruin M. L. - Traceability of biopharmaceuticals in spontaneous reporting systems: a cross-sectional study in the FDA Adverse Event Reporting System (FAERS) and EudraVigilance databases. *Drug Safety,* 2013, 36, 617–625.

*** - ISO 8402:1994 Quality management and quality assurance - Vocabulary - https://www.iso.org/standard/20115.html

*** - CX / CAC/GL 60-2006 - Principles for Traceability/Product Tracing as a Tool within a Food Import and Export Certification System - http://www.fao.org/fao-who- codexalimentarius

*** - ISO 22005 : 2007 Traceability in the feed and food chain - General principles and basic requirements for system design and implementation - https://www.iso.org/obp/ui/#iso:std:iso:22005:ed-1:v1:en

*** - Food Traceability, *IUFoST Scientific Information Bulletin* , March, 2012

*** - FAO - Food traceability guidance, Santiago, 2017 - http://www.fao.org/3/i7665en/I7665EN.pdf

IDENTIFICATION AND CHARACTERIZATION OF SIALYLATED GLYCOLIPIDS IN TLR2D KNOCKOUT GENE

Raluca ICĂ[1], Mirela SÂRBU[1], Kristina MLINAC-JERKOVIĆ[2], Svjetlana KALANJ-BOGNAR[2], Roxana Biricioiu[1,3], Alina ZAMFIR[1,4]

[1]*Department of Condensed Matter, National Institute for Research and Development in Electrochemistry and Condensed Matter, 300224 Timisoara, 1 Plautius Andronescu Street, Romania;*
[2]*Department for Chemistry and Biochemistry & Croatian Institute for Brain Research, School of Medicine, Zagreb University, 10000 Zagreb, Pierottijeva 6, Croatia;*
[3]*West University of Timisoara, Faculty of Physics, Vasile Parvan, 4, 300223, Timisoara; Romania*
[4]*Department of Technical and Natural Sciences, "Aurel Vlaicu" University of Arad, 310130, Arad, Romania;*
email: *raluca.ica@gmail.com*

Abstract

Gangliosides, complex glycosphingolipids essential for the central nervous system, play crucial roles in cellular processes such as cell adhesion, signal transduction, and cell-to-cell communication. Alterations in ganglioside composition are associated with various neurological disorders, underscoring the importance of studying these molecules for a better understanding of neural function and pathology. This study characterized the ganglioside profiles in mouse brain tissues from four distinct groups: wild-type females (WF), knockout females (KF) with the TLR2D gene inhibited, wild-type males (WM), and knockout males (KM).

Introduction

Gangliosides are vital for maintaining the structural integrity of neural cells and facilitating synaptic plasticity [1]. Changes in their composition have been implicated in neurological diseases such as Alzheimer's disease, Parkinson's disease, and multiple sclerosis [2]. Moreover, gangliosides are known to modulate immune responses in the nervous system, making them significant for studying neuroinflammatory conditions [3]. The TLR2D gene plays a crucial role in regulating immune responses by facilitating the recognition of pathogen-associated molecular patterns and modulating inflammatory signaling pathways, thereby influencing the overall immune activity within the nervous system [4].

Experimental

To characterize the ganglioside profiles, we analyzed brain tissues from four groups of mice: WF, KF with TLR2D gene inhibition, WM and KM also with TLR2D inhibition. Brain tissues were harvested and subjected to a lipid extraction process using organic solvents to isolate gangliosides from other lipid components. Ion Mobility Mass Spectrometry (IMS) with Electrospray Ionization (ESI) was employed using a Synapt G2S mass spectrometer in negative ion mode, which enhances the sensitivity for detecting various ganglioside species. Multiple runs were conducted to ensure the reproducibility of results.

Results and Discussion

Our analysis revealed 175 ganglioside species in the KF samples, a significant increase compared to 130 species in the WF samples. Similarly, 140 species were detected in the KM samples, while only 115 were identified in the WM samples. This increase in the knockout groups suggests that TLR2D gene inhibition may lead to metabolic shifts that promote the

synthesis or accumulation of specific gangliosides. We also observed complex structural modifications indicative of biological adaptations or compensatory mechanisms.

Data analysis focused on comparing the diversity and composition of gangliosides across the groups and included structural elucidation through Collision-Induced Dissociation (CID) MS/MS to identify specific modifications such as *O*-fucosylation and *O*-acetylation. Significant variations in glycosphingolipid composition were noted among the groups, with KM samples showing greater diversity of GD1 species compared to KF samples. Conversely, KF samples exhibited a higher abundance of GD2 species, indicating potential sex-specific differences in ganglioside metabolism. Detailed structural analysis using IMS CID MS/MS of the $[M\text{-}2H^+]^{2-}$ ion detected in KM at *m/z* 917.471, corresponding to GD1 (d18:1/18:0), confirmed the presence of the GD1b isomer, providing deeper insights into the specific ganglioside structures present in the knockout groups.

Conclusion

This study highlights significant differences in ganglioside profiles among WF, WM, KF, and KM mice, with a notable increase in diversity observed in the knockout groups. Inhibition of the TLR2D gene appears to induce metabolic or regulatory shifts in ganglioside composition, which could have important implications for understanding the role of these lipids in neural function and pathology. The application of IMS MS has proven to be a powerful tool for elucidating these complex lipid profiles, paving the way for future research into their biological significance and potential therapeutic targets for neurological disorders.

Acknowledgements

References

[1] Itokazu Y, Tsai YT, Yu RK. Glycoconj J. 34 (2017) 749-756.
[2] Furukawa K, Ohmi Y, Tajima O, et al. Prog Mol Biol Transl Sci. 156 (2018) 265-287
[3] Galleguillos D, Wang Q, Steinberg N, Zaidi A, et al.,J Neuroinflammation 19 (2022) 1-9.
[4] Seoudi N, Bergmeier LA, Hagi-Pavli E, et al. Innate Immun. 20 (2014) 412-422.

DETERMINATION OF PARACETAMOL FROM PARACETAMOL-IBUPROFEN MIXTURES USING ZERO, FIRST AND SECOND DERIVATIVE OF UV-VIS SPECTRA

Ioana M.C. Ienaşcu[1,2], Adina Căta[1], Antonina Lazăr[1], Nick S. Ţolea[1], Dan Roşu[1]

[1]National Institute of Research and Development for Electrochemistry and Condensed Matter, Dr. A. P. Podeanu 144, 300569, Timişoara, Romania
[2] "Vasile Goldiş" Western University of Arad, Faculty of Pharmacy, Liviu Rebreanu 86, 310045, Arad, Romania

Abstract
Ibuprofen, 2-(4-isobutylphenyl)-propionic acid, an AINS drug, available in a variety of preparations, is commonly used in the treatment of pain and inflammation in rheumatoid arthritis and other musculoskeletal disorders [1]. Paracetamol, acetaminophen, is a worldwide used drug with analgesic and antipyretic activity [2]. There are several pharmaceuticals that contain both substances, along with several excipients. Thus, simple, rapid and low-cost methods for quantitative determination of such compounds in mixtures are needed.
The aim of the present study was to determine the conditions for quantitative analysis of paracetamol in mixtures with ibuprofen using the UV-VIS spectrophotometric method. Optimizing the conditions and validating the developed analytical procedure will allow the determination of the active substance content in pharmaceutical preparations. Based on the zero, first and second derivative of UV-Vis spectra [3], the paracetamol content of different synthetic mixtures with ibuprofen and also of some commercial available drugs (Synocam, Paduden Duo) was determined. When using first and second derivative spectra for synthetic mixtures, small amounts of paracetamol (2.5-5 μg/mL) could be accurately quantified compared with zero derivative spectra. Also, good recoveries with small standard deviations (100.12±3.69 – for first derivative spectra; 100.81±3.93 – for second derivative spectra) were obtained which indicated the high repeatability and accuracy of the two proposed methods. In the case of the analysis of the selected pharmaceutical preparations, the determined active ingredient content varies from the value declared by the manufacturers, depending on the applied method.
The presented techniques are fast and economical method for the quantitative determination of selected drugs and can be successfully applied in laboratories.

References
[1] S.S. Adams, P. Bresloff, C.G. Mason, J. Pharm. Pharmacol. 28 (1976) 256.
[2] M.J. Hamm, Crit. Care Nurse 20 (2000) 69.
[3] Y.M. Issa, S.I.M. Zayed, I.H.I. Habib, Arab. J. Chem. (2011) 4, 259–263.

PHENOLIC CONTENT AND ANTIOXIDANT ACTIVITY EVALUATION OF SOME SALIX,VIBURNUM AND ALNUS PLANT EXTRACTS

Antonina Lazăr[1], Neli K. Olah[2,3], Adina Căta[1], Nick S. Țolea[1], <u>Dan Roşu[1]</u>, Ioana M.C. Ienaşcu[1,2]

[1]National Institute of Research and Development for Electrochemistry and Condensed Matter, Dr. A. P. Podeanu 144, 300569, Timişoara, Romania
[2]"Vasile Goldiş" Western University of Arad, Faculty of Pharmacy, Liviu Rebreanu 86, 310045, Arad, Romania
[3]SC PlantExtract SRL, Radaia 46, 407059, Cluj county, Romania
e-mail: antonina_pop@yahoo.com

Abstract
This study examines the phenolic content and antioxidant activity of some hydroethanolic extracts and/or glycerine macerates of *Salix alba* (cortex, buds, catkins*), Salix purpurea* (cortex), *Viburnum prunifolium* (fruits) and *lantana* (buds)*,* and *Alnus glutinosa* (buds) obtained according to *European Pharmacopoeia* 11th. These plants are not only used in traditional medicines but also in some pharmaceutical products, due to their proved bioactivity. Medicinal plants emerged as alternatives to synthetic products.
Willow bark extract has been used for thousands of years as an anti-inflammatory, antipyretic, and analgesic product [1]. Viburnum plants are considered abundant resource of bioactive natural products with diverse pharmacological properties, i.e. antioxidant, antibacterial, anti-inflammatory, cytotoxic, and anticancer [2]. Alnus species have been used for the treatment of rheumatism, hemorrhoids and for wound healing in folk medicine [3].
The antioxidant activity of phenolic compounds is the chemical feature that has received great attention in the recent years. The phenolics content was determine using Folin Ciocalteu method [4] and the antioxidant effect was investigated using the DPPH [5], ABTS [6] and FRAP [7] assays. The total phenolic content ranged between 3412.12 - 9210.42 mg GAE/L for Salix alba, and 2703.87 - 3175.90 mg GAE/L for Viburnum species. Alnus glutinosa phenolic content was 4800 mg GAE/L and the highest content was obtained in case of Salix purpurea 15417.09 mg GAE/L. Except for Salix purpurea, good correlations (R^2 = 0.937 – 0.975) were obtained between antioxidant activities determined by the three methods and total phenolics content.

References
[1] M. Shara, S.J. Stohs, Phytother. Res. 29 (2015) 1112–1116.
[2] J. Sharifi-Rad, C. Quispe, C. V. Vergara, D. Kitic, M. Kostic, L. Armstrong, Z.K. Shinwari, A.T. Khalil, M. Brdar-Jokanović, B. Ljevnaić-Mašić, E.M. Varoni, M. Iriti, G. Leyva-Gómez, J. Herrera-Bravo, L.A. Salazar, W.C. Cho, Hindawi, Oxid. Med. Cell. Longev., Volume 2021, Article ID 3095514.
[3] Ç. Altınyay, I. Süntar, L. Altun, H. Keleş, E. K. Akkol, J. Ethnopharmacol. 192 (2016) 148–160.
[4] A.L. Waterhouse. Unit I1.1. Polyphenolics. Determination of Total Phenolics.In *Current Protocols in Food Analytical Chemistry*; John Wiley & Sons, Inc.: New York, USA, 2002; p. I1.1.1-I1.1.8.
[5] W. Brand-Williams, M.E. Cuvelier, C. Berset, LWT - Food Sci. Technol. 28 (1995) 25-30.
[6] M. Ozgen, R.N. Reese, A.Z. Tulio Jr, J.C. Scheerens, R. Miller, J. Agric. Food Chem. 54 (2006) 1151-1157.
[7] I.F.F. Benzie, J.J. Strain, Anal. Biochem. 239 (1996) 70-76.

SOLID STATE SYNTHESIS OF UNDOPPED $Zn_3Nb_2O_8$ AND DOOPED WITH Er^{3+}

<u>Liviu Mocanu</u>, Mina-Ionela Morariu, Mircea Nicolaescu, Mihaela Birdeanu

National Institute for Research and Development in Electrochemistry and Condensed Matter, Timisoara, PlautiusAndronescu Str. No. 1, RO-300224, Timisoara, Romania
e-mail: mocanuliv@gmail.com

Abstract

The present work focused on the synthesis in solid state of the undoped and doped pseudo-binary oxides $Zn_3Nb_2O_8$ with different concentrations of Er^{3+}, used in the study of luminescence properties.

Introduction

The optical properties of materials are applicable in a wide range of fields, both consumer (solar cells) and highly specialized (photoreceptors, radiant surfaces). Among the recent studies on semi-constrictor ternary oxides of the spinelic type, those according to which they are a viable alternative in applications such as electronic devices, light-emitting diodes, electromagnetic screens, rechargeable batteries, chemical sensors, biosensors stand out. A special interest is aroused by pseudo-binary oxides, such as $Zn_3Nb_2O_8$ compounds with wide bandwidth, having phosphorescent properties, effective for flat screens or emission in electric field, used at low acceleration voltages, ensuring high stability to electron flow irradiation. The design of the method of obtaining nanomaterials must take into account the structural factors (crystalline or amorphous), dimensional dispersion, shape and chemical properties. All of them are affected by the kinetics of the chemical synthesis process. The reaction rate depends on the concentration of the reactants, the temperature and the pH of the solution.

Results and Discussions

Figure 1 shows the RX diffraction spectra of undoped and Er^{3+}-doped $Zn_3Nb_2O_8$ nanocrystals (in molar ratio Zn:Nb:Er 1:3:0.01; 0.1; 0.2). The synthesis in solid state was performed in the SNOL calcination furnace at a temperature of 1100 0C, for 4 h, at a rate of 50 C/min, both for heating and cooling. After the introduction of Er^{3+}, a displacement of the angle 2θ is observed due to the difference in ionic radius between the element substituted in the lattice and the ion Er^{3+}, which led to the modification of the lattice parameters. The degree of displacement being strongly dependent on the degree of doping.
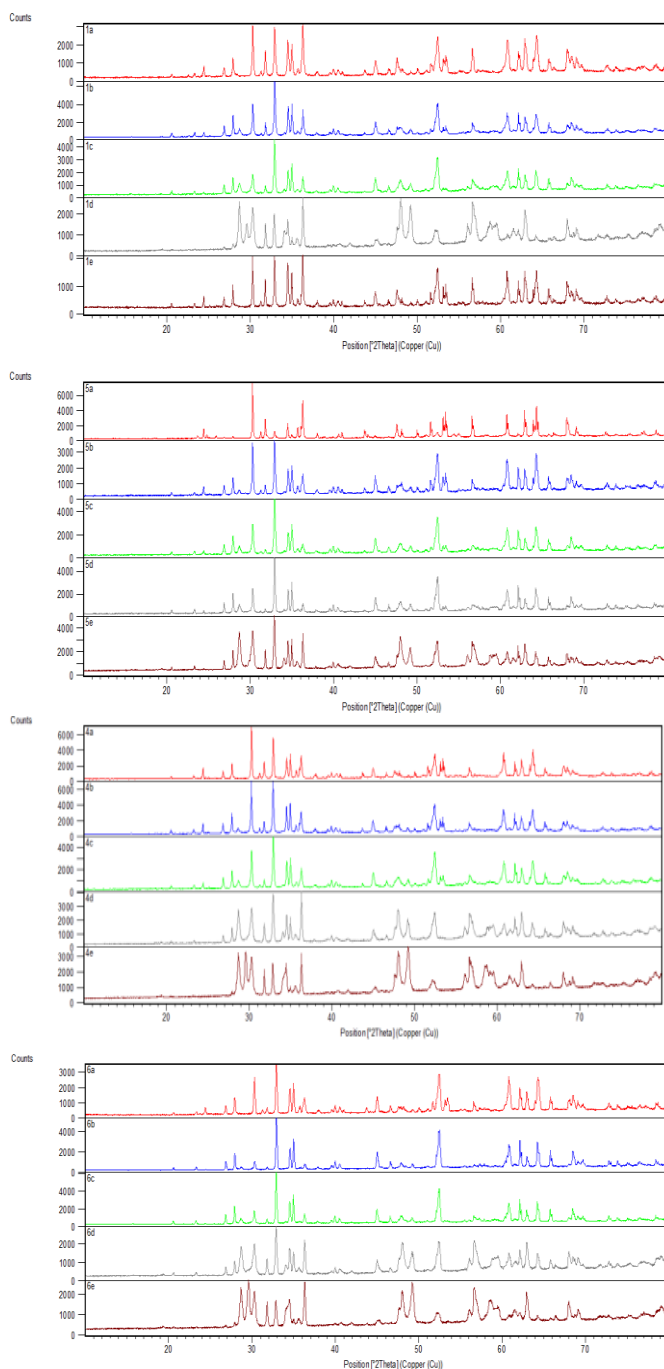
Figure 1.XRD spectra of non-doped and Er^{3+}-doped $Zn_3Nb_2O_8$ pseudo-binary oxide materials (molar ratio Zn:Nb:Er 1:3:0.01; 0.1; 0.2) obtained by synthesis from solid state.

The symmetry of the group implies a complex polyhedral structure, with [ZnO4] tetrahedral and [ErO6] octahedral. Each octahedral layer [ErO6] is located between two layers of tetrahedra with irreducible positions of the ions of Zn, [Zn(1)O4] and [Zn(2)O4] respectively.

Figure 2. Primitive cell $Zn_3Nb_2O_8$ with Zn1 substitued by Er^{3+}

Primitive cell $Zn_3Nb_2O_8$ Zn2 substitued by Er^{3+}
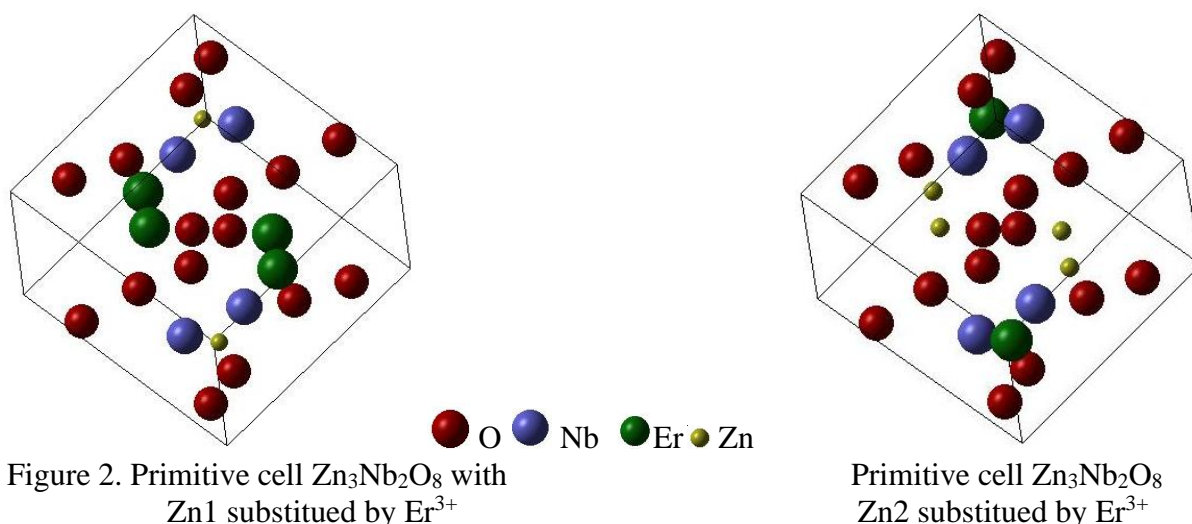
Using the electron density functional (DFT) method of the Crystal 14 Package, it was possible to evaluate both the substitutional positions and the interstitial one that the dopant can occupy, so that the crystal structure could preserve its symmetry, a relevant fact also in RXD spectra.In the DFT calculation, only the valence electrons were taken into account; The inner ones played the role of a screen for the nuclear charge, thus generating an effective pseudopotential. The ionic configuration of the elementary cell was evaluated starting from the asymmetric unit, consisting of 7 ions, of which 4 ions of Oxygen, 2 ions of Zn occupying two symmetrically irreducible positions and the ion of Er.In following the symmetry operations applied to the asymmetric unit, specific to the spatial group C2/c, the primitive cell contains 4 ions of Er, 2 ions of Zn(1), 4 ions of Zn(2) and 16 ions of O, a total of 26 ions.

Conclusion

The paper presented the conditions for obtaining and characterizing the $Zn_3Nb_2O_8$ crystal structure doped with Er^{3+} by solid state synthesis.

Acknowledgements

References

[1]M. Birdeanu,I.Fratilescu,C.Epuran,.Mocanu,C.Ianasi,A.Lascu,E.Fagadar-Cosma, International Journal of Molecular Sciences, 2023,24,8920.
[2] M. Birdeanu, A. Bîrdeanu, M. Vaida, D. Milovanovic, A. Lascu, E. Fagadar-Cosma, Phys. Scr. 94, 075702, (2019)

SOME NUTRITIONAL PROPERTIES OF COW CHEESE
WITH GOJI FRUITS ADDED

Ariana-Bianca Velciov[1], Antoanela Cozma[2], Georgeta-Sofia Popescu[1], Daniela Stoin[1], Andreea Petcov[3], Corina Megyesi[1], Laura Rădulescu[1], Iasmina-Mădălina Anghel[4], Marioara Drugă[1], Maria Rada[5*]

[1]*University of Life Sciences "King Michael I" Timisoara, Faculty of Food Engineering, Food Science Department, Calea Aradului, 300645, Timisoara, Romania*
[2]*University of Life Sciences "King Michael I" Timisoara, Faculty of Agriculture, Department of Soil Sciences, Calea Aradului, 300645, Timisoara, Romania*
[3]*University of Life Sciences "King Michael I" Timisoara, Faculty of Engineering and Applied Technologies, Department of Soil Sciences, Calea Aradului, 300645, Timisoara, Romania*
[4]*Politehnica University of Timişoara, Materials and Manufacturing Engineering Department, 300222, Timişoara, Romania*
[5]*University of Medicine and Pharmacy "Victor Babes", 2 EftimieMurgu Sq., 300041, Timisoara, Romania*
e-mail: radamariam@gmail.com

Abstract

A number of previous studies have shown that cheese-fruit combinations with synergistic effects could be considered functional foods with potential to promote health. This study aims to obtain and determine some nutritional parameters of cow's milk cheese with goji berries addition, to identify if the combination of cheese – goji fruits can improve the nutritional properties of the cheese. The obtained results showed that the analyzed parameters have the following value limits: 22.58 - 23.65% moisture, 75.32 - 78.65% dry matter, 3.04 - 3.76% minerals (ash), 17.21 - 18.88% fat and 11.91 - 13.25% protein. Compared to plain cheese, the cow cheese with goji added is richer in dry matter (10.95%), minerals (12.60%) and proteins (5.65) and lower amounts of fat (17.13%). In addition, according to some studies, the cheese combined with goji fruits significantly improve the antioxidant, α-glucosidase inhibitory, antimicrobial and immunomodulatory properties of plain cheese. Therefore, cow's cheese with goji added could be an attractive functional food option.

Introduction

Dairy products and fruits are essential components of the diet. Dairy products (milk and milk products) are an excellent good source of calcium and a good source of bioactive compounds that have many health benefits. Fruits provide vitamins and minerals and are also a rich source of phytochemicals that act as antioxidants, which can help prevent chronic diseases. Combining fruit and dairy has the potential to promote synergistic health benefits. [1,2]
Goji berries have been used for thousands of years as a medicinal plant in Asian countries due to their rich nutritional value, medicinal properties and biological properties. Several studies have highlighted the pro-health effects of goji berries, particularly in terms of their antioxidant, antitumor, antimicrobial, hypoglycemic, hypolipidemic, antimutagenic, immunomodulatory, prebiotic, anti-aging, anti-fatigue, anti-fatigue and neuroprotective effects. [3,4]
The aim of this work was to obtain a cheese assortment with the addition of goji fruits and to determine its nutritional parameters. In the context of this paper, the term "cheese" has been used for the designation of cheese made from cow's milk with or without added goji berries.

Experimental

2.1. Materials

The following ingredients were used to make the cheese with added goji berries: whole cow's milk, rennet, salt and dehydrated goji berries. Except for the goji fruit, which is imported, the milk, rennet and salt are local (domestic) products. The following recipe was used to make 1 kg of cheese with added goji fruit: 9.5 l whole cow's milk, 2 ml rennet, 20 g salt and 30 g dehydrated goji fruit. At the same time, a control sample of curd cheese without added goji fruit was obtained.

Cow's curd cheese is made from 1 kg of curd (left to ferment for 3 days at a temperature of 25 ⁰C), 30 g of dehydrated fruit, namely goji berries. The first step in making the curd cheese is curd scalding. Heat the water to a temperature of 85 ⁰C, then scald the curd together with the dehydrated fruit, all mixed in the same pot. The scalded paste is stirred with a spatula until it becomes uniform, with a soft consistency, which is kneaded and well bound so that it can be put into molds. Once in the molds, prick to release the whey and avoid any holes. The molds are turned 3-4 times every hour, kept in the molds for 12 hours, then placed in 20% brine for several hours. Remove from the molds, drain and put in the rinsing. Leave to mature for 20 days.

Samples of cow cheeses, i.e. plain cheese (PCC) and cheese with goji fruits (GCC) were used for analysis. Moisture content, dry matter content, total mineral content, fat content and protein concentration were determined.

2.2. Methods

The determination of the nutritional composition of the plain cow cheese and cow cheese with goji fruits was performed according standard to official methods used by Velciov et al., 2022.[5] For moisture content, the cheeses were dried in an oven at 105 ^{0}C to constant mass. The mineral substances (ash) were determined by the calcination method at 550 °C. The protein content was determined by the Kjeldahl method, using a conversion factor for nitrogen of 6.25. The crude fat was determined using the Soxhlet method with hexane as solvent. All the analyses were done in triplicate.

Results and discussion

The results obtained when analyzing the cheese samples studied for this experiment are presented in Table 1 and illustrated in Figure 1.

Table 1. Some nutritional properties of cottage cheese with goji added compared to plain cottage cheese

Cheese type	Specification	Moisture, %	Dry matter, %	Minerals (ash), %	Fat, %	Protein, %
Cow cheese with goji added (GCC)	Limits	22.08-23.75	75.32-78.65	3.04-3.76	17.11-18.56	11.91-13.25
	Mean values	23.05±0.68	76.95±2.86	3.38±0.36	18.00±0.65	12.52±0.69
Plain cow cheese (PCC)	Limits	27.08 - 28.56	70.86-73.11	2.67-3.38	20.89-22.76	11.11-12.65
	Mean values	27.94 ± 0.60	72.06±0.93	3.00±0.29	21.72±0.78	11.85±0.63

It can be observed that the nutritional parameters of GCC and PCC, show values within the following concentration limits: 22.58 - 23.75% moisture, 75.32 - 78.65% dry matter, 3.04 - 3.76% minerals, 17.11 - 18.56% fat, 11.91 - 13.25% protein, respectively 27.08 - 28.56% moisture, 70.86 - 73.11% dry matter, 2.67 - 3.38% minerals, 20.89 - 22.76% fat, 11.11 - 12.65%. Comparing the average nutritional values of GCC: $23.05 \pm 0.68\%$ moisture, $76.05 \pm 0.93\%$ dry matter, $3.38 \pm 0.36\%$ minerals, $18.00 \pm 0.65\%$ fat, $12.52 \pm 0.69\%$ protein with those of PCC: $27.94 \pm 0.60\%$ moisture, $72.06 \pm 0.93\%$ dry matter, $3.00 \pm 0.29\%$ minerals, $21.72 \pm 0.78\%$ fat, $11.85 \pm 0.63\%$ protein, we observe obvious differences (table 1 and figure 1),
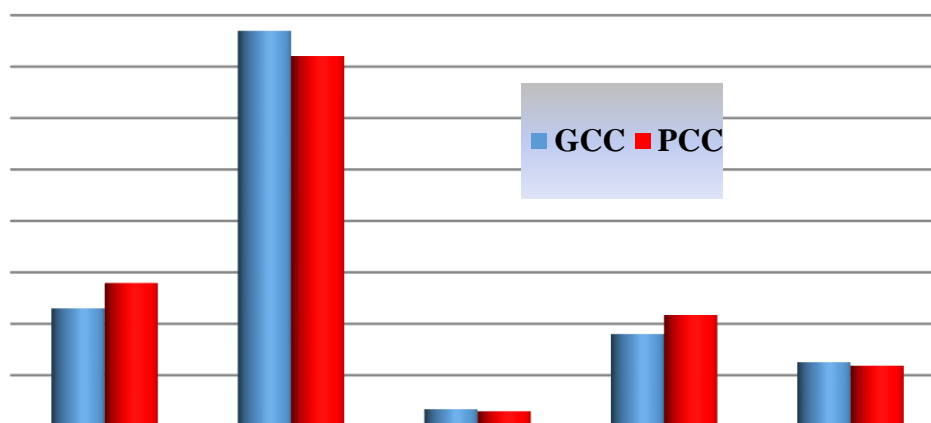
Figure 1. The nutritional parameters of cow cheese goji added (GCC) versus plain cow cheese (PCC)

Compared to PCC, GCC cheese is richer in dry matter (with 10.95%), minerals (with 12.60%) and proteins (with 5.65) and lower amounts of fat (with 17.13%) These differences are due to the addition of dried goji fruits , which contains higher amounts of minerals, dry matter and proteins and reduced amounts of proteins. Therefore, the addition of goji fruits contributes to increasing the mineral and protein intake, but also to reducing the water content of cow cheese added. Also, the lower fat content recommends the introduction of this in the diet of elderly adults. In addition, due to the increased content of biologically active substances goji fruit have the potential to improve the antioxidant, antidiabetic and antimicrobial properties of cow's cheese.

Conclusion
Experimental results show that compared to cow plain cheese, the cow cheese whit goji is richer in dry matter (with 10.95%), minerals (with 12.60%) and proteins (with 5.65%) and lower in fat (with 17.13%). Combining goji fruit and cow cheese has the potential to promote synergistic health benefits. Therefore, cow's cheese with goji added could be an attractive functional food option.

References
[1] Genet, B.M.L., Sedó Molina, G.E., Wätjen, A.P., Barone, G.; Albersten, K., Ahrné, L.M., Hansen, E.B., Bang-Berthelsen, C.H., **2023**, Hybrid Cheeses, Supplementation of Cheese with Plant-Based Ingredients for a Tasty, Nutritious and Sustainable Food Transition, *Fermentation 9*, 667, https://doi.org/10.3390/fermentation9070667;

[2] Plante, A. M., McCarthy, A. L., Lacey, S., & O'Halloran, F. (2021). Investigating The Bioactive Properties of Cheese-Fruit Combinations Following In Vitro Digestion Using an Elderly Model. Current Research in Nutrition and Food Science Journal, 9(2), 465-478;

[3]Ili´c, T., Dodevska, M., Marˇceti´c, M., Boži´c, D., Kodranov, I., Vidovi´c, B., **2020,** Chemical characterization, antioxidant and antimicrobial properties of goji berries cultivated in Serbia, *Foods 9*, 1614;

[4] Jiang, Y., Fang, Z., Leonard, W., Zhang, P., **2021**, Phenolic compounds in Lycium berry: Composition, health benefits and industrial applications, J. *Funct. Foods 77*, 104340;

[5] A.B. Velciov, A. Riviş, D. Lalescu, G-S Popescu, A. Cozma, A-A. Kiss, A-M. Gherman, I-M. Anghel, R-E. Simescu, M. Rada., Determination of some nutritional parameters of dark chocolate, Journal of Agroalimentary Processes and Technologies 2021, 27(3), 271-276.

NOVEL THIOPHENE-CONTAINING COMPOUNDS OBTAINED BY USING 5-BROMO-2-THIOPHENECARBOXYLIC ACID AS SCAFFOLD

Bogdan Mara, Liliana Cseh

"Coriolan Dragulescu" Institute of Chemistry, Timişoara, România
e-mail: bogdanmara54@gmail.com

Abstract

Cancer renders as one of the greatest therapeutical challenges not only due to the high uncertainty of the underlying causing mechanisms but as well as the fact that cancer is not considered a well-defined and isolated single disease but rather a group of diseases [1]. Thiophene and its derivatives have emerged as promising candidates for the development of new anticancer drugs [2]. Therefore, the present work reports the synthesis and characterization of novel series of compounds based on thiophene scaffold (Scheme 1 and Scheme 2).
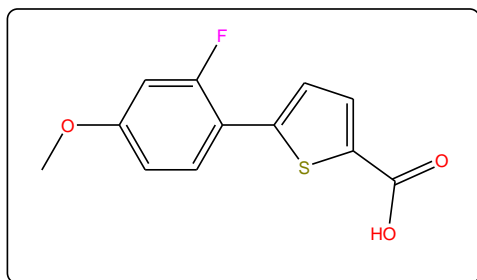
Scheme 1. Chemical structure of 5-(2-fluoro-4-methoxyphenyl) thiophene-2-carboxylic acid
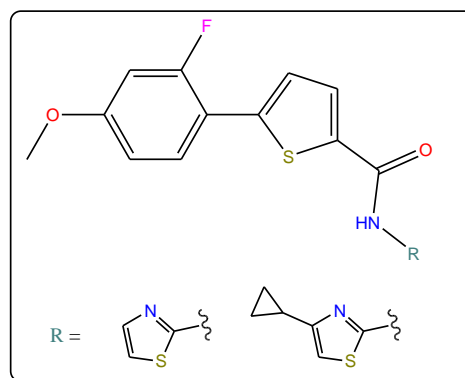
Scheme 2. Chemical structure of 5-(2-fluoro-4-methoxyphenyl)thiophene-2-carboxamide compounds

Acknowledgements

References

[1] Zhao M., Cui Y., Zhao L., Zhu T., Lee R.J., Liao W., Sun F., Li Y., Teng L., ACS Omega 2019, 4, 5, 8874-8880.
[2] Archna, Pathania S., Chawla P.A., Bioorg. Chem., 2020, 101, 104026.

SENSORIAL AND PHYSICOCHEMICAL CHARACTERIZATION OF PASTA FROM DURUM WHEAT FLOUR ENRICHED WITH CHESTNUT FLOUR

Corina-Iuliana Megyesi[1*], Ariana-Bianca Velciov[1], Laura Rădulescu[1], Bujancă Gabriel[2], Alexandru Rinovetz[1]

[1] *University of Life Sciences "King Michael I" Timisoara, Faculty of Food Engineering, Food Science Department, Calea Aradului, 300645, Timisoara, Romania*
[2] *University of Life Sciences "King Michael I" Timisoara, Faculty of Food Engineering, Food Control and Expertise Department, Calea Aradului, 300645, Timisoara, Romania*
e-mail: corina.megyesi@usvt.ro

Abstract
The present study aimed to perform the sensory and physicochemical characterization of some pasta samples, obtained from durum wheat flour enriched with chestnut flour and to highlight the beneficial effects of this pasta on the human body. The recipe for obtaining this type of pastas was presented, creating a new product, as natural and healthy as possible.
Chestnut flour does not contain gluten, but unlike other gluten-free flours, which are sometimes low in nutrients, chestnut flour has a high nutritional value. It is rich in dietary fiber, essential amino acids (due to its protein content), fatty acids (omega 3 and 6), vitamins (C and B group) and also provides important minerals needed by the body (calcium, magnesium, potassium).
The sensory analysis of the pasta samples enriched with chestnut flour was carried out with the help of 10 tasters, who analyzed the appearance, consistency and preservation of the shape, taste and smell of the samples. Two types of samples were tested: samples purchased from the local markets and samples obtained at home, after an own recipe. The sensory analysis highlighted that artisanal (home-made) pasta outperformed commercial pasta, with a total average score of 4.88 points, compared to 4.34 points. The physicochemical analysis of the pasta samples followed the determination of humidity, the increase in volume, as well as the determination of the sediment resulting after the cooking. Artisanal pasta showed higher values than commercial pasta, both for humidity (11,2%) and for the volume of sediment (15,7%). Regarding the increase in volume (after boiling) of the analyzed pasta samples, the highest value (225%) was recorded for commercial pasta, and for those obtained at home it was determined an increase of 202%.

Introduction
Pasta is one of the most common and popular staple foods due to its sensory and nutritional value but also due to its versatility. It is reported that approximately 14.3 million tons of pasta are produced annually worldwide. The main producer is Italy, followed by the United States, Brazil, Turkey and Russia. Italians are the main consumers of pasta, with 23.1 kg per capita per year, followed by Tunisians (17 kg), Venezuelans (12 kg) and Greeks (11.4 kg). [1,4]
According to Italian law, "dry pasta" must be produced with water and durum wheat (*Triticum durum*) (ie semolina, coarse semolina or whole semolina). It is well known that only durum semolina can ensure the best pasta quality in terms of dough rheological properties, cooking quality and consumer acceptance. [1,2]
One of the main reasons for pasta's success is its nutritional profile. Pasta is generally very nutritious due to its low-fat content and easily digestible carbohydrates. In addition, pasta can provide healthy components such as fiber or prebiotics. The low cost and long shelf life of pasta make it popular among many diverse consumer groups. [3,4,8]

Most of the studies carried out on flour pasta focus on its preparation, including the addition of different flours from grains other than durum wheat (or their fractions) or other ingredients (including vegetables) to improve the nutritional profile of the pasta. [5,6,7,9]

Experimental
2.1. Materials
Home-made durum wheat pasta enriched with chestnut flour was obtained using the following ingredients: durum flour, chestnut flour, eggs and water. These materials, except water (which was tap water), were purchased from supermarkets or local markets. Also, a commercial durum wheat pasta enriched with chestnut flour was purchased from a local market.
The pasta sample was produced by mixing all the ingredients by hand, the dough being passed through a pasta machine, several times, until the desired thickness was obtained. After shaping, the pasta was boiled (for 10 minutes) in salted water, then poured into a sieve and drained.

2.2. Methods
The two types of pasta (commercial and home-made) were analyzed from a sensory and physicochemical point of view.
The sensory analysis of the samples was carried out by the scoring scale method, using a panel of 10 tasters. The sensory characteristics evaluated were: appearance, consistency and shape retention, taste and smell. 5 points were awarded for maximum attributes.
The physicochemical analysis of the pasta samples consisted of: determining the water content, the increase in volume and the sediment. To determine the moisture content of durum wheat pasta samples with the addition of chestnut flour, the thermobalance method was used, according to SR 90/2007. Determining the increase in volume of the pasta samples (according to STAS 756/3-1985) is done by placing the pasta in a graduated cylinder before and after boiling, to measure their volume. The determination of the sediment is carried out according to STAS 756/3-1985. Thus, the pasta is subjected to boiling, observing its behavior: the consistency, the appearance of the water after boiling, the volume of sediment in the boiling water. When the pasta is "al dente" it is strained, and the water in which the pasta was boiled is transferred to the Imhoff cones. The volume of the sediment is read the next day and is related to the total volume of water in which the pasta was boiled. The physicochemical analyses were done in triplicate.

Results and discussion
The interpretation of the results obtained for commercial durum wheat pasta enriched with chestnut flour, highlights the fact that the most appreciated characteristics of this pasta were the taste and smell with an average score of 4.7 points, followed in order by shape keeping (4.3 points), color (4.2 points) and appearance (3.8 points).
The characteristics most appreciated in the case of home-made durum wheat pasta enriched with chestnut flour were smell and taste (all tasters giving a maximum score of 5 points for these two characteristics). It was followed by color (with an average score of 4.9 points), appearance (4.8 points) and shape keeping (4.7 points).
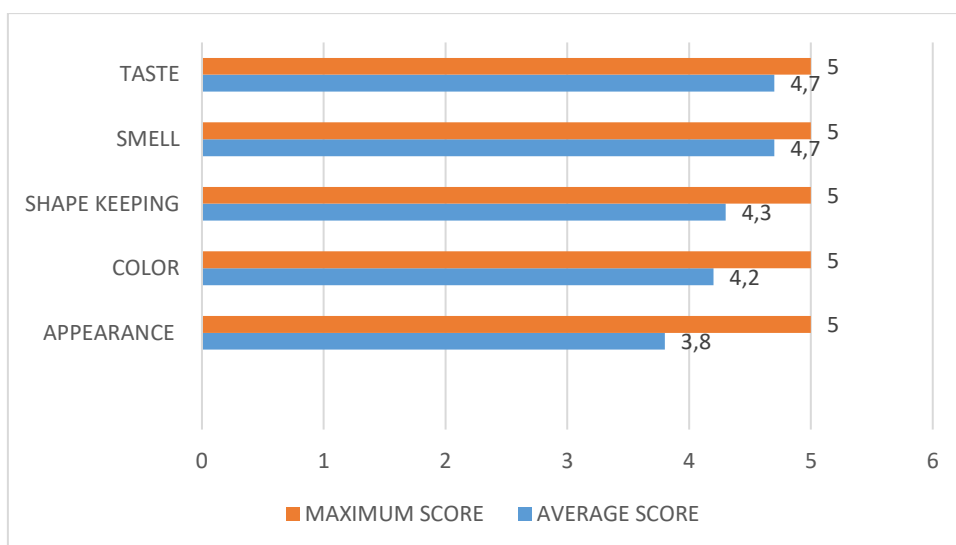
Figure 1. Sensory characterization of commercial durum wheat flour pasta enriched with chestnut flour
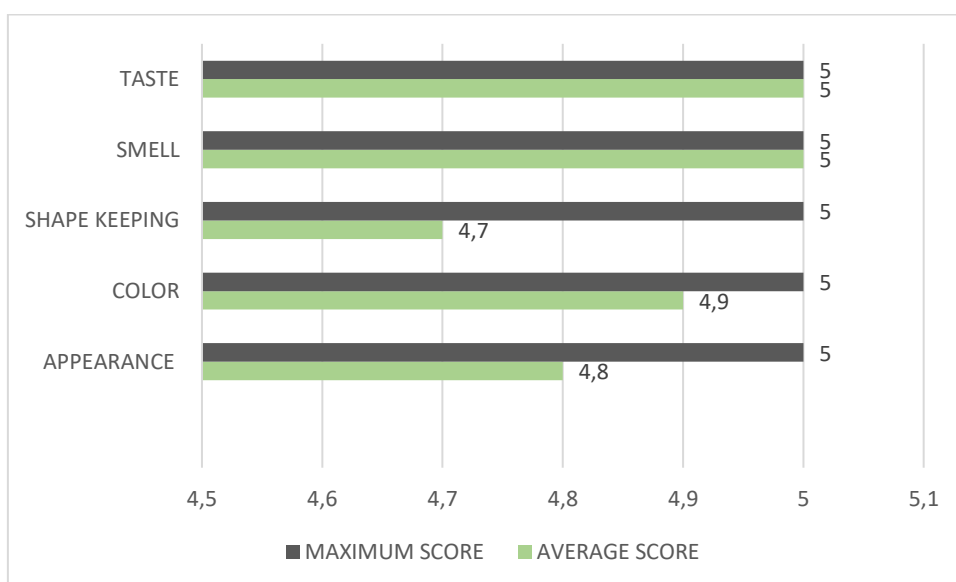
Figure 2. Sensory characterization of home-made durum wheat flour pasta enriched with chestnut flour

The results of the physicochemical analysis for the 2 varieties of pasta are presented in the table below.

Table 1. The results of the physicochemical analyzes for the 2 varieties of pasta

Physicochemical analysis	Commercial durum wheat flour pasta enriched with chestnut flour	Home-made durum wheat flour pasta enriched with chestnut flour
Water content (%)	8,3	11,2
Increase in volume (%)	225	202
Volume of sediment (%)	12,5	15,7

Conclusion

Pasta products tend to be energy dense foods but low in micronutrients or bioactive compounds such as dietary vitamins and minerals. For this reason, pasta is fortified with various substances, such as chestnut flour.

The two types of durum wheat flour pasta enriched with chestnut flour were characterized from a sensory point of view, the most appreciated being home-made pasta with a total average score of 4.88 points, compared to commercial pasta, with a total average score of 4.34 points.

The moisture content of the flour pasta samples analyzed was below the maximum limits allowed for this parameter of 13%, the highest value (11.2%) being recorded for home-made pasta. This type of pasta also recorded the highest value for the volume of sediment resulting from boiling, namely 15.7%. Increase in volume of the analyzed pasta samples, shown a higher value (225%) for commercially purchased pasta, while the home-made pasta showed a value of 202%.

References

[1] Padalino, L.; Mastromatteo, M.; Lecce, L.; Spinelli, S.; Contò, F.; Del Nobile, M.A., **2014**, Effect of durum wheat cultivars on physicochemical and sensory properties of spaghetti, *J. Sci. Food Agric., 94*, 2196–2204;

[2] Giannetti, V.; Mariani, M.B.; Marini, F.; Biancolillo, A., **2021**, Effects of thermal treatments on durum wheat pasta flavour during production process: A modelling approach to provide added-value to pasta dried at low temperatures, *Talanta*, *225*, 121955;

[3] Oliviero, T.; Fogliano, V., **2016**, Food design strategies to increase vegetable intake: The case of vegetable enriched pasta, *Trends Food Sci. Technol., 51*, 58–64;

[4] Wahanik, A.L.; Chang, Y.K.; Clerici, M.T.P.S, **2018**, How to make pastas healthier?, *Food Rev. Int., 34*, 52–69;

[5] Mercier, S.; Moresoli, C.; Mondor, M.; Villeneuve, S.; Marcos, B., **2016**, A meta-analysis of enriched pasta: What are the effects of enrichment and process specifications on the quality attributes of pasta?, *Compr. Rev. Food Sci. Food Saf., 15*, 685–704;

[6] Li, M.; Zhu, K.X.; Guo, X.N.; Brijs, K.; Zhou, H.M., **2014**, Natural additives in wheat-based pasta and noodle products: Opportunities for enhanced nutritional and functional properties, *Compr. Rev. Food Sci. Food Saf., 13*, 347–357;

[7] Fuad, T.; Prabhasankar, P., **2010**, Role of ingredients in pasta product quality: A review on recent developments, *Crit. Rev. Food Sci., 50*, 787–798,

[8] Marti, A.; Cattaneo, S.; Benedetti, S.; Buratti, S.; Abbasi Parizad, P.; Masotti, F.; Iametti, S.; Pagani, M.A., **2017**, Characterization of whole grain pasta: Integrating physical, chemical, molecular, and instrumental sensory approaches, *J. Food Sci., 82*, 2583–2590;

[9] Sissons, M., **2008**, Role of durum wheat composition on the quality of pasta and bread, *Food, 2*, 75–90.

SOIL RESOURCES AND LIMITING FACTORS IN SĂVÂRŞIN, ARAD COUNTY

Mihuţ Casiana[1], Okros Adalbert[1], Cozma Antonela[1], Duma Copcea Anişoara[1], Mircov Vlad Dragoslav[2], Durău Carmen[1], Eremi Ovidiu[1]

[1]*Department of Soil Sciences, University of Life Sciences "King Mihai I" from Timişoara, Calea Aradului nr.119, 300645 Timişoara, country Timiş, România*
[2]*Department of Agricultural Technologies University of Life Sciences "King Mihai I" from Timişoara, Calea Aradului nr.119, 300645 Timişoara, country Timiş, România*
e-mail:adalbertokros@usvt.ro

Abstract
The purpose of this study is to present the soil resources in Săvârşin, Arad County, to identify limiting factors and to establish improvement measures. The objectives envisage the following stages: the study of the natural framework of soil formation and evolution; establishing limiting factors; establishing the necessary measures.
The paper addresses a common problem in soils on the territory of Romania in general and those located near the main rivers in our country, namely the presence of factors that limit their fertility. The study was carried out in the village of Săvârşin in Arad County, which is located on the left bank of the Mureş River. The research carried out allows us to formulate the following assessments related to the soils of this area: there are a number of limiting factors that seriously affect natural fertility, namely: soil reaction, high clay content, low humus reserve, gleaning, stagnogleization, salinization and alkalinization. The main types of soils found in this area are: Lithosols, Regosols, Gleic Alluvials, Luvosols, Eutricambosols and Preluvosols [10].

Introducere
Ianoş, Gh., et al. (1997), specifies that in the formation of the soil cover, in addition to the pedogenetic processes, there are also some geological processes, which interfere with the formation of the soil cover and which he calls pedogeological processes [2].
In order to explain the genesis of soils and to establish their evolution time, both in natural conditions and in the conditions of their use by man, it is necessary to analyze the specific and combined actions of all the factors that intervene in these processes [3,4,5].
The studies were carried out in Săvârşin, a locality located in Western Romania, respectively in the south-east of Arad County, from which it is separated by 87 km[1]. The locality is located on the corridor of the Mureş River. The nearest town is the town of Lipova, 53 km away (fig. 1.).

Figure 1. Geographical location of Săvârşin

The E68 international road passes through the locality, a road that connects Romania - through Hungary - with the center of Europe.

As can be seen from the county map, the Mureș corridor is delimited in the southern part by the Poiana Ruscă Mountains and the Lipova Hills and in the northern part by the Zărand Mountains[6, 14].

The relief of the area is made up of hills and the Mureș meadow. Between the two mountains (Poiana Ruscă and Zărandului Mountains), the landscape of the locality is made up exclusively of hills and the Mureș meadow has been transformed into land for agriculture[8,12].

Experimental

The studies were carried out both in the field and in the laboratory and are based on the methodology and standards imposed by the soil analysis laboratories. From the data taken from the previous studies, the Săvârșin City Hall, the Forest District and OSPA Arad and from the field observations, the presence of certain pedogenesis processes that affected the soils in the area was observed [1,7].

Certain characteristics of climate, soil, relief, drainage, are limiting factors for agricultural production.

The main constraints or restrictions (limiting factors) will be grouped differently according to their nature and intensity, according to indicator 271 of the methodology for the elaboration of pedological studies part III, depending on the soil and land units encountered in the analyzed territory [5,9,10].

Results and discussions

The locality, due to its geographical location and the special complexity given by its hydrography, of the solification processes as essential elements for defining the living environment of the plants, is practically made up of a mosaic of soils, as they are presented in table 1.

Table 1.

The main types and associations of soils in Săvârșin, Arad County
(ha and % of agricultural area)

Nr crt	Main types of soil (after SRTS 2012)	Surface	
		Ha	%
1	Lithosols	150	1,30
2	Regosols	281	12,1
3	Gleic alluvial soil	496	38,54
4.	Luvosols	767	14,91
5.	Eutricambosols	457	33,6
6	Preluvosols	288	12,5
TOTAL		**4463**	**100**

A detailed analysis of each type of soil highlights the following aspects regarding the current state of nutrient supply of agricultural land in Săvârșin locality.

The main factors identified relate to the following:

Restrictions caused by soil salinization

This happens when there are two types of causes in the same territory: natural and man-made. 3,778 ha, respectively 6.9%, is affected by a series of salting and/or alkalization processes.

Restrictions generated by certain chemical properties of the soil: The area -374.32 ha of the studied area, respectively 0.69% presents these risks.

In this group we have identified the following limitations:

Restrictions caused by the decrease in humus reserve: Both must be seen as limiting factors of soil fertility. 59.67 hectares, respectively 0.11% of the total studied area, includes land with soils that have a humus reserve below 120 t/ha in the first 50 cm and that require the application of organic fertilizers.

Restrictions due to a high concentration of CaCO3 (risk of chlorosis). 314.65 ha, respectively 0.58% of the mapped area, includes land with a CaCO3 content higher than 16% in the first 50 cm and which requires the application of chemical fertilizers with physiologically acidic reaction for the characterization of Ca carbonates.

Limitations due to some physical characteristics of the soil. Out of the total area of 4463 ha, 4181.75 ha, which represents about 83.1%, includes land with soils that present one or more such limitations, due to: the fine texture in Ap, compactness, settlement, etc. to which, depending on the nature of the limiting factor, we can distinguish:

Restrictions caused by fine texture in Apa: The total area affected by these processes is 1328 ha, representing 29.47% of the studied area, in which there are soils with a medium fine texture (clay-clay) in Apa (with content between 33-46% colloidal clay).

Limitations due to soil compactness:

The total area affected by these phenomena is 4152.28 ha, i.e. 83.23% of the studied area and includes land with soils with a weak-strong compaction level between 20-75 cm (equal to or greater than 1%) that require subsoiling and/or deep loosening works to improve the aerohydraulic regime.

Restrictions caused by land cover or unevenness (U). 16,020.03 ha fall into this category, i.e. 29.53% of the area. It groups a series of soils located on terrain with uneven relief with level differences of over 0.29 m, which are presented in the form of crovs, valleys, ponds, pits and other forms of microdepressions, as well as areas with gilgoi microrelief that require modeling works or complete leveling.

Limitations due to excess moisture (poor drainage). In Romania in recent years, specific operations have been carried out on about 5 million hectares to eliminate excess moisture in our country. A surplus of moisture can be interpreted in two different ways: one in the hydroameliorative context and the other in the pedoagronomic context.

Quantitatively speaking, the high level of moisture or excessive presence of water in the soil are considered: the level of moisture that is greater than 30% in the soil, water or air; humidity level above the ventilation limit.

515.5 ha, respectively 28.60% of the total area of the studied area is affected by these limitations. This category includes land with soils that have a moderate to excessive excess of surface moisture (i.e. the soils are very wet for more than 5 days), divided according to the limiting factor (excess moisture) into:

Limitations due to excess groundwater: The area of 455.71 hectares, represents 0.84% of the total area and includes groundwater land at a depth of 0-1.5 m in the medium and fine textured soils in the control section, and at a depth of 0-1.0 m in the coarse-textured soils in the control section, which were separated according to the depth of the groundwater.

Soils with water table at extremely shallow depths (0.5-1 m) with a medium and fine texture in the analysis area. Area - 146.48 ha, 0.27% of the mapped area;

Soils with an extremely shallow water table (1-1.5 m) with intermediate and fine texture in the monitoring area: Area of 309.23 hectares, representing 0.57 % of the total area.

The limitations on the occurrence of excess stagnant moisture are obvious. The total area of distribution is 15,320.21 hectares, representing 28.24% of the measured area.

Restrictions due to moderate moisture levels on the surface. Approximately 11886.18 hectares, representing 21.91% of the area of the locality are affected by this process.

Limitations due to strong excess water on the surface: Limitations occur due to a large amount of moisture from the surface of the land. The total affected area is 3,434.03 ha, representing 6.33% of the total area.

Limitations due to climate (moisture deficit): Area -38,365.6 ha, i.e. 70.72% of the area. Group soils with low to excessive moisture deficit

By the intensity of the manifestation of moisture deficiency, we distinguish:

Low moisture deficit:

Sometimes, soil moisture can reach such a low level that it leads to wilting of the upper root for periods of more than 5-15 days. During these periods, many crops suffer from lack of water, with reduced harvests. Irrigation is essential for intensive agriculture.

Affected area = 16,036.8 ha, 41.8%.

Moderate moisture deficit:

The total affected area is 10,957.2 hectares, representing 28.56% of the mapped area.

Large (strong) moisture deficit:

Total affected area: 134.28 hectares, 0.35% of the total.

Conclusions

The researches presented in the paper were carried out in the locality of Săvârșin, which is located in the western part of Romania, in the south-east of Arad County, 87 km from it, on the course of the Mureș River. Along the Mureș River there are oak, ash and elm forests.

The relief is characterized by a high complexity of morphological forms and geological structure. The climate has many macroclimatic characteristics, which are influenced by its geographical location.

The morphological, physical and chemical description of the main soil types correctly reflects the current level of available nutrients: humus, nitrogen, phosphorus and potassium. The best soil types are preluvosols and alluvial soils. The geographical location and the complex hydrography of the locality make the soils and the solification processes essential elements in defining the living environment of the plants, creating a mosaic of soils, such as: lithosols, regosols, gleic alluvials, luvosols, eutricambosols and preluvosols.

The main limiting factors present in the studied area were produced by:

Restrictions due to soil salinization. These limits have been defended for two reasons: natural and anthropogenic causes. 3,778 hectares, i.e. 6.9% of the area, are affected by salting and/or alkalization processes.

Restrictions caused by certain chemical characteristics of the soil:

374.32 ha were affected, respectively 0.69% by these problems.

Restrictions caused by certain physical aspects of the soil: 4181.75 ha i.e. approx. 83.1% of the soils have a fine texture on the surface and are affected by these processes.

There are various levels of compaction determined by the intensity of the pressure exerted on the soil, namely:

- *Poorly compacted soils* (degree of compaction between 1 and 10%). On approximately 43,052.8 ha of land, i.e. 79.36% of the entire land.

- *Heavily compacted soils* (degree of compaction 11-18%). Approximately 2,099.48 hectares, i.e. 3.87% of the total studied area are affected;

Restrictions caused by land cover or inequality (U): 16,020.03 ha fall into this category, i.e. 29.53% of the area of the locality.

Restrictions caused by the large amount of humidity (insufficient drainage,) can be:

- moisture level exceeding 30% in soil, water or air;

- the humidity level exceeds the ventilation limit.

515.5 hectares, i.e. 28.60% of the area of the analyzed area, is affected by such restrictions.

Restrictions caused by the excess amount of groundwater: 455.71 hectares (0.84%) of the surface of the locality are affected by these restrictive factors.

Weather-related restrictions (lack of moisture): 38,365.6 hectares, which represents 70.72% of the area, is affected.

Depending on how strongly the lack of moisture manifests itself, we have:

- Soils with low humidity: 16,036.8 hectares, representing 41.8% of the total;
- Soils with moderate humidity: 134.28 hectares, representing 0.35% of the total.

Most plants suffer from a lack of water, which leads to significant decreases in the harvest. Irrigation is essential to have efficient agriculture and to achieve high yields.

BIBLIOGRAFIE

[1] Băcăuanu, V., 1989, Geomorphology (Geomorfologie), „Al. I. Cuza" University Press House, Iaşi, pp. 103-104.

[2] Ianoş, Gh., Puşcă, I., Goian, M., 1997, Banat soils - natural conditions and fertility (Solurile Banatului-condiţii naturale şi fertilitate), Mirton Publishing House, Timişoara, pp. 96-98.

[3] Ianoş, Gh., Goian, M., 1992, Influence of the agriculture systems on the soils quality from Banat. Problems of Theoretical and Applied Phytotechnique in Banat (Influenţa sistemelor de agricultură asupra calităţii solurilor din Banat. Probleme de agrofit. teor. şi aplic.), ICCPT Fundulea, Vol. 14(3-4), pp. 116-119.

[4] Mihuț, C., Niță L., 2018, Atmospheric Factors used to characterize soil resources https://www.rjas.ro/issue_detail/44, Timișoara, pag. 114-120.

[5] Mihuț C., Mateoc-Sîrb N., Duma Copcea A., Niță L., Ciolac V., Okros A., Popa D. (2022). Assessment of soil quality limitative factors. A case study: Secaş, Timiş County, Romania. *Scientific Papers Series Management, Economic Engineering in Agriculture and Rural Development* Vol. 22, Issue 1, Page 413-419, WOS:000798307300049.

[6] Okros, A., Pirsan, P., Borcean, A., Mihut, C., Nita, S., Mircov, V.D., Shahzod, H., Abdumanon, G., 2019, Intensive Agriculture Management In The North-West Area Of The Banat Region Under The Influence Of Different Bio-Pedo-Climatic Conditions. Proceedings of the InternationaL Conference on Life Sciences. Proceedings Edition July, 2020, pp. 176-178.

[7] O.S.P.A. Archive, Arad, 2020, 2021, 2022.

[8]Răuţă, C., Cârstea, S., 1993, Soil - the essential resource of the sustainable development, Soil Science, 1993 p. 104.

[9] Răuţă, C., Sustainable agriculture in Romania. Soil Science, Series III, Vol. XXXI, no. 1, 1997, and vol. XXIX no. 1, 1995, p. 21.

[10] Rogobete, Gh., Ianos, Gh., Implementation of the Romania System of Taxonomy of the soild for the West part of Romania. (Implementarea Sistemului Român de Taxonomie a solurilor pentru partea de vest a României).

[11] Șmuleac, L., Rujescu, C., Șmuleac, A., Imbrea, F., Radulov, I., Manea, D., Ienciu, A., Adamov, T., Pascalau, R., 2020, Impact of climate change in the Banat Plain, Western Romania, on the accessibility of water for crop production. Agriculture, 10(10), p. 437, 2020.

[12] Ţărău, D., Luca, M., 2002, Panopticon of Banat communes fro pedological perspective (Panoptic al comunelor bănăţene din perspectiva pedologică), Marineasa Publishing House, Timișoara, p. 181.

[13] Vass, H., Mănescu, C., Murg-Sicoe, O., Mateoc, T., Mateoc-Sîrb, N., 2021, Study on climate change issue and environmental degradation in Romania, Management Agricol, Lucrări Științifice Seria I, Vol. 23(2), 89-96.

[14] Vintilă, I., Borlan, Z., Răuţă, C., Daniliuc, D., Ţigănaş, L., 1984, Agrochemical situation of Romania's soils. Present and future (Situatia agrochimica a solurilor din România. Prezent si viitor), In Romanian. Ceres Publishing House, Bucuresti, p.43.

CLASSIFICATION OF MELANOMA PATIENTS TREATED BY IMMUNOTHERAPY

Srđan Milićević, **Buda Bajić, Katarina Vidojević, Marija Delić**

Department of Fundamental Sciences Faculty of Technical Sciences, University of Novi Sad, 21000 Novi Sad, Trg Dositeja Obradovića 6, Serbia
e-mail: srdjan88@uns.ac.rs

Abstract

This paper presents the classification of melanoma patients treated with immunotherapy, based on percentiles of standardized uptake value. The effects of therapy treatment on three organs of interest, lung, thyroid, and bowel are divided into two categories: with and without immune-related adverse events. Three well-known classification methods were used: logistic regression, support vector machine, and k-nearest neighbors. Due to the small data set and class imbalance, the emphasis was on choosing the appropriate metric. For testing, K-fold cross-validation was implemented and the obtained numerical results were analyzed and discussed.

Introduction

New cancer treatment with Immune Checkpoint Inhibitors (ICI) has improved the median overall survival rate for patients in various malignancies ([1], [2]). Although this treatment significantly improved outcomes, it often puts some patients at high risk of developing severe serious side effects, named immune-related adverse events (irAE), where an immune response is generated against healthy tissue [3]. The most common side effects include pneumonitis, colitis, thyroiditis, and many others which can disrupt the quality of a patient's life ([4], [5]).

One aspect of treatment that needs to be improved is minimizing the proportion of patients who experience side effects. Toxicity levels depend on the type of therapy but can occur in both monotherapy and a combination of immunotherapies. For combined therapies, adverse events are generally more frequent and serious. Hribernik et al. [6] have recently reported that irAE occurred in 63%. patients, while 8.7% patients experienced grade 3-4, and 11.6% patients need to discontinue the treatment, due to toxicity level.

Patients on ICI therapies are constantly monitored, before and during the therapy, with whole-body ^{18}F-fluorodeoxyglucose positron emission tomography/computed tomography (^{18}F-FDG PET/CT). It was shown that ^{18}F-FDG PET/CT is sensitive to inflammation of the pathogenesis of irAE [7] and has been successfully utilized for advanced metastatic melanoma staging and therapy response evaluation [8].

In this study, we first categorized the data based on patients diagnosed with pneumonitis, thyroiditis, and colitis in two classes: the Normal Control (NC) with patients who are not affected by irAE, and the Adverse Event (AE) group with those that experienced irAE. This selection is done based on biomarker values (SUV percentiles) extracted from the patient's images before and during the therapeutic process, and by looking at the medical data of the conducted retrospective study. classification assessment in a case study of immunotherapy treatment of metastatic melanoma patients.

The paper is organized as follows. Section II introduces methods, Section III presents data, experiments, and obtained results, while Section IV gives the conclusion of the conducted research.

Methods

A. Logistic Regression

Logistic regression $(\mathbf{LR})$ represents the data analysis technique specialized for classification and prediction. It is used to describe the relationship between an independent variable (X) and a dichotomy outcome variable (Y) that can have only two values. In our model, X represents biomarker values and Y has values 0 for $\mathbf{NC}$ and 1 for $\mathbf{AE}$ group of patients. The logistic regression function is given by

$$p(x) = \frac{e^{\beta_0 + \beta_1 x}}{1 + e^{\beta_0 + \beta_1 x}},$$

where β_0 and β_1 represent the intercept and rate parameters, respectively (see [10]). The values of parameters are estimated by the Maximum likelihood estimation (MLE) method. We assume that outcome variable Y has the predicted value 1 if $p(x) \geq 0.5$ and 0 if $p(x) < 0.5$.

B. Support Vector Machine

A support vector machine (SVM) is machine-learning algorithm for solving complex classification or regression problems. In this paper, we consider the SVM model specialized for the classification (see [11]). The idea of the model is to find a hyperplane that separates data into two classes with a maximal margin.

In the linear case, the equation of the hyperplane is given by $g(x) = w^T x + b$. For a given set of data points $\{(x_i, y_i)\}$, $i \in \{1, 2, \ldots, N\}$, $x_i \in R^n$, $y_i \in \{-1, 1\}$, (-1 for NC and 1 for AE), the primal formulation of SVM is given by:

$$min \, f(w, \xi) = \frac{1}{2}||w||^2 + C \sum_{i=1}^{N} \xi_i$$

$$y_i(w^T x_i + b) \geq 1 - \xi_i, \; \xi_i \geq 0,$$

where $\xi = (\xi_1, \xi_2, \ldots, \xi_N)$ is the vector of slack variables and C is the regularization term or box constraint. When the value of C increases, a tighter margin will be obtained. The role of slack variables is to allow errors in misclassification. In practice, instead of primal, it is easier and more sufficiently to solve dual problem, which is convex and has unique solution. Sometimes, the data is not linearly separable in input space. In that case, Kernel function can be used to transform the data in higher-dimensional space. Some examples of Kernel functions are: linear $(K(x, u) = x^T u)$, polynomial $(K(x, u) = (ax^T u + c)q, \; a, c \in R, \; q > 0)$, Gaussian radial basis $(K(x, u) = e^{||x - \mu||}, \; \mu \in R, \; \sigma > 0)$, etc.

C. K-Nearest Neighbors Algorithm

K-nearest neighbors algorithm (KNN) is one of the most fundamental algorithms for classification (see [12]). Due to its simple implementation, KNN is one of the first choices for classification, especially in cases where we do not know the data distribution.

Let $\{(x_i, y_i)\}$, $i \in \{1, 2, \ldots, N\}$, $x_i \in R^n$, $y_i \in \{0, 1\}$, be the given data set, where y_i are the labels corresponding to values x_i. First, we choose the values of k which represent the number of nearest neighbors needed to make a decision on class membership. Then, we measure the distance from test point x and training points. Then, k nearest points from x are selected. The class with the most members in the set of its k nearest neighbors of x is the predicted class for x. The choices of value of k and metrics are crucial for the algorithm. In the case of two classes, it is recommended that k be an odd number (to avoid equal voting). For data with outliers, it is better to use higher values for k. To measure distaces between points, commonly used is Minkowski distance:

$$d(x, x_i) = \left(\sum_{i=1}^{N} |x - x_i|^p \right)^{\frac{1}{p}}, \qquad p \geq 1.$$

Results and discussion

A. Data

In this work, we study data from patients who have metastatic melanoma and were treated with immunotherapy at the Institute of Oncology Ljubljana (OIL), Slovenia, or at the University of Wisconsin Carbone Cancer Centre (UW), Madison, WI, USA. In total 58 metastatic melanoma patients were retrospectively analyzed to see whether they developed irAE or not. From ^{18}F-FDG PET/CT scans of patients, SUV percentiles are used as an imaging biomarker (for more details see [13]). We analyze in this work three target organs, which are commonly exhibiting irAE (typically serious inflammations): the lung (irPneumonitits), bowel (irColitis), and thyroid (irThyroiditis). All patients are labeled either as NC if they did not encounter irAE in the organ of interest, or AE if they developed an adverse event.

Based on extracted biomarkers, we aim to perform binary classification and try to find the decision boundary between NC and AE groups for each of the three organs separately. For our sample of the size $N = N_{NC} + N_{AE} = 58$ for each organ, (x_i, y_i) $i \in \{1, 2, ..., N\}$, is the pair of the scalar value of SUV percentile imaging biomarker (x_i) and corresponding binary label $y_i \in \{0, 1\}$, where 0 stands for NC class (this holds for **LR** and **KNN** whereas for **SVM** is -1) and 1 for AE class belongingness.

A summary of data used in experiments is given in Table I. For all three organs NC class has more samples than AE class, meaning that we have to deal with an imbalanced dataset with a limited size. In particular, due to the small dataset size, we are able to only consider the simplest classification methods (briefly introduced in Section 2) with a small number of parameters to avoid overfitting. In addition, due to the small dataset size, we cannot split the dataset into training, validation, and test subsets, so we perform Fold cross-validation instead. **K**-Fold cross-validation scheme starts with the division of all samples into **K** groups, called folds. In our experiments, we set **K**=4.

Organ	N_{NC}	N_{AE}
Lung	53	5
Bowel	52	6
Thyroid	49	9

Table I. Number of patients in normal control (NNC) and adverse event.

C. Evaluation metrics

In order to measure classification performances, several well-known measures are frequently used such as accuracy, precision, recall, F_1 score, and others. Most of them are derived from elements of the confusion matrix, as shown in Fig. 3. In the case of imbalanced classes, accuracy, the most frequently used classification performance measure, is not a good choice since for the dominant class most of the instances will be correctly classified and accuracy will be close to 1. For imbalanced classes better is to consider precision or recall, or their harmonic mean, so-called F_1 score. In our experiments, we will compute both precision and recall, as well as F_1 score.
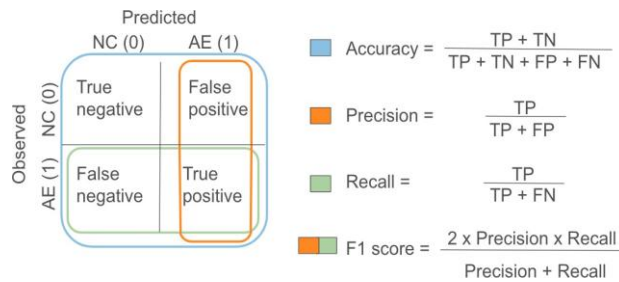
Figure 3. Illustration of confusion matrix.

D. Results

We perform binary classification using three different basic machine learning methods - LR, SVM, and KNN. We do it independently for all three organs of interest. SVM is estimated with Gaussian radial basis kernel and KNN with 3 neighbors and Minkowski distance. A cross-validation scheme with 4 folds is used for the evaluation of each method. As we are interested in average precision, recall, and F_1 score, for some of the methods and some of the folds it happens that some of that measure cannot be computed due to division with zero. Therefore, instead of computing for each fold these three measures and averaging them, we computed the "average" confusion matrix from confusion matrices corresponding to all 4 folds. From such an "average" confusion matrix we further computed precision, recall, and F_1 score. Results for all three methods and three considered organs are given in Table II.

	Lung			Bowel			Thyroid		
	LR	SVM	KNN	LR	SVM	KNN	LR	SVM	KNN
Precision	0.5	0.67	0.8	0.5	0.5	-	0.75	0.57	0.57
Recall	0.4	0.4	0.8	0.44	0.42	-	0.33	0.44	0.44
F_1 score	0.44	0.5	0.8	0.47	0.45	-	0.46	0.5	0.5

Table II. Classification performance for three different methods for lung, bowel, and thyroid based on SUV percentiles.

Conclusion

In this work, we perform binary classification of biomarker value, the so-called SUV percentile, based on ^{18}F-FDG PET/CT images of melanoma patients going through immunotherapy. Three organs that are most commonly negatively affected by therapy, lung, thyroid, and bowel, for 58 patients in total are monitored, and based on SUV percentile value we try to estimate the decision boundary between those who do not have therapy side effects and those who have. Due to the limited dataset size, the simplest classification methods are considered: logistic regression, support vector machine and k-nearest neighbors, and K-Fold cross-validation is performed. The real clinical dataset we consider in this study is heavily imbalanced and as such, it requires special attention on classification performance measures. Instead of accuracy, we used precision, recall, and F_1 score which aggregates precision and recall. No uniform conclusion is derived - for classification related to lung k-nearest neighbors was the most effective, whereas for bowel and thyroid, almost all methods exhibit similar performance. Future work will be to try to construct new classification measures by aggregating precision and recall in a way that better suits the application of interest.

Acknowledgements

References

[1] D. Wolchok, V. Chiarion-Sileni, R. Gonzalez, P. Rutkowski, J-J. Grob, C.L. Cowey, C.D. Lao, J. Wagstaff, D. Schadendorf, P.F. Ferrucci and others, Overall survival with combined nivolumab and ipilimumab in advanced melanoma, New England Journal of Medicine, vol. 377, num. 14, 2017, pp. 1345–1356.

[2] D. Wolchok, V. Chiarion-Sileni, R. Gonzalez, J-J. Grob, P. Rutkowski, C.D. Lao, C.L. Cowey, D. Schadendorf, J. Wagstaff, R. Dummer and others, Long-term outcomes with nivolumab plus ipilimumab or nivolumab alone versus ipilimumab in patients with advanced melanoma, Journal of Clinical Oncology, vol. 40, num. 2, 2022, pp. 127.

[3] N. Gandy, M.A. Arshad, K.L. Wallint, S. Dubash, S. Khan and T.D. Barwick, Immunotherapy-related adverse effects on [18]F- FDG PET/CT imaging, The British Journal of Radiology, vol. 93, num. 1111, 2020, pp. 20190832.

[4] D.Y. Wang, J-E. Salem, J.V. Cohen, S. Chandra, C. Menzer, F. Ye, S. Zhao, S. Das, K.E. Beckermann, L. Ha and others, Fatal toxic effects associated with immune checkpoint inhibitors: a systematic review and meta-analysis, JAMA oncology, vol. 4, num. 12, , 2018, pp. 1721–1728.

[5] N. Eshghi, L.L. Garland, E. Nia, R. Betancourt, E. Krupinski and P.H. Kuo, ^{18}F-FDG PET/CT can predict development of thyroiditis due to immunotherapy for lung cancer, Journal of nuclear medicine technology, vol. 46, num. 3, 2018, pp. 260–264.

[6] N. Hribernik, M. Boc, J. Ocvirk, J. Knez-Arbeiter, T. Mesti, M. Ignjatovic and M Rebersek, Retrospective analysis of treatment-naive Slovenian patients with metastatic melanoma treated with pembrolizumab–real-world experience, Radiology and Oncology, 2020, pp. 119–127.

[7] N. Aide, A. Iravani, K. Pringent, D. Kottler, R. Alipour and R.J. Hicks, PET/CT variants and pitfalls in malignant melanoma, Cancer imaging, vol. 22, num. 1, 2022.

[8] L. Filippi, F. Bianconi, O. Schillaci, A. Spanu and B. Palumbo, The Role and Potential of ^{18}F-FDG PET/CT in Malignant Melanoma: Prognostication, Monitoring Response to Targeted and Immunotherapy, and Radiomics, Diagnostics, vol. 12, num. 4, 2022.

[9] S. Nadaraja, J. Helsing, M. Naghavi-Behzad, L. Land, C. Ruhlmann, O. Gerke and M.G. Hildebrandt, Value of 2- [^{18}F]FDG-PET/CT in identifying immune-related adverse events in patients with melanoma or non-small cell lung cancer: a systematic scoping review, Clinical and Translational Imaging, vol. 12, 2024, pp. 187–195.

[10] H-A. Park, An Introduction to Logistic Regression: From Basic Concepts to Interpretation with Particular Attention to Nursing Domain, J Korean Acad Nurs, 2013, pp. 153-164.

[11] M. Awad and R. Khanna, Support Vector Machines for Classification, Apress open, 2005.

[12] L.E. Peterson, L.E, K-nearest neighbor, Scholarpedia, vol. 4, 2009.
R. Jeraj and M. Reberšek, Quantitative imaging biomarkers of immune-related adverse events

[13] D.T. Huff, P. Ferjancic, M. Namias, H. Emamekhoo, S. Perlman and R. Jeraj, Image intensity histograms as imaging biomarkers: application to immune-related colitis, Biomedical physics & engineering express, IOP publishing, vol. 7, 2021, pp. 065019.

THE USE OF HYBRID MATERIALS (Mg3AL-LDH/IONIC LIQUIDS/CHITOSAN) IN THE RECOVERY PROCESS OF Pd IONS FROM AQUEOUS SOLUTIONS

Emilia Milos[1], Laura Cocheci[1], Adriana Popa[2], Anca Filimon[3], Lavinia Lupa[1]

[1] *Faculty of Industrial Chemistry and Environmental Engineering, Politehnica University Timisoara*

[2] *"Coriolan Dragulescu" Institute of Chemistry, Timisoara*

[3] *Polycondensation and Thermostable Polymers Department, "Petru Poni" Institute of Macromolecular Chemistry*

Abstract

In this work, studies were carried out on the recovery of palladium ions from aqueous solutions by adsorption on hybrid materials, Mg_3Al-LDH/ionic liquids/ chitosan.

To synthesize the double layered hydroxide, Mg_3Al, the coprecipitation method at low supersaturation was used , using as sources of metal ions $Mg(NO_3)_2 \cdot 6H_2O$ and $Al(NO \cdot 9H_2O)$, the ratio between the cations being Mg^{2+}/Al^{3+} =3:1.

Regarding obtaining the functionalized compound with 10% ionic liquid, the same method was used, specifying that the mixture of nitrates was added, dropwise, to the ionic liquid solution, dissolved in acetone, the ratio between them being ionic liquid:acetone =1g/50mL. To maintain the pH in the desired range, a NaOH solution was used , prepared from boiled and cooled water, and the mechanical strength of the obtained adsorbents (Mg_3Al and Mg_3Al-IL) was increased by dispersing them in chitosan solution dissolved in 1% acetic acid, obtaining the hybrid materials: Chitosan / Mg_3Al, Chitosan / Mg_3Al-IL, Chitosan / Mg_3Al/IL. The hybrid materials were characterized by X-ray diffraction, Fourier transform IR spectroscopy (FTIR) and scanning electron microscopy (SEM) coupled with an energy dispersive X-ray detector (EDX).

The X-ray spectrum of the Mg_3Al sample, obtained by co -precipitation at low supersaturation, suggests a good compatibility of chitosan with LDH, which leads to the formation of porous networks.

For all studied materials and for all initial palladium concentrations, the adsorption capacity of the studied materials increases with increasing contact time, up to 60 minutes, after which it remains practically constant.

To clarify the palladium adsorption mechanism on the three studied materials, three kinetic models were used: the pseudo-first-order kinetic model, the pseudo-second-order kinetic model and the intraparticle diffusion model (Weber-Morris), the pseudo-order kinetic model second order being the one that confirmed, the best, the experimental data, value of the correlation coefficients R^2, being approximately 1, regardless of the working temperature.

In order to study the nature of the palladium adsorption process on the studied materials, the thermodynamic parameters were calculated: enthalpy, entropy, Gibbs free energy, activation energy, the results confirming that the reactions are spontaneous, endothermic, and the palladium adsorption process on the studied materials corresponds a chemosorption.

In order to identify the mechanism of the process and evaluate, theoretically, the adsorption capacity at equilibrium, the Langmuir, Freundlich , Temkin and Redlich-Peterson isotherms were used , finding that the Langmuir isotherm best describes the palladium adsorption process on synthesized materials.

It is recommended to add the ionic liquid in the synthesis process of the hybrid material, not in the synthesis process of the LDH.

Introduction

In the conditions where the primary reserves are continuously depleted, palladium's applications are multiple, and the price of the metal in a fluctuating increase, its recovery from secondary products and waste becomes imperative. The recovery processes are multiple: melting, chlorination, dissolution in acids, co-precipitation, ion exchange, adsorption, etc. Particular attention is paid to adsorption, being one of the most promising methods due to its simplicity and high efficiency, attributes that determine the widespread use of this recovery method.

As a result, in the present work the possibility of recovering palladium ions from residual aqueous solutions was studied, by adsorption on hybrid materials, Mg3Al-LDH/ionic liquids/chitosan, proving that all the raw materials used to obtain the adsorbents proved their effectiveness.

Experimental

To synthesize the double layered hydroxide, $Mg_{3\,Al,\,the}$ coprecipitation method at low supersaturation was used , using as sources of metal ions $Mg(NO_3)_2 \cdot 6H_2O$ and $Al(NO \cdot 9H_2O)$, the ratio between the cations being $Mg^{2+}/Al^{3+} = 3:1$.

Regarding obtaining the functionalized compound with 10% ionic liquid, the same method was used, specifying that the mixture of nitrates was added, dropwise, to the ionic liquid solution, dissolved in acetone, the ratio between them being ionic liquid:acetone =1g/50mL. To maintain the pH in the desired range, a NaOH solution was used , prepared from boiled and cooled water, and the mechanical strength of the obtained adsorbents (Mg_3Al and Mg_3Al-IL) was increased by dispersing them in chitosan solution dissolved in 1% acetic acid, obtaining the hybrid materials: Chitosan / Mg_3Al, Chitosan / Mg_3Al-IL, Chitosan / Mg_3Al/IL. The hybrid materials were characterized by X-ray diffraction, Fourier transform IR spectroscopy (FTIR) and scanning electron microscopy (SEM) coupled with an energy dispersive X-ray detector (EDX).

To explain the mechanism of the adsorption process, kinetic, thermodynamic and equilibrium studies were carried out.

Results and discussion

The X-ray spectrum of the Mg_3Al sample, obtained by co -precipitation at low supersaturation, suggests a good compatibility of chitosan with LDH, which leads to the formation of porous networks.

For all studied materials and for all initial palladium concentrations, the adsorption capacity of the studied materials increases with increasing contact time, up to 60 minutes, after which it remains practically constant.

The structural and morphological characterization of the synthesized materials was achieved by: X-ray diffraction (XRD); Fourier transform IR spectroscopy (FTIR); scanning electron microscopy (SEM);

Diffractograms of the synthesized hybrid samples were compared with the X-ray diffractograms of the raw materials used (chitosan , Mg_3Al, Mg_3Al-IL). The X-ray spectrum of the Mg_3Al sample obtained by co -precipitation at low supersaturation confirms the fact that layered double hydroxide was obtained as the main crystalline phase, being able to highlight the specific basal peaks of planes (003) and (006) at the angle 2Ө=11, 5°, respectively 2Ө=22.8° and the non-basal peaks corresponding to planes (110) and (113) present at angles 2Ө around 60 degrees. In the case of the layered double hydroxide sample functionalized with

methyl trialkyl ammonium chloride (Mg 3 Al-IL), was observed a shift of the basal peaks to smaller 2Ө angles, a decrease in their intensity and an increase in the base indicating the intercalation of the ionic liquid between the LDH layers. X-ray diffraction studies of pure chitosan show very broad peaks at the angles 2Ө = 10° and 2Ө = 20°, results similar to the data presented in the specialized literature . In hybrids samples are observed disappearance of chitosan peak at 2 Ө = 10°, and the very wide peak from 2 Ө = 20° became weak. These results suggests that chitosan has a good compatibility with LDH, which leads to formation of some porous network of chitosan and LDH, respectively IL, demonstrating that the preparation method was effective for obtaining the studied hybrid materials.

While the chitosan particles have a very smooth surface, the morphology of the Mg3Al sample is in the form of hexagons arranged neatly in overlapping layers, typical of layered double hydroxides. By functionalizing it with methyl trialkyl ammonium chloride through co - synthesis, it is observed that the layers are disordered due to the penetration of the ionic liquid between the layers, the surface of the sample appearing in the form of cotton flowers. The synthesized hybrid samples show very different surface morphologies, with more compact surfaces containing small, well-dispersed LDH particles. EDX spectra confirm the obtaining of hybrid materials.

To clarify the palladium adsorption mechanism on the three studied materials, three kinetic models were used: the pseudo-first-order kinetic model, the pseudo-second-order kinetic model and the intraparticle diffusion model (Weber-Morris), the pseudo-order kinetic model second order being the one that confirmed, the best, the experimental data, value of the correlation coefficients R^2, being approximately 1, regardless of the working temperature.

In order to study the nature of the palladium adsorption process on the studied materials, the thermodynamic parameters were calculated: enthalpy, entropy, Gibbs free energy, activation energy, the results confirming that the reactions are spontaneous, endothermic, and the palladium adsorption process on the studied materials corresponds a chemosorption.

In order to identify the mechanism of the process and evaluate, theoretically, the adsorption capacity at equilibrium, the Langmuir, Freundlich , Temkin and Redlich-Peterson isotherms were used , finding that the Langmuir isotherm best describes the palladium adsorption process on synthesized materials.

Conclusion

It can be found that the functionalization of the adsorbent materials with the studied ionic liquid leads to an increase in their adsorptive efficiency, which means that the functional groups in the ionic liquid contribute to the palladium removal process from aqueous solutions. It is found that the method of obtaining the adsorbent material also influences the efficiency of the Pd recovery process from aqueous solutions, so it is recommended to functionalize the adsorbent material with the studied ionic liquid in the hybrid materials synthesis process, not in the LDH synthesis.

References

[1] Jayanudin,J, Lestari, Retno S. D., Kustiningsih, I., Irawanto, D., Rozak, R, Wardana, Reyonaldo L. A., and Muhammad, F, *Sustainable material for urea delivery based on chitosan cross-linked by glutaraldehyde saturated toluene: Characterization and determination of the release rate mathematical model*, Karbala International Journal of Modern Science 2022, Vol. 8 : Iss. 4 , Article 9.
[2] Kumar, S., Koh, J. *Physiochemical, Optical and Biological Activity of Chitosan-Chromone Derivative for Biomedical Applications*, Int. J. Mol. Sci. 2012, 13, 6102-6116.

[3] Morsy, M., Mostafa, K., Amyn, H., El-Ebissy, A., Salah, A., Youssef, M. ,*Synthesis and Characterization of Freeze Dryer Chitosan Nano particles as Multi functional Eco-Friendly Finish for Fabricating Easy Care and Antibacterial Cotton Textiles*, Egyptian Journal of Chemistry, 2019, 62(7), pp. 1277-1293.

[4] Fernandes Queiroz, M., Melo, K.R.T., Sabry, D.A., Sassaki, G.L., Rocha, H.A.O., *Does the Use of Chitosan Contribute to Oxalate Kidney Stone Formation?* Mar. Drugs 2015, 13, pp.141-158.

[5] Drabczyk, A., Kudłacik-Kramarczyk, S., Głąb, M., Kędzierska, M., Jaromin, A., Mierzwiński, D., Tyliszczak, *B., Physicochemical Investigations of Chitosan-Based Hydrogels Containing Aloe Vera Designed for Biomedical Use. Materials* 2020, *13*, 3073.

[6] Mikkola, J.P.,Virtanen, P., Sjöholm ,R. ,*Aliquat 336 – a versatile and affordable cation source for an entirely new family of hydrophobic ionic liquids*, Green. Chem., 8, 250–255, (2006).

[7] Kloprogge, J.T.,Frost, R.L., *Fourier Transform Infrared and Raman Spectroscopic Study of the Local Structure of Mg-, Ni-, and Co-Hydrotalcites*, J. Solid State Chem.,146(2), 506–515, (1999).

[8] Haro, N. K., Del Vecchio, P., Marcilio, N.R., Feris, L.A., *Removal of atenolol by adsorption - Study of kinetics and equilibrium, Journal of Cleaner Production*, 154: 214-219, (2017).

[9] Cocheci, L., Lupa, L., Tolea, N.S., Lazău, R., Pode R., *IL-Functionalized Mg$_3$Al-LDH as New Efficient Adsorbent for Pd Recovery from Aqueous Solutions*. *Int. J. Mol. Sci.* **2022**, *23*, 9107.

[10] Kumar, K. V.,Sivanesan, S., *Prediction of optimum sorption isotherm: Comparison of linear and non-linear method, Journal of Hazardours Materials* 123: 198, (2005).

[11] Wang, J., Xu, J.,Xia, J., Wu, F., Zhang, Y., *A kinetic study of concurrent arsenic adsorption and phosphorus release during sediment resuspension, Chemical Geology*, 495: 67-75, (2018).

CLIMATIC INTERPRETATION OF METEOROLOGICAL ASPECTS IN THE SATU MARE AREA OVER A PERIOD OF THREE YEARS

Mircov Vlad Dragoslav[1], Mihuț Casiana[2], Okros Adalbert[2], Cozma Antonela[2], Duma Copcea Anişoara[2]

[1]*Department of Agricultural Tehnologies University of Life Sciences "King Mihai I" from Timişoara, Calea Aradului nr.119, 300645 Timişoara, country Timiş, România*
[2]*Department of Soil Sciences, University of Life Sciences "King Mihai I" from Timişoara, Calea Aradului nr.119, 300645 Timişoara, country Timiş, România*
e-mail: mihut_casiana@usvt.ro, vlad.mircov@yahoo.com

Abstract
The study of weather-climatic phenomena, especially the extremes that have become more and more frequent, has acquired increased significance, given the increasing awareness of the importance of preventing material damage, but especially of the human victims they cause. The monitoring and analysis of atmospheric risk phenomena thus comes to the aid of local and national authorities whose duty is to protect the population and goods of any kind, and early warning of the occurrence of such a phenomenon is useful to each individual [6,7].
The west and north-west of Romania, like the whole country, due to its geographical position - in the temperate zone, is exposed to a wide range of weather-climatic risk phenomena with the potential to occur throughout the year.

Introduction
The city of Satu Mare benefits from a moderate temperate continental climate. The winter periods, due to the northern location, are longer and colder in Satu Mare, the average thermal value of the cold season being lower, -17°C, than the values recorded in the other cities in the west, for example -15°C in Oradea and -12°C in Timisoara [11]. The annual average temperature is 9.6°, and the atmospheric humidity is quite high [8]. The wind regime is characterized by the predominance of currents from the north-western sector, which bring precipitation in spring and summer [1,2]. The hydrographic network in the area of the city of Satu Mare is represented by the Someş river, in the north by the Sar stream, and in the south by the Homorod stream [5,9]. The constitution and evolution of the municipality of Satu Mare was closely linked to the Someş river, which, apart from the favorable conditions for the settlement of a human community around it, offered, starting from the early Middle Ages, the possibility of intense commercial links with the riparian regions of this water, favored the practice of milling, fishing, etc. [3,10].

Figure 1 Northern Transylvania Regional Meteorological Center

Experimental

The purpose of this work is to identify some indicators that most accurately express the extreme nature of the manifestations of some meteorological parameters, and through the Banat Crisana and Transilvania Nord Meteorological Centers, we highlighted the period 2019-2021, but also the summary evolution of certain parameters over a period of forty years, between 1961 and 2000 [4,12,14]. Ocna Șugatag and Cluj-Napoca weather stations are included in the international Regional Basic Synoptic Network, while Bistrița and Cluj-Napoca weather stations are included in the international [13].

Results and discussions

The table below shows the differences between the monthly averages of the daily minimums, over a period of forty years, from the stations located in the west and east of the country, it can be seen that, in general, in winter and at the beginning of spring, these differences are positive, and summer and early autumn are negative. As in the case of the average of the maximum and the average of the minimum, it is generally higher at the stations in the west of the country, by several tenths of a degree, compared to the stations in the east of the country, the causes being the same.

Table1.

Difference between monthly and annual averages of minimum daily temperatures from meteorological stations located in the west of the country (°C)

Stațiile	lunile											
	I	II	III	IV	V	VI	VII	VIII	IX	X	XI	XII
Satu Mare	0,3	0,6	1,0	-0,1	-0,6	-0,9	-1,1	-0,8	-0,5	-0,5	0,7	0,4
Oradea	1,6	1,6	1,4	0,1	-0,4	-0,9	-0,9	-0,4	0,2	0,3	1,0	1,1
Sannicolau-Mare	1,4	1,5	1,2	0,4	-0,1	-0,4	-0,4	0,0	0,7	0,7	0,9	1,2
Banloc	1,2	1,3	1,0	0,4	-0,1	-0,8	-1,3	-0,9	-0,1	-0,1	1,1	1,0

The dates of production of absolute maximum temperatures on the territory of our country depend a lot on the landforms. The maximum temperature in Romania during the period under consideration, between 1961 and 2000, was 43.5°C recorded in Giurgiu, on July 5, 2000. As is known, the highest absolute maximum temperature in our country recorded since the beginning meteorological observations and until now it is 44.5°C reported on August 10, 1951, in the town of Ion Sion. In these conditions, the circulation of air from the lower layers of the troposphere, having a northeast to southwest direction, determines the penetration of cold arctic continental air masses of Siberian origin into our country, in the form of the Crivățului. These air masses cause cold and dry weather in the south and east of the country and something warmer, quiet

and with more frequent snow in the Transylvanian Plateau and in the mountain area. The high mountain area is characterized by less cloudiness and a greater number of clear days. Next, we present the maximum temperature values from meteorological stations representative of the studied area.

Table 2

Maximum monthly temperature recorded during the period 1961-2000

Stațiile		Lunile											
		I	II	III	IV	V	VI	VII	VIII	IX	X	XI	XII
	°C	17,4	20,5	28,0	30,6	34,3	37,5	39,5	39,5	33,8	30,5	24,8	17,9
Timișoara	zi	29	28	24	27	12	14	6	22	19	2	14,8	16
	an	1979	1994	1977	1992	1968	2000	1988	2000	1961	1965	1997	1989
	°C	14,7	17,9	26,0	28,8	31,4	36,3	37,2	38,8	33,8	27,9	24,2	18,0
Satu Mare	zi	31	26	21	30	18	23	24	21	14	2	4	17
	an	1990	1989	1974	1969	1994	2000	1987	2000	1994	1965	1968	1989
	°C	13,8	19,0	27,0	28,2	33,1	35,3	37,7	36,8	34,0	28,2	23,3	17,2
Târgu Mureș	zi	24	28	31	26	16	30	25	22	15	14	6,1	11
	an	1971	1994	1975	1968	1969	1963	1987	2000	1994	1993	63,90	1982

In the Transylvanian Plateau and Maramureș, in terms of cloudiness, apart from the maximum in December and the minimum in August, there is a secondary maximum in April and a secondary minimum in March. For the Getic Subcarpathians (with southern exposure), the secondary maximum is recorded in February-March, and the secondary minimum in January. If during the main maximum (December) the average values of total cloudiness, in the hill and plateau regions, oscillate between 7.0-7.9 tenths, during the secondary maximum they are only 6.1-6.5 tenths.

Table 3.

Monthly and annual averages of total cloudiness

Stațiile	Lunile	I	II	III	IV	V	VI	VII	VIII	IX	X	XI	XII
Timișoara		7,2	6,8	6,4	6,4	6,0	5,6	4,6	4,3	4,9	5,0	6,9	7,6
Satu Mare		2,3	6,9	6,4	6,3	5,9	5,6	5,1	4,7	5,2	5,5	7,3	7,7
Tg. Mureș		7,4	6,8	6,2	6,4	6,0	5,7	5,1	4,6	5,1	5,1	6,8	7,9

During the analyzed interval, the amounts of both monthly and annual precipitation showed important variations in all areas of the country, as can be seen from the table below in the period 1961-2000, the highest annual amount of precipitation was recorded in Stana of 370 mm, in 1980, and the lowest, 137.6 mm, in Sulina in 2000. On large geographical areas, the maximum annual precipitation amounts reached 950-1,100 mm in the Romanian Plain, 850-1,000 mm in Moldova, 1,000-1,300 mm in Transylvania and the Western Plain, while in Dobrogea the highest annual amounts did not exceed 700 mm. In the mountainous areas, they exceeded 2,000 mm.

Regarding the rainfall regime recorded in Satu Mare, in recent years, respectively in 2019 and 2020, differences of approximately 200 mm have appeared between the two years studied, concretely, in 2019 515.7 mm were recorded, and in 2020 record amount for Satu Mare, i.e. 706.1 mm. There were enormous differences in the summer months, from June, July, August and until September, it rained approximately 350 mm in the 4 months, in 2020, compared to only 150 mm recorded in 2019. Regarding the thermal regime for the period 2019-2021 we can say that the values showed small deviations, in the winter of 2020, the difference being from 0.8 degrees C to 1.2 degrees C, values recorded in the months of January, March and April. In the conditions of our country, the regime of atmospheric precipitation is characterized by a

more pronounced variability, as is natural during the warm period of the year. The high variability of the annual quantities was realized both in the phenomenon of drought and in excess rainfall. Thus, the years 1961, 1983, 1986, 1990, 1992, 1993, 1994 and 2000 stand out as dry years in a large part of the country, and the period 1983-1992 as dry decades. They are known as years with excess rainfall 1969, 1970, 1975, 1991-1992, 1997, and as rainy decades 1966-1975.

The period 1961-2000 is characterized by lower annual amounts, this deficit is the result of the very small amounts that fell in the period 1980-2000, in the intervals January-April in the west of the country and June-December, in the south and east of the country. In the Transylvanian Plateau, with the exception of December, there is a moderate decrease in precipitation throughout the year. The end of spring was marked by a pluviometric surplus throughout the country. The rainfall deficit, generalized in the reference period, overlaps the intervals warmer than the multiannual average, which include the second half of the winter and the spring season.

Conclusions

Regarding the rainfall regime recorded in Satu Mare, during the years 2019-2021, respectively in 2019 and 2020, there were differences of approximately 200 mm between the two years studied, concretely, in 2019 515.7 mm were recorded , and the following year the record amount for Satu Mare, i.e. 706.1 mm, while 2021 brought approximately 640 l/m2. There were enormous differences in the summer months, from June, July, August and until September, it rained approximately 350 mm in the 4 months, in 2020, compared to only 150 mm recorded in 2019.

Also, the maximum daily amount of precipitation in 2019 was 22.6 mm, on 27.07, compared to 45.4 mm, in 2021, and also in July, more precisely, on 03.07.

We can say that it was a beneficial year for most of the agricultural crops in our area, we can say that the thermal values were not strongly felt, although there were warm periods, the thermal maxima of the two years being, on 29.06.2020, 32 degrees was recorded, and the same maximum value of 32.2 degrees, all the month of July, more precisely on 02.07.2021, at an interval of 70 h. The rainfall deficit, generalized in the reference period, overlaps the intervals warmer than the multiannual average, which include the second half of the winter and the spring season. Based on the analysis of the daily maximum precipitation regime and over longer intervals, we took into account the rainfall data from both the meteorological stations and those from the rainfall stations for a significant period of operation. The accumulation of exceptional amounts of precipitation over the intervals of 24, 48 and 72 hours is random, both in time and in space, and falls under the category of climatic hazards, with major negative effects on the most important economic and social fields.

From the values shown in certain tables in the paper, it can be seen that, in the territorial distribution of the respective parameters, the distance from the sea, the altitude and the Fohn effect will be taken into account, causes that play the main role. The air descent specific to both the proximity to the sea and the Fohn phenomenon also cause small differences in the average of the maximum amounts over different time intervals.

BIBLIOGRAFIE

[1] Barbu, I., Popa, I. (2003), Monitoringul secetei în padurile din România. Edit.Tehnica Silvica, Câmpulung Moldovenesc, 128 p..

[2] Bogdan, Octavia, Niculescu, Elena, (1999), Riscurile climatice din România, Ed. Sega-International, București.

[3] Mihuț C., Mateoc-Sîrb N., Duma Copcea A., Niță L., Ciolac V., Okros A., Popa D. (2022). Assessment of soil quality limitative factors. A case study: Secaş, Timiş County, Romania.

Scientific Papers Series Management, Economic Engineering in Agriculture and Rural Development Vol. 22, Issue 1, Page 413-419, WOS:000798307300049.

[4] Vlad Dragoslav Mircov, Casiana Mihuț, Antoanela Cozma (2024), Climate changes and its effects on soils and agriculture in Western and South-Western Romania. Scientific Papers. Series B. Horticulture Vol. l 68, No. 1, București

[5] Vlad Dragoslav Mircov, Adalbert Okros, Casiana Doina Mihut, Anisoara Duma Copcea, Codruța Chis (2023), Interpretarea factorilor de risc climatici pentru perioada 2019-2022 în zona de Vest a României. GeoConferință științifică internațională multidisciplinară: SGEM, Vol. 23 No. 4.1 Pag. 301-306

[6] Moldovan, F., (2003), Fenomene climatice de risc, Editura Echinox, Cluj-Napoca.

[7] Munteanu, Rodica, (2001), Geografia fizică a României, Editura Mirton, Timișoara,

[8] Nichita, C., (2011), Utilizarea radarului doppler în gestionarea fenomenelor meteorologice periculoase în sud-vestul României – teză de doctorat, Universitatea de Vest din Timișoara.

[9] Okros, A., Pirsan, P., Borcean, A., Mihut, C., Nita, S., Mircov, V.D., Shahzod, H., Abdumanon, G., 2019, Intensive Agriculture Management In The North-West Area Of The Banat Region Under The Influence Of Different Bio-Pedo-Climatic Conditions. Proceedings of the InternationaL Conference on Life Sciences. Proceedings Edition July, 2020, pp. 176-178.

[10] Oncescu, N., (1965), Geologia României, Editura Tehnică, București.

[11] Ujvári, I., (1972), Geografia apelor României, Editura Științifică, București.

[12] ***, Date furnizate de catre Centrul Meteorologic Regional Transilvania Nord.

[13] ***, (2008),Clima României, Administrația Națională de Meteorologie, București.

[14] . ***, Arhiva Centrului Meteorologic Regional Banat-Crișana din Timișoara.

COMPARATIVE MORPHO-STRUCTURAL AND ELECTROCHEMICAL CHARACTERIZATION OF FTO-BASED OXIDE FILMS CORRELATED WITH SYNTHESIS METHOD

Mina-Ionela Morariu (Popescu)[1,2] , Mircea Nicolaescu[1], Corina Orha[1] , Carmen Lazau[1] Cornelia Bandas[1]*

[1]National Institute for Research and Development in Electrochemistry and Condensed Matter, Department of Condensed Matter Timisoara, e-mail: cornelia.bandas@gmail.com
[2]"Politehnica" University of Timisoara, e-mail: mina.popescu37@gmail.com
*Correspondence author: cornelia.bandas@gmail.com

Abstract

Thin films based on gallium oxide (β-Ga_2O_3) and mesoporous titanium oxide (TiO_2 (MZ)) were successfully obtained by deposition on fluorine-doped tin oxide (FTO) conductive glass, using Doctor Blade method in two steps. Firstly, the β-Ga_2O_3 powders was synthesized by a simple and rapid microwave-assisted hydrothermal method followed by the calcination at 900° C for 3 hours. For the TiO_2 (MZ) powders a sol-gel method was chosen to obtain the crystalline materials. Secondly, a stock pasta based on as-synthesized powders and a mixed solution of ethyl cellulose and α-terpineol was used for deposition of thin films by Doctor Blade method, obtaining the FTO/β-Ga_2O_3 and FTO/TiO_2(MZ) thin films. The as-obtained structures were assessed for structural, optical, and morphological properties by X-ray diffraction, Ultraviolet-visible spectroscopy and SEM microscopy. The electrochemical properties were investigated by EIS and CV in 1M Na_2SO_4 supporting electrolyte at scan range -0.3 V/SCE and 0.5 V/SCE. These obtained results provide new insights into the development of high-performance and cost-effective FTO-based oxide thin films for electrochemical applications.

1. Introduction

Recently, Ga_2O_3 and TiO_2 has been widely used with excellent results in electrochemical sensors, as cancer treatment, electronics, photocatalysis, photo and electrochemistry because of the good thermal, chemical stability, high crystallinity/surface and low-cost chemical [1-3]. TiO_2 could be obtained in different crystalline phases, known as anatase and rutile (tetragonal), brookite (orthorhombic) and TiO_2-B (monoclinic) [4] by several synthesis methods as, sol-gel [5] , precipitation [6], hydrothermal/ microwave-assisted hydrothermal [7-8] and chemical vapor deposition [9]. On the other way, Ga_2O_3 has a total of five polymorphs phases, α-corundum, β-monoclinic, γ-defective spinel, δ-cubic, and ϵ-orthorhombic structures, the most popular being β-Ga_2O_3-monoclinic phase because is the most thermodynamically stable phase among them [10]. Regarding the synthesis methods, the researchers were used various methods or processes to synthesize Ga_2O_3, the most popular being sol-gel [11], hydrothermal [10], microwave-assisted hydrothermal method [12], contactless technique (CZ) and continuous growth direction perpendicular (EFG method) [13], atomic layer deposition [14], etc. Among all the methods, the main advantages of using microwave-assisted hydrothermal method consists in: a reproducible method due to uniform working conditions; the heating is uniform, efficient and fast; the kinetics of the chemical reactions are accelerated leading to the obtaining of pure crystalline phases; the expenses, times and energy consumption are much decreased in comparison to other methods; the tools are simple to use and maintain. Our research group previously obtained other structures using the microwave-assisted hydrothermal method, some composite structure based on Ti-TiO2-rGO suitable for electrochemical application [7]. The progress and novelty of this work consisted of the comparative evaluation of the thin films

based on FTO/β-Ga$_2$O$_3$ and FTO/TiO$_2$(MZ), respectively, obtained by a simple and effective Doctor Blade method.

2. Experimental

2.1.Reagents

Synthesis reagents as follows, gallium (III) nitrate hydrate (Ga (NO$_3$)$_3$x H$_2$O), titanium issopropoxide (TTIP, 98%), alpha-terpinol, ammonium hydroxide (NH$_4$OH), ethyl cellulose (EC), polymer Pluronic 123(P$_{123}$), nitric acid (HNO$_3$) and ethyl alcohol were purchased from Sigma-Aldrich Company and used without any pre-treatment.

2.2.Development of the FTO/β- Ga$_2$O$_3$ and FTO/TiO$_2$ (MZ) thin films

The schematic representation for development of FTO/β-Ga$_2$O$_3$ and FTO/TiO$_2$(MZ) thin films is illustrated in Figure 1. As shown, the synthesis protocol consists in two stages: the obtaining of the β-Ga$_2$O$_3$ and TiO$_2$(MZ) powders and deposition by Doctor Blade method on FTO conductive glass.

(a)

(b)
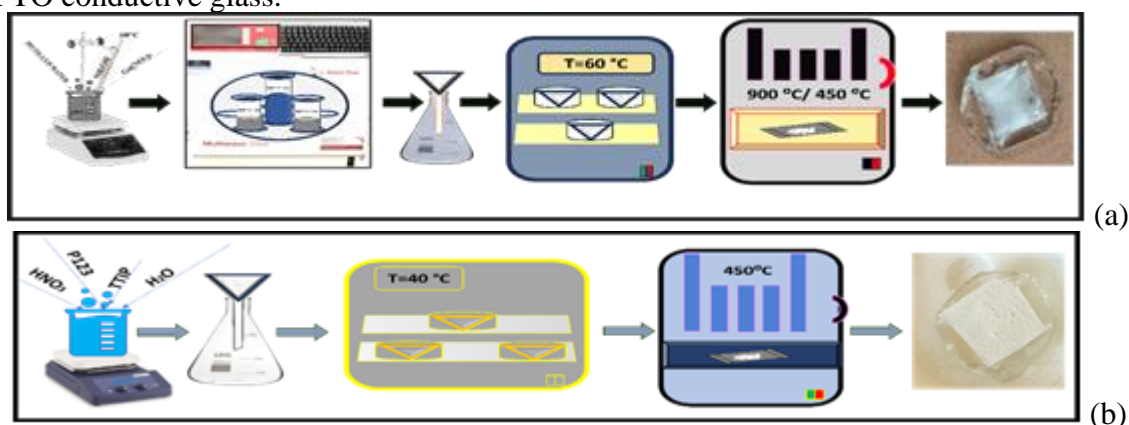
Figure 1. *Schematic representation of the synthesis process for FTO/β- Ga$_2$O$_3$ (a) and FTO/TiO$_2$(MZ) (b)*

2.2.1. Obtaining of β-Ga$_2$O$_3$ powder: The synthesis of GaOOH nanorods was carried out by microwave-assisted hydrothermal method. Briefly, an aqueous solution consisting an amount of Ga(NO$_3$)$_3$xH$_2$O was continuous stirring for 3 hours at 60°C. Afterwards, the homogenous solution was introduced into a Teflon autoclave with 75% fullness degree in a microwave-assisted hydrothermal reaction (*Anton Paar Multiwave 3000 Microwave Digestion Oven, USA*), at a temperature of 180°C for 1 hour. Finally, after the system cooling the as-obtained powders were washed with distilled water and dried at 60° C for 6 hours. The washed samples were calcinated in oven at 900° C for 3 hours to obtain β- Ga$_2$O$_3$ powders.

2.2.2. Obtaining of TiO$_2$(MZ) powder: The TiO$_2$(MZ) powder consists of mixing 10 mL of TTIP in an aqueous solution at pH 1 under continuous stirring, followed by addition of the P$_{123}$ polymer that was previously dissolved in ethanol. The final solution was stirred for 4 hours at room temperature. After that, the precipitate was dried at 40°C for 48 hours, and treated in an oven at 400°C for 4 hours.

2.2.3. Fabrication of FTO/β-Ga$_2$O$_3$ and FTO/ TiO$_2$(MZ) films: The as-synthesized β-Ga$_2$O$_3$ and TiO$_2$(MZ) powders were used to obtain stock paste, by mixing an aqueous solution of 0.15 g ethyl cellulose and 1 mL of α-terpineol at a room temperature under continuous stirring for 20 minutes. Finally, an amount of β-Ga$_2$O$_3$ powder, and TiO$_2$(MZ) respectively, was added into the homogenous solution under continuous mixing. In the end, the as-obtained stock paste was

used for film deposition by Doctor Blade method on FTO glass followed by calcination at a temperature of 450 °C for 1 hour.

3. Results and discussion

The morphologies by scanning electron microscopy (*SEM, FEI Inspect S model, Eindhoven, The Netherlands*) of the as-obtained films are presented in Figure 2. As observed in Figure 2a, the SEM morphology shows an agglomeration of particles and the shape as nanorods for the FTO/β-Ga$_2$O$_3$ film, formed with a slender cocoon-shaped[14]. Instead, for the FTO/TiO$_2$(MZ) the images shows that shows that the mesoporous TiO2 has a well-defined spherical shape and numerous nanoparticles are present on the rough surface. Both the as-obtained films are homogenous, uniform and cracks-free.

(a)　　　　　　　　　　　　　　　　　　　(b)
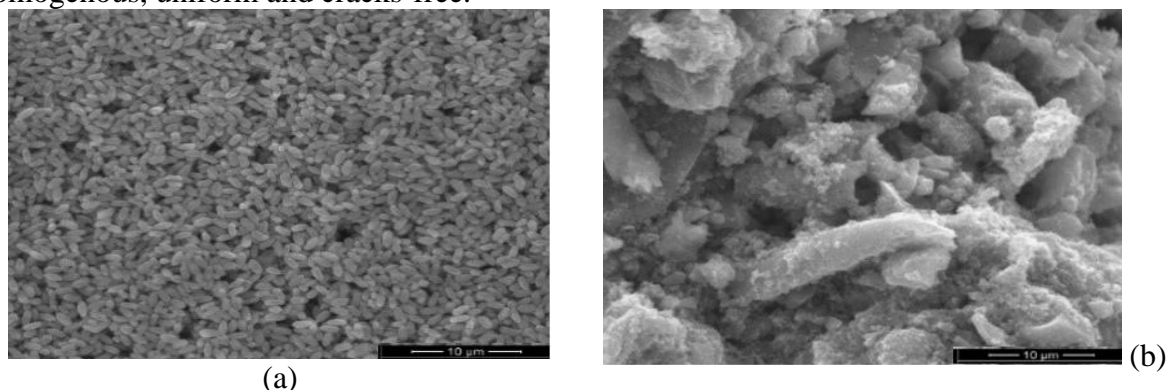
Figure 2. SEM morphologies for a) FTO/β-Ga$_2$O$_3$ and b) FTO/TiO$_2$(MZ) films

For the structural investigations, X-ray diffraction analysis (*XRD, PANalyticalX'Pert PRO MPD Diffractometer, Almelo, The Netherlands*) was used, the X-ray patterns for both β- Ga$_2$O$_3$ and TiO$_2$(MZ) powders are presented in Figure 3. It can be seen the presence of a strong peaks at value of *2theta*: 30.49º, 31.73º, 33.46º, 35.17º, 37.38º, 38.39º and 64.67º (JCPDS 01-075-0573) confirming the monoclinic crystalline phase of β-Ga$_2$O$_3$ sample (Figure 3a). The anatase-TiO$_2$ phase is also confirmed by the presence of strong peaks at *2theta*: 25.35º, 37.93º, 48.10º and 55.29º (JCPDS 00-002-0387) (Figure 3b).

(a)　　　　　　　　　　　(b)
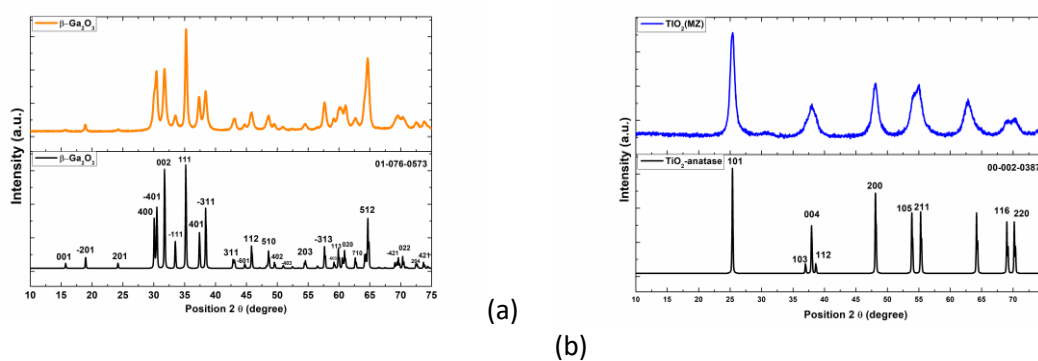
Figure 3. X-ray patterns for as-synthesized powders β-Ga$_2$O$_3$ (a) and TiO$_2$(MZ) (b)

The structural properties of the powders are confirmed by the optical analysis performed by UV-visible spectroscopy (*PerkinElmer Lambda 950 UV/Vis spectrophotometer, Shelton*) in the range of 200–800 nm for as-obtained FTO/β-Ga$_2$O$_3$ and FTO/TiO$_2$(MZ) films. For both samples the strong absorption is in the UV region, respectively for FTO/β-Ga$_2$O$_3$ the corresponding wavelength was about 220 nm, with an estimated band gap of 4.92eV calculated with *Tauc* method, which is in accordance the literature data [15]. For FTO/TiO$_2$(MZ) film the absorbance is slightly increased to 350nm, with a bandgap value of about 3.48eV [16,17].

(a)   (b)
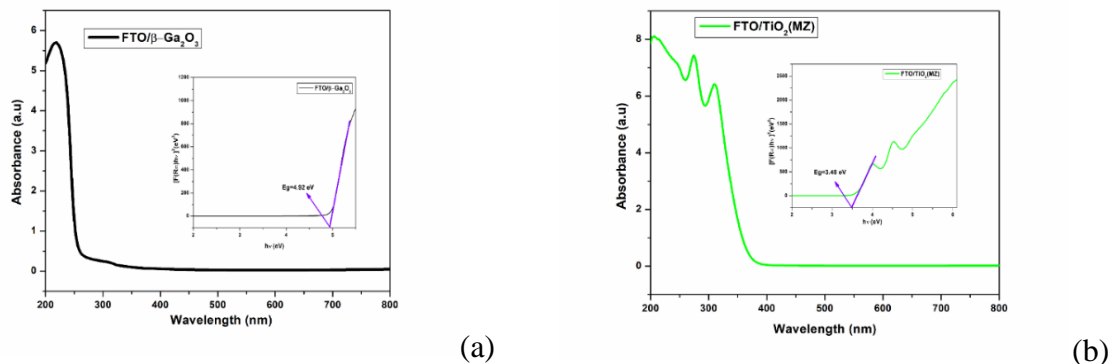
Figure 4. UV-Vis spectra and band-gap calculation using the *Tauc* method for as-obtained films

The electrochemical behavior of FTO/β-Ga$_2$O$_3$ and FTO/TiO$_2$(MZ) was investigated using cyclic voltammetry (Figure 5) with a potential window range of -0.3 to 0.5 V in 1M Na$_2$SO$_4$ electrolyte support, where the measurements were conducted at a scan rate of 5, 10, 20, 50, 100 mV s^{-1}. For both as-obtained films based on the CV measurements, the current increased with higher scan rates indicating the capacitive nature of the films.

(a)   (b)
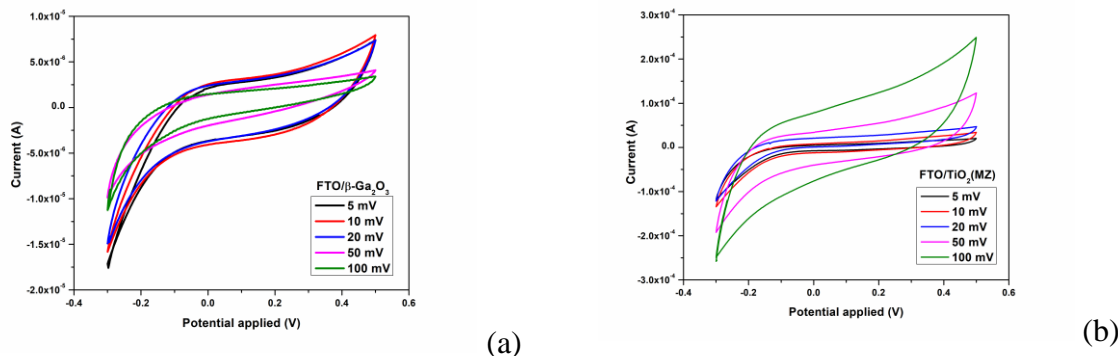
Figure 5. Cyclic voltammograms of supporting electrolyte for the FTO/β-Ga$_2$O$_3$ (a) and FTO/TiO$_2$(MZ) (b) at different scan rates

Electrochemical impedance spectroscopy (EIS) over a frequency range of 0.1 Hz to 10.000 Hz, with an amplitude of 0.01 V, using a three-electrode cell was recorded for both as-obtained films (Figure 6). Therefore, the semicircle portion diameter is a demonstration of the charge transfer resistance FTO/TiO$_2$(MZ) films and the straight line represents the Warburg impedance for the samples (Randles circuit).

(a)

(b)
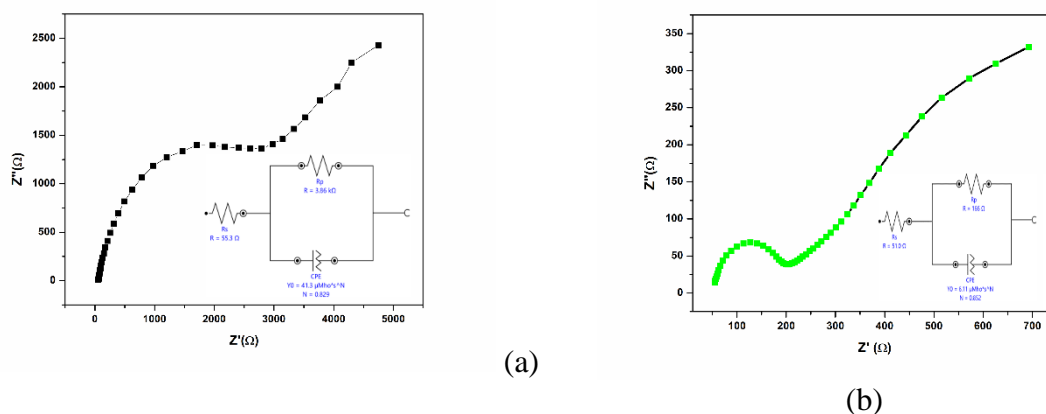
Figure 6. Nyquist plots of as-obtained (a) FTO/β-Ga$_2$O$_3$ and (b) FTO/TiO$_2$(MZ) films

4. Conclusion

Thin films based on FTO/β-Ga_2O_3 and FTO/TiO_2(MZ) were successfully achieved by a simple and effective Doctor Blade method. Also, the β-Ga_2O_3 powder by microwave-assisted hydrothermal method was synthesized. The as-obtained films were structurally, morphologically, and electrochemically characterized by specific methods. The SEM micrographs revealed that the FTO/β-Ga_2O_3 and FTO/TiO_2(MZ) films are uniformly coated and crack-free on the FTO support. These obtained results provide new insights into the development of high-performance and cost-effective FTO-based oxide thin films for electrochemical applications.

5. Acknowledgements

6. References

[1] M. Suarez, A. Arias, J.R. Castillo Saenz, M. Curiel-Alvarez, O. Perez-Landeros, D. Mateos, E. Martinez-Guerra, A. Concha-Balderrama, B. Valdez-Salas, N. Nedev, Ceramics International 48 (2022) 25322-25325.

[2] K. Lan, R. Wang, W. Zhang, Z. Zhao, A. Elzatahry, X. Zhang, Y. Liu, D. Al-Dhayan, Chem, 4 (2018), 2436-2450.

[3] H.J. Bae, T.H Yoo, Y. Yoon, I.G Lee, J.P. Kim, B.J. Cho, W-S. Hwang, Nanomaterials 8, (2018), 594.

[4] M.T. Noman, M.A Ashraf, A. Ali, Environmental Science and Pollution Research, (2018).

[5] C. Lăzău, C. Ratiu, C. Orha , R. Pode, F. Manea, Materials Research Bulletin 46, (2011), 1916-1921.

[6] Z. Wang, S. Liu, X. Cao, S. Wu, C. Liu, G. Li, W. Jiang, H. Wang, N. Wang, W. Ding, Ceramics International 46 [10], (2020)15333–15341.

[7] C. Lazau, M. Nicolaescu, C. Orha, A. Pop, S. Caprarescu, C. Bandas, Coatings, 12, (2022), 1805.

[8] C. Bandas, C. Lazau, M. Nicolaescu, C. Orha, A. Pop, S. Căprărescu, Chapter 2 Current Topics and Emerging Issues in Materials Sciences Vol. 1, Print ISBN: 978-81-19217-34-2, eBook ISBN: 978- 81-19217-35-9.

[9] I.F. Mironyuk, L.M. Soltys, T.R. Tatarchuk, Kh.O. Savka, Review, 21, (2020), 462-477.

[10] N. Badiei, A. Tarat, L. Li, AIP Advances 12, (2022), 085118.

[11] Y. Kakubun. K. Miura, F. Endo, S. Makagomi, Appl. Phys. Lett 90 (2007) 031912.

[12] N.C. Gatsi, G.H. Mhlongo, N. Moloto, R.M. Erasmus, P. Mashazi, T. Nyokong, O.M. Ntwaeaborwa, Materials Today Comunications, 33, (2022), 104808.

[13] X T Tao, J. Semicond., 40, (2019) 010401.

[14] F.K Shan, G.X Liu, W.J. Lee, G.H. Lee, I.S. Kim B.C. Shin, Appl.Phys., 98, (2005) 023504.

[15] L.S. Reddy, Y.H. Ko, J.S. Yu, Nanoscale Research Letters 10 (2015) 364.

[16] K.V. Vinutha, K.B. Naveen Kumar, M.K. Tejas, B. Jai Kumar, D. Sumanth Kumar, H.M. Mahesh, Imperial Journal of Interdisciplinary Research, 2 (2016).

[17] N. Santhosh, K. B. Bhojanaa, P. Vijayakumar, M. Senthil Pandian, P. Ramasamy, A. Pandikumar, Journal of Materials Science: Materials in Electronics 31 (2020), 3910–3923.

ASSESSMENT OF Y_2SiO_5:Pr^{3+} COMPOUND TOXICITY ON *E. coli*

Cristina Mosoarca[1,] **Radu Banică**[1,] **Vetési Ramona**[2,] **Željka Antić**[1,3,] **Miroslav D. Dramićanin**[1,3]

[1]National Institute of Research and Development for Electrochemistry and Condensed Matter, INCEMC, Timisoara, Romania
[2]Water Quality Control Laboratory, Aquatim S.A., Timisoara, Romania
[3]Centre of Excellence for Photoconversion, Vinča Institute of Nuclear Sciences - National Institute of the Republic of Serbia, University of Belgrade, Belgrade, Serbia
e-mail: m.crristina@gmail.com

Abstract

In this study, the characterization of the Y_2SiO_5:Pr^{3+} material and microbiological toxicity tests are presented. The sample was characterized by XRD [1], PL spectroscopy [1] and FT-IR. Microbiological assays having the purpose to evaluate the material toxicity effect on bacteria were conducted on *Escherichia coli* ATCC 8739.

Introduction

Ultraviolet light is a non-chemical disinfection method that employs extremely rapid physical light energy to eliminate microorganisms. UV radiation at 254 nm effectively destroys the DNA of microorganisms [1,2]. In the food industry [2], UV light is widely used for antimicrobial purposes, including the disinfection of water, air, food preparation surfaces, and containers. UV light leaves no residues, is not subjected to legal restrictions, and does not require extensive safety equipment. Given the rising prevalence of MRSA bacterial infections, there is a need to explore novel approaches for producing and maintaining aseptic surfaces. One way to produce UVC radiation is by utilizing UC materials that generate light in the germicidal spectrum [1,3]. These materials have the property of amplifying the energy of the photons emitted when illuminated with mono- and polychromatic light [4]. Spectroscopic studies for this type of material are generally conducted using laser radiation as the excitation source [5]. Therefore, the evaluation of the composite material's resistance to heating needs to be studied. This paper presents the FT-IR characterization of Y_2SiO_5:Pr^{3+}, and toxicity assays on the compound using the reference strain *E. coli* ATCC 8739.

Experimental

The Y_2SiO_5:(0.5-1.5) mol% Pr^{3+} sample was synthesized using a Pechini-type polymerized complex route. FT-IR spectra were obtained on a Vertex70 instrument from Bruker using KBr pellets. Specific culture medium for E. coli and coliform bacteria, Chromocult® Coliform Agar, prepared as per the manufacturer's instructions, was used. The experiments were conducted using the reference strain E. coli ATCC 8739, with a concentration of 5.8 x 10³ CFU per pellet. The strain was hydrated for one hour in 10 ml of peptone water prior to testing. E. coli bacterial suspension and a mixture of Y_2SiO_5:Pr^{3+} and bacteria was inoculated on Petri dishes and incubated for 24 hours at 37°C. The microbiological experiments were performed in duplicate.

Results and discussion

The XRD and photoluminescence characterization was presented in our previous work [1]. The FTIR spectrum, figure 1 a, shows the lower peaks positioned at about 455 cm^{-1} corresponding to Si–O bending modes. The peak at 580 cm^{-1} have been assigned to Si–O

symmetric stretching mode. The band at 1509 cm^{-1} and 1629 cm^{-1} could be attributed to Pr–O vibrations. The bands at 860–1020 cm^{-1} confirm the presence of the SiO_4 group. The broad band with a maximum at 3434 cm^{-1} is due to the adsorption of water on the oxide material. Several other unidentified peaks can be observed in the spectrum.

a)

b)

c)

d)
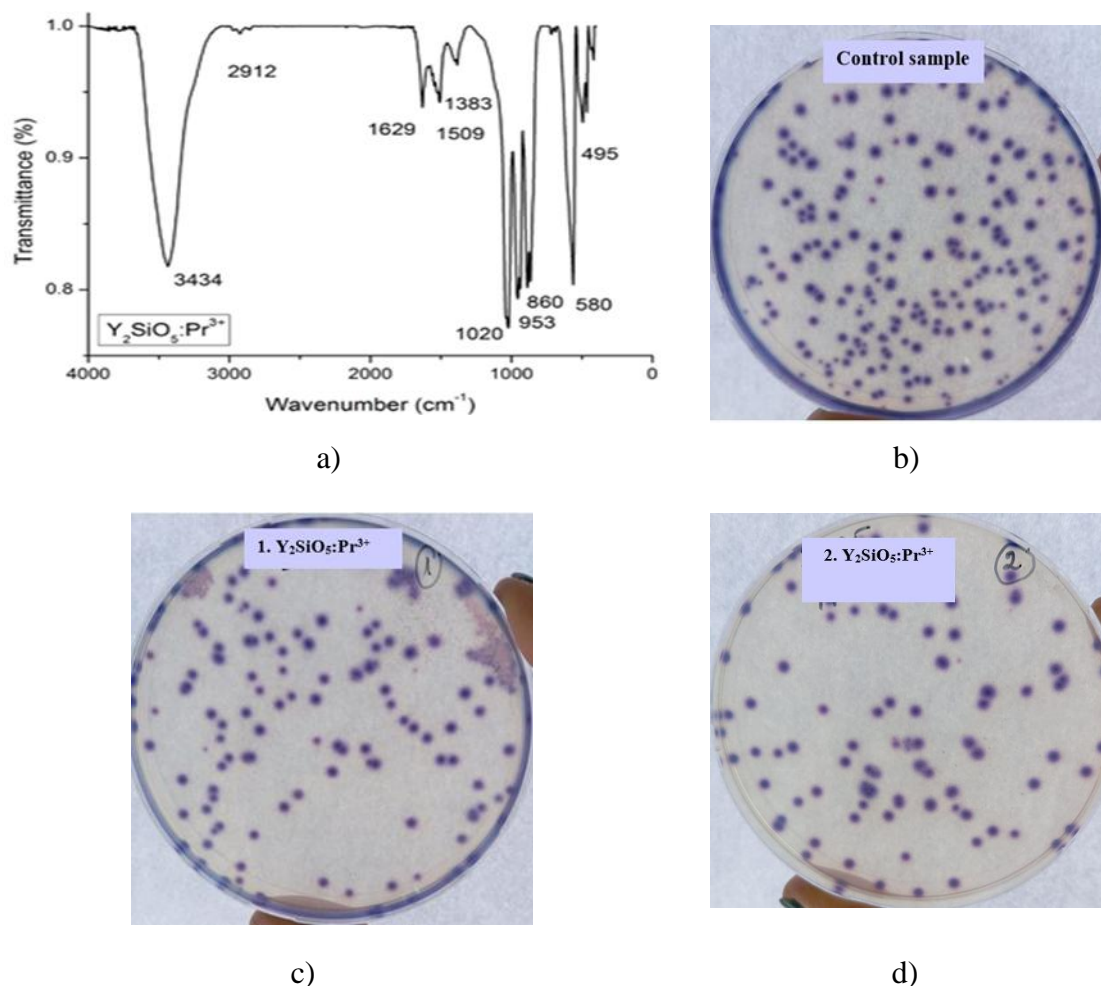
Figure 1. a) FTIR spectrum of Y_2SiO_5:Pr3+ compound and images of plates inoculated with *E. coli* (purple being the specific color of these colonies on Chromocult medium): b) control; c) mixed with Y2SiO5:Pr3+; d) duplication of previous.

Microbiological assays were carried out using the reference strain *E. coli* ATCC 8739 and Chromocult® Coliform Agar, streaking was conducted using the flooding technique with 0.6 ml of the aqueous solution on plates. After the incubation period (24 hours), macroscopic cultures are observed to determine the growth rate as shown in figure 1 b, c, d, the control sample exhibited a larger number of CFU compared with the sample mixed with our compound. The control sample, after counting had a total number of 219 CFU, while the first and second sample, both containing the bacterial solution and 6 mg of Y_2SiO_5:Pr^{3+} each, had a 53% decrease in the number of CFU. In the plate culture method, there may be toxicity upon contact with the substance, which is present at a relatively high concentration. Although, in the plate culture method, colony growth is limited by direct contact with the solid on the surface of the culture medium, the toxicity of our compound was clearly detected. This demonstrates the possibility of obtaining surfaces with germicidal effects upon contact, even in the absence of excitation with visible light.

Conclusion

$Y_2SiO_5:Pr^{3+}$ compound synthesis was successful, exhibiting UVC light emission [1] under visible light excitation. $Y_2SiO_5:Pr^{3+}$ exhibited a noticeable bacterial growth inhibition upon *E. coli* ATCC 8739.

Acknowledgements

References

[1] R. Banică, Ž. Antić, M.D. Dramićanin, C. Moșoarcă, M.I. Iorga, TIM 24 Physics Conference, (2024), Timisoara, Romania.
[2] X. Fan, R. Huang, H. Chen, Trends Food Sci Technol. 70 (2017) 9–19.
[3] N. Kandoth, S. Barman, A. Chatterjee, S. Sarkar, A. K. Dey, S. K. Pramanik, A. Das, Adv. Funct. Mater. 31 (2021) 2104480.
[4] S. He Guang, L.S. Tan, Q.D. Zheng, P.N. Prasad, Chem. Rev. 108 (2008) 1245.
[5] E.L. Cates, M. Cho, J. H. Kim, Environmental science & technology, (2011)

CONTROL OF *CACOPSYLLA PYRI* USING CHLORANTRANILIPROLE AND DELTAMETHRIN

Đura Nađ[1], <u>Antonije Žunić</u>[1], Dušan Marinković[1], Vojislava Bursić[1], Gorica Vuković[2], Bojana Špirović Trifunović[3]

[1]*University of Novi Sad, Faculty of Agriculture, Trg Dositeja Obradovića 8, Novi Sad, Serbia*
[2]*Field Test, Vinogradarska 150b, Belgrade, Serbia*
[3]*University of Belgrade, Faculty of Agriculture, Nemanjina 6, Zemun, Serbia*
e-mail: djuranadj01@gmail.com

Abstract
During the 1960s, the pear psyllid (*Cacopsylla pyri*) became the most significant pest of pear in many European countries. This pest is particularly problematic in intensive pear orchards due to its rapid development of resistance to insecticides and its production of large amounts of honeydew, which complicates control efforts. Changes in production technology and orchard structure led to the emergence of ecologically unstable agricultural systems that favored the development of R-selected organisms, including the pear psyllid. Attempts to control this pest using insecticides showed limited effectiveness, prompting research to focus on their application strategies. Therefore, a comprehensive strategy that involves novel insecticides and developing more effective control methods is necessary to reduce the impact of this pest on pear production. In this article susceptibility of *C. pyri* to chlorantraniliprol and deltamethrin was investigated in order to assess their efficacy. Experiments were conducted in accordance with standard OEPP/EPPO methods, in field trials on test site in the Republic of Serbia (Kula), during 2021. Results of the field trials indicate good efficacy for all variants in pear psyllid control in pear orchards. The high efficacy ranging from 86 to 93%, was achieved 7 and 14 days after treatment, for both insecticides. Based on the obtained results it can be concluded that the high efficacy of the researched insecticides is a good indicator of *C. pyri* susceptibility in pear orchards.

Introduction
Numerous studies conducted over many years for control of *C. pyri* have primarily focused on the use of insecticides. However, over time, it has become evident that pear psyllid rapidly develop resistance to the used insecticides, and due to the large amount of honeydew produced by the insects, these treatments do not yield satisfactory results [1]. For these reasons, scientific and professional attention is now directed toward finding more effective methods for controlling *C. pyri*. The pear psyllid represents a pest of significant economic importance for pear orchards Serbia due to the direct damage and its role as a vector for certain pear pathogens. This pest has multiple generations, a high reproductive potential, and lives either hidden or semi-hidden, regularly multiplying. Unfortunately, natural predators, parasitoids, and disease agents do not significantly reduce its population.
The pear psyllid inflicts both direct and indirect damage. Its larvae (Figure 1) and adults feed on young leaves, buds, and fruits by sucking sap. Their intensive feeding can lead to leaf and bud drop, disrupting assimilation and affecting shoot growth [2, 3]. The basic strategy of *C. pyri* suppression deeply relies on the use of chemical insecticides with different mechanisms of action, but with a large number of generations, it makes this pest very difficult to control. It should be taken into account that pear psyllid very easily develops resistance to insecticides, so it must be properly and timely applied [4].

Figure 1. Larvae (L4) of *Cacopsylla pyri on pear leaf*

Experimental

In order to determine the efficacy of chlorantraniliprole and deltamethrin in the management and control of pear psyllid (*C. pyri*) in pear orchards, the experiments were set up at site Kula (45°38'27.8"N; 19°30'35.7"E) which is located in Vojvodina province, Serbia. At the time of treatment (2021) the orchard was 12 years old, with the represented pear cultivar variety „Williams". For the biologIcal efficacy, experimental design and data analysis standard OEPP/EPPO methods PP 1/44(2) PP 1/152(4) [4, 5] were used. Foliar treatments were performed using a back sprayer with a water consumption of 1 000 L/ha. The preparations based on the active substance chlorantraniliprole (Coragen SC, a.i. 200 g/L) and deltamethrin (Decis EC, a.i. 25 g/L) were applied in a concentration of 0.02% and 0.05%, respectively. Preparations were applied before flowering (phases 56–60 BBCH scale), at the time of emergence of L1 grade larvae. The number of larvae aged L1–L3 and L4–L5 was observed visually on the outside of the tree, slightly before treatment in order to review the abundance of *C. pyri* larvae and determine timely treatment. During the experiment, three observations were performed (slightly before treatment, seven and 14 days after treatment). Field trial results were presented as the absolute and mean values for the number of larvae, standard deviation from the average values (SD), the efficacy according to Henderson-Tilton (1955) and statistically analyzed by an ANOVA and the Fisher LSD test for the confidence interval of 95%, in the statistical program R (version 4.1.0).

Results and discussion

Controlling *C. pyri* can be quite challenging due to its resistance to many insecticides. However, both chlorantraniliprole and deltamethrin have shown good effectiveness in managing this pest. Based on experiments conducted during 2021, the number of larvae of the pear psyllid aged L1–L3 immediately before treatment was at the same level of significance in all variants and it ranged from 31–39.5, while the number of L4–L5 larvae was also at the same level of significance in all variants and ranged from 17–18.0.

Seven days after treatment (Table 1), the number of larvae of pear psyllid aged L1–L3, in all variants was significantly reduced compared to the control variant and the efficacy ranged from 86 to 89.5%. The same can be concluded for the L4–L5 aged larvae, where the efficacy of the applied preparations was 89.5% to 93.2%. Two weeks after treatments, the number of L1–L3 larvae was significantly lower in all variants compared to the control, in both localities. The preparation based on delzsmethrin showed the lower efficacy in relation to chlorantraniliprol, and it ranged from 90.3–91.3%. Chlorantraniliprol showed slightly higher efficacy ranging from 90.7–91.8% for all larval stages.

Table 1. The number of *Cacopsylla pyri* larvae 7 and 14 days after treatment (Kula, 2021)

Insecticide	7 days				14 days			
	L_1-L_3		L_4-L_5		L_1-L_3		L_4-L_5	
	x±SD	E(%)	x±SD	E(%)	x±SD	E(%)	x±SD	E(%)
chlorantraniliprole	3.0±0.9[b]	89,5	1.7±0.6[b]	93.2	3.5±0.5[b]	90.7	2.0±0.9[b]	91.8
deltamethrin	5.7±1.3[b]	86.0	3.2±0.5[b]	89.5	3.2±0.7[b]	90.3	2.5±1.3[b]	91.3
Control	41.2±7.8[a]	-	23.7±2.9[a]	-	50.5±9.6[a]	-	25.2±3.4[a]	-
LSD	6.5		4.7		5.9		3.2	

*E-efficacy; LSD- Fisher least significance diference test; a,b- significant difference

Conclusion

The high efficacy of chlorantraniliprol and deltamethrin was achieved at Kula locality 7 and 14 days after treatment during 2021 field trials. According to the performed tests and the obtained results on the performance evaluation of insecticides for the control of pear psyllid (*C. pyri*) in Serbian pear orchards (locality Kula) it can be concluded that there are obvious significant differences in efficiency that largely depend on the larval stage of the insect and also it can be noted that high sensitivity of pear psyllid populations depends on the applied insecticides. The results of our experiments indicate that chlorantraniliprol and deltamethrin have the potential for the significant suppression of *C. pyri* populations in pear orchards.

Acknowledgements

References

[1] D. Jerinić-Prodanović, L. Protić, L. Mihajlović, Pes & Phytomed., 25 (2010) 29.
[2] F. Erler, Phytoparasitica, 32 (2004) 295.
[3] L. Sigsgaard, P. Esbjerg, H. Philipsen, J. Fruit & Ornam. Plant Res., 14 (2006) 89.
[4] E. Pasqualini, S. Civolani, G. Corelli, Bull. Insect. 55(2002) 39.
[5] OEPP/EPPO PP 1/152(4) – Design and analysis of efficacy evaluation trials. Bulletin 42 (2012) 367.
[6] OEPP/EPPO PP 1/44(2) – Cacopsylla spp.: Efficacy evaluation of plant protection products. European and Mediterranean Plant Protection Organization, 3 (2004) 64.

Cu₂O/CuO(NW) FLEXIBILE SUPERCAPACITOR ELECTROD FABRICATD ON COPPER MASH

Mircea Nicolaescu[1], Mina-Ionela Morariu (Popescu)[1,2], Narcis Duţeanu[2], Iosif Hulka[3], Corina Orha[1], Carmen Lăzău[1], Cornelia Bandas[1],

[1]*Department of Condensed Matter, National Institute for Research and Development in Electrochemistry and Condensed Matter Timisoara, 300224 Timisoara, Romania*
[2]*Department of Applied Chemistry and Engineering of Inorganic Compounds and Environment, Politehnica University of Timisoara, 300223 Timisoara, Romania*
[3]*Research Institute for Renewable Energies, Politehnica University of Timisoara, 300501 Timisoara, Romania*
e-mail: nicolaescu.mircea13@yahoo.com

Abstract

Recent research highlights the potential of transition metal oxides like MnO_2, NiO, Co_3O_4, and Fe_3O_4 as efficient, low-cost, and environmentally stable electrode materials for energy storage applications [1]. Copper oxides played an important role in this advancement in the research for advanced materials for energy storage applications. The supercapacitors-based CuO and Cu_2O are researched due to their affordability, lower toxicity, and high theoretical capacity [2]. One of the simple approaches for producing a supercapacitor electrode based on copper oxides is to use metal foil both as a metal contact and as a precursor in the formation of the metal oxide[3]. For integration in advances application, the weight is one of most important factors for that utilization of cooper mash is one of most promising approaches for this supercapacitor application. Over time, different methods of obtaining copper-based oxide structures on Cu mesh was find. In our research approach we used thermal oxidation in other to synthesis $Cu_2O/CuO(NW)$ on copper mash surfaces[4].

This metal/oxide composite electrode presented a good supercapacitor behaver. Furthermore, the supercapacitor electrode establishes a flexible supercapacitor behaver, and for that, these electrodes can be incorporated in advanced application. In Figure 1a is presented the morpho-structural analysis of the surface of Cu mash following thermal growth of CuO nanowires. In figures 1b, an electrochemical behaver of the influence of capacitance depending on electrode bending from CV analysis is presented.
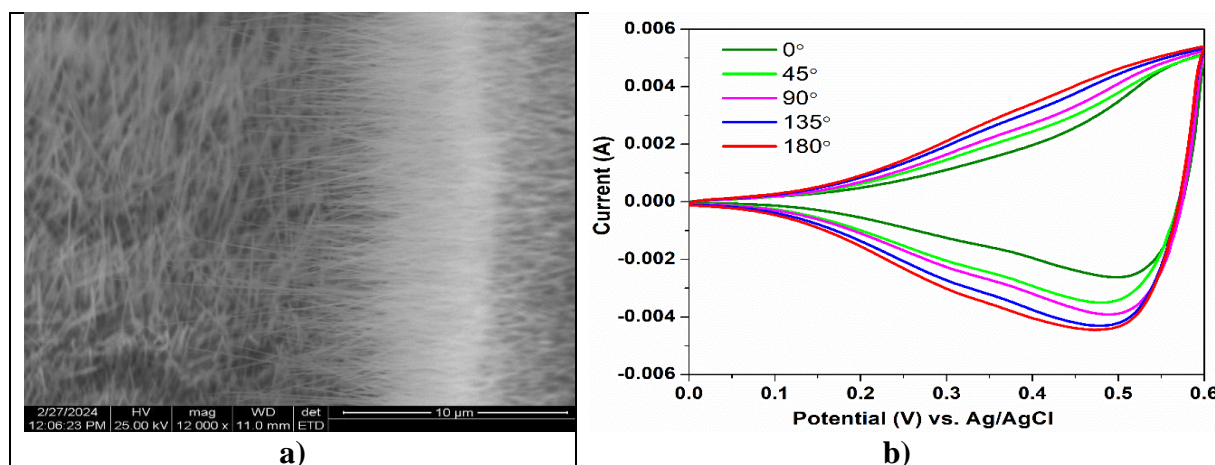
Figure 1a) Morpho-structural analysis of as growth CuO(NW); 1b) CV analysis for capacitance behaver depending on bending angle for Cu₂O/CuO(NW) electrode

References

[1] C. An, Y. Zhang, H. Guo, Y. Wang, Nanoscale Advances 1 (2019) 4644-4658.

[2] X. Du, C. Xia, Q. Li, X. Wang, T. Yang, F. Yin, Materials Letters 233 (2018) 170-173.

[3] D. Majumdar, S. Ghosh, Journal of Energy Storage 34 (2021) 101995.

[4] M.-I. Morariu, M. Nicolaescu, I. Hulka, N. Duţeanu, C. Orha, C. Lăzău, C. Bandas, Batteries 10, (2024).

GENERAL ASPECTS OF THE COAGULATION PROCESS FOR THE REMOVAL OF ARSENIC FROM SIMULATED GROUNDWATER

Adina Pacala[1], Dorian-Gabriel Neidoni[1], Sorina-Claudia Negrea[1], Lidia-Ani Diaconu[1], Anda-Gabriela Tenea[2], Cristina Dinu[2], Mihai Stefanescu[2]

[1]*National Research and Development Institute for Industrial Ecology ECOIND, Timisoara Subsidiary, 300431 Timisoara, Bujorilor u. 115, Romania*
[2]*National Research and Development Institute for Industrial Ecology – ECOIND Bucharest, 060652 Bucharest, 57-73 Drumul Podu Dambovitei, district 6, Romania*
e-mail: adina.pacala@ecoind.ro

Abstract

Removal of As from the simulated groundwater contaminated with arsenic by coagulation process was examined in the present study using Jar-test procedure. Aluminium sulfate, polyaluminium chloride, ferric chloride and ferric sulfate were comparatively tested as coagulants, in order to investigate their performance on arsenic removal.
The experimental study results have showed that all the coagulants tested are found to be effective in removing As from simulated groundwater with initial As concentration of 20 μg L^{-1}, the best results being obtained with ferric chloride.

Introduction

Providing drinking water with safe arsenic levels in the West Region of Romania is a current challenge, due to arsenic's presence in some specific groundwater sources.
Low-cost, easy to use, efficient, and sustainable solutions are needed to supply arsenic safewater to the rural and peri-urban population in the affected areas [1,7].
Various technologies are available for the removal of arsenic from contaminated groundwater using physicochemical methods including oxidation, chemical precipitation or coagulation-flocculation, adsorption, lime softening, ion exchange, and membrane separation processes like reverse osmosis, nanofiltration and electrodialysis [2,3,4].
Coagulation is a simple method for As removal process from contaminated groundwater and most used coagulants are aluminum salts such as aluminum sulfate [$Al_2(SO_4)_3.18H_2O$] and ferric salts such as ferric chloride [$FeCl_3$] or ferric sulfate [$Fe_2(SO_4)_3.7H_2O$]. Ferric salts have been found to be more effective than alum removing As on a weight basis and effective over a wider pH range. With low cost and relative ease of handling in arsenic removal by this process, the coagulants transform dissolved arsenic into an insoluble solid which is precipitated later. Dissolved arsenic may also be adsorbed on the solid hydroxide surface site and be coprecipitated with other precipitating species [4] and the solids can be removed through sedimentation and/or filtration. Optimized operating coagulants doses needed are dependent on the matrix quality of the groundwater source.
Groundwater monitoring is nowadays mandatory in all member state level in European Union [6,7] and our previous studies was focused to act in accordance with the legal provisions of this directive adopted. After an adequate conventional monitoring in groundwater, in the Western Region of Romania, in the catchment areas for abstraction points, or in groundwater sources, of some relevant parameters, substances or pollutants, we concluded that the groundwater sources from the West Region of Romania that require water treatment, are generally characterized by high concentrations of iron and manganese, also arsenic being present in fairly high concentrations and in certain situations exceedances may occur for ammonium [5].

Based on these results, the present study investigates the treatment of a simulated groundwater contaminated with arsenic (20 µg L^{-1}) by using a coagulation process, using Jar-test procedure and aluminium sulfate, polyaluminium chloride, ferric chloride and ferric sulfate as coagulants.

Experimental

Coagulants and water samples

For comparison purposes, commercially available PAC (>19% Al_2O_3, basicity >80,0%, density >1.20 kg/dm^3) was a UNICHEM product (Hungary). Alum stock solution was prepared from liquid aluminium sulphate (approximately 339 g/L $Al_2(SO_4)_3.18H_2O$) obtained from a local Bega water treatment plant. $FeCl_3$ stock solution (approximately 40%) and $Fe_2(SO_4)_3$ stock solution (approximately 40%) were prepared by adding commercial $FeCl_3$ product (Chimcomplex S.A. Borzesti, Romania), respectively $Fe_2(SO_4)_3.7H_2O$ (Kemwater Cristal, Romania).

The simulated groundwater chemistry composition was given by 4 simulated pollutants added: arsenic (20 µg L^{-1}), iron (0,4 mg L^{-1}), manganese (0,2 mg L^{-1}), and ammonium (0,5 mg L^{-1}), into deionized water. After that, this simulated groundwater was stirred for 5 min., at 300 rpm.

Experimental and analytical methods

Coagulation experiments were carried out at room temperature using Jar-test on a six-paddle gang stirrer (Floculator Jar-test, WiteStir JT M6). The 800mL simulated groundwater was added into the 1000mL beaker. A measured amount of coagulant was added by a calibrated pipette (Multipette stream Electronic hand dispenser, Eppendorf, Germany) into the working simulated groundwater under rapid stirring. The simulated groundwater was stirred rapidly at 150 rpm for 2 min after coagulant dosing, followed by slow stirring at 45 rpm for 10 min.

For 20 min after settling, supernatants were collected to measure residual turbidity using a Turbidimeter (HI 88713, HANNA Instruments). Total organic carbon (TOC) was analyzed after filtration through a 0.45 mm membrane and were determined using a TOC Analyzer (Multi N/C 2100 S, Analytik Jena). pH and conductivity were determined on a laboratory pH-meter (Thermo Orion, Cole-Parmer) and conductometer (Starter 3100C, Ohaus). Colour in Hazen units and residual aluminium was measuring using a photometer (Move 100, Merck). The absorbance at 254 nm (due to the Natural Organic Matter/NOM content) was measured with a Spectrofotometer UV-VIS (Specord 205, Analytik Jena), using a 1 cm path length quartz cuvette. The detection technique used for As was Inductively Coupled Plasma Optical Emission Spectrometry (ICP-OES Avio 500, Perkin-Elmer) and the concentration of iron and manganese were determinated with a Spectrofotometer (sAA-280FS, Agilent).

Results and discussion

The comparison of the efficiency of the coagulation-flocculation process by using the 4 types of coagulants (selected according to the data from the specialized literature) was carried out by the Jar-test method, in 2 situations, respectively without and with pre-oxidation with sodium hypochlorite applied as oxidant before coagulation.

Sodium hypochlorite (concentration 14.6%) was added to each sample before the introduction of coagulants, pre-oxidation which was practically carried out under continuous stirring at a speed of 600 rpm for 2 minutes.

Added doses (similarly established with documented literature data) are specified on each work set in Tables 1,2.

Coagulants were added under rapid stirring simultaneously to all samples using the automatic dosing pipette. Three sets of analysis were performed for each type of coagulant.

Table 1: Comparative analysis for quality parameters of AS1 (simulated groundwater) treated with coagulants SA, PAC, $FeCl_3$, $Fe_2(SO_4)_3$.

Parameter, unit	AS1	SA	PAC	FeCl₃	Fe₂(SO₄)₃
Dose, mg/L	-	10	10	10	10
Turbidity, NTU	0,79	0,48	0,24	0,84	0,316
pH	7,54	7,24	7,16	6,206	6,239
Temperature, °C	22	22	22	22	22
Color, grd. Hz	<25	38	<25	32	27
Conductivity, µs/cm	258	228	234	247	249
MTS, mg/L	<2	8,1	11,5	34,8	26,4
UV_{254nm}, cm^{-1}	0,050	0,031	0,023	0,028	0,051
Aluminium dissolved, µg/L	-	<20	<20	-	-
Iron dissolved, mg/L	0,40	0,32	0,268	0,293	0,123
Manganese dissolved, mg/L	0,20	0,20	0,20	0,20	0,20
Amonium, mg/L	0,50	0,50	0,50	0,50	0,50
Arsen, µg/L	20	<2	<2	<2	<2

The application of preoxidation with sodium hypochlorite (doses of 0.1 mg/L NaOCl) also significantly improved the degree of reduction of iron, manganese and ammonium ions (table 2).

Table 2: Comparative analysis for quality parameters of AS1 (simulated groundwater) after peroxidation with 0.1 mg/L NaOCl and treated with coagulants SA, PAC, FeCl₃, Fe₂(SO₄)₃.

Parameter, unit	AS1	SA	PAC	FeCl₃	Fe₂(SO₄)₃
Dose, mg/L	-	10	10	10	10
Turbidity, NTU	0,79	0,32	0,21	0,54	0,286
pH	7,54	6,58	6,75	6,17	5,99
Temperature, °C	22	22	22	22	22
Color, grd. Hz	<25	37	34	30	28
Conductivity, µs/cm	258	266	283	293	298
MTS, mg/L	<2	7,3	9,9	38,9	21,8
UV_{254nm}, cm^{-1}	0,050	0,040	0,032	0,031	0,067

Aluminium dissolved, µg/L	-	33	<20	-	-
Iron dissolved, mg/L	0,40	0,27	0,218	0,18	0,178
Manganese dissolved, mg/L	0,20	0,18	0,16	0,176	0,18
Amonium, mg/L	0,50	<0,028	0,043	0,060	0,040
Arsen, µg/L	20	<2	<2	<2	<2

Conclusion

Concluding this study results:

- Differences were observed between the performances of arsenic removal for the four coagulants compared, ferric chloride proven to be the most effective coagulant.

- However, the degrees of reduction to match the quality of the coagulated and then decanted water within the norms required by the drinking water standards were not achieved, even for iron chloride coagulant applied to treat the simulated selected chemistry matrix for groundwater, with similarity into part of the underground aquifer in the West region of Romania.

- Continue research are needed in finding the best available and cost-effective treatment process to remove As and its co-contaminants, for As-free safe and healthy drinking water.

Acknowledgements

References

[1] Guidelines for drinking-water quality: fourth edition Incorporating the first and second addenda. Chemical fact sheets: Arsenic, World Health Organization (2022).

[2] B.M. Baskan, A. Pala, Desalination, 254(1-3), (2010), 42-48.

[3] E.E.C. Kurz, V.T. Luong, U. Hellriegel, F. Leidinger, T. L. Luu, J. Bundschuh, J. Hoinkis, Water Research, 181, (2020) 115929.

[4] A.M. Ingallinela, V.A. Pacini, R.G. Fernandez, R.M. Vidoni, G. Sanguinetti, J. Environmental Science and Health Part A Toxic/Hazardous Substances & Environmental Engineering, 46, (2011), 1288-1296.

[5] A. Pacala, M. Stefanescu, G.G. Vasile, Proceedings of 29th ISAEP, Szeged, Hungary, (2023), 254-257.

[6] EU, 2020, Directive (EU) 2020/2184 of the European Parliament and of the Council of 16 December 2020 on the quality of water intended for human consumption.

[7] EC, 2014, Directive 2006/118/EC of the European Parliament and of the Council of 12 December 2006 on the protection of groundwater against pollution and deterioration.

ANTIOXIDANT ACTIVITY DETERMINATION OF HOT TRUB EXTRACTS USING GREEN EXTRACTION METHODS

Jelena Pejin*, Teodora Subić, Milana Pribić, Lenka Grubač, Sanja Milošević, Danica Božović, Branimir Pavlić

Faculty of Technology Novi Sad, University of Novi Sad,
Bulevar cara Lazara 1, 21 000 Novi Sad, Serbia
e-mail: jpejin@uns.ac.rs

Finding sustainable solutions for the utilization of agro-industrial residues is essential to reduce their environmental footprint, making it necessary to explore various alternatives for their use. During brewery process, large amounts of organic by-products are produced, such as brewer's spent grains, spent yeast, and hot trub. While in recent years, research has primarily focused on the utilization of spent grain and spent yeast, hot trub remain relatively underexplored despite his considerable potential. Hot trub is a precipitation product of the wort boiling process that includes insoluble hop materials, large amounts of proteins, and phenolic compounds derived from the formation of protein-polyphenol complexes created during wort boiling after adding the hops, and isomerised hop acids. All of these compounds have biological activity such as antioxidant, antimicrobial, antifungal, antiviral, anti-inflammatory, and anticancer, which gives hot trub a great potential for application in the pharmaceutical and food industries.

The aim of this study was to examine antioxidant activity of the extracts from hot trub using novel extraction techniques with special emphasis on green and environmental aspects. Ultrasound-assistant extraction (at 30 ºC for 20 minutes) was performed to obtain the hot trub extracts. The effect of different ethanol concentrations (20, 40, 60, 80, 96%), as an extraction solvent, on antioxidant activity of hot trub extracts was investigated. The antioxidant activity of obtained extracts was tested *in vitro* by DPPH, FRAP, and ABTS tests. The highest ability to neutralize DPPH radicals (DPPH test) had the sample obtained using ethanol concentration of 60% (11.1911 µM TE/g). Also, this ethanol concentration yielded the sample with the highest reducing capacity (21.4113 µM Fe^{2+}/g). The highest ability to neutralize $ABTS^+$ radicals (ABTS test) was found in the sample obtained by extraction with 80% ethanol (31.5927 µM TE/g). This results suggest that using this extraction technique has a significant potential for valorization of hot trub as a brewery stream in isolation of novel extracts with biological activity.

Acknowledgements

IN SILICO EVALUATION OF TETRAHYMENA PYRIFORMIS TOXICITY FOR TWO SERIES OF NOVEL SUCCINIMIDE DERIVATIVES

Damir Pinter[1], Maja Milanović[1], Jelena Kvrgić[2], Dunja Vidović[1], Nataša Milošević[1], Nataša Milić[1], Nebojša Banjac[3]

[1]University of Novi Sad, Faculty of Medicine, Department of Pharmacy, Hajduk Veljkova 3, 21 000, Novi Sad, Serbia
[2]University Business Academy in Novi Sad, Faculty of Pharmacy Novi Sad, Heroja Pinkija 4, 21101 Novi Sad, Srbija,
[3]University of Belgrade, Faculty of Agriculture, Nemanjina 6, 11081 Belgrade-Zemun, Serbia
e-mail: 904009d23@mf.uns.ac.rs

Abstract
An important issue in environmental protection is risk assessment of pollutants and hazardous chemicals including pharmaceuticals. Tetrahymena species are model organism in toxicological assessment of xenobiotics extensively used in various toxicological and environmental studies. Quantitative structure–toxicity relationship (QSTR) models are often applied as green alternatives for predicting the toxicological potential of newly synthesized compounds. In this study 24 newly synthesized succinimide derivatives were evaluated for Tetrahymena pyriformis toxicity in silico. Online tools pkCSM was applied for determining the concentration of the compounds required to inhibit 50% growth of T. pyriformis. Online tools SwissADME and PreADMET were applied to determine the physicochemical descriptors of the analysed compounds. Moreover, the obtained toxicity was associated with the previously quantified lipophilicity of the analysed molecules. All compounds of both analysed series have pIGC50 for T. pyriformis above -0.5 log μg/L indicating their potential aquatic toxicity. The predicted toxicity was positively correlated with molecular weight (p=0.025) and molar and negatively associated with the polar surface area (p=0.005). The toxicity given as pIGC50 was positively correlated with predicted logD values on pH 7.4 (p<0.001), log P (p<0.001) as well as with R_M^0 values obtained with acetone-water mixture (p<0.001) and acetonitrile-water as mobile phase (p<0.001) respectively and negatively associated with the in silico predicted solubility expressed as logS (p<0.001). The toxic effect of the analysed succinimide derivatives increased with the increment of the lipophilicity of the succinimide core by adding more lipophilic substituents and by decrement of their aquatic solubility.

Introduction
Tetrahymena species abundance indicates a healthy aquatic environment. It is used to evaluate the toxic potential of different toxicants, pollutants and contaminants, suggests their cumulative effect and thus it is referred as an indicator of water pollution and a test system for health risk assessment [1]. Succinimide derivatives have exhibited various effects including analgetic [2], anticonvulsive [3], proapoptotic [4], antifungal [5], antibacterial and cytotoxic [6] anticancer [7,8], and also have anticholinesterase and antioxidative activity [9,10]. Two novel series of succinimide derivatives (Table 1) were tested for their antiproliferative activity and are candidates for further studying. In order to compete as drug candidates, except being safe and effective, the molecules are tested also as possible environmental pollutants together with their ability to accumulate in the environment. Assessing the risks of newly synthesized compounds to human health as well as the environmental hazards that a substance may cause is a key point for further safe application. The experimental toxicity evaluation of chemicals is not only time-consuming process with high cost but also can be ethically limited. In silico tools such as

quantitative structure–toxicity relationship (QSTR) models are applied to evaluate the toxic end-points for new or even yet not-synthesized molecules [11]. Thus, in this study 24 newly synthesized compounds were analysed for their Tetrahymena pyriformis toxicity in silico and their potential for aquatic toxicity was associated to their structural changes and physicochemical properties.

Experimental
Twenty-four newly synthesized succinimide derivatives of two series (thirteen from the series C and eleven from the series D, Table 1) were evaluated for their T. Pyriformis toxicity by the free online platform pkCSM (http://biosig. unimelb.edu.au/pkcsm/prediction).

Table 1. The structures of the observed succinimide derivatives
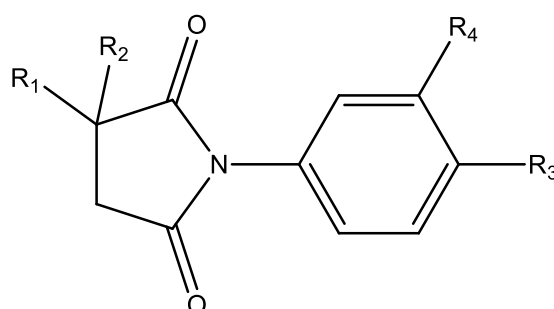
Compound	R_1	R_2	R_3	R_4
C1	-CH_3	-H	-H	-H
C2	-CH_3	-H	-CH_3	-H
C3	-CH_3	-H	-OCH_3	-H
C4	-CH_3	-H	-OH	-H
C5	-CH_3	-H	-COOH	-H
C6	-CH_3	-H	-H	-$COCH_3$
C7	-CH_3	-H	-$COCH_3$	-H
C8	-CH_3	-H	-NO_2	-H
C9	-CH_3	-H	-Cl	-H
C10	-CH_3	-H	-Br	-H
C11	-CH_3	-H	-I	-H
C12	-CH_3	-H	-H	-Cl
C13	-CH_3	-H	-H	-Br
D1	-C_2H_5	-CH_3	-H	-H
D2	-C_2H_5	-CH_3	-OH	-H
D3	-C_2H_5	-CH_3	-OCH_3	-H
D4	-C_2H_5	-CH_3	-COOH	-H
D5	-C_2H_5	-CH_3	-CN	-H
D6	-C_2H_5	-CH_3	-CH_3	-H
D7	-C_2H_5	-CH_3	-NO_2	-H
D8	-C_2H_5	-CH_3	-Cl	-H
D9	-C_2H_5	-CH_3	-Br	-H
D10	-C_2H_5	-CH_3	-H	-Cl
D11	-C_2H_5	-CH_3	-H	-Br

The method is based on the concentration of 1571 compounds which was required to inhibit 50% growth of T. Pyriformis (IGC50). For each compound the pIGC50, which is a negative logarithm of the concentration required to inhibit 50% growth in log μg/L, was predicted.

Values above -0.5 log μg/L are considered to be toxic. All compounds were drawn as 2D in ChemDraw Professional (version 16.0) their Simplified Molecular-Input Line-Entry System (SMILES) specifications were generated in order to use them for further predictions. The free online software SwissADME (http://www.swissadme.ch/index.php) and PreADMET (https://preadmet.bmdrc.kr/adme/) were applied to determine the physicochemical descriptors of the analysed compounds including molecular weight (MW), polar surface are (PSA) molar refractivity (MR), lipophilicity (logP and log D on pH= 7.4) and aqueous solubility (logS, mol/L on pH 7.4). Moreover, the toxicity was related to previously experimentally evaluated lipophilicity of the analysed compounds given as retention constants R_M^0 obtained on thin-layer reversed-phase chromatography with acetone-water and acetonitrile-water mixtures as mobile phases, respectively [12]. The statistical analysis was conducted with OriginPro 8.

Results and discussion

The T. pyriformis toxicity for all analysed compounds is given on Figure 1. All observed compounds have pIGC50 for T. pyriformis above -0.5 log μg/L. The most polar compounds C5 and D4 with carboxylic functional group in their structure however have been predicted with the lowest toxicity levels. The predicted toxicity was positively correlated with molecular weight (adj. r^2=0.172, p=0.025) and molar refractivity (adj. r^2=0.118, p=0.056) respectively, while it was negatively correlated with the polar surface area (adj. r^2=0.271, p=0.005). Lipophilicity obtained both in silico and experimentally had the most significant relations indicating the lipophilicity as one of the most important descriptors for toxicity predictions. Namely, pIGC50 was positively correlated with predicted logD values on pH 7.4 (adj. r^2=0.864, p=3.2×10^{-11}, Figure 2) and log P (adj. r^2=0.506, p=5.92×10^{-5}) respectively, as well as with R_M^0 values obtained with acetone-water mixture as mobile phase (adj. r^2=0.700, p=2.09×10^{-7}) and acetonitrile-water as mobile phase (adj. r^2=0.801, p=2.10×10^{-9}, Figure 3) respectively. The toxicity pIGC50 of the analysed compounds on the other hand was negatively associated with the in silico predicted solubility expressed as logS (adj. r^2=0.680, p=4.30×10^{-7}).
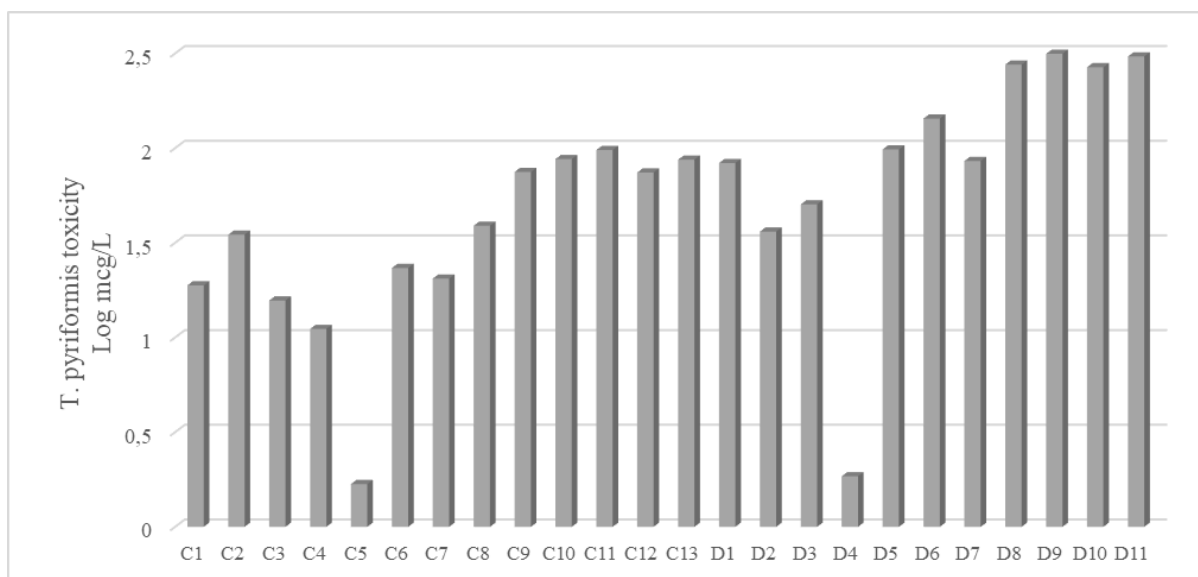
Figure 1. T. pyriformis toxicity of the analysed compounds obtained through pkCSM online tool
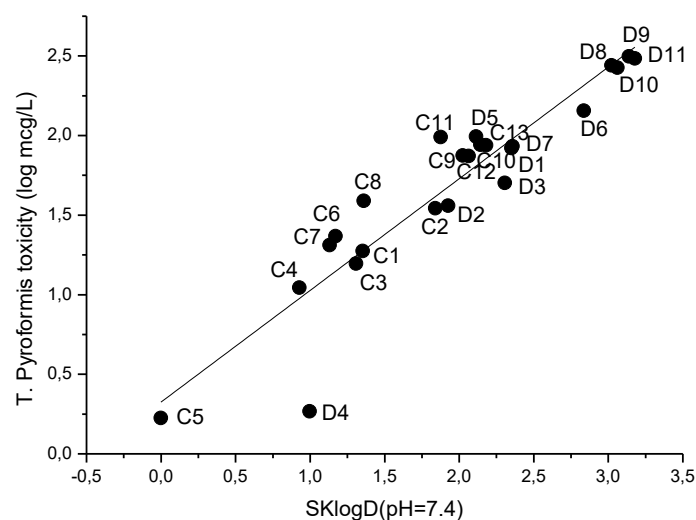
Figure 2. Correlation of T. pyriformis toxicity of the analysed compounds with in silico predicted lipophilicity expressed as logD
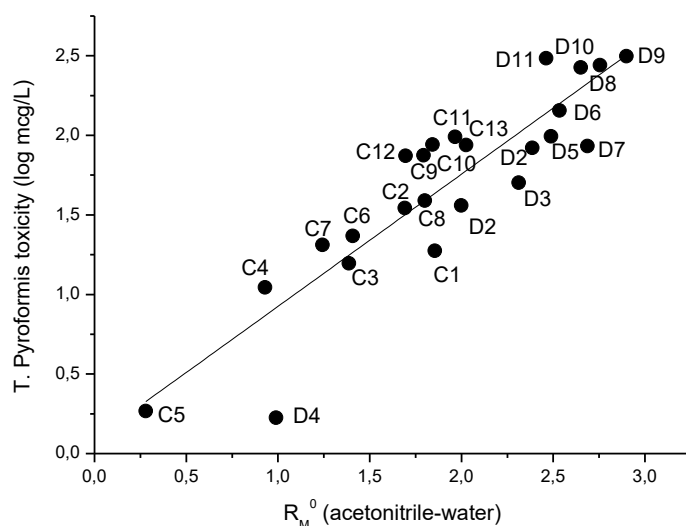
Figure 2. Correlation of T. pyriformis toxicity of the analysed compounds with experimentally obtained lipophilicity expressed as R_M^0

Conclusion

Succinimide derivatives based on QSTR analysis are expected to have pIGC50 for T. pyriformis above -0.5 log μg/L. The calculated pIGC50 values for the analysed 24 succinimide derivates can be positively associated to their lipophilicity obtained both experimentally and predicted in silico as well as negatively associated to their predicted aqueous solubility. The results indicated increased toxic effect of the compounds on T. pyriformis with the increment of their lipophilicity and decrement of their solubility, respectively.

References
[1] R. Maurya, A.K. Pandey. Sci. Total Environ. 741 (2020) 140058.

[2] R. Correa, V. Cechinel Filho, P. Rosa, C. Isolani Pereira, V. Schlemper, R.J. Nunes. Pharm. Sci. 3 (1997) 67–71.

[3] R.R. Goehring, T.D. Greenwood, J.S. Pisipati, J.F. Wolfe. J. Pharm. Sci. 80 (1991) 790–792.

[4] B. Kuran, M. Krawiecka, J. Kossakowski, M. Koronkiewicz, Z. Chilmonczyk. Acta Pol. Pharm. 70 (2013) 459–468.

[5] M. Sortino, A. Postigo, S. Zacchino. Molecules 18 (2013) 5669–5683.

[6] F. Zentz, R. Le Guillou, R. Labia, D. Sirot, B. Linard, A. Valla. Farmaco 59 (2004) 879–886.

[7] E.L. Luzina, A.V. Popov, J. Fluor. Chem. 168 (2014) 121–127.

[8] N. P. Milosevic, V. Kojic, J. Curcic, D. Jakimov, N. Milic, N. Banjac, G. Uscumlic, R. Kaliszan. J. Pharm. Biomed. Anal. 137 (2017) 252-257.

[9] A.J. Guevara-Salazar, M. Espinoza-Fonseca, H.I. Beltrán , J. Correa-Basurto, D. Quintana Zavala, J.G. Trujillo-Ferrar, JG. J. Mex. Chem. Soc. 51 (2007) 222–227.

[10] A. Sadiq, F. Mahmood, F. Ullah, M. Ayaz, S. Ahmad, F. Ul Haq, G. Khan, M. Saeed Jan. 9 (2015) 31.

[11] F. Abbasitabar, V. Zare-Shahabadi. Chemosphere. 172 (2017) 249-259.

[12] S. Kovačević, M.K. Banjac, N. Milošević, J. Ćurčić, D. Marjanović, N. Todorović, J. Krmar, S. Podunavac-Kuzmanović, N. Banjac, G. Ušćumlić. J. Chromatogr A. 1628 (2020) 461439.

QSTR STUDY FOR TWO SERIES OF NOVEL SUCCINIMIDE DERIVATIVES – EVALUATION OF IN SILICO MINNOW TOXICITY

Damir Pinter[1], Nataša Milošević[1], Nataša Milić[1], Jelena Kvrgić[2], Dunja Vidović[1], Nebojša Banjac[3], Maja Milanović[1]

[1]*University of Novi Sad, Faculty of Medicine, Department of Pharmacy, Hajduk Veljkova 3, 21 000, Novi Sad, Serbia*
[2]*University Business Academy in Novi Sad, Faculty of Pharmacy Novi Sad, Heroja Pinkija 4, 21101 Novi Sad, Srbija,*
[3]*University of Belgrade, Faculty of Agriculture, Nemanjina 6, 11081 Belgrade-Zemun, Serbia*
e-mail: 904009d23@mf.uns.ac.rs

Abstract
Fathead minnow (Pimephales promelas) test are applied for the evaluation of aqueous toxicity of xenobiotics. The environmental hazardous effect of newly synthesized compounds and drug candidates can also be evaluated in silico since many quantitative structure–toxicity relationship (QSTR) models are recognized as less expensive alternatives. In this study two series of succinimide derivatives were assessed for Minnow toxicity in silico by applying pkCSM online tool. Minnow toxicity was quantified as logLC50 (mM) value for all analysed compounds whereas LC50 is the concentration of a molecules necessary to cause the death of 50% of the Flathead Minnows. Physicochemical descriptors of the analysed compounds such as molar weight, molar refractivity and polar surface area were determined by the SwissADME online platform, while the lipophilicity (logD, logP) and aqueous solubility (logS) were quantified by the application of PreADMET online tool. The predicted toxicity was correlated to literature experimentally obtained lipophilicity for the observed molecules. The minnow logLC50 for all twenty-four succinimide derivatives was above -0.3 indicating very low acute toxicity. The compounds of the series C in comparison to the series D compounds had statistically significant higher minnow logLC50 (p=0.007) indicating lower toxic potential. The predicted toxicity was negatively correlated with molar weight (p=1.45×10^{-4}) and molar refractivity (p=8.21×10^{-4}) respectively. Minnow logLC50 values were negatively associated with both in silico (logD values on pH 7.4 and logP, respectively, p<0.001 for both relations), and experimentally quantified lipophilicity (R_M^0 values with acetone-water mixture, p<0.001 and acetonitrile-water as mobile phase p<0.001, respectively). Aqueous solubility was positively associated with minnow logLC50 (p<0.001) indicating lower toxicity for more soluble compounds. Despite the higher aquatic solubility, the compounds of the series C are recognized as less toxic molecules in comparison to the compounds of the series D.
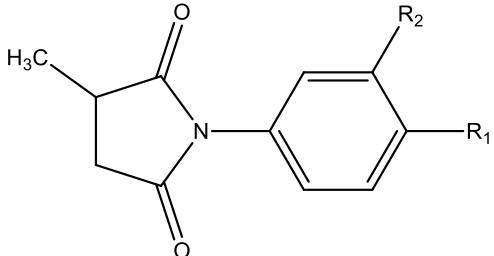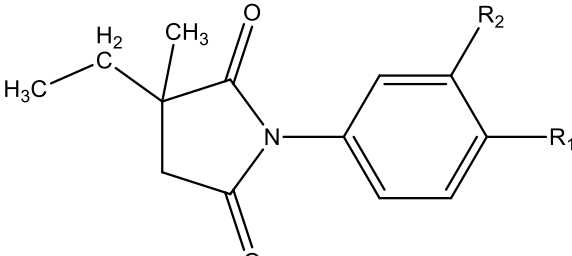
Introduction
Fathead minnow (Pimephales promelas) as a small fish model is applied for risk assessment for various chemicals, xenobiotics and pollutants in the aquatic environment. Lethality test, partial and full life-cycle assays with the fathead minnow are used for the evaluation of aqueous toxicity of new chemicals and are routinely applied for regulatory programs aimed at assessing environmental risks of chemicals. Moreover, minnow is recognized as an excellent model for identification of sensitive life-stages for chemicals, predicting population-level effects and understanding the role of genomics [1,2]. Both natural compounds and synthetic drugs often contain heterocyclic core with succinimide moiety as building blocks [3]. A five-member heterocyclic lipophilic ring containing a nitrogen atom and two carbonyl groups as polar attachments is the core of the succinimides compounds [4]. Substituents with alkyl or aryl

groups attached to the carbon or nitrogen of the succinimides core increase the lipophilicity of the compounds whereas the two carbonyl groups and polar substituents contribute to increased polarity and aqueous solubility [5]. Twenty-four newly synthesized succinimide derivatives from two series (Table 1) are observed as potential drug candidates due to their antiproliferative effect. In order to fully express their potential as drugs, the compounds should be also eliminated as potential environmental hazards. Quantitative structure–toxicity relationship (QSTR) studies allow in silico prediction of toxic end-points for various xenobiotics based only on their structure and molecular descriptors [6]. The Minnow toxicity for two series of succinimide derivatives (Table 1) was evaluated in silico and their logLC50 values were associated to their structural features.

Experimental

Two series of newly synthesized succinimide derivatives (Table 1) were analysed for their Minnow toxicity through the free online software program pkCSM (http://biosig.unimelb.edu.au/pkcsm/prediction).

Table 1. The structures of the analyzed succinimide derivatives

Series C			Series D		
Compound	R₁	R₂	Compound	R₁	R₂
C1	-H	-H	D1	-H	-H
C2	-CH₃	-H	D2	-OH	-H
C3	-OCH₃	-H	D3	-OCH₃	-H
C4	-OH	-H	D4	-COOH	-H
C5	-COOH	-H	D5	-CN	-H
C6	-H	-COCH₃	D6	-CH₃	-H
C7	-COCH₃	-H	D7	-NO₂	-H
C8	-NO₂	-H	D8	-Cl	-H
C9	-Cl	-H	D9	-Br	-H
C10	-Br	-H	D10	-H	-Cl
C11	-I	-H	D11	-H	-Br
C12	-H	-Cl			
C13	-H	-Br			

The method is based on the lethal concentration values (LC50) measurements for 554 compounds where LC50 represents the concentration of a molecules necessary to cause the death of 50% of the Flathead Minnows. For a given compound a logLC50 is predicted and values below 0.5 mM (log LC50 < -0.3) are recognized as high acute toxicity. The Simplified Molecular-Input Line-Entry System (SMILES) specifications were generated with ChemDraw Professional (version 16.0) for all observed compounds after they were drawn as 2D and afterwards were used for further calculations. The free online platform SwissADME (http://www.swissadme.ch/index.php) was used to determine the molecular weight (MW),

polar surface area (PSA) and molar refractivity (MR) of the compounds analysed. The online tool PreADMET (https://preadmet.bmdrc.kr/adme/) was applied to determine the physicochemical descriptors including lipophilicity (logP and log D on pH=7.4) and aqueous solubility (logS, mol/L on pH 7.4). Finally, literature data on the experimentally obtained lipophilicity of the analysed compounds were used for comparison. The experimental lipophilicity was presented as retention R_M^0 values calculated by thin-layer reversed-phase chromatography when acetone-water and acetonitrile-water mixtures were applied as mobile phases respectively [7]. The statistical analysis was performed by the use of OriginPro 8.

Results and discussion

The Minnow toxicity for all twenty-four succinimide derivatives is given on Figure 1. All analysed succinimide derivatives have logLC50 which is far above -0.3 indicating very low acute minnow toxicity. The predicted Minnow toxicity LC50 were statistically significant higher for less lipophilic compounds of the series C in comparison to the series D structures (p=0.007, Figure 2) indicating lower toxicity for the compounds of the series C. Given the fact that the compounds of the C series are more polar and less lipophilic, their permeability through biological membranes is restricted which may be the key factor for limited toxicity in the aqueous environment. The predicted toxicity was negatively correlated with molar weight (adj. r^2=0.465, p=1.45×10^{-4}) and molar refractivity (adj. r^2=0.378, p=8.21×10^{-4}) respectively, while no statistically significant association with the polar surface area (p=0.103) was obsrved. In silico and experimentally quantified lipophilicity was negatively associated with minnow logLC50 values confirming that the more lipophilic compounds have higher toxic potential. Thus, logLC50 was statistically significant correlated to predicted logD values on pH 7.4 (adj. r^2=0.764, p=1.48×10^{-8}) and log P (adj. r^2=0.762, p=1.60×10^{-8}) respectively and also with R_M^0 values obtained with acetone-water mixture as mobile phase (adj. r^2=0.767, p=1.16×10^{-8}, Figure 3) and acetonitrile-water as mobile phase (adj. r^2=0.575, p=1.05×10^{-5}) respectively. The minnow logLC50 values for the analysed compounds had positive correlation with logS values (adj. r^2=0.567, p=1.33×10^{-5}) which indicates increased toxic potential for compounds with lower aqueous solubility.
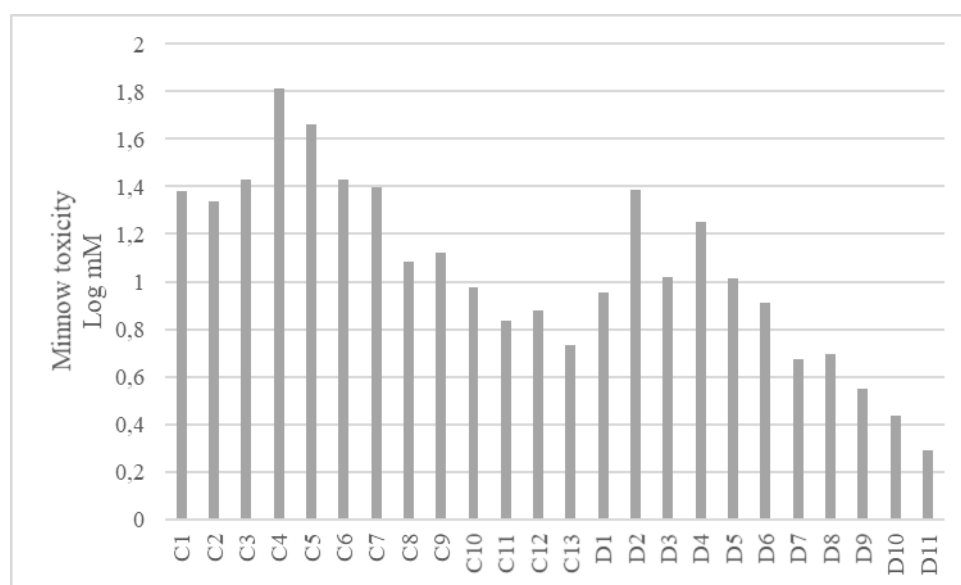
Figure 1. Minnow toxicity of the analysed compounds obtained through pkCSM online tool
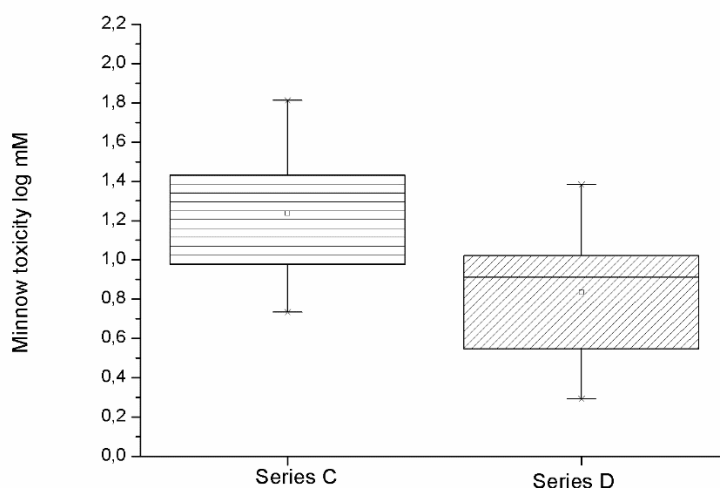
Figure 2. Statistically significant higher minnow LC50 values for compounds of the series C in comparison to series D molecules indicating lower toxicity
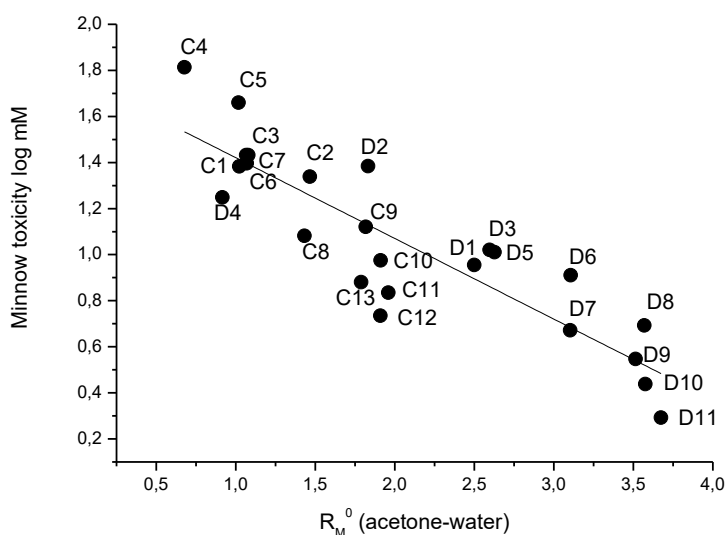
Figure 3. Correlation of Minnow toxicity of the analysed compounds
with experimentally obtained lipophilicity expressed as R_M^0

Conclusion

The QSTR analysis indicated that the analysed succinimide derivatives have minnow logLC50 above -0.3 log mM values suggesting low acute minnow toxicity. The compounds of the series C despite their higher aquatic solubility are less toxic as less lipophilic molecules in comparison to the compounds of the series D.

References

[1] G.T. Ankley, D. L. Villeneuve. The fathead minnow in aquatic toxicology: past, present and future. Aquat. Toxicol. 78 (2006) 91-102.
[2] X. Wu, Q. Zhang, J. Hu. SAR QSAR Environ. Res. 27 (2016) 147-164.

[3] E. Jafari, N. Taghi Jarah-Najafabadi, A. Jahanian-Najafabadi, S. Poorirani, F. Hassanzadeh, S. Sadeghian-Rizi. Res. Pharm. Sci. 12 (2017) 526–534,

[4] B. Bozdoğan, M. Erşatır, O. Demirkol, D. Akbaşlar, E. Sultan Giray. Synth. Commun. 47 (2017) 217–223,

[5] A. Torregrosa-Chinillach, A. Moragues, H. Pérez-Furundarena, E. Gómez-Bengoa R.Chinchilla, G. Guillena. Molecules 23 (2018) 3299.

[6] L. Tarko, M.V. Putz, C. Ionascu, A.M. Putz. Curr. Comput. Aided Drug Des. 10 (2014) 99-106.

[7] S. Kovačević, M.K. Banjac, N. Milošević, J. Ćurčić, D. Marjanović, N. Todorović, J. Krmar, S. Podunavac-Kuzmanović, N. Banjac, G. Ušćumlić. J. Chromatogr A. 1628 (2020) 461439.

DEVELOPMENT OF INNOVATIVE FORMULAS OF VERMOUTH WITH PARTICULAR PROPERTIES

Diana Moigradean[1], Mariana-Atena Poiana[1]*, Liana-Maria Alda[1], Despina-Maria Bordean[1], Daniela Stoin[1], Simion Alda[2], <u>Florina Radu[1]</u>

[1]Faculty of Food Engineering, University of Life Sciences „King Michael I" from Timisoara, Romania, Aradului Street No 119, 300645 Timisoara, Romania
[2]Faculty of Engineering and Applied Technology, University of Life Sciences „King Michael I" from Timisoara, Romania, Aradului Street No 119, 300645 Timisoara, Romania
* corresponding author e-mail: <u>marianapoiana@usvt.ro</u>

Abstract
The aim of the study was to presents practical aspects of the production and characterisation under physico-chemical and sensory aspects of an aromatized white Vermouth wine. Aromatized vermouth wine which is a special wine obtained from basic white wine, sugar, hydroalcoholic macerates and citric acid. A hydroalcoholic maceration of dried herbs, dried fruit, citrus peel and spices was used to prepare the vermouth recipe. The hydroalcoholic macerate represents 2% of the volume of white vermouth prepared. Vermouth is available in a very wide range of varieties, depending on the amount of sugar and alcohol it contains. In terms of sugar content, it can be dry (20 g/L) to very sweet (180 g/L). Alcohol levels range from 14.5 - 20% (v/v). Total acidity is low (2-3.5 g/L H_2SO_4) and volatile acidity is below 0.5 g/L H_2SO_4. The white vermouth obtained in our study has the following characteristics: alcoholic degree 18% (v/v), sugar content 100 g/L and total acidity 4.0 g/L H_2SO_4. The resulting product belongs to the class of flavoured aperitif wines. The information obtained from this study contributes to the extension of knowledge in the field of designing white flavored wine formulations with particular properties.

Introduction
Aromatized wines are also known as aperitif wines and are made from wine with added sugar or must, wine distillate or food alcohol and flavoring substances obtained from various herbs. The Vermouth must be at least 70% wine. Under the current legislation [10], aromatized wines belong to the category of special wines. They are made from must or wine to which special, authorized treatments are applied during or after processing. Aromatized wines have specific characteristics, determined by the technological properties of the raw material and the technology applied during processing [3].
Vermouth is a special wine, aperitif and tonic made from white or red wines, with the addition of alcohol, sugar, herbal macerate and other ingredients [6]. The name comes from the German word "Wermuth" meaning wormwood; the wormwood is the main herb used to make this product [9]. The main characteristics of vermouth are the following: alcoholic strength 16-18% (v/v) and sugar content 40-180 g/L; characteristic bitter herbal aroma. Vermouth can be made from white or red wine, to which rectified ethyl alcohol, sugar syrup, herbal macerate and sometimes citric acid are added [8, 9]. The following conditions are required for the preparation of vermouth: (i) the raw material-wine must be old (2-3 years) and have an alcoholic strength of at least 12% vol; (ii) the sugar must be of good quality, contain a minimum of 99.8% sucrose and have a maximum moisture content of 0.2%; (iii) the alcohol must be rectified and have an alcoholic strength of at least 96% vol; (iv) the citric acid must be crystallized and free from impurities; (v) the plants must be well preserved and free of foreign tastes and odors; (vi) the

equipment must be chemically inert so as not to enrich the wine with toxic or mutagenic compounds [8].

The design of flavored wine types with specific properties is a current concern in the field of producing prototypes with distinct identity. In this respect, the aim of this study consists in the design and characterization under physico-chemical and sensory aspects of a variety of aromatized white wine, of Vermouth type [9].

Experimental

There are two main stages in the production of vermouth: preparation of the wine and auxiliary materials (syrup, macerate, citric acid solution) and production of the technological mixture.

The raw wine must be healthy, moderately alcoholic, not very extractive and low in total acidity. For better preservation, it is recommended that when the wine is not used immediately in the preparation of vermouth, it should be sweetened and alcoholized to near the concentrations of the finished product [5]. The alcohol used in the preparation of vermouth must have an alcoholic strength of not less than 96°, must be free of foreign taste or odor, must not contain furfural and must not contain methyl alcohol. The sugar used to sweeten the vermouth must be white in color, with a gloss and crystals as uniform as possible, dry and not sticky, and must give a clear solution with water, free of extraneous tastes and odors [1]. The quality of the vermouth depends to a large extent on the number and proportion of herbs and spices used in the manufacturing recipe [2].

In order to prepare the vermouth recipe, a hydroalcoholic maceration was conducted using dried medicinal plants, dehydrated fruits, citrus peels and spices, in accordance with the information presented in Table 1.

Table 1. Quantity of plant material (medicinal, citrus, spices) used to obtain the hydroalcoholic macerate

Plant name	Plant parts (peel, leaves, flower)	Weight (g)*
Achillea millefolium	flower	2
Citrus paradisi	peel	20
Artemisia absinthium	stem	20
Citrus limon	peel	10
Syzygium aromaticum	flower	20
Citrus × sinensis	peel	18
Carum carvi	seeds	10
Thymus serpyllum	flower	10
Urtica dioica	leaves	5
Hippophae	fruit	20
Hyssopus officinalis	flower	15
Ocimum basilicum	leaves	1
Silybum marianum	fruit	5
Cinnamomum verum	peel	7
Foeniculum vulgare	fruit	5
Mentha	leaves	10
Origanum vulgare	leaves	10
Salvia Rosmarinus	stem	15
Cynara cardunculus var. Scolymus	flower	15
Coriandrum sativum	fruit	15

* 2000 mL of aqueous solution 45% (v/v) of absolute alcohol to the plant material has been added

Innovativeness

The white aromatized wine of the Vermouth type obtained is based on the premise of inserting innovative aspects into the classic technology of making aromatized wines. The innovative aspects of the product are: (i) the selection of plant material (medicinal plants, spices and fruit) and hydroalcoholic maceration techniques to obtain a hydroalcoholic macerate with a high content of bioactive compounds; (ii) the valorization of the varietal character of the white base wine, obtained from NOVA grapes in the hilly area in the south of the country in order to adapt to the tastes of the modern consumer who explores new flavor combinations, focusing on sustainability and health, thus meeting contemporary demands; (iii) the design of the assortment was based on technological calculations of total and partial material balance in the useful components: ethyl alcohol and sugar.

The process of manufacturing the white vermouth wine type

The white aromatized wine of the Vermouth type is a distinctive alcoholic beverage appreciated for its complexity and refinement. It is obtained by fortifying the basic white wine with sugar and natural plant and fruit extracts in the form of hydroalcoholic macerate [5].

Selection of the base wine: white wine from the NOVA grape variety (harvested year 2021) was used, with a neutral flavor profile to allow the hydroalcoholic macerate to stand out. Addition of the macerate: the macerate, added at a rate of 2% of the final volume of the Vermouth obtained, imparts unique flavors and olfactory and gustatory complexity.

Sweetening: the sweetening was achieved by adding edible sugar to balance the bitterness due to the botanical ingredients from which the macerate was prepared [4].

Maturation: the technological blend was matured for 30 days at a temperature of 15-20°C, allowing the aromas to harmonize. After this time, the hydroalcoholic macerates were filtered and incorporated into the basic white wine [5].

Analytical methods of white Vermouth wine

The following chemical analyses were carried out according to the International Organization of Vine and Wine methodology (OIV) [7]. These included determinations of total acidity, alcohol degree, sugar contents, total dry extract and non-reducing dry extract. All chemicals and reagents were purchased from Merck, Fluka, Sigma. The bidistilled water used.

Results and discussion

Aromatized wines are aperitif, tonic, pleasantly aromatic and bitter-tasting. Both the aromas and the taste come from certain plants and ingredients, the number and proportions of which are often manufacturing secrets. These products are obtained either by the infusion of aroma and taste constituents during must fermentation, or from wine by the addition of sugar or must, wine distillate or refined food alcohol, citric acid and macerates of plants and fruits [4].

The quantities of raw materials required for the preparation of 5000 mL of white Vermouth were calculated using a material balance. This comprised a total material balance and partial material balance in alcohol and sugar (Table 2). Citric acid is used to correct wine acidity [6].

Table 2. The materials needed to make 5000 mL of white Vermouth

Materials	Values
Basic wine NOVA (mL)	3868
Alcohol 96% v/v (mL)	407
Sugar (g)	529
Hydroalcoholic macerate of plants (mL)	100
Water (mL)	296
Citric acid (g)	6.5

Table 3 shows the characteristics of white wine from the NOVA grape variety.

Table 3. The base wine physicochemical characteristics

Physicochemical characteristics	Values
Total acidity (g/L H_2SO_4)	4.0
Alcohol (%, v/v)	12.0
Sugar (g/L)	1.50
Total dry extract (g/L)	24.10
Non-reduccing dry extract (g/L)	22.60

A sensory analysis provides insights into the provenance and maturation of a given wine, offering a comprehensive representation of its intrinsic characteristics [2]. The sensory properties of white Vermouth type wine are presented in Table 4 and Table 5 shows the physicochemical characteristics of this drink.

Table 4. The sensory properties of white Vermouth type wine

Sensory properties	Description
appearance	clear, without suspended particles or sediment
color	gold yellow with an amber tint
taste	pleasant taste, with a slightly bitter distinct aroma by fruit, flower and vegetable notes (derived from the macerate extract)
odor	pleasant, characteristic of aromatized wine

Table 5. The physicochemical characteristics of white wine Vermouth type

Physicochemical characteristics	Values
Total acidity (g/L H_2SO_4)	4.0
Alcohol (%, v/v)	18.0
Sugar (g/L)	100
Total dry extract (g/L)	116.46
Non-reduccing dry extract (g/L)	16.46

This assortment is a special, flavored aperitif wine [6]. This flavored wine is suitable for special occasions and is an excellent choice for events and social gatherings, bringing an element of elegance [3].

Conclusion
Thanks to the combination of herb, spices and fruit, Vermouth offers a multifaceted taste experience that can satisfy even the most demanding palate. Consumed moderately, this flavored wine may have digestive benefits due to the herbs and botanicals used in the preparation of the macerate. The white Vermouth-type aromatized wine obtained is based on the premise of inserting innovative aspects into the traditional technology of making aromatized wines. The aspects that support the innovativeness of the product consist in capitalizing on the varietal character of the basic white wine in order to adapt it to the tastes of the modern consumer who is exploring new flavor combinations, focusing on sustainability and health. The design of the assortment was based on technological calculations of total and partial material

balance in useful components: ethyl alcohol and sugar. The techniques accessed in the direction of obtaining special white wine of Vermouth type are relatively simple, easy to apply, being recommended for the purpose of expanding the assortment of flavored wines.

References

[1] D.J.W. Burns, A.C. Noble, J Texture Stud. 16 (1985) 365-381.

[2] R. Culea, M. Radiana, R.M Tamba-Berehoiu, C. Popa, Scientific Papers Series Management, Economic Engineering in Agriculture and Rural Development. 1 (2015) 147-152.

[3] V.K. Joshi, D.K., Sandhu, B.A.B.T. 43(5) (2000) 537-545.

[4] V.M. Kiselev, T.F. Kiseleva, A.V. Petropavlovskaya, L.P. Lipatova, M.A. Nikolaeva, in BIO Web of Conferences, EDP Sciences, vol. 103, 2024, pp.96.

[5] A. Morata, C. Vaquero, F. Palomero, I. Loira, M.A. Banuelos, J.A. Suárez-Lepe, Alcoholic Beverages, Volume 7: The Science of Beverages. 2019, pp.35-63.

[6] E. Mudura, T.E. Coldea, Bulletin UASVM Food Science and Technology, 73(1) (2016), 28-32.

[7] OIV (Organisation Internationale de la Vigne et du Vin), Compendium of International Methods of Wine and Must Analysis, 2008. vol.1, Paris

[8] P.S. Panesar, N. Kumar, S.S. Marwaha, V.K. Joshi, Nat. Prod. Radiance. 8(4) (2009) 334-344.

[9] P.S. Panesar, V.K. Joshi, R. Panesar, G.S. Abrol, Adv Food Nutr Res. 63 (2011) 251-283.

[10]***Order No. 142 from February 29, 2008, published in The Official Gazette of Romania No. 565 from July 28, 2008, http://old.madr.ro/pages/inspectii/ordin-142-din-2008.pdf.

SYNTHESIS, STRUCTURAL AND OPTICAL PROPERTIES OF BIRNESSITE-TYPE POTASSIUM MANGANESE OXIDE MATERIALS

Maria Poienar[1], Gabriel Buse[1], Paula Svera[2]

[1]ICAM, West University of Timişoara, Bd. V. Pârvan no.4, 300223 Timisoara, Romania;
[2]National Institute for Research and Development in Electrochemistry and Condensed Matter, Timisoara, P. Andronescu no.1, 300224, Romania
e-mail: maria.poienar@e-uvt.ro

Abstract

Mixed-valence manganese oxides play important roles and have many promising applications in catalysis, electronics, sensors, etc [1-4]. These materials are abundant, low-cost, and have unique properties due to different valence states of Mn cations: Mn^{3+}, Mn^{4+} and Mn^{2+}. Our attention has been focused to potassium-containing manganese oxide materials as recently they have shown to present for example excellent catalytic performance for soot combustion with high resistance to H_2O and SO_2 [5] and moreover are promising cathodes for potassium ion batteries [6].

In this work, facile, fast, high-yield and low-cost solid-state methods for preparation of birnessite-type KMnO materials have been developed. The factors that affect the formation processes: change in the precursor's ratio, the reaction temperature and reaction time have been analysed. The as-synthesized compounds have been characterized by X-ray diffraction (XRD), Raman spectroscopy, thermogravimetric analysis and the optical absorption properties of the compounds were evaluated in this research work. The structure-properties relationships are investigated for these materials in order to address their potential use in different applications.

Acknowledgements

References

[1] B. Dutta et al. Nat.Commun. 10 (2019) 655
[2] B. Zhang et al. Nat. Commun. 10 (2019) 2980
[3] B. Lin et al., Adv. Mater., 31 (2019) 1900060
[4] H. Zhao et al. Appl. Catal. B: Environ. 268 (2020) 118422
[5] D. Yua et al. Applied Catalysis B: Environmental 285 (2021) 119779
[6] J. Wenga, et al. Chemical Engineering Journal 392 (2020) 123649

STYRENE-DIVINYLBENZENE COPOLYMERS FUNCTIONALIZED WITH GLYCINE GROUPS AND IMPREGNATED WITH Zn(II) FOR THE PHOTOCATALYSIS OF CONGO RED DYE

Laura Cocheci[1], Aurelia Visa[2], Bianca Marenescu[3]. Lavinia Lupa[1], Ecaterina Stela Dragan[4], <u>Adriana Popa[2]*</u>

[1] *Politehnica University Timisoara, Faculty of Industrial Chemistry and Environmental Engineering, 6 Vasile Parvan Blvd., 300223, Timisoara, Romania*
[2] *"Coriolan Drăgulescu" Institute of Chemistry, 24 Mihai Viteazul Blvd., 300223, Timisoara, Romania,*
[3] *Faculty of Chemistry, Biology, Geography, 16 Pestalozzi Str., 300115 Timisoara, Romania*
[4] *Petru Poni Institute of Macromolecular Chemistry, 41A Aleea G. Gh Voda, Iasi, Romania*
*e-mail: apopa_ro@yahoo.com; apopa@acad-icht.tm.edu.ro

Abstract

The ecotoxicological impact of dyes can be mitigated by textile wastewater pollution control, making sure that the issue of wastewater discharge directly into the environment is resolved.

In this work, water contaminated with Congo red dye was decontaminated using two new compounds of the glycine type pendant groups grafted on S-DVB copolymer.

A potential class of adsorbents are polymeric ones because they can form a large variety of porous shapes inside a particular chemical system. Enhancing the surface chemistry of polymer supports to get superior adsorption capabilities against certain contaminants is a commonly employed method that involves chemically altering polymer matrices with pendant functional groups [1]. Considerable attention has been paid to polymeric matrices with pendant functional groups as matrices for heterogeneous photocatalyst design [2]. A serious ecological issue has arisen in recent years as a result of the industrial sector's use of a wider range of artificial dyes that are harmful to the environment [3, 4].

In the present study, two novel compounds of glycine type pendant groups grafted on S-DVB copolymer were used for the decontamination of Congo red dye polluted water. They were characterized by FTIR spectroscopy, scanning electron microscopy, EDX spectroscopy, thermogravimetric analysis. Photocatalysis was used in the photodegradation process for both polymer-supported glycine groups (Code: AP2) and polymer-supported glycine-Zn(II) (Code: AP2-Zn(II)). The efficiencies obtained after 30 min of dark adsorption were 8.17% in the case of AP2 material, and 17.5% in the case of AP2-Zn(II) material, respectively. By using 25 mg/L initial concentration of Congo red dye and a catalyst concentration of 1 g/L and 240 min of irradiation, a photocatalysis efficiency of 86.7% in the case of glycine pendant groups grafted on styrene-6.7% divinylbenzene copolymer (AP2), and of 80.7% in the case of glycine-Zn(II) pendant groups grafted on styrene-6.7% divinylbenzene copolymer (AP2-Zn(II)), respectively, was achieved.

Acknowledgements

References

[1] A. Popa, L. Cocheci, , L. Lupa, A. Pop, A. Visa, Appl. Sci. 13 (2023) 2025.

[2] Y. Orooji, R. Akbari, Z. Nezafat, M. Nasrollahzadeh, T.A. Kamali, J. Mol. Liq. 329 (2021) 115583.

[3] I.A. Salem, H.A. El-ghamry, M.A. El-ghobashy, J. Basic Appl. Sci. 3 (2014) 186.

[4] E.R. Shilpa, V. Gayathri, J. Saudi Chem. Soc., 22(6) (2018) 678.

ANTIOXIDANT CAPACITY AND POLYPHENOLS CONTENT FOR SOME MEDICINAL PLANTS

<u>Georgeta-Sofia Popescu</u>[1*], Florina Radu[,1*], Ariana-Bianca Velciov[1], Antoanela Cozma[2], Luminita Pirvulescu[3], Lia Sanda Rotariu[3], Daniela Stoin[1], Despina Bordean[1]

[1]Faculty of Food Engineering, University of Life Sciences "King Michael I" from Timisoara, 300645, Timisoara, Romania
[2]Faculty of Agriculture, University of Life Sciences "King Michael I" from Timisoara, 300645, Timisoara, Romania
[3]Faculty of Management and Rural Tourism, University of Life Sciences "King Michael I" from Timisoara, 300645, Timisoara, Romania
*Corresponding author, e-mail: sofiapopescu@yahoo.com , florinaradu@usvt.ro

The purpose of this study is to determine antioxidant and total phenolic contents of the ethanol extracts obtained from some medicinal and aromatic plants collected from Timis County.

A medicinal plant is that species of the plant kingdom, whose parts (flowers, leaves, roots, stems, fruits, or seeds) are directly used or used in some preparation as a medicine to treat a condition or disease. Medicinal plants are traditionally used in folk medicine as natural healing remedies with therapeutic effects. Medicinal plants represent as an alternative treatment to various diseases, and their use is increasingly prevalent throughout the world. Due to the large number of plant species with medicinal properties, some sciences have emerged such as medicinal herbalism, which has allowed the wide development of traditional medicine in some countries. Herbal teas are a popular beverage, that can be prepared very easily (by pouring hot water on various dried herbs).

We studied four types of medicinal plant: peppermint (*Mentha piperita* L.), sage (*Salvia officinalis* L.), thyme (*Thymus vulgaris* L.), and lavender *(Lavandula angustifolia* Mill.). The ethanol (70%) extraction was carried at 40 °C for 2 h. The antioxidant activities of these extracts were determined by the methods of DPPH and polyphenols were determined by the Folin Ciocâlteu method.Total phenolic content (TPC) of the extracts were between 3-32 mg gallic acid equivalents (GAE) per g of plant, respectively.

The bioactivity in medicinal herbs shows significant variations determined by the nature and type of herbal tea and bio-elements investigated.

NITROGENOUS PROFILE OF WORT PRODUCED FROM NATIVE TRITICALE

Milana Pribić[*], Lenka Grubač, Jelena Pejin

*Department of Biotechnology, Faculty of Technology Novi Sad, University of Novi Sad,
Bulevar cara Lazara 1, 21 000 Novi Sad, Serbia
e-mail:milana.pribic@uns.ac.rs*

Abstract

Beer, one of the oldest human-controlled processes, has been a companion to mankind since ancient times. In recent decades, the growing demand for a wider variety of beer has posed new challenges for brewers, prompting the need for extensive research and the integration of innovative technologies. To remain competitive in this ever-evolving market, brewers are increasingly experimenting with novel ingredients and techniques to create beers that go beyond traditional styles. The primary ingredients in beer production are cereals, water, hops, and yeast, with barley being the preferred starch source. However, over 80% of global beer production now incorporates alternatives to barley malt, and this trend continues to grow. Triticale, the first man-made hybrid, was developed by crossing wheat with rye. Its brewing potential is particularly notable in its malted form, which is characterized by high α-amylase and proteolytic activities, as well as an optimal starch gelatinization temperature. However, research indicates that even in its unmalted form, triticale exhibits significant enzymatic activity.

The objective of the study was to examine the effects of mashing with unmalted triticale variety 'Odisej,' approved in Serbia, at different proportions (10%, 30%, and 50%), along with the addition of the commercial enzyme Shearzyme® 500L to reduce wort viscosity, with an emphasis on the nitrogenous profile. The viscosity of the triticale-based produced worts exceeded the specified range (1.45-1.60 mPa·s, MEBAK 2011) when no enzyme was added. In contrast, all analysed worts treated with Shearzyme® 500L met the prescribed requirements. Addition of commercial enzyme also enhanced proteolytic process, as free amino nitrogen (FAN) content in wort treated with enzyme was higher in every ratio than that without enzyme addition. In this study, the highest FAN content was observed in the wort prepared from 10% triticale in the grist with enzyme addition (192.18 mg/L), which is approximately 2.0% lower than the content noted in the reference sample – all malt wort. In addition to FAN, total nitrogen content of the worts was investigated. This parameter is crucial for both yeast nutrition and foam stability in beer. Triticale worts with 10% and 30% grists exhibited slightly higher total nitrogen content than the reference sample ($0.12 \pm 0.01\%$ (w/w)). Notably, the triticale wort with 10% grist had the highest total nitrogen content, which was also observed with FAN. Additionally, soluble nitrogen content was investigated, and it was found that worts produced with 30% and 50% triticale met standard values (0.55–0.75%). However, the wort produced with 10% triticale showed a higher concentration of 0.89%. The obtained results indicate that triticale variety ‚Odisej' had good technological parameters and could be used as a partial substitute for barley malt in beer production.

DIFFERENCES IN NITROGEN AND PHOSPHORUS CONCENTRATIONS IN THE WHOLE GRAIN OF *AEGILOPS* AND *TRITICUM* SPECIES

Putnik-Delić Marina[1], Maksimović Ivana[1], Kastori Rudolf[1], Milan Mirosavljević[2]

[1]*University of Novi Sad, Faculty of Agriculture, Trg Dositeja Obradovića 8, Novi Sad, Serbia,*
[2]*Institute of Field and Vegetable Crops, Novi Sad, Serbia*
putnikdelic@polj.uns.ac.rs

Abstract
This study examined the accumulation of nitrogen (N) and phosphorus (P) in the grain of *Aegilops* and *Triticum* species bearing different genomes (AA, BB, BBAA, BBAADD and DD). Twenty different genotypes were included in a two-year field experiment. The highest concentrations of N and P were found in the grain of *Aegilops* and lower in modern cultivated *Triticum* genotypes. There was a negative relationship between N and P concentrations in the grain and in thousand-grain weight (TGW).

Introduction
Wheat is one of the most important cultivated plants, since it covers the the largest area harvested worldwide, at just over 219 million hectares (in 2022), and it is one of the basis of human nutrition. The increase in yield in the modern common hexaploid wheat has been accompanied by a reduction in the content of important nutrients proteins, minerals, vitamins, etc. (dilute effect) in the grain, with negative consequences for its nutritional quality. This can be remedied by biofortification - cultivating wheat genotypes with higher nutrient accumulation in the seed (Biel et al., 2021). This has led to interest in the wild diploid *Aegilops* species which are less productive, but have a grain of higher nutritional value. The knowledge of the genetic variability of wheat grain nutrient content is important for the success of developing new wheat cultivars with nutrient-rich grain.

Material and methods
Six diploid genotypes of wheat with different genomes (BB, AA, or DD), five tetraploids (BBAA), and nine hexaploids (BBAADD) were used in the experiment. Among the diploid wheat, four were wild and one (*Triticum monococcum* var. monococcum) was a primitive cultivated wheat. Among the tetraploids, two genotypes were cultivated. All hexaploids were cultivated genotypes. This choice of genotypes allowed an evaluation of the variation of grain nitrogen and phosphorus accumulation ability in wild and primitive genotypes compared to modern wheat cultivars (Tab. 1).
The experiments were established on calcareous, gleyic chernozem. Nitrogen concentration was assessed by the method of Kjeldahl, phosphorus by the vanadate-molybdate method, and TGW in dry grains.
Statistical analyses of data were carried out using Statistica 14 software. All data were subjected to ANOVA and comparison of means was done using Duncan's least significant difference test. Relation between the concentrations of elements and TGW were analyzed by calculating correlation coefficients.

Table 1. Genotypes of *Aegilops* and *Triticum* species examined in the experiment

No	Species and subtaxa	Genome	No	Species and subtaxa	Genome	No	Species and subtaxa	Genome
1	*Aegilops speltoides* TAUSCH var. *speltoides*	BB (D)*	8	*Triticum turgidum* L. var. *rubralbum*	BBAA (RS)	15	*Triticum aestivum L.*	BBAADD (RUS)
2	*Aegilops speltoides* TAUSCH var. *speltoides*	BB (D)	9	*Triticum turgidum* L. var. *turgidum*	BBAA (RS)	16	*Triticum aestivum L.*	BBAADD (MEX)
3	*Triticum urartu* THUM	AA (RS)	10	*Triticum turgidum* L.	BBAA (D)	17	*Triticum aestivum L.*	BBAADD (D)
4	*Triticum monococcum* L.	AA (RS)	11	*Triticum durum* DESF. var. *pseudosalomonis*	BBAA (RS)	18	*Triticum aestivum* L. var. *aestivum*	BBAADD (F)
5	*Triticum monococcum* L. var. *monococcum*	AA (RS)	12	*Triticum spelta* L. var. *duhamelianum*	BBAADD (RS)	19	*Triticum aestivum L.*	BBAADD (AUS)
6	*Aegilops tauschii* COSS.	DD (D)	13	*Triticum aestivum* L. var. *lutescens*	BBAADD (RS)	20	*Triticum aestivum L.*	BBAADD (TR)
7	*Triticum dicoccoides* (KOERN) SCHWEINF.	BBAA (D)	14	*Triticum aestivum* L. var. *lutescens*	BBAADD (H)			

* In the brackets is the label of the country from whose collection the seeds were taken for the experiment

Results and discussion

The highest concentration of N and P was found in the wild *Aegilops speltoides* (BB genome) and *Triticum turgidum* L. (BBAA genome), whereas hexaploids had lower and similar values (Fig. 1 and 2). The TGW and grain morphology in wheat depend on genetic, ecological, and agrotechnical factors.
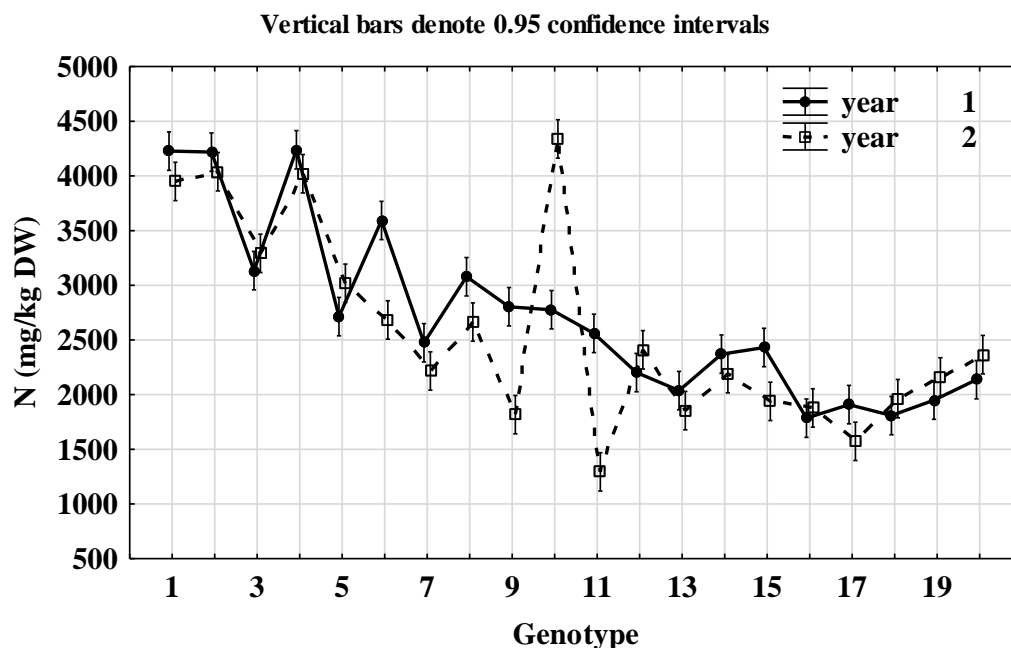
Figure 1. Nitrogen concentration of whole grains of *Aegilops* and *Triticum* species over 2 years

Vertical bars denote 0.95 confidence intervals
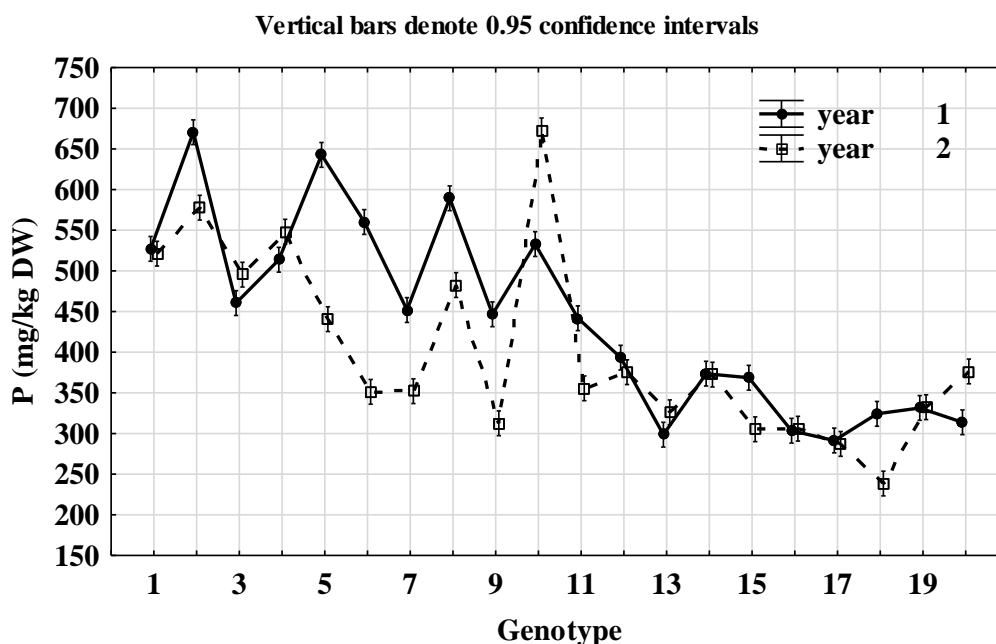
Figure 2. Phosphorus concentration of whole grains of *Aegilops* and *Triticum* species over 2 years

The TGW depends primarily on the grain size and to a lesser extent on its chemical composition. According to Simmonds et al. (2016), a splice acceptor site mutation in TaGW2-A1 gen increases TGW in tetraploid and hexaploid wheat through wider and longer grains. The TGW varied significantly among the examined genotypes (Fig. 3).

Vertical bars denote 0.95 confidence intervals
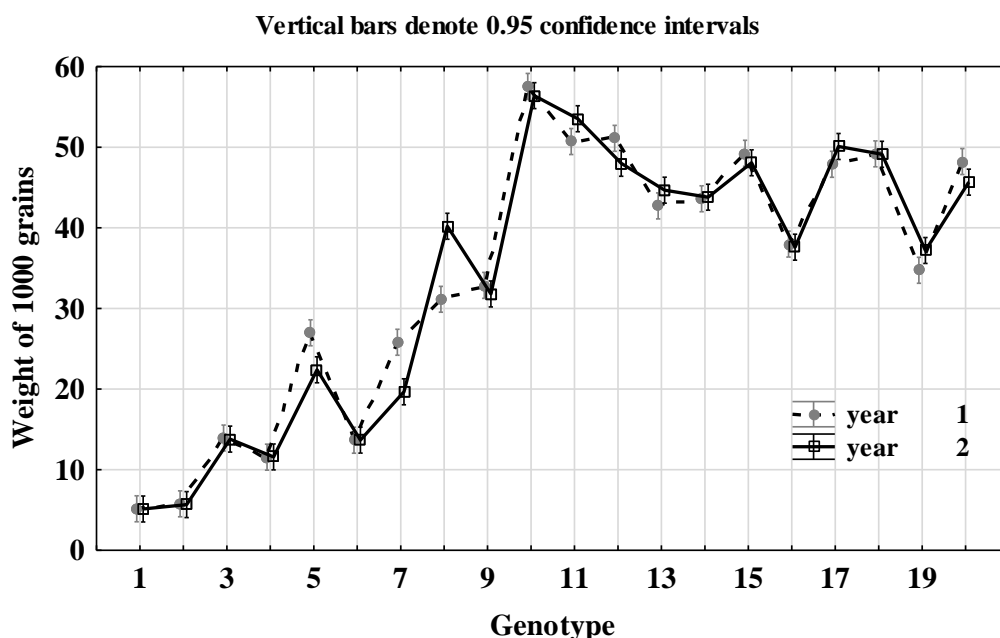
Figure 3. Weight of 1000 grains of *Aegilops* and *Triticum* species over 2 years.

It was the lowest in ancient diploid species, and the highest in cultivated hexaploid genotypes. There was a negative correlation between TGW and the concentration of N and P in grain (Fig. 4 and 5). The highest N and P concentration was found in grains of ancient species whose average TGW was the lowest.

Scatterplot: N (mg/kg DW) vs. weight of 1000 grains (g) (Casewise MD deletion)
weight of 1000 grains (g) = 68.774 - .0131 * N (mg/kg DW)
Correlation: r = -.6754
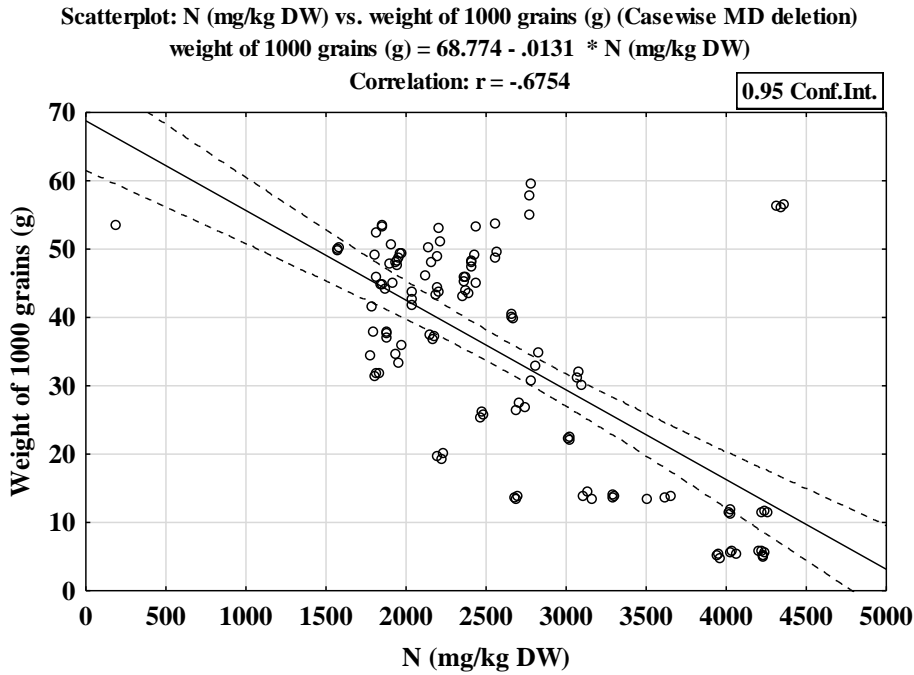
Figure 4. Relation between nitrogen concentration in whole grains of *Aegilops* and *Triticum* species and weight of 1000 grains over 2 years

The concentration of mineral substances in whole grains depends also on the ratio of the peripheral part (seed coat and aleuron layer) and endosperm because in wheat grains the mineral substances are concentrated in the peripheral part of the grain (Khalid et al., 2023). The smaller the grain, the greater the mass of the peripheral part in the total mass of the grain, which can contribute to a higher concentration of minerals in the grain as a whole.

Scatterplot: P (mg/kg DW) vs. weight of 1000 grains (g) (Casewise MD deletion)
weight of 1000 grains (g) = 63.931 - .0711 * P (mg/kg DW)
Correlation: r = -.4991
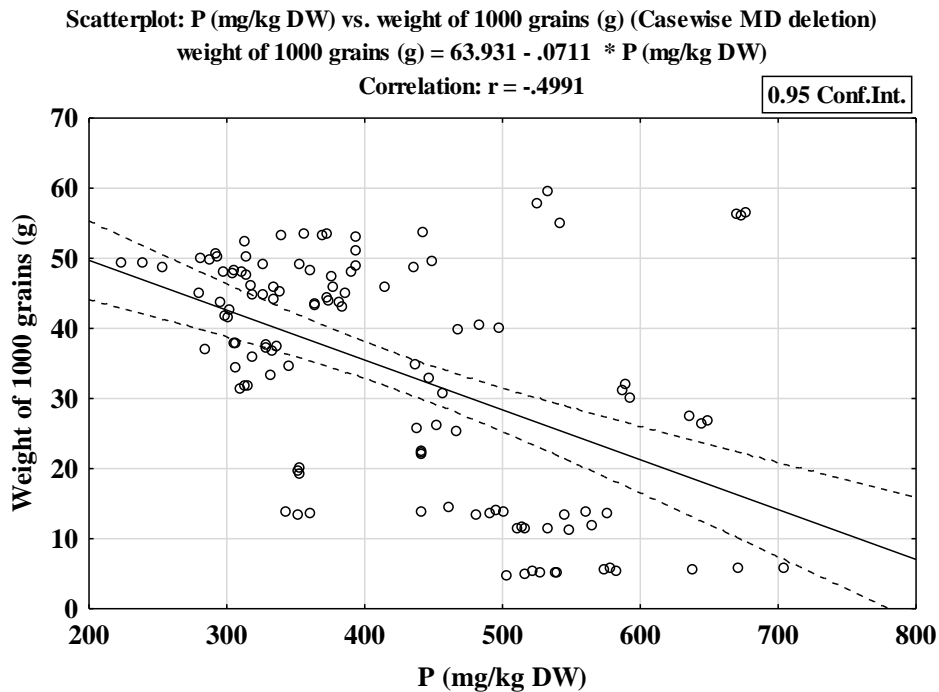
Figure 5. Relation between phosphorus concentration in whole grains of *Aegilops* and *Triticum* species and weight of 1000 grains over 2 years

Higher concentrations in smaller wheat grains were reported also for microelements (Svečnjak et al.,2013), aluminum (Maksimović et al., 2020), and iron (Kastori et al., 2021).

Conclusion

The analyzed *Aegilops* and *Triticum* genotypes differ significantly with respect to the N and P accumulation in grains, which can be used in breeding to increase its concentration in wheat cultivars. The highest concentration of N and P was found in the wild primitive diploid *Aegilops* species. The presence of lower N and P concentrations in the grains of tetraploid and hexaploid species with respect to diploid ancestors suggests that during the increase in ploidy and higher productivity, its concentration decreases (dilution effect). There was a negative correlation between N and P concentration in grain and TWG.

Acknowledgements

References

[1] Kastori R., Maksimović I., Momčilović V., Mirosavljević M., Putnik-Delić M., Daničić, M., Acta Agric. Serb. (2021), 26, 103-110.
[2] Biel W., Jaroszewska A., Stankowski S., Sobolewska M., Kepinska-Pacelik J., Eur. Food Res. Technol., (2021), 247, 1525-1538.
[3] Khalid A., Hameed A., Farrukh Tahir M., Front Nutr., (2023), 10:1053196 doi: 10.3389/ fnut. 2023.1053196.
[4] Maksimović I. Kastori R., Putnik-Delić M., Momčilović V., Denčić S., Mirosavljević M., Plant Soil Environ., (2020), 66, 351-356.
[5] Simmonds J., Scott P., Brinton J., Mestre TC., Bush M., Blanco A., Dubcovsky J., Uauy C., Theor. Appl. Genet., (2016), 129, 1099-1112.

PHYTOCHEMICAL AND ANTIOXIDANT PROPERTIES OF DIFFERENT PARTS OF ROUMANIAN CUMIN (*CUMINUM CYMINUM L.*) ESSENTIAL OILS

Florina Radu[1], Mariana-Atena Poiană[1*], Daniela Stoin[1], Diana Moigrădean[1], Antoanela Cozma[2], Georgeta-Sofia Popescu[1]

[1]Faculty of Food Ingeneering, University of Life Sciences „King Mihai I" from Timişoara, Calea Aradului nr. 119, 300645, Timişoara, Romania
[2]Faculty of Agriculture, University of Life Sciences „King Mihai I" from Timişoara, Calea Aradului nr. 119, 300645, Timişoara, Romania
e-mail: florinaradu@usvt.ro

Abstract

Essential oils are concentrated extracts from plants, recognized for their intense aromas and therapeutic properties. They are used in aromatherapy, cleaning (in natural cleaning products for their antimicrobial properties), natural fragrances and also as preservatives in meat and cheese industries. Essential oils obtained by hydro-distillation from flowers and seeds of cumin were investigated. Gas chromatography-mass spectrometry (GC/MS) was used for the identification of the volatile compounds. The Folin-Ciocalteu method was chosen for determination of total phenol content (TPC). The antioxidant activity of *C. cyminum* essential oils were assessed using 1,1-diphenyl-2-picrylhydrazyl (DPPH) assay. Essential oil yields were 1.75% in flowers, and 3.63% in seeds. Major components of the oils were γ-terpinene (20.2%) in flowers and cumin aldehyde (36.1%) in seeds, respectively. The total phenol content of the essential oils of different parts of cumin ranged from 10.3 to 17.8 mg of GAE/g of dw. The antioxidant activity of the cumin essential oils obtained from flowers was found to be lower than synthetic antioxidant butylated hydroxytoluene (BHT).

Introduction

Chinese, Indian, Korean and North African civilizations considered aromatic plants as the major source of phytomedicines providing written evidence regarding the applications of these specific plants for the treatment of infectious diseases [1]. Medicinal plants are the source of many compounds that can play an important role in improving health, and the phytomedicinal system is the result of extraction procedures from seeds, leaves, fruits, bark, roots and flowers, etc. *Cuminum cyminum* L. (english cumin, Roman caraway) belongs to the Apiaceae family, is a leafy plant that grows at ground level in China, India, the Middle East, and the Mediterranean region [1]. The plant blooms in June, its flowers being white or pink, type 5, arranged in compound umbrellas; the fruits are ellipsoidal diachene, slightly arched, grayish-brown, aromatic [2, 3]. The fruits of the plant are basically cumin seeds, popular around the world in the form of a spice. Its have a strong, sweet flavor with a slight bitter and spicy tinge [4]. The cumin seeds essential oil composition has been exhaustively studied and did not give homogenous results. A detailed analysis of the essential oil composition revealed the prevalence of cumin aldehyde, p-cymene, γ-terpinene, safranal, β-pinene and terpenoids [5,6]

Most of the benefits of cumin are related to digestion, the immune system and circulation. Thus, the dynamic components of the cumin plant are used as: (1) moderate antibacterials for a number of bacterial infections; (2) can relieve diseases caused by elevated cholesterol levels respectively glucose; (3) weight loss; (4) milk production stimulants in women; (5) insecticides and (6) cancer prevention agents. Some benefits have been demonstrated through clinical trials, while others are based solely on anecdotal evidence and therefore remain difficult to prove

[7,8,9]. Because of the presence of different active compounds such as flavonoids, alcohols, terpenes and poliphenols, cumin essential oil is considered as highly antioxidant [10].

The aim of the study was to evaluated the essential oil composition and antioxidant activity from seeds and flowers of *Cuminum cyminum* L. cultivated in Roumania, in order to highlight the qualitative and quantitative changes of the above vegetal parts.

Experimental

Chemicals and reagents. All chemicals (methanol, hexan, dichloromethan, DPPH, Folin-Ciocalteu reagent, Na_2CO_3, butylated hydroxytoluene (BHT) ($C_{15}H_{24}O$), gallic acid ($C_7H_6O_5$)) used for analyses were of an analytical grade and purchased from Sigma Chemical Co. (Sigma-Aldrich GmbH, Stern-heim, Germany)

Plant Material. Samples of flowers of cumin (*Cuminum cyminum L.*) were collected at flowering stage from Zalau area (North-westhern Roumania) on May 2023. After harvest, samples were transported from the field to laboratory at +4°C. Samples were washed by distilled water, dried at 20°C for 1 week in a well-ventilated room and storage in plastic bags before being treated. Cumin seeds came from S.C. Pronatura S.R.L. Zalău (certified seeds, purity 90%, germination capacity 65% and MMB 7.5 g); the cumin seeds were manually sorted, dried at room temperature and stored in sealed plastic bags until their analysis. The cumin essential oils yields (%) were calculated using the following equation:

$$\% \text{ Yield} = \text{Weight of dried crude extracts g /Weight of dried plant sample taken g } 100$$

Obtaining of essential oils. The essential oils were obtained by the hydrodistillation of 100 g plant material in a Clevenger apparatus, the extraction time being 4 hours. Afterwards, the distillate was extracted in dichloromethane after a preliminary saturation with sodium chloride. The organic layer of dichloromethane and essential oil was then dehydrated by passing it over a layer of anhydrous sodium sulfate. The extraction solvent was removed by evaporation under vacuum in a Buchi rotary evaporator, at a temperature of 18°C. The obtained volatile oil was collected in a brown vial, hermetically sealed and kept refrigerated at +4°C until analysis.

GC-MS analysis of essential oils. The identification and quantification of volatile compounds from cumin essential oils were performed by GC/MS, using a Hewlett Packard 5890 II gas chromatograph coupled with a mass detector, HP 5972, a capillary column model HP-5 MS (30 m×0.25 mm id, film thickness 0.25 μm). The ionization mode was EI type at a value of 70 eV, scan time of 1.5 s and a mass range of 40–300 amu. The carrier gas was He at a flow rate of 1.2 ml/min. Injector and transfer line temperatures were fixed at 250 and 280°C, respectively. The oven temperature setting program was as follows: hold for 10 min at 55°C, schedule to reach 160°C at a rate of 20°C /min, hold at this temperature for 10 min and then increase the temperature to 220°C with a speed of 10°C/min. The samples to be analyzed were diluted in hexane at a ratio of 1:100, and the injection volume was 1.0 μl.The identification of the compounds from the analyzed samples was carried out by comparing the mass spectra with those existing in the spectrum library in the software of the device. The content of various compounds present in the extracts was determined as a relative percentage of the area of the peaks related to TICs. A mixture of n-alkanes was used as a reference in the calculation of relative retention indices (RRIs).

Determination of total phenols content (TPC). The TPCs of cumin essential oils were determined using the Folin–Ciocalteu colorimetric method as described by Singleton and Rossi [11]. The TPCs were expressed as mg gallic acid equivalent per gram of dry weight plant material (mg GAE/g dw) and ±SD (standard deviation) for three replicate analyses.

Antioxidant activity, DPPH radical scavenging assay. The DPPH method is based on the reduction of the stable free radical 1,1-diphenyl-2-picrylhyrazyl by the addition of a radical species or an antioxidant, which is accompanied by the discoloration of the purple DPPH solution, as described by Blois [12].

Results and discussion

Cumin essential oils appear as pale-yellow liquids, transparent and having values of the main physical characteristics shown in Table 1.

Table 1. Physical and chemical characteristics of essential oil of *Cuminum cyminum L.*

No.	Parameter	Seeds EO	Average	Flowers EO	Average
1.	Color	Pale yellow		Pale yellow	
2.	Odor	Strong aromatic with a slight bitter tinge		Sweet Flavor with a slight spicy tinge	
3.	Yield	3.62 - 3.66	3.63%	1.65 - 1.85	1.75%
4.	Specific gravity	0.8596 - 0.8792	0.8694	0.8654 - 0.8670	0.8662
5.	Refractive Index	1.495 - 1.502	1.499	1.492 - 1.500	1.496
6.	Peroxide value (meq.O_2/Kg oil)	0.020 - 0.040	0.030	0.018 – 0.042	0.030

 Conventional extraction (steam distilation) was carried out to extract the volatile compounds from the seeds, and flowers of C. Cyminum with a percentage yield of 3.63% and 1.75% (v/w). The essential oil is gradually produced as the fruit develops, its quantity being lower in the flowers. On the other hand, as the fruit reaches maturity, the amount of essential oil increases, reaching a maximum just before the fruit's maturity stage. The essential oil characteristics (specific gravity, refractive index) showed no significant differences between cumin seeds and flowers. The specific gravity ranged between 0.8694 in seeds EO to 0.8662 in flowers EO samples. Refractive index ranged between 1.499 (seeds EO) to 1.496 (flowers EO). The average peroxide value was the same for both essential oil categories (0.030 meq.O_2/Kg oil).

The chemical composition of Cumin Cyminum essential oils is shown in Table 2. GC-MS analysis revealed the presence of 30 compounds representing over 99% of the total volatiles in seeds EO content, among which the most abundant were αmin aldehyde (36.1%), β-pinene (15.6%), γ-terpinene (11.8%), γ-terpinene-7-al (2.4%) and p-cymene (5.7%). In the case of flowers EO, GC-MS analysis detected 22 compounds representing over 97% of the oil content. Regarding the chemical composition of the essential oil obtained from cumin flowers, it can be found that the most abundant volatile compound was γ-terpinene (20.2%), γ-terpinene-7-al (18.2%) and p-cymene (13.7%). The volatiles compound can be classified into monoterpenes, sesqui-, diterpenes and heterogeneous groups. Monoterpenes were found as the main components in both types of essential oil (over 55.67%). Sesquiterpenes levels were lower than monoterpenes (18.5%). The amount of oxygenated monoterpenes in seeds EO (38.7 %) was higher than in flowers EO (22.46%). The results of our study are in line with the findings of various studies on the chemical components of cumin [6, 8, 9]. In general, the chemical differences between different parts of the cumin plants are inevitable, these differences being caused by a series of factors among which we can mention genetic, geographical, climatic, seasonal conditions, and harvesting time.

Table 2. Essential oil compounds of *C. Cyminum L.* from seeds and flowers

No.	Components Name	Seeds EO		Flowers EO	
		RI	%	RI	%
1.	α-thujene	934	nd	934	0.31± 0.08
2.	α-pinene	951	0.855 ± 0.04	951	0.11 ± 0.002
3.	sabinene	973	0.688 ± 0.01	973	0.724 ± 0.023
4.	β-pinene	978	15.6 ± 0.89	978	9.81 ± 0.25
5.	β-myrcene	989	0.61± 0.04	989	0.76± 0.02
6.	α-phellandrene	1000	5.6 ±0.03	1000	2.9 ± 0.01
7.	δ-3-carene	1006	0.04 ± 0.02	1006	0.04 ± 0.01
8.	α-terpinene	1013	2.34 ± 0.03	1013	1.23 ± 0.02
9.	limonene	1018	6.71 ± 0.04	1018	1.45 ± 0.03
10.	p- cymene	1026	5.78 ± 0.02	1026	13.7 ± 1.03
11.	β-phellandrene	1030	0.60 ± 0.01	1030	0.21 ± 0.003
12.	*cis*-ocimene	1236	0.18± 0.01	1236	nd
13.	γ-terpinene	1040	11.8 ±1.23	1040	20.2 ± 1.73
14.	terpinene-4-ol	1180	0.1± 0.01	1180	nd
15.	cumin aldehyde	1223	36.1± 2.56	1223	19.4 ± 0.01
16.	α-terpinene-7-al	1274	1.41± 0.11	1274	7.52± 0.18
17.	γ-terpinene-7-al	1280	2.4 ± 0.23	1280	18.2 ± 2.03
18.	o-cymene	1281	4.90 ± 0.02	1281	0.45± 0.31
19.	3-caren-10-al	1291	0.45± 0.01	1291	nd
20.	Eugenol	1356	0.21± 0.01	1356	nd
21.	cis-Carvyl acetate	1364	0.30± 0.01	1364	nd
22.	Isocaryophyllene	1410	0.18± 0.01	1410	nd
23.	thujopsene	1429	0.27± 0.01	1429	nd
24.	β-Caryophyllene	1431	0.23± 0.01	1431	nd
25.	γ-elemene	1434	0.32± 0.01	1434	nd
26.	α-Caryophyllene	1454	0.18± 0.01	1454	nd
27.	α-Humulene	1467	0.21± 0.01	1467	nd
28.	Valencene	1490	0.32± 0.01	1490	nd
29.	α- Farnesene	1509	1.22± 0.01	1509	nd
30.	Trans-Nerolidol	1563	0.25± 0.01	1563	nd

The total phenol content of the cumin essential oils was determined to be 17.82 mg GAE/g dw in seeds EO and 10.3 mg GAE/g dw in flowers EO (Table 3). Despite dilution effect, comparable results were obtained for seeds and flowers EOs. For example, Milan and others 2008, [13], reported a total phenol content of 0.21 ± 0.01 mg/g in cumin essential oil from India. Ho and others 2008, [14] found total phenolics of cumin methanolic extracts to be 75 ± 1 mg GAE/mg extract solids

Table 3. TPCs of *C. Cyminum L.* essential oils and mean inhibition of DPPH free radical (%)

Parameter	Seeds EO	Seeds EO*(1:5)	Flowers EO	Flowers EO (1:5)	BHT (1mM)
mg GAE/g dw	17.82 ± 1.5	3.45 ± 0.6	10.3 ± 2.2	2.31 ± 0.4	-
DPPH inhibition (%)	44.56 ± 2.1	23.56 ± 2.6	12.36 ± 1.7	9.12 ± 2.7	20.24 ± 2.3

The free radical DPPH scavenging ability assay was used to estimate the antioxidant activity of the cumin EOs. The results presented in Table 3, demonstrate that all the studied essential oils exhibited high (seeds EO) and moderate antioxidant activities. Scavenging efficacy of cumin EOs was compared with the butylated hydroxytoluene (BHT), a standard commercial synthetic antioxidant. From the data it was evident that the seeds EO exhibited high antioxidant efficacy (44.56%) than the standard BHT (20.24%), on the contrary flowers EO (12.36%) exhibited weak antioxidant efficacy. The high antioxidant activity of seeds EO can be correlated to the high phenolic content.

Conclusion

Cuminum cyminum L is a plant that has been used since ancient times both in natural therapy and in the gastronomy of peoples from different regions of the world. Its aromatic properties due especially to secondary metabolites from the class of terpenes and terpenoids have drawn the attention of food processors to the huge potential of using cumin essential oil as a preservative for food of animal origin with a short shelf life.
These results indicate that the cumin seeds essential oil is an excellent source of natural antioxidants, that could be used for food preservation and health benefits.

References

[1] P.M. Dewick, Medicinal natural products: a biosynthetic approach, John Wiley & Sons.183(9): 445-446, (2002).
[2] G.A. Holt and A. Chandra, Clinical Research and Regulatory Affairs 19(1), 83-107, (2002).
[3] S.I. Shivakumar, A.A. Shahapurkar, K.V. Kalmath, B. Shivakumar, Der Pharm Lett 2(1), 22-24, (2010)
[4] V.S. Rana, Journal of Medicinal Plants and By-products 2, 207-210. (2014)
[5] V.D. Zheljazkov, S. Shiwakoti, T. Astatkie, I. Salamon, D. Grul'ová, S. Mudrencekova, andV. Schlegel, Hort Science, 50(8), 1213-1217, (2015)
[6] S.D. Patil, P.P. Maknikar, S.J. Wankhade, C.S. Ukesh and M.K. Rai, Acta Univ. Cibiniensis, Ser. E: Food Technol. 20(2), 39-52. (2016)
[7] R.P.Singh, et al., Pharmacognosy Journal 9(3), 256-261, (2017)
[8]]. T. Krupodorova, M. Sevindik, AgroLife Sci. Journal 9 (1), 186–191, (2020)
[9] A.K. Behera, P. Bhadra, Indian J Nat Sci 9 (4), 156, (2020)
[10] R. Ranjbar, E. Zarenezhad, A. Abdollahi, et al., Journal of Tropical Medicine (2023), https://doi.org/10.1155/2023/5075581.
[11] V.L. Singleton, J.A. Rossi, Am J Enol Vitic., 16(3), 144–58, (1965)
[12] M.S. Blois, Nature. 181(4617), 1199–200, 1958, doi: 10.1038/ 1811199a0
[13] K.S.M. Milan, H. Dholakia, P.K. Tiku, P. Vishveshwaraiah, Food Chem 110, 678–83, (2008)
[14] D. Huang, O.U. Boxin, R.L. Prior, J Agric Food Chem 53, 1841–56, (2008)

THE IMPACT OF THE ŽELJEZARA LANDFILL ON THE ENVIRONMENT

Nada Markovic[1], Nebojsa M. Ralevic[2], Vladimir Dj. Djakovic[3]

[1,2,3] *University of Novi Sad, Faculty of Technical Sciences, Novi Sad, Serbia*
e-mail: nadamarkovic71@t-com.me, nralevic@uns.ac.rs, v_djakovic@uns.ac.rs

Abstract
Montenegro faces significant problems in the management of all types of waste, a particular problem in the environment, in several locations are represented by PCBs (Polychlorinated biphenyls), extremely toxic chlorinated industrial chemicals, classified as POPs (Persistent Organic Pollutants) substances. Due to the aforementioned properties, the production of these compounds is prohibited in most developed countries [3], however, despite the cessation of production in numerous countries since the mid-seventies, PCBs are still pollutants that cause great concern at the international level [1]. Today, the use of PCBs in open systems is prohibited, so the current sources of PCBs are primarily landfills. Significant amounts of PCBs in equipment are still in use, there are certain amounts that are waiting for treatment in warehouses [17]. Illegal landfills in Montenegro represent a problem that has been fought for years, the data on illegal landfills are not complete, it is believed that there are about 400 illegal landfills in the country. Despite the strict provisions of the law, this problem is being solved slowly. For this work, soil analysis was performed near the industrial waste landfill in Nikšić, the analyzes were performed at the Center for Ecotoxicological Testing of Montenegro. The aim of this paper is to point out the importance of the presence of PCBs in Montenegro, which can lead to progress in their detection and removal from the environment. The results showed that the soil near the Željezara landfill in Nikšić is highly contaminated, in soil samples from the Nikšić Željezara landfill, concentrations of PCBs, congener 138 of 0.253 mg/kg, and congener 101 at a concentration of 0.111 were determined.

Introduction
In the first half of the last century, 209 different PCB-compounds, known as congeners, were synthesized, the physical and chemical properties as well as the toxicity of PCB-s congeners are different [6]. Congeners 18, 28, 52, 101, 118, 138, 153 and 180 are very toxic, they belong to compounds similar in toxicity to dioxins. Other PCBs do not have toxicity similar to dioxins, but they have a harmful effect on the organism, they are classified in the group of indicator PCBs. PCBs are substances that, when they enter the environment, remain unchanged for a long period of time [16]. In the environment, they spread over large areas, and through the soil, water and air, they enter the food chain and accumulate in the fatty tissues of living organisms chemical characteristics of the soil, as well as the concentration and properties of PCBs, [4]. High octanol-water distribution coefficients of PCBs indicate the affinity of PCBs for organic matter, which can affect the high content of PCBs in the soil [7]. Accumulation of PCBs in soil can cause long-term contamination. Tests carried out by [19] showed that tri-CB, tetra-CB and penta-CB are the congeners that evaporate and settle on the soil most easily. Scientific studies conducted around the world have confirmed the harmful effects of these compounds on human health, it is believed that the level of an individual compound does not necessarily lead to harmful effect, but the effect of several congeners together can be of toxicological significance [14].
PCBs cause neurotoxicity, carcinogenicity, reproductive disorders, several studies have shown their negative impact on the endocrine system, the most significant endocrine effects of PCBs are disruption of thyroid hormones. They are most often detected in food of animal origin (meat,

eggs and dairy products), a particularly high risk for human health is the consumption of food of animal origin from animals that move close to waste dumps.

The use of PCBs began in 1929, it is assumed that the quantities produced in the world amount to about 2.5 million tons [18]. They were used in dielectric fluids, they proved to be excellent in places where the risk of fire is high, in installations of various plants, also in cooling systems, paints, adhesives [8]. PCBs are mainly synthetic compounds, unintentional formation of PCBs can occur in some thermal and chemical processes [10], as well as in the production of polymer resins [13]. It was established that PCB 11 can be formed during product pigmentation and can also be found in soil and atmosphere during wastewater treatment [12]. After the end of use, these products often ended up in "wild" waste dumps, so high concentration levels of PCBs were identified near old warehouses, then in land near industrial waste dumps, in places of former chemical industries and in large industrial centers, [5] which was also shown in this work. It is considered that the PCBs that were released into nature as part of the transformer oil spill were mostly concentrated in the soil (about 90%) and a much smaller part in the groundwater [2]. The low solubility of PCBs in water leads to the conclusion that small amounts of PCBs can be expected in underground and surface waters [9]. In the environment, PCBs bind to sediments and organic matter, they are difficult to decompose, the half-life of PCBs in the soil is several years, and in water and air it is much shorter, depending on the position of Cl-atoms and the prevailing conditions in the environment, [15]. Biodegradation of PCBs with more chlorine atoms is anaerobic, while mono and dichlorine PCBs are degraded under aerobic conditions. Plants take up little PCBs from the soil, mainly by adsorption [11].

1

PCBs in the soil of Montenegro

Production of PCBs did not occur in Montenegro, but they were imported for accompanying energy equipment within the power industry, military and PTT facilities, where they were mainly used as insulating liquids [11]. Interest in researching these compounds arose in Montenegro due to increased soil pollution in industrial areas, intoxication of aquatic organisms, and negative impact on both humans and the environment.

Production of PCBs did not take place in Montenegro, but they were imported for accompanying energy equipment within the power industry, military and PTT facilities, where they were mainly used as insulating liquids [1]. At a distance of about six kilometers from the center of Nikšić, on one and the other side of the road leading to the local community of Župa, there is a landfill of the Nikšić - Halda Railway. This hazardous waste landfill was created in the production process of the Nikšić Ironworks, it was formed in another half of the last century, and it still represents a great danger for the health of citizens and the heart of life. It presents a very bad image of the landfill, which has long since exceeded the available capacity of the land for receiving waste.

The landfill contains a mixture of waste materials dominated by loose ash. It is not properly secured and is accessible to passers-by. Its southern part descends into the very bed of the Gračanica river, and due to its large slope, it is subject to erosion, and as the Gračanica river is torrential during heavy rainfall, it is loose and dangerous waste easily spreads downstream, which leads to much wider pollution than the location itself. How dangerous is the waste the results of this soil analysis at the location of the Željezara - Halda landfill, as well as in the nearby Rubeža settlement, also show.

Material and working methods

For this work, an analysis of the soil 200m away from the Halda Iron and Steel dump was carried out, tests were carried out for the following PCB congeners 18, 28, 31, 44, 52, 101, 118, 138, 149, 153, 180, 194. Analyzes were performed at the Center for Ecotoxicological Testing

in Podgorica. Sample preparation for the analysis of this paper consisted of the following steps: extraction, sample purification and analyte concentration.

After grinding the soil to a granular granulation, extraction was started using the solvent hexane and dichloromethane in a ratio of 1:1, the samples were purified with sodium sulfate, after evaporation to an amount of 2-3 ml, the samples were washed with hexane (2 ml) and then evaporated in a stream of nitrogen to 4 ml, of which 1 ml was taken for analysis.

The extraction was carried out with the solvent of hexane and dichloromethane in a ratio of 1:1. 8 g of the sample was separated, quartz sand and the sample were added to the extractor tube, the process was carried out in the "speed" extractor and lasted 1h and 17 min., then the sample was purified with Na2 SO4, after which the sample was evaporated on a rotary evaporator to an amount of 2-3 ml, then it was washed with 1-2 ml of hexane, then it was evaporated under a stream of nitrogen to 4 ml, of which 1 ml was separated for the column, the column was eluted with 40 ml of hexane, all 40 ml of hexane and the sample were collected in a conical vessel of 50 ml, the sample was reduced to 2 ml, washed and transferred to a vial, the vial with 1 ml of the sample was introduced into the reading apparatus. For each individual sample as well as for a series of samples, a blind test was performed. An acid-base column was used.

A combined gas chromatograph-mass spectrometer instrument was used for the detection of PCBs in the soil, the mass spectrometer was used as a gas chromatograph detector. A gas chromatograph separates the components in a mixture, while a mass spectrometer enables the identification of each component separately. Based on the intensity of the peaks on the chromatogram, the presence of PCBs in the samples was determined by calculation based on the internal standard. The data obtained from this analysis were processed using a suitable computer system. The test results were compared with the maximum allowed concentration of MDK, according to the Rulebook on permitted quantities of hazardous and harmful substances in the soil and methods for their testing (Official Gazette of Montenegro No. 18/97). This rulebook prescribes the maximum allowed concentration of dangerous and harmful substances that can be found in the soil, for PCB-s congeners 18, 28,31, 44, 52, 101,118, 138,149, 153,180, 194 is 0.004 mg/kg in agricultural I 33 mg/kg in industrial soil.

Examination results and discussions

In Nikšić, soil was sampled from several locations: arable land sampled at a distance of 200 m from the Željezara landfill (Halda landfill), while in other cities the results of this analysis do not show that the soil samples contain PCBs above the MDK. Table 1 shows the concentrations of PCBs in the soil samples near the Halda landfill. Based on the presented results, we notice that the dominant presence of toxic congeners 153,138 and 180, similar in toxicity to dioxins, is the highest concentration of hex PCB congener 138, near the Halda landfill in Nikšić, Fig. 1. The results from Nikšić showed that in the soil samples near the Halda landfill, in addition to the dominant presence of congeners fig. dioxins, which is most likely a consequence of the impact of the industrial waste dump, the presence, in a higher concentration, of ongeners with fewer chlorine atoms, which is the result of biological decomposition of congeners with a higher chlorine content, was also detected.

Table 1. Results of soil samples from Nikšić. Source: Authors.

Depth		0-30cm		0-30cm	Measurement results 0-30cm	0-30 cm	
PCB 18	mg/kg	<0,002		0.023±0.003		<0.002	
PCB 31	mg/kg	<0.002		0.110±0.013		0.0020±0.0002	
PCB 28	mg/kg	<0.002		0.115±0.013		0.0020±0.0002	
PCB 52	mg/kg	<0.002		0.094±0.012		<0.002	
PCB 44	mg/kg	<0.002		0.066±0.008		<0.002	
PCB 101	mg/kg	<0.002		0.111±0.012		0.0100±0.0011	
PCB 149	mg/kg	<0.002		0.075±0.008		0.0220±0.0022	
PCB 118	mg/kg	<0.002		0.238±0.024		0.0079±0.0007	
PCB 153	mg/kg	<0.002		0.212±0.021		0.0230±0.023	
PCB 138	mg/kg	<0.002		0.253±0.023		0.0250±0.025	
PCB 180	mg/kg	<0.002		0.117±0.018		0.018±0.027	
PCB 194	mg/kg	<0.002		0.019±0.003		0.0030±0.0004	

Conclusion

The need to solve this problem has existed for half a century, but there is still no concrete progress. Montenegro adopted a new Law on Waste Management and a set of corresponding strategies and by-laws, which established a solid legal framework that is in line with European Union (EU) legislation.The hazardous waste management model must be harmonized with European ones, and the rehabilitation of this landfill is urgent.

The legal obligation of competent inspection authorities, at the local and state level, is to monitor whether waste is disposed of at the location determined by spatial planning regulations and to control whether waste is managed in accordance with the law.

It is necessary to react urgently at all levels, both local and central, because the waste pollution that we are witnessing today in Montenegro is a matter of national interest, it affects public health, the natural environment, the Montenegrin economy, tourism, thus on all aspects of life, Climate change which we witness are largely caused by human activities, primarily through the emission of gases with the greenhouse effect. Competent authorities should invest efforts in strengthening infrastructure, education and implementation of legislation for efficient waste management and emission reduction, as well as that when making important decisions about how to set up waste management in the country, hierarchy and relevant independent sources of information should always be consulted.

Acknowledgements

References

[1] Allen, A (2000) Containment landfills: the myth of sustainability. *Engineering geology 60 (1- 4), 3-19.*

[2] Asif Z, Chen Z. (2016) Multimedia environmental analysis of PCBs fate and transport mechanism through a case study of transformer oil leakage. *International Journal of Environmental Science and Technology.* 2016;13(3):793–797.

[3] Baibergenova A, Kudyakov R, Zdeb M, Carpenter DO (2003): Low birth weight and residental proximity to PCB-contaminated waste sites. *Environmental Health Perspectives 111(10), 1352-1357*

[4] Bielská L, Šmidová K, Hofman J. (2013) Supercritical fluid extraction of persistent organic pollutants from natural and artificial soils and comparison with bioaccumulation in earthworms. *Environmental Pollution.* 2013; 176:48–54. Doi: 10.1016/j.envpol.2013.01.005

[5] Brunner PH, Fellner J. (2007): *Setting priorities for waste management strategies in developing countries. Waste Management and Research 25, 234-240*

[6] Chen L., Yang Y., Chen J., Gao S., Qi S., Sun C., Shen Z. (2017) Spatial-temporal variability and transportation mechanism of polychlorinated biphenyls in the Yangtze River Estuary. *Science of The Total Environment, 598, 12, 2017.*

[7] Cordellicchio N, Buccolieri A, Giandomenico S, Lopez L, Pizzulli F, Spada L. (2007) Organic pollutants (PAHs, PCBs) in sediments from the Mar Piccolo in Taranto (Ionian sea, Southerne Italy). *Mar. Pollu. Bull. 55 451-458*

[8] Duan X., Li Y., Li X., Li M., Zhang D. (2013) Distributions and sources of polychlorinated biphenyls in the coastal East China Sea sediments. *Science of The Total Environment, 463, 894,*

[9] Eriksson P, Fischer C, Fredriksson A. (2006) Polybrominated diphenyl ethers, a group of brominated flame retardants, can interact with polychlorinated biphenyls in enhancing developmental neurobehavioral defects. *Toxicol Sci 2006; 94(2): 302- 9.*

[10] Foster G.D., Walls C., Mceachern P.R., Huff T.B., (2019) Mcbride R. Sedimentary profiles of pollution marker chemicals along a large tributary of Chesapeake Bay (mid-Atlantic USA). *Journal of Soils and Sediments, 19 (3), 1511, 2019.*

[11] Fu C, Wu S. (2006) Seasonal variation of the distribution of PCB in sediments and biota in a PCB contaminated estuary. *Chem 62 1786-1794.*

[12] Gabryszewska M. and Barbara Gworek, (2021) Municipal waste landfill as a source of polychlorinated biphenyls releases to the environment. *Natural Library of Medicine, Natural Center for Biotechnology information,*

[13] Herkert, N.J., Jahnke, J.C., Hornbuckle, K.C., (2013) Emissions of tetrachlorobiphenyls (PCBs 47, 51, and 68) from polymer resin on kitchen cabinets as a non-Aroclor source to residential air. Environ. Sci. Technol. 52 (9), 5154–5160.

[14] Jankovic S, Jurčić M, Radičević T, Stefanović S, Lenhardt M, Durgo K, Antonijević B. (2010) Non-dioxin-like PCBs in ten different fish species from the Danube river in Serbia. Environ Monit Assess 2010; 181(1-4): 153-63.

[15] Kanzari F, Syakti A D, Asia L , Malleret L, Piram A, Mille G, Doumenq P. (2014) Distributions and sources of persistent organic pollutants (aliphatic hydrocarbons, PAHs, PCBs and pesticides) in surface sediments of an industrialized urban river (Huveaune), *France. Science of the Total Environment 478 141–151*

[16] Kaya D, Imamoglu I, Sanin FD, Sowers KR. (2013) A comparative evaluation of anaerobic dechlorination of PCB-118 and Aroclor 1254 in sediment microcosms from three PCB-impacted environments. *Journal of Hazardous Materials.* 2018; 341:328–335.

[17] Klanova J, Eupr P, Kohoutek J, Harner T (2008): Assessing the influence meteorological parameters on the performance of polyurethane foambased passive air samplers.

[18] Kodavanti P. R. (2017.) *Reference module in neuroscience and biobehavioral psychology.* Amsterdam: Polychlorinated Biphenyls (PCBs) Encyclopedia of the Neurological Sciences; pp. 917–921

[19] Li Q, Yang K, Wang Y, Jin B, Luo C, Li J, Zhang G. (2018) Environmental behaviour of polychlorinated biphenyls in a paddy field: impact factors and canopy effects. *Science of the Total Environment.* 2018;637–638:50– 57.

CITRIC ACID ROLE: METALS CORROSION INHIBITOR OR ACCELERATOR

Nataliia Rudenko[1], George-Daniel Dima[2], Mircea Laurențiu Dan[2]

[1]Innovation and Technology Transfer Center, University Politehnica Timisoara 2 V. Parvan, 300223 Timisoara, Romania
[2]Faculty of Industrial Chemistry and Environmental Engineering, University Politehnica Timisoara, 6 V. Parvan, 300223 Timisoara, Romania
e-mail: mircea.dan@upt.ro

Abstract

Citric acid, a naturally occurring component and common metabolite in plants and animals, is the most versatile and widely utilized organic acid, with primary applications in the food industry (60%) and pharmaceuticals (10%). It is also used in a variety of other fields.

Citric acid is widely used in the food industry to stabilize or preserve medicines and as a disinfectant. Because of it acidic, sour-tasting nature, citric acid is predominantly used as a flavoring and preserving agent, especially in carbonated drinks and candies.

Also, the action of the different chemical components in sweetened drinks foods in general is bound to be dependent on the metal or alloy. For example, because citric acid is described to inhibit the corrosion of aluminium [1,2,3,4,5], carbon steel [6] and stainless steel [7], it is also reported to enhance the corrosion of tin in similar media [8].

The aim of this work is to investigate how the addition of citric acid with different concentrations affects the corrosion process of samples from carbon steel, aluminium and copper in neutral environment.

Citric acid ($C_6H_8O_7$) has IUPAC name 2-hydroxy-1,2,3-propanetricarboxylic acid and its chemical structure is shown in Figure 1.
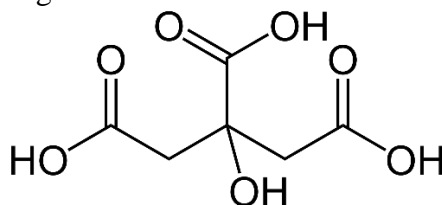
Figure 1. Citric acid chemical structure

In this study, potentiodynamic polarization and chronoamperometry techniques were employed to assess the inhibition efficiency of citric acid in test solutions. The electrochemical behavior of citric acid in basic solution was researched using cyclic voltammetry on a platinum electrode. Additionally, the Tafel method was used to determine the kinetic parameters for the corrosion process under investigation. To better understand the behavior of citric acid in a neutral solution during corrosion studies on various metal surfaces, an electrical equivalent circuit was modeled based on data from electrochemical impedance spectroscopy (EIS) spectra. Potential interactions between citric acid molecules and the metal surfaces of the tested materials were analyzed using quantum chemical calculations and molecular modeling.

The aim of this article is the studying the corrosion of metal samples in neutral environment (basic solution 0.25 mol L^{-1} Na_2SO_4 solution-a base solution). Also was studied effect of citric acid (inhibitor or accelerator) on the investigated materials. During investigations a range of solutions with concentrations of citric acid 0.25; 0.5; 1; 2.5; 5; 7.5; 10 g /L was used. The corrosion test electrode was made from different metals. Experimental equipment consists of classic electrolytic cell with three electrodes: graphite counter electrodes, working electrodes

(OLC 52, Al, Cu) and reference electrode Ag/AgCl, which was connected to a Biologic SP150 potentiostat/galvanostat.

References
1. R. Solmaz, G. Kardaş, B. Yazıcı, M. Erbil, Corros. Eng. Sci. Technol. 43 (2008) 186–191.
2. E.E. Abd El Aal, S. Abd El Wanees, A. Farouk, S.M. Abd El Haleem, Corros. Sci. 68 (2013) 14-24
3. M. Šerug, D. Hasenay, J. Appl. Electrochem. 31 (2001) 961–967.
4. B. Müller, Corros. Sci. 46 (2004) 159–167.
5. Zh. Wang, Zh. Cai, X. Han, H. Zhang, Zh. Shao, K. Xiao, Y. Fan, Sh. Wang, Int. J. Electrochem. Sci. 18:4 (2023) 100073.
6. H. Ashassi-Sorkhabi, E. Asghari, M. Mohammadi, J. Mater. Eng. Perform. 23 (2004) 2992–3000.
7. A. T. da Costa, M. C. Lopes de Oliveira, R. A. Antunes, Surf. Interface Anal., 53:3 (2021) 374-384.
8. M.S.S. Morad, A.A. Hermas, J. Chem. Technol. Biotechnol. 76 (2001) 401–410.

COMPREHENSIVE ANALYSIS OF THE EFFECT OF RENEWABLE ENERGY ON THE STABILITY OF THE ENVIRONMENT

Ahmed Salah Ahmed[1], Mohamed Saad[2]

[1]Department of chemical engineering, Atatürk University, 25030 Yakutiye, Erzurum, Turkey.
[2]Department of Chemical Engineering, Cairo University, Arab Republic of Egypt
e-mail: ahmedsalah221994@yahoo.com

Abstract
This work represents a review of the effect of renewable energy on the stability of the environment through generating clean energy with no greenhouse gas emissions and lowering some types of air pollution by using comprehensive analysis of the processes such as consumption and production. It aims to audit the research articles in addition to the aspects and opinions to scrutiny and handle the challenges. Besides, creating an extensive vision aimed at completing research development by analyzing the published papers, patents, and industrial designs in this field. Furthermore, this present study aims to highlight on the efficient energy conversion systems, sources of greenhouse gas emissions as an attempt to reach an optimal solution to preserve the environment and climate through modern technologies. Renewable energy has unstable and indirect performance due to changing of the climate in the current era. The unstable characteristics lower the popularization and use of renewable energy resources. According to the energy consumption, analysis and studies of management system refer to the generation of photovoltaic power and wind power capacity data are predicted accurately by multiple models which are combined with an optimal control solution equation to manage it scientifically with high efficiency. In addition, the output of generating solar energy, wind power, or photovoltaic power can be flexibly selected and applied to the maximum extent. On the other hand, the energy consumption cost is minimized. So, the utilization efficiency of renewable energy sources by electricity will be improved and made considerable contributions to improving the capacity of green energy and keeping the environment lower polluted.

Introduction
Our world is facing many important environmental challenges due to the use of non-renewable energy sources and fossil fuels which have major damage and threaten stability of the environment. Carbon dioxide and other greenhouse gases are released into the atmosphere when fossil fuels such as coal and oil are burned, leading to non-equilibrium in the environmental system and climate change.The continuous use of non-renewable energy sources leads to environmental pollution and produces emissions such as carbon dioxide (CO_2), methane (CH_4), nitrous oxide (N_2O), hydrochlorofluorocarbons (HCFCs), hydrofluorocarbons (HFCs), and ozone (O_3). These gases are the principal greenhouse gases whose concentrations are increasing in the lower atmosphere [1]. To mitigate these critical challenges, renewable energy resources are considered as more ecologically friendly alternatives to traditional energy sources. Currently, climate and integrated assessment models are used to estimate this effect on essential renewables through scientific statistics and costs are quantified across recent technologies. This review paper presents a comprehensive analysis of the effect of renewable energy on the stability of the environment "ecological stability". There are many types of resources of renewable energy such as solar, biomass, geothermal, wind and other resources.

Experimental

Renewable energy resources are derived from natural resources that replenish themselves over time, such as sunshine, water, and wind. In this era, these renewable resources are getting more significant in total primary energy supply (TPES) nearly 15% of the global primary energy as follows: bioenergy (10%) and hydropower (3%), and the rest in other renewables (2%) such as photovoltaic (PV) and wind energy. By 2040, renewables may supply 20-30% of the world's primary energy. The modern studies suggest that the world will move toward a completely renewable energy system by 2050. Environmental deterioration and greenhouse gas emissions are the new millennium's issues. Rapid economic expansion endangers humanity by depleting resources, polluting the environment, and causing climate change [2]. To meet these global issues, the UNFCCC (United Nations Framework Convention on Climate Change) has evolved an essential framework for international collaboration close to declining environmental quality. Energy consumption is a requirement for economic growth and is seen as a key part of economic growth. Around the world, fossil fuels, often known as conventional energy sources, are the major source of energy. Almost 85% of total energy demands are met by fossil fuels, which also account for increasing greenhouse gas emissions (CO_2 equivalent).

Results and discussion

As known, the use of renewable energy recourses has advantages and disadvantages. All dimensions must be put in order to reach the optimal using of these recourses and benefit to individuals, societies and preserving the environment. Some advantages of renewable energy are [5]:

1. Sustainability: renewable energy sources can be used indefinitely without decreasing the environment's natural resources.

2. Reduction of Greenhouse Gases (GHG): Renewable energy resources produce almost no greenhouse gases, which are a major driver of climate change, which occurs when changes in the Earth's climate system led to new climate patterns that persist over long periods of time. the period can be only a few tens of years or millions of years.

3. Economical: The cost of renewable energy sources has decreased significantly in recent years, making them more cost-effective and competitive compared to traditional energy sources.

4. Employment opportunities: are created by the renewable energy sector, including production, installation and maintenance.

5. Energy Independence: The use of renewable energy technologies can help the world become energy independent and less dependent on imported oil and gas.

On the other hand, some of disadvantages of renewable energy:

1. Intermittency: Renewable resources like wind and solar are intermittent. Solar and wind farms power manufacturing in Europe were acknowledged to differ among zero to 23 and 24 GW of power respectively all through top times.

2. High upfront costs: The initial cost of installing renewable energy technologies such as solar panels and wind turbines can be high, although the cost has decreased in recent years.

3. Land use: Renewable energy technologies such as wind turbines and solar panels require large amounts of land, which can be a challenge in densely populated areas.

4. Wildlife impact: Renewable energy technologies can have a negative impact on wildlife, particularly birds and bats, which can be killed or injured by wind turbines.

5. Energy storage: Renewable energy technologies require energy storage systems to store excess energy generated during periods of high availability, which can be costly and present technical challenges.

Figure 1. Multi-model mean change in climate patterns and yields determining renewable energy potential for RCP6.0
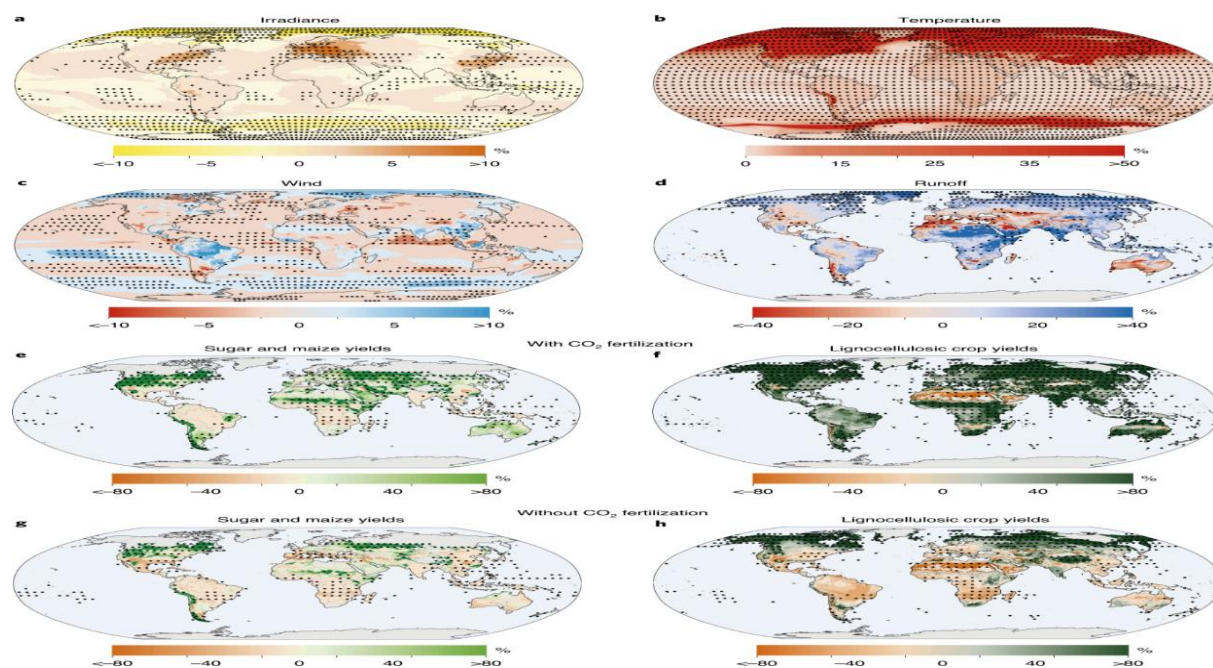
Conclusion

Renewable energy provides a lot of environmental benefits for instance:

1- Reducing greenhouse gas emissions: One of the primary drivers of climate change is the use of fossil fuels for energy. Renewable energy sources, on the other hand, such as solar, wind, hydropower, and geothermal, emit no greenhouse emissions during operation. We can dramatically cut greenhouse gas emissions and alleviate the consequences of climate change by lowering our reliance on fossil fuels and increasing our usage of renewable energy sources.

2- Improving air quality: The combustion of fossil fuels generates a variety of damaging pollutants into the atmosphere, including sulfur dioxide, nitrogen oxides, and particulate matter. These contaminants can be harmful to one's health.

3-Water resource conservation: Many types of renewable energy, such as solar and wind energy, do not use water to create power. This is significant since many parts of the world are suffering from water scarcity, and traditional power plants that rely on water for cooling might compound the situation.

4-Reduced land usage: Traditional power plants sometimes need extensive land use for mining, drilling, and extraction of fossil fuels. Renewable energy sources, on the other hand, may be put in a considerably smaller footprint, which means they have a lower impact on wildlife habitats and natural ecosystems.

5-Long-term energy security: fossil fuels are finite resources that will run out someday. Renewable energy sources, such as solar and wind energy, on the other hand, are nearly limitless. We can assure a more secure and sustainable energy supply for future generations by shifting to renewable energy sources.

Acknowledgements

period. His/her expertise and wisdom were an invaluable asset to this project. I am grateful to the Atatürk University for offering facilities and resources for this project. Their support facilitated the smooth execution of the research.

References

1-WMO Greenhouse Gas Bulletin (GHG Bulletin), No.17: The State of Greenhouse Gases in the Atmosphere Based on Global Observations, 2020.

2-Report of IEA. World Energy Outlook (International Energy Agency, 2017).

3-Fang Wang, Technologies and perspectives for achieving carbon neutrality, Volume 2, Issue 4, 28 100180, November. 2021.

4-Dario Maradin, Advantages and Disadvantages of Renewable Energy Sources Utilization, University of Rijeka, International Journal of Energy Economics and Policy-Vol 11 - Issue 3, April 2021.

5-Kenneth Hansen, K., Breyer, C. & Lund, H. J. E. Status and perspectives on renewable energy systems. Energy 175, 471–480 (2019).

6-Ali Q. Al-Shetwi, Sustainable development of renewable energy integrated power sector: Trends, environmental impacts, and recent challenges, Elsevier Journal, Volume 822, 20 May 2022, 153645.

7-Bin Zheng, Sheng Wang and Jingxin Xu, A Review on the CO2 Emission Reduction Scheme and Countermeasures in China's Energy and Power Industry under the Background of Carbon Peak, MDPI Sustainability 2022, 14(2), 879 January 2022.

8-Mousa Gowfal Selmey & Ahmed A Elamer, Economic policy uncertainty, renewable energy and environmental degradation: Evidence from Egypt, Environmental Science and Pollution Research, 58603–58617 (2023).

9-"Climate change impacts on renewable energy supply", nature climate change, 119-125 January (2021).

10-Muhammad Kamran, Muhammad Rayyan Fazal, Chapter 2, Thermodynamics for renewable energy systems, Renewable Energy Conversion Systems, 2021, Pages 1-19, May 2021.

THE WEEDS IN SOYBEAN AND THE EFFICACY OF THEIR CONTROL BY FLUMIOXAZIN 510 g/kg WG

Nataša Samardžić[1], <u>Bojan Konstantinović</u>[1], Milena Popov[1], Tijana Stojanović[1], Stefan Ugrinov[1], Milana Vučković[1], Savka Blagojević[1]

[1]*University of Novi Sad, Faculty of Agriculture, Department of Environmental and Plant Protection, Trg Dositeja Obradovića 8, 21000 Novi Sad, Republic of Serbia*
e-mail: bojan.konstantinovic@polj.edu.rs

Abstract
Soybean is one of the most important agricultural crops and one of the leading problems in the soybean production is the presence of the weeds. The weed species are, for the most part, controlled by herbicides. The use of soil herbicides, as well as the subsequent application of the corrective foliar herbicides, reduces the amount of the potential weeds on the field. During the vegetative period in 2023, the number of the weed species was monitored at four localities in the Republic of Serbia (Stara Pazova, Kać, Despotovo and Čurug), after which the efficacy of different application rates of flumioxazine 510 g/kg WG was compared. At the application rates of 0.12 and 0.16 kg/ha, the studied herbicide had high level of efficacy in the control of: *A. retroflexus*, *D. stramonium*, *C. hybridum*, *H. trionum*, *S. glauca*, *S. arvensis* and *S. nigrum*, satisfactory efficacy in case of *C. album* and *B. convolvulus*, poor to satisfactory efficacy in case of *S. halepense* and low efficacy in the control of *A. theophrasti*, *A. artemisiifolia*, *C. arvense*, *C. arvensis* and *X. strumarium*. The standard showed the same results as the tested herbicide. The phytotoxicity was not observed.

Introduction
Soybean, scientifically known as *Glycine max* (L.) Merrill, is one of the oldest cultivated plants, with roots tracing back to the Far East around 3000 BC. Renowned for its high protein and oil content, along with essential minerals and vitamins, soybean is a crucial agricultural resource for both human and animal nutrition, as well as various industrial applications. Despite its nutritional importance, soybean has not always received the recognition it deserves in agricultural production. Originating in China, the plant later spread to southern China, Korea and Japan, which are considered the secondary centers of its development. The soybean gained wider awareness in the West during the 18th century due to advancements in maritime transport, leading to its introduction in European and American botanical gardens. Benjamin Franklin is credited with bringing soybean to America. By the 19th century, soybean began to proliferate globally, solidifying its role in modern agriculture [1]. For successful soybean production, it is essential to adhere to all recommended agronomic practices, with weed control playing a critical role. Soybean, like the other field crops, is particularly vulnerable to competition with the weeds during the early growth stages, when the greatest struggle occurs for available space, sunlight, water and nutrients [2]. In soybean, as in the other row crops, a wide range of different weed species can be encountered. Some of the most prevalent broadleaf weeds in soybean are: *Abutilon theophrasti* Medik., *Amaranthus retroflexus* L., *Ambrosia artemisiifolia* L., *Chenopodium album* L., *Cirsium arvense* (L.) Scop., *Convolvulus arvensis* L., *Datura stramonium* L., *Hibiscus trionum* L., *Polygonum convolvulus* L., *Sinapis arvensis* L., *Solanum nigrum* L., *Xanthium strumarium* L., etc., while the important grass weeds which can occur are: *Agropyrum repens* L., *Digitaria sanguinalis* (L.) Scop., *Echinochloa crus-galli* (L.) P.Beauv., *Panicum* sp., *Setaria* sp. and *Sorghum halepense* L. [3]. The objective of the research was to identify and monitor weed vegetation in soybean crops at four studied localities under the

conditions of chemical control. The aim of the study was to determine and evaluate the efficacy of the tested herbicide for the weed control in soybean.

Experimental

During the growing season in 2023 (in May and June) the study conducted on the weed flora in soybean crops at four localities in the Republic of Serbia (Stara Pazova, Kać, Despotovo and Čurug) was carried out. The assessment of the weed species in soybean fields involved counting the weeds in randomly chosen 1 m² quadrants within each 25 m² plot. This method allowed for a systematic evaluation of weed diversity in the crop. The identification of the weed species was done according to the literature sources [4,5]. The experiment was conducted using a randomized block design with four replicates, which included a standard treatment (the herbicide with the same formulation and equivalent amount of active ingredient as the one being tested) and a control group (untreated plots), following EPPO guidelines [6,7]. Weather conditions throughout the experiment were optimal for the effective performance of the herbicides under investigation. The results were compiled and analyzed at the University of Novi Sad, Faculty of Agriculture, Department of Environmental and Plant Protection, using MS Excel and Statistica 10. This analysis was based on the average values from four plots for each treatment, including the control. The efficacy of the studied herbicide was assessed using the following categories: poor efficacy (less than 75%), satisfactory efficacy (75-90%) and high efficacy (greater than 90%). Phytotoxicity was visually assessed on a scale from 0 to 100% during the efficacy evaluation, where 0% indicates no visible signs of phytotoxicity and 100% signifies complete plant degradation. Flumioxazin 510 g/kg WG was applied at two application rates: 0.12 and 0.16 kg/ha, while the standard was applied at the rate 0.16 kg/ha. Table 1 provides the details of the field sites and the experiment.

Table 1. The overall information about the field sites and the experiment

Locality	Stara Pazova	Kać	Despotovo	Čurug
Coordinates	44°58'59''N 20°11'19''E	45°20'18''N 19°52'23''E	45°27'52''N 19°34'13''E	45°31'33''N 20°01'45''E
Crop variety	Dukat	Rubin	Wendy	Rubin
Sowing time	20.04.2023.	30.04.2023.	30.04.2023.	01.05.2023.
Date of application	22.04.2023.	04.05.2023.	05.05.2023.	04.05.2023.
Temperature atmoa* [C°]	15.87	15.60	17.09	15.53
Humidity atmoa [%]	42.85	76.06	84.66	77.36
Amount of water used [l/ha]	300	300	300	300
First assessment	06.05.2023.	22.05.2023.	22.05.2023.	22.05.2023.
Second assessment	13.05.2023.	05.06.2023.	29.05.2023.	05.06.2023.

*atmoa – at the moment of application

Results and discussion

Flumioxazin is a selective, contact (foliar) herbicide from the chemical group of N-phenylphthalimides. Flumioxazin is used for post-emergence control of annual broadleaf weeds. Its mode of action affects the chlorophyll biosynthesis and inhibits the PPO (protoporphyrinogen oxidase) activity, leading to the irreversible damage to the function and structure of the lipid membranes [8].

Efficacy of flumioxazin 510 g/kg WG at Stara Pazova locality. The results of flumioxazin 510 g/kg WG efficacy at Stara Pazova locality are shown in Table 2.

Table 2. The efficacy of flumioxazin 510 g/kg WG at Stara Pazova locality.

Weed species	Control	Flumioxazin 510 g/kg WG 0.12 kg/ha		Flumioxazin 510 g/kg WG 0.16 kg/ha		Standard 510 g/kg WG 0.16 kg/ha	
	No./m²*	No./m²	Eff.*	No./m²	Eff.	No./m²	Eff.
First assessment							
Abutilon theophrasti	3.25	1.25	61.54	1.00	69.23	1.00	69.23
Ambrosia artemisiifolia	4.00	1.50	62.50	1.25	68.75	1.25	68.75
Chenopodium album	4.75	1.00	78.95	0.75	84.21	0.50	89.47
Cirsium arvense	4.75	2.00	57.89	1.25	73.68	1.50	68.42
Datura stramonium	4.00	0.25	93.75	0.00	100.00	0.25	93.75
Solanum nigrum	3.50	0.00	100.00	0.00	100.00	0.00	100.00
Second assessment							
Abutilon theophrasti	4.50	1.75	61.11	1.50	66.67	1.25	72.22
Ambrosia artemisiifolia	6.00	3.00	50.00	2.00	66.67	2.25	62.50
Chenopodium album	6.25	1.50	76.00	1.00	84.00	0.75	88.00
Cirsium arvense	6.00	2.75	54.17	2.00	66.67	2.25	62.50
Datura stramonium	6.50	0.50	92.31	0.00	100.00	0.25	96.15
Solanum nigrum	5.50	0.25	95.45	0.00	100.00	0.00	100.00

*No./m² – number per m²; Eff. – efficacy

Flumioxazin 510 g/kg WG applied at the rates 0.12 and 0.16 kg/ha at Stara Pazova locality had high efficacy in the control of *D. stramonium* and *S. nigrum*, satisfactory efficacy in case of *C. album* and poor efficacy for the remaining three weed species.

Efficacy of flumioxazin 510 g/kg WG at Kać locality. The results of flumioxazin 510 g/kg WG efficacy at Kać locality are shown in Table 3.

Table 3. The efficacy of flumioxazin 510 g/kg WG at Kać locality.

Weed species	Control	Flumioxazin 510 g/kg WG 0.12 kg/ha		Flumioxazin 510 g/kg WG 0.16 kg/ha		Standard 510 g/kg WG 0.16 kg/ha	
	No./m²*	No./m²	Eff.*	No./m²	Eff.	No./m²	Eff.
First assessment							
Ambrosia artemisiifolia	4.75	1.75	63.16	1.25	73.68	1.25	73.68
Chenopodium album	4.25	0.00	100.00	0.00	100.00	0.00	100.00
Sinapis arvensis	4.00	0.00	100.00	0.00	100.00	0.00	100.00
Solanum nigrum	3.75	0.25	93.33	0.00	100.00	0.00	100.00
Xanthium strumarium	5.00	2.00	60.00	1.75	65.00	1.50	70.00
Second assessment							
Ambrosia artemisiifolia	7.25	3.00	58.62	2.25	68.97	2.00	72.41
Chenopodium album	5.00	0.25	95.00	0.00	100.00	0.00	100.00
Sinapis arvensis	6.25	0.50	92.00	0.25	96.00	0.00	100.00
Solanum nigrum	5.50	0.50	90.91	0.00	100.00	0.25	95.45
Xanthium strumarium	6.75	2.50	62.96	2.00	70.37	2.25	66.67

*No./m² – number per m²; Eff. – efficacy

Flumioxazin 510 g/kg WG applied at the rates 0.12 and 0.16 kg/ha at Kać locality had poor efficacy in the control of *A. artemisiifolia* and *X. strumarium*, as well as the high efficacy in case of the remaining three weed species.

Efficacy of flumioxazin 510 g/kg WG at Despotovo locality. The results of flumioxazin 510 g/kg WG efficacy at Despotovo locality are shown in Table 4.

Table 4. The efficacy of flumioxazin 510 g/kg WG at Despotovo locality.

Weed species	Control	Flumioxazin 510 g/kg WG 0.12 kg/ha		Flumioxazin 510 g/kg WG 0.16 kg/ha		Standard 510 g/kg WG 0.16 kg/ha	
	No./m^{2*}	No./m^2	Eff.*	No./m^2	Eff.	No./m^2	Eff.
First assessment							
Ambrosia artemisiifolia	4.25	2.25	47.06	2.00	52.94	1.75	58.82
Chenopodium album	3.75	0.75	80.00	0.50	86.67	0.50	86.67
Convolvulus arvensis	4.25	2.00	52.94	1.75	58.82	1.50	64.71
Setaria glauca	3.50	0.25	92.86	0.00	100.00	0.00	100.00
Sorghum halepense	4.25	2.00	52.94	1.50	64.71	1.25	70.59
Xanthium strumarium	3.00	1.50	50.00	1.00	66.67	1.00	66.67
Second assessment							
Ambrosia artemisiifolia	5.75	3.50	39.13	2.75	52.17	2.50	56.52
Chenopodium album	4.75	1.00	78.95	0.75	84.21	0.75	84.21
Convolvulus arvensis	6.50	3.25	50.00	2.75	57.69	2.50	61.54
Setaria glauca	4.25	0.25	94.12	0.00	100.00	0.00	100.00
Sorghum halepense	6.50	3.50	46.15	2.50	61.54	2.00	69.23
Xanthium strumarium	5.50	2.75	50.00	2.00	63.64	2.25	59.09

*No./m^2 – number per m^2; Eff. – efficacy

Flumioxazin 510 g/kg WG applied at the rates 0.12 and 0.16 kg/ha at Despotovo locality had high efficacy in the control of *S. glauca*, satisfactory efficacy in case of *C. album* and poor efficacy for the remaining four weed species.

Efficacy of flumioxazin 510 g/kg WG at Čurug locality. The results of flumioxazin 510 g/kg WG efficacy at Čurug locality are shown in Table 5.

Table 5. The efficacy of flumioxazin 510 g/kg WG at Čurug locality.

Weed species	Control	Flumioxazin 510 g/kg WG 0.12 kg/ha		Flumioxazin 510 g/kg WG 0.16 kg/ha		Standard 510 g/kg WG 0.16 kg/ha	
	No./m^{2*}	No./m^2	Eff.*	No./m^2	Eff.	No./m^2	Eff.
First assessment							
Amaranthus retroflexus	5.00	0.25	95.00	0.00	100.00	0.00	100.00
Ambrosia artemisiifolia	3.50	1.25	64.29	1.00	71.43	1.00	71.43
Bilderdykia convolvulus	4.25	0.75	82.35	0.50	88.24	0.50	88.24
Datura stramonium	4.00	0.25	93.75	0.00	100.00	0.25	93.75
Hibiscus trionum	3.50	0.25	92.86	0.00	100.00	0.00	100.00
Sorghum halepense	4.75	1.00	78.95	0.75	84.21	0.50	89.47
Second assessment							
Amaranthus retroflexus	6.50	0.50	92.31	0.00	100.00	0.00	100.00
Ambrosia artemisiifolia	5.50	2.00	63.64	1.50	72.73	1.75	68.18
Bilderdykia convolvulus	5.75	1.00	82.61	0.75	86.96	1.00	82.61
Datura stramonium	6.00	0.50	91.67	0.25	95.83	0.50	91.67
Hibiscus trionum	5.50	0.50	90.91	0.00	100.00	0.25	95.45
Sorghum halepense	6.25	1.50	76.00	1.00	84.00	0.75	88.00

*No./m^2 – number per m^2; Eff. – efficacy

Flumioxazin 510 g/kg WG applied at the rates 0.12 and 0.16 kg/ha at Čurug locality had poor efficacy in the control of *A. artemisiifolia*, satisfactory efficacy in case of *B. convolvulus* and *S. halepense*, as well as the high efficacy for the remaining three weed species.

The results obtained in this study are similar to those from the research published by [9], in which flumioxazin had high efficacy in the control of the majority of the broadleaf weeds, such as *A. retroflexus* and *H. trionum*, even in case of *A. theophrasti* and *C. album* for which, in our study, the efficacy was poor or satisfactory.

Conclusion

According to the obtained results it can be concluded that the flumioxazin 510 g/kg WG at the application rates of 0.12 and 0.16 kg/ha had high level of efficacy in the control of: *A. retroflexus*, *D. stramonium*, *C. hybridum*, *H. trionum*, *S. glauca*, *S. arvensis* and *S. nigrum*, satisfactory efficacy in case of *C. album* and *B. convolvulus*, poor to satisfactory efficacy in case of *S. halepense* and low efficacy in the control of *A. theophrasti*, *A. artemisiifolia*, *C. arvense*, *C. arvensis* and *X. strumarium*. The standard showed the same results as the tested herbicide. The phytotoxicity was not observed.

References

[1] B. Vlahović, S. Ilin, A. Puškarić, Status and perspectives of soybean production worldwide and in the Republic of Serbia, Economic Insights – Trends and Challenges 2(1) (2013), pp. 38-46.

[2] M. Vučković, Weeds in soybean at the localities Stara Pazova and Kać and the possibilities of their control, Master thesis, University of Novi Sad, Faculty of Agriculture, Department of Environmental and Plant Protection, Novi Sad, Republic of Serbia, 2023.

[3] S. Blagojević, Korovi u usevu soje na lokalitetima Despotovo i Čurug i njihovo suzbijanje, Bachelor's thesis, University of Novi Sad, Faculty of Agriculture, Department of Environmental and Plant Protection, Novi Sad, Republic of Serbia, 2023.

[4] M. Josifović (Ed.), Flora SR Srbije I-X, SANU, Belgrade, Republic of Serbia, 1970-1986.

[5] T. Šarić, Atlas korova: 100 najvažnijih korovskih biljaka u Jugoslaviji, Svjetlost, Sarajevo, Bosnia and Herzegovina, 1991.

[6] European and Mediterranean Plant Protection Organization (EPPO), Guideline for the efficacy evaluation of plant protection products, Phytotoxicity assessment, PP 1/135 (4), EPPO Bulletin 44(3) (2014), pp. 265-273.

[7] European and Mediterranean Plant Protection Organization (EPPO), Guideline for the efficacy evaluation of herbicides, Weeds in soybean, PP 1/305 (1), EPPO Bulletin 47(3) (2017), pp. 342-345.

[8] Tim priređivača, Pesticidi u poljoprivredi i šumarstvu u Srbiji, Dvadeset prvo, izmenjeno i dopunjeno izdranje, Društvo za zaštitu bilja Srbije, Belgrade, Republic of Serbia, 2022.

[9] M.C. Oliveira, D. Feist, S. Eskelsen, J.E. Scott, S.Z. Knežević, Weed control in soybean with preemergence- and postemergence-applied herbicides, Crop, Forage & Turfgrass Management 3 (2017), pp. 1-7.

THE VALUE OF WORKPLACE ENVIRONMENT IN THE HOSPITALITY INDUSTRY: EMPLOYEE PERSPECTIVES

Selena Samardžić[1], Nenad Novaković[2], Robert Laktoš[1], Aleksandra Mihailović[1], Savka Adamović[3]

[1]Department of Fundamental Disciplines, University of Novi Sad, Faculty of Technical Sciences Trg Dositeja Obradovića 6, Serbia
[2]Department of Industrial Engineering and Engineering Management, University of Novi Sad, Faculty of Technical Sciences, Trg Dositeja Obradovića 6, Serbia
[3]Department of Graphic Engineering and Design, University of Novi Sad, Faculty of Technical Sciences, Trg Dositeja Obradovića 6, 21000 Novi Sad, Serbia
e-mail: selena@uns.ac.rs

Abstract
Employees are valuable assets for organizations, and their well-being is crucial for productivity and success. The workplace environment significantly affects employees' cognitive and emotional states, behavior, engagement, performance, and productivity. Factors such as room design, layout, cleanliness, equipment quality, temperature, ventilation, lighting, noise levels and air quality all play a crucial role in creating a comfortable and engaging workplace environment. This study highlights the importance of these factors and underscores the potential benefits of further research on how they impact employee productivity in hospitality organizations. The findings suggest that lighting quality significantly influences employees' perception of working conditions, while noise levels positively correlate with productivity and employee health.

Introduction
Employees and their skills are valuable intangible assets for an organization. A successful organization prioritizes the well-being of its employees by providing a high-quality, enjoyable, and safe work environment, recognizing that employees spend a significant amount of time at work. The workplace environment not only dramatically influences the cognitive and emotional states, concentration, behavior, actions, and abilities of employees across various organizations, but also plays a crucial role in their well-being. It significantly impacts employee engagement, performance, and overall productivity and profitability of the organization. The potential benefits of a high-quality work environment are vast, offering the promise of enhanced employee well-being and organizational success.
Clements-Croome [1] reports that providing a healthy working environment for employees is crucial in enhancing human productivity. Failing to do so could negatively affect employee health, such as reduced concentration, fatigue, and increased absenteeism [2].
Essential factors of the workplace environment include room design, workplace layout, cleanliness, equipment quality, temperature, ventilation, lighting, noise, vibration, radiation, and air quality. A comfortable physical workplace environment encourages employee mobility, higher concentration, sensory and physical connection to work roles, and engagement. It also improves their physical and mental well-being.
Ambiental factors such as noise, temperature, lighting, and air quality can significantly influence people's behavior in indoor spaces [3]. Considering that physical factors impact the behavior of individuals in enclosed environments, this research raises the question of whether these factors also affect employees' productivity in hospitality organizations. This study

underscores the need for further research, sparking curiosity and the desire for a more comprehensive understanding.

Materials and Methods

The research was conducted in October 2021 on 66 employees of different socio-demographic characteristics in three catering establishments from the territory of the City of Novi Sad. The structure of the sample was observed according to the following independent variables: part of the day in which the questionnaire was filled out, gender, age, education, total length of service, length of service at the current job, size of the room where the work is done and part of the catering facility where work tasks are performed.

The newly developed questionnaire Ambient Factors at Work Scale (AFWS) consisted of 41 items, each rated on a 5-point Likert scale ranging from strongly disagree to strongly agree. The survey covered a range of productivity and performance at work regarding environmental conditions and surroundings. All analyses were run in IBM SPSS v.26 [4].

Results and discussion

The provided table (Table 1) offers an overview of the central tendency and variability measures for the subjective assessments of ambient factors in the catering facility, as reported by the respondents. The range of values for individual ambient factors was consistently between 1 and 5. Upon analyzing the results and computing the average values along with their accompanying standard deviations, it is evident that the respondents expressed the highest satisfaction with the lighting quality. Conversely, the research conducted in hospitality facilities highlighted air quality as the most challenging ambient factor.

Figure 1. Subjective assessment of the respondents on ambient factors

	N	Minimum	Maximum	AS	SD
Lightening	66	3.00	5.00	4.15	0.827
Noise	66	1.00	5.00	3.18	1.006
Air quality	66	1.00	5.00	2.51	1.361
Temperature	66	1.00	5.00	3.15	1.140

The general hypothesis related to establishing the connection between ambient factors through the subjective evaluations of respondents and operationalization through questions on the questionnaire with working conditions, employee productivity and employee health. In the table, the first four variables - lighting quality, noise intensity, air quality and temperature adequacy refer to the subjective assessment of the respondents. In comparison, the remaining three variables were measured through statements on the questionnaire. In order to investigate the correlation between variables, Pearson's correlation was performed.

Figure 2. The correlation between ambient factors and working conditions, productivity and health of employees

		Work conditions	Productivity	Health
Air quality	r	0.021	-0.096	-0.115
	p	0.865	0.442	0.356
Noise	r	-0.146	0.623**	0.631**
	p	0.243	0.000	0.000
Temperature	r	-0.398**	-0.175	-0.143

	p	0.001	0.161	0.252
Lightening	r	0.417**	0.512**	0.373**
	p	0.001	0.000	0.002

Upon analyzing the results, it becomes apparent that lighting and air quality emerge as prominent ambient factors. Specifically, lighting exhibits the highest quality rating, while air quality garners the lowest. Concerning the impact of these independent variables on working conditions, productivity, and employee health, it is noteworthy that lighting demonstrates a statistically significant correlation with all three dependent variables. Moreover, temperature significantly influences working conditions, with higher temperatures exerting a negative impact on productivity. Conversely, noise in catering establishments yields a positive and statistically significant effect on productivity and employee well-being.

Conclusion

The findings suggest that ambient factors significantly influence the work environment and its various facets. Therefore, regular monitoring of these physical factors is imperative to foster an optimal working environment for specific tasks. On the other hand, the employees' opinions, as the main contributors to every work process, are also crucial.

However, in order to draw robust conclusions, it is imperative to conduct research involving a larger group of participants using a standardized questionnaire and to accurately measure these physical parameters. This will thereby facilitate the generalization of the findings and take specific action in that direction.

Acknowledgements

References

[1] Clements-Croome, Derek John. Specifying indoor climate data. Naturally Ventilated Buildings (2002) 35.
[2] Seppanen, Olli A., and William J. Fisk. Summary of human responses to ventilation.(2004).
[3]Jazizadeh, Farrokh, Franco Moiso Marin, and Burcin Becerik-Gerber. A thermal preference scale for personalized comfort profile identification via participatory sensing. Building and Environment 68 (2013): 140-149.
[4] IBM Corp. Released 2019. IBM SPSS Statistics for Windows, Version 26.0. Armonk, NY: IBM Corp

DISCOVERY OF GANGLIOSIDE BIOMARKERS IN BRAIN METASTASIS OF LUNG ADENOCARCINOMA BY TRAVELLING-WAVE ION MOBILITY SEPARATION MASS SPECTROMETRY

Mirela Sarbu[1], Željka Vukelić[2], David E. Clemmer[3], Alina D. Zamfir[1,4]

[1]Department of Condensed Matter, National Institute for Research and Development in Electrochemistry and Condensed Matter, 300224 Timisoara, 1 Plautius Andronescu Street, Romania
[2]Department of Chemistry and Biochemistry, University of Zagreb, 10000 Zagreb, Pierottijeva 6, Croatia
[3]Department of Chemistry, The College of Arts & Science, Indiana University, 47405-7102 Bloomington, 800 E. Kirkwood Ave., Indiana, USA
[4]Department of Technical and Natural Sciences, "Aurel Vlaicu" University of Arad, 310330 Arad, 2-4 Elena Dragoi Street, Romania
e-mail: mirela.sarbu86@yahoo.co.uk

Abstract

High performance travelling-wave ion mobility separation mass spectrometry (TWIMS MS) was thoroughly optimized to allow the discovery of brain metastasis of lung adenocarcinoma (BMLA)-specific structures and the assessment of their roles as tumor markers or possible associated antigens. Ganglioside (GG) separation by TWIMS according to the charge state, carbohydrate chain length, degree of sialylation and ceramide composition, led to the identification of no less than 151 distinct components. The detected GGs and asialo-GGs were found characterized by a high heterogeneity in their ceramide and glycan compositions, encompassing up five Neu5Ac residues. The tumor was found dominated by GM3 and GT1 forms, with a particular incidence of C26 fatty acids in the ceramide.

Introduction

Lung adenocarcinoma is a type of non-small cell lung cancer (NSCLC), which contains certain distinct malignant tissue architectural, or molecular features, and accounts for about 40% of all lung cancers. NSCLC, the leading cause of cancer death in the United States, has a high risk of brain metastasis that reportedly reaches up to 50% in brain autopsy [1]. The outcome for patients with brain metastasis is poor, with median survival time of 3–6 months [2,3]. Gangliosides (GGs), sialic acid-containing glycosphingolipids, are known to be involved in the invasive/metastatic behavior of brain tumor cells. Hence, the research nowadays is focused on the determination of the molecular mechanisms related to BMLA tumor invasion and the discovery of innovative approaches for invasiveness suppression. Since GGs are tumor-associated antigens, we introduced here TWIMS MS platform to discover possible biomarkers that can be used in the early diagnosis of the secondary tumor (metastasis cerebral).

Experimental

GGs were extracted and purified from a brain tumor localized in the cerebellar vermis of a 73-y-old male patient, previously operated for lung tumor removal. The pathohistologic examination of surgical removed tumor tissue confirmed the diagnosis of adenocarcinoma brain metastasis. The extracted GGs were dissolved in methanol to the concentration of 5 pmol/mL and infused into a Synapt G2S instrument. The signal was acquired for two minutes in the negative ion mode at 1.5kV ESI voltage and 45 V cone voltage respectively. To enhance the separation, IMS wave velocity was set at 650 m/s and IMS wave height at 40 V. MS/MS

was performed by collision-induced dissociation (CID) after mobility separation in the transfer cell, using energies between 30-35eV.

Results and discussion
The 2D data set of GGs from BMLA patients revealed their separation into mobility families based on their charge state, carbohydrate chain length, and the degree of sialylation. TWIMS MS offered a reliable separation, given the detection and identification in BMLA of 164 ions, corresponding to over 150 distinct glycoforms. NanoESI ionization followed by TWIMS separation and MS screening revealed the predominance of GM3 species, followed by the GM1, GT1 and GD1 type species with different compositions of the ceramide part. However, almost half of the total ions detected in brain metastatic tissue represent monosialylated components of GM1, GM2, GM3 and GM4 type with ceramide of variable constitutions. A special feature arising from the interpretation of the MS data is the identification of several GalNAcGalGlc-Cer species; such structures correspond to asialo GA1 and GA3. Under identical experimental conditions, TWIMS MS analysis of a normal tissue sample revealed that unlike metastatic tissue, the healthy cerebellar sample is dominated by mono- to hexasialylated structures with higher expression of GD, GT and GQ type. Observed differences in ceramide structures and altered sialylation patterns have been attributed to tumor-related changes in human carcinomas. Gangliosidic components modified by Fuc or *O*-Ac could also be detected, but in a specific pattern for adenocarcinoma, which was not found in other tissues. Most *O*-acetylated gangliosides are short GT3 type, while fucosylated components are represented by monosialo species of GM3 and GM4 structure, di- and trisialylated GT1 and GT3 exhibiting heterogeneity in their ceramide motifs. By the occurrence of only one mobility feature and the diagnostic fragment ions, the TWIMS tandem MS conducted using CID achieved a complete structural characterization of species with short oligosaccharide chains and reduced overall sialic acid content associated with brain metastasis of lung adenocarcinoma.

Conclusion
We have optimized and applied here TWIMS MS to identify the ganglioside pattern uniquely developed in BMLA. TWIMS in combination with highly sensitive (-) nanoESI and tandem MS by CID, provided an exhaustive structural and compositional investigation of BMLA gangliosides due to the advantages of the platform. The major outcome of this study is that, by TWIMS MS and CID MS/MS various novel species could be identified and added to the currently existing panel of BMLA tissue-associated structures.

References
[1]. S. Page, C. Milner-Watts, M. Perna, et al., Eur. J.Cancer 132 (2020) 187-198.
[2]. L.E. Gaspar, M.P. Mehta, R.A. Patchell, et al., J. Neurooncol. 96 (2010) 17–32.
[3]. Kalkanis, S.N., D. Kondziolka, L.E. Gaspar, et al., J. Neurooncol. 96 (2010) 33–43.

MERCURY EXPOSURE AND LUNG CANCER-URINARY LEVELS IN FEMALES WITH ADENOCARCINOMA

<u>Mirjana Ševo</u>[1,2], Danica Sazdanić Velikić[1,3], Nataša Milošević[1], Maja Milanović[1], Danijela Lukić[4], Milorad Španović[1,5], Jan Sudji[1,5], Nataša Milić[1]

[1]*Faculty of Medicine, University of Novi Sad, 21000 Novi Sad, Serbia*
[2]*IMC Banja Luka-Center of Radiotherapy, Part of Affidea Group, 78000 Banja Luka, Bosnia and Herzegovina*
[3]*Institute for Pulmonary Diseases of Vojvodina, Clinic for Pulmonary Oncology, 21204 Sremska Kamenica, Serbia*
[4]*Institute of Public Health of Vojvodina, 21000 Novi Sad, Serbia*
[5]*Institute of Occupational Health Novi Sad, 21000 Novi Sad, Serbia*
e-mail: 902012d23@mf.uns.ac.rs

Abstract

It is predicted that one out of 17 women will develop lung cancer during the lifetime. Adenocarcinoma is recognized as the most frequent subtype of non-small lung cancers with almost 40% of total lung cancer and is more common in women than in men. Apart from cigarette smoking, secondhand smoking, and a lung cancer family history, environmental determinants of lung cancer are poorly understood. Although cadmium exposure is considered as a risk factor for lung cancer onset as well as mortality, the data about carcinogenic mercury (Hg) effects are still scarce.

In order to evaluate Hg exposure in lung cancer, 27 female patients (older than 18) with inoperable IIIB and IV stadium of adenocarcinoma, diagnosed in the Institute for Pulmonary Diseases of Vojvodina, Serbia, were enrolled. The women were interviewed about their exposure to chemicals during lifetime and the presence of amalgam dental fillings. The body mass index (BMI) and waist-to-height ratio were calculated based on current weight, height and waist circumference for each patient. Total Hg levels were determined by inductively coupled plasma mass spectrometry (ICP-MS) in the morning spot urine samples after the microwave digestion with nitric acid. The urinary Hg levels was expressed in terms of µg/g creatinine (Cre). Based on the obtained results, 52.26% (16/27) women were detected with Hg in urine samples above the limit of detection (1.9 µg/L) in the range 2.18 to 197.6 µg/gCre. There were no statistical differences in the mean values of urinary Hg between women with amalgam dental fillings in comparison to those without dental fillings i.e. 34.39 ± 66.46 versus 11.29 ± 8.56 µg/gCre (p=0.346). One should note that although no statistical differences were observed, women without dental fillings had higher Hg urinary levels indicating other sources of exposure. In addition, the obesity nor central obesity had no influence on urinary Hg concentration. There were no differences in Hg urinary levels between normal weight (BMI$\leq$25kg/m^2) and overweight (BMI>25kg/m^2) women (p=0.548). Moreover, no statistically significant variations in urinary Hg levels were registered between women with healthy waist-to-height ratio below 0.5 and those with values above 0.5 (p=0.168).

The obtained results could enable a better understanding of heavy metal exposure as environmental determinants of lung cancer.

RARE EARTH DOPED LaMnO₃ NANOMATERIALS: COMPLEMENTARY EFFECT TOWARDS AN ENHANCED PHOTOCATALYTIC PERFORMANCE

Paula Sfirloaga, Ionel Balcu, Corina Macarie, Doru Buzatu

National Institute for Research and Development in Electrochemistry and Condensed Matter, str. Dr. A. Paunescu Podeanu 144, 300569 Timisoara Romania
e-mail: paulasfirloaga@gmail.com

Abstract

In the context of fast-growing technologies, there is a strong drive to develop innovative functional materials that can be used in multiple applications to fulfill needs. Because of their architectural, thermal durability, ionic conductivity and catalytic, perovskite oxide has attracted a lot of interest for use in a wide range of fields, such as gas detecting, fuel cells, visible light photo-catalysis, magnetic memory devices, photovoltaic cells, metal-air batteries, and pseudo-capacitors [1,2]. Rare-earth-containing perovskite materials have attracted great attention in the different fields because of their unique adjustable crystal structures and the coexistence of various valence states [3]. To enhancing and adjusting the physico-chemical properties, controllable elemental doping/alloying is a key strategy, which dictates the future applications of the synthesized materials. In order to study the photocatalytic properties of the materials studied doped lanthanum manganite was synthesized by sol-gel technique. The crystal phase of the products was investigated by a PANalytical diffractometer, with Cu-Kα radiations (λ = 0.15406 nm) in a 2θ range from 15° to 80°, and the FT-IR analysis was accomplished in the 400–4000 cm^{-1} range, in KBr pellets. The X-ray diffraction spectra of the perovskite materials doped with 1% rare earths showed that all the samples have a well-crystallized perovskite type structure, with no detectable secondary phases. The structural parameters were refined using the X'Pert HighScore Plus program. The diffraction picks for all materials can be indexed to the orthorhombic phase, space group P n m a (62), according to JCPDS card No. 01-089-0680. The surface morphology, the EDX spectrum and the elements map were made for all the synthesized samples. Thus, from the analysis of the EDX spectra, it can be seen that the obtained materials are pure, and the quantification of the elements shows that the stoichiometry of the ABO₃ perovskite material has been preserved.

Acknowledgements

References
[1] A. Ray, A. Roy, S. Saha, M. Ghosh, S. Roy Chowdhury, T. Maiyalagan, S. K. Bhattacharya, S. Das, Langmuir 35 (2019) 8257.
[2] A. Roy, A. Ray, P. Sadhukhan, S. Saha, S. Das, Mater. Res. Bull. 107 (2018) 379.
[3] B.Z. Zheng, J.Y. Fan, B. Chen, X. Qin, J. Wang, F. Wang, R.R. Deng, X.G. Liu, Chem. Rev. 122 (2022) 5519.

RED KIDNEY BEAN FLOUR AND RICE FLOUR: POTENTIAL INGREDIENTS IN THE PRODUCTION OF GLUTEN-FREE PASTA WITH FUNCTIONAL QUALITY

Daniela Stoin [1*], Calin Jianu [1], Ariana Velciov [1], Mariana-Atena Poiana[1], Antoanela Cozma [1], Florina Radu[1], Diana Moigradean[1], Sofia Popescu[1], Alexandru Rinovetz[1]

[1]*Faculty of Food Engineering, University of Life Sciences „King Michael I" from Timisoara, Romania, Aradului Street No 119, 300645 Timisoara, Romania*
[2] *Faculty of Agriculture, Banat's University of Life Sciences „King Michael I" from Timisoara, Romania, Aradului Street No 119, 300645 Timisoara, Romania*
[*]*author's email address:* danielastoin@usvt.ro

Abstract

The present studies relates to the development of a gluten-free pasta enriched with bioactive compounds, proteins, fibers, and minerals through the addition of red kidney bean flour in varying proportions. Four samples of gluten-free pasta were produced using different ratios of rice flour (RF) and red kidney bean flour (RKBF): 100:0%, 90:10%, 85:15%, and 80:20%. Standard laboratory procedures were used to evaluate the proximate composition, cooking properties, sensory characteristics, total phenolic content (TPC), total flavonoids content (TFC), and antioxidant activity (AA) of gluten-free pasta samples. The results demonstrate that the studied gluten-free pasta samples have a superior nutritional profile, with higher protein, fiber, ash, and fat content, and lower carbohydrate content. The pasta samples showed an increase in cooking time and cooking losses, resulting in a decrease in overall acceptability. However, the functional attributes of the gluten-free pasta samples with added red kidney bean flour significantly increased in proportion to the percentage of added red kidney bean flour, compared to the control sample.

Keywords: *red kidney bean flour, gluten-free pasta, high nutritional value*

Introduction

In the contemporary era, consumers globally are susceptible to a plethora of ailments, including diabetes, as a consequence of obesity, elevated cholesterol, cardiovascular disease, hypertension, and erratic glycemic levels. These risk factors are attributable to inadequate dietary habits characterized by a paucity of essential nutrients, such as protein, dietary fiber, phytochemicals, and antioxidants. Functional foods offer health benefits and help prevent disease by incorporating nutraceutical ingredients and other essential nutrients [1]. The most important recommendation is to reduce macro- and micronutrient deficiencies through nutrition education programmes that help people choose a balanced diet [2, 3]. There has been a notable increase in interest in recent years with regard to the potential replacement of wheat flour with alternative types of flours in the production of bakery products and pasta, including noodles. The focus has been on starchy roots and tubers (e.g., cassava, sweet potato), protein-rich flours (e.g., soybeans, peas, beans), and cereals (e.g., rice, maize, sorghum) [4]. Similarly, pasta can be considered a complete source of protein when combined with other plant foods, such as legumes, to compensate for lysine deficiency. Furthermore, protein and fibre isolated from legumes have been demonstrated to confer a range of health benefits [5]. The flours employed in this study to produce gluten-free pasta with functional potential were rice flour (RF) and red kidney bean flour (RKBF). The incorporation of RKBF in varying proportions in the manufacture of gluten-free pasta through partial substitution of RF is substantiated by their intricate chemical composition, implicitly from their nutritional and biological value. Red kidney bean flour is a gluten-free flour that is a good source of 57.7% total carbohydrates,

22.7% protein, 1% fat, 5.1% crude fiber, 3.5% minerals, unsaturated fatty acids, vitamins, and numerous biologically active compounds (such as phenolic acids and flavonoids) [5, 6]. Therefore, identifying new viable raw materials and efficiently using them to produce flour-based products could be a suitable option for establishing a sustainable economy. The inclusion of legumes in food products helps to improve the diet pattern of consumers as some do not consume these ordinarily and it also provides a good and non-expensive source of protein in the diets [4, 7]. This study is being carried out to use RKBF as a good and non-expensive source of protein to fortify the RF used for pasta production. Effect of replacement levels on pasta nutritional parameters, functional attributes, cooking quality and sensory characteristics were studied. The general objective of this study is to determine the quality characteristics and consumer acceptability of pasta fortified with RKBF.

Experimental
Materials
Rice flour, red kidney bean flour and the other ingredients used in this study were purchased from local market in Timisoara town, Romania.

Technological process for obtaining pasta samples
Gluten-free pasta samples were prepared according to the AACC International Method 10-50.05 with minor modifications. For each sample, the RF and RKBF were mixed with water until the dough reached the desired consistency, as for the control sample, only RF was mixed with water. Then, each sample was kneaded into a firm and homogeneous dough and allowed to rest for 1 hour. Subsequently, the sheet of dough was passed through a hand-operated pasta machine which cut the dough into strips of 5 mm width that was hung on glass rods and steamed at 70ºC. The pasta produced were then transferred to a cabinet dehydrator and dried at 70ºC for 12h. Thereafter, cooled to room temperature, placed in sealed plastic bags until further Analysis [6].

Analytical procedures
The proximate composition, cooking properties, TPC, TFC and AA of the gluten-free pasta samples using standard laboratory procedures [8-12], were evaluated. All determinations were performed in triplicate, calculating their arithmetic mean of three separate determinations. The data were statistically analyzed using the program Microsoft Excel.

Sensory evaluation
Cooked coded pasta samples were presented to twenty panelists and they scored the following attributes: color, appearance, odor, flavor and overall acceptability of the products using a 9-point hedonic scale, in which 1 represents extreme dislike and 9 represents like extremely. 100% RF pasta was used as control [12].

Results and discussion
Proximate composition of pasta samples
In *Table 1* are shown the results obtained from the proximate analysis of cooked pasta. The obtained pasta formulas (P10RKBF, P15RKBF, P20RKBF) have a superior nutritional profile compared to PC, a profile correlated with the percentage of RKBF compared to RF. The moisture content decreased significantly with the increase in the content of RKBF and the decrease in the amount of RF in the pasta sample. The highest moisture content was observed in the control sample of pasta made from 100% RF (26.65 ± 0.57%), while the lowest moisture content was recorded in the noodle sample made with 20% RKBF (23.44 ± 0.04%).

Table 1. Proximate composition of gluten-free pasta samples

Proximate composition (%)	Gluten-free pasta samples			
	PC	P10RKBF	P15RKBF	P20RKBF
Moisture	26.65 ± 0.57	25.32 ± 1.29	24.71 ± 0.09	23.44 ± 0.04
Fat	2.17 ± 0.04	2.32 ± 0.12	2.42 ± 0.14	2.54 ± 0.18
Protein	8.82 ± 0.17	10.26 ± 0.22	10.66 ± 0.21	11.93 ± 0.44
Crude fiber	1.96 ± 0.22	3.25 ± 0.14	3.55 ± 0.21	4.32 ± 0.59
Ash	1.65 ± 0.21	3.60 ± 0.15	3.84 ± 0.05	4.08 ± 0.05
Carbohydrates	58.75 ± 0.08	55.25 ± 0.55	54.82 ± 0.25	53.69 ± 0.33

All determinations were done in triplicate and the results were reported as average value ± standard deviation (SD). **PC** – *Pasta control sample made from 100% RF;* **P10RKBF** - *Pasta made from 90% RF + 10% RKBF;* **P15RKBF** - *Pasta made from 85% RF + 15% RKBF;* **P20RKBF** - *Pasta made from 80% RF + 20% RKBF.*

Pasta samples with the addition of RKBF are distinguished by higher contents of proteins, fibers, lipids and mineral substances compared to PC, these increased with the proportion of RKBF added to RF. The pasta formulas obtained in this research proved to be a good source of protein, thus the protein content ranged from 10.26% in P10RKBF to 11.93% in P20RKBF. The same upward trend was recorded in the case of fiber and ash content, which ranged from 3.25% to 4.32%, respectively form 3.60% to 4.08%, compared to 1.96% and 1.65% in PC, which can be considered products with high potential, being important sources of fiber and mineral substances. These results are similar to the studies made by Ramírez-Jiménez et al. (2018) [12], Yahya et al. (2021) [13] and Stoin et al. (2022) [14] and show the potential of using bean flour in supplementing various food products with proteins.

Table 2. Cooking properties of gluten-free pasta samples

Treatments	Gluten-free pasta samples			
	PC	P10RKBF	P15RKBF	P20RKBF
Cooking time (min)	5.26 ± 0.11	5.84 ± 0.09	6.45 ± 0.21	7.53 ± 0.24
Cooked weight (g)	4.46 ± 0.08	3.77 ± 0.38	3.42 ± 0.22	3.12 ± 0.09
Cooking loss (%)	3.42 ± 0.24	4.34 ± 0.08	4.62 ± 0.05	4.87 ± 0.22

In terms of cooking time, an increase was observed as the percentage of RKBF used increased. Therefore, the shortest cooking time was found in the control sample, 5.26±0.11 minutes, and the longest cooking time in the pasta sample with 20% RKBF, 7.53 ± 0.24 minutes. These differences in cooking time are due to the different gelatinization temperatures of the starches from flours [12, 14]. In the case of the cooking weight, it can be observed that it decreases with increasing the amount of RKBF used. Thus, the highest cooking weight was observed in the control sample, of 4.46 ± 0.08 g, this gradually decreased with increasing percentage of RKBF used, the lowest value being 3.12 ± 0.09 g, obtained by the noodle sample with 20% RKBF. As in the case of cooking time, an increase in cooking loss was also observed with the increase in the amount of RKBF and the decrease in the amount of RF used in the pasta recipe. The lowest cooking loss was 3.42 ± 0.24 % in the control sample, while the highest cooking loss was 4.87 ± 0.22 in the noodle sample with 20% RKBF. These results are consistent with the results obtained in other studies, such as those of Stoin et al. (2022) [14] and Too et al (2022) [15]. Regarding the color, no big differences were found between the samples, however, a greater appreciation was observed with the increase in the amount of RKBF in the recipe, the best result being obtained by the pasta sample with 20% RKBF (5.62±0.02), and the lowest by the control sample, made from 100% WF (5.52 ± 0.02).

Table 3. Sensory evaluation of gluten-free pasta samples

Sensory evaluation	Gluten-free pasta samples			
	PC	P10RKBF	P15RKBF	P20RKBF
Color	5.24 ± 0.87	5.36 ± 1.22	5.40 ± 0.13	5.52 ± 0.02
Appearance	5.49 ± 0.14	4.88 ± 0.12	4.46 ± 0.04	4.08 ± 0.14
Odor	5.26 ± 0.17	4.48 ± 0.36	4.08 ± 0.11	3.93 ± 0.33
Flavor	5.76 ± 0.47	4.72 ± 0.13	4.10 ± 0.55	3.86 ± 0.09
Overall acceptance	5.34 ± 0.33	4.45 ± 0.14	4.32 ± 0.26	4.19 ± 0.41

Regarding the other evaluated aspects, on the other hand, the panelists preferred the pasta sample made from 100% RF, as a decrease in the values regarding appearance, odor, flavor and overall acceptance was observed with the increase in the amount of RKBF in the pasta. Thus, the values varied between 4.08 ± 0.14 and 5.49 ± 0.14 in terms of appearance, between 3.93 ± 0.33 and 5.26 ± 0.17 in terms of odor, between 3.86 ± 0.09 and 5.76 ± 0.47 in terms of flavor and between 4.19 ± 0.41 and 5.34 ± 0.33 in terms of overall acceptance, the lowest values being obtained by the pasta sample with 20% RKBF, and the highest values by the control sample. The results obtained are consistent with other studies, which reported the same decrease in sensory properties of the products with the replacement of RF, in pasta with flour from other vegetables or beans, such as the studies carried out by Ramírez-Jiménez et al. (2018) [12] and Yahya et al. (2021) [13].

Table 4. Phytochemical content and antioxidant activity of pasta samples

Gluten-free pasta samples	Phytochemical parameters		
	TPC (mg GAE/100g DW)	TFC (mg QE/100 g DW)	AA (µM TE/100g DW)
PC	21.27 ±0.41	21.48 ± 0.31	23.21 ± 0.09
P10RKBF	35.33 ± 0.13	27.66 ± 0.03	34.22 ± 0.03
P15RKBF	47.75 ± 0.22	36.22 ± 0.11	44.66 ± 0.08
P20RKBF	59.02 ± 0.04	48.64 ± 0.08	52.94 ± 0.44

The obtained results shown that the content of TPC, TFC and AA increased with the level of RKBF added in the pasta samples. Thus, in the case of pasta samples the highest TPC and TFC content was found in P20RKBF (59.02 ± 0.04 mg GAE/100g DW and 48.64 ± 0.08 mg QE/100 g DW), while the lowest value was recorded for the PC (21.27 ±0.41 mg GAE/100g DW and 21.48 ± 0.31 mg QE/100 g DW). The same trend was maintained for antioxidant activity (AA), thus, in the case of pasta samples, the highest AA was recorded for P20RKBF (52.94 ± 0.44 µM TE/100g DW), while the lowest value was recorded for the PC (23.21 ± 0.09 µM TE/100g DW) [7, 15].

Conclusions
The results obtained from this study show that the use of RKBF in the production of flour pasta results in obtaining a flour product with improved functionality. Sensory evaluation of RF and RKBF-based pasta shows that the use of up to 15% RKBF in the recipe, results in increased consumer acceptance. The content of phenolic compounds, total flavonoids content as well as the antioxidant activity of the gluten-free pasta increased considerably. The overall nutritional, physical, phytochemical and sensory evaluation of the obtained pasta showed that RKBF can represent a valid vegetal source in the formulation of new food products with improved functionality.

References
[1] K.N. Pakhare, A.C. Dagadkhair, I.S. Udachan, R.A. Andhale, Studies on preparation and quality of nutritious noodles by incorporation of defatted rice bran and soy flour; Journal of Food Processing and Technology., 7(10), 2016.
[2] O.H. Adejunwon, A.I.O. Jideani, K.O. Falade, Quality and Public Health Concerns of Instant Noodles as Influenced by Raw Materials and Processing Technology, Food Reviews International, 2019.
[3] A. Shehzad, U.M. Chander, M.K. Sharif, A. Rakha, A. Ansari, M.Z. Shuja, Nutritional, functional and health promoting attributes of red kidney beans, A review, PAK. J. FOOD SCI., 25(4), 2015.
[4] O.H. Adejunwon, A.I.O. Jideani, K.O. Falade, Quality and Public Health Concerns of Instant Noodles as Influenced by Raw Materials and Processing Technology, Food Reviews International, 2019.
[5] T.M. Chepkosgei, I. Orina, Quality and sensory properties of instant fried noodles made with soyabean and carrot pomace flour; African Journal of Food Science.,15(3):92-99, 2021.
[6] O. R. Adegbanke, Quality characteristics and consumer acceptability of noodles produced from wheat flour fortified with kidney bean (Phaseolus vulgaris L.) flour, Acta Scientific Nutritional Health 6.9, 2022.
[7] B.C. Too, N.V. Tai, N.M. Thuy, Formulation and quality evaluation of noodles with starchy flours containing high levels of resistant starch. Acta Sci. Pol. Technol. Aliment., 21(2), 145–154, 2022.
[8] A.O.A.C., "Official Methods of Analysis" Association Official Analytical Chemists of the 16" Ed. International, Washington, D.C., U.S.A., 1995.
[9] AOAC (Association of Official Analytical Chemists) Official Methods of Analysis International. 17th, Ed. Washington, DC: AOAC, 2000.
[10] A. Bouasla, A. Wojtowicz, M.N. Zidoune, Gluten-free precooked rice pasta enriched with legumes flours: physical properties, texture, sensory attributes and microstructure, LWT - Food Science and Technology, 75, 569-577, 2017.
[11] M. A.Poiana, E. Alexa, I. Radulov, D.N. Raba, I. Cocan, M. Negrea, G. Suster, G., Strategies to Formulate Value-Added Pastry Products from Composite Flours Based on Spelt Flour and Grape Pomace Powder. Foods, 12(17), 3239, 2023.
[12] F. Yahya, Y.K Xiang., M.K. Zainol, M. Hasmadi, Effect of different ratios of wheat flour to black bean (Phaseolus vulgaris L.) flour on physicochemical properties and sensory acceptability of cooked noodle, Food Research, 6(2), 457 – 464, 2021.
[13] A.K. Ramírez-Jiménez, M. Gaytán-Martínez, E. Morales Sánchez, G. Loarca-Piña, Functional properties and sensory value of snack bars added with common bean flour as a source of bioactive compounds, LWT-Food Science and Technology, 89, 674-680, 2018.
[14] D. Stoin, D.L. Vîrsta, R. Robert, O.M. Bicu, C. Jianu, A.B. Velciov, M.A. Poiană, Quality evaluation of noodles based on black bean flour and wheat flour, Journal of Agroalimentary Processes and Technologies, 28(4), 292-298, 2022.
[15] B.C. Too, N.V. Tai, N.M. Thuy, Formulation and quality evaluation of noodles with starchy flours containing high levels of resistant starch. Acta Sci. Pol. Technol. Aliment., 21(2), 145–154, 2022.
[16] N.M.B.Barreto, N.G. Pimenta, B.F. Braz, A.S. Freire, R.E. Santelli, A.C. Oliveira, L.H.P. Bastos, M.H.W.M. Cardoso, M. Monteiro, M.E.L. Diogenes, D. Perrone, Organic Black Beans (*Phaseolus vulgaris* L.) from Rio de Janeiro State, Brazil, Present More Phenolic Compounds and Better Nutritional Profile Than Nonorganic, Foods, 10(4), 900, 2021.

TRANSMISSION ELECTRON MICROSCOPY INVESTIGATION OF A PORPHYRIN-CONTAINING ORGANIC-INORGANIC HYBRID NANOMATERIAL

Bogdan-Ovidiu Taranu

National Institute of Research and Development for Electrochemistry and Condensed Matter, Dr. A.P. Podeanu street, No. 144, 300569, Timisoara, Romania
e-mail: b.taranu84@gmail.com

Abstract

An organic-inorganic hybrid nanomaterial containing the A_3B-type free-base porphyrin 5-(4-carboxyphenyl)-5,10,15-tris(4-phenoxyphenyl)-porphyrin, the polysaccharide *k*-carrageenan and Fe_3O_4 magnetic nanoparticles was successfully synthesized and analyzed using Transmission Electron Microscopy (TEM). Different operating modes – TEM Bright Field, High-Resolution TEM and Scanning Transmission Electron Microscopy – were employed during the investigation. The recorded images provide morphological and structural data concerning the detailed understanding of the hybrid in ways that are specific to the aforementioned characterization technique. The results of the study complement the scientific knowledge relevant to domains of current interest for researchers, such as porphyrin chemistry and the nanomaterials field.

Introduction

The naturally occurring and artificially synthesized members of the class of organic compounds known as porphyrins all share a macrocyclic aromatic structure comprised of four pyrrole groups interconnected in the α position *via* methine bridges [1]. Substitution with functional moieties in the *meso* and β positions of the porphyrin macrocycle leads to porphyrin derivatives with properties that make them promising candidates for a wide variety of applications in which they can be used individually or combined with a wide range of materials [2-8]. Concerning the fitness of porphyrins when utilized as components of hybrid nanomaterials with applicative potential, Mak *et al.* [9] reported a study in which different multifunctional compounds containing 5-(4-carboxyphenyl)-5,10,15-tris(4-phenoxyphenyl)-porphyrin and iron oxide magnetic nanoparticles (MNPs) were evaluated for their CO_2 sensing property and were shown to display comparable efficiency. One of these organic-inorganic hybrids consisted of the specified A_3B free-base porphyrin in combination with the Fe_3O_4 MNPs, as well as with the linear sulfated polysaccharide *k*-carrageenan. During that study, this nanomaterial was characterized by means of several physicochemical methods, including TEM. However, because the main focus of the investigation was on the compound's applicative potential, the performed TEM analysis was sufficient for gathering only basic morphological data.

To the best of the author's knowledge, no detailed TEM characterization of the porphyrin-polysaccharide-Fe_3O_4 magnetic nanoparticles hybrid has been reported. In light of this, the present work aims to provide a more detailed understanding of the compound by using the same microscopy investigation technique. The transmission electron microscope employed in the study was operated in three different modes that ensured the collection of different types of data. The acquired information revealed intricate morphological and structural features of the samples.

Experimental

The 5-(4-carboxyphenyl)-5,10,15-tris(4-phenoxyphenyl)-porphyrin (CPTPPP) was laboratory-synthesized *via* the Adler-Longo multicomponent reaction [10], as previously reported [11], and its chemical structure is presented in Scheme 1. The Fe_3O_4 MNPs and the CPTPPP–*k*-carrageenan–Fe_3O_4 MNPs hybrid nanomaterial were also obtained based on published procedures [9,12]. For comparative purposes, a hybrid containing only the porphyrin and the polysaccharide was prepared as well.
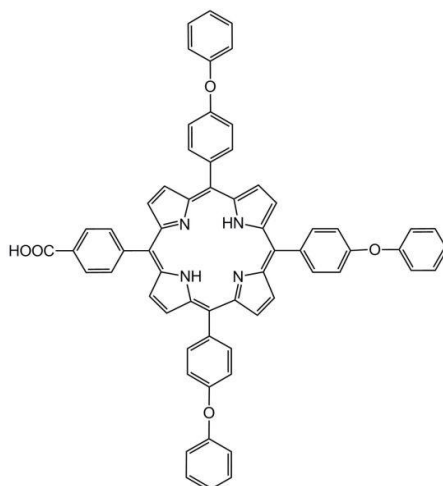
Scheme 1. The chemical structure of CPTPPP

Tetrahydrofuran (THF) and dimethylsulfoxide (DMSO) – purchased from Sigma Aldrich (Saint Louis, MO, USA) and Merck (Darmstadt, Germany) – were employed in the study to obtain the samples for the TEM analysis. Copper grids (200 mesh type) covered with continuous or lacey carbon films served as the supports on the surface of which the investigated compounds were deposited by means of the subsequently described step-by-step procedure. Firstly, suspensions in THF and DMSO of the synthesized structures were obtained. Secondly, the suspensions were thoroughly mixed with a vortex mixer. Thirdly, volumes of 5 µL were collected from the suspensions and drop-casted onto the carbon film covering the copper grids. Fourthly, a solvent evaporation stage at 23 ± 2 °C led to the desired samples.

The TEM analysis was performed with a Titan G2 80–200 microscope (FEI Company, The Netherlands) at accelerating voltages of 80 and 200 kV and by using the Digital Micrograph v. 2.12.1579.0 and TEM Imaging & Analysis v. 4.7 software. The different operating modes employed during the study are TEM Bright Field, High-Resolution TEM (HR-TEM), and Scanning Transmission Electron Microscopy (STEM).

Results and discussion

The HR-TEM image recorded on the CPTPPP-polysaccharide hybrid and shown in Figure 1 contains a structure bearing close resemblance to carbon nano-onions [13]. Measurements performed on the neighboring layers of the carbon onion-like structure reveal that the distance between 10 shells is 3.5 nm. The spacing of 3.5 Å corresponding to two neighboring layers is the same as the one measured by Papaioannou *et al.* [14] for a type of glucose-derived carbon nanodot displaying the standard carbon onion pattern. An important difference between the TEM analysis from that study and the present one is that the Fast Fourier Transform (FFT) recorded in the former case shows an amorphous structure, while the FFT inserted in Figure 1 outlines the crystalline nature of the formation identified in the current investigation.

Another feature of the CPTPPP-polysaccharide hybrid worthy of mention is that the distance between two neighboring layers is about the same as the spacing between two crystal planes – an observation that has also been made for carbon nano-onions [15,16].

In terms of crystal plane indexing, the spacing of 3.5 Å may correspond to the (–210) crystal plane (JCPDS file 00-001-0330).
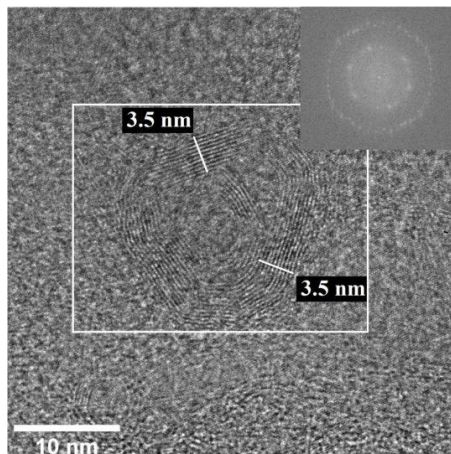
Figure 1. HR-TEM image recorded on the CPTPPP-polysaccharide hybrid. The inset shows the FFT obtained for the area enclosed in the rectangle

The HR-TEM and TEM Bright Field images shown in Figure 2 were recorded on the CPTPPP–polysaccharide–Fe_3O_4 MNPs hybrid. The features similar to the walls of single- and multi-walled carbon nanotubes [17] that can be observed in Figure 2a are layers having the same spacing as the one measured for the layers belonging to the structure from Figure 1. Many such arrangements can be seen in Figure 2b and are part of carbon onion-like architectures such as the one in Figure 1. With regard to the Fe_3O_4 MNPs, they can be seen in Figure 2c as embedded in the organic component of the investigated compound.

(a) (b) (c)
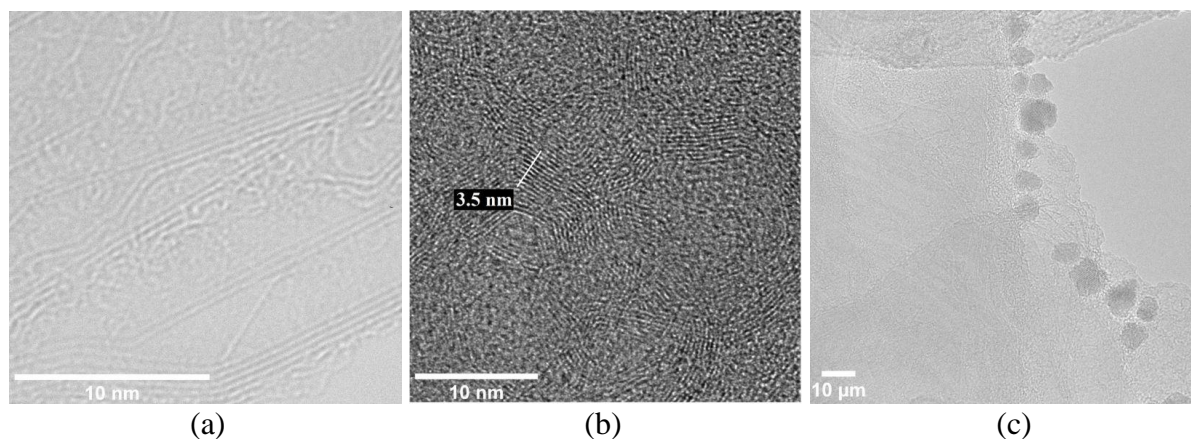
Figure 2. TEM images recorded on the CPTPPP–polysaccharide–Fe_3O_4 MNPs hybrid (a-c)

To provide a more detailed characterization of the nanoparticles, several images were acquired at different magnifications and are provided in Figures 3 and 4. An agglomeration of this type of structures is visible in Figure 3a and some have been singled out so as to make them easier to identify. By approximating these arrangements to spherical objects, it became possible to measure their diameters which were between 6 and 8 nm. The values are close to that reported by Mak *et al.* for Fe_3O_4 MNPs [9].

Figures 3b and 3c show HR-TEM images of the nanoparticles, outlining their features down to the atomic level. Measurements carried out on some of them indicate a distance of 3.42 nm for 10 interplanar spacings. With the aid of the JCPDS file 00-001-1111 for magnetite, it was found that the spacing of 3.42 Å corresponds to the (211) crystal plane. The file was selected because it can be used to index the planes corresponding to the diffraction peaks from the previously published XRD pattern of Fe_3O_4 MNPs [9].

| (a) | (b) | (c) |
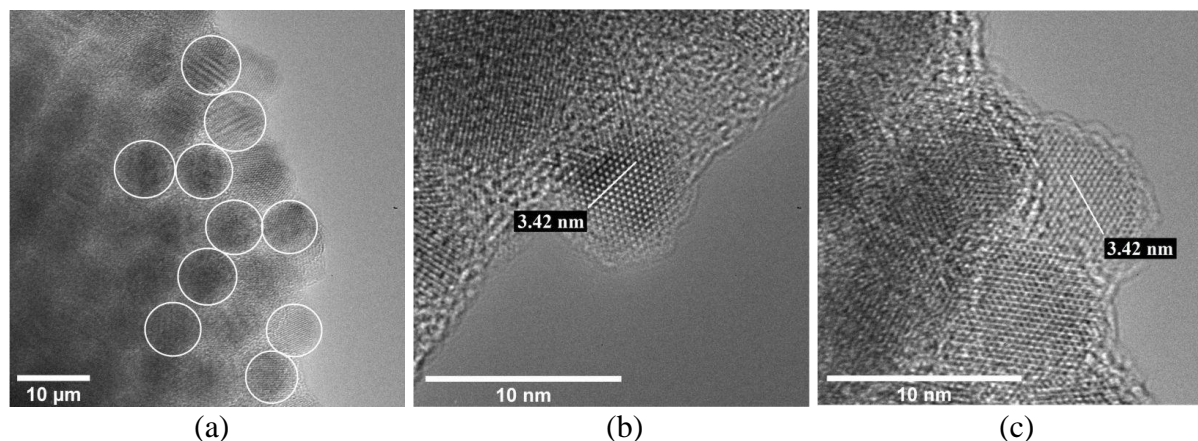
Figure 3. TEM images recorded on the CPTPPP–polysaccharide–Fe_3O_4 MNPs hybrid that highlight the Fe_3O_4 MNPs (a-c)

Another Fe_3O_4 MNP can be observed in detail in Figure 4a. Performed measurements reveal a distance of 2.95 nm for 10 interplanar spacings. The interplanar spacing of 2.95 Å is very close to the d-spacing of 2.97 Å from the previously mentioned JCPDS file for magnetite which corresponds to the (220) crystal plane.

The STEM image in Figure 4b was recorded at a relatively low magnification so as to provide an overview of the sample. Because of the Z-contrast, the differences between the organic and inorganic components of the hybrid are quite clear. The former has a fog-like appearance, while the latter looks solid. The image also reveals the tendency of the inorganic nanoparticles to form clusters by showing several such formations.

| (a) | (b) |
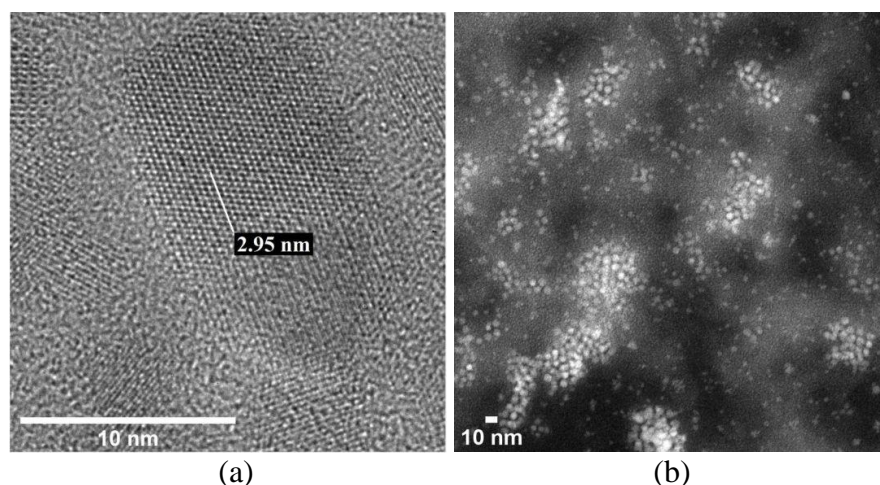
Figure 4. HR-TEM image (a) and STEM image (b) recorded on the CPTPPP–polysaccharide–Fe_3O_4 MNPs hybrid

Conclusion

The TEM Bright Field, HR-TEM and STEM detailed analysis of a laboratory-synthesized hybrid nanomaterial, comprised of an asymmetrically substituted free-base porphyrin, *k*-carrageenan and Fe_3O_4 magnetic nanoparticles, was successfully performed. Two types of data – morphological and structural – were acquired. These provide an in-depth understanding of the compound in ways that are characteristic of techniques belonging to the electron microscopy field. Furthermore, the obtained data complement the scientific knowledge pertinent to porphyrin chemistry and the nanomaterials domain.

Acknowledgements

References

[1] E. Fagadar-Cosma, D. Vlascici, G. Fagadar-Cosma, Porfirinele de la sinteză la aplicații, Eurostampa, Timisoara, Romania, 2008, pp. 10.
[2] G. Fagadar-Cosma, M. Birdeanu, E. Fagadar-Cosma, J. Res. Updates Polym. Sci. 5 (2016) 39.
[3] M. Imran, M. Ramzan, A.K. Qureshi, M.A. Khan, M. Tariq, Biosensors (Basel) 8 (2018) 95.
[4] N.S. Lebedeva, Y.A. Gubarev, M.O. Koifman, O.I. Koifman, Molecules 25 (2020) 4368.
[5] J.M. Park, K.-I. Hong, H. Lee, W.-D. Jang, Acc. Chem. Res. 54 (2021) 2249.
[6] Y. Shi, F. Zhang, R.J. Linhardt, Dyes and Pigm. 188 (2021) 109136.
[7] L.B. Silva, K.A.D.F. Castro, C.E.A. Botteon, C.L.P. Oliveira, R.S. da Silva, P.D. Marcato, Front. Bioeng. Biotechnol. 9 (2021) 679128.
[8] C.J.P. Monteiro, M.A.F. Faustino, C. Serpa, Molecules 28 (2023) 7108.
[10] E. Fagadar-Cosma, L. Cseh, V. Badea, G. Fagadar-Cosma, D. Vlascici, Comb. Chem. High Throughput Screen. 10 (2007) 466.
[11] D. Vlascici, E. Fagadar-Cosma, I. Popa, V. Chiriac, M. Gil-Agusti, Sensors 12 (2012) 8193.
[9] C.A. Mak, M.A. Pericas, E. Fagadar-Cosma, Catal. Today 306 (2018) 268.
[12] P. Riente, C. Mendoza, M.A. Pericas, J. Mater. Chem. 21 (2011) 7350.
[13] J.K. McDonough, Y. Gogotsi, Electrochem. Soc. Interface 22 (2013) 61.
[14] N. Papaioannou, A. Marinovic, N. Yoshizawa, A.E. Goode, M. Fay, A. Khlobystov, M.-M. Titirici, A. Sapelkin, Sci. Rep. 8 (2018) 6559.
[15] O. Mykhailiv, H. Zubyk, M.E. Plonska-Brzezinska, Inorg. Chim. Acta 468 (2017) 49. [16] R. Bacon, J. Appl. Phys. 31 (1960) 283.
[17] P.J.F. Harris, Journal of Carbon Research 4 (2018) 4.

OPTICAL MICROSCOPY ANALYSIS OF ELECTRODEPOSITED HYDROXYAPATITE COATINGS ON Ti SUPPORT BY PATENTED METHOD

Bogdan-Ovidiu Taranu, Alexandra Ioana Bucur

National Institute of Research and Development for Electrochemistry and Condensed Matter, Dr. A.P. Podeanu street, No. 144, 300569, Timisoara, Romania
e-mail: b.taranu84@gmail.com

Abstract

A previously reported [1,2] and recently patented [3] electrochemical deposition method for hydroxyapatite (HA) on metal supports has been used to modify Ti discs with the specified ceramic material. The method differs from the standard approach by ensuring that only one of the two HA precursors – $Ca(NO_3)_2 \cdot 4H_2O$ and $(NH_4)_2HPO_4$ – is introduced into the electrolysis cell before the coating process begins. The other precursor is added drop by drop and concurrently with the application of a constant electrochemical potential (E). By changing the order in which the precursors are added, as well as the electrodeposition duration, four samples were obtained and were labeled as follows: P1-1h, P2-1h, P1-4h, and P2-4h. Where, P1 = the Ca-based precursor and P2 = the P-based precursor. 1h and 4h refer to the duration of the experiments of one hour and four hours, respectively. The precursor mentioned in the labels is the added precursor. The HA electrochemical coating was carried out at 80 °C and – 1.5 V was the applied and maintained E value. The preparation process of the Ti disks utilized in the study was previously reported [2]. The electrogenerated HA layers were analyzed *via* optical microscopy and the observations made for each sample are presented in what follows. In the case of P1-1h, the noticed HA amount was insufficient to substantially cover the Ti support. Island-like formations with micrometric dimensions were evidenced during the investigation, together with more extended but discontinuous patches of electrocoated material. Similar arrangements were revealed for P2-1h. Isolated structures with sizes in the micrometric range and wide HA-covered areas were observed. The P1-4h and P2-4h samples, which resulted from experiments lasting four times longer, contained a higher amount of generated material and displayed morphological differences. In the first case, most of the HA layer was riddled with crevices and near the edge of the Ti support it became thinner and less discontinuous. In the second case, the electrodeposited material had a cauliflower-like aspect. Higher magnification images show knob-like formations with sizes higher than 10 µm. These structures become smaller and sparser near the edge of the Ti disk, but the presence of a thin HA layer is noticed between them. The results of the optical microscopy analysis of the electrochemically formed HA coatings on Ti support using the mentioned patented method indicate that a deposition time of 1 h is insufficient for covering the metal substrate. However, durations of 4 h avoid this issue and thus display a higher potential of finding application in the fields of dentistry or orthopedics.

Acknowledgements

References

[1] B.-O. Taranu, P. Ianasi, S.F. Rus, A.I. Bucur, Coatings 12 (2022) 288.
[2] A.I. Bucur, E. Linul, B.-O. Taranu, Appl. Surf. Sci. 527 (2020) 146820.
[3] A.I. Bucur, B.-O. Taranu, OSIM patent no. RO133673 B1, 2023.

REMOVAL OF PARACETAMOL AND ASPIRIN TRACES FROM WATER BY ADSORPTION ON SOME NATURAL AND SYNTHETIC CLAY MINERALS

Nick S. Țolea[1], Antonina Lazăr[1], Marina A. Tudoran[1], Ioana M.C. Ienașcu[1,2], Dan Roșu[1], Adina Căta[1]

[1]*National Institute of Research and Development for Electrochemistry and Condensed Matter, Dr. A. P. Podeanu 144, 300569, Timişoara, Romania*
[2]*"Vasile Goldiş" Western University of Arad, Faculty of Pharmacy, Liviu Rebreanu 86, 310045, Arad, Romania*
e-mail: samy_nick2008@yahoo.com

Abstract

The presence of pharmaceutical contaminants in surface waters and drinking water is a major concern worldwide, due to the fact that they can produce various physiological effects in humans and animals even at low concentrations. The widespread presence of pharmaceutical residues in environmental compartments challenged the scientific researchers to find effective solutions for the removal of these pollutants. Adsorption of contaminants on the surface of solids is one of the best alternatives for the removal of organic contaminants due to its low cost, simple design, and ease of use [1]. Clay mineral adsorbents are considered as readily available natural materials that can be used to remove pharmaceutical micropollutants from wastewaters [2]. In addition, clay minerals are chemically and physically stable, have low toxicity and can be easily regenerated [3].

The aim of this work was to study the efficiency of removing aspirin and paracetamol from water using some natural clay minerals (montmorillonite, sepiolite) and a synthetic layered double hydroxide (Mg_3Al-LDH) as adsorbents. The adsorption experiments were conducted using ultrasounds at 40 kHz and room temperature. Different contact times (5-30 min) between mineral clays and drug solutions were applied. The change in the concentration of drug solutions was followed spectrophotometrically at 293 nm for paracetamol and 314 nm for aspirin. The concentration of drug solutions was 0.5 g/L and that of the clay minerals was 2 g/L of drug solution.

The adsorption capacity of mineral clays toward aspirin decreased in the following order: LDH>sepiolite>montmorillonite, while the paracetamol was better removed from solution when sepiolite was used as adsorbent. Generally, adsorption equilibrium was reached after 5 minutes of ultrasonication.

References

[1] O. Fraiha, N. Hadoudi, N. Zaki, A. Salhi, H. Amhamdi, E.H. Akichouh, F. Mourabit, M. Ahari, Desalin. Water. Treat. 317 (2024) 100114.
[2] M. Kryuchkova, S. Batasheva, F. Akhatova, V. Babaev, D. Buzyurova, A. Vikulina, D. Volodkin, R. Fakhrullin, E. Rozhina, Int. J. Mol. Sci. 22 (2021) 9670.
[3] G.G. Hacıosmanoğlu, C. Mejías, J. Martín, J.L. Santos, I. Aparicio, E. Alonso, J. Environ. Manage. 317 (2022) 115397.

AB INITIO AND DFT CALCULATION ON 2,7,12,17-TETRA-TERT-BUTYL-5,10,15,20-TETRAAZA-21H,23H-PORPHINE

Marina Alexandra Tudoran, Bogdan-Ovidiu Taranu

National Institute of Research and Development for Electrochemistry and Condensed Matter, Dr. A. Paunescu Podeanu Street, No. 144, 300569 Timisoara, Romania
e-mail: r_alliy@yahoo.com

Abstract
The integration of computational chemistry with experimental analysis is becoming an increasingly prevalent approach in the chemical sciences. This path offers insights into molecular structures and chemical reaction mechanisms that cannot be discerned through observation alone. In light of these considerations, the present study employs quantum mechanical calculations to investigate the 2,7,12,17-tetra-tert-butyl-5,10,15,20-tetraaza-21H,23H-porphine. *Ab initio* and DFT calculations, performed using Gaussian 03 software, were employed to predict the optimized geometrical parameters and electronic and thermodynamic properties. The results from this theoretical study would be instrumental in guiding the development of novel porphyrazines for energy production applications.

Introduction
Porphyrins are a class of natural macrocyclic compounds that fulfill an important role in various biological processes; they can also be obtained artificially by employing one of several laboratory synthesis methods; their shared characteristic is the porphyrin macrocycle made of four pyrrolic rings connected in the *α* position by four methine groups; the N atoms in the center of the macrocycle are responsible for the amphoteric nature of porphyrins and the macrocycle can be peripherally substituted with a wide variety of functional groups with the formation of porphyrin derivatives having different properties and applications [1]. The aza-analogues of porphyrins are porphyrazines, or tetraazaporphyrins, and they differ by containing N atoms in the *meso*-positions of their macrocycle (as opposed to C atoms) [2]. They can display exceptional photochemical and electrochemical properties and have been studied in the field of sensors, as photosensitizers in PTD, as solar cell dyes and as catalysts [2,3]. Given the significance of porphyrazines and their derivatives, the present work offers a theoretical *ab initio* and DFT analysis of the tetraazaporphyrin molecule 2,7,12,17-tetra-tert-butyl-5,10,15,20-tetraaza-21H,23H-porphine (tBuTAP). The objective of this study is to provide an understanding of the structure and properties of the functionalized porphyrazine that will inform the design and synthesis of new derivatives with potential applications in the energy field.

Experimental
All theoretical calculations for the 2,7,12,17-tetra-tert-butyl-5,10,15,20-tetraaza-21H,23H-porphine were carried out using Gaussian 03W software package at Restricted Hartree-Fock (STO basis set) and Density Functional Theory (B3LYP – STO basis set) levels of theory [4]. Hartree-Fock (HF) is considered the basic *ab initio* model, which employs the approximation that the Coulombic electron-electron repulsion can be averaged. In its restricted form, the same orbital spatial function is utilized for electrons within the same pair. The Density Functional Theory (DFT) method employs the electron density in order to calculate the molecule's energy [5]. In the context of quantum mechanical calculations, the Becke's three-parameter hybrid exchange functional combined with the Lee-Yang-Parr gradient-corrected correlation hybrid functional (B3LYP) is arguably the most common functional used. This approach provides a

reasonable degree of accuracy with an affordable computational cost [6,7]. The geometries of tBuTAP were fully optimized *in vacuo* by minimizing the energies using the default convergence criteria, without the imposition of any molecular symmetry constraints [8,9]. The frequency calculations were conducted at the same levels of theory to confirm that the optimized geometry represents a real minimum on the potential energy surface, with no imaginary frequency. The electronic populations of the highest occupied molecular orbital (HOMO) and the lowest unoccupied molecular orbital (LUMO), the energy gap, the total dipole moment, and thermodynamic parameters were calculated based on the optimized geometry obtained at the HF/STO and DFT-B3LYP/STO levels. The GaussView 6.0 program was used for the molecular visualization of the calculated structure.

Results and discussion

The optimized molecular structure of tBuTAP, obtained through the application of the HF and DFT methods, and the selected atomic labelling scheme, are depicted in Figure 1. A summary of the predicted bond lengths, bond angles, and Mulliken charges is provided in Table 1. The results demonstrate that the introduction of the tert-butyl group and the replacement of C atoms by N atoms in the porphyrin molecule led to a deformation of the molecular geometry. To illustrate, both the $C_\alpha - C_\beta$, and $C_{\alpha'} - N_{\alpha'}$ bonds exhibit slightly elevated values when compared to the $C - C$ (1.465 Å) and $C - N$ (1.371 Å) bonds that are characteristic of porphyrins [7], as determined through experimental analysis by Chen & Tulinsky [10]. Additionally, the $C - N - C$ angle exceeds the $C - C - C$ angle within the porphyrin molecule ($90.00 \pm 0.42°$) [11].

Table 1. Selected bond length, bond angle and Mulliken charge of tBuTAP calculated by HF/STO and DFT B3LYP/STO

Bond length (Å)			Bond Angle (°)			Mulliken charge		
	HF	*DFT*		*HF*	*DFT*		*HF*	*DFT*
$C_\alpha - C_\beta$	1.491	1.469	$N_f - C_\alpha - N_\alpha$	127.984	124.598	C_α	0.200	0.151
$C_\alpha - N_\alpha$	1.311	1.415	$N_f - C_{\alpha'} - N_{\alpha'}$	129.419	124.637	C_β	-0.095	-0.93
$C_\alpha - N_f$	1.430	1.390	$C_\alpha - N_f - C_{\alpha'}$	118.872	113.751	N_f	-0.295	-0.226
$N_f - C_{\alpha'}$	1.295	1.389	$C_\alpha - C_\beta - C_\gamma$	107.758	107.805	$C_{\alpha'}$	0.530	0.149
$C_{\alpha'} - C_{\beta'}$	1.515	1.487	$C_\beta - C_\alpha - N_\alpha$	113.595	110.394	$C_{\beta'}$	0.015	-0.004
$C_{\alpha'} - N_{\alpha'}$	1.402	1.416	$C_{\alpha'} - C_{\beta'} - C_{\gamma'}$	107.724	105.525	N_α	-0.326	-0.286
$N_{\alpha'} - H$	1.018	1.258	$C_{\beta'} - C_{\alpha'} - N_{\alpha'}$	105.584	110.723	$N_{\alpha'}$	-0.359	-0.285

The results of the Mulliken population analysis, obtained with HF and DFT, revealed that the atomic charges of nitrogen are exclusively negative, a consequence of their high electronegativity, which results in some charge accumulation [12]. In contrast, the atomic charges of carbon are both positive and negative. The carbon atoms bonded to the two nitrogen atoms have a positive charge, whereas the carbon atom bonded to the hydrogen has a negative one. The carbon atom bonded to the tert-butyl group yielded positive results when analyzed using the HF method and negative results when analyzed using the DFT method.

The electronic characteristics and stability of compounds are evaluated using the energies of HOMO, LUMO, and their corresponding energy gap. In the context of electron transfer, the ability of an electron to donate or accept is described by the E_{HOMO} and E_{LUMO} – these parameters being of great importance in elucidating the nature of intermolecular interactions. The frontier gap plays a pivotal role in elucidating both the chemical reactivity and the electron conductivity, which in turn inform our understanding of the molecular electrical transport [13,14].

Table 2. Calculated energy values of HOMO (E_{HOMO}), LUMO (E_{LUMO}), and energy gap (ΔE_{HL}) of tBuTAP in gas phase using HF and DFT methods

Parameter	HF	DFT
E_{HOMO} (eV)	-5.45125956	-3.89694445
E_{LUMO} (eV)	3.1674068	-1.03757064
ΔE_{HL} (eV)	8.61866641	2.85937381

The results of the HOMO and LUMO energies and the energy gap, computed at HF/STO and DFT/B3LYP-STO levels of theory in gas phase are presented in Table 2. Figure 2 illustrates the frontier molecular orbital diagrams, which reveal that orbitals are delocalized over the macrocycle and are responsible for $\pi\rightarrow\pi*$ transitions, as observed in other porphyrinoid systems [15].
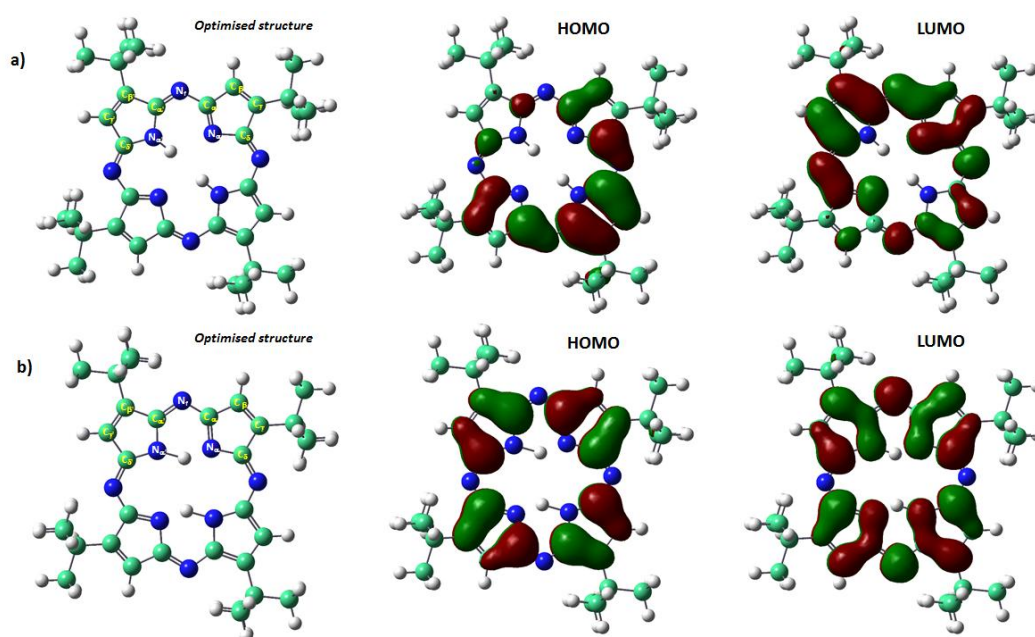
Figure 1. Atomic labelling scheme for the optimized structures and molecular orbitals of tBuTAP corresponding to a) HF and b) DFT calculations

Molecular electrostatic potential (MEP) employed to investigate the relationship between molecular structures and the correlation between molecular physiochemical properties. Additionally, this methodology elucidates molecular interactions with other molecules and within the molecule. The MEP map provides data regarding the presence of both positive and negative charged regions within a given molecule, this information being used to predict the reactivity of individual atoms in response to electrophilic and nucleophilic interactions [9, 16]. In terms of the local electrostatic potential, the color scheme employed is as follows: red and yellow are used to indicate negative regions associated with electrophilic reactivity, while blue denotes positive regions related to nucleophilic reactivity. Neutral regions are represented in green [9,17]. The MEP map presented in Figure 2 indicates that the red and yellow regions surrounding the nitrogen atoms correspond to the electrophilic center of the tBuTAP.
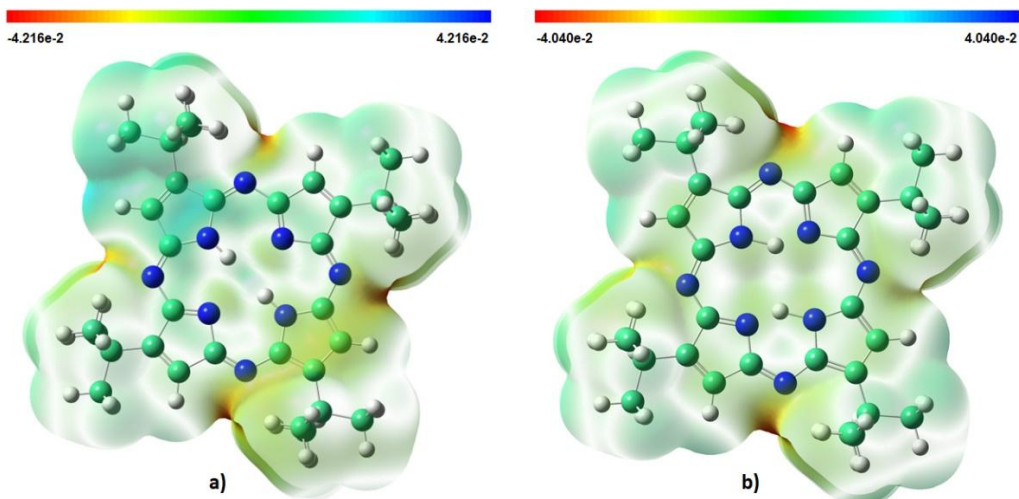
Figure 2. Molecular electrostatic potential (MEP) map of tBuTAP in gas phase calculated by a) HF and b) DFT methods

A statistical thermochemical analysis was conducted on the tBuTAP, with the assumption that the molecule was at room temperature (298.150 K) and 1 atm. The data presented in Table 3 provides a summary of the calculated thermodynamic parameters, including thermal energy, constant volume heat capacity, entropy, and dipole moment. The findings indicate that the ZPVE energy is considerably higher in the HF method in comparison to the B3LYP method (515.14482 kcal/mol *vs.* 466.28333 kcal/mol). Conversely, the total thermal energy and the dipole moment are observed to decrease with an increase in the basis set dimension, the result obtained with HF being smaller than those obtained with DFT. The two calculation methods yield comparable values for heat capacity and entropy [18].

Table 3. Calculated thermodynamic parameters of tBuTAP using HF and DFT methods

Parameter		HF/STO	DFT/B3LYP-STO
Zero-point vibrational energy (kcal/mol)		515.14482	466.28333
Rotational constant (GHz)	*X*	0.07985	0.08238
	Y	0.07966	0.07571
	Z	0.04135	0.04092
Thermal energy (kcal/mol)	*Total*	538.074	490.772
	Translational	0.889	0.889
	Rotational	0.889	0.889
	Vibrational	536.297	488.994
Constant volume heat capacity (cal/mol-Kelvin)	*Total*	141.350	152.333
	Translational	2.981	2.981
	Rotational	2.981	2.981
	Vibrational	135.389	146.372
Entropy (cal/mol-Kelvin)	*Total*	219.884	229.724
	Translational	44.736	44.736
	Rotational	38.344	38.374
	Vibrational	136.804	146.614
Dipole Moment (Debye)		2.627384	0.005660

Conclusion

In this study, the *ab initio* and DFT methods are employed for theoretical investigation of the 2,7,12,17-tetra-tert-butyl-5,10,15,20-tetraaza-21H,23H-porphine molecule. The electronic and thermodynamic properties of optimized structures have been obtained using the STO basis set.

The theoretically calculated values of both bond lengths and bond angles in the minimum energy structure reveals a slight increase in both parameters in the tetraazaporphyrin relative to the unfunctionalized porphyrin. As evidenced by the Mulliken population analysis, there are notable distinctions between the HF and DFT methods with respect to the $C_{\beta'}$ atom. The HOMO-LUMO energy gap was determined to be 8.619 eV (HF) and 2.859 eV (DFT), the frontier orbitals being delocalized over the compound's core. The MEP plot indicates that the most favorable atomic sites for electrophilic attack are the negative regions present at the nitrogen atoms level. In order to elucidate the internal energy system and achieve a deeper understanding of the molecular structure of the porphyrazine, the thermodynamic properties and dipole moment have also been calculated.

References

[1] E. Fagadar-Cosma, D. Vlascici, G. Fagadar-Cosma, Porfirinele de la sinteză la aplicații, Eurostampa, Timisoara, Romania, 2008, pp. 10.

[2] A. Rusanov, N. Chizhova, N. Mamardashvili, Molecules 27 (2022) 8619.

[3] S. Yamazaki, M. Asahi, N. Taguchi, et al., ACS Catalysis 10 (2020) 14567.

[4] M. J. Frisch, G.W. Trucks, H.B. Schlegel, et al., Gaussian 03 (Gaussian, Inc., Wallingford, CT, 2003).

[5] A. Tomberg, Gaussian 09w tutorial. An Introduction to Computational Chemistry Using G09W and Avogadro Software, 2013, pp. 1-36.

[6] X. Gu, Q. Sun, Phys. Chem. Chem. Phys. 15 (2013) 15434.

[7] C.K. Tai, W.H. Chuang, B.C. Wang, J. Lumin. 142 (2013) 8.

[8] M.P. Balanay, D.H. Kim, Phys. Chem. Chem. Phys. 10 (2008) 5121.

[9] S.D. Kanmazalp, Karaelmas Sci. Eng. J., 7 (2017) 491.

[10] B.M.L. Chen, A. Tulinsky, J. Am. Chem. Soc. 94 (1972) 4144.

[11] L.P. Cook, G. Brewer, W. Wong-Ng, Crystals 7 (2017) 223.

[12] M.S. Liao, S. Scheiner, J. Chem. Phys. 117 (2002) 205.

[13] P. Govindasamy, S. Gunasekaran, S. Srinivasan, Spectrochim. Acta A Mol. Biomol. Spectrosc. 130 (2014) 329.

[14] M.A. Sakr, M.A. Saad, J. Mol. Struct., 1258 (2022) 132699.

[15] F. Sabuzi, M. Stefanelli, D. Monti, et al., Molecules 25 (2019) 133.

[16] A.K. Shukla, A.P. Chaudhary, J. Pandey, Heliyon 6 (2020) e05016.

[17] T.C. Zeyrek, J. Korean Chem. Soc. 57 (2013) 461.

[18] A. Hassan, A.S. Gidado, FUDMA J. Sci. 3 (2019) 268.

METAL-ORGANIC FRAMEWORKS AS ELECTRODE'S MODIFIER FOR DOPAMINE DETECTION

<u>Alexandra Belcovici</u>[1], Davide Tocco[2], Andrea Salis[2], Graziella Liana Turdean*,[1]

[1]*"Babes-Bolyai" University, Faculty of Chemistry and Chemical Engineering, Department of Chemical Engineering, Laboratory of Electrochemical Research and Nonconventional Materials, Arany Janos 11, RO-400028 Cluj-Napoca, Romania*
[2]*Università degli Studi di Cagliari, CSGI, and CNBS, Dipartimento di Scienze Chimiche e Geologiche, Cittadella Universitaria SS 554 bivio Sestu, 09042, Monserrato, Cagliari, Italy*
* graziella.turdean@ubbcluj.ro

In the human body, dopamine (DA) plays an important role as a neurotransmitter in the central nervous system (CNS) and, also, is a key factor in the function of renal and cardiovascular systems. Thus, the normal clinical concentration of DA in mamalians typically ranges from 10^{-8} M to 10^{-6} M. Therefore, the selective and sensitive detection of DA in biological systems is of great clinical importance for correct diagnosis. The electrochemical method that uses chemically modified electrodes is an alternate method for the quantitative determination of DA by liquid chromatography, capillary electrophoresis, chemiluminescence, and colorimetry [1].

In this context, metal-organic frameworks (MOFs) – a new widely researched class of porous materials constituted by a metal node/cluster and an organic ligand linked through coordination bonds – could play the role of modifier for developing chemically modified electrodes [2].

Consequently, composite materials consisting of zeolitic imidazolate frameworks (a subclass of MOFs, e.g., ZIF-8) [3] and reduced graphene oxide (rGO) were immobilized using Nafion polymer on the glassy carbon electrode surface. The following modified electrode architectures were prepared: rGO–Nafion/GCE, ZIF-8–Nafion/GCE and ZIF-8–rGO–Nafion/GCE, and investigated by electrochemical methods. The influence of experimental parameters (scan rate, pH of electrolyte, etc) leads to the estimation of the electrochemical parameters.

The ZIF-8–rGO–Nafion/GCE modified electrode shows the following analytical parameters: sensitivity of 0.348 A/M and limit of detection (signal/noise = 3) of 0.098 μM dopamine.

Thus, the obtained results recommend the ZIF-8–rGO–Nafion/GCE modified electrode as a robust and performant alternative for dopamine detection.

References

[1] G. Yu, J. Xia, F. Zhang, Z. Wang, J. Electroanal. Chem. 2017, 801, 496–502.
[2] S. R. Batten, N. R. Champness, X.-M. Chen, J. Garcia-Martinez, S. Kitagawa, L. Öhrström, M. O'Keeffe, M. P. Suh, J. Reedijk, Cryst Eng Comm 2012, 14, 3001.
[3] T. T. H. Ngo, T. H. Y. Pham, N. T. Dang, N. T. V. Hoan, T. H. Pham, G. L. Turdean, Studia Universitatis "Babes-Bolyai" Chemia, 2023, 68(1), pp. 7–17.

THE INHIBITORY EFFECT OF WHITE ALDER EXTRACT ON LOW-CARBON STEEL CORROSION IN SULFURIC ACID

Cristian George Vaszilcsin[1], George-Daniel Dima[1,2], Nataliia Rudenko[3], Mircea Laurenţiu Dan[2]

[1]National Institute of Research and Development for Electrochemistry and Condensed Matter, Dr. A. P. Podeanu 144, 300569, Timişoara, Romania
[2]University Politehnica Timisoara, Faculty of Industrial Chemistry and Environmental Engineering, Laboratory of Electrochemistry, Corrosion and Electrochemical Engineering, 6 Pârvan, 300223 Timisoara, Romania
[3]University Politehnica Timisoara, Innovation and Technology Transfer Center, 2 V. Pârvan, 300223 Timisoara, Romania
e-mail: cristi_vasz@yahoo.com

Abstract

One potential way to reduce corrosion expenses is to utilize corrosion inhibitors. Recently, most of the research has focused on corrosion inhibitors with a minimal environmental effect, with plant extracts being particularly popular [1,2]. The study's goal is to determine the inhibitory impact of a commercial alcoholic extract of white alder (Alnus incana) on OL48 steel corrosion in an H_2SO_4 media.

To assess the stability of the active components in the inhibitor structure, cyclic voltammograms were plotted on the Pt electrode on the potential range between the release of hydrogen and oxygen, at polarization rates of 500, 100, and 5 mV s^{-1}, in the absence and presence of 2.5, 7.5, and 10 mLL^{-1} extract. The effect of extract additions on the corrosion process of OL48 steel, which was used as a working electrode, was investigated using linear voltammetry, chronoamperometry, and the representation of electrode potential vs. time at a temperature of 293 K for extract concentrations of 1.25, 5, 2.5, 3.75, 5, 7.5, and 10 mL/L.

To conclude the research, molecular modeling of the extract's first two main natural compounds was performed. The structures were optimized using the DFT method on a B3LYP function, on the basis set 6-31G*, based on which the plotting of the Frontier orbitals and the molecular descriptors such as the energy of the HOMO orbital (E_{HOMO}), the energy of the LUMO orbital (E_{LUMO}), their difference in absolute value E_{GAP}, the molecule hardness, and softness, the electronegativity χ, the dipole moment μ, respectively the QSAR properties related to the surface and molecular volume. All of thesementioned is consistent with the electrochemical measurements and explains the formation of covalently coordinating bonds between non-participating electrons of polar functional groups and iron's vacant orbital, allowing for the formation of a protective layer that prevents further corrosive attacks [3].

References

[1] A. Zakeri, E. Bahmani, A. Sabour Rouh Aghdam, Plant extracts as sustainable and green corrosion inhibitors for protection of ferrous metals in corrosive media: A mini review, Corros. Commun., 5 (2022) 25-38.

[2] R. O. Medupin, K. O. Ukoba, K. O. Yoro, T.-C. Jen, Sustainable approach for corrosion control in mild steel using plant-based inhibitors: a review,Mater Today Sustain, 22 (2023), 100373.

[3]E.Alibakhshi, M.Ramezanzadeh, G.Bahlakeh, B.Ramezanzadeh, M.Mahdavian, M.Motamedi, J. Mol. Liq., 255 (2018) 185–198.

IDENTIFICATION AND STRUCTURAL CHARACTERIZATION OF CHONDROITIN SULFATE DISACCHARIDES IN HUMAN BIGLYCAN BY NANOELECTROSPRAY IONIZATION-ION MOBILITY TANDEM MASS SPECTROMETRY

Mirela Sarbu[1], Raluca Ica[1], Roxana Biricioiu[1,2], David E. Clemmer[3], <u>Alina D. Zamfir</u>[1,4]

[1]Department of Condensed Matter, National Institute for Research and Development in Electrochemistry and Condensed Matter, 300224 Timisoara, 1 Plautius Andronescu Street, Romania
[2]Faculty of Physics, West University of Timisoara, 300223 Timisoara, 4 Vasile Parvan Blvd., Romania
[3]Department of Chemistry, The College of Arts & Science, Indiana University, 47405-7102 Bloomington, 800 E. Kirkwood Ave., Indiana, USA
[4]Department of Technical and Natural Sciences, "Aurel Vlaicu" University of Arad, 310330 Arad, 2-4 Elena Dragoi Street, Romania
e-mail: alina.zamfir@uav.ro

Abstract

We have implemented a superior glycomics method based on ion mobility separation (IMS) mass spectrometry (MS) and tandem MS (MS/MS) to characterize the chondoritin sulfate (CS) disaccharide domains in human biglycan (BGN). The high separation efficiency and sensitivity of IMS MS technique allowed the discrimination of five distinct CS motifs, of which four irregulated in their sulfation pattern. The structural investigation by IMS MS/MS disclosed that in one or both of the CS/DS chains, the non-reducing end is 3-*O*-sulfated GlcA in a rare bisulfated motif having the structure 3-*O*-sulfated -GlcA-4-*O*-sulfated GalNAc. Considering the role played by BGN in cancer cell spreading, the influence on this process of the newly identified sequences is to be investigated in the future.

Introduction

Biglycan (BGN) is a small leucine-rich repeat proteoglycan involved in a variety of pathological processes including malignant transformation, for which the upregulation of BGN was found related to cancer cell invasiveness. Since the functions and interactions of BGN are mediated by its chondroitin/dermatan sulfate (CS/DS) chains through the sulfates, the determination of CS/DS sulfation pattern is of major biological importance [1]. In the past years, ion mobility separation (IMS) combined with mass spectrometry (MS) has emerged as a reliable analytical platform able to separate and identify isomers, isobars, and conformers, thus decoding the structural information of functional components in biological mixtures [2]. In this context, in the present study we have implemented IMS MS and tandem MS (MS/MS) for the characterization of CS disaccharide domains in BGN, with a particular emphasis on the determination of the sulfation code *i.e.* the number of the sulfate groups and their exact location.

Experimental

CS/DS chains were released from HEK293 cells BGN by β-elimination and submitted to partial depolymerization with AC I lyase. The mixture was fractionated on a Superdex Peptide HR10/30 column. Following the purification, the pooled disaccharide fraction was dissolved in pure methanol to a concentration of 10 pmol/μL and infused by negative ion nanoelectrospray (nanoESI) into a Synapt G2S (Waters, Manchester, UK) mass spectrometer at a nanoESI potential of 1.4 kV, a cone voltage of 15 V, IMS gas flow 90 mL/min, IMS wave velocity 650

m/s and IMS wave height 40 V. MS/MS experiments were performed by collision induced dissociation (CID) at collision energies ramped from 25 to 35 eV.

Results and discussion

The CS disaccharide pool infused by (-) nanoESI was subjected to a two dimensional separation of the ions: the initial separation took place in the IMS sector according to the mobilities of the ions under the electric field, while the second separation occurred in the TOF analyzer according to *m/z* values of the ions. The generated ion mobilograms revealed that BGN: a) contains heterogeneous CS disaccharide domains and b) the species were separated not only according to their charge state but also to the number of the sulfate groups and the saturated (GlcA) or unsaturated (4,5-Δ-GlcA) type of glucuronic acid. Ten molecular ions corresponding to five distinct disaccharides differing in the number of sulfate groups and the saturated/unsaturated type of GlcA were discovered. As expected, the most abundant ions correspond to [4,5-Δ-GlcAGalNAc], the regularly sulfated unsaturated disaccharide, containing one SO_3 group. Except for the regularly sulfated species a non-sulfated [4,5-Δ-GlcAGalNAc] and a series of three oversulfated structures bearing two or three sulfate groups were also identified. According to mass calculation, the monodeprotonated species at *m/z* 538.021 corresponds to the unsaturated bisulfated-[4,5-Δ-GlcAGalNAc] whereas the [M-H]$^-$ detected as an ion of fair abundance at *m/z* 617.970 is attributable to the unsaturated trisulfated-[4,5-Δ-GlcAGalNAc]. The latter domain is among the CS disaccharides containing the highest number of sulfates ever detected by MS. Of a particular importance is the discovery of the saturated bisulfated-[GlcAGalNAc], which might originate from the terminus of the original chain. The detailed structural analysis carried out by IMS CID MS/MS disclosed that one or both of the non-reducing ends of BGN consist of an atypical oversulfated motif having the structure 3-*O*-sulfated GlcA-4-*O*- sulfated GalNAc.

Conclusion

We have reported here on the discovery of CS disaccharide domains in BGN by one of the most advanced glycomics methods based on IMS MS and CID MS/MS. Considering the role of BGN in the biological processes related to malignant transformation, the novel structural CS domains of irregular sulfation, discovered here, are to be further investigated from this perspective. Such domains may influence, by triggering or obstructing, the functional interactions of BGN involved in tumour growth.

Acknowledgements

References

[1].V. Kram, R. Shainer, P. Jani, et al., J. Histochem. Cytochem. 68 (2020) 747–762.
[2]. R.L. Miller, S.E. Guimond, R. Schwörer, et al., Nat. Commun. 11 (2020) 1481-1492.

ASSESSING LEVEE INTEGRITY: SIMULATING FLOOD CONDITIONS WITH TIME-LAPSE ERT FOR ENHANCED RISK MANAGEMENT

Ahmed M. Ali[1,2], Attila Timar[3], Enas Abdelsamei[1,2], Diaa Sheishah[1,2], Alexandru Hegyi[4], György Sipos[1*]

[1]*University of Szeged, Department of Geoinformatics, Physical and Environmental Geography, 6722 Szeged, Egyetem u. 2-6., Hungary*
ahmed.mahmoud@nriag.sci.eg, enas.mohammed@nriag.sci.eg, geo_diaa@nriag.sci.eg, gysipos@geo.u-szeged.hu
[2]*National Research Institute of Astronomy and Geophysics, 11421, El Marsad st., Helwan, Cairo, Egypt*
enas.mohammed@nriag.sci.eg, geo_diaa@nriag.sci.eg , ahmed.mahmoud@nriag.sci.eg
[3]*Körös District Water Directorate, Department of Flood Protection and River Engineering, 5700 Gyula, Városháza u. 26., Hungary atimar82@gmail.com*
[4]*Applied Geomorphology and Interdisciplinary Research Centre (CGACI), Department of Geography, West University of Timisoara, 300223 Timisoara, Romania*
alexandru.hegyi89@e-uvt.ro
Corresponding author email: gysipos@geo.u-szeged.hu

Abstract
Aging levees, particularly those without detailed construction data, pose a growing risk to flood-prone regions. As these critical structures deteriorate over time, subsurface leakage paths can develop, compromising their stability. Detecting these leakage paths before they lead to catastrophic failure is crucial, but real-time assessment during flood conditions remains a significant challenge. Electrical resistivity tomography (ERT) offers a non-invasive way to identify potential weak spots within levees, but its use during actual flood events is limited by logistical difficulties and insufficient data. To bridge this gap, this study simulates flood conditions on a 40-meter section of an artificial levee in Békés, Hungary, providing valuable insights into levee behavior under stress.

The experiment, conducted during the summer of 2023, used time-lapse ERT measurements to monitor how potential leakage pathways evolve within the levee's mixed fluvial soils under both dry and wet conditions. Core samples were collected to obtain key physical parameters, including grain size, hydraulic conductivity, porosity, density, and water content, which were used to cross-validate the ERT data. The results, processed through integrated 2D and 3D inversion models, identified areas where resistivity values fell below 10 $\Omega \cdot m$, indicating zones of saturated soil that could act as conduits for water movement.

The findings revealed significant leakage zones concentrated at the crest of the levee, with water migrating laterally through the crest and toward the protected side. Three distinct pathways for water passage were identified, suggesting potential weak points that could exacerbate flooding during high water events. These results underline the importance of targeted monitoring for levee health.

This study provides a practical framework for using ERT in controlled environments to evaluate the integrity of aging levees. By offering a clear method for periodic levee health assessments, this approach can guide more effective flood risk management strategies, helping engineers and policymakers make informed decisions to safeguard vulnerable communities from the increasing threat of floods.

OPTIMIZATION OF MASS SPECTROMETRY MEASUREMENTS FOR MONITORING DEUTERIUM PRODUCTION IN NANOPLASMONIC LASER FUSION

Á. Bélteki[1,2], D.J. Palásti[1,2], M. Aladi[2], M.Á. Kedves[2], A. Bonyár[2,3], M. Szalóki[2,4], M. Veres[2], N. Kroó[2], T. Bíró[2], G. Galbács[1,2]

[1]*Department of Molecular and Analytical Chemistry, University of Szeged, H-6720 Szeged, Dóm tér 7, Hungary*
[2]*HUN-REN Wigner Research Centre for Physics, NAPLIFE, H-1525 Budapest, P.O.B 49. Hungary*
[3]*Department of Electronics Technology, Budapest University of Technology and Economics, H-1111 Budapest, Egry József u. 18., Hungary*
[4]*Department of Biomaterials and Prosthetic Dentistry, University of Debrecen, H-4032, Debrecen, Nagyerdei krt. 98., Hungary*
e-mail: adamteki@chem.u-szeged.hu

Abstract

Nanoplasmonic laser fusion is a new concept in energy production. Our research project utilizes focused, high intensity femtosecond laser pulses to initiate nuclear fusion between hydrogen isotopes in special polymer targets, which contain carefully distributed gold nanorods (nanoantennas) of the proper dimensions [1]. An important task of this project was to develop suitable analytical methods that allow the sensitive monitoring of the chemical products of the reaction. Laser-induced breakdown spectroscopy, mass spectrometry and Raman spectroscopy was selected for this purpose [2]. The present contribution reports about the process of the development and performance of the mass spectrometry method created for detecting deuterium. This includes a.) the construction of the measurement system, centered around a ultra high intensity Coherent Hidra-25 Ti:Sapphire fs laser, a high vacuum processing chamber and Hiden DLS-20 ultra high resolution quadruple mass spectrometer; b.) the detailed optimization of the experimental parameters influencing system performance (e.g. pressure, laser focusing, ionization, ion signal recording mode, etc.) and c.) the assessment of the analytical figures of merit. In our presentation, we will also describe the characteristics of the laser targets used [3-4], the assignation of the mass signals to hydrogen-containing species as well as the present status of the project.

Acknowledgment

References

[1] T. S. Biró, N. Kroó, L. P. Csernai, M. Veres, M. Aladi, I. Papp, et al.; Universe, 2023, 9, 233.
[2] N. Kroó, M. Aladi, M. Kedves, B. Ráczkevi, A. Kumari, P. Rácz, et al.; Sci. Reports, 2024, 14, 1828.
[3] D.J. Palásti, O. Urbán, F.A. Casian-Plaza, J. Kámán, et al.; Polymer Testing, 2024, 139, 108565.
[4] A. Bonyár, M. Szalóki, A. Borók, I. Rigó, J. Kámán, et al.; Int. J. Mol. Sci. 2022, 23, 13575.

COMPARISON OF THE EFFICIENCY OF MERCURY VAPOR AND EXCIMER LAMPS EMITTING IN THE UV-C RANGE FOR UV/H_2O_2 AND UV/PDS PROCESSES

Réka Biró, Tünde Alapi, Anett Covič

Department of Molecular and Analytical Chemistry, University of Szeged, H-6720 Szeged, Dóm tér 7., Hungary

Nowadays, more and more persistent micropollutants (i.e. pharmaceuticals and cosmetics) are entering our waters, and reaching the drinking water supply, causing serious health and environmental problems. The conventional water treatment process is not effective enough to remove them, thus, the application of additional processes is required. Advanced Oxidation Processes (AOPs) based on $SO_4^{\bullet-}$ and $^{\bullet}OH$ generation using a combination of UV light and appropriate oxidants offer a promising solution.

This study investigated the efficiency of UV/H_2O_2 and UV/PDS methods using trimethoprim antibiotic as an organic model compound and two light sources. The low-pressure mercury vapor lamp emits 254 nm, a widely used light source in water treatment. It was compared to the 222 nm emitting KrCl excimer lamp, which could be an alternative to mercury-containing UV lamps. KrCl excimer lamps became widespread during the 2019 Covid pandemic, due to their excellent disinfection properties. The effect of inorganic ions (Cl^- and HCO_3^-) and the matrix (biologically treated wastewater) were also investigated.

First, the photolysis of oxidizing agents was investigated and compared at different wavelengths. Although the photon flux of the mercury vapor lamp is an order of magnitude greater than the photon flux of the excimer lamp, the conversion rate of oxidants for 254 nm photolysis is only twice that of 222 nm photolysis due to the significant difference in molar absorbance at the emission wavelengths. The molar absorbance of H_2O_2 and PDS at 222 nm (79 and 172 M^{-1} cm^{-1}, respectively) highly exceeds the value determined at 254 nm (17 and 21 M^{-1} cm^{-1}). Trimethoprim transformation rate was negligible at 254 nm, but direct photolysis was observed at 222 nm. The oxidizing agent increased the rate of transformation of trimethoprim; the magnitude of the effect increased with H_2O_2 and PDS concentration. At 222 nm, due to the higher molar absorbance of trimethoprim, a stronger competition for photon absorption between oxidant and trimethoprim was established. Despite their radical scavenging capacity, inorganic ions only slightly altered the transformation rate, but the matrix (biologically treated domestic wastewater) significantly reduced the efficiency of both methods due to its organic matter content. The efficiency of mineralization was also reduced by the matrix. The role of secondary radicals formed from inorganic ions in the matrix must also be considered in the case of both processes.

Despite the limitations of the 222 nm KrCl excimer lamp, it can be a good alternative to the mercury vapor lamp used in water treatment for UV/PDS and UV/H_2O_2 processes. However, due to the shorter wavelength and the higher molar absorbance of the inorganic and organic matrix components, the competition for photons between the oxidizing agents and the matrix components is more pronounced than in the case of the 254 nm photolysis. All this must be taken into account in terms of optimizing the operating parameters and the formation of secondary radicals.

PLASTIC POLLUTION FROM COVID-19 PERSONAL PROTECTIVE EQUIPMENT CAN CAUSE CHANGES IN PLANT ROOT GROWTH AND SOIL HEALTH

Klaudia Hoffmann[1], Enikő Mészáros[2], Kamilla Kovács[2], Etelka Kovács[1], Katalin Perei[1], Gábor Feigl[2*], <u>Attila Bodor[1,3*]</u>

[1]*Department of Biotechnology and Microbiology, University of Szeged, H-6726 Szeged, Közép fasor 52, Hungary*
[2]*Department of Plant Biology, University of Szeged, H-6726 Szeged, Közép fasor 52, Hungary*
[3]*Department of Physiology, Anatomy, and Neuroscience, University of Szeged, H-6726 Szeged, Közép fasor 52, Hungary*
e-mail: bodora@bio.u-szeged.hu
*These authors contributed equally to this work.

Background

The COVID-19 pandemic significantly increased plastic pollution from improperly disposed single-use personal protective equipment (PPE), particularly polypropylene (PP) surgical masks and disposable protective gloves (DPGs) [1-4]. Notably, PPE, like other conventional plastics with limited degradability, are not environmentally inert and can release secondary fragments (*e.g*., macro-, meso-, and microplastics) or leach harmful components, potentially disrupting local ecosystems [3-5]. While scientists agree that the burden of PPE waste is inevitably of global concern due to environmental pollution [6], its exact effects on plant growth and development, as well as on the soil environment, has not yet been examined.

Aims and methods

In this study, a soil-filled rhizotron model system (Fig. 1.) was used to investigate the effects of soil plastic pollution from PPE fragments on plant development and soil health parameters. The soils were supplemented with macro-sized (2.5 cm), meso-sized (2 cm, 1 cm, 0.5 cm), or micro-sized (<0.5 cm) fragments of PPE—latex DPGs, nitrile DPGs, and PP surgical masks. The applied concentrations of 0.5% and 1% plastic fragments were chosen to model less severe and environmentally realistic plastic pollution scenarios, respectively. After the 14-days cultivation period of oilseed rape (*Brassica napus* L.), plant primary root lengths and lateral root numbers were measured to calculate lateral root density (lateral roots per 1 cm of the primary root).
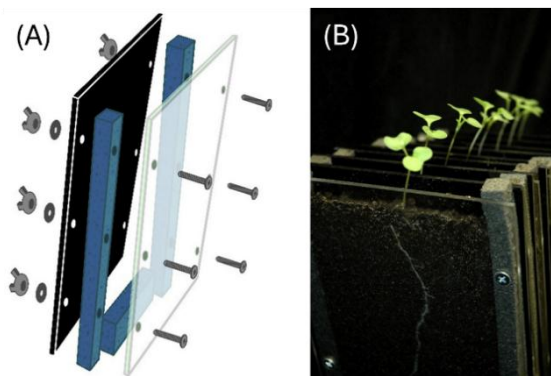
Figure 1. (A) Schematic rhizotron design and (B) oilseed rape (*B. napus*) seedlings growing in soil-filled, non-contaminated control rhizotrons [7].

Soil biology parameters, including the cell count of aerobic heterotrophic bacteria (AHB) and soil health indicator soil enzyme activities [catalase (CAT) and dehydrogenase (DH)], were also assessed.

Results and discussion

Plant root growth parameters are shown in Figure 2.
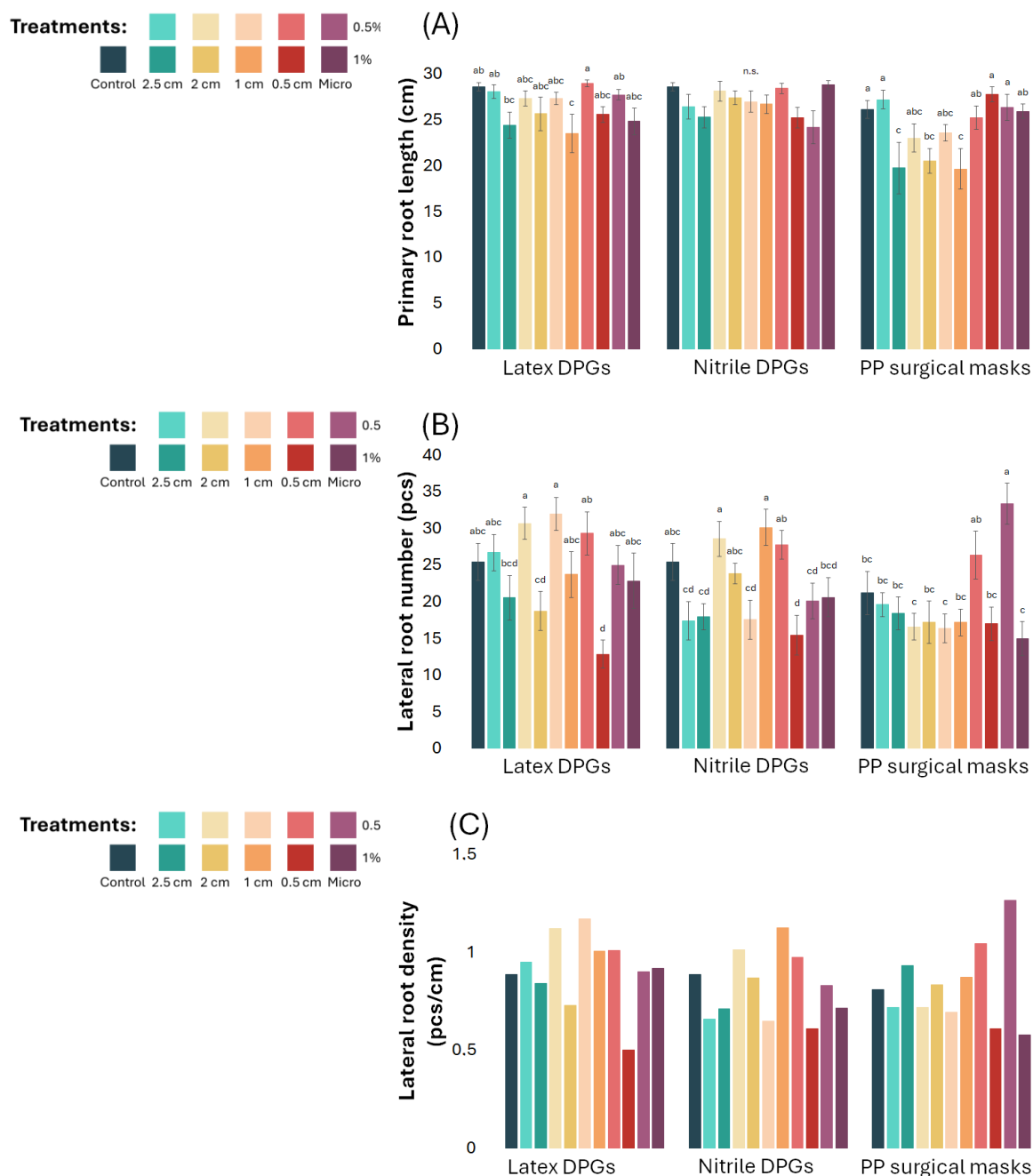
Figure 2. Root growth parameters of 14-days-old *Brassica napus* seedlings grown in rhizotron soils supplemented with plastic fragments from latex protective disposable gloves (DPGs), nitrile DPGs, or polypropylene (PP) masks of various sizes (2.5, 2, 1, 0.5, and <0.5 cm) at 0.5% and 1% concentrations: (A) primary root lengths, (B) lateral root numbers, and (C) lateral root density.

Different letters in each treatment indicate significant differences according to Duncan's test (p≤0.05), n.s.: no significant difference.

Soil biology parameters are shown in Figure 3.
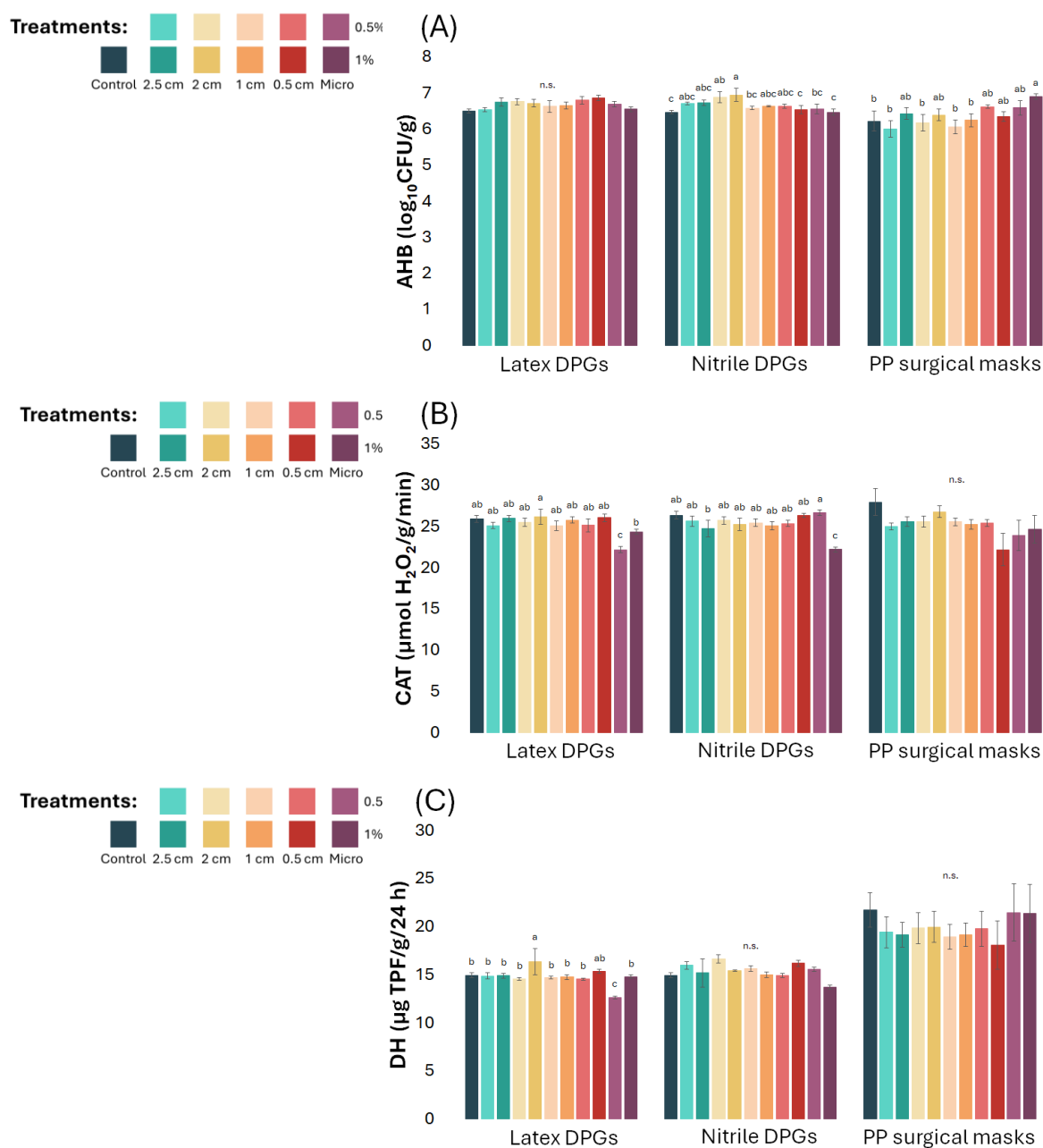
Figure 3. Soil biology parameters measured, after the 14-days cultivation period, from the rhizotron soils supplemented with plastic fragments from latex protective disposable gloves (DPGs), nitrile DPGs, or polypropylene (PP) masks of various sizes (2.5, 2, 1, 0.5, and <0.5 cm) at 0.5% and 1% concentrations: (A) colony forming units (CFUs) of aerobic heterotrophic bacteria (AHB), (B) soil catalase (CAT) activity, and (C) soil dehydrogenase (DH) activity. Different letters in each treatment indicate significant differences according to Duncan's test (p≤0.05), n.s.: no significant difference.

Conclusions

Both PP mask and DPG fragments caused morphogenic responses in the root system of B. napus, including variations in the of primary root length, lateral root numbers, and lateral root density. Larger mask fragments inhibited primary root length at 1% concentration, while smaller mask fragments altered lateral root numbers in a concentration-dependent manner. The effects of latex and nitrile DPG fragments were less pronounced. Additionally, PPE contamination affected the soil microbiota, altering soil enzyme activities and biomass depending on fragment type and concentration, which may indicate degraded soil quality as stress markers.

Acknowledgements

References

[1] Silva, A.L.P., Prata, J.C., Duarte, A.C., Barcelò, D. and Rocha-Santos, T., 2021. An urgent call to think globally and act locally on landfill disposable plastics under and after covid-19 pandemic: Pollution prevention and technological (Bio) remediation solutions. *Chemical Engineering Journal*, 426, p.131201.

[2] Aragaw, T.A. and Mekonnen, B.A., 2021. Current plastics pollution threats due to COVID-19 and its possible mitigation techniques: a waste-to-energy conversion via Pyrolysis. *Environmental Systems Research*, 10, pp.1-11..

[3] Shams, M., Alam, I. and Mahbub, M.S., 2021. Plastic pollution during COVID-19: Plastic waste directives and its long-term impact on the environment. *Environmental Advances*, 5, p.100119.

[4] Jędruchniewicz, K., Ok, Y.S. and Oleszczuk, P., 2021. COVID-19 discarded disposable gloves as a source and a vector of pollutants in the environment. *Journal of Hazardous Materials*, 417, p.125938.

[5] Bodor, A., Feigl, G., Kolossa, B., Mészáros, E., Laczi, K., Kovács, E., Perei, K. and Rákhely, G., 2024. Soils in distress: The impacts and ecological risks of (micro) plastic pollution in the terrestrial environment. *Ecotoxicology and Environmental Safety*, 269, p.115807.

[6] Mészáros, E., Bodor, A., Szierer, Á., Kovács, E., Perei, K., Tölgyesi, C., Bátori, Z. and Feigl, G., 2022. Indirect effects of COVID-19 on the environment: How plastic contamination from disposable surgical masks affect early development of plants. *Journal of Hazardous Materials*, 436, p.129255.

[7] Feigl, G., Molnár, Á., Szőllősi, R., Ördög, A., Törőcsik, K., Oláh, D., Bodor, A., Perei, K. and Kolbert, Z., 2019. Zinc-induced root architectural changes of rhizotron-grown B. napus correlate with a differential nitro-oxidative response. *Nitric Oxide*, 90, pp.55-65.

PREPARATION AND CHARACTERIZATION OF CHITOSAN ENCAPSULATED KARRIKIN 2

Tamás Bodor[1,2], Kolbert Zsuzsanna[2], Kónya Zoltán[3], Andrea Rónavári[3]

[1]Department of Plant Biology, University of Szeged, Szeged, Hungary
[2]Doctoral School of Biology, Faculty of Science and Informatics, University of Szeged, Szeged, Hungary
[3]Department of Applied and Environmental Chemistry, University of Szeged, Szeged, Hungary
e-mail: ronavari@chem.u-szeged.hu

Abstract
The aim of this study was to encapsulate karrikin 2 (KAR 2) molecules, a class of plant regulator butenolides, in low molecular weight chitosan microcapsules. Karrikin 2, known for its stimulating effects on seed germination in certain plant species, was selected as the active ingredient. Chitosan, a biodegradable and biocompatible polymer, was chosen for its ability to form micro- and nanoparticles and its environmentally friendly production. The encapsulation process was expected to increase the bioavailability and retention of karrikin 2, allowing for a more controlled and sustained release in biological systems. The microcapsules were characterized to assess the success of the encapsulation. These characterizations are vital for understanding the performance of the microcapsules in practical applications and for optimizing the encapsulation process for potential use in agriculture and plant biotechnology.

Introduction
Plant growth regulators are organic substances that can either be naturally produced by plants, known as phytohormones, or synthesized in laboratories. These compounds can influence or control one or more physiological processes in plants, affecting growth, development, or maturation. Depending on the type and concentration, regulators can either promote or inhibit plant growth and modify various aspects of plant behavior or the characteristics of plant products. Karrikins are a family of plant regulator butenolid molecules, produced by the combustion of cellulose [1] (Fig. 1.). Karrikinolide (KAR 1) was first identified in 2003 [2], [3]. Subsequently, the structure of KAR 1 was confirmed by a separate group of molecules that have been demonstrated to stimulate seed germination. However, different karrikins may exert varying effects on different plant species. For instance, KAR 2 has been shown to be the most active member of the family in terms of promoting germination in Arabidopsis thaliana L, but is considerably less active compared to KAR 1 in other species [1].

Despite its bioactivity, the practical application of KAR 2 in agriculture faces challenges, including rapid degradation and limited bioavailability in natural environments. Therefore, encapsulation was proposed as a strategy to overcome these limitations. Encapsulation technology is a process whereby a matrix is added to a solution of an active ingredient, which is then becomes encapsulated and protected by the membrane ensured the increase of the bioavailability and retention of the bioactivity of chemical compounds [4]. Furthermore, the encapsulation process can slow down the release of the active agent, allowing for the effect to be measured over an extended period of time. This can be of particular significance in the context of biological samples, where the treatment materials may potentially cause damage at higher concentrations.

In the present study, low molecular weight chitosan was employed for the encapsulation of karrikins (Fig. 2.). Chitosan is chemically inert, biodegradable, and biocompatible. It exhibits

KAR 1   KAR 2

KAR 3   KAR 4
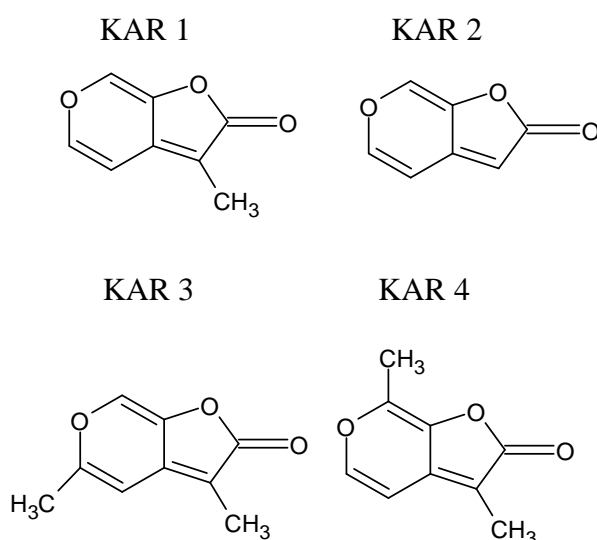
Fig. 1.: Chemical structures of karrikines

film-, fiber-, and micro/nanoparticle-forming properties and can be produced in an environmentally friendly manner using chitin derived from eukaryotic organisms, including crustaceans, insects and fungi [5]. Chitosan is prepared by N-deacetylation of chitin, resulting in the formation of a copolymer comprising the repeating units 'β-[1f 4]-linked 2-acetamido-2-deoxy-D-glucopyranose and 2-amino-2-deoxy-D-glucopyranose (Fig 1.). The encapsulation process was expected to improve the bioavailability of karrikin 2 by protecting it from environmental degradation, The obtained microcapsules were characterized to ascertain the size and optical properties.
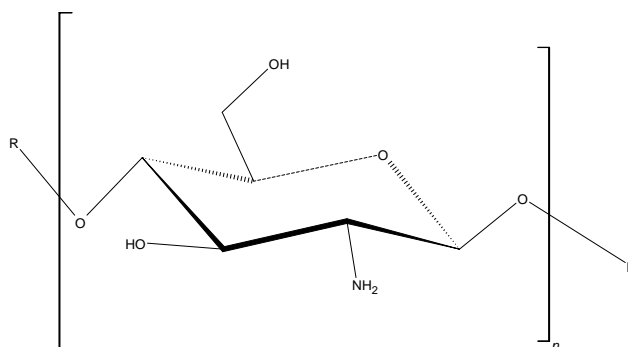
Fig. 2.: Chemical structures of chitosan

Experimental

For the encapsulation of Karrikin 2 into chitosan nanoparticles (CHIT NPs), the ionic gelation method based on the process of Calvo et. al. was used [6]. The initial step is to prepare an 1% polymeric solution of low molecular weight chitosan. This is achieved by mixing the chitosan with an aqueous solution of acetic acid and allowing the mixture to stand overnight. Subsequently, the solution was diluted to a concentration of 0.5%, and 1 ml of NaOH was added to 24 ml of the solution. Then 1 mg of KAR 2 and 16,5 ml of tripolyphosphate (TPP, 0.25 m/v%) were added to the CHIT solution dropwise. The interaction between tripolyphosphate anions and positive charges in CHIT chains occurs through two bonding configurations (both H- and T- link configuration) produces the nanoparticles. The final mixture was stirred further

for 45 min at room temperature, leading to the formation of the aqueous suspension of CHIT NPs and CHIT-KAR 2 NPs (Fig. 3.).
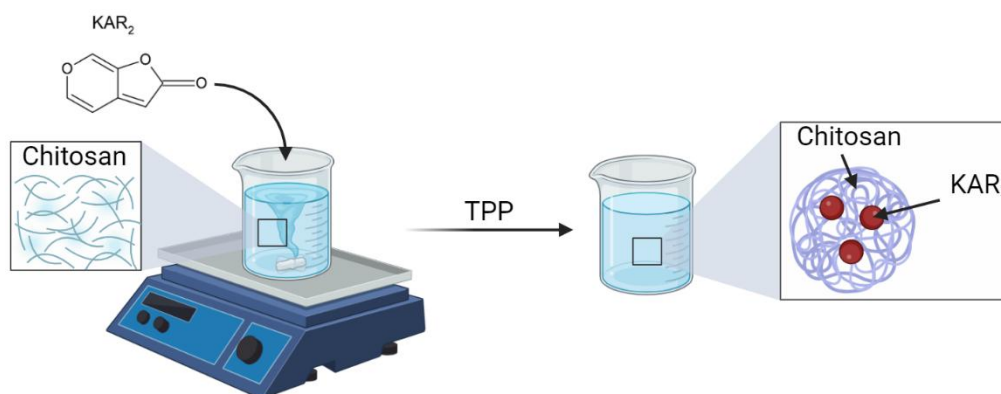
Fig. 3.: Sematic figure of ionic gelation method based on the process of Calvo et. al.

To ensure the success of the synthesis, the obtained nanoparticles were characterized. A transmission electron microscope (TEM) was used to investigate the morphology and particle size of the prepared nanoparticles. The investigation was carried out using a FEI Tecnai G^2 20× microscope at an acceleration voltage of 200 kV. The optical properties of nanoparticles were studied by spectral analysis. The absorbance spectra of nanoparticles were recorded within the range from 200 to 800 nm using an Ocean Optics 355 DH-2000-BAL UV–VIS spectrophotometer and a 10-mm path length quartz cuvette.

Results and discussion

The success of the syntheses was confirmed by TEM and UV-Vis measurements. Transmission electron microscopy (TEM) was employed to ascertain the size and morphological characteristics of the nanoparticles. The results of the TEM analysis are presented in Fig. 4. The CHIT NPs was roundish, while the filled nanoparticles exhibited a homogeneous morphology with a spherical shape with an average size of approximately 36 nm. The use of UV–Vis spectroscopy enabled the measurement of the localized surface plasmon resonance. The peaks were observed at 238 nm for CHIT NP, at 245 nm, 325 nm and 356 nm for KAR 2 and at 237 nm, 326 nm, and 358 nm in case of CHIT-KAR 2 NPs. In case of filled chitosan nanoparticles, the first peak is similar to the peak of chitosan nanoparticles, as observed by Agarwal et al. [7]. The other two are identical to those measured from the karrikin 2 stock solution. Additionally, the first peak of the karrikin 2 spectrum was around 245 nm, but it overlapped with the chitosan spectrum (Fig. 4).
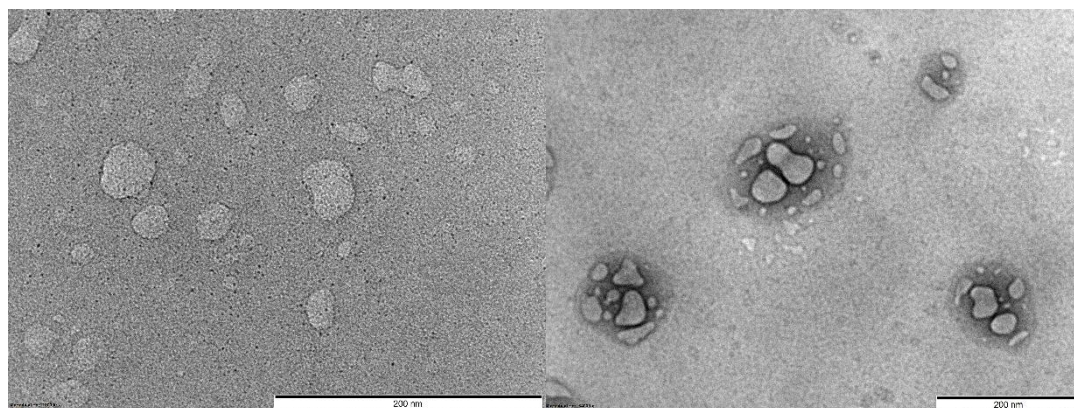
Fig. 4.: TEM pictures of CHIT NPs and CHIT-KAR 2 NPs
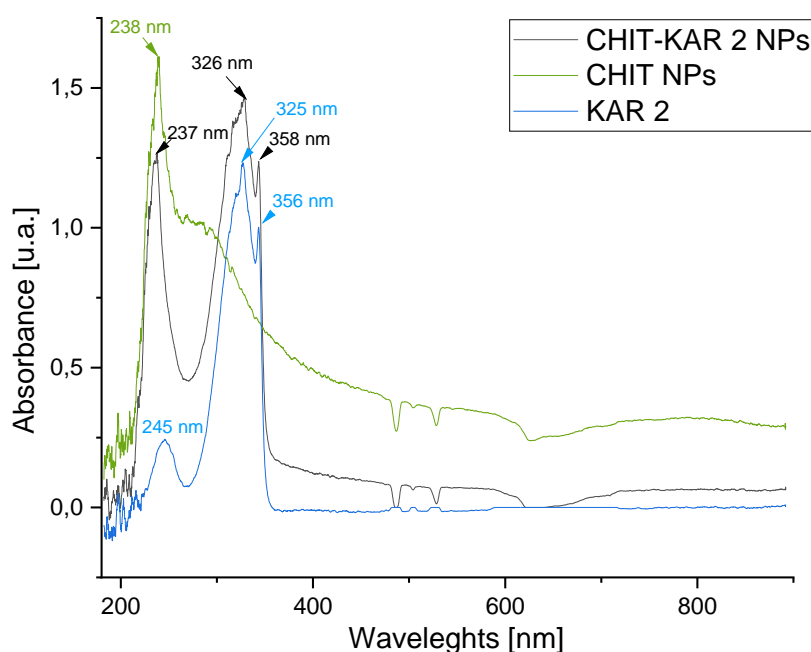
Fig. 5.: UV-VIS spectra of CHIT NPs (1.) filled CHIT-KAR 2 NPs and KAR 2 molecules (2.)

Conclusion

In conclusion, this study demonstrated the succesful encapsulation of karrikin 2 using low molecular weight chitosan, highlighting its potential as an effective polymeric matrix for enhancing the bioavailability of bioactive compounds. Nanoparticle formed were majorly homogeneous and spherical microcapsules, which were verified by UV-VIS spectroscopy and transmission electron microscopy (TEM) measurements. The characterisation results showed distinct spectral peaks corresponding to both CHIT and KAR 2, suggesting the successful incorporation of the bioactive molecules. Further investigation is needed to verify the structure of the obtained nanoparticles. This research anticipates the promising applications of chitosan-based microencapsulation in plant growth and development via the functional benefits of karrikins.

Acknowledgements

References

[1] Chiwocha, S., Dixon, K., Flematti, G., Science, (2009). Karrikins: a new family of plant growth regulators in smoke.
[2] Flematti, G., Ghisalberti, E., Dixon, K., Science, (2004). A compound from smoke that promotes seed germination.
[3] Marciniak, P., Sochacki, D., & Nowakowska, K., (2023). Karrikins–effect on plants, interaction with other growth regulators, and potential use in horticulture
[4] Bychkova, E., Sin, A., Belyakova, D. & Kotova, Y., (2021). Development of microcapsulationtechnology

[5] Malerba, M., sciences, R. C.-I. journal of molecular, (2016). Chitosan effects on plant systems.

[6] Calvo, P., Remunan-Lopez, C., Vila-Jato, J. L., & Alonso, M. J. (1997). Novel hydrophilic chitosan-polyethylene oxide nanoparticles as protein carriers.

[7] Agarwal, M., Agarwal, M. K., Shrivastav, N., Pandey, S., Das, R., & Gaur, P. (2018). Preparation of chitosan nanoparticles and their in-vitro characterization.

MULTI-MYCOTOXIN ANALYSIS OF *ALTERNARIA* MYCOTOXINS IN WHEET: CROSSTOX RECOVERY ASSESSMENT

Vojislava Bursić[1], Gorica Vuković[2], Tijana Stojanović[1], Bojan Konstantinović[1], Milena Popov[1], Nataša Samardžić[1], Nikola Puvača[3]

[1]*University of Novi Sad, Faculty of AgricultureTrg Dositeja Obradovića 8, 21000 Novi Sad, Serbia*
[2]*Institute of Pharmaceutical Chemistry, University of Szeged, H-6720 Szeged, Eötvös u. 6, Hungary*
e-mail: vojislava.bursic@polj.edu.rs

Abstract
A liquid chromatography-tandem mass spectrometry method for the determination of <u>Alternaria</u> toxins, including AME (Alternariol Monomethyl Ether), AOH (Alternariol) and TEN (Tentoxin) in wheat was validated using multi mycotoxin sample preparation. Nameli, the QuEChERS SPE method for mycotoxins – CrossTOX, which proved to give high recoveries for many mycotoxins. The recovery was assessed by analysis of spiked samples with a mixture of standard solutions of all three mycotoxins at two spiking levels (0.02 and 0.1 mg kg^{-1}) in six replicates. The obtained average recoveries and precisions (expressed as the RSDr, %) for Crosstox method were 102.1% (RSDr of 11.84%) for AME, 96.1% (RSDr of 16.10%) for AOH, and 95.9% (RSDr of 9.04%) for TEN. All the obtained recoveries were in accordance with the Commission Implementing Regulation (EU) 2023/2782.

Introduction
Alternaria species, ubiquitous fungal pathogens and saprophytes of the division Ascomycota, exhibit a remarkable ability to proliferate even under low-temperature conditions. These fungi have been isolated from diverse agricultural products, including fruits, vegetables, cereals and oilseeds. Of particular concern is *A. alternata*, a prolific producer of over seventy distinct secondary metabolites. The studies have elucidated the chemical structures of several of these metabolites, revealing their mycotoxic properties detrimental to both human and animal health [1]. *Alternaria* mycotoxins are classified into five structural groups: perylene quinones (altertoxins I-III [ATX I-III]), dibenzo-α-pyrones (alternariol monomethyl ether [AME], alternariol [AOH]), tetramic acid derivatives (tenuazonic acid [TeA]), *A. alternata* f. spp. *Lycopersici* toxins (AAL-toxins) and miscellaneous structures (tentoxin [TEN]). Notably, AME, AOH and TeA are the most significant contaminants, frequently found in the cereals and animal feed [2].
Mycotoxins are naturally toxic compounds with a low molecular weight and a high bioaccumulation ability and thermal stability which is very important for wheat and other cereals during the processing. According to literature, among more than 400 identified secondary compounds, deoxynivalenol, ochratoxin A, zearalenone and aflatoxins were renowned as the most studied mycotoxins and are considered a hazard to human or animal health [3]. *Alternaria* mycotoxins showed notably toxicity, such as mutagenicity, carcinogenicity, induction of DNA strand break, sphingolipid metabolism disruption, or inhibition of enzymes activity and photophosphorylation [4], which caused their massive research during past years.
Josef Hauptmann said: "Using the new CrossTOX® columns has made our mycotoxin multi-method much more effective, especially in terms of time and the use of consumables", indicate that this columns are good for the extraction of many mycotoxins including aflatoxins B1, B2,

G1, G2, sterigmatocystin, ochratoxin A, fumonisine B1 and B2, deoxynivalenol, nivalenol, 15-acetyl DON, 3-acetyl DON, DON-3-GLC, zearalenon, T-2 and HT-2, citrinin and diacetoxyscirpenol [5]. It was a reason to apply CrossTOX® in the analysis of Alternaria mycotoxins in wheat as part of the research.

Experimental

Reagents, solvents and equipment

The analytical standards of the AOH, TEN and AME were purchased from Romer Labs Biopure (Romer Labs Division Holding GmbH, Getzersdorf, Austria). The standards were reconstituted with 1 mL of the methanol to obtain 0.1 mg mL^{-1} stock solutions. All stock solutions were kept at 4 °C. The mixtures of all the toxins were prepared in acetonitrile (MeCN) in the final concentrations of 1 and 10 µg mL^{-1}. These solutions were used for spiking the blank samples for the recovery analyses.

The methanol and acetonitrile were LC-MS grade obtained from J.T.Baker. The ammonium formiate and acetic acid were analytical grade purchased from Merck (Darmstadt, Germany). The Zorbax Eclipse Plus C18 column Rapid Resolution HD (50x2.1mm, 1.8 µm particle size) and regenerated cellulose syringe filters (13 mm, 0.45 µm) were obtained from Agilent (Agilent Technologies, Inc, US). CrossTOX columns were obtained by LCTech (LCTech GmbH Obertaufkirchen, Germany).

The HPLC system was coupled to an Agilent 6475B LC/TQ triple quadrupole mass spectrometer with AJS ESI (Jet Stream Technology Ion Source). A Zorbax Eclipse Plus C18 column was used for the chromatographic separation. The column temperature was held at 35°C and the injection volume for the LC system was 2 µL. The chromatographic separation of the AOH, TEN and AME was carried out with mobile phase consisted of water (A) and acetonitrile (B), both containing 10 mM ammonium formiate, in a gradient mode and flow rate of 0,3 mL min^{-1}. A gradient elution started at 10% of B and composition was increased to 50% B at 3 min, 95% B at 6 min and held for 3 min. The composition of the mobile phase returned to the initial conditions in 1 min and the system was equilibrated during 3 min. The total running time was 10 min. The ESI source was used with the following settings: drying gas (nitrogen) temperature 220 °C, drying gas flow rate 10 L min^{-1}, nebulizer pressure 40 psi, sheath gas temperature of 250 °C, sheath gas flow 12 L min^{-1} and capillary voltage 3000 V. The detection was performed using the dynamic multiple reactions monitoring mode (dMRM). The Agilent MassHunter software (version 10.1 Agilent Technologies, 2006-2020) was used for the optimization and quantification.

The MRM mode was applied in the MS/MS detector and two ion transitions (quantifier and qualifier) were recorded for AOH, TEN and AME. The selected ion transitions with the optimized fragmentation (Frag) and collision energies (CE) are summarized in Table 1.

Table 1. Acquisition parameters for MS/MS determination

Compound	Molecular mass	Precursor ion [M – H]$^-$ (*m/z*)	Product ions (*m/z*)	Frag (V)	CE (eV)
AOH	256.0	257	215	120	23
			147		23
TEN	412.3	413	271	120	17
			215		23
AME	270.0	271	256	135	23
			228		30

Spiking samples and extraction

Homogenized blank wheat samples were spiked at two levels 0.02 and 0.1 mg kg^{-1} in six replicates. After spiking the blank samples, the extraction of the AOH, TEN and AME was performed (Figure 1).

Figure 1. Extraction of *Alternaria* mycotoxins
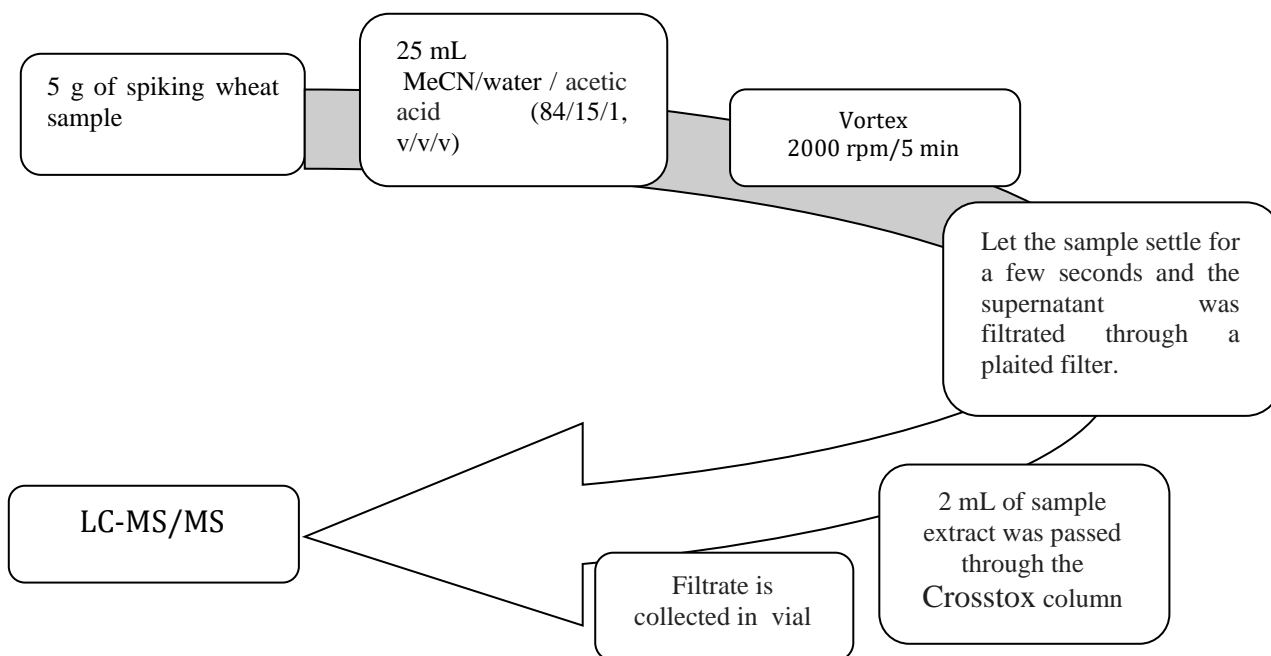
Results and discussion

The extraction of AOH, TEN and AME from wheat spiking samples using the CrossTox columns, proved to be a very simple, i.e. the described method for the extraction of the investigated mycotoxins uses a relatively small amount of organic solvents and thus protects the environment, while, on the other hand, it is not time consuming, which means that a large number of samples can be done in a short time.

The obtained average recoveries (Rec) and precision when the blank wheat samples were spiked at 0.02 and 0.1 mg kg^{-1} in six replicates are shown in Figure 2.

Figure 2. Rec (%) and RSD (%) of *Alternaria* mycotoxins
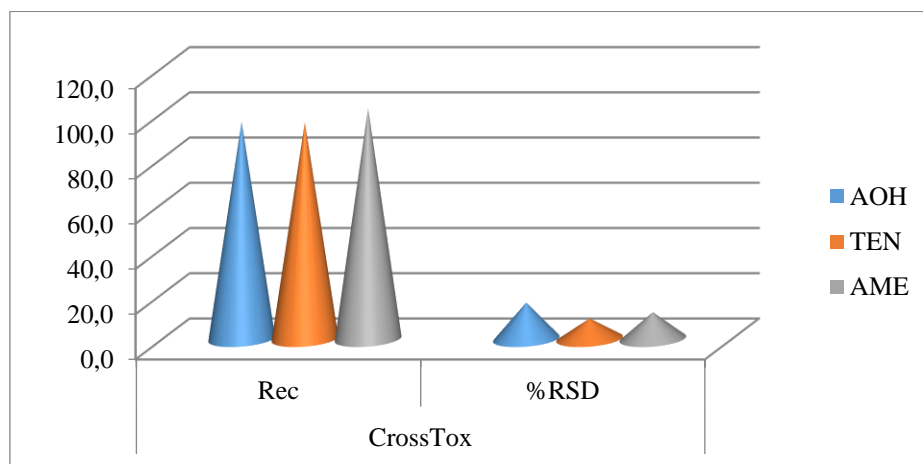
The obtained recovery values for all investigated *Alternaria* mycotoxins were in accordance with the Commission Implementing Regulation (EU) 2023/2782 (the average recovery should be between 70 and 120% and RSDr $\leq$ 20 %).

Conclusion

The wheat contributes 30% of the world's average crop consumption and is cultivated in most of the countries worldwide. According to the Republic of Serbia's statistical calendar, the estimated wheat production for this year is 2,901,000 tonnes, which is a 15.9% decrease compared to the last year's yield. Ensuring the wheat is free from contaminants, particularly mycotoxins, is crucial. The analysis of *Alternaria* mycotoxins using the CrossTOX method demonstrated the excellent recovery rates for AOH, TEN and AME.

Acknowledgements

References

[1] S. De Berardisa, E.L. De Paola, G. Montevecchi, D. Garbinid, F. Masino, A. Antonelli, D. Meluccia Food Res. Int. 106 (2018) 677.
[2] X. Mao, W. Chen, H. Wu, Y. Shao, Y. Zhu, Q. Guo, Y. Li, L. Xia. Toxins (Basel). 4 (2023)15(8):495.
[3] S. Smaoui, O.B. Braiek, H.B. Hlima. J. Food Quality. 2020 (2020) 23.
[4] L. Escrivá, S. Oueslati, G. Font, L. Manyes, J. Food Quality. 2017 (2017) 1569748.
[5] LCTech https://www.lctech.de/en/products/mycotoxin-products/crosstox
[6] Commission Implementing Regulation (EU) 2023/2782

ADVANCED LASER-INDUCED BREAKDOWN SEPCTROSCOPY-BASED QUALITATIVE ANALYTICAL METHODOLOGIES FOR FOOD AND PLANT-RELATED APPLICATIONS

Fernando A. Casian Plaza[1], Patrick M. Janovszky[1], Dávid J. Palásti[1], Selahattin Kondak[2], Zsuzsanna Kolbert[2], Gábor Galbács[1*]

[1]Department of Molecular and Analytical Chemistry, University of Szeged, H-6720 Szeged, Dóm sq. 7, Hungary
[2]Department of Plant Biology, University of Szeged, H-6726, Közép fasor 52., Szeged, Hungary
e-mail: galbx@chem.u-szeged.hu

Abstract

There is a growing need for the non-destructive, simple, cost-effective and fast inspection of products in the agricultural and food industry for quality control. Laser-induced breakdown spectroscopy (LIBS) has a great potential in this application. This research was focused on three main methodologies: a) the qualitative discrimination of plants in a fast, non-contact and microdestructive way; b) method development of spatially resolved LIBS elemental mapping of plant species for nanoparticles (NPs) detection; and c) the identification of harmful contaminants (e.g. pesticides, heavy metals, NPs).

Introduction

LIBS is a micro-analytical technique that uses short laser pulses as an energy source to produce a microplasma on the surface of a solid sample, which breaks down sample material and thermally excites the atoms generated to produce an atomic emission spectrum. Nowadays LIBS is being applied in many research fields due to its unique set of characteristics. It is a rapid, sensitive, versatile analytical method, which provides quantitative (ppm level) or qualitative information about the sample, is micro-destructive and requires practically no sample preparation, therefore allows fast and direct analysis of solid and liquid (even gaseous) samples in a non-contact manner. LIBS spectra are rich in spectral lines (and bands) and hence in analytical information, therefore can successfully be used for sample or contaminant identification or classification. Furthermore, the application of chemical imaging methods or elemental mapping provides a spatial distribution of a single chemical species within a complex sample, obtaining information in the form of 2D (or 3D) images and also offering a high degree of discrimination between different sources [1-4].

Plant analysis by LIBS can potentially be used to study their nutritional composition, detect adulteration, assess toxicology status, and identify contaminants. However, these analytical also pose significant challenges. The soft and humid nature of these samples affects their physical properties, which in turn influences laser energy absorption, material ablation, and plasma formation. Therefore, a thorough method development is needed prior to any plant analysis by LIBS. Elemental mapping of plants by LIBS offers an innovative analytical tool for high-resolution (microscale) multielemental plant bioimaging on a large scale. It allows for the evaluation of distribution, bioaccumulation, uptake, and translocation of analytes of interest; providing detailed information on the spatial distribution of elements.

One of the key advantages of LIBS is its requirement for little to no sample preparation. However, this advantage does not fully extend to biological samples. For these, the most common, efficient, and cost-effective approach involves drying the samples and carefully fixing them in a transparent hard polymer or onto glass slides. Additionally, the spatial resolution of

LIBS analysis will need to be adjusted according to the sample size and the size of the specimen. Hence, optimizing the sample preparation process is essential and should be prioritized [5-7].

In food science, LIBS studies can be conducted through either a qualitative or quantitative way. Qualitative investigations involve comparing spectra or emission intensities, and utilizing chemometric tools to enable discrimination, classification, identification, and imaging. As a consequence of this, LIBS measurements can provide large datasets for data evaluation by chemometric or multivariate statistical methods to be used towards the identification, comparison and classification of foodstuff. Such information can be used for monitoring of food safety and quality control in the food and agricultural industry; among others, the adulteration, counterfeiting or contamination of plants and other edible products [8-10].

In the present work we set three goals of investigating the applicability of LIBS for agricultural and food related applications: 1) a method development for the qualitative discrimination analysis of aromatic plants (herbs) based on their LIBS spectra (with the aim of identifying adulteration or counterfeiting); 2) developing new sample preparation and data collection methodologies for the inspection of the uptake and distribution of some elements and nanoparticles (NPs) in plants; and 3) developing tools and methodology for the detection and qualitative discrimination analysis of organo-chlorine and -fluorine pesticides on fruits.

Experimental

LIBS measurements were performed using a J200 LIBS/LA tandem instrument (Applied Spectra, USA) equipped with a Q-switched Nd:YAG laser source operating at 266 nm with a pulse duration of 6 ns. The LIBS detection system consisted of a six-channel CCD spectrometer with a spectral coverage of 190 to 1040 nm and a resolution of 0.07 nm. The system was controlled by Applied Spectra's Axiom LA 2.4 operation software, typically employing a 0.5 µs gate delay and 1 ms gate width. A laser pulse energy of 15 mJ and a focal spot diameter of 60 µm was employed.

Qualitative discrimination analysis of aromatic plants: we have grown five herbs (parsley, basil, cilantro, mint, rosemary) in our lab and investigated the influence of LIBS experimental parameters (e.g. laser pulse energy, focal spot size, repeated pulses, etc.) on the information content of their LIBS spectra and the accuracy and repeatability of the classification on both fresh and dry plants. The performance of three multivariate chemometric methods, namely principal component analysis (PCA), linear discriminant analysis (LDA), and random forest (RF) were evaluated, also employing optimization involving normalization and variable selection approaches.

Spatial elemental distribution in plants by LIBS: Plants of *O. lesbiaca* (Loutra ecotype) a Ni hyperaccumulator species, were used to assess spatial Ni distribution in order to get information about the uptake of Ni and other macro-elements through the whole plant. Plants were fed with aqueous solutions of $NiCl_2$ or NiO NP suspension [7]. Each plant was washed, dried and embedded in a one-component photopolymerizing resin Technovit 7200 (Kulzer GmbH, Germany) glued onto a glass slide using a precision adhesive press Exakt 402 (Exakt Advanced Technologies GmbH, Germany) allowing a bubble-free adhesion via acrylic block kept at vacuum with an adjustable contact pressure with a light polymerization unit. Before the LIBS analysis itself, a microscopic image of each plant was obtained with an Olympus BX43 (Evident, Japan) microscope equipped with an Olympus DP-73 camera. LIBS mapping measurements were carried out employing stepwise scans with non-overlapping 100 µm spot sizes, giving the lateral resolution; using a laser pulse energy of 14 mJ and a repetition rate of 10 Hz. From each plant, multiple layers were ablated in order to analyze the whole plant sample;

then the spectra were aggregated in each location vertically. Spectral intensity-based elemental maps for Ni I 352.4 nm spectral line were visualized using ImageLab (Epina GmbH, Austria) on the basis of the measured net signal intensity.

Qualitative discrimination analysis of pesticides in a closed ablation cell: We developed a closed, sample-holding (ablation) cell in which hazardous substances can be LIBS analyzed. Six halogen-containing (Cl, F) analytical standard solid pesticides were chosen: acetamiprid, chlorpyrifos, cyhalothrin, tebuconazole and tefluthrin (Lab. Instruments S.r.l., Italy). Solid pesticides were put onto a 6 mm diameter 99.9% purity zinc substrates. The closed ablation cell consisted of aluminum, with 8 lockable wells with a 6 mm depth and a diameter of 8 mm. A 2 mm thick quartz slide (Ted Pella, Inc., USA) covering the wells was employed for the laser light absorption. 50-50 LIBS spectra was collected for each analyte to classify pesticides by applying chemometric data evaluation procedures (e.g. LDA and RF) and comparing the entire spectrum.

Results and Discussion

Regarding the discrimination analysis of aromatic plants; by using the linear correlation function it was shown that the dry stem is the best for recording the spectra, due to its robustness, larger analytical signal and good repeatability (R^2 of 0.90). We also studied the effectiveness of the chemometric methods for classification based on the LIBS spectra. PCA was found to be inefficient, but LDA and RF provided decent cumulative accuracies in training, reaching 78% and 100%, respectively. The accuracy of PCA could be further improved by data pre-treatment (normalization and spectral reduction) to 92%.

We developed a new sample preparation method for plant samples for LIBS-based analysis of trace element distribution. By comparing several methods, we found that the best sensitivity and lateral resolution can be achieved by using a photopolymer embedding approach and an aggregated multilayer laser ablation. LIBS elemental mapping was capable of detecting the spatial distribution of Ni in the planlets (Fig. 1). We also measured the distribution of K, Na, Mg, and Ca simultaneously. Our developed LIBS measurement methodology provided valuable analytical data for plant biological studies, the purpose of which was to examine the absorption of NPs and the stress tolerance of plants for trace elements. This approach provides spatial information about the distribution of elements, and these results support the possibility that LIBS is suitable for the visualization of macroelement and microelement distributions mainly in the shoot of Ni hyperaccumulator seedlings.
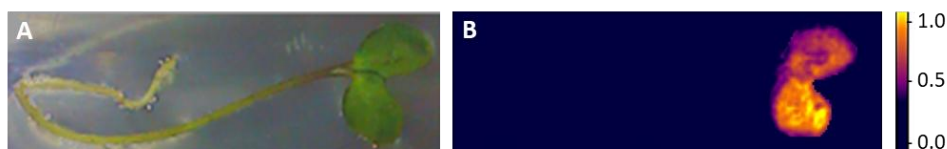
Figure 1. Representative LIBS elemental map demonstrating the nickel distribution in the ecotype of Loutra seedling cultivated with 250 mg/mL of NiCl$_2$. The pixel color scale in the map shows the net emission intensity of the Ni I 352.4 nm spectral line, which is proportional with the concentration.

During the pesticides analysis, we performed the classification in two ways; one by scaling the entire data set to the C 247.8 nm line and the other by employing the normal data (no scaling). However, in some cases the Zn spectral lines appeared in the pesticides spectra (besides the pesticide grains, the substrate was also ablated), therefore it was necessary to mask-out the spectra from the Zn lines. From the point of view of the masking of the spectra, we examined three cases: processing the entire set of spectra without masking ("full spectra"),

cutting out the Zn lines ("without Zn"), and using only those parts of the spectrum in which only lines characteristic of one of the pesticides appeared ("only pesticide"). A total of 12 combinations of these conditions were reported. During our calculations data sets were randomly split in a 2:1 ratio into training and validations sets. Average and standard deviation values were obtained from repeating the above calculations five times. In general, when analyzing the raw data, LDA was significantly less accurate than the RF method. The latter procedure was always able to perfectly separate the pesticides from each other during training (100% accuracy). It is also shown that the accuracy of both methods proved to be quite insensitive to the masking of the spectra. Scaling clearly helped the accuracy in the case of the LDA method, but significantly worsened the results during validation; the effectiveness of the RF did not improve as a result. According to the values in the confusion matrix, only chlorpyrifos was identified with almost 100% accuracy, which can be due to its significantly different structure (no aromatic ring) and its other heteroatom content (phosphorus). Acetamiprid was most often mistakenly identified as tebuconazole by our algorithm, which we attributed to the high nitrogen content of the molecules and their similar molecular structure. The same case exists for the pair cyhalothrin - tefluthrin, that the algorithm mainly confuses the two pesticides with each other. Their distinctiveness from other molecules can primarily be attributed to their fluorine content.

Conclusion
LIBS was found to be effectively useable for food safety investigations providing an alternative method for analyzing plant samples with little to no sample preparation. In addition, LIBS has the ability to provide qualitative results for plant samples due to the fact that LIBS spectra are line-rich and sensitive, but is both beneficial and problematic during discrimination analysis of biological samples, since the sensitivity of the method can be a limitation factor for the performance, as deviations in the growing conditions or between sub-species of plants can result in a decreased accuracy of classification. On the other hand, elemental mapping by LIBS provides an innovative and unique capability for analyzing and mapping every element in a sample at each spatial location, providing and easy and rapid elemental distribution assessment in plants.

References
[1] G. Galbács, Anal. Bioanal. Chem. (2015) 407, 7537–17562.
[2] D. Cremers, R. Multari, A. Knight, Encyclopedia of Analytical Chemistry. (2006) 1-24.
[3] A. Limbeck, L. Brunnbauer, H. Lohninger, P. Pořízka, P. Modlitbová, J. Kaiser, P. Janovszky, A. Kéri, G. Galbács, Anal. Chim. Acta. (2021) 1147, 72-98.
[4] L. Jolivet, M. Leprince, S. Moncayo, L. Sorbier, C.-P. Lienemann, V. Motto-Ros, Spectrochim. Acta B. (2019) 151, 41-53.
[5] P. Modlitbová, P. Pořízka, J. Kaiser, TrAC, Trends Anal. Chem. (2020) 122, 115729.
[6] P. Modlitbová, P. Pořízka, J. Kaiser, Bioimaging in laser-induced breakdown spectroscopy. In: V.K. Singh, D.K. Tripathi, Y. Deguchi, Z. Wang (Eds.), Laser Induced Breakdown Spectroscopy (LIBS) Concepts, Instrumentation, Data Analysis and Applications, volume 2, Wiley, New Jersey, 2023, pp. 729-740.

[7] S. Kondak, P. Janovszky, R. Szőllősi, Á. Molnár, D. Oláh, O. Adedokun, P.G. Dimitrakopoulos, A. Rónavári, Z. Kónya, L. Erdei, G.Galbács, Z. Kolbert, Environ. Pollut. (2024) 341, 122874.

[8] J. Naozuka, A.P. Oliveira, Laser-induced breakdown spectroscopy in food sciences. In: V.K. Singh, D.K. Tripathi, Y. Deguchi, Z. Wang (Eds.), Laser Induced Breakdown Spectroscopy (LIBS) Concepts, Instrumentation, Data Analysis and Applications, volume 2, Wiley, New Jersey, 2023, pp. 781-806.

[9] D. Santos, L.C. Nunes, G.G. de Carvalho, M. da Silva, P.F. de Souza, F. de Oliveira, L.G. dos Santos, F.J. Krug, Spectrochim. Acta B. (2012) 71, 3-13.

[10] D.J. Palásti, A. Metzinger, T. Ajtai, Z. Bozóki, B. Hopp, É. Kovács-Széles, G. Galbács, Spectrochim. Acta B. (2019) 153, 34-41.

THE PM10 EXPOSURE DURING POOL CONSTRUCTION
IN NOVI SAD, SERBIA

Aleksandra Čavić[1], Marko Carić[1], Jelena Kiurski[1], Snežana Aksentijević[2],
Boris Obrovski[3], Dunja Istrat[3], Miljan Šunjević[3]

[1]*University Business Academy in Novi Sad, Faculty of Economy and Engineering*
Management in Novi Sad, 21000 Novi Sad, Cvecarska 2, Serbia
[2]*Business Technical College, Trg Svetog Save 34, 31000 Uzice, Serbia*
[3]*Department of Environmental Engineering and Occupational Safety and Health,* Faculty of
Technical Sciences, University of Novi Sad, Trg Dositeja Obradovića 6, Novi Sad, Serbia
e-mail: aleksandra.cavic22@gmail.com

Abstract
The local impacts of construction site activity should be taken into account in order to properly address the risks to human health, particularly within vulnerable and sensitive urban areas. The paper presents a particulate matter (PM10) exposure assessment during a construction project in a mixed-use area including medical center, an elementary school, sports centers, and residential houses. The average PM10 concentration modeled was 171.25 μg/m³, using the EMEP/EEA Tier 1 methodology. Risk assessment was based on dose-response functions and Time-Weighted Average (TWA), Occupational Exposure Limits (OEL) and the Air Quality Index (AQI) value. Risk elements are highly expressed, especially for certain groups: children, patients, and residents. The research revealed rapid need for application of effective dust control measures that will avert the PM10 emission impact on workers carrying out the project and people in the vicinity of the construction site.

Introduction
Air pollution, including particulate matter suspended in the air, has currently emerged as both an important environmental and public health issue in urban areas across the world. Among the various kinds of pollutants Particulate Matter (PM) smaller than 10 micrometers, referred to as PM10, poses a major threat to health because of the way these particles can enter the respiratory system and travel down to the lungs. Several research studies prove that exposure for a long time to high levels of PM10 is very dangerous and may result in a variety of health problems such as respiratory and cardiovascular diseases and ultimately may lead to high mortality rates [1–4]. That is why urban transformation activities need to be clearly marked as crucial sources of PM10 emissions, especially in densely populated regions where they can seriously degrade air quality and affect public health [5, 6].
Earth excavation, material handling, demolition, and use of heavy machinery are among the major dust and particulate matter sources in construction activities [7]. Without effective dust control, emitted particulate matter can stay airborne for a long time and travel long distances, resulting in increased concentrations of PM10 [8, 9]. The associated health risks are extended by the exposure of children, the elderly, and persons with existing respiratory health problems [10].
The paper observes a construction project of pool center within a mixed-use area. The construction site urban characteristics are important for detailed assessment of PM10 emissions. Proximity to hospitals increases the population's risk of being sensibly exposed to high levels of PM10, which has the effect of compounding or inducing cardiovascular or respiratory conditions [11]. The sports centers and residential areas are also at a greater risk because during

the period of construction, active individuals as well as residents would be exposed to harmful air.

The World Health Organization (WHO) and the European Environment Agency (EEA) have laid down guidelines to limit concentrations of particulate matter to safeguard human health. WHO specifies that particulate matter concentration by mass should not exceed on average 20 µg/m³ annually and 50 µg/m³ in 24 hours [1, 2].In many urban construction sites across the globe, the levels of PM10 are high above these limit values [12–14]. The main concern is the long-term health impact it may have on the workers. While developed countries are under strict air quality monitoring, the developing countries such is Serbia still lack legislation.

Material and methods

Location
The construction project is in an urban area surrounded by critical infrastructures; these include a medical center, an elementary school, several sports centers, and residential housing. These facilities are within a 500-m radius which classifies the area as very sensitive to air quality changes. Construction activities involve earth excavation and building development over 12 months. The proximity of sensitive receptors, such as patients at the hospital, and children at the school or playground, as well as elderly residents in surrounding houses, requires special attention to PM10 exposure.
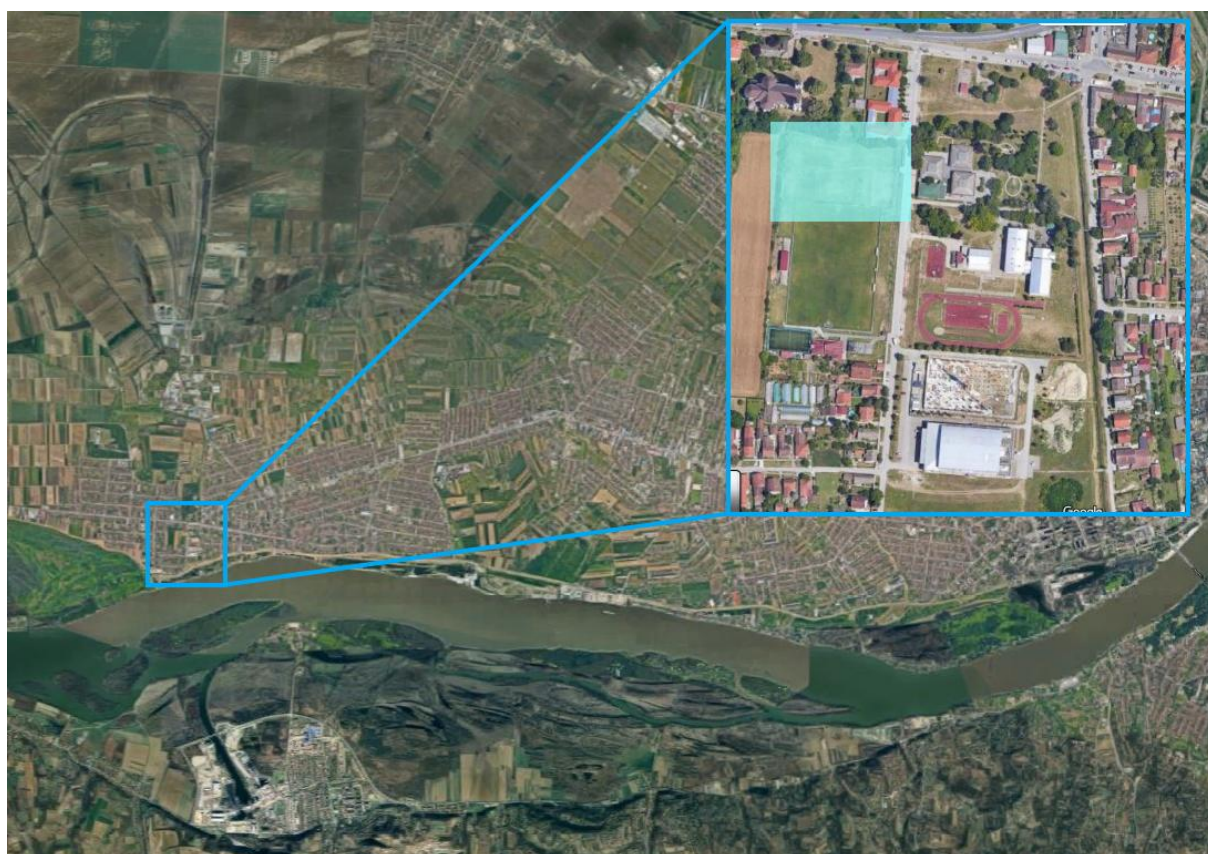
Figure 3. Pool construction in Novi Sad, Serbia

PM10 emission modeling

The EMEP/EEA Tier 1 methodology model was applied in modeling average PM10 concentrations [15]. The method uses emission factors and activity data for estimating levels of PM10 on selected location. Key input parameters include a silt content of 35.4% [16]. The modeled average concentration of PM10 for pool construction project is 171.25 µg/m³. Since the site is close to different receptors, such a concentration is of great concern to public health.

Dose - response calculation

The dose-response function is used to calculate the relative risk (RR) of respiratory diseases due to PM10 exposure. With the concentration of PM10 increasing per 10 µg/m³, the risk of respiratory diseases RR increase by 0.6%. At an average PM10 concentration of 171.25 µg/m³ with a baseline reference level of 20 µg/m³, the relative risk (RR) at this site is 1.9075. This means that the likelihood of respiratory complications increases by 90.75%.

Occupational exposure limit (OEL)

For modeled PM10, the Time-Weighted Average (TWA) concentration for worker exposure is given as TWA = C × T / Ttotal, where C is the concentration, 171.25 µg/m³, T is the duration of the work shift, 8 hours, and Ttotal is the total shift length, 8 hours. The TWA was 171.25 µg/m³ for this project, 3.425 times the Occupational Exposure Limit (OEL) of 50 µg/m³. This indicates very major risks to the occupational health of workers.

Air quality index (AQI)

From the average modeled PM10 concentration, the AQI was calculated to 115, putting the air quality into the "Unhealthy for Sensitive Groups" category. This indicates that under prolonged exposure, members of sensitive populations (children, patients, elderly) may experience effects that are unhealthy, and members of the general population may be lightly affected.

Results and discussion

At 171.25 µg/m³, the modeled concentration significantly exceeds the WHO's 24-hour recommended limit of 50 µg/m³ [2]. The high level of PM10 is very risky, especially for sensitive populations around the construction site. For instance, patients in the medical center are already at risk of developing a disease associated with PM pollution, which is primarily linked to heart or respiratory conditions. Onsite school-going children are more susceptible to developing asthma and other related respiratory issues due to their developing lungs. Equally, athletes involved in different sports and who frequently attend training sessions may note a reduction in their lung capacity as well as feeling exacerbated signs during high-level physical activities in a polluted environment.

Table 1. *Research results*

Applied model	Average PM10	Dose-response	OEL	AQI
Results	171.25 µg/m³	1.9075	3.425	115

TWA calculation indicates that workers are exposed to PM10 levels that are 3.425 times the OEL. Continued exposure to such high levels increases the likelihood of an individual developing chronic respiratory conditions. The conditions may manifest as bronchitis or lung dysfunction. The different conditions further call for strict workplace safety measures, which include personal protective equipment (PPE) and dust suppression systems. Use of PPE reduces the level at which workers may be exposed to risky conditions.

With an AQI value of 115, this location is slightly within the "Unhealthy for Sensitive Groups" category. Because it is close to the medical center and elementary school, immediate mitigations are very important: water spraying for dust control, covering exposed soil, and also scheduling high-dust activities so that they take place during off-peak hours when the surrounding areas are less occupied.

Conclusion

On the pool construction site, PM10 emissions are discovered to be tightly connected with health risks. The recently allowed average PM10 concentration in this atmosphere is surpassed by 171.25 μg/m³, an issue of great concern related to public health. Vulnerable populations that is located in the vicinity of the construction site present a much higher risk of contracting respiratory diseases. In addition, workers are exposed to levels close to four times the recommended OEL, which therefore calls for dust control and personal protection strategies to ensure worker safety. The most effective ways the risks associated with such exposure occur only during working hours and would need complete dust control and personal protection strategies to be put in place.

Acknowledgement

References

1. EEA (2021) Air quality in Europe 2021. European Environment Agency
2. WHO (2021) WHO global air quality guidelines. Coast Estuar Process 1–360
3. Lu F, Xu D, Cheng Y, Dong S, Guo C, Jiang X, Zheng X (2015) Systematic review and meta-analysis of the adverse health effects of ambient PM2.5 and PM10 pollution in the Chinese population. Environ Res 136:196–204
4. Brook RD, Rajagopalan S, Iii CAP, et al (2010) Particulate Matter Air Pollution and Cardiovascular Disease An Update to the Scientific Statement From the American. https://doi.org/10.1161/CIR.0b013e3181dbece1
5. Cohen AJ, Brauer M, Burnett R, et al (2017) Estimates and 25-year trends of the global burden of disease attributable to ambient air pollution: an analysis of data from the Global Burden of Diseases Study 2015. Lancet 389:1907–1918
6. Shaddick G, Thomas ML, Green A, et al (2018) Data integration model for air quality: a hierarchical approach to the global estimation of exposures to ambient air pollution. J R Stat Soc Ser C Appl Stat 67:231–253
7. Zuo J, Rameezdeen R, Hagger M, Zhou Z, Ding Z (2017) Dust pollution control on construction sites: Awareness and self-responsibility of managers. J Clean Prod 166:312–320

8. Pereira P, Monkevičius A, Siarova H (2014) Public Perception of Environmental, Social and Economic Impacts of Urban Sprawl in Vilnius. Soc Stud 6:259–290
9. Wu Z, Zhang X, Wu M (2016) Mitigating construction dust pollution: State of the art and the way forward. J Clean Prod 112:1658–1666
10. Van Den Heuvel R, Den Hond E, Govarts E, Colles A, Koppen G, Staelens J, Mampaey M, Janssen N, Schoeters G (2016) Identification of PM10 characteristics involved in cellular responses in human bronchial epithelial cells (Beas-2B). Environ Res 149:48–56
11. Pope CA, Dockery DW (2006) Health effects of fine particulate air pollution: Lines that connect. J Air Waste Manag Assoc 56:709–742
12. Yan H, Ding G, Li H, Wang Y, Zhang L, Shen Q, Feng K (2019) Field evaluation of the dust impacts from construction sites on surrounding areas: A city case study in China. Sustain 11:1–19
13. Li J, Chen H, Li X, et al (2019) Differing toxicity of ambient particulate matter (PM)in global cities. Atmos Environ 212:305–315
14. Chaudhary IJ, Rathore D (2018) Suspended particulate matter deposition and its impact on urban trees. Atmos Pollut Res 9:1072–1082
15. EEA (2019) 2.A.5.b Construction and demolition. EMEP/EEA Air Pollut. Emiss. Invent. Guideb.
16. Sunjevic M, Reba D, Rajs V, Vujic B, Ninkov M, Vojinovic-Miloradov M (2023) Assessment of detected in situ and modeled PM10/2.5 concentration levels during the urban transformation process in Novi Sad, Serbia. Therm Sci 27:2275–2286

EVALUATION OF EXTRACTION METHODS OF GALICJANKA CHOKEBERRY POMACE ON THE ANTHOCYANINS AND ANTIOXIDANT CAPACITY

Efaishe Kavela, Mónika Máté, Lilla Szalóki-Dorkó

Department of Fruits and Vegetables Processing Technology, Institute of Food Science and Technology, Hungarian University of Agriculture and Life Sciences, H-1118, Budapest, Villányi street 29-43, Hungary
e-mail: Kavela.Efaishe.Tweuhanga.Angaleni@phd.uni-mate.hu

Abstract
Chokeberry pomace is an abundant source of anthocyanins. Anthocyanins are important phenols, which give berries the red, purple, and dark colour. The anthocyanins found in the chokeberry pomace have the potential to be used in the food industry as a natural food additive, however, the effectiveness will depend on the level of anthocyanins in the extract. This study evaluated the level of anthocyanins and antioxidant capacity found in samples extracted from Galicjanka Polish variety chokeberry pomace, extracted with 50% ethanol + 1% citric acid and 50% glycerol +1% citric acid, at 50 and 60 °C for 60 and 120 minutes. The results indicated a significantly higher (P< 0.05) level of anthocyanins with 50% ethanol + 1% citric acid (ranged from 1546 ±5 4 mg/100g to 1680 ± 36 mg/100g DW) than 50% glycerol 1% citric acid (ranged from 1355 ±73 mg/100g DW to 1456 ± 48 mg/100g DW) at all extraction conditions, with the highest level yielded at 50 °C at 120 minutes. The 50% ethanol +1 citric acid has also yielded the highest antioxidant capacity with both DPPH and TEAC, at 60 °C for 120 minutes. This study reveals that 50% ethanol +1% citric acid, 50-60 °C, and 120 minutes serve as a potent solvent, incubation temperature, and duration respectively, for obtaining extracts containing a high level of anthocyanins, antioxidant capacity, and good colour intensity.

Introduction
In connection with saving the planet and human health, the interest in utilizing by-product extracts as natural food additives and pharmaceutical active agents has increased globally [1]. Chokeberry pomace is a by-product produced after juice extraction from the chokeberry fruits. Chokeberries have been identified as rich in phytochemicals including anthocyanins [2]. Anthocyanins are polyphenols that contribute to the dark purple colour of chokeberry. This distinctive colour can be utilized in the food industry as a natural colourant. Anthocyanins are attributed to the predominant percentage of total phenolic compounds found in fruits, ranging between 25-50% [3]. Several studies have identified cyanidin-3-galactoside, cyanidin-3-arabinoside, and cyanidin-3-xyloside as predominant anthocyanins in chokeberry extracts accounting for proximately 90% of the total anthocyanins [4–6]. Anthocyanins are also identified with antioxidant effects, which play a significant role in inhibiting oxidation reactions and delaying ripening in fruits [7,8]. However, the effective utilization of anthocyanins is determined by their concentration in the extracts. Anthocyanins are not so stable and can easily be affected by many factors including temperature, solvents used, and the extraction duration. Therefore, this study aimed to study the effectiveness of 50% ethanol +1 citric acid and 50% glycerol +1 citric acid in extracting anthocyanin and the antioxidant capacity under different extraction conditions.

Material and methods
Garijanca (Polish) variety chokeberry fruits collected from a farm located near Lajosmizse (47∘02′44.4″ N 19∘35′14.8″ E) in Hungary in 2023, were pressed under controlled conditions

in the laboratory to produce juice and pomace. The produced pomace was lyophilized using a Leybold Heraeus Lyovac CT2 freeze dryer (Labexchanger, Burladingen, Germany), and ground into 2.2 mm powder, then used to extract bioactive compounds. The extraction was carried out with 50% ethanol and 50% glycerol all acidified with 1% citric acid (to stabilize anthocyanins), at 50 and 60 °C incubation temperature each for 60 and 120 minutes. This was then assisted by sonication for 15 minutes. These extraction conditions were selected based on our previous studies' results [5]. Thereafter, samples were centrifuged at 4500 rpm for 5 minutes, then the supernatant was collected and measured for total anthocyanins, antioxidants capacity (FRAP and TEAC), and colour parameters. Extraction and all tests were done in triplicate.

The total anthocyanin concentration was spectrophotometrically measured following the pH differential method [9]. The antioxidant capacity was evaluated following the Ferric Reducing Ability of plasma (FRAP) assay [10], and Trolox equivalent antioxidant capacity (TEAC) assay as indicated by Müller et al. [11] with some modifications. The colours intensity of samples was measured with a digital colourimeter (Konika Minolta, Chroma-400). The differences in colour (ΔE) between ethanol and glycerol samples were evaluated and reported by looking at the noticeability level (0 - 0.5 = not noticeable, 0.5 - 1.5 = slightly noticeable, 1.5 - 3.0 = noticeable, 3.0 - 6.0 = clearly visible, and 6.0 - 12.0 = great visibility) described by Lukács [12]

Statistical Analysis

The IBM SPSS statistics software, version 27 (IBM Corp., New York, NY 10022, USA, 2020) was used to analyse the mean difference between samples, using a one-way analysis of variances (ANOVA) post-hoc test (Turkey's, and Games' Howell). The normality of error for different analyses was proved by Skewness, Kurtosis, and Kolmogorov-Smirnova ($P > 0.05$). Levene's test was used to test the homogeneity of variances between the mean values of the samples. The significant difference between factors was determined at the interval level of $P < 0.05$.

Results and Discussions

Total anthocyanins

The mean values of total anthocyanins between samples were compared between the solvents (50% ethanol and 50% glycerol samples all acidified with 1%) and the extraction conditions (50 °C and 60 °C each at 60 minutes and 120 minutes) to determine the solvent and extraction conditions giving the highest level of anthocyanin from Galicjanka variety. The results are indicated in Figure 1. Based on the results 50% ethanol has given significantly ($P < 0.05$) higher levels of anthocyanins at all extraction conditions (ranging from 1546 ±5 4 mg/100g to 1680 ± 36 mg/100g DW) compared to 50% glycerol (ranging from 1355 ±73 mg/100g DW to 1456 ± 48 mg/100g DW). The highest levels of anthocyanins from ethanol (1680 ± 36 mg/100g DW) and glycerol (1456 ± 48 mg/100g) extracts were obtained at 50 °C incubation temperature for 120 minutes. These results are in line with our previous findings [5], in which 50% ethanol + 1% citric acid yielded a higher level of anthocyanins compared to other solvents including 50% glycerol + 1% citric. Our previous study has also found 50 °C at 120 optimal for anthocyanins and TPC extraction with ethanol and glycerol respectively. However, both solvents are green solvents that can extract a significant yield of anthocyanins that can used as a natural food additive.
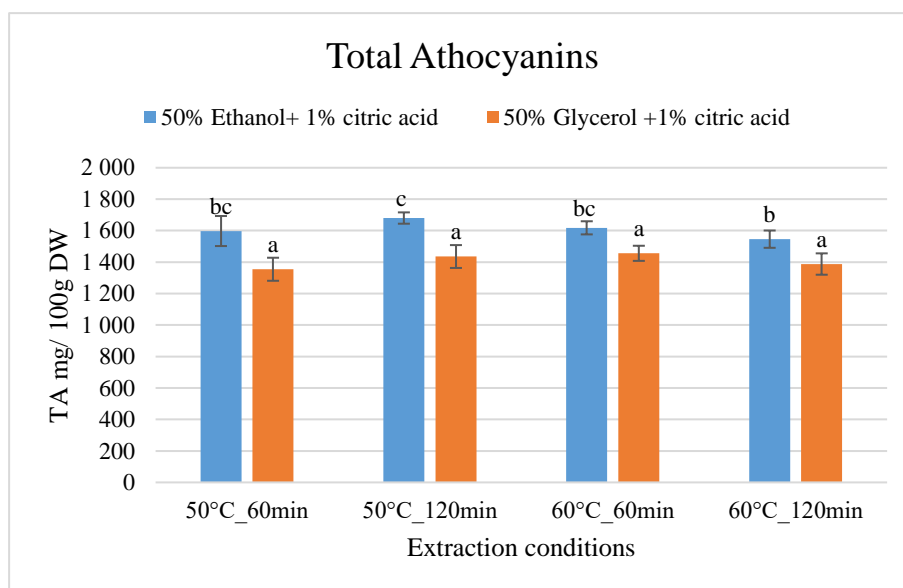
Figure 1. Anthocyanin mean values obtained with 50% ethanol +1% citric acid and 50% glycerol +1% citric acid at different extraction conditions. Different letters indicate significant differences (0.95 confidence interval) between treatments. Error bars the standard deviation.

In a study done by Kowalska et al. [13] 65% glycerol at 80 °C was found optimal in extracting anthocyanins. This could mean that 50% glycerol + 1% citric acid concentration might be too low to dissolve a high quantity of anthocyanins. The plant properties matrices, anthocyanin solubility, and polarity can influence anthocyanin yield.

Antioxidant capacity

The level of antioxidant capacity of polyphenols obtained from the chokeberry pomace using 50% ethanol and 50% glycerol acidified with 1% citric acid is indicated in Figures 2 and 3. Regarding FRAP (Figure 2), 50% ethanol has yielded a significantly higher (P< 0.05) level of antioxidant activity (4476 ± 488 mg AA/100g DW) compared to glycerol at 60 °C for 120 minutes. However, glycerol yielded a significantly higher (P< 0.05) level of antioxidant activity (3662 ± 439 mg AA/100g DW) at 50 °C and 120 minutes.
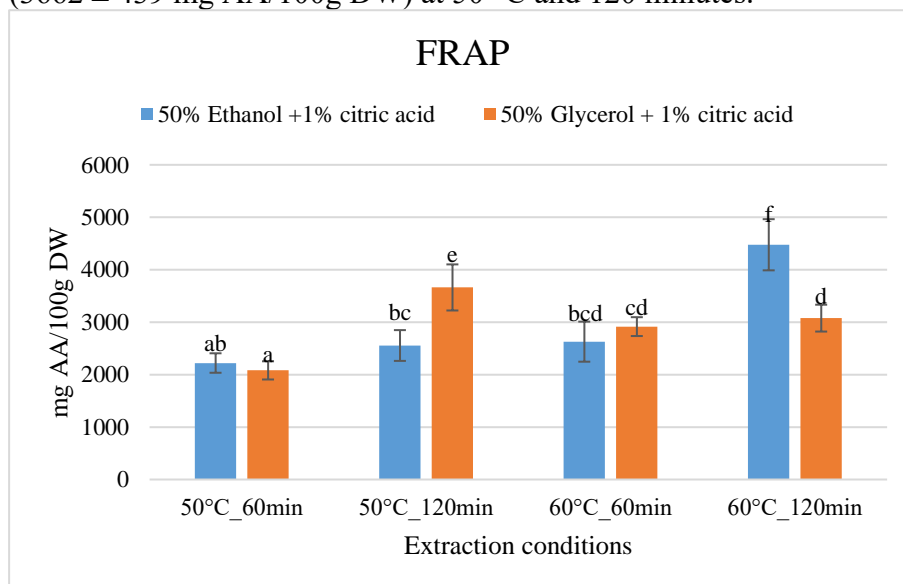
Figure 2. FRAP mean values obtained with 50% ethanol +1% citric acid and 50% glycerol +1% citric acid at different extraction conditions. Different letters indicate significant differences (0.95 confidence interval) between treatments. Error bars the standard deviation.

TEAC results (Figure 3) have also indicated ethanol extracts to yield a higher level of antioxidant capacity compared to glycerol, and the highest was obtained at 60 °C for 120 minutes similar to FRAP. the efficiency of ethanol in yielding extracts with high antioxidants over other solvents has been reported by [11]. Extracts with a higher antioxidant capacity are

needed for utilization in the food industry as anti-senescence, antibacterial, and to prevent oxidation.
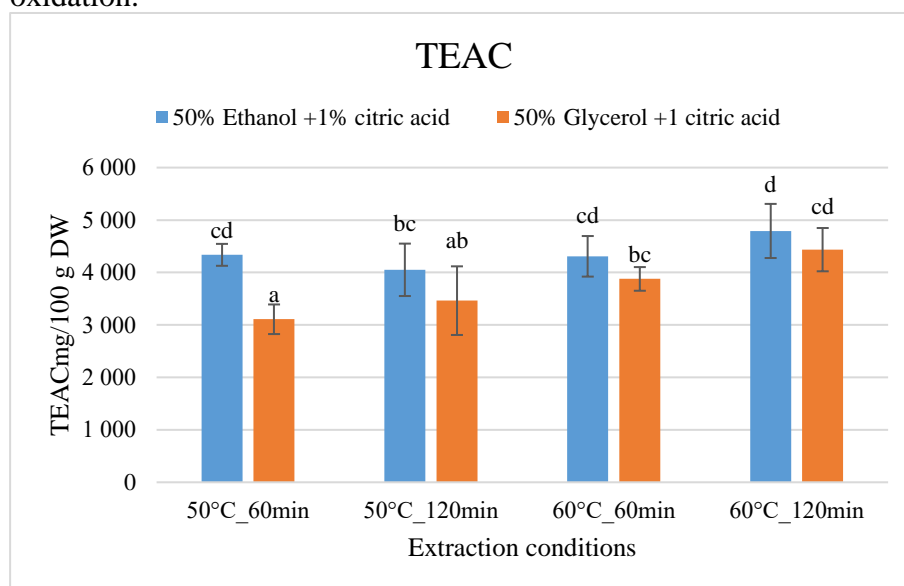
Figure 3. TEAC mean values obtained with 50% ethanol +1% citric acid and 50% glycerol +1% citric acid at different extraction conditions. Different letters indicate significant differences (0.95 confidence interval) between treatments. Error bars the standard deviation.

Colour Differences

The colour differences between 50% ethanol + 1% citric acid and glycerol +1% citric acid at each extraction condition were evaluated, and the results are given in Table 1. The difference in colour between the two solvents was noticeable. These results align with the anthocyanins results, in which 50% ethanol + 1% citric acid extracts have yielded the highest level of anthocyanins.

Table 1. The colour differences between 50% ethanol +1% citric acid and 50% glycerol + 1% citric acid

Extraction conditions	Ethanol			Glycerol			ΔE*	Evaluation
	L*	a*	b*	L*	a*	b*		
50°C_60min	9,07	1,59	-0,40	10,49	1,93	-0,31	1,46	Noticeable
50°C_120min	9,05	1,56	-0,44	10,90	1,69	-0,50	1,85	Noticeable
60°C_60min	9,06	1,38	-0,43	10,67	1,49	-0,51	1,619	Noticeable
60°C_120min	9,03	1,37	-0,46	10,44	1,45	-0,49	1,41	Noticeable

Conclusion

This study assessed the level of anthocyanins and antioxidant capacity in samples extracted with 50% ethanol and 50% glycerol all acidified with 1% citric acid at different extraction conditions previously known to yield a high level of polyphenols. In overall, 50% ethanol +1% citric acid has given the maximum yield for anthocyanins, antioxidant capacity and the colour. For the extraction conditions, the highest anthocyanins were obtained at 50 °C for 120 minutes, whereas at 60°C for 120 minutes extracts yielded the highest antioxidant capacity. Therefore, this study suggests these two extraction settings can be suitable for extracting a high level of anthocyanins and antioxidant compounds.

References

[1] Jurendić, T., & Ščetar, M. (2021). Aronia melanocarpa Products and By-Products for Health and Nutrition: A Review. *Antioxidants*, *10*(7), 1052. https://doi.org/10.3390/antiox10071052

[2] Kaloudi, T., Tsimogiannis, D., & Oreopoulou, V. (2022). Aronia Melanocarpa: Identification and Exploitation of Its Phenolic Components. *Molecules*, *27*(14), 4375. https://doi.org/10.3390/molecules27144375

[3] Jakobek, L., Drenjančević, M., Jukić, V., & Šeruga, M. (2012). Phenolic acids, flavonols, anthocyanins and antiradical activity of "Nero", "Viking", "Galicianka" and wild chokeberries. *Scientia Horticulturae*, *147*, 56–63. https://doi.org/10.1016/j.scienta.2012.09.006

[4] Gao, N., Shu, C., Wang, Y., Tian, J., Lang, Y., Jin, C., Cui, X., Jiang, H., Liu, S., Li, Z., Chen, W., Xu, H., & Li, B. (2024). Polyphenol components in black chokeberry (*Aronia melanocarpa*) as clinically proven diseases control factors—An overview. *Food Science and Human Wellness*, *13*(3), 1152–1167. https://doi.org/10.26599/FSHW.2022.9250096

[5] Kavela, E. T. A., Szalóki-Dorkó, L., & Máté, M. (2023). The Efficiency of Selected Green Solvents and Parameters for Polyphenol Extraction from Chokeberry (Aronia melanocarpa (Michx)) Pomace. *Foods*, *12*(19), 3639. https://doi.org/10.3390/foods12193639

[6] Lubana Shahin, Shreriff S. Phaal, Brajesh N. Vaidya, James E. Brown, & Nirmal Joshee. (2019). *Aronia (Chokeberry: An underutilized, highly nutraceutical plant*. https://doi.org/10.7275/Q651-2W57

[7] Chen, J., Li, Y., Li, F., Hong, K., & Yuan, D. (2022). Effects of procyanidin treatment on the ripening and softening of banana fruit during storage. *Scientia Horticulturae*, *292*, 110644. https://doi.org/10.1016/j.scienta.2021.110644

[8] Babaoğlu, A. S., Unal, K., Dilek, N. M., Poçan, H. B., & Karakaya, M. (2022). Antioxidant and antimicrobial effects of blackberry, black chokeberry, blueberry, and red currant pomace extracts on beef patties subject to refrigerated storage. *Meat Science*, *187*, 108765. https://doi.org/10.1016/j.meatsci.2022.108765

[9] Lee, J., Durst, R., & Wrolstad, R. (2005). *AOAC 2005.02: Total Monomeric Anthocyanin Pigment Content of Fruit Juices, Beverages, Natural Colorants, and Wines- pH Differential Method* (pp. 37–39).

[10] Benzie, I. F. F., & Strain, J. J. (1996). The Ferric Reducing Ability of Plasma (FRAP) as a Measure of "Antioxidant Power": The FRAP Assay. *Analytical Biochemistry*, *239*(1), 70–76. https://doi.org/10.1006/abio.1996.0292

[11] Müller, L., Gnoyke, S., Popken, A. M., & Böhm, V. (2010). Antioxidant capacity and related parameters of different fruit formulations. *LWT - Food Science and Technology*, *43*(6), 992–999. https://doi.org/10.1016/j.lwt.2010.02.004

[12] Lukács, G. (1982). Color Measurement. *Műszaki Könyvkiadó, Budapest*, 140–165.

[13] Kowalska, G., Wyrostek, J., Kowalski, R., & Pankiewicz, U. (2021). Evaluation of glycerol usage for the extraction of anthocyanins from black chokeberry and elderberry fruits. *Journal of Applied Research on Medicinal and Aromatic Plants*, *22*, 100296. https://doi.org/10.1016/j.jarmap.2021.100296

SURFACE MODIFICATION OF POLYVINYLIDENE DIFLUORIDE (PVDF) MICROFILTRATION MEMBRANES BY POLYDOPAMINE GRAFTING FOR MORE EFFECTIVE FILTRATION OF OIL EMULSIONS

<u>Ákos Ferenc Fazekas</u>[1,2], Sándor Beszédes[1], Szabolcs Kertész[1], Cecilia Hodúr[1], Zsuzsanna László[1], Gábor Veréb[1]

[1]*Department of Biosystems Engineering, Faculty of Engineering, University of Szeged, Moszkvai Blvd. 9., H-6725 Szeged, Hungary*
[2] *Doctoral School of Environmental Sciences, University of Szeged, Rerrich Béla Sq. 1, H-6720 Szeged, Hungary*
e-mail: fazekas@mk.u-szeged.hu

Abstract
Membrane separation has several advantages (e.g. excellent cleaning efficiency, chemical-free and easy operation) that allow it to be used effectively in oily wastewater treatment. However, during the operation of the membranes their pores can easily become fouled by the hydrophobic pollutants, which ends up in reduced lifetime. Consequently, it is necessary to increase the antifouling properties of the membranes.

Polydopamine-based membrane modification can be used to form a thin layer on the membrane surface, which due to its excellent adhesion properties can result in a stable, homogeneous, hydrophilic surface, thus reducing the adhesion of the contaminants (e.g. the oil droplets). The advantage of this method (compared to other membrane modification by chemical "grafting") is that the polymerization takes place spontaneously in one step, no need for radical formation (UV light) and for additives (initiator, cross-linking reagent) for the reaction to occure, thus it is a cheaper, faster and more scalable technique [1].

In the present study, the surface of a PVDF microfiltration membrane was grafted with polydopamine for different reaction times (1-8h) in order to improve their filtration parameters (flux, filtration resistance) during the separation of oil-water emulsions (c=400 ppm).

The water contact angle results show that compared to the neat PVDF membrane a slightly more hydrophilic surface (81.1° vs 76.2°) was obtained with 1h of polydopamine modification, while after 8h of reaction time the contact angle was reduced even more to 51.1°. The significantly more hydrophilic membrane surfaces resulted an improvement in filtration of the oil emulsion: the flux was increased by 140% after 8h of modification, compared to the unmodified membrane (36 vs 88 L/m^{2}h) and a significant increase in the flux recovery ratio (29.2 to 71.7%) was also observed indicating the elevated cleanability of the modified membranes. The modification with polydopamine also improved the purification efficiency of the effluent, reaching 99.9% reduction of the turbidity and more than 96% reduction of the chemical oxygen demand (COD) by using the 1h-grafted membrane, while for the unmodified membrane these values were 98.3% and 94.1%, respectively.

References
[1] Susan D., Mohammadreza O., Simin S. (2021) Role of polydopamine in the enhancement of binding stability of TiO$_2$ nanoparticles on polyethersulfone ultrafiltration membrane. Colloids and Surfaces A: Physicochemical and Engineering Aspects, 622, 126694

IMPACT OF PERSONAL PROTECTIVE EQUIPMENT LEACHATES ON EARLY PLANT DEVELOPMENT

Enikő Mészáros[1], Kamilla Kovács[1], Etelka Kovács[2], Klaudia Hoffmann[2], Katalin Perei[2], Attila Bodor[2,3], <u>Gábor Feigl</u>[1]

[1]*Department Plant Biology, University of Szeged, H-6726 Szeged, Közép fasor 52, Hungary*
[2]*Institute of Biotechnology and Microbiology, University of Szeged, H-6726 Szeged, Közép fasor 52, Hungary*
[3]*Department of Physiology, Anatomy and Neuroscience, University of Szeged, H-6726 Szeged, Közép fasor 52, Hungary*
e-mail: feigl.gabor@szte.hu

Abstract
The increased disposal of personal protective equipment, such as face masks and gloves, during the global pandemic caused by the novel coronavirus (Covid-19) has led to a notable rise in plastic pollution, which represents a significant ecological threat. This study examines the impact of leachates from polypropylene masks and both latex and nitrile gloves on the early development of twelve plant species, utilising an *in vitro* semi-hydroponic system. The germination and root growth of the plants were assessed, and Fourier transform infrared spectroscopy was employed to analyse the ageing of the materials.
The findings revealed a range of effects of leachates on plant development. The root growth of species such as crimson clover, radish, and buckwheat was found to be inhibited, while other species, including rapeseed, white mustard, and cress, exhibited enhanced growth. The germination index, which integrates relative germination and root length, was utilised to evaluate plant responses. The Brassicaceae species exhibited distinctive responses, with radish displaying high sensitivity to glove leachates, while rapeseed, white mustard, and cress frequently demonstrated growth stimulation. At the family level, legumes exhibited the greatest sensitivity, while monocotyledons were minimally affected, and growth of the Brassicaceae family was generally enhanced. The least reduction in the germination index was observed in the case of mask leachates, in comparison to latex and nitrile gloves. Furthermore, a correlation was identified between root growth responses and material ageing, indicating that masks exhibiting minimal signs of ageing had a comparatively reduced impact on early root development in comparison to aged gloves.
The findings of this study emphasise the intricate relationships between plastic leachates from personal protective equipment and plant growth, underscoring the necessity for further investigation in this field.

Introduction
In addition to the conventional abiotic stresses that can impede plant root development, the impact of rising plastic pollution in the environment, including the vast quantity of personal protective equipment (PPE) utilized during the Covid-19 pandemic, represents a pressing yet under-researched topic in plant biology.
The rapid spread and high mortality rate of the SARS-CoV-2 pandemic caused considerable concern globally, leading to the introduction of various restrictions and prevention strategies to reduce the rate of virus transmission [1,2]. Face masks and disposable gloves became the most widely accepted tools for infection prevention, and thus the demand for gloves increased, leading to their excessive daily use. Consequently, the elevated volume of disposable protective equipment has imposed a significant burden on the disposal and management of plastic waste.

One estimate suggests that 1.5 billion units of personal protective equipment were produced globally between March 2020 and November 2021, with a total weight of 87 thousand tonnes [3]. Similarly, like other traditional plastics, protective equipment is not environmentally inert and can accumulate various harmful substances, including heavy metals and organic pollutants [4,5]. Such substances have the potential to adsorb, accumulate and, when transported by plastic, to pollute water and soil [6-8]. The gradual release of these pollutants has the potential to disrupt wildlife and ecosystem functioning.

Experimental

This study examined the impact of leachates from polypropylene (PP) masks, latex, and nitrile gloves on the early development of twelve plant species. An *in vitro* semi-hydroponic system was employed to assess the effects of these leachates.

Prior to the experiments, surgical mask, nitrile and latex glove pieces with an edge length of 1 cm were soaked in sterile distilled water at concentrations of 0.5% and 1% (w/v) in flasks for 72 h at room temperature with shaking at 100 rpm [9], and subsequently leachate free of plastic pieces was used.

The impact of the leachate was evaluated on the following plant species: *Trifolium pratense* L. (red clover, Rédei Kertimag Zrt., Altaswede), *Trifolium incarnatum* L. (crimson clover, Rédei Kertimag Zrt., Cantea), *Trifolium repens* L. (white clover, Rédei Kertimag Zrt., Romena), *Brassica napus* L. (rapeseed, GK Gabriella), *Medicago sativa* L. (medicago, Rédei Kertimag Zrt., Plato), *Sinapis alba* L. (white mustard, Rédei Kertimag Zrt., Marci), *Lepidium sativum* L. (garden cress, Rédei Kertimag Zrt., 539001), *Raphanus sativus* L. (radish, Rédei Kertimag Zrt, 629000), *Linum usitatissimum* L. (flax, GK Helga), *Oryza sativa* L. (rice, NAIK ÖVKI M-488), *Sorghum vulgare* L. (sorghum, GK Emese), *Fagopyrum esculentum* Moench (buckwheat, GK Oberon).

In the course of the experiments, 10 seeds were germinated in glass Petri dishes on two layers of sterile filter paper in 5 mL of leachate for a period of five days [10].

The germination and growth of the seeds were observed, and germination index (GI) was calculated from the germination data (expressed as a percentage in comparison to the control) and the relative root length (also expressed as a percentage in comparison to the control) [11]. Furthermore, in addition to measuring the pH and conductivity of the leachates, Fourier-transform infrared spectroscopy was utilised to examine the effects of ageing of the materials. The ageing of plastics was characterised by the ageing index (AI), which was calculated from Fourier transform infrared spectroscopy (FTIR) absorbance spectra. This value is calculated in a manner analogous to that employed in the characterisation of plastics, as represented by the carbonyl index, as outlined by Zhao et al. [12].

The results are presented as mean ± standard error. Pairwise comparisons were conducted using Student's t-test in Microsoft Excel 2016, with a significance level of $P \leq 0.05$, $P \leq 0.01$, and $P \leq 0.001$, respectively.

Results and discussion

The results demonstrated that leachate had a variable effect on plant development. Some species, including crimson clover, radish and buckwheat, exhibited inhibited root growth, while others, such as oilseed rape, white mustard and cress, demonstrated enhanced growth (Fig. 1-2).
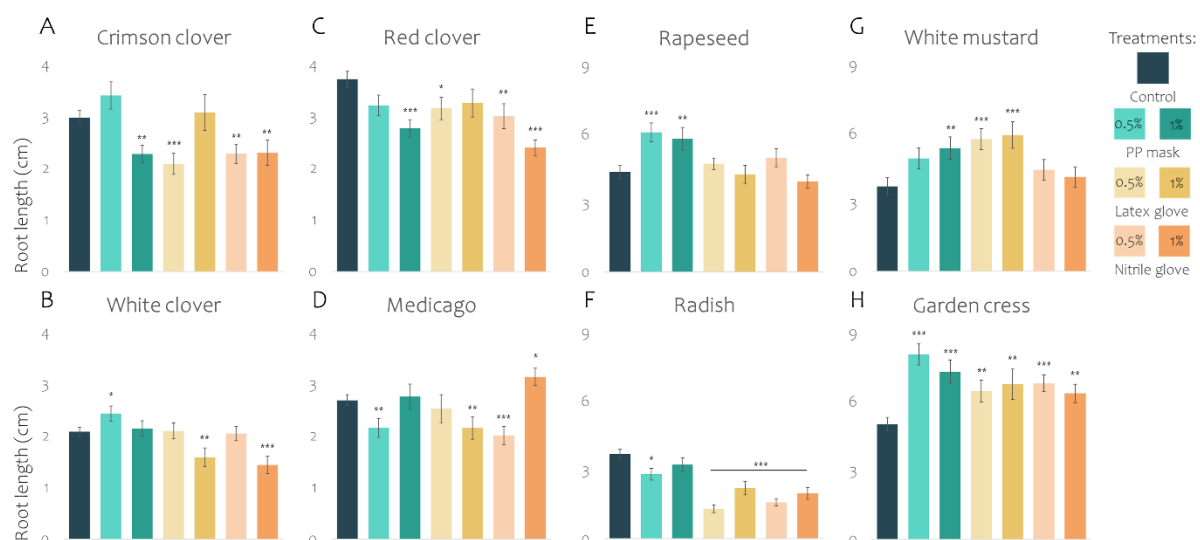
Figure 1. Primary root length of 5-day-old legume (A-D) and crucifer (E-H) seedlings grown on leachate from PP mask, latex and nitrile gloves. Results are expressed as mean ± standard error. Pairwise comparisons were performed using Student's t-test (*$P \leq 0.05$; **$P \leq 0.01$; ***$P \leq 0.001$).
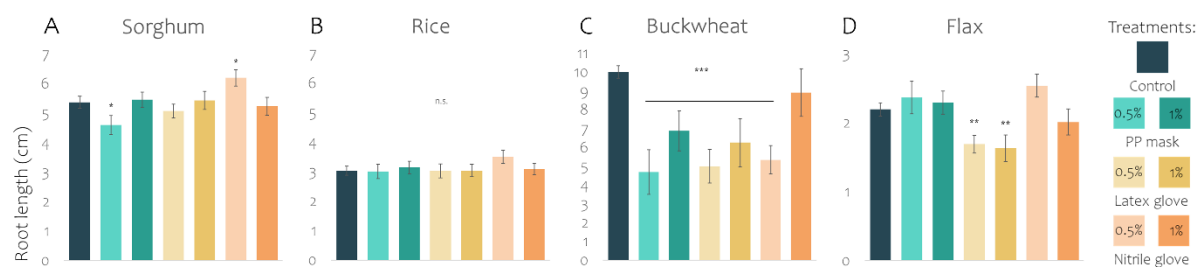
Figure 2. Primary root length of 5-day-old monocot (A-B), buckwheat (C) and flax (D) seedlings grown on leachate from PP mask, latex and nitrile gloves. Results are expressed as mean ± standard error. Pairwise comparisons were performed using Student's t-test (*$P \leq 0.05$; **$P \leq 0.01$; ***$P \leq 0.001$).

	Control	PP mask 0.5%	PP mask 1%	Latex glove 0.5%	Latex glove 1%	Nitril glove 0.5%	Nitril glove 1%
Crimson clover	100	92	56	65	55	61	64
Red clover	100	72	67	85	79	73	64
White clover	100	113	107	90	79	98	61
Medicago	100	69	85	71	69	64	101
Rapeseed	100	134	108	104	87	110	74
White mustard	100	144	151	168	186	124	115
Radish	100	71	88	36	60	43	55
Garden cress	100	161	146	129	130	135	127
Rice	100	88	92	89	93	107	90
Sorghum	100	89	98	98	98	115	94
Buckwheat	100	23	48	27	47	35	58
Flax	100	89	101	77	61	112	85

Figure 3. Germination index of 5-day-old seedlings grown on leachate from PP mask, latex and nitrile gloves.

In addition to root length, the germination index, which combines relative germination and root length, was also used to characterize the response of the plant species.

The average GI of the different families (considering all three leachate types at both concentrations) indicates that the legumes were the most sensitive, while the monocots exhibited no significant inhibition, and the crucifers demonstrated the capacity to stimulate growth (Fig. 3). Upon examination of the impact of leachate from disparate protective devices, it was observed that the PP masks elicited the least pronounced reduction in GI values across all plant species and both concentrations. In contrast, the two types of gloves produced exhibited a greater reduction in GI, with an average reduction of 13% for latex glove leachate and 14% for nitrile.
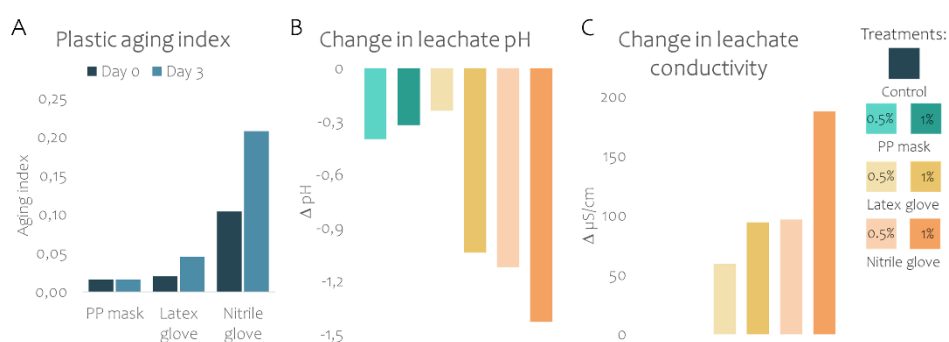
Figure 4. (A) Plastic aging index before and after leachate preparation. Changes in leachate parameters: pH (B) and conductivity (C), after 3 days of leachate preparation.

It is noteworthy that alterations in GI values are associated with fluctuations in the AI values of the test substances, as well as with the pH and conductivity of the leachates. (Fig. 4). The AI value of the PP mask remained unaltered throughout the three-day soaking period. The leachate, which exhibited a similar pH and conductivity after the 72-hour soaking duration, also demonstrated a negligible impact on the mean GI value of the plants. In contrast, the AI value of the two types of gloves approximately doubled after three days of soaking, resulting in a greater decrease in the GI values of the plants. It can also be seen that although the AI values of the nitrile glove pieces were an order of magnitude higher, this only caused a significant difference in the case of leachate from 1% of its concentration, i.e. a higher AI value of the plastic does not necessarily lead to a higher toxicity of the leachate from it.

Conclusion

Among the plant families, the species belonging to the Brassicaceae displayed distinct responses. The radish was observed to be highly sensitive to the leachates from gloves, while the rapeseed, white mustard, and cress often exhibited growth stimulation. The mean GI analysis demonstrated that legumes exhibited the greatest sensitivity, while monocotyledons demonstrated minimal inhibition, and growth in the Brassicaceae family was stimulated.

The least reduction in GI was observed in the case of mask leachates, in comparison to latex and nitrile gloves. The different levels of material ageing and the resultant varying leachate parameters may be responsible for the varying degrees of impact observed with different PPEs.

Acknowledgements

References

[1] Gostin, L. O., & Wiley, L. F. (2020). Governmental public health powers during the COVID-19 pandemic: stay-at-home orders, business closures, and travel restrictions. *Jama*, 323(21), 2137-2138.

[2] Acter, T., Uddin, N., Das, J., Akhter, A., Choudhury, T. R., & Kim, S. (2020). Evolution of severe acute respiratory syndrome coronavirus 2 (SARS-CoV-2) as coronavirus disease 2019 (COVID-19) pandemic: A global health emergency. *Science of the Total Environment*, 730, 138996.

[3] Wise, J. (2022). Covid-19: Pandemic waste threatens human and environmental health, says WHO. *BMJ*, 376:o266, doi: https://doi.org/10.1136/bmj.o266.

[4] Albertsson, A. C., & Karlsson, S. (1993). Aspects of biodeterioration of inert and degradable polymers. *International biodeterioration & biodegradation*, 31(3), 161-170.

[5] Elizalde-Velázquez, A., Subbiah, S., Anderson, T. A., Green, M. J., Zhao, X., & Cañas-Carrell, J. E. (2020). Sorption of three common nonsteroidal anti-inflammatory drugs (NSAIDs) to microplastics. *Science of the Total Environment*, 715, 136974.

[6] Jędruchniewicz, K., Ok, Y. S., & Oleszczuk, P. (2021). COVID-19 discarded disposable gloves as a source and a vector of pollutants in the environment. *Journal of hazardous materials*, 417, 125938.

[7] Garçon, M., Sauzeat, L., Carlson, R. W., Shirey, S. B., Simon, M., Balter, V., & Boyet, M. (2017). Nitrile, latex, neoprene and vinyl gloves: a primary source of contamination for trace element and Zn isotopic analyses in geological and biological samples. *Geostandards and Geoanalytical Research*, 41(3), 367-380.

[8] Reichel, C. (2012). Mass spectrometric analysis of EPO IEF-PAGE interfering substances in nitrile examination gloves. *Drug Testing and Analysis*, 4(10), 761-774.

[9] Bejgarn, S., MacLeod, M., Bogdal, C., & Breitholtz, M. (2015). Toxicity of leachate from weathering plastics: An exploratory screening study with Nitocra spinipes. *Chemosphere*, 132, 114-119.

[10] Mészáros, E., Bodor, A., Szierer, Á., Kovács, E., Perei, K., Tölgyesi, C., ... & Feigl, G. (2022). Indirect effects of COVID-19 on the environment: How plastic contamination from disposable surgical masks affect early development of plants. *Journal of Hazardous Materials*, 436, 129255.

[11] Bodor, A., Feigl, G., Kolossa, B., Mészáros, E., Laczi, K., Kovács, E., ... & Rákhely, G. (2024). Soils in distress: The impacts and ecological risks of (micro) plastic pollution in the terrestrial environment. *Ecotoxicology and Environmental Safety*, 269, 115807.

[12] Zhao, Z. Y., Wang, P. Y., Wang, Y. B., Zhou, R., Koskei, K., Munyasya, A. N., ... & Xiong, Y. C. (2021). Fate of plastic film residues in agro-ecosystem and its effects on aggregate-associated soil carbon and nitrogen stocks. *Journal of Hazardous materials*, 416, 125954.

PERFORMANCE EVALUATION OF A 3D-PRINTED PLASTIC V-GROOVE NEBULIZER FOR TRACE ANALYTICAL USE IN ICP-MS

Almachiusi Rwegasira Rweyemamu[1], Gyula Kajner[1], **Ádám Bélteki[1], Tibor Ajtai[3],**
Martin Cseh[2], Zsolt Geretovszky[2,3], Gábor Galbács[1*]

[1]Department of Molecular and Analytical Chemistry, University of Szeged,
H-6720 Szeged, Dóm tér 7, Hungary
[2]Center of Excellence for Interdisciplinary Research, Development and Innovation, 3D
Centre Universty of Szeged, Tisza Lajos Boulevard 107, H-6725 Szeged, Hungary
[3]Department of Optics and Quantum Electronics, University of Szeged, Dom Square 9, H-
6720 Szeged, Hungary
*e-mail: galbx@chem.u-szeged.hu

Abstract
In this study, we demonstrated the feasibility and reliability of using 3D printing to create a low-cost, customized plastic V-groove nebulizer. Triplicates of plastic V-groove nebulizer were fabricated using multijet 3D-printing technology and tested for analytical performance using ICP-MS. The nebulizers were validated by optimizing key parameters and aerosol quality monitored by an optical particle counter (OPC). On average, all nebulizers generated aerosol droplets in the feasible range of diameters suitable for analytical use. Calibration curves for all nebulizers showed excellent linearity ($r^2 > 0.998$), with detection limits in the sub-ppb range.

1. Introduction

The advancement of additive manufacturing, commonly known as 3D printing, has opened new possibilities for the design and fabrication of complex, precise, and customizable devices for spectroscopic instruments in analytical chemistry. Among the few innovations highlighted in the literature is the development of 3D-printed nebulizers [1,2] for use in analytical instruments such as ICP-MS. Nebulizers converts liquids into fine aerosol droplets. The quality of these aerosols, particularly the size distribution and consistency of the droplets, is critical for a nebulizer in achieving high analytical accuracy, sensitivity, and reproducibility of the measurements. Studies have shown that 3D-printed plastic nebulizers can as good as standard nebulizers if geometries are well optmized [2]. The standard glass nebulizers are expensive, fragile and some can easily clog when handling complex or high-matrix samples. However, the use of 3D printing technologies allows one to create nebulizers from durable, chemically resistant plastic materials that are cost-effective, so their replacement is easy [3,4]. A V-groove nebulizer has features of a specific geometry where a liquid sample is funnelled into a small groove shaped like a "V," which interacts with a pressurized gas stream to create an aerosol. With 3D printing technology such as multijet technology, it is possible to precise control over this geometry by optimizing aspects such as the angle of the groove, which have impact in aerosol characteristics. In this study, we described the design, manufacturing process, and the characterization of the 3D-printed plastic V-groove nebulizers with ICP-MS.

2. Experimental
2.1 Instrumentation

An inductively coupled plasma mass spectrometer (ICP-MS) of the Agilent 7700X model (Agilent, Santa Clara, CA, USA) was used in this experiment experiments. The instrument operated with an R.F. forward power of 1550 W and a plasma gas flow rate of 15 L.min^{-1}, with the sampling depth set at 10 mm. For sample introduction, a Peltier-cooled Scott spray chamber

(Glass Expansion, Port Melbourne, Australia) was coupled with a 3D-printed V-groove nebulizer. The properties of the primary aerosols generated by the nebulizers were studied by using an optical particle counter (OPC, model 1.109), manufactured by Grimm Aerosol Technik (Ainring, Germany).

2.2 Matrials used
During the experiments, a high purity argon gas supplied by Messer Hungarogáz (Budapest, Hungary was used. This instrument was calibrated with solutions prepared from 10 ppm multielement ICP-MS standard (Inorganic Ventures, Christiansburg, VA, USA). For sample dilution, trace quality diionized water sourced from a MilliPore Elix 10 system fitted with a Synergy polishing unit (Merck, Darmstadt, Germany) was used.

2.3 Statistical software
The 3D model of the V-groove nebulizer was created using AutoCAD, an engineering design software developed by Autodesk Inc. (San Francisco, CA, USA). Data acquisition and management in all ICP-MS experiments was performed by Agilent MassHunter software (Agilent Technologies, Santa Clara, CA, USA). The recorded data were subsequently processed and analyzed using Microsoft Excel (Microsoft Corp., Redmond, WA, USA) alongside with Origin software (OriginLab Corp., Northampton, MA, USA).

2.3 3D-printing
The 3D-printing was carried out using a ProJet MJP 3600 MAX professional 3D printer which contains a VisiJet M3 resin cartridge (3D Systems, Rock Hill, SC, USA). The printer was operated in XHD mode, with a nominal layer thickness of 16 micrometers and an x and y resolution of 750 dpi. Three repricates of the V-groove nebulizers were printed and cleaned from any residual support resin (VisiJet S300) by keeping them in a laboratory oven set at 75 °C. Following the melting and draining of most of the waxes, the parts were placed in a sonicated bath filled with EZ Rinse liquid (3D Systems, Rock Hill, SC, USA) for 10 minutes at 65 °C. The prints were rinsed with trace quality diionized water (Analytical grade) and dried.

3. Results and discussion
The drop size distributions of the aerosols produced by tripricates of 3D-printed plastic V-groove nebulizer (**Fig.1**) were assessed and compared to each other.

Figure 1. 3D-printed plastic V-groove nebulizer

The primary aerosols generated by each nebulizer were directly sampled by the OPC from the nebulizer tip, without spray chamber. This approach was deliberately chosen to focus on the characteristics of primary aerosols. Each measurement was conducted at different nebulizer gas flow rates; 0.5, 1.0, 1.5, 2.0 and 2.5 L·min^{-1} and liquid flow rates; 0.1, 0.2, 0.3 and 0.4 mL·min^{-1} in order to find the best conditions. The V-groove nebulizers were able to produce practically useful aerosol droplets with diameters of ca. 10 µm using gas flow rates between 1 and 2.5 L.min^{-1} at all liquid flow rates. On other hand, nebulizers produced larged liquid droplets with diameter reaching up to 30 µm. When the gas flow rate was 0.5 L.min^{-1}, all nebulizers performed poorly (**Fig 2**). On average, nebulizers demonstrated equal eficiency in aerosol generation which indicates a fairly good reproducibility of 3D-printing.
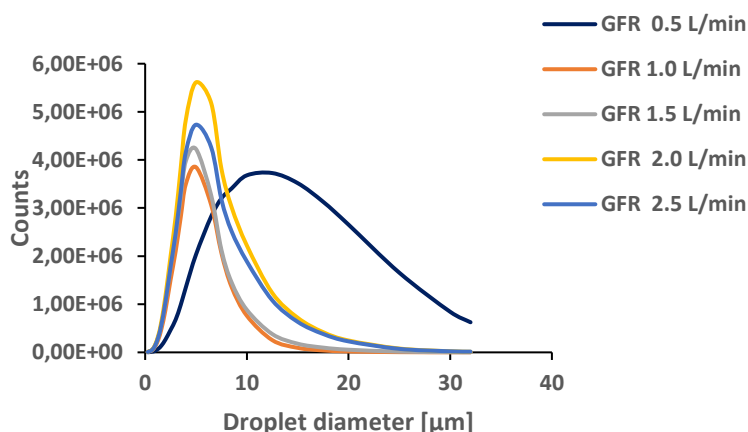
Figure 2. The droplet size distribution of the 3D-printed plastic V-groove nebulizer recorded at different gas flow rates (GFR) and at 0.2 mL.min^{-1} liquid flow rate

We also assessed the elemental contaminations of resin materials. This is an important detail for trace analysis, but it often not disclosed by commercial resin manufacturers since the resins are mainly meant for technical use. Using Milli-Q deionized water, the background contamination of the 3D-printed V-groove nebulizer was assessed with ICP-MS and compared to a conventional concentric glass nebulizer (**Fig.3**). The results showed that only a slight elevation in the background intensites occurred, which indicates that the resin is sufficiently pure and suitable for trace metal analysis.
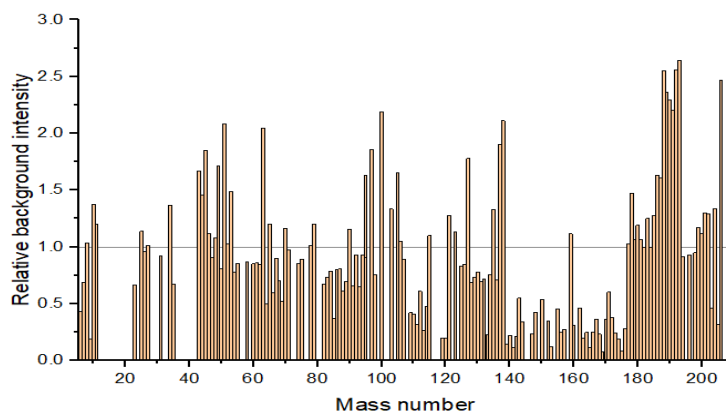
Fig 3. Background signals of 3-printed V-groove nebulizer relative to the values recorded with standard MicroMist cencentric nebulizer (as a reference) used in ICP-MS

Similarly, we evaluated the ICP-MS performance of the three 3D printed V-groove nebulizers by conducting a five-point calibration using a series of standard solutions with concentrations of 0.0, 1.0, 5.0, 10.0, and 50.0 µg·L^{-1} for six elements. They were detected at their ^{9}Be, ^{23}Na, ^{63}Cu, ^{66}Zn, ^{107}Ag and ^{208}Pb isotopes. All three nebulizers exhibited relatively low detection limits in, the hudreths of ppb range. The detection limits for ^{23}Na were at least ten times higher than that of other elements, but this is a fairly typical behaviour for this element in ICP-MS analysis. The detection limits showed a slight variation across the three V-groove nebulizers. This could be due to differences in the nebulization efficiency as a result of small deviations in reproduction of the geometry with 3D printing.

Conclusion

Results obtained in this study clearly demonstrate that 3D-printing is a viable and feasible method for producing cost-effective and customizable nebulizers from plastic materials for analytical applications. The aerosol characterization results suggest that with proper material selection and design adjustments, 3D-printed V-groove nebulizers can achieve a performance which is comparable to the that of traditional glass nebulizers. Further refinement in material properties and printing techniques can enhance their efficiency and widen their application in analytical intruments.

Acknowledgements

References

[1] Kajner, G., Bélteki, Á., Cseh, M., Geretovszky, Z., Ajtai, T., Barna, L., & Galbács, G.(2023). Design, optimization, and application of a 3D-printed polymer sampleintroduction system for the ICP-MS analysis of nanoparticles and cells. *Nanomaterials*, *13* (23), 3018

[2] Garcia-Montoto, V., Mallet, S., Arnaudguilhem, C., Christensen, J. H., & Bouyssiere, B. (2020). 3D-printed total consumption microflow nebuliser development for trace element analysis in organic matrices via inductively coupled plasma mass spectrometry. *Journal of Analytical Atomic Spectrometry*, *35*(8), 1552-1557.

[3] Grajewski, M., Hermann, M., Oleschuk, R. D., Verpoorte, E., & Salentijn, G. I. (2021). Leveraging 3D printing to enhance mass spectrometry: A review. *Analytica Chimica Acta, 1166*, 338332

[4] Rösch, M., & Cziczo, D. J. (2020). Aqueous particle generation with a 3D printed nebulizer. *Atmospheric Measurement Techniques*, *13*(12), 6807-6812.

DEVELOPMENT OF A HEALTHIER BREAD RECIPE: IMPACT OF FLOUR TYPE AND FERMENTATION ON BREAD QUALITY IN KOSOVO

<u>Njomza Gashi</u>[1,2]*, Jehona Latifi[1], Fjolla Hoxha[1], Dhurata Mani[1], Dejsi Qorri[3], Salih Salihu[1]

[1]*Department of Food Technology with Biotechnology, Faculty of Agriculture and Veterinary, University of Prishtina "Hasan Prishtina", Prishtina 10 000, Kosovo*
[2]*Faculty of Agricultural and Food Sciences and Environmental Management, University of Debrecen, H-4032 Debrecen, Hungary*
[3]*Institute of Economics, Department of Agricultural Economics, Faculty of Economics and Business, University of Debrecen, 4032 Debrecen, Hungary*
*Corresponding author: nj.gashi2@gmail.com

Abstract
Bread is a fundamental part of the daily diet in Kosovo, with white bread being one of the most consumed products. Given its high carbohydrate content, regular consumption may impact public health, necessitating the development of healthier alternatives. This study aimed to create a nutritionally improved bread recipe by using both market-purchased and self-milled wheat and rye flours. Two fermentation methods were compared: one involving 30- and 50-minute rest intervals, and another with a 20+40-minute combination. Water absorption of the flours was measured using a Promylograph.
Bread quality was assessed through multiple parameters: weight was determined using a precision scale, volume through the seed displacement method with amaranth seeds, and porosity and color were evaluated visually. Significant differences in weight and porosity were observed between the different bread samples ($p<0.05$). The comparison between bread made from imported and local flours revealed significant variations in volume ($p<0.05$) but no differences in other attributes ($p>0.05$). Additionally, variations in porosity were detected between the two fermentation processes ($p<0.05$), highlighting the role of fermentation in influencing bread texture.
The new formulation resulted in a bread with favorable sensory characteristics, including texture and taste, while introducing healthier ingredients. These findings suggest that incorporating locally milled flours and optimizing fermentation processes can lead to bread with enhanced quality, offering a viable alternative to conventional white bread commonly consumed in Kosovo.

Keywords: healthier bread, bread quality, wheat flour, rye flour, fermentation.

THE ROLE OF SOIL MICROBIOME ON WHEAT NUTRITIONAL PROFILE

Njomza Gashi[1,3*], Péter Fauszt[1], Péter Dávid[1], Zsombor Szőke[1], Judit Remenyik[1], László Stündl[2], and Melinda Paholcsek[1]

[1] *Center for Complex Systems and Microbiome Innovations, Faculty of Agricultural and Food Sciences and Environmental Management, University of Debrecen, 4032 Debrecen, Hungary*
[2] *Institute of Food Technology, Faculty of Agricultural and Food Sciences and Environmental Management, University of Debrecen, 4032 Debrecen, Hungary*
[3] *Department of Food Technology with Biotechnology, Faculty of Agriculture and Veterinary, University of Prishtina "Hasan Prishtina", 10 000 Prishtina, Kosovo*
*Corresponding author: njomza.gashi@agr.unideb.hu

Abstract
Wheat is a key global food source, offering energy through its carbohydrates and significant health benefits due to its proteins, vitamins, and dietary fibers. The rapid expansion of agriculture has led to increased use of agrochemicals and varied tillage methods, both of which impact soil microbial communities and, consequently, wheat's nutritional composition. This study aimed to evaluate the nutritional value of wheat cultivated under different fertilization regimes and tillage systems, with a focus on the relationship between soil microbial composition and wheat nutrition.
Wheat and soil samples were collected from two tillage systems: ploughing and deep loosening, and treated with two nutrient settings: 100 kg/ha N, 50 kg/ha P_2O_5, 70 kg/ha K_2O (A) and 150 kg/ha N, 100 kg/ha P_2O_5, 120 kg/ha K_2O (B). Nutritional content was analyzed using chromatographic and spectrophotometric methods, assessing fat- and water-soluble antioxidants, as well as protein content. Soil microbial composition was examined via 16S rRNA sequencing.
The results showed no significant differences in wheat nutritional values between tillage methods, though nutrient distribution varied across systems. Similarly, fertilization systems demonstrated differential nutrient spread. Correlation analysis revealed positive correlations between certain microbial members and both fat- and water-soluble antioxidants, while negative correlations were observed with a larger number of microbial species. This suggests that soil microbiota play a critical role in influencing wheat's nutritional outcomes.

Keywords: wheat, soil microbiome, nutritional composition, 16s RNA sequencing, tillage, fertilization.

IMINO SEMICARBAZIDES AND THEIR METAL COMPLEXES: SOLUTION STABILITY, REDOX AND ANTICANCER PROPERTIES

Gerda T. Gátszegi[1], Tatsiana V. Petrasheuskaya[1], Bálint Hajdu[1], Vladimir B. Arion[2], Gabriella Spengler[3], and Éva A. Enyedy[1]

[1]Department of Molecular and Analytical Chemistry, University of Szeged, Dóm tér 7-8, H-6720 Szeged, Hungary
[2]Institute of Inorganic Chemistry, University of Vienna, Währinger Strasse 42, A-1090 Vienna, Austria.
[3]Department of Medical Microbiology, University of Szeged, Semmelweis u. 6, H-6720 Szeged, Hungary

The administration of anticancer drugs in chemotherapy is often limited by the occurrence of serious side effects and resistance. These issues have led to the development of new potential active compounds, including metal complexes. Thiosemicarbazone (TSC) derivatives and their metal complexes have been extensively studied in the literature due to their potential pharmacological activities, such as antimicrobial, antiviral, antitumor, and antioxidant effects [1]. It has been established that both the coordinating donor set and the substituents on the TSC scaffold strongly influence the stability and biological activity of their metal complexes [2]. Previously, salicylidene-imino semicarbazide (IS) Schiff base metal complexes with {O,N,N} coordinating sites were investigated to study the effect of $C=S \rightarrow C=NH$ isosteric replacement on coordination and biological properties [3].

In this study, various 2-acetylpyridine-imino semicarbazide Schiff base derivatives bearing an {N,N,N} donor set, along with their Cu(II) and Fe(II) complexes, were investigated. To analyze their solution equilibrium and redox properties, pH-potentiometric, UV-visible spectrophotometric and cyclic voltammetric measurements were used. The reactivity of the Cu(II) complexes with physiological reducing agents was also investigated by spectrophotometric methods.

We found that the ligands are predominantly positively charged at physiological pH. The formation constants obtained show that low stability complexes are formed with both Cu(II) and Fe(II/III) ions. In the human cancer cells studied (Colo205, Colo320, MCF7), the ligands were not cytotoxic, but their Cu(II) complexes exhibited moderate activity. In summary, the replacement of the thione sulfur atom by imino nitrogen results in complexes with lower stability and anticancer activity.

References
[1] V. Singh, et al., Polyhedron 2023, 245, 116658.
[2] V. Pósa, et al., J. Inorg. Biochem. 2022, 231, 1111786.
[3] O. Dömötör; et al., Molecules 2022, 27, 2044.

IMPACT OF NATURAL ACEROLA EXTRACTS ON THE QUALITY OF CANNED VEGETABLES

Bálint Góczán[1], Bernadett Mohácsi[1], Judit Friedrich-Ivanics[1], Mónika Máté[1]

[1]*Department of Fruit and Vegetable Processing Technology, Institute of Food Science and Technology, Hungarian University of Agriculture and Life Sciences, H-1118 Budapest, Villányi út 29-43., Hungary*
e-mail: balint.goczan@gmail.com

Abstract

Applying natural origin additives in the creation of consumer-accepted food items is becoming more and more crucial for food producers. The aim of this study was to evaluate the efficacy of several organically derived plant extracts in place of ascorbic acid and determine whether or not they might be used in a canned mixture of red beans and supersweet corn. In this experiment, the samples were examined for pH, water-soluble dry matter content, color (L*, a*, b*, ΔE*), total polyphenol content (TPC), and antioxidant capacity (FRAP).

The samples were prepared using two separate source of acerola extract. During the color test, the product with the plant extracts added showed a discernible change in color, however, the samples with the extracts typically had a high polyphenol content and antioxidant potential. Based on the test results, natural acerola extracts could be a viable substitute for ascorbic acid, which is utilized in the canned mixture of red beans and super sweet corn.

Introduction

Consumer worry of the food sector is on the rise, primarily because of worries about additive usage. Many people are skeptical of the long-term impact of artificial chemicals on well-being and are afraid of the possible health effects. The lack of transparency displayed by food manufacturers, who frequently withhold information about the source of additives, increases this mistrust. As a result, while choosing foods, people are becoming more and more drawn to natural components. Customers are looking for products with identifiable natural components because they want transparency and simplicity, which is in line with the broader drive towards a more mindful and healthful approach to eating. This development emphasizes the necessity for the food business to prioritize consumer concerns, encourage greater transparency, and prioritize the use of natural, healthful ingredients. Many spices, herbs, fruits, vegetables, cereals, cocoa shells, grain, enzymes, and proteins are natural sources of antioxidants [1]. Numerous studies have demonstrated the high concentrations of ascorbic acid, phenolic compounds, and antioxidant activity found in acerola [2].

Experimental

The industrial canning process' technological procedures were followed in the preparation of the samples. The samples were created in a pilot lab, and the procedure was modeled. The brines for the trials were made when the preparation of sweet corn and beans were ready. After that, the samples were filled with the necessary amoung of brine and the prepared cans were filled with the raw materials in the exact amounts. Sample C was prepared with water as it were (control), sample AC1, AC2 were prepared with different concentrations of acerola extracts from different suppliers. The amount of ingredients was determined at different concentrations.

Table 1. Amount of ingredients and water per 0.5 liter of brine

	C (control)	AC1	AC2
Water (g)	500	475.1	479
Salt (g)		19	19
Acerola extract 1 (g)		5.9	
Acerola extract 2 (g)			2

The preparation of sweetcorn and red kidney beans was the first step in sample preparation. As both corn and red kidney beans were frozen, the vegetables only needed to be blanched for 3 minutes, then strained and the appropriate amount filled into the cans. After filling the cans, the composition of the brine given in Table 1 was prepared and heated to 60 °C. The required amount of brine was then poured into the cans. Cans were double-seamed in vacuum chamber using a laboratory seaming machine. The cans were then marked, and heat treated, and the conformity of the heat treatment was checked by an F_0 probe at the cold point of the product. After processing, the samples were stored for 6 months to check the parameters.

Testo digital pH meter was used to determine the pH value from the juice of the product. The water soluble solids content was measured with an ATAGO DBX-55 digital refractometer. Konica Minolta CR 400 digital colorimeter was used to determine the value of color coordinate based on CIELab system: L* (lightness factor), the a* (the transition from red to green) and the b* (from blue to yellow) were measured. The color difference parameter (ΔE*) was calculated according to Equation:

$$\Delta E^* = \sqrt{\Delta L^{*2} + \Delta a^{*2} + \Delta b^{*2}} \quad [3]$$

Evaluation of ΔE * using in Table 2.

Table 2. Summary of color difference [3]

ΔE*	Color difference
0-0.5	Not noticed
0.5-1.5	Hardly noticeable
1.5-3.0	Noticeable
3.0-6.0	Clearly visionable
>6.0	Great difference

The browning index (BI) was calculated according to equation [4]:

$$BI = \frac{100(x - 0.31)}{0.17}$$

where

$$x = \frac{a + 1.75L}{5.645L + a - 3.012b}$$

Gallic acid was applied as the calibration curve for the Folin-Ciocalteu method, which was used to analyze the total phenolic content (TPC) in accordance with Singleton and Rossi [5]. The

results were represented as grams of gallic acid equivalent per 100 g (mgGA 100 g-1). At 765 nm, absorbance was measured with a Hitachi U-2900 spectrophotometer.

The methodology of Benzie and Strain [6] was applied to measure antioxidant activity using the ferric reducing ability of plasma (FRAP). The calibration curve was created using ascorbic acid, and the results were presented as milligrams of ascorbic acid equivalent per 100 grams (mgAA g-1). The Hitachi U-2900 spectrophotometer was used to perform the FRAP test at 593 nm.

Results and discussion

The pH values were evaluated after 1 and 6 months of storage. Based on the pH measurements, the pH of sample C was the highest at 6.53 1 month after sample preparation. Sample AC1 showed the lowest value of 6.25. After 6 months of storage the pH values of the samples showed a decrease. The largest decrease was observed for sample C, but even then sample C had the highest value of 6.45.

The highest water-soluble solids content was found in sample AC1 (10.3%) and the lowest in sample C (control) (8.73%) after 1 month of preparation. Tests at month 6 showed that the water-soluble solids content increased in different levels.

The ΔE* color difference calculated from L*, a* and b* data after 0 and 6 months of storage is shown in Table 3. The values shown are from samples of corn kernels. The value of ΔE* at moment 0 was found to be greater than 0.5 for all samples, so the colour change is noticeable, but to different degrees. After 6 months of storage the difference is clearly visionable.

Table 3. Colour difference [ΔE*] of samples of corn kernels compared to each other

ΔE*	0 month		6 months	
	AC1	AC2	AC1	AC2
C (control)	1.20	1.91	3.02	5.60
AC1		2.13		3.31

The colour difference [ΔE*] of the corn kernels after 6 months of storage compared to the time of production is classified as noticeable and clear visionable according to Table 4.

Table 4. Colour difference [ΔE*] of samples of corn kernels each sample is compared to its own value at month 0 in month 6

6 months / 0 month	C (control)	AC1	AC2
C (control)	5.14		
AC1		2.89	
AC2			2.80

In terms of browning index results, sample AC2 gave similar results to sample C (control) after the storage test, as shown in Fig 1.

Figure 1. Browning index [BI] of samples of corn kernels in month 6
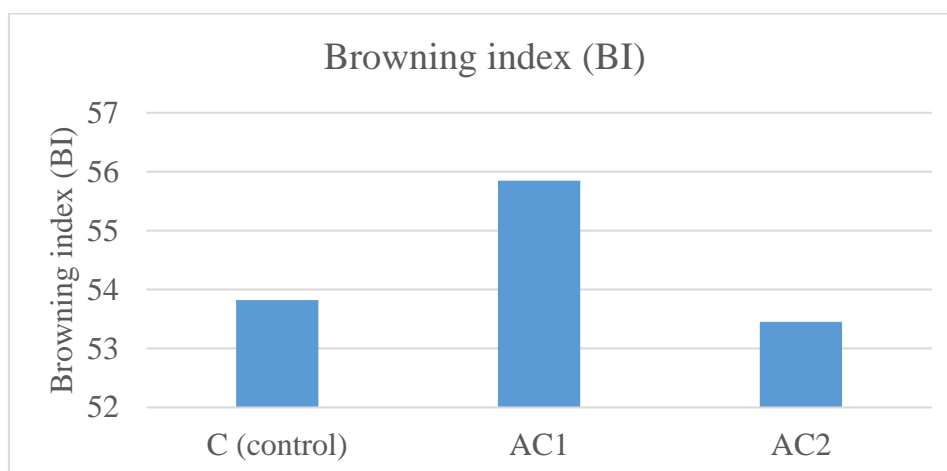
The polyphenol content was found to be higher in all samples containing plant extracts than in sample C (control) (Figure 2). The highest value was measured in sample AC2 (108.7 mgGA 100g^{-1}) After 6 months of storage, the values decreased in all samples, with the least change being observed in sample AC1.

Figure 2. Total polyphenol content of samples at months 0 and 6
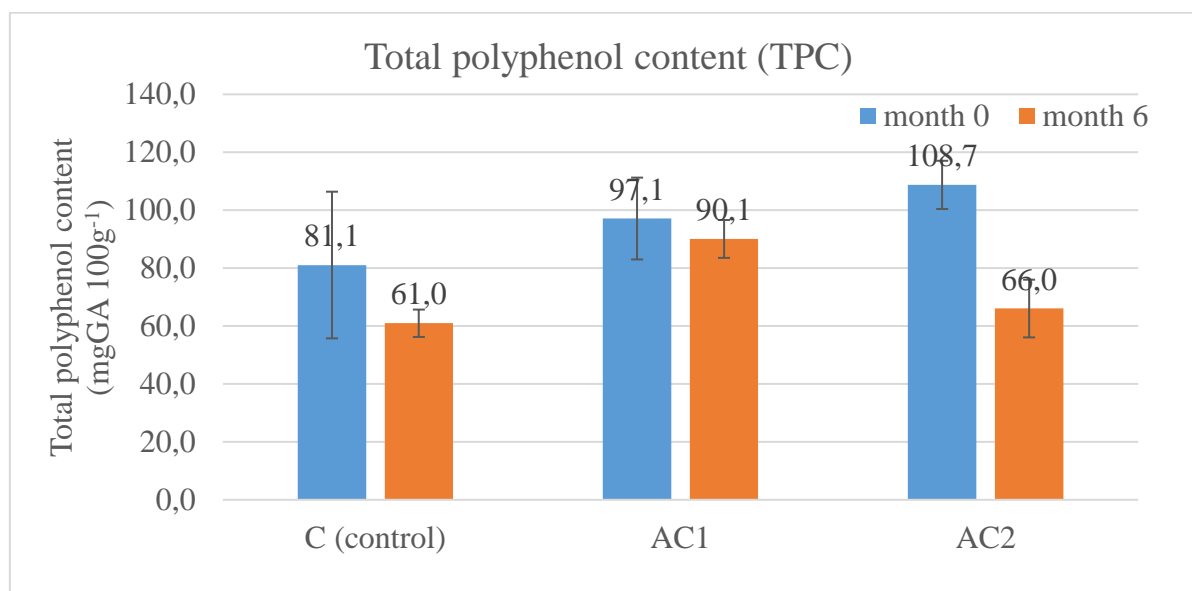
The antioxidant capacity test showed that the values measured in the samples containing acerola extracts were higher than those of the C (control) sample (Figure 3). The highest values were obtained for the AC1 sample. After 6 months storage, a minimal decrease in antioxidant capacity values was observed for all samples.

Figure 3. FRAP of samples at months 0 and 6

Antioxidant capacity (FRAP)
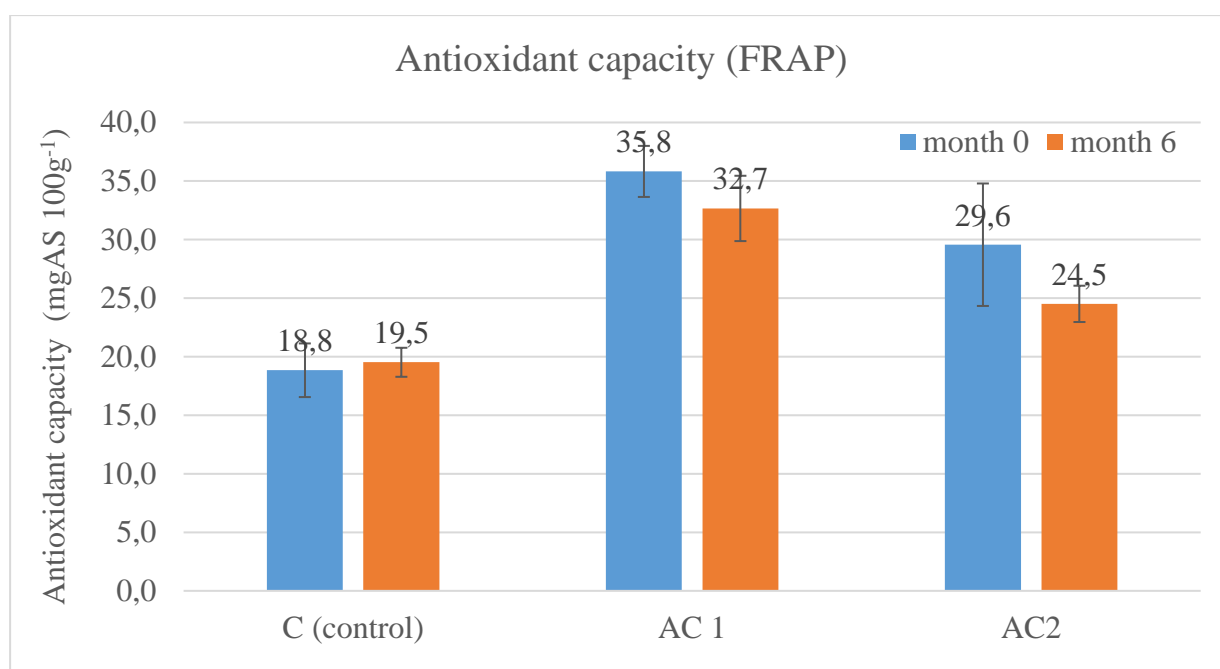
Conclusion

The study showed that natural acerola extracts could be a potential alternative to the currently used ascorbic acid in the canned mixture of supersweet corn and red beans. Samples prepared with acerola extract achieved promising results. After longer-term storage, further evaluation of the trials is necessary to draw longer-term conclusions.

Acknowledgements

References

[1] Yanishlieva, N. V. and Marinova, E. M. 2001. Stabilisation of edible oils with natural antioxidants. European Journal of Lipid Science and Technology, 103 (11): 752-767.

[2] Chang, S. K., Alasalvar, C., Shahidi, F. 2019. Superfruits: Phytochemicals, antioxidant efficacies, and health effects–A comprehensive review. Critical Reviews in Food Science and Nutrition, 59 (10): 1580-1604.

[3] M. B. Lalit, A. Kar, S. Satya and N. N. Satya "Kinetics of Colour Change of Bamboo Shoot Slices during Microwave Drying," International Journal of Food Science & Technology,Vol.46, No. 4, 2011, pp. 827-833.

[4] Klimczak, I. and Gliszczyńska-Świgło, A. 2017. Green tea extract as an anti-browning agent for cloudy apple juice. Journal of the Science of Food and Agriculture. 97(5): 1420-1426.

[5] Singleton, V. L. and Rossi, J. A. 1965. Colometry of total phenolics with phosphomolybdic phosphotungstic acid „reagents", American Journal of Enology and Viticulture. 16, 144-158.

[6] Benzie, I.I.F. and Strain, J.J. 1996. The ferric reducing ability of plasma (FRAP) as a measuring of "antioxidant power": The FRAP assay. Annal. Biochem. 239(1): 70-76.

IMPACT OF ASCORBIC ACID ON THE LEVEL OF ANTHOCYANINS AND POLYPHENOLS IN ARONIA JUICE DURING HEAT TREATMENT

Meriem Serine Hamaidia[1], Mónika Máté[1], Judit Friedrich-Ivanics[1], Nikolett Kalamár[1], Márta Ladányi[2,] Lilla Szalóki-Dorkó[1]

[1]Department of Fruits and Vegetables Processing Technology, Institute of Food Science and Technology, Hungarian University of Agriculture and Life Sciences, H-1118, Budapest, Villányi út 29-43, Hungary

[2]Department of Applied Statistics, Institute of Mathematics and Basic Science, Hungarian University of Agriculture and Life Sciences, Villányi út 29-43, 1118 Budapest, Hungary
e-mail: hamaidiameriemserine@gmail.com

Abstract

This study examines the effects of 1% ascorbic acid and varying heat treatments (60°C and 80°C) on total anthocyanin content (TAC), total phenolic content (TPC), and antioxidant capacity (FRAP) in Aronia juice. The results show that ascorbic acid and temperature had minimal impact on total anthocyanin content (TAC), with no significant differences observed between the 0% and 1% ascorbic acid treatments at both 60°C and 80°C (p>0.05). Meanwhile the TPC results show that adding 1% ascorbic acid significantly increased total phenolic content (TPC) at both 60°C and 80°C, with the highest values at 10 minutes for 60°C (4142.63±85.77 GAE mg/L) and 30 minutes for 80°C (3660±229.19 GAE mg/L), while 60°C consistently yielded higher TPC than 80°C. Additionally, the antioxidant capacity values indicate that 1% ascorbic acid significantly increased (FRAP) values compared to 0% at both 60°C and 80°C, with the highest value at 60 minutes (12.865.69±527.08 mg/L at 60°C), while (FRAP) values at 80°C were significantly lower than those at 60°C. In conclusion, while ascorbic acid and temperature had minimal effects on total anthocyanin content (TAC), the addition of 1% ascorbic acid significantly boosted total phenolic content (TPC) and antioxidant capacity (FRAP), particularly at 60°C. These findings highlight the potential of ascorbic acid in enhancing the antioxidant properties of Aronia juice during heat treatment.

Introduction

Black chokeberry (*Aronia melanocarpa* (Michx.) Elliott), native to North America and now cultivated in Eastern Europe, is not commonly consumed as a table fruit due to its astringent taste but is widely used in food production like jams, wines, dietary supplements, and particularly for juices and natural food coloring due to its deep violet color. Black Chokeberry and its processed products are highly regarded for their abundance of bioactive compounds that provide exceptional biological and nutritional value such as polyphenols such as anthocyanins, procyanidins, phenolic acids, flavonols, and flavanols, compared to other dark berries [1-2]. Studies results have shown that different juice processing conditions like heat treatment, have significant effects on the content of polyphenols and the antioxidant activity, also on other parameters in black chokeberry [3-4]. Thus, current research is exploring the use of external antioxidants to preserve native compounds in food products [5]. Recently, there has been considerable focus on incorporating natural and synthetic antioxidants into food products to delay or prevent the autoxidation of other compounds and neutralize free radicals. This approach is widely applicable in the food processing industry to inhibit oxidation and improve flavor, aroma, and color [6-7]. Ascorbic acid (Vitamin C), a fundamental exogenous vitamin and a free radical scavenger, is widely recognized for its powerful antioxidant properties [8]. Despite ascorbic acid's recognized antioxidant properties, its effectiveness in safeguarding other bioactive compounds during food processing remains relatively unexplored. Therefore, the aim

of this study was to investigate the impact of 1% of ascorbic acid on the phenolic content and the antioxidant levels of Aronia juice subjected to heat treatment (60°C and 80°C) over different durations (5, 10, 30, 60, 120 min).

Experimental

In the extraction process, the first step involves grinding the Aronia berries to break them down into smaller pieces. The resulted mash was placed in the juice presser. Then, the 1% of Ascorbic acid was added to the Aronia juice samples, which then was placed in the water bath for the heat under controlled different temperature (60°C and 80°C) at different durations (5, 10, 30, 60, 120 min). After that, the tubes were immediately cooled in ice water to stop further thermal degradation. The investigation included quantification of Toal Anthocyanins Content (TAC) as described in the Association of Official Foods 2023, 12, 3639 Agricultural Chemists (AOAC) Method 2005:07 [9], Total Phenolic Content (TPC) by Singleton and Rossi method [10], and the Antioxidant capacity by Benzie and Strain method [11].

Results and Discussion

Total Anthocyanins content (TAC)

The results indicate that there is no significant difference between the samples treated with 0% of ascorbic acid and the ones with 1% at 60°C except at 120min (63.34 ± 3.08 vs 54.72 ± 2.70 mg/L, respectively); similarly at 80°C, there was no significant difference between the samples treated with 0% and 1% of ascorbic acid ($p > 0.05$), except at 5 and 60 min (66.18 ± 7.67 vs 43.47 ± 9.55 and 39.41 ± 4.29 vs 61.34 ± 2.11 mg/L, respectively). Furthermore, no significant difference was observed between the TAC values of the 0% samples treated at 60°C and 80°C ($p > 0.05$), except at 120min (63.34 ± 3.08 vs 44.09 ± 4.01 mg/L, respectively). Similary, no significant difference was observed between the TAC values of the 1% samples treated at 60°C and 80°C ($p > 0.05$), except at 30 min (77.48 ± 7.44 vs 54.66 ± 7.29 mg/L, respectively). In conclusion, ascorbic acid had insignificant effect on total antioxidant content (TAC, ANOVA: $F_{(1;40)} = 0.04$, $p = 0.84$), and the effect of temperature was significant ($F_{(1;40)} = 16.78$, $p < 0.01$), though both results were moderated by the highly significant interaction effect of ascorbic acid treatment and temperature ($F_{(1;40)} = 7.50$, $p < 0.001$). This suggests that ascorbic acid and temperature has limited effect on TAC under the conditions tested.
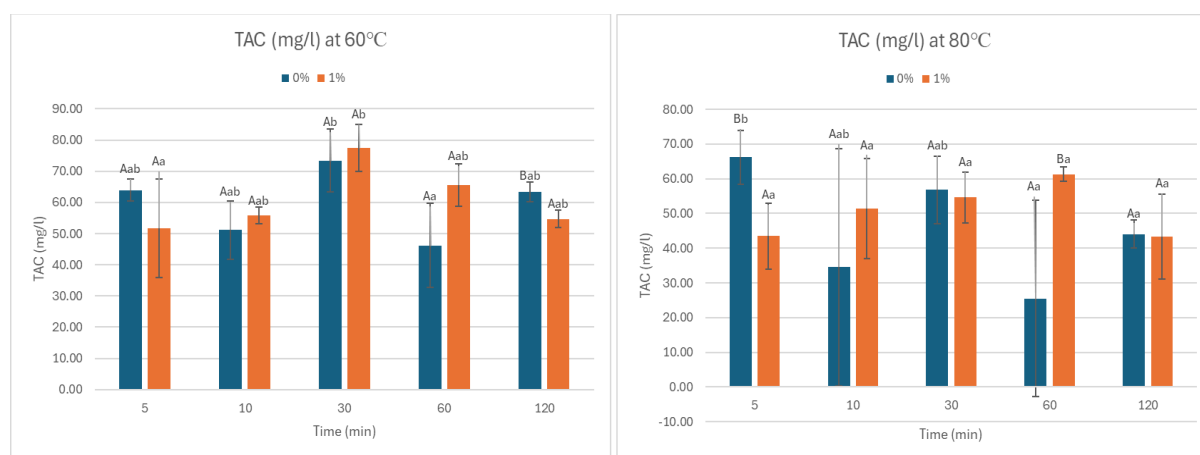
Figure1. Total Anthocyanins Content (TAC), Different letters denote significantly different groups; lower case: comparison of time levels at fixed temperature; upper case: comparison of samples treated with 1% ascorbic acid with control at fixed time level (Tukey's, $p < 0.05$). Error bars = Standard deviation

Total Phenolic Content (TPC)

The results show that TPC values in samples treated with 1% ascorbic acid are significantly higher than those treated with 0%, at 5, 10, and 30 minutes at 60°C, with the highest value recorded at 10 minutes (4142.63±85.77 GAE mg/L); and similarly, at 80°C, the 1% ascorbic acid samples had elevated TPC levels significantly at 5, 10, 30, and 60 minutes, with a peak at 30 minutes (3660±229.19 GAE mg/L) (ANOVA $F_{(1;40)}$=89.67, $p<0.001$). Additionally, no significant difference was observed between the TPC values of the 0% samples treated at 60°C and 80°C ($p>0.05$), except at 30 minutes (2553.46±8.99 vs 3002.74±226.92 GAE mg/L, respectively). However, in the 1% ascorbic acid samples, the TPC values at 80°C were significantly lower than those at 60°C ($p>0.05$), except at 60 minutes of treatment (3444.18±239.04 vs 3789.48±106 GAE mg/L, respectively). In conclusion, adding 1% ascorbic acid consistently boosted total phenolic content (TPC), particularly at shorter times. The best results were observed at 60°C, which yielded higher TPC than 80°C. Thus, optimizing both factors temperature ($F_{1;40}$=18.80; $p<0.001$) and time ($F_{(4;40)}$=10.96; $p<0.001$) is essential for effective phenolic extraction.
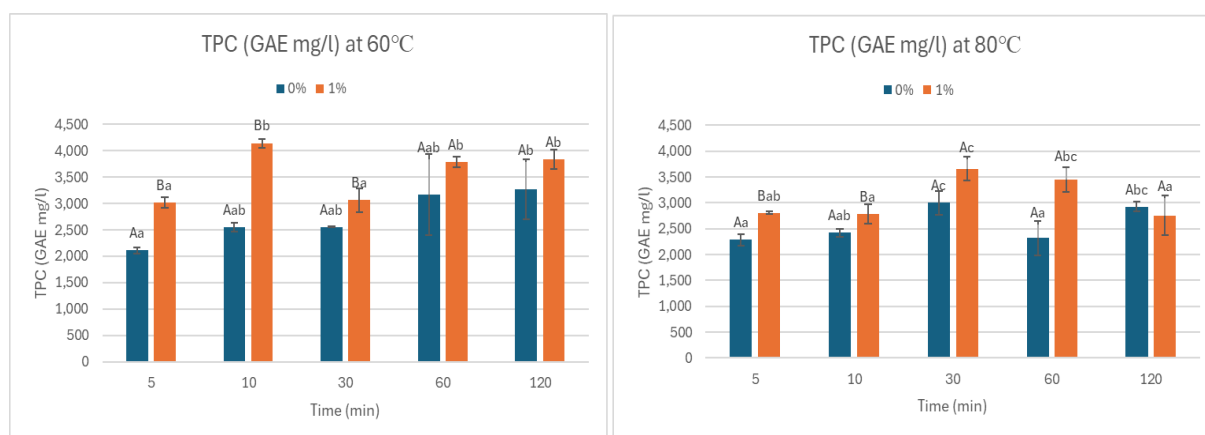
Figure2. Total Phenolic Content (TPC), Different letters denote significantly different groups; lower case: comparison of time levels at fixed temperature; upper case: comparison of samples treated with 1% ascorbic acid with control at fixed time level (Tukey's, $p<0.05$). Error bars = Standard deviation

Antioxidant capacity by Ferric Reducing Ability of Plasma (FRAP)

The results indicate that, the 1% concentration consistently showed significantly higher FRAP values than 0% at both temperatures, at 5, 10, 30 and 60 minutes at 60°C, with the highest value at 60 minutes being 12865.69±527.08 mg/L compared to 8312.69±749.43 mg/L for 0%, meanwhile, at 80°C, the 1% TPC values were significantly higher than the 0% treated samples, except at 120 minutes (ANOVA $F_{(1;40)}$=181.65, $p<0.001$). Furthermore, no significant difference was observed between the FRAP values of the 0% samples treated at 60°C and 80°C ($p>0.05$). However, in the 1% ascorbic acid samples, the FRAP values at 80°C were significantly lower than those at 60°C ($p<0.05$). Statistical analysis confirmed significant differences between concentrations across most time points, highlighting the impact of concentration of ascorbic acid, temperature ($F_{1;40}$=217.58; $p<0.001$), and time ($F_{(4;40)}$=14.32; $p<0.001$) on antioxidant activity of the Aronia juice, with optimal results at 60 minutes at 60°C.
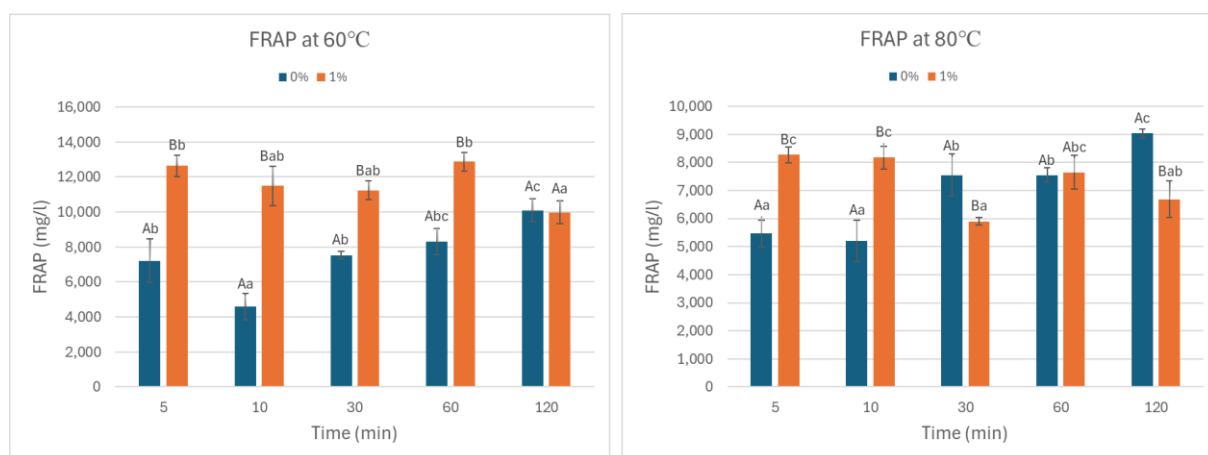
Figure3. Ferric Reducing Ability of Plasma (FRAP), Different letters denote significantly different groups; lower case: comparison of time levels at fixed temperature; upper case: comparison of samples treated with 1% ascorbic acid with control at fixed time level (Tukey's, $p < 0.05$). Error bars = Standard deviation

Conclusion

In conclusion, the study highlights the significant influence of ascorbic acid concentration, temperature, and heat treatment time on the total anthocyanin content (TAC), total phenolic content (TPC), and antioxidant capacity (FRAP) in Aronia juice. While ascorbic acid had a minimal impact on TAC, it notably enhanced TPC and FRAP values, especially at 60°C, with shorter extraction times yielding the best results. The 1% ascorbic acid treatment consistently outperformed the control, demonstrating its effectiveness in boosting phenolic content and antioxidant activity.

References

[1] M. Oziembłowski. M. Trenka, M. Czaplicka, D. Maksimowski, A. Nawirska-Olszańska. Appl. Sci. (2022) 12, 7008.

[2] B. Kapci, E. Neradová, H. Čížková, M. Voldřich, A. Rajchl, E. Capanoglu. Journal of food and nutrition research. (2013) 52(4), 219-229.

[3] Z. Kobus, R. Nadulski, K. Wilczyński, M. Kozak, T. Guz, L. Rydzak. PLOS ONE. (2019). 14(7): e021 9585.

[4] K. Wilkes, L. Howard, C. Brownmiller, L. Ronald. Journal of Agricultural and Food Chemistry. (2016). 62(18): 4018–25.

[5] L. Pedrouso, María, J.M. Lorenzo, D. Franco. Antioxidants. 2022. 11(9): 1825.

[6] S. C. Lourenço, M. Moldão-Martins, V.D. Alves. Molecules. 2019. 24(22): 4132.

[7] A. Uzombah, Thomas. In Natural Food Additives. (2022) 328.

[8] A. Gęgotek, E. Skrzydlewska. Vitamins and Hormones. 2023. Elsevier, 247–70.

[9] J. Lee, R. Durst, R. Wrolstad. In Official Methods of Analysis of AOAC International; AOAC International: Rockville, MD, USA. (2005). pp. 37–39.

[10] VL. Singleton, J.A. Rossi. Am. J. Enol. Vitic. (1965). 16, 144.

[11] I.F.F. Benzie, J.J. Strain, Methods in Enzymology. 1999. 299, 15-27.

NOVEL FLUORESCENT-LABELED ESTRADIOL DERIVATIVES

Tamás Hlogyik[1], Máté Vágvölgyi[1], Labos Péter[2], Noémi Bózsity[2], István Zupkó[2], Attila Hunyadi[1], Erzsébet Mernyák[1]

[1]*Department of Pharmacognosy, University of Szeged, Szeged H-6720, Hungary*
[2]*Department of Pharmacodynamics and Biopharmacy, Szeged H-6720, Hungary*
e-mail: hlogyik@chem.u-szeged.hu

Abstract

The overproduction of the female sex hormone 17β-estradiol (E2) can lead to various hormone-dependent diseases, including tumors. Due to its biological activity in reproductive tissues and the nervous system, understanding its mechanisms of action and protein interactions is of significant importance. Fluorescent labeling methods are becoming increasingly favored over radiochemical techniques for making E2 detectable, as they offer more environmentally friendly alternatives. We published recently E2–BODIPY conjugates, labeled at the phenolic hydroxy function of the steroid, that retained estrogenic activity despite modifying the estradiol structure. Here we explored certain organic dyes suitable for fluorescent labeling, focusing on compounds, which provide tunable optical properties, high photostability, and physiological stability. A rhodamine, a rosamine and an *aza*-BODIPY dye were conjugated to an estradiol derivative bearing a four carbon-long linker at its 3-hydroxy group. We emphasized green chemistry approaches, including supercritical fluid chromatography, one-pot reactions, and microwave-assisted methods.

Introduction

The overproduction of the female hormone 17β-estradiol (E2) can lead to the development of various hormone-dependent diseases, including tumors. It can exert its biological activity in both reproductive tissues and the nervous system, making it crucial to understand the mechanisms of action, investigate its interactions with proteins, and uncover biological behavior. Nowadays, radioisotope labeling techniques are increasingly being replaced by more environmentally friendly methods based on fluorescence detection. However, several criteria should be considered when choosing the right fluorescent dye. The ideal candidates should have tunable absorption/emission wavelengths, high photostability, high absorption coefficient, and physiological stability [1]. BODIPY (4,4-difluoro-4-bora-3a,4a-diaza-*s*-indacene) dyes meet the above requirements, and possess easily modifiable structure. Recently, we synthesized an E2–BODIPY conjugate, where the dye and the estrogen are linked *via* their phenolic hydroxy groups through an ether bond, connected by a 4-carbon linker. Despite modifying the aromatic –OH group of estradiol (Figure 1.), the labeled hormone retained its estrogenic activity [2].
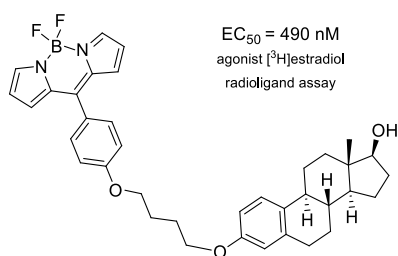
Figure 1. Structure of the estrogenic BODIPY-labeled E2 derivative [2]

Rhodamines and rosamines, which belong to the xanthene dye group, possess excellent photophysical properties and are widely used in imaging techniques [3]. The advantage of rosamines over rhodamines is the lack of a carboxyl group at the C-2', thus they do not form non-fluorescent lactone derivatives. Rhodamines, due to their favorable and pH-dependent optical properties [4], are known as pH sensors, since their spirolactone form is non-fluorescent [5].

In recent years, *aza*-BODIPY-based red-emitting fluorophores have received special attention, as these compounds have additional advantageous properties. As IR-emitting dyes, they possess deeper tissue penetration, making their utilization less invasive and facilitating special detection [6].

The development and application of green chemical synthetic methods is a highly important task nowadays. Utilization of one-pot processes is solvent- and energy-efficient. Microwave irradiation saves a considerable amount of energy and reduces the application of harmful solvents. The latter can be achieved by using supercritical chromatography as well [7].

Based on our recent results and the favorable application opportunities of the above-mentioned dyes, we aimed to label E2 with three different fluorophores by the same strategy. A rosamine, a rhodamine, and an *aza*-BODIPY were synthesized and connected to E2 through a C4-alkyl linker with ether or triazole coupling moieties. We placed great emphasis on applying green chemical synthetic protocols. We planned to perform the compound purifications by high-performance supercritical liquid chromatography.

Results and Discussion
Firstly, the starting materials were prepared. We introduced a C4-alkyl linker onto the phenolic hydroxy group of E2 (compound **1**) *via* Williamson ether synthesis. The condensed ring structure of the rosamine dye was constructed by reacting 4-(diethylamino)salicyl aldehyde (**2**) with 3-(dimethylamino)phenol (**3**) under microwave irradiation (Figure 2.), followed by purification by supercritical liquid chromatography (Figure 3.). The resulting dye (**4**) was then conjugated to the E2 derivative *via* subsequent ether synthesis.
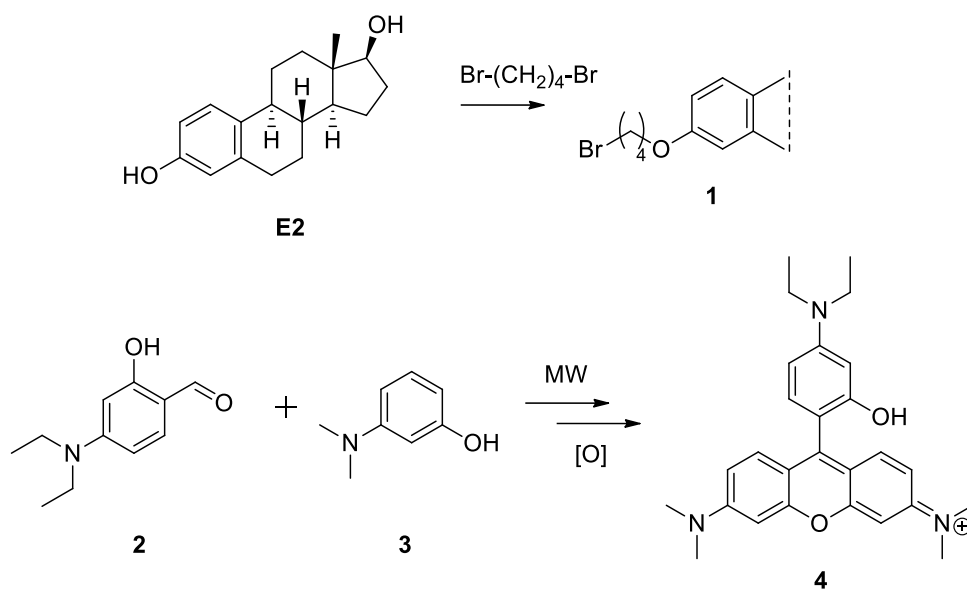
Figure 2. Synthesis of the starting steroid (**1**) and the rosamine dye (**4**)
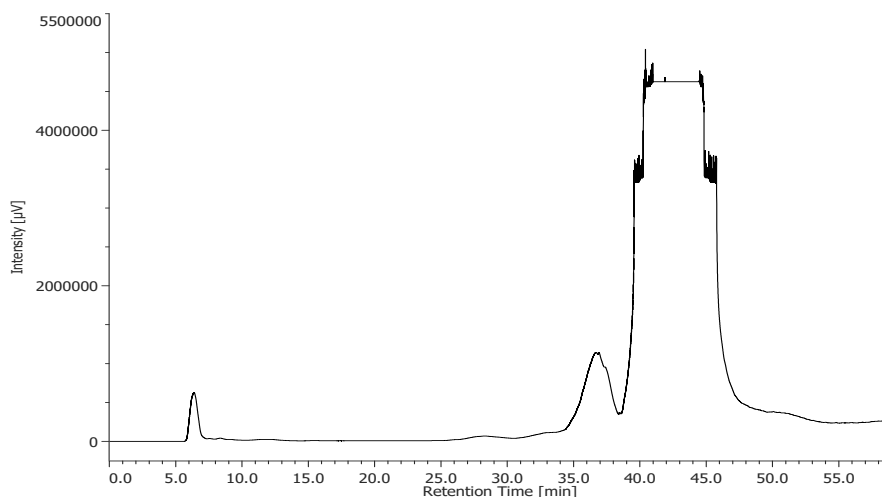
Figure 3. Chromatogram of compound **4** after preparative SFC purification

For further conjugations, we subjected E2 bearing the bromoalkyl linker (**1**) to a substitution with sodium azide, in order to obtain a starting azide (**5**) for copper-catalyzed azide-alkyne cycloaddition (CuAAC). Terminal alkyne counterparts were synthesized starting from the rhodamine dye (**6**) or the tetraphenyl-*aza*-BODIPY carboxylic acid derivative (**7**), previously synthesized by our research group, using propargylamine as a reagent (Figure 4.).
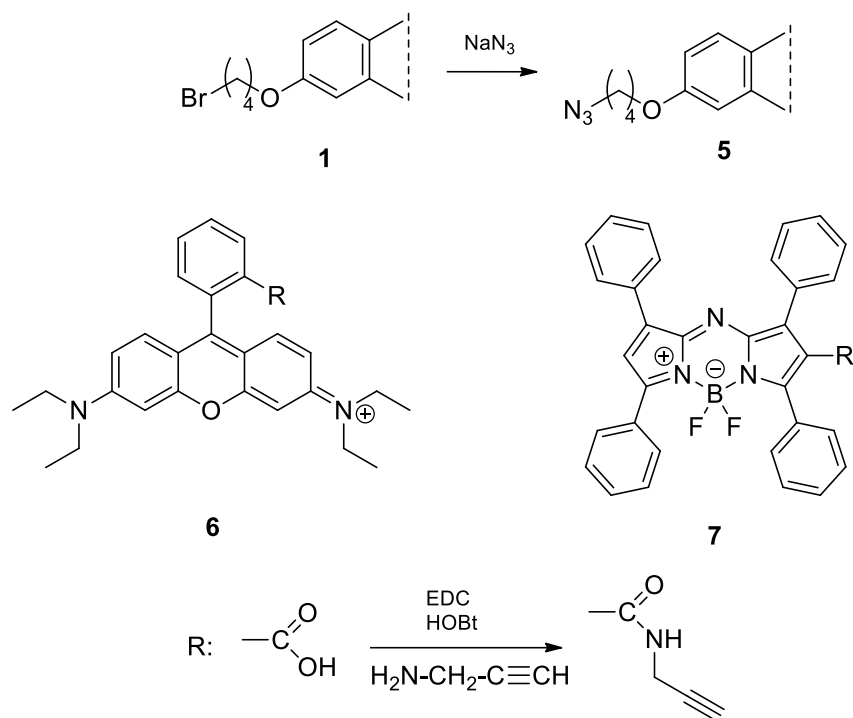
Figure 4. Synthesis of the azide (**5**) and alkyne (**6**, **7**) coupling partners

The newly synthesized labeled E2 derivatives were subjected to determination of their estrogenic activity by utilizing a luciferase reporter assay in T47D cells. The investigations are still in progress, however compound **8** showed highly promising results, with estrogenic activity in the nanomolar range (EC_{50} = 86.36 nM) (Figure 5.).
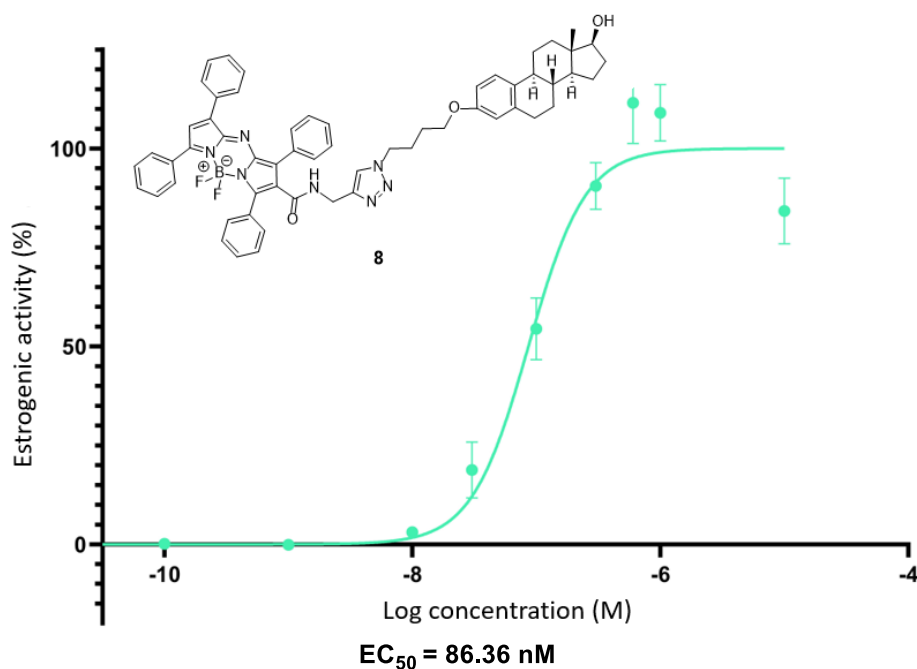
Figure 5. Estrogenic activity of the *aza*-BODIPY labeled E2 derivative **8**

Conclusion

We synthesized novel fluorescent labeled estradiol conjugates. The syntheses were controlled to comply with the principles of green chemistry. Owing to its IR-emitting and estrogenic nature, the newly synthesized *aza*-BODIPY conjugate might be suitable for studying estrogen uptake or transport in cells, as well as for examining estrogen-binding proteins.

Acknowledgements

References

[1] Kaur, P., & Singh, K., J. Mater. Chem. C, 7 (2019) 11361-11405.
[2] Perina, M.; Börzsei, R.; Ágoston, H.; Hlogyik, T.; Poór, M.; Rigó, R.; Özvegy-Lacka, Cs.; Batta, Gy.; Hetényi, Cs.; Vojácková, V.; Jorda, R.; Mernyák, E. Eur. J. Pharm. Sci., 199 (2024) 106813.
[3] Arambula, C.; Rodrigues, J.;Jae Koh, J.; Woydziak, Z. J. Org. Chem. 86 (2021) 17856–17865
[4] Shuang, Z.; Xiaosheng, L.; Yves, S. K.; Heejeong, K.; Jingyun, W.; Xiaojun, P.; Haidong, L.; Juyoung, Y. Chem. Soc. Rev., 52 (2023) 5607-5651.
[5] Srivastava, P.; Fürstenwerth, P. C.; Witte, J. F.; & Resch-Genger, U. New J. Chem., 45 (2021) 13755-13762.
[6] Loaeza, L.; Corona-Sánchez, R.; Castro, G.; Romero-Ávila, M.; Santillan, R.; Maraval, V.; Chauvin, R.; Farfán, N. Tetrahedron, 83 (2021) 131983.
[7] Welch, C. J.; Leonard, W. R.; DaSilva, J. O.; Biba, M.; Albaneze-Walker, J.; Henderson, D. W.; Laing, B.; Mathre, D. J. LC GC Europe, 18 (2005) 264-272.

EFFECTIVE DECOMPOSITION OF LIGNOCELLULOSE BY ANAEROBIC FUNGI

Annabella Juhász-Erdélyi[1], Etelka Kovács[1], Roland Wirth[2], Gergely Maróti[2], Zoltán Bagi[1,2], Kornél L. Kovács[1,2]

[1]Department of Biotechnology and Microbiology, Faculty of Science and Informatics, University of Szeged;
[2]Institute of Plant Biology, HUN-REN Biological Research Centre, Szeged

Abstract

Starch and cellulose are the primary energy sources of herbivores. These polymeric carbohydrates are decomposed by enzymes and microorganisms in the rumen. To promote the complex process, the microbes and enzymes involved need to be comprehended in details (1). Similar microbial community degrades the cellulose-rich biomass in biogas reactors for efficient and sustainable renewable energy generation. Methane is an undesirable by-product in the rumen, whereas it is the main target commodity in the biogas technology. Dissecting the details of the metabolic pathways in the two systems can lead to the identification of the regulatory elements governing the bioconversion of lignocellulosic biomass (2). An important difference between the ruminal and biogas microbial communities is the high abundance of anaerobic fungi (AF) in the rumen and their scarce incidence in the biogas producing community. Therefore, we intend to explore the potential beneficial interactions between AF and methanogens to augment biogas/biomethane production.

Introduction

Anaerobic digestion (AD) of lignocellulosic biomass is cost-effective but usually low yield strategy for biomethane production, which provides great potential to convert biomass into renewable energy. The recalcitrance of lignocellulosic biomass makes it resistant to microbial hydrolysis, which reduces the bioconversion efficiency of organic matter into biogas (3). Anaerobic fungi (AF) from the phylum Neocallimastigomycota are natural inhabitants of the digestive tract of herbivorous animals. AF decompose a large share of the ingested forage, i.e. around 30%. The mobile AF zoospores anchor themselves to the plant material and crack the fibres mechanically by growth and expansion of their rhizoids or bulbous holdfasts (4). Although it is rather cumbersome to work with anaerobic fungi, they can break down plant fibers more efficiently and generate suitable sugar rich substrate for the bioconversion reactions. Their synthrophic cooperation with methanogens is more effective than the more complex metabolic network developing between bacteria and methanogens (5,6). From a scientific point of view, the synthrophic interaction between the Eukaryote AF and the methanogens, which are members of the Archaea kingdom, is particularly intriguing.

Materials and Methods

A 500mL blue cap ISO glass vessels were filled with 350 mL of Medium C, which is favored by both anaerobic fungi and methanogens (7). The vessels were equipped with a pre-prepared, specifically designed double bag structure. The bags were made of inert polymeric textile of about 100 μm pore size, which allowed the trafficking of AF, bacteria and methanogenic archaea through the barrier easily. Both bags contained sterile wheat straw particles of about 2 mm in length. The reaction vessel was supplemented with 20 g of fresh rumen contents, comprising the particulate fraction and were shaken at 75rpm at 39°C with 5 g of glass beads to ensure that the fungal/bacterial/methanogen associations were adequately separated from the inoculum particles. The microbes capable to participate in the straw degradation and digestion

were thus separated from the biofilm forming particles present in the rumen content. The microbes thus inflicted to planktonic lifestyle migrated through the bag wall barrier towards the straw particles driven by the chemical gradients of chemical attractant gradient of the fresh wheat straw (8). This way the lignocellulose degrading zoospore-bacteria teams were enriched in the inner plastic bag for further analysis. Samples were taken from both the outer and inner bags after 24, 48, and 72 hours. During incubation, the pH was continuously monitored to avoid acidification. Methane production was determined using gas chromatography (9). High-performance liquid chromatography (HPLC) provided information about the volatile fatty acid productions (9). Samples were also subjected to scanning electron microscopy (SEM) in order to visualize the microbial communities present on the internal straw biofilms. The abundant members of the developed biofilms we identified by metagenomic sequencing.

Results

The pH remained in the range of 6.6-6.8 maintaining a suitable environment for all members of the consortia, and pH induced inactivation of diminishing activity of the microbial community was not observed. Artificial growth control of any taxa in the system was not executed by antibiotics. The complex microbial community was capable of effectively degrade cellulose under these conditions. The degradation/fermentation products composed primarily of volatile fatty acids (Acetic acid: 1.8-3.9 g/L, propionic acid: 0.3-0.9 g/L). Continuous gas production, comprising primarily methane and carbon dioxide was observed indicating an intimate and effective syntrophic interaction between the AF and methanogens. Scanning electron microscopic images further confirmed the presence of anaerobic fungi and bacteria, as well as their temporal changes (Fig. 1.). Further, more focused studies will disclose the spatial and taxonomical microbial niche around the anaerobic fungi responsible for the major contribution of these poorly characterized microbes to the overall carbon cycles of biomass on Earth.
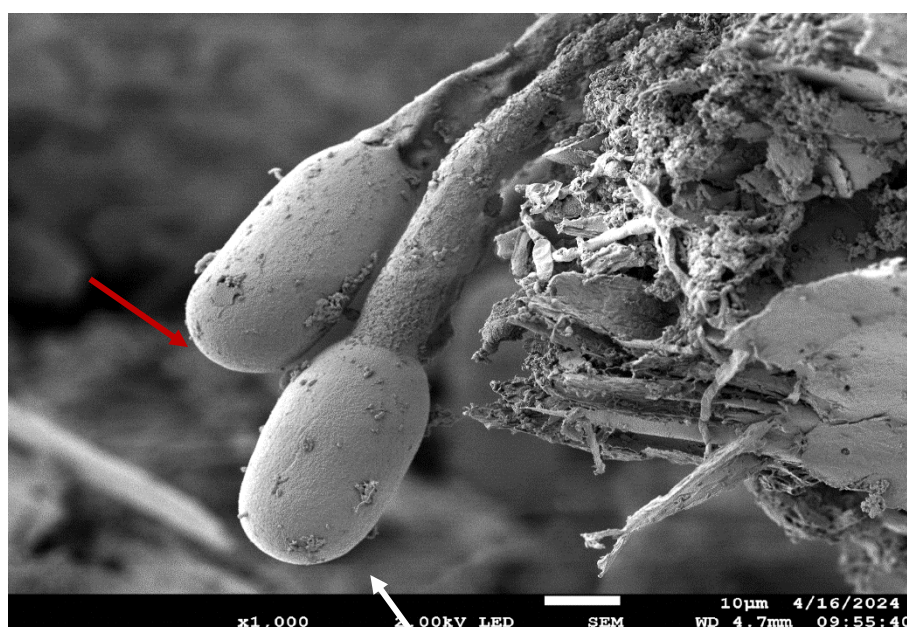
Figure 1. SEM image of the microbial community on the surface of a straw particle after 72 hours of enrichment and colonization. The anaerobic fungi are marked with red arrows, the accompanying bacteria/archaea are indicated with white arrows in the enlarged insert.

Acknowledgements

References

1. Hua, D., Hendriks, W. H., Xiong, B., Pellikaan, W. F. Starch and cellulose degradation in the rumen and applications of metagenomics on ruminal microorganisms. (2022). Animals, 12 (21):3020. doi: 10.3390/ani12213020

2. Chettri1, D., Verma, A. K., Ghosh, S., Verma, A. K. Biogas from lignocellulosic feedstock: current status and challenges. (2024). Env. Sci. and Pollution Res., 31:39037–39062. https://doi.org/10.1007/s11356-023-29805-x

3. Bhat, M. K. Cellulases and related enzymes in biotechnology. (2000). Biotechnol. Adv., 18 (5):355- 383. doi: 10.1016/S0734-9750 (00) 00041-0

4. Bauchop, T., Mountfort, D.O. Cellulose fermentation by a rumen anaerobic fungus in both the absence and the presence of rumen methanogens. (1981). Appl. Environ. Microbiol., 42 (6):1103-1110.

5. Joblin, K.N., Campbell, G.P., Richardson, A.J. et al. Fermentation of barley straw by anaerobic rumen bacteria and fungi in axenic culture and in co-culture with methanogens. (1989). Lett. Appl. Microbiol. 9:195–197.

6. Jin, W., Cheng, Y-F., Mao, S-Y., Zhu, W-Y. Isolation of natural cultures of anaerobic fungi and indigenously associated methanogens from herbivores and their bioconversion of lignocellulosic materials to methane. (2011). Bioresour. Technol., 102 (17):7925-7931. 10.1016/j.biortech.2011.06.026

7. Peng X, Swift C. L., Theodorou M. K., O'Malley M. A. Methods for Genomic Characterization and Maintenance of Anaerobic Fungi (2018) Methods in Molecular Biology,1775.

8. Wubah D. A., Kim D. S.H. Chemoattraction of anaerobic ruminal fungi zoospores to selected phenolic acids (1996) Microbiol. Res. 151, 257 – 262

9. Kovács E.,Wirth R.,Maróti G.,Bagi Z.,Rákhely G., Kovács K.L. Biogas Production from Protein-Rich Biomass: Fed-Batch Anaerobic Fermentation of Casein and of Pig Blood and Associated Changes in Microbial Community Composition (2013) PlosOne https://doi.org/10.1371/journal.pone.0077265

NATURAL DEEP EUTECTIC SOLVENTS (NADES) AS A GREEN STRATEGY FOR THE EXTRACTION OF ROSMARINIC ACID FROM SOME LAMIACEAE SPECIES

Tatjana Jurić, Ružica Ždero Pavlović, Denis Uka, Boris Popović

Chemistry Laboratory, Department of Field and Vegetable Crops, Faculty of Agriculture, University of Novi Sad, 21000 Novi Sad, Trg Dositeja Obradovića 8, Serbia
e-mail: tatjana.juric@polj.uns.ac.rs

Abstract
The plants from Lamiaceae family are widely distributed and used in food, cosmetics, and as therapeutics in medicine. Many phenolic compounds known for their broad spectrum of biological activities are found in Lamiaceae species, particularly rosmarinic acid (RA). Growing interest in novel green solvents for extracting bioactives from plants is driven by a shift towards minimizing harmful organic solvents. Natural deep eutectic solvents (NADES) are a promising option, composed of naturally occurring substances that form a transparent liquid when combined at specific molar ratios.

The aim of this study was to explore the effectiveness of choline chloride-based natural deep eutectic solvents (NADES) for the extraction of RA from *Melissa officinalis* and *Thymus serpyllum*, followed by HPLC-PDA analysis for quantification and assessing antioxidant activity through DPPH, FRAP, and ORAC methods. Comparisons were made with conventional (70% ethanol) extracts.

Four NADES were prepared via microwave irradiation, combining choline chloride with citric acid, 1,2-propanediol, urea, or fructose at a 1:1 molar ratio, with the addition of 20% water (w/w). The extraction process involved sonication of plant material (solid-liquid ratio 1:10 (g/mL)) for two hours at 40 °C.

HPLC-PDA analysis revealed that RA was the main compound in all extracts. Overall, NADES yield similar or greater amounts of RA than 70% ethanol ($p \leq 0.05$; Tukey test). Specifically, NADES extracted nearly 25% more RA from *M. officinalis* than ethanol. For *T. serpyllum*, 50% higher RA yields were achieved using NADES containing citric acid and 1,2-propanediol. Additionally, NADES extracts demonstrated superior antioxidant activity in reducing ferric ions and neutralizing DPPH radicals compared to ethanol ($p \leq 0.05$), except in the ORAC assay. Our results confirm the potential of NADES as effective green solvents for the extraction of bioactive compounds from plants. Future work will focus on optimizing the extraction process to maximize RA yield from other Lamiaceae species.

INTERPRETATION OF RETENTION BEHAVIOR OF *s*-TRIAZINE DERIVATIVES IN RP-UHPLC SYSTEM FROM THE ASPECT OF REACTIVITY DESCRIPTORS

Milica Karadžić Banjac[1], **Strahinja Kovačević[1]**, **Jasmina Anojčić[2]**, **Benjamin Salaković[1]**, **Sanja Podunavac-Kuzmanović[1]**, **Lidija Jevrić[1]**

[1]Department of Applied and Engineering Chemistry, Faculty of Technology Novi Sad, University of Novi Sad, Bulevar cara Lazara 1, 21000 Novi Sad, Serbia
[2]Department of Chemistry, Biochemistry and Environmental Protection, Faculty of Sciences, University of Novi Sad, Trg Dositeja Obradovića 3, 21000 Novi Sad, Serbia
e-mail: mkaradza@uns.ac.rs

Abstract
The present study deals with the interpretation of the retention data of a series of *s*-triazine derivatives from the aspect of reactivity descriptors, including highest occupied molecular orbitals (HOMO), lowest unoccupied molecular orbitals (LUMO), the difference between HOMO and LUMO energies (HOMO-LUMO gap – Egap), chemical potential (μ) and electrophilicity index (ω). The retention behavior of the studied compounds was determined by using RP-UHPLC system with phenyl column and methanol/water mobile phase and it was expressed as capacity factor ($logk_0$) obtained based on extrapolation of the linear dependence between the volume fraction of modifier in the mobile phase (φ) and capacity factor ($logk$). The relationships between the retention parameters and reactivity descriptors were examined by univariate linear approach. Statistical characteristics of the resulting relationships provided an insight into the influence of the molecular characteristics on the retention behavior of the studied compounds in the applied chromatographic system. The established linear quantitative structure-retention relationships (QSRRs) can be considered to be preliminary ones, taking into account the limited number of compounds, however they could be significant guidelines for further detailed examination of the retention mechanisms.

Introduction
The application of *s*-triazine derivatives in agriculture is well-known. Some of the triazine derivatives are used as effective herbicides and fungicides [1]. Considering the fact that some of the triazine derivatives are persistent in environment, their efficient analysis is quite important task.
Chromatographic analysis provides an efficient, fast and precise determination of many compounds. One of the aspects of application of chromatographic approaches is examination of certain molecular properties that can be estimated based on their retention behavior in particular chromatographic system. Quantitative structure-retention relationship (QSRR) approach is a chemometric approach that integrates the molecular properties and retention behavior in the form of mathematical models [2]. QSRR approach is based on linear or non-linear approaches. These linear or non-linear relationships can correlate the retention behavior with various types of molecular descriptors, including physicochemical, topological, biological, etc [3].
The present study is based on univariate linear QSRR approach for examination of the influence of some reactivity descriptors, including highest occupied molecular orbitals (HOMO), lowest unoccupied molecular orbitals (LUMO), the difference between HOMO and LUMO energies (HOMO-LUMO gap – Egap), chemical potential (μ) and electrophilicity index (ω), on the retention behavior of a series of *s*-triazine derivatives in reversed-phase ultra high performance liquid chromatography system (RP-UHPLC) with phenyl column and methanol/water mobile

phase. The aim of the present study is contribution to the understanding of retention mechanisms of *s*-triazines in RP-UHPLC system from the aspect of the reactivity descriptors.

Experimental

The molecular structures of the series of the studied *s*-triazines are presented in Figure 1. The studied molecules are based on 6-chloro-1,3,5-triazine structure with acyclic and cyclic substituents. The compounds were synthesized at the Faculty of Technology and Metallurgy, University of Belgrade, following the procedures described in literature [4].
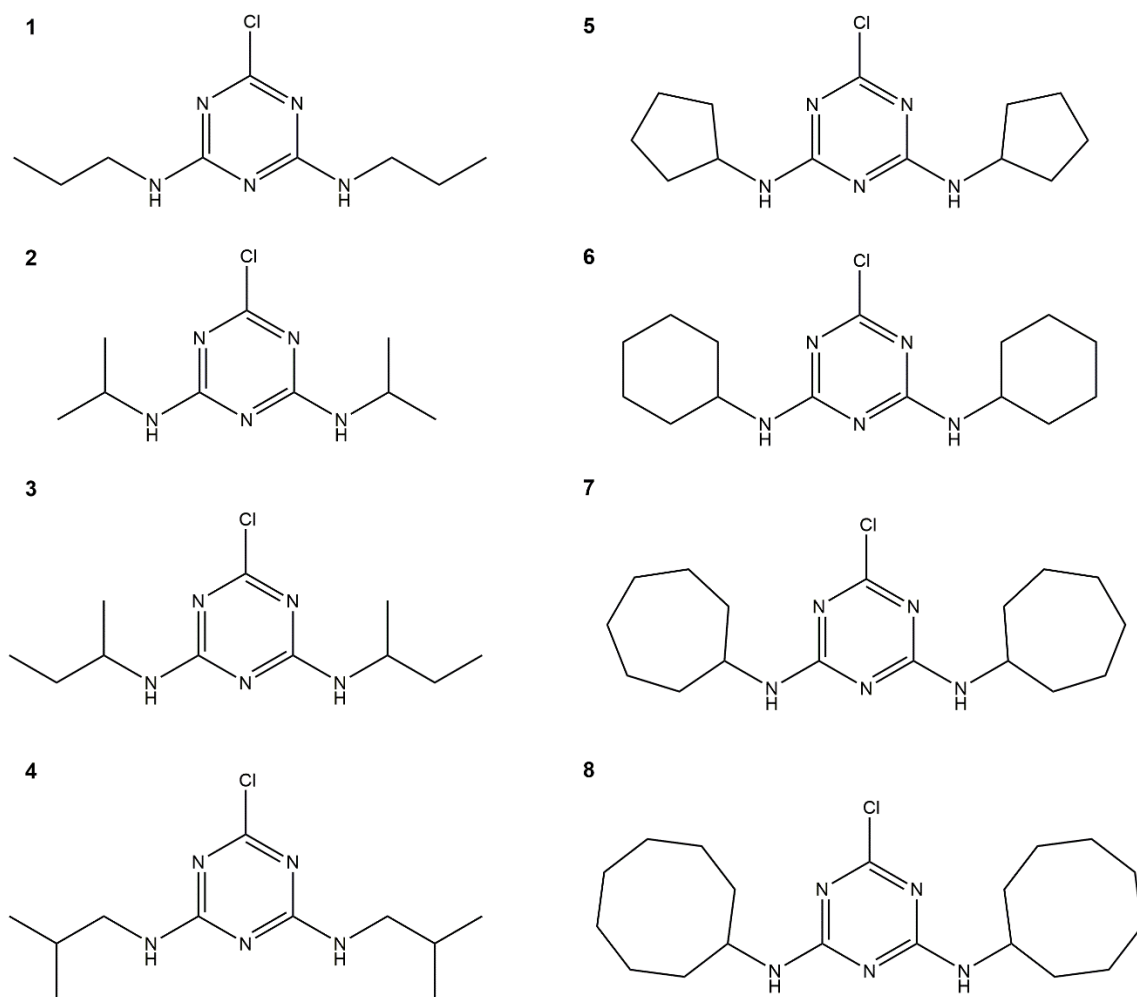
Figure 1. Molecular structures of the studied *s*-triazine derivatives

The chromatographic analysis was done by using UHPLC Agilent 1290 Infinity LC system with Diode Array Detector. The applied column was ZORBAX Eclipse XDB-Phenyl, 95 Å, 2.1 × 150 mm, 5 μm. The mobile phase was methanol/water mixture. The chromatographic analysis and determination of retention parameters ($logk_0$) are described in detail in a previous study [5]. The reactivity molecular descriptors were calculated by Gaussian 16 program. HOMO and LUMO descriptors represent the ability to donate and ability to receive an electron, respectively, whilst Egap is the energy difference between the HOMO and LUMO energies. Chemical potential (μ) represents the entropy change after addition of a particle to a system. Electrophilicity index (ω) measures the energy stabilization when the system gains an additional electronic charge in the environment.

Results and discussion

The molecular descriptors were obtained based on 2D molecular structures and their values are given in Table 1. Also, the retention data in the form of capacity factor obtained by extrapolation are provided in Table 1. Observing the values of the calculated molecular descriptors, it can be seen that the compounds with acyclic substituents (compounds **1**-**4**) possess generally lower HOMO energies and μ values, and higher Egap and ω values, than compounds with cyclic substituents (compounds **5**-**8**). There is no strict separation between these two groups of compounds regarding their LUMO energies. In order to examine their influence on the retention behavior of the studied compounds in RP-UHPLC system, the correlation analysis was performed. Electron excitations become easier as the Egap narrows. Increased mobility of π electrons in extensive conjugated π orbital systems enhances energy distribution throughout the molecule, thereby stabilizing it. Consequently, smaller Egap values are associated with greater stability, which is the case with *s*-triazine derivatives with cyclic substituents (**5**-**8**).

Table 1. Retention data and molecular descriptors of the analyzed *s*-triazine derivatives

Comp.	$logk_0$ [5]	HOMO	LUMO	Egap	μ (eV)	ω (eV)
1	1.379	-9.657	3.214	12.871	-3.22147	0.806
2	0.790	-9.628	3.199	12.826	-3.21457	0.806
3	2.147	-9.598	3.222	12.820	-3.18805	0.793
4	2.947	-9.614	3.178	12.792	-3.21807	0.810
5	4.068	-9.538	3.220	12.758	-3.15931	0.782
6	4.455	-9.552	3.199	12.751	-3.17644	0.791
7	5.331	-9.535	3.225	12.761	-3.15498	0.780
8	6.061	-9.504	3.260	12.764	-3.12172	0.763

The univariate linear relationships between HOMO, LUMO and Egap energies are presented in Figure 2. Here, it can be seen that there is a strong influence of HOMO and Egap energies on the retention parameters of the studied *s*-triazine derivatives considering significantly high correlation coefficients of the relationships. On the other hand, there is a weak correlation between LUMO energy and retention parameters.

The obtained results indicate that higher retention in the applied chromatographic system is associated with high HOMO energies and low Egap energies. Having in mind that the applied chromatographic system has a phenyl column as a stationary phase, it can be assumed that π-π interactions occur during the chromatographic separation.

LUMO energies are associated with higher retention, however there are some exceptions such as the compound **3** that has higher LUMO energy but lower retention parameter than compounds **4**, **5** and **6** which possess lower LUMO energies but higher retention parameters.

Since the chromatographic separation is a quite complex process, the retention behavior can rarely be explained by only one variable. Usually, it is explained by more complex mathematical equations (QSRR models) based on multivariate regression (multiple linear regression, partial least squares regression, principal component regression, etc.). However, there is the limitation in the present study since it was impossible to apply multivariate regression due to limited number of compounds. Nevertheless, the obtained results can be considered a preliminary ones and further investigation is needed to confirm the possibility of precise prediction of the retention parameters based on reactivity descriptors by establishing the QSRR models with strictly defined applicability domain and evaluated predictive ability based on internal and external validation procedures.
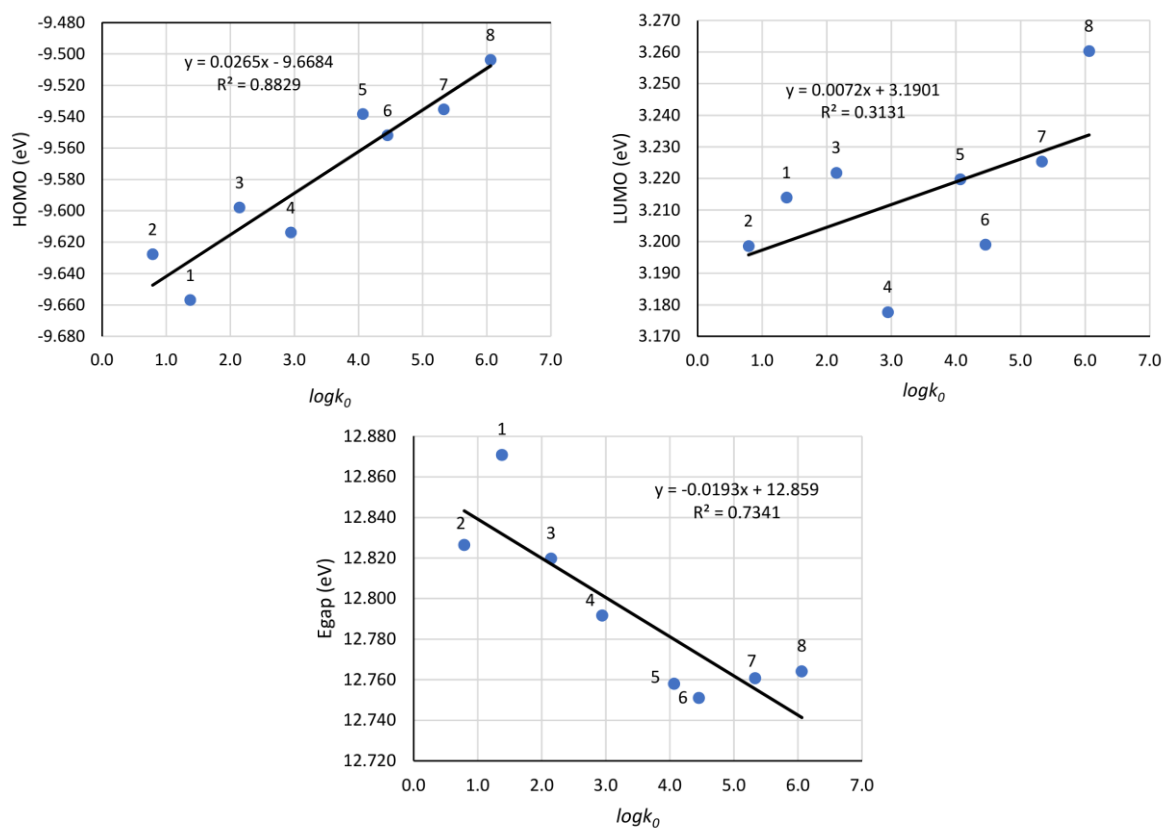
Figure 2. Linear relationships between retention data ($logk_0$) and HOMO, LUMO and Egap molecular descriptors

Linear relationships between the retention parameters and chemical potential and electrophilicity index are presented in Figure 3. There is a significant influence of these two chemical properties on the retention behavior of the studied derivatives, considering high regression coefficient.
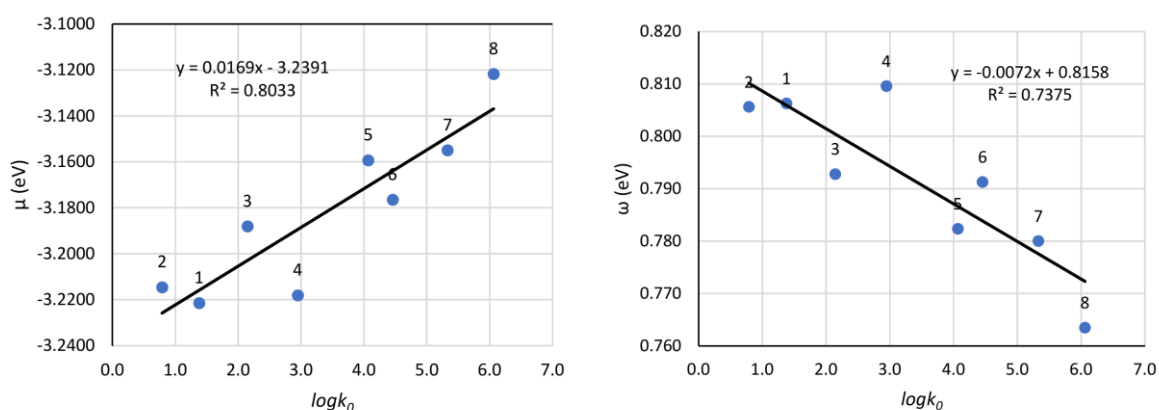
Figure 3. Linear relationships between retention data ($logk_0$) and μ and ω molecular descriptors

Statistical parameters of the established preliminary QSRR models are presented in Table 2. Based on the presented statistical data, it can be concluded that only the influence of the LUMO energies on the retention is questionable considering small determination coefficient (R^2),

adjusted determination coefficient (R^2adj), cross-validation determination coefficient (R^2_{CV}) and *F-test*. Those parameters indicate poor fitting of the data between retention parameter and LUMO energies. The other models have acceptable statistical parameters and can be considered statically significant, but with limited predictive ability.

Table 2. Statistical parameters of the established QSRR models

Parameter	Model 1	Model 2	Model 3	Model 4	Model 5
x	$logk_0$	$logk_0$	$logk_0$	$logk_0$	$logk_0$
y	HOMO	LUMO	Egap	μ	ω
R^2	0.8829	0.3131	0.7341	0.8033	0.7375
R^2adj	0.8635	0.1922	0.6882	0.7706	0.6939
R^2_{CV}	0.7919	-0.2455	0.4665	0.6670	0.5556
F-test	45.3	2.7	16.4	24.5	16.9

Conclusion

The presented results indicate the importance of reactivity descriptors in retention mechanism of the studied series of *s*-triazine derivatives in the applied RP-UHPLC system with phenyl column and methanol/water mobile phase. Particular influence of HOMO, Egap, μ and ω descriptors on the retention behavior of the studied compounds was confirmed by correlation analysis. Considering the aforementioned descriptors, there is a clear separation between the derivatives with acyclic and cyclic substituents. The compounds with cyclic substituents possess higher HOMO and μ descriptors than the derivatives with acyclic substituents. There is no clear separation among the derivative with acyclic and cyclic substituents regarding LUMO energies. HOMO and μ descriptors have the highest influence on the determined retention parameters ($logk_0$) of the studied compounds determined in the applied chromatographic system.

References
[1] B. Salaković, S. Kovačević, M. Karadžić Banjac, S. Podunavac-Kuzmanović, L. Jevrić, I. Pajčin, J. Grahovac, Processes 11 (2023) 358.
[2] R. Kalizsan, Chem. Rev. 107 (2007) 3212-3246.
[3] S. Kovačević, M. Karadžić Banjac, N. Milošević, J. Ćurčić, D. Marjanović, N. Todorović, J. Krmar, S. Podunavac-Kuzmanović, N. Banjac, G. Ušćumlić, J. Chromatogr. A 1628 (2020) 461439
[4] D. Antonović, G. A. Bončić-Caričić, J. Serb. Chem. Soc. 59 (1994) 993-996.
[5] S. Kovačević, M. Karadžić Banjac, J. Anojčić, V. Banjac, P. Ilić, B. Salaković, S. Podunavac-Kuzmanović, L. Jevrić, Agriculture 13 (2023) 2212.

CASCADE MEMBRANE SYSTEM FOR EFFECTIVE COD REMOVAL FROM DAIRY BY-PRODUCT

Hadid Sukmana, Adrienn Fejős, Anikó Birkásné Nagypál, Dorottya Csenki, József Csanádi, Szabolcs Kertész*

Faculty of Engineering, University of Szeged, H-6725 Szeged, Moszkvai krt. 9, Hungary
*e-mail: kertesz@mk.u-szeged.hu

Abstract
The dairy industry is highly water-intensive, producing wastewater characterized by elevated organic loads, suspended solids, and a pH range of 7–8, which varies based on specific processes (e.g., milk processing, dairy products, cheese whey). Wastewater from both the dairy sector and chemical industries generally requires treatment before discharge to mitigate environmental impact. Dairy processing effluents are notably distinct from other industrial wastewaters, exhibiting high concentrations of chemical oxygen demand (COD), which can severely disrupt ecosystems. Membrane filtration technology has increasingly gained traction as an advanced method for water purification and to decrease COD to a desirable level.

This study provides a comparative analysis of ultrafiltration membranes for COD removal from dairy by-products. A cascade membrane system is utilized, incorporating several sequential stages: initial milk fat separation using microfiltration (MF) membranes with pore sizes of 0.1/0.2/0.5 μm, followed by protein-selective ultrafiltration (UF) with membranes of 100–150 kDa molecular weight cut-offs, and subsequent protein concentration using a 10 kDa UF membrane. The 150 kDa UF membrane exhibited superior performance, achieving higher flux and 33% COD removal. Meanwhile, the result showed that the COD removal of 10 kDa UF membrane was achieved at 40%. However, further investigation is necessary to evaluate long-term filtration performance and the effects of multiple cleaning cycles.

Keywords: Cascade membrane system, COD removal, Dairy by-product, Membrane filtration, UF membrane

IMPACT OF SPACER GEOMETRY ON ULTRAFILTRATION PERFORMANCE IN A FILTER MODULE

Imre Vajk Fazekas[1], Aws N. Al-Tayawi[1], József Richárd Lennert[2], Sándor Beszédes[1], József Csanádi[3], Cecilia Hodúr[1], Gábor Veréb[1], Zsuzsanna László[1], Szabolcs Kertész[1]*

[1]*Department of Biosystems Engineering, Faculty of Engineering, University of Szeged, Szeged H-6725, Hungary*
[2]*Department of Power Electronics and E-Drives, Audi Hungaria Faculty of Automotive Engineering, Széchenyi István University, Győr H-9026, Hungary*
[3]*Department of Food Engineering, Faculty of Engineering, University of Szeged, Szeged H-6725, Hungary*
Corresponding author: *kertesz@mk.u-szeged.hu

Abstract

In our research, we aimed to explore how the filtration efficiency of a specialized membrane filtration device could be enhanced using custom-made, 3D-printed spacers with various geometric designs. We performed experiments using model dairy wastewater with an average load, a polyethersulfone (PES) ultrafiltration membrane, and a membrane filtration device. The tests were performed with (and without) different spacer configurations.

During the experiments, we evaluated several factors, including the permeate flux, membrane retentions, resistances, and specific energy consumption. Our measurements clearly showed that the use of 3D-printed spacers significantly improved the filtering efficiency, with some geometric configurations yielding better results.

Introduction

In today's world, wastewater management poses a significant challenge due to limited resources, making it essential to treat and recycle as much waste as possible. Among the various wastewater treatment methods, membrane filtration holds the most potential [1]. This process uses semi-permeable membranes to filter water, allowing water molecules to pass through while retaining solid particles [2]. In our research, we focused on ultrafiltration (*UF*), a pressure-driven filtration process. *UF* effectively removes suspended particles, bacteria, and viruses, but cannot filter out sugars or mono- and multivalent ions. A key drawback of membrane filtration is the inevitable fouling of the membranes. As filtered solids accumulate on the membrane's surface and within its pores, permeate flux decreases, and energy consumption rises [3]. To address this, several mitigation strategies exist, such as backwashing, chemical cleaning, and the use of module vibrations or flow diverter spacers [4]. Our study focused on the impact of the last method. We conducted tests with flow diverter spacers, which were designed based on our own plans using reference models and produced via *FDM* (Fused Deposition Modeling) 3D printing. This manufacturing method was ideal for our research, as 3D printing technology has seen rapid advancements in recent years and is now widely applied not only in industry but also in everyday life [5]. Additionally, 3D printing allowed us to quickly modify and produce new models based on insights gained from previous tests and experiences.

Experimental

The tests were conducted on a 10 liters of a model dairy wastewater solution consisting of skimmed milk powder, with a mass concentration of 5 g/L, cleaning detergent, with 0.5 g/L and room temperature tap water. A *VSEP* Series L membrane filtration module was employed,

maintaining two constant parameters: a transmembrane pressure of 8 bars and a volumetric flow rate of 4 *GPM* (approximately 15.14 L/min) (New Logic Research, Inc., USA).

Throughout 5 experiments, we analyzed various factors, including permeate flux, membrane retention, resistance, and specific energy consumption. The experiments used four variations of spacers: Sp.1-4. (Table 1.) The spacers were 3D-printed using *PETG* and *PCTG* plastic filaments on our in-house 3D printer (filaments: Filatikum, Hungary; *FDM* printer: Creality CR-10S Pro V2, China).

During the 2-hour experiment processes, 9 samples were collected in each case at different time intervals (2 feed solutions, 4 permeates, and 3 concentrates). Each sample was analyzed for total dissolved solids (*TDS*), pH level, conductivity, and turbulence. The final permeates and concentrate samples were also tested for chemical oxygen demand (*COD*), milk fat, protein, lactose with an infrared device (Bentley Instruments, Inc., USA), and protein values with Kjeldahl method (Foss, Britain).

Results and discussion

In figure 1. the permeate fluxes and in figure 3. the specific energy consumption results were plotted. Values were compared over time and over volume reduction ratio (VRR). First, it can be concluded that the use of spacers produced better results compared to the control measurements. One of the designs, Sp.1 yielded the best overall performance across all parameters, including permeate flux, retention, resistance, and specific energy consumption.
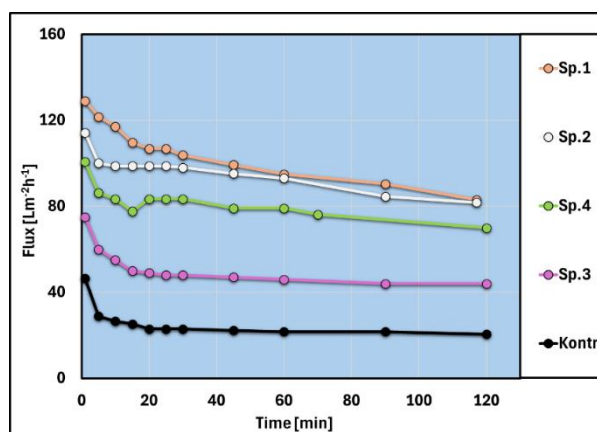
Figure 1. Permeate fluxes as a function of time (TMP=0.8MPa, q_{vrec}=15.14L/min, T=25±1°C)
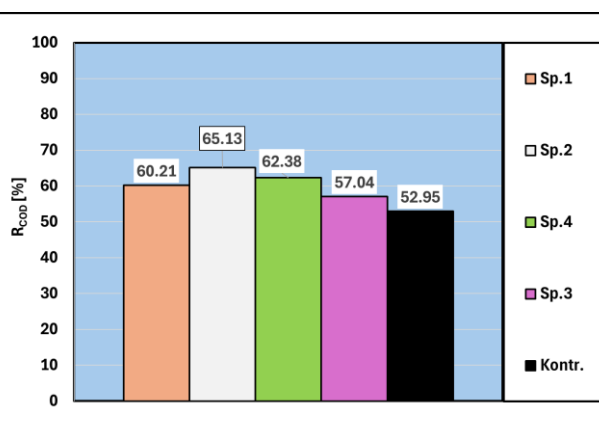
Figure 2. Retentions compared within each spacer (TMP=0.8MPa, q_{vrec}=15.14L/min, T=25±1°C)
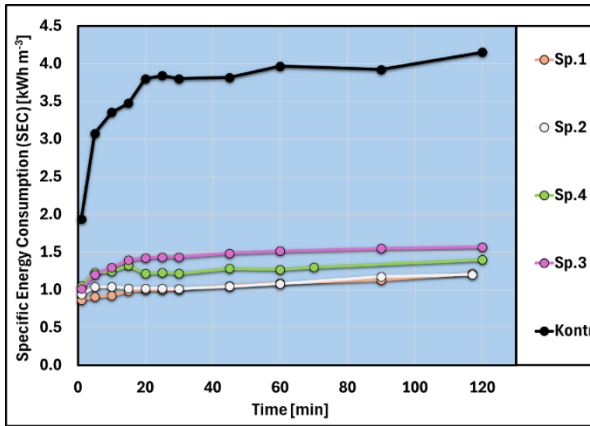
Figure 3. Specific energy consumption as a function of time (TMP=0.8MPa, q$_{vrec}$:4, T=25±1°C)
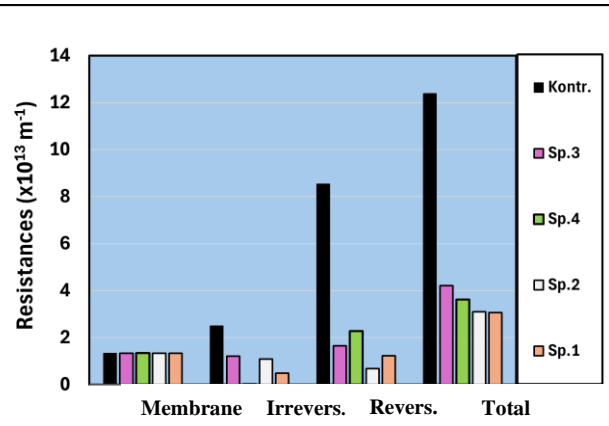
Figure 4. Irreversible and reversible resistances compared to total resistance (TMP=0.8MPa, q$_{vrec}$:4, T=25±1°C)

Differences between the geometric spacer designs were observed. The first two designs (Sp.1 and Sp.2) significantly outperformed the latter two (Sp.3 and Sp.4) based on the flux results. However, it's important to highlight that Sp.3 and Sp.4 required considerably less plastic for the printings. Furthermore, it can be seen from Figure 3 that the use of spacers reduced the specific energy consumption values by about one third. The fourth figure shows that the value of the total

resistances have also been greatly reduced compared to the control measurements. In addition, the first two designs gave better results than the third and fourth, as the resistances were the lowest.

***Sp.1** – First design*
***Sp.2** – First design, cone variant*
***Sp.3** – Tesla-valve inspired design*
***Sp.4** – Strengthened Tesla-valve inspired design*

Table 1. Spacer designs meanings

Conclusion

The key finding from our results is that to achieve optimal performance, a spacer with a certain geometry should be used. This approach significantly boosts the initial flux and extends the time before a substantial drop in performance occurs. As a result, the filtration process becomes more efficient, reducing the time required to treat a given volume of wastewater and lowering overall energy consumption. The average of flux values taken with the best spacer indicate a staggering 309% improvement when compared to the average of the control measurements. In the case of energy consumption, an 70% decrease is observable, when compared to the control values.

Given the lower resource and energy demands of the latter designs, it warrants further investigation to determine whether their reduced performance is offset by these savings. Future studies should assess whether the decreased performance of Sp.3 and Sp.4 can be justified by their more efficient material and energy use, particularly for large-scale applications.

Further research should also explore the combination of using multiple anti-fouling techniques, such as using spacers and module vibrations simultaneously. Our preliminary experiments in

this area have shown highly promising results, warranting continued investigation. Future studies will focus on further examining this approach.

Acknowledgements

References

[1]   J. F. J. Chimuca, C. S. A. do Canto, J. T. de Sousa, V. D. Leite, and W. S. Lopes, "Anaerobic dynamic membrane bioreactor applied to wastewater treatment: a review," *Afinidad*, vol. 80, no. 598, pp. 20–34, 2022, doi: 10.55815/413319.

[2]   S. Mulyati *et al.*, "Enhancing the Anti-Fouling Property of Polyethersulfonebased Membrane using Chitosan Additive from Golden Snail (Pomacea canaliculata) Shell Waste for Water Purification," *ASEAN J. Chem. Eng.*, vol. 23, no. 2, pp. 224–239, 2023, doi: 10.22146/ajche.79643.

[3]   M. S. Amiraftabi, N. Mostoufi, M. Hosseinzadeh, and M. R. Mehrnia, "Reduction of membrane fouling by innovative method (injection of air jet)," *J. Environ. Heal. Sci. Eng.*, vol. 12, no. 1, pp. 1–8, 2014, doi: 10.1186/s40201-014-0128-0.

[4]   S. G. Szerencsés *et al.*, "Effect of vibration on the efficiency of ultrafiltration," *Analecta Tech. Szeged.*, vol. 15, no. 1, pp. 37–44, 2021, doi: 10.14232/analecta.2021.1.37-44.

[5]   T. Templom, T. I. Erdei, and G. Husi, "Delta tripod robot FDM típusú 3D nyomtató tervezése Open-Source Arduino fejlesztőplatform felhasználásával," *Recent Innov. Mechatronics*, vol. 5, 2018, doi: 10.17667/riim.2018.si/10.

A SHORT OVERVIEW OF BIOSENSOR TECHNIQUES FOR THE DETECTION OF CHEMICAL COMPOUNDS AND BIOMARKERS DURING ECOTOXICOLOGICAL TESTING

Szandra Klátyik[1], Eszter Takács[1], Alexei Nabok[2], András Székács[1]

[1]*Institute of Environmental Sciences, Hungarian University of Agriculture and Life Sciences, H-2100 Gödöllő, Páter Károly u. 1., Hungary*
[2]*Materials and Engineering Research Institute, Sheffield Hallam University, City Campus, Howard Street, Sheffield, S1 1WB, United Kingdom*
e-mail: klatyik.szandra@uni-mate.hu

Abstract
Different biosensors, along with ecotoxicological tools such as bio-analytical systems, bioassays, and biomarkers, serve as early detection systems to indicate potential environmental damage. Early recognition can help prevent further harm to environmental and ecological matrices. The application of biosensors in ecotoxicology has gained increasing attention over the past few decades as traditional chemical analysis methods are often expensive and time-consuming. The development of biosensor methods for detecting of environmentally relevant pollutants (e.g., pesticide residues, mycotoxins, heavy metals, pharmaceuticals) and ecotoxicologically important indicator compounds (e.g., heat shock proteins) is advantageous because biosensors offer faster, more sensitive, and environmentally friendly methods for identifying and monitoring various pollutants in environmental and biological samples. The presence of pesticide and pharmaceutical residues in the environment is a complex problem (e.g., environmental and health risks, toxicological effects). Therefore, to protect ecological sustainability, environmental and human health, early and reliable detection of contaminants, even in the case of low concentrations, is of particular importance. A persistent challenge remains to identify relevant interpretation and risk assessment tools within the context of reference areas for the environment.

Introduction
According to the recommendation of IUPAC (International Union of Pure and Applied Chemistry), "biosensors are integrated devices capable of providing specific quantitative or semi-quantitative analytical information using a biological recognition element (biochemical receptor) that is in direct spatial contact with an electrochemical transducer element" [1–3]. In other words, biosensors are devices that use biological materials or living organisms to detect environmental effects or pollutants. Biosensors find extensive applications primarily in analytical chemistry and biochemistry, ranging from clinical practice to food and environmental analysis. However, in toxicology, their use is almost exclusively for analytical purposes, rarely applied to detect biological endpoints. Biosensor techniques have shown significant potential in ecotoxicity testing as they can detect specific chemical compounds (e.g., pesticide active ingredients, mycotoxins, heavy metals, pharmaceuticals) and biological markers (e.g., heat shock proteins, glutathione-S-transferase, vitellogenin) present in environmental and biological samples, thereby contributing to the assessment of toxic effects on ecosystems [4]. Yet, in ecotoxicology, the widespread application of biosensors offers numerous possibilities and advantages, as biosensors can be extremely sensitive and selective, enabling reliable detection of environmental pollutants at low concentrations, which is particularly important in ecotoxicological studies.

Structure and operating principle of biosensors

Based on the definition, biosensors are analytical instruments that integrate a biological element such as microorganisms, organelles, cell receptors, enzymes, antibodies, or nucleic acids, along with a physicochemical transducer [1,2]. For instance, an enzyme-linked recombinant receptor assay qualifies as a biosensor under this definition, where the enzyme serves as the biological component and the optical element acts as the transducer. Although biosensors, combined with effect-related parameters or biochemical responses, can be complex tools for environmental monitoring, they provide a clear and comprehensive assessment of the condition and possible risks of the investigated system [3,4]. Biosensors consist of two main parts: bioreceptors that specifically bind to target molecules, and a transducer unit that converts the interaction with the bioreceptor into an electrical, optical, or other type signal [1,5]. This signal conversion allows the concentration of the detected substance to be monitored in real-time [5,6]. Biosensors used in ecotoxicological studies can be based on various mechanisms, including enzyme-based, microorganism-based, and DNA-based biosensors. Enzyme-based sensors typically rely on enzyme inhibition, while microorganism-based biosensors measure changes in microbial metabolic activity in the presence of a toxicant [7].

Application areas and types of biosensors

Biosensors are versatile tools with a wide range of applications, from medical diagnostics to environmental monitoring. Based on the biological component used and the transduction method, biosensors can be classified into several types. The type of biosensor chosen depends on the specific application, the analyte of interest, and the desired sensitivity. Enzyme-based, microbial, DNA-based, immunosensors, cell-based, aptamer-based, and nanomaterial-based biosensors each have distinct advantages and limitations, contributing to their relevance in different fields of science and technology [5].

Enzyme-based biosensors

Enzyme-based biosensors use enzymes as the biological recognition element. Enzymes are highly specific catalysts for biochemical reactions, making them ideal for detecting particular substrates. The interaction between the enzyme and the analyte results in the production of a measurable product, often detected electrochemically, optically, or calorimetrically. A common example is the glucose biosensor, which uses glucose oxidase to measure blood glucose levels in medical diagnostics [2]. The primary advantages of enzyme-based biosensors include their high specificity and the rapidity of the reaction. However, they may suffer from limited stability, as enzymes can be sensitive to environmental factors such as temperature and pH [8].

Microbial biosensors

Microbial biosensors use whole microorganisms (bacteria, fungi, or yeasts) as the biological component. These biosensors rely on the metabolic activity of microorganisms, which can be altered in the presence of specific substances like pollutants, heavy metals, or organic compounds. Changes in microbial metabolism can be measured electrochemically or via changes in optical properties [3,9,10]. Microbial biosensors are commonly used in environmental monitoring (e.g., detection of heavy metals, assessment of water and soil quality). One key advantage of microbial biosensors is their robustness, as microorganisms can tolerate a wide range of environmental conditions [11,12].

DNA-based biosensors

DNA-based biosensors, also known as genosensors, use single-stranded DNA (ssDNA) or RNA sequences as the biorecognition element. These sensors detect complementary nucleotide

sequences by hybridization. DNA-based biosensors can be used to detect specific genetic materials, making them highly useful in pathogen detection, genetic screening, and environmental monitoring (e.g., for genetically modified organisms) [13]. The DNA-based biosensors are highly specific due to the sequence-based recognition mechanism. However, DNA-based sensors require careful handling to avoid degradation, and they may be sensitive to temperature changes [13,14].

Antibody-based biosensors (immunobiosensors)
Immunosensors use antibodies or antigens as the biological component to detect specific molecules based on the highly specific antigen-antibody interaction. These biosensors are commonly employed in medical diagnostics, food safety testing, and environmental monitoring for detecting toxins, pathogens, or allergens [15-17]. The high specificity of immunosensors allows for the detection of very low concentrations of the target analyte. However, the production of antibodies and the stability of the biosensor over time can pose challenges [18].

Cell-based biosensors
Cell-based biosensors use whole cells as the biorecognition element. Cells, like microorganisms, can detect a wide range of substances based on their metabolic or physiological responses. These biosensors are often used in drug testing, toxicity screening, and environmental monitoring to assess the effects of chemicals on living organisms [19,20]. A particular area is the use of cell-based biosensors to detect cellular interactions, cell attachment processes to surfaces, or cell signaling. Cell-based biosensors are advantageous because they can provide comprehensive information about the toxic effects of a compound, but they may have slower response times compared to other biosensors [21].

Aptamer-based biosensors
Aptamer-based biosensors utilize aptamers, which are short sequences of nucleic acids or peptides that can bind to specific targets, including proteins, small molecules, and cells. Aptamers have advantages over antibodies, such as ease of synthesis, high stability, and the ability to bind non-immunogenic targets [22]. These biosensors are gaining popularity in medical diagnostics, environmental monitoring, and food safety. For instance, they can be used to detect biomarkers in cancer patients or monitor contaminants in water [23].

Nanomaterial-based biosensors
Nanomaterial-based biosensors incorporate nanomaterials like carbon nanotubes, nanoparticles, or graphene into the transducer. Therefore, novel nanomaterials utilized in these biosensors do not typically contribute to the core molecular recognition process. Instead, the applied nanomaterials enhance the sensitivity and speed of the biosensor by increasing the surface area, allow physicochemical stabilization or delivery of the analytes, or facilitating electron transfer in electrochemical sensors [24,25]. Nanomaterial-based biosensors are highly sensitive and are employed in detecting low concentrations of analytes in medical diagnostics and environmental monitoring. However, challenges remain in terms of cost and scalability for widespread commercial use [26].

The application of biosensors in ecotoxicology
The use of biosensors in ecotoxicology can improve the detection of contaminants in real-time, with advantages such as sensitivity, selectivity, and rapid response time [3,6]. For example, biosensors can be employed to measure levels of heavy metals, pesticides, and pharmaceuticals, which are often implicated in environmental degradation and exert adverse effects on wildlife,

biodiversity, and human health [27]. The integration of biosensor technology in ecotoxicological testing not only enhances the ability to monitor environmental health but also aids in regulatory compliance by providing rapid and reliable data necessary for risk assessments [4,6,28]. The continuous advancement of biosensor technologies, including nanomaterials and microfluidics, promises to further improve their application in ecological monitoring and pollutant detection in the near future [29]. One of the most commonly used areas for ecotoxicological biosensors is water pollution monitoring (e.g., detection of heavy metals such as mercury or cadmium, as well as pesticide residues) [3,29]. The application of biosensors is capable for the detection of pollutants at low concentrations and provides immediate warnings to environmental authorities [3]. Furthermore, the detection of biomarkers, such as stress proteins in aquatic organisms, can provide insights into the biological impacts of pollutants [30]. Another important application area is the determination of soil pollution, where biosensors can detect various organic and inorganic pollutants [29,31]. For example, biosensors using *Pseudomonas fluorescens* bacteria can measure changes in soil biological activity in response to pollutants [32].

The advantages of biosensors include rapid measurement, small size, and ease of portability, allowing for field applications during environmental monitoring [2,3]. Moreover, they can directly measure biological effects, which is particularly useful in ecotoxicological studies, as this more accurately indicates the impact of pollutants on living organisms [8]. However, there are limitations to the ecotoxicological application of biosensors. One of the biggest challenges is the limited lifespan and stability of biosensors, especially in polluted environments [3]. In addition, the sensitivity and specificity of sensors may need improvement in certain cases to avoid false positive or even more false negative results [15].

Conclusion

In conclusion, the application of biosensor techniques plays a crucial role in advancing ecotoxicological testing by enabling the efficient detection of chemical compounds and biomarkers. Moreover, the use of biosensors supports our better understanding and management of environmental pollutants and their effects on biological systems. However, challenges remain, technological advancements may open new opportunities for the rapid and effective detection of ecological risks. In the future, biosensor applications in ecotoxicology are expected to further expand, particularly with the integration of new materials and technologies such as nanotechnology. The use of nanoscale components can lead to the development of even more sensitive and specific biosensors, capable of detecting the smallest contaminants.

Acknowledgements

References

[1] D.R. Thévenot, K. Toth, R.A. Durst, G.S. Wilson, Biosens. Bioelectron. 16 (2001) 121-131.
[2] A.P.F. Turner, I. Karube, G.S. Wilson, Biosensors: fundamentals and applications, Oxford University Press, Oxford, 1990, pp. 786.

[3] C.W. Huang, C. Lin, M.K. Nguyen, A. Hussain, X.T. Bui, H.H. Ngo, Bioengineered 14 (2023) 58-80.

[4] P.-D. Hansen Eng. Life Sci. 8 (2008) 26-31.

[5] V. Naresh, N. Lee, Sensors (Basel) 21 (2021) 1109.

[6] S. Nath, Sustainable Food Technol. 2 (2024) 976-992.

[7] C.S. Pundir, N. Chauhan, Anal. Biochem. 429 (2012) 19-31.

[8] A. Sassolas, L.J. Blum, B.D. Leca-Bouvier, Biotechnol. Adv. 30 (2012) 489-511.

[9] S.F. D'Souza, Biosens. Bioelectron. 16 (2001) 337-353.

[10] H. Abu-Ali, A. Nabok, T.J. Smith, Anal. Bioanal. Chem. 411 (2019) 7659-7668.

[11] L.D. Mello, L.T. Kubota, Food Chem. 77 (2002) 237-256.

[12] Z. Ma, C. Meliana, H.S.H. Munawaroh, C. Karaman, H. Karimi-Maleh, S.S. Low, P.L. Show, Chemosphere 306 (2022) 135515.

[13] A. Sassolas, L.J. Blum, B.D. Leca-Bouvier, Chem. Rev. 108 (2008) 109-139.

[14] M. Yu, T. He, Q. Wang, C. Cui, Biosensors 13 (2023) 889.

[15] S. Piermarini, L. Micheli, N.H.S. Ammida, G. Palleschi, D. Moscone, Biosens. Bioelectron. 22 (2007) 1434-1440.

[16] N.B. Ramírez, A.M. Salgado, B. Valdman, Braz. J. Chem. Eng. 26 (2009) 227-249.

[17] A. Nabok, A.M. Al-Jawdah, A. Tsargorodska, Sens. Actuators B Chem. 247 (2017) 975-980.

[18] F.S. Felix, L. Angnes Biosens. Bioelectron. 102 (2018) 470-478.

[19] N. Gupta, V. Renugopalakrishnan, D. Liepmann, R. Paulmurugan, B.D. Malhotra, Biosens. Bioelectron. 141 (2019) 111435.

[20] E. Farkas, A. Székács, B. Kovács, M. Oláh, R. Horvath, I. Székacs, J. Hazard. Mater. 351 (2018) 80-89.

[21] F. Lagarde, N. Jaffrezic-Renault, Anal. Bioanal. Chem. 400 (2011) 947-964.

[22] S. Song, L. Wang, J. Li, C. Fan, J. Zhao, Trends Anal. Chem. 27 (2008) 108-117.

[23] T. Hianik, J. Wang, Electroanalysis 21 (2009) 1223-1235.

[24] J. Wang, Analyst, 130 (2005) 421-426.

[25] J. Wang, Electroanalysis 17 (2005) 7-14.

[26] S. Malik, J. Singh, R. Goyat, Y. Saharan, V. Chaudhry, A. Umar, A.A. Ibrahim, S. Akbar, S. Ameen, S. Baskoutas, Heliyon 9 (2023) e19929.

[27] K.R. Rogers, Anal. Chim. Acta 568 (2006) 222-231.

[28] A. Baldassarre, N. Mucci, L.I. Lecca, E. Tomasini, M.J. Parcias-do-Rosario, C.T. Pereira, G. Arcangeli, P.A.B. Oliveira, Int. J. Environ. Res. Public Health 17 (2020) 2461.

[29] S. Gavrilaș, C.S. Ursachi, S. Perța-Crișan, F.D. Munteanu, Sensors (Basel) 22 (2022) 1513.

[30] S.E. Hook, E.P. Gallagher, G.E. Batley, Integr Environ Assess Manag. 10 (2014) 327-341.

[31] A. Thakur, A. Kumar, Sci. Total Environ. 834 (2022) 155219.

[32] T. Petänen, M. Romantschuk, Anal. Chim. Acta 456 (2002) 55-61.

QUINCE BIOWASTE FOR PRODUCTION OF GRAPHENE-BASED NANOMATERIALS USED FOR ELECTROMAGNETIC SHIELDING

Mila Milenković[1], Warda Saeed[2], Muhammad Yasir[2], Duška Kleut[1], Svetlana Jovanović[1]

[1]*Vinča Institute of Nuclear Sciences-National Institute of the Republic of Serbia, University of Belgrade, P.O. Box 522, 11000 Belgrade, Serbia*
[2]*Carl von Ossietzky Universität Oldenburg, 26111 Oldenburg, Germany*
duska@vin.bg.ac.rs

Abstract

This paper investigates the potential of using fruit biowaste as a starting material for producing new, environmentally friendly electromagnetic interference (EMI) shielding materials. Specifically, we selected distillery stillage, a by-product of fruit schnapps distillation, which distilleries discharged in large quantities [1]. For every liter of alcohol produced, between 8 and 15 liters of stillage are generated. Due to the high levels of nitrogen compounds and various organic molecules, these waste materials require proper management, leading to additional disposal or treatment costs. One common solution for stillage management is converting it into low-value products such as fertilizer or livestock feed. Our research explores graphene fabrication from biomass-derived sources obtained by the pyrolysis of quince biowaste under inert atmosphere.

In this study, we utilized stillage collected after the distillation of quince schnapps, which was then pyrolyzed at 850°C. We analyzed the resulting graphene-based materials' structural and morphological properties of the and their ability to block electromagnetic waves (EMWs) in the X-band frequency region [2]. Previous studies have shown that biochar produced from lignin can increase the shielding efficiency of cement [3], while sewage sludge biochar has demonstrated shielding effectiveness (SE) values greater than 10 dB [4]. By exploring the possibility of converting quince stillage into value-added, highly demanded materials, this study addresses the need for new sustainable products and provides a novel approach to reducing the environmental burden of stillage discharge.

Acknowledgements

References

[1] G.D. Gebreeyessus, A.Mekonnen, E. Alemayehu, Journal of Cleaner Production 232 (2019) 295
[2] S. Jovanović, M. Huskić, D. Kepić, M. Yasir, M. K. Haddadi, Graphene and 2D Materials, 8 (2023) 59
[3] M.Yasir, D. di Summa, G. Ruscica,I. Natali Sora, P. Savi, Electronics, 9 (2020) 819.
[4] P. Savi, M. Yasir, Microwave technology, 56 (2020) 335

BETTI BASES AS CHIRAL LIGANDS IN THE ENVIRONMENTALLY BENIGN ENANTIOSELECTIVE TRANSFER HYDROGENATION

<u>Lili Kóczán</u>,[1,*] György Szőllősi,[2] István Szatmári,[1,2]

[1]*Institute of Pharmaceutical Chemistry, Faculty of Pharmacy, University of Szeged, Eötvös utca 6, Szeged, 6720, Hungary.*
[2]*ELKH-SZTE Eötvös Loránd Research Network, Stereochemistry Research Group, Institute of Pharmaceutical Chemistry, Faculty of Pharmacy, University of Szeged.*
Corresponding author: lilikoczan@gmail.com

Abstract

There is a great need for enantioselective synthesis of biological active compounds, since in many cases only one of the stereoisomers can be used as pharmaceutical. Enantioselective transfer hydrogenations of ketones usually catalysed by metal complexes formed with bifunctional ligands, such as 1,2-aminoalcohols, are convenient methods of obtaining chiral alcohols. Our aim was to apply in the enantioselective reduction of a ketone an easily obtained Betti base as chiral ligand, which have not yet been employed in these reactions. During the present study we have obtained complete conversions and high enantioselectivities, up to 96%, in an environmentally friendly aqueous solvent mixture with the simplest Betti base enantiomers prepared from benzaldehyde, ammonia and β-naphthol. We hope that our results will pave the way of the application of 1,3-aminohydroxyl derivatives as chiral ligands in other asymmetric catalytic processes as well.

Introduction

Asymmetric synthesis procedures are of paramount importance in many fields of the fine chemical especially in the pharmaceutical industry, since often only one of the enantiomers of a compound is effective. Enantioselective reduction of unsaturated compounds such as ketones has a significant role in producing biologically active molecules [1]. Notable, the stereoselective transfer hydrogenation of carbonyl compounds can also be observed in nature using oxidoreductase like alcohol dehydrogenase as catalyst, cofactors like NADH or NADPH as donor. The above-mentioned biochemical process can also be mimicked by asymmetric chemical synthesis using chiral metal complexes as catalysts.

In 2001 the Nobel prize was awarded to Knowles, Noyori and Sharpless for developing catalysts for enantioselective metal catalysed reactions. These catalysts are highly effective, but many of them are very expensive, sensitive, hard to be removed from the reaction mixture, cannot be reused and their use needs special equipment. Because of the above mentioned disadvantages it can be useful to develop other organic ligands, meanwhile keeping the important molecular properties of the efficient chiral compounds. According to the so far obtained results the ligands must bear both a primary amine and a hydrogen-bond donor group [2,3]. Betti base derivatives seem to be a proper choice for these purposes, because they are bearing such functional groups, moreover, scarcely have been tested as chiral auxiliaries. To our knowledge complexes of these easily prepared optically pure compounds have not yet been applied as ligands in the enantioselective transfer hydrogenations so far.

Experimental
Preparation of the Betti base enantiomers

7.2 g (50 mmol) of β-naphthol (**1**) and 10.68 g (100 mmol) of bezaldehyde (**2**) were placed in a round-bottom flask and dissolved in 10 mL of 95% ethanol and then 10 mL of 95% ethanol

saturated with ammonia was added. The reaction mixture was allowed to stand at room temperature (rt) for two hours. Then the excess of ammonia was let to evaporate. The precipitate was filtered, the product mixture (**3a** and **3b**) resulted in 85% yield. 3.0 g of the above mixture (9 mmol) was dissolved in 50 mL 37% aqueous HCl solution and stirred at 100°C for an hour. After cooling to rt the precipitate was filtered and washed with cold water. The desired HCl salt (**4**×HCl) resulted in 94% yield. 1.0 g (3.5 mmol) of the salt was dissolved in 20 mL of EtOAc and 20 mL of 30% aqueous ammonia solution was added in a separatory funnel, the organic phase was collected, dried over Na_2SO_4, filtered and evaporteted, resulting in the racemic Betti-base (*rac*-**4**) in 20% total yield.

A solution of (2*R*,3*R*)-tartaric acid (**5**) (1.5 g, 10.0 mmol) in an 95% ethanol / methanol mixture (6.6/3.3 mL) was added dropwise to a solution of *rac*-**4** (2.5 g, 10.0 mmol) in 80 mL 95% ethanol. The mixture was stirred for 6 h at rt and then filtered. Methanol (10 mL) was added to the less soluble salt and the suspension was stirred for 3 h at rt. The salt was filtered and collected (1.8 g, 4.5 mmol, 45%). The mother liquor was evaporated to dryness under reduced pressure, producing an orange residue, which was washed with CH_2Cl_2, yielding a white crystalline powder (1 g, 2.5 mmol, 25%). Each diastereomeric salt was suspended in water (10 mL/g salt) and a 2 M Na_2CO_3 solution was added (10 mL/g salt). After 45 min, the mixtures were extracted with diethyl ether and dried (Na_2SO_4). The solvent was evaporated to give resolved (*S*)-**4** or (*R*)-**4** (both in 95% yield), which were further purified by washing with a small amount of diethyl ether. The optical purities of the separated enantiomers were determined by liquid chromatography (HPLC) using Chiralcel OD-H chiral column.

Catalytic transfer hydrogenations, general method

The transfer hydrogenations were carried out in 4 mL closed glass vials using magnetic stirring. In a typical reaction 0.00625 mmol of [Ru(*p*-cymene)Cl$_2$]$_2$ and 0.0125 mmol Betti base were suspended in 0.25 mL solvent by stirring for 1 h followed by addition of 1.25 mmol of HCOONa hydrogen donor and 0.25 mmol 4-chromanone (**6**). After the given reaction time the mixtures were diluted to 1 mL with water and the products were extracted with 3×2 mL EtOAc. The unified organic solution was dried and analysed by gas-chromatography (GC-FID) using chiral capillary column to determine the conversion and the enantiomeric excess of the product 4-chromanol (**7**), given by the formula: ee (%) = 100 × |[(*R*)-**7**]-[(*S*)-**7**]/([(*R*)-**7**]+[(*S*)-**7**]). The excess enantiomers were identified based on previous studies [4].

Results and discussion

First of all we synthesized based on a literature procedure the Betti base in a one-pot reaction using compound **1** and **2** dissolved in methanol saturated with ammonia (see Scheme 1.) resulting in the desired racemic aminonaphthol derivative *rac*-**4** [5]. Then we separated the obtained racemic mixture to the corresponding enantiomers, (*S*)-**4** and (*R*)-**4**, by resolution using L-tartaric acid (**5**), which yielded the close to optically pure enantiomers, as determined by HPLC [6]. These optically pure 1,3-aminohydroxyl derivatives we hope to be appropriate chiral ligands in metal catalysed enantioselective reactions.

Next we attempted to use the optically pure Betti bases, (*S*)-**4** and (*R*)-**4**, as ligands in the enantioselective transfer hydrogenation of a prochiral ketone using ruthenium catalyst. These experiments were carried out in conventional magnetically stirred batch reactors. For the transfer hydrogenation we choose as a test reaction the enantioselective reduction of 4-chromanone (**6**), using [Ru(*p*-cym)Cl$_2$)]$_2$ metal precursor and HCOONa as a hydrogen donor (Scheme 2). We started to optimize of the reaction conditions using the (*R*)-**4** enantiomer, which was obtained in higher yield after resolution of the racemic Betti base.
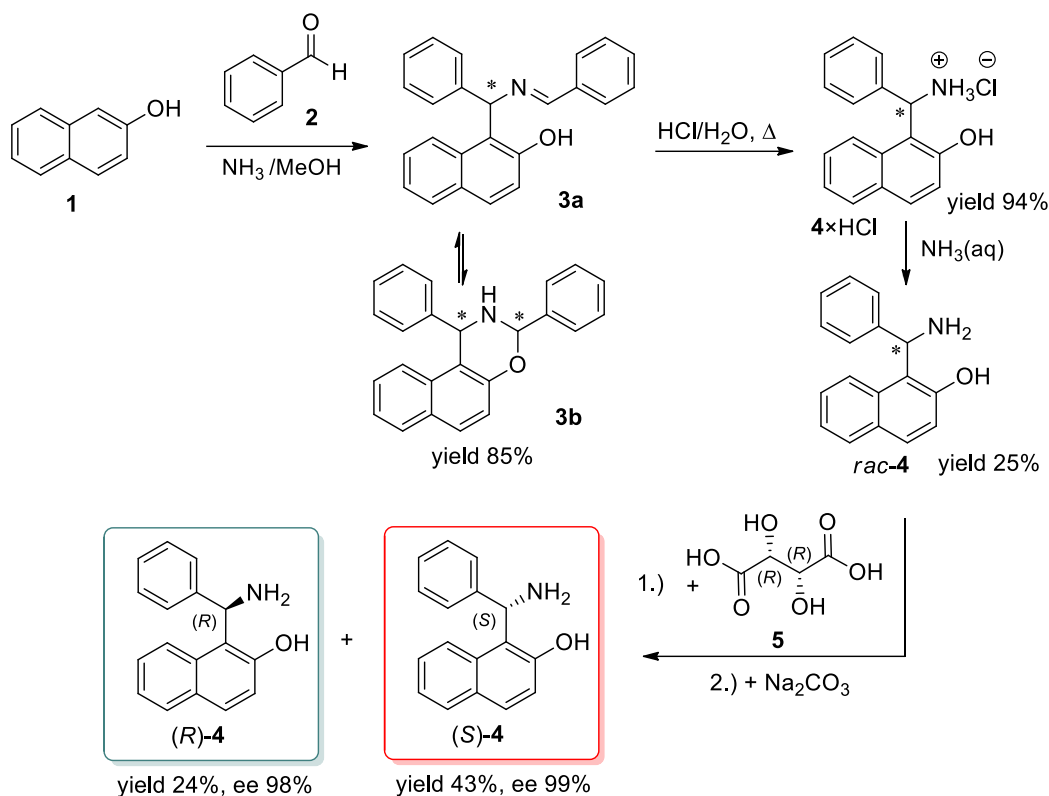
Scheme 1. Preparation of Betti-base enantiomers through the reaction of benzaldehyde (**2**), ammonia and β-naphthol (**1**) and resolution using (2*R*,3*R*)-tartaric acid.

Finding the right solvent or solvent mixture is crucial to obtain high conversions and enantiomeric excesses, so we started to screen few solvent, among which were water and few polar, water miscible organic solvents, such as isopropanol (*i*PrOH). Using only water as a solvent gave promising results, however, based on results obtained previously in transfer hydrogenations of prochiral ketones [4] and due to solubility problems of the reactant and the products, we have decided to test the effect of the addition of *i*PrOH to the water. Results obtained using different water/*i*PrOH ratios are presented in Figure 1. As one can see a small amount of *i*PrOH (20 vol%) can slightly increase the conversion, however, using higher amounts decreased significantly the conversion. Moreover, very low transformation of **6** was obtained in pure *i*PrOH. The amount of the alcohol hardly had any effect on the enantiomeric excess, except in pure *i*PrOH, in which a decrease to 91% was recorded.
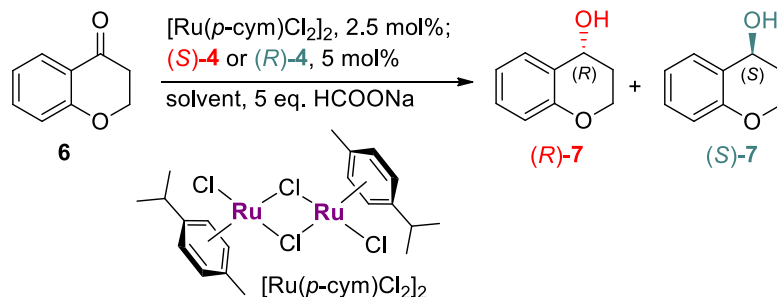
Scheme 2. Enantioselective transfer hydrogenation of 4-chromanone (**6**) using *in situ* formed chiral ruthenium complexes applying enantiomerically pure Betti bases as ligands.
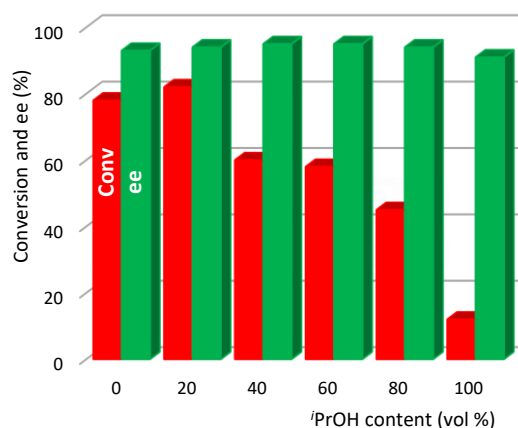
Figure 1. Effect of the ^{i}PrOH content (vol %) in the water on the conversion (red bars) and ee (green bars) obtained in the transfer hydrogenation of **6** using (*S*)-**4** as ligand. *Reaction conditions*: 0.00625 mmol [Ru(*p*-cym)Cl$_2$]$_2$; 0.0125 mmol (*S*)-**4**, 0.25 mmol **6**; 0.25 mL solvent; 1.25 mmol HCOONa, rt, 6h.

As we have seen a small amount of ^{i}PrOH had positive effect on the conversion (compare Table 1, entries 1 and 3) In continuation of our study we also tried other polar protic (EtOH, MeOH) and polar aprotic solvents (acetonitrile (MeCN), *N,N*-dimethylformamide (DMF)) mixed with water (entries 9, 10). The tests have shown that EtOH proved to be more efficient than ^{i}PrOH when using 20 vol% (entry 4). Using DMF in the solvent mixture was also highly effective, however, due to difficulties in removing the solvent residues (high boiling point) and due to our goal to use an environmentally benign system, we decided to use in the followings EtOH as solvent mixture component. The latter besides being non-toxic and safe, may also be obtained from renewable sources.

Table 1. Enantioselective transfer hydrogenation of **6** using chiral ruthenium complex formed with (*S*)-**4** as ligand[a]

Entry	Solvent	Ligand	Time (h)	Conv. (%)[b]	ee (%)[b]
1	H$_2$O	(*S*)-**4**	6	**78**	**93** (*R*)
2	^{i}PrOH	(*S*)-**4**	6	**12**	**91** (*R*)
3	H$_2$O/^{i}PrOH 8/2	(*S*)-**4**	6	**82**	**94** (*R*)
4	H$_2$O/EtOH 8/2	(*S*)-**4**	6	**91**	**94** (*R*)
5	H$_2$O/EtOH 8/2	(*S*)-**4**	18	**>99**	**94** (*R*)
6	H$_2$O/EtOH 4/6	(*S*)-**4**	18	**45**	**94** (*R*)
7[c]	H$_2$O/EtOH 8/2	(*S*)-**4**	24	**91**	**95** (*R*)
6	H$_2$O/MeOH 8/2	(*S*)-**4**	6	**82**	**94** (*R*)
9	H$_2$O/MeCN 8/2	(*S*)-**4**	6	**32**	**93** (*R*)
10	H$_2$O/DMF 8/2	(*S*)-**4**	6	**96**	**93** (*R*)
11	H$_2$O	(*R*)-**4**	6	**95**	**95** (*S*)
12	H$_2$O/EtOH 8/2	(*R*)-**4**	6	**98**	**96** (*S*)
13[c]	H$_2$O/EtOH 8/2	(*R*)-**4**	24	**97**	**96** (*S*)

[a] *Reaction conditions*: 0.00625 mmol [Ru(*p*-cym)Cl$_2$]$_2$; 0.0125 mmol ligand, 0.25 mmol **6**; 0.25 mL solvent; 1.25 mmol HCOONa, rt.
[b] Conversion (Conv.) and enantiomeric excess (ee) determined by GC-FID, in brackets the configuration of the excess enantiomer.
[c] Reaction at 4 °C

By examining the effect of increasing ratio of EtOH in H$_2$O/EtOH mixture, we experienced decreasing conversion similarly as in case of ^{i}PrOH (entry 6). Although 6 h were not sufficient to obtain complete transformation of **6**, in 18 h close to full conversion was obtained (entry 5). By decreasing the reaction temperature to 4°C in a 24 h reaction the enantiomeric excess was slightly better, but the conversion decreased (entry 7). According to the above results the water/EtOH solvent mixture is the most appropriate, thus we employed the (*R*)-**4** Betti base under these conditions. We got slightly better results with this enantiomer as with (*S*)-**4**, however the opposite enantiomer, *i.e.* (*S*)-**7** resulted in excess (entries 11-13).

Based on the above presented results and the structures of the transition states suggested previously with the use of other bifunctional ligands, we propose that transition states of the structures sketched in Figure 2 are formed during the reduction of **6**. These may rationalize the formation of one product enantiomer in large excess with the optically pure Betti base ligands.
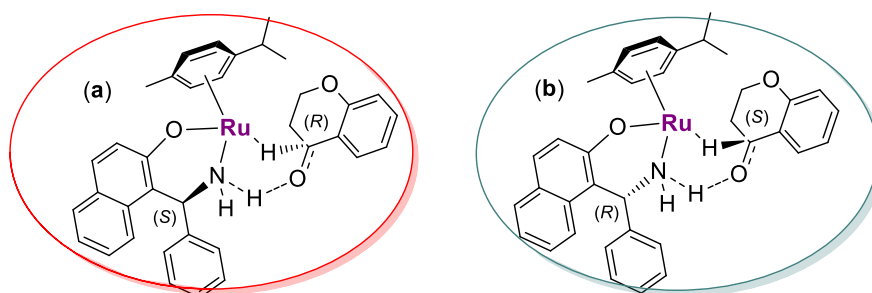
Figure 2. Structures of the possible *pro-R* (**a**) and *pro-S* (**b**) transition states using (*S*)-**4** and (*R*)-**4** ligands in the transfer hydrogenation of **6**.

Conclusion

In summary, we synthesized the Betti base enantiomers known from the literature in order to use them as chiral ligands in transfer hydrogenations. Our aim was also to use environment friendly solvents. According to the results water with a small amount of EtOH (20 vol%) proved to be the most effective solvent mixture for obtaining high conversion and enantioselectivity in the reduction of 4-chromanone. Both Betti base enantiomers performed similarly, giving the opposite 4-chromanol enantiomers in up to 98/2 ratio. Our study is the first in which easily prepared Betti base enantiomers were used as chiral ligand in transfer hydrogenation in an environmentally benign solvent mixture.

Acknowledgements

References

[1] T. Akiyama, I. Ojima (Eds.), Catalytic Asymmetric Synthesis, John Wiley & Sons, Hoboken, New Jersey, 2022.
[2] R. Noyori, A. Fujii, J. Takehara, T. Ikariya, S. Hashiguchi, J. Am. Chem. Soc. 117 (1995) 7562.
[3] V. Ratovelomanana-Vidal, P. Phansavath (Eds.), Asymmetric Hydrogenation and Transfer Hydrogenation, Wiley-VCH, Weinheim, 2021.
[4] Gy. Szőllősi, V. Kolcsár, ChemCatChem 11 (2019) 820.
[5] M. Betti, Org. Synth. 9 (1929) 60.
[6] C. Cardelliccio, G. Ciccarella, F. Naso, E. Schingaro, F. Scordari. Tetrahedron: Asymmetry 9 (1998) 3667.

THE EFFICACY OF THE WEED CONTROL IN MAIZE BY TWO DIFFERENT HERBICIDES AT TWO LOCALITIES IN THE REPUBLIC OF SERBIA

Bojan Konstantinović[1], Nataša Samardžić[1], Milena Popov[1], Tijana Stojanović[1], Stefan Ugrinov[1], Mirjana Vratunić[1]

[1]*University of Novi Sad, Faculty of Agriculture, Department of Environmental and Plant Protection, Trg Dositeja Obradovića 8, 21000 Novi Sad, Republic of Serbia*
e-mail: natasa.samardzic@polj.edu.rs

Abstract

During the vegetative period in 2021, the number of the weed species in the mercantile maize was monitored at two localities in the Republic of Serbia (Despotovo and Čurug), after which the efficacy of two different herbicides (isoxaflutole+thiencarbazone-methyl+cyprosulfamide - ITC and mesotrione+nicosulfuron - MN) was compared. ITC had satisfactory to high efficacy in case of *X. strumarium*, satisfactory efficacy in the control of *S. glauca* and *S. annua*, low efficacy in case of *C. arvensis*, and high efficacy in the control of the remaining eight weed species. MN had low efficacy in case of *C. arvensis* and *H. trionum*, low to high efficacy in the control of *A. artemisiifolia*, low to satisfactory efficacy in case of *P. lapathifolium*, and high efficacy in the control of the remaining seven weed species. In case of *S. halepense*, ITC and MN applied at 0.7 l/ha application rate, showed high efficacy at Despotovo locality, and low efficacy at Čurug locality.

Introduction

Maize (*Zea mays* L.) is native to the Americas and ranks among the most significant cereal crops globally. When Europeans arrived in America, they introduced maize to various continents, including Europe, Africa, and Asia, where it underwent diverse adaptation and breeding processes. Today, maize serves as a fundamental food source in numerous countries. Beyond its role as a staple, it is also utilized for animal feed, biofuel production, as well as a raw material for a wide range of industrial products. In 2018, global maize production reached approximately 1.147 million tons, with the leading producers being the United States, China, and Brazil [1]. Maize production in the Republic of Serbia has increased by 2.5 times over the past fifty years. With the expansion of the area cultivated with this crop, the issue of weeds has become increasingly prevalent. In addition to preventive and mechanical measures, chemical weed control is essential in maize cultivation [2]. The losses of the maize yield caused by the weeds are more pronounced on smaller cultivated areas and can reach up to 99% [3]. The weeds cause the most significant damage during the early growth stages of maize, specifically from the third to the eighth leaf stage [4]. In the Republic of Serbia, a total of 213 weed species have been identified in maize crops, among which some of the dominant species include: *Abutilon theophrasti* Medik., *Amaranthus retroflexus* L., *Ambrosia artemisiifolia* L., *Chenopodium album* L., *Cirsium arvense* (L.) Scop., *Convolvulus arvensis* L., *Cynodon dactylon* (L.) Pers., *Datura stramonium* L., *Hibiscus trionum* L., *Polygonum lapathifolium* L., *Setaria* sp., *Solanum nigrum* L., *Sorghum halepense* L. and *Xanthium strumarium* L. [5]. The objective of the research was to identify and monitor weed vegetation in maize crops under conditions of chemical control at two studied localities. The aim of the study was to evaluate the efficacy of two different herbicides applied at different application rates for the control of annual and perennial grass and broadleaf weeds.

Experimental

In May and June of the 2021 growing season, a study was conducted to examine the weed flora in maize crops at two localities in the Republic of Serbia: Despotovo and Čurug. The assessment involved counting weed species within randomly selected 1 m² quadrants across each of the 25 m² plot, enabling a systematic analysis of weed diversity. The identification of the weeds was performed based on the established literature sources [6,7]. The experiment was designed as a randomized block system with four replicates. It included a standard treatment, which consisted of a herbicide with the same formulation and equivalent active ingredient as the tested one, as well as a control group comprising untreated plots, in accordance with the EPPO guidelines [8,9,10]. The weather conditions during the experiment were ideal for the effective application of the tested herbicides. The data were collected and analyzed at the University of Novi Sad, Faculty of Agriculture, Department of Environmental and Plant Protection, utilizing MS Excel and Statistica 10. The analysis focused on the average values derived from four plots for each treatment, including the control group. The efficacy of the herbicides was categorized as follows: poor (<75%), satisfactory (75-90%), and high (>90%). Isoxaflutole+thiencarbazone-methyl+cyprosulfamide (ITC) was applied at the application rate of 0.45 l/ha, while mesotrione+nicosulfuron (MN) was applied at 0.7 and 1.3 l/ha application rates. The phytotoxicity was assessed visually on a scale from 0 (no visible phytotoxic effects) to 100% (complete degradation of the plants). The details regarding the localities and the experiment can be seen in Table 1.

Table 1. The details regarding the localities and the experiment

Locality	Despotovo	Čurug
Coordinates	45°25'28.26''N	45°28'08.82''N
	19°31'50.16''E	19°57'52.64''E
Crop variety	DKC5031	P0164
Sowing time	16.04.2021.	17.04.2021.
Date of application	11.05.2021.	11.05.2021.
Temperature atmoa* [C°]	22.58	21.45
Humidity atmoa [%]	48.06	46.29
Amount of water used [l/ha]	300	300
First assessment	28.05.2021.	28.05.2021.
Second assessment	11.06.2021.	11.06.2021.

*atmoa – at the moment of application

Results and discussion

ITC and MN are selective, systemic herbicides which can control both grass and broadleaf annual and perennial weeds in maize. The first is applied when the maize is in the stage of up to 3 leaves, while the second is the most efficient when applied at 2-8 leaf stage of maize. Both herbicides are selective for maize if they are applied in accordance with the manufacturer's recommendations [2].

Efficacy of the tested herbicides at Despotovo locality. Before the application of the tested herbicides the presence of ten weed species was observed, with the mean value of their occurrence being as follows: *A. theophrasti* (3.75-6.00), *A. retroflexus* (3.25-4.75), *A. artemisiifolia* (3.00-5.75), *D. stramonium* (3.75-6.00), *H. trionum* (4.00-5.50), *P. lapathifolium* (3.25-4.25), *S. glauca* (3.00-4.25), *S. nigrum* (3.50-5.50), *S. halepense* (3.75-10.00) and *X. strumarium* (3.75-5.00). The efficacy of ITC is shown in Table 2, while the efficacy of MN can be seen in Table 3.

Table 2. The efficacy of ITC at Despotovo locality.

Weed species	Control	ITC (0.45 l/ha)		Standard (0.45 l/ha)	
	No./m²*	No./m²	Eff.*	No./m²	Eff.
First assessment					
Abutilon theophrasti	8.25	0.25	96.97	0.00	100.00
Amaranthus retroflexus	5.25	0.00	100.00	0.00	100.00
Ambrosia artemisiifolia	6.75	0.25	96.30	0.00	100.00
Datura stramonium	7.00	0.00	100.00	0.00	100.00
Hibiscus trionum	6.75	0.00	100.00	0.25	96.30
Setaria glauca	6.50	0.75	88.46	1.00	84.62
Polygonum lapathifolium	6.25	0.25	96.00	0.00	100.00
Sorghum halepense	5.75	0.25	95.64	0.50	91.30
Solanum nigrum	7.25	0.00	100.00	0.00	100.00
Xanthium strumarium	7.25	0.75	89.66	1.00	96.21
Second assessment					
Abutilon theophrasti	10.75	0.50	95.35	0.25	97.67
Amaranthus retroflexus	7.50	0.00	100.00	0.00	100.00
Ambrosia artemisiifolia	9.00	0.50	94.44	0.25	97.22
Datura stramonium	8.75	0.25	97.14	0.00	100.00
Hibiscus trionum	8.00	0.25	96.88	0.50	93.75
Setaria glauca	9.25	1.50	93.78	1.75	81.08
Polygonum lapathifolium	10.50	0.75	92.86	0.50	95.24
Sorghum halepense	7.75	0.50	93.55	0.75	90.32
Solanum nigrum	9.25	0.00	100.00	0.00	100.00
Xanthium strumarium	10.50	1.50	85.71	1.75	83.33

*No./m² – number per m²; Eff. – efficacy

Table 3. The efficacy of MN at Despotovo locality.

Weed species	Control	MN (0.7 l/ha)		MN (1.3 l/ha)		Standard (1.3 l/ha)	
	No./m²*	No./m²	Eff.*	No./m²	Eff.	No./m²	Eff.
First assessment							
Abutilon theophrasti	5.25	0.25	95.24	0.00	100.00	0.00	100.00
Amaranthus retroflexus	7.00	0.00	100.00	0.00	100.00	0.00	100.00
Ambrosia artemisiifolia	5.75	1.50	73.91	0.50	91.30	0.25	95.65
Datura stramonium	8.25	0.00	100.00	0.00	100.00	0.00	100.00
Hibiscus trionum	6.75	2.00	70.37	1.75	74.07	1.75	74.07
Setaria glauca	5.50	0.25	95.45	0.00	100.00	0.00	100.00
Polygonum lapathifolium	5.25	1.50	71.43	1.00	80.95	0.75	85.71
Sorghum halepense	9.50	0.25	97.37	0.00	100.00	0.00	100.00
Solanum nigrum	6.00	0.00	100.00	0.00	100.00	0.00	100.00
Xanthium strumarium	5.75	0.25	95.65	0.00	100.00	0.00	100.00
Second assessment							
Abutilon theophrasti	7.50	0.50	93.33	0.00	100.00	0.00	100.00
Amaranthus retroflexus	8.25	0.25	96.97	0.00	100.00	0.00	100.00
Ambrosia artemisiifolia	7.75	2.25	70.97	0.75	90.32	0.50	93.55
Datura stramonium	9.50	0.25	97.37	0.00	100.00	0.00	100.00
Hibiscus trionum	9.25	3.25	64.96	2.75	70.27	2.50	72.97
Setaria glauca	7.00	0.50	92.86	0.00	100.00	0.25	96.43

Polygonum lapathifolium	7.50	2.25	70.00	1.50	80.00	1.50	80.00
Sorghum halepense	11.00	0.75	93.18	0.25	97.73	0.50	95.45
Solanum nigrum	7.75	0.50	93.55	0.25	96.77	0.00	100.00
Xanthium strumarium	8.00	0.50	93.75	0.25	96.88	0.00	100.00

*No./m^2 – number per m^2; Eff. – efficacy

Efficacy of the tested herbicides at Čurug locality. Prior to the application, seven weed species were noted, with their average occurrence measured as follows: *A. artemisiifolia* (3.50-5.25)*, C. arvensis* (3.00-4.50)*, D. stramonium* (3.50-5.25), *S. glauca* (3.00-4.75), *Sinapis arvensis* L. (3.50-4.75)*, S. halepense* (3.00-4.50) and *Stachys annua* (L.) L (4.00-4.50). The efficacy of ITC is shown in Table 4, while the efficacy of MN is stated in Table 5.

Table 4. The efficacy of ITC at Čurug locality.

Weed species	Control	ITC (0.45 l/ha)		Standard (0.45 l/ha)	
	No./m^{2*}	No./m^2	Eff.*	No./m^2	Eff.
First assessment					
Ambrosia artemisiifolia	5.25	0.25	95.24	0.50	90.48
Convolvulus arvensis	7.25	2.00	72.41	2.50	65.52
Datura stramonium	6.25	0.25	96.00	0.00	100.00
Setaria glauca	5.75	0.75	86.96	0.75	86.96
Sinapis arvensis	5.00	0.25	95.00	0.25	95.00
Sorghum halepense	5.25	2.00	61.90	1.50	71.43
Stachys annua	6.25	0.75	88.00	1.00	84.00
Second assessment					
Ambrosia artemisiifolia	7.75	0.50	93.55	0.75	90.32
Convolvulus arvensis	9.25	3.25	64.86	4.00	56.76
Datura stramonium	8.00	0.50	93.75	0.25	96.88
Setaria glauca	7.75	1.25	93.87	1.50	80.65
Sinapis arvensis	7.00	0.50	92.86	0.50	92.86
Sorghum halepense	7.75	3.25	58.06	3.00	61.29
Stachys annua	8.50	1.25	85.29	1.75	79.41

*No./m^2 – number per m^2; Eff. – efficacy

Table 5. The efficacy of MN at Čurug locality.

Weed species	Control	MN (0.7 l/ha)		MN (1.3 l/ha)		Standard (1.3 l/ha)	
	No./m^{2*}	No./m^2	Eff.*	No./m^2	Eff.	No./m^2	Eff.
First assessment							
Ambrosia artemisiifolia	5.75	1.50	73.91	0.50	91.30	0.25	95.65
Convolvulus arvensis	6.00	2.00	66.67	1.75	70.83	1.75	70.83
Datura stramonium	7.25	0.25	96.55	0.00	100.00	0.00	100.00
Setaria glauca	5.50	0.00	100.00	0.00	100.00	0.00	100.00
Sinapis arvensis	5.75	0.25	95.65	0.00	100.00	0.00	100.00
Sorghum halepense	6.25	1.75	72.00	0.50	92.00	0.25	96.00
Second assessment							
Ambrosia artemisiifolia	7.75	2.25	70.97	0.75	90.32	0.75	90.32
Convolvulus arvensis	8.00	3.25	59.38	2.75	65.63	2.50	68.75
Datura stramonium	9.25	0.50	94.59	0.25	97.30	0.00	100.00
Setaria glauca	7.75	0.00	100.00	0.00	100.00	0.00	100.00
Sinapis arvensis	7.50	0.50	93.33	0.25	96.67	0.00	100.00

Sorghum halepense	8.50	2.50	70.59	0.75	91.18	0.50	94.12

*No./m^2 – number per m^2; Eff. – efficacy

ITC had satisfactory to high efficacy in case of *X. strumarium*, satisfactory efficacy in the control of *S. glauca* and *S. annua*, low efficacy in case of *C. arvensis*, and high efficacy in the control of the remaining eight weed species. MN had low efficacy in case of *C. arvensis* and *H. trionum*, low to high efficacy in the control of *A. artemisiifolia*, low to satisfactory efficacy in case of *P. lapathifolium*, and high efficacy in the control of the remaining seven weed species. In case of *S. halepense*, ITC and MN applied at 0.7 l/ha application rate, showed high efficacy at Despotovo locality, and low efficacy at Čurug locality.

Conclusion

ITC at both studied localities had: high efficacy in the control of: *A. artemisiifolia*, *A. theophrasti*, *A. retroflexus*, *D. stramonium*, *H. trionum*, *P. lapathifolium*, *S. arvensis* and *S. nigrum*, satisfactory to high efficacy in case of *X. strumarium*, satisfactory efficacy in the control of *S. glauca* and *S. annua*, as well as the low efficacy in the control of *C. arvensis*. MN at both studied localities had: high efficacy in the control of: *A. theophrasti*, *A. retroflexus*, *D. stramonium*, *S. glauca*, *S. arvensis*, *S. nigrum* and *X. strumarium*, low efficacy in case of *C. arvensis* and *H. trionum*, while, depending on the application rate, it had low to high efficacy in the control of *A. artemisiifolia*, as well as the low to satisfactory efficacy in case of *P. lapathifolium*. Interesting results were obtained regarding *S. halepense*, in case of which ITC, as well as MN applied at 0.7 l/ha application rate, showed high efficacy at Despotovo locality, and low efficacy at Čurug locality.

References

[1] L.G. Ranilla, The application of metabolomics for the study of cereal corn (*Zea mays* L.), Metabolites 10(8) (2020), 300.

[2] M. Vratunić, Weeds in maize in Despotovo and Čurug and their control, Master thesis, University of Novi Sad, Faculty of Agriculture, Department of Environmental and Plant Protection, Novi Sad, Republic of Serbia, 2022.

[3] M. Fanadzo, C. Chiduza, P.N.S. Mnkeni, Effect of inter-row spacing and plant population on weed dynamics and maize (*Zea mays* L.) yield at Zanzokwe irrigation scheme, Eastern Cape, South Africa, African Journal of Agricultural Research 5(7) (2010), pp. 518-523.

[4] R. Bernik, F. Vučajnk, Postupci uništavanja korova u kukuruzu, Poljoprivredna tehnika 31(2) (2006), pp. 95-100.

[5] L. Stefanović, S. Ajder, M. Kojić, Korovska vegetacija u usevu kukuruza u uslovima primene herbicida na različitim tipovima zemljišta Kraljevačkog područja, Fragmenta herbologica Jugoslavica 19(1) (1990), pp. 31-49.

[6] M. Josifović (Ed.), Flora SR Srbije I-X, SANU, Belgrade, Republic of Serbia, 1970-1986.

[7] T. Šarić, Atlas korova: 100 najvažnijih korovskih biljaka u Jugoslaviji, Svjetlost, Sarajevo, Bosnia and Herzegovina, 1991.

[8] European and Mediterranean Plant Protection Organization (EPPO), Guideline for the efficacy evaluation of plant protection products, Phytotoxicity assessment, PP 1/135 (4), EPPO Bulletin 44(3) (2014), pp. 265-273.

[9] European and Mediterranean Plant Protection Organization (EPPO), Guideline for the efficacy evaluation of herbicides, Weeds in maize, PP 1/050 (3), EPPO Bulletin 37 (2007), pp. 40-43.

[10] European and Mediterranean Plant Protection Organization (EPPO), Guideline for the efficacy evaluation of herbicides, Weeds in maize, PP 1/050 (4), EPPO Bulletin 51(1) (2021), p. 92.

MECHANOCHEMICALLY ASSISTED, ENVIRONMENTALLY BENIGN HETEROGENEOUS ASYMMETRIC MICHAEL ADDITION TO MALEIMIDES

Kristóf András Kőszegi,[1],* Márton Szabados,[1] György Szőllősi[2]

[1]*Department of Molecular and Analytical Chemistry, Institute of Chemistry, Faculty of Science and Informatics, University of Szeged, Dóm tér 8, Szeged, 6720, Hungary.*
[2]*HUN-REN-SZTE, Stereochemistry Research Group, Institute of Pharmaceutical Chemistry, Eötvös utca 6, Szeged, 6720, Hungary.*
*Corresponding author: kristofkoszegi03@gmail.com

Abstract

Chiral *N*-substituted succinimides are widely used intermediates in the pharmaceutical industry. The Michael additions of various nucleophiles to maleimides results in such compounds. In the industry, since the upraise of environmental awareness, there is a huge demand of sustainable synthetic methods. Therefore, efficient alternative reaction activations are highly examined. Asymmetric catalytic processes have been developed for Michael additions to maleimides under batch conditions using organocatalysts. Our aim was to implement mechanochemical activation in these reactions because of its huge benefits over the conventional methods, *i.e.* the possibility of applying solvent-free conditions and the significantly reduced reaction times. We set the goal to prepare *N*-substituted succinimides with high yields and enantioselectivity using isobutyraldehyde as nucleophile and L-phenylalanine adsorbed on the surface of inorganic oxides (Bentolite H and Laponite RD) as heterogeneous organocatalyst. *N*-methylmaleimide as reactant was used to optimise the reaction and milling parameters. We also studied the structure of the catalyst using different methods to examine the deposition of L-Phe on the inorganic oxide. As a result of our studies, optimal conditions were determined to carry out the preparation of various *N*-substituted succinimides, which may be a significant step in the development of sustainable industrial synthetic methods.

Introduction

Asymmetric catalytic reactions are of high importance since the synthesis of optically pure compounds is crucial for the pharmaceutical industry [1]. Among these catalytic procedures, because of their environmental benefits, numerous organocatalytic methods have been developed. Asymmetric Michael additions of aldehydes to maleimides catalysed by bifunctional organocatalysts result in chiral succinimide derivatives that can be found as building blocks in biologically active natural products and pharmaceuticals [2]. Amino acids, their simple derivatives and oligopeptides as organocatalysts were successfully used in these reactions achieving outstanding conversion and enantiomeric excess values [3-7]. Out of several examined amino acids, L-phenylalanine (L-Phe) was found to be the most advantageous because of its natural occurrence and provided both great conversion and enantioselectivity. Based on these studies, efficient recyclable heterogenized organocatalysts have been developed in our research group by adsorbing amino acids on the surface of inorganic oxides [8]. These experiments were carried out in conventional batch reactors, using various solvents and needed long reaction times. However, numerous alternative activation methods can be applied, such as microwave or ultrasound assisted reactions or using mechanochemical energy transmission, to decrease the necessary time and to increase the sustainability of the processes.

Mechanochemistry bears several major advantages over the conventional activation such as significantly reduced reaction time, solvent-free conditions and relatively simple scale-up potential. It is considered a green chemical method; hence it implies great industrial relevance. The necessary energy in these alternative methods is provided by the collisions and

friction between the grinding media, the components and the wall of the jar. Although, various asymmetric organocatalytic reactions have been carried out in the last few decades using mechanochemistry [9-12], up to our work there are no reports on the enantioselective Michael addition of aldehydes to maleimides by mechanochemical activation.

In the present work our aim was to examine the use of heterogeneous organocatalyst in the asymmetric Michael addition reaction of an aldehyde, *i.e.* isobutyraldehyde to *N*-substituted maleimides using mechanochemical activation. After optimizing the parameters of the milling and the reaction, we hoped to achieve similar enantioselectivities and conversions as were observed under batch circumstances in previous works, however under environmentally benign conditions, such as without using a solvent and in shorter reactions.

Experimental

The L-phenylalanine (L-Phe), Bentolite H (Ben) (68,1% SiO_2, 13,5% Al_2O_3, 2,9% MgO, 0,7% Fe_2O_3, 0,9% CaO, 3,5% Na_2O, 0,1% K_2O, 0,2% TiO_2; pH = 9,5), Laponite RD (Lap) (59,5% SiO_2, 27,5% MgO, 0,8% Li_2O, 2,8% Na_2O; pH = 9,8; specific surface: 370 m^2/g), isobutyraldehyde (**1**) and *N*-methylmaleimide (**2a**) were obtained from commercial sources and were used as received. The other N-substituted maleimides either were commercial products or were prepared during our previous study. The mechanochemical reactions were carried in 10 cm^3 ZrO_2 grinding jars with milling balls of 3, 5, 12 and 15 mm diameter made from the same material. First the L-Phe, Lap or Ben were measured into to the jars, then the necessary number of balls were added, followed by introducing the given amount of maleimide and **1**. The mixture was agitated in a Retsch Mixer Mill MM 400 instrument at the desired frequency for the desired time. Products were dissolved in 3 cm^3 EtOAc, the catalyst was separated by centrifugation and washed twice with EtOAc. The combined organic phase was analysed by gas-chromatography using a chiral capillary column (GC-FID), and the products were identified using mass spectroscopy (GC-MS). The conversion and enantiomeric excess (ee) were determined based on the results obtained by GC-FID. The conventional magnetically stirred batch reactions were carried out the same way but in closed glass vials. Products were purified by column chromatography using hexane/EtOAc eluent to determine the yields of the reactions. The identity and purity of isolated succinimides was determined by ^{1}H- and ^{13}C-NMR spectroscopy.

Results and discussion

As a test reaction we chose the addition of **1** to **2a** resulting in the formation of the succinimide derivative 2-methyl-2-(1-methyl-2,5-dioxopyrrolidin-3-yl) propanal (**3a**), using L-Phe adsorbed on the surface of Ben or Lap as heterogeneous organocatalyst (Scheme 1.).
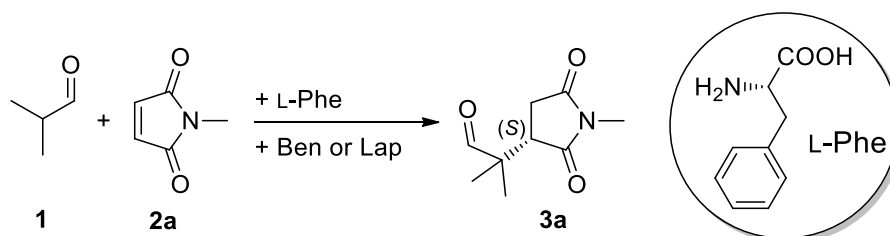
Scheme 1. Michael addition of isobutyraldehyde (**1**) to *N*-methylmaleimide (**2**) catalysed by L-Phe adsorbed on the surface of Ben or Lap.

First, we compared the conventional magnetic stirring with mechanochemical activation in this reaction without the use of solvent (Table 1.). From the results it can be concluded that the use of additive is required (entry 1) for the reaction. As observed, mechanochemical activation provided similarly high enantioselectivity as magnetic stirring though the former

afforded high conversions in significantly shorter reaction times. With the use of Lap, we could reach an almost complete conversion of **2a** in 30 minutes with ball milling while the batch system afforded lower than 50 % conversion in 90 minutes. According to these results, the implementation of mechanochemistry in this reaction seemed promising, thus in our further studies we attempted to optimise the reaction and milling parameters. From these experiments, we concluded that working with Lap as additive is more promising since it afforded higher conversion and only slightly lower enantioselectivity than Ben.

Table 1. Comparison of magnetic stirring and ball milling in the asymmetric Michael addition of isobutyraldehyde (**1**) to *N*-methylmaleimide (**2a**).[a]

Entry	Reaction activation	Additive[b]	Time (min)	Conv (%)[c]	ee (%)[c]
1	Magnetic stirring	–	90	0.5	46
2	Magnetic stirring	Lap	90	47	93
3	Magnetic stirring	Ben	90	42	95
4	Mechanochemical	Lap	30	97	93
5	Mechanochemical	Ben	30	72	95

[a] *Reaction conditions*: 0.03 mmol L-Phe, 100 mg additive, 0.3 mmol **2a**, 1.2 mmol **1**; room temperature, magnetic stirring: 800 rpm; mechanochemical activation: one Ø 15 mm ZrO_2 grinding ball, milling frequency 24 Hz.
[b] Additives: Laponite RD (Lap), Bentolite H (Ben).
[c] Conversion (Conv) and enantiomeric excess (ee) determined by gas-chromatography (GC-FID), *S* enantiomer in excess.

Further, we have examined the structure of the heterogeneous chiral organocatalyst with various methods. By infrared spectroscopy, we identified L-Phe deposited on Lap. X-ray diffractometry (XRD) measurements carried out using the parent Lap and the catalyst before and after use showed that L-Phe crystals are not deposited on the surface. However, the diffraction corresponding to the (001) plane appears at lower angles upon adsorption of the amino acid (Figure 1). This means that the interlamellar distance increases following adsorption of L-Phe, which implies that the intercalation of a part of the amino acid between the layers of Lap occurred. After using four times the catalyst, we found that this distance approaches that characteristic of Lap, *i.e.* the L-Phe is removed from the layers. Although the catalyst remained active, the conversion decreased gradually, which showed that mainly the amino acid adsorbed on the outer surface is responsible for catalysing the reaction and the role of the less accessible intercalated L-Phe is to restore the activity of the surface from which the amino acid has leached during reaction by supplying additional chiral compound.
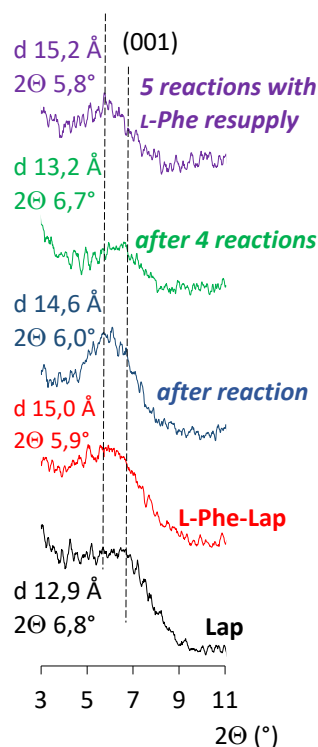
Figure 1. XRD patterns of Lap and L-Phe deposited on Lap before and after use.

After finding the optimal reaction conditions, we examined the performances of our catalytic system in the Michael addition of various *N*-substituted maleimides as shown in Table 2. These reactions were carried out at a three-fold scale compared to the optimization measurements. High, almost complete conversions and great enantioselectivities were reached with derivatives containing short aliphatic *N*-substituents, which allowed isolation of the products in good yields (up to 98% in case of *N*-allyl derivative) (entries 1, 2, 6). Increase in chain length or α-branching had negative impact on the conversion as seen with **2d**, **2e**, **2g, 2h,** however the *ee* values remained high (94-98%). *N*-phenylmaleimide (**2j**), *N*-benzylmaleimide (**2m**) and the latter's substituted derivative (**2l**) were almost completely transformed and high yields (90-94%) were obtained with great enantioselectivities (97-98%). The fluorine substituent on the phenyl ring in *para* position decreased slightly the conversion, however, afforded high, 96 % ee (**2j**, entry 10). These reactions were carried out under the same conditions and applying the same milling times in order to examine the effect of the substituents. These conditions were appropriate to the reaction of the most reactive *N*-methylmaleimide. However, by extending the reaction or increasing the grinding frequency it is also possible to transform the less reactive maleimide derivatives. Accordingly, the mechanochemical process may be applied to obtain a large variety of *N*-substituted succinimides, regardless on the nature of the *N*-substituent.

Table 2. Asymmetric addition of **1** to various *N*-substituted maleimides using mechanochemistry.[a]

Entry	Product; R	Conv (Yield)[b] (%)	*ee* (%)
1	**3a**; CH_3	>99 (88)	94
2	**3b**; $CH_3CH_2CH_2$	96 (90)	96
3	**3c**; $CH_3(CH_2)_2CH_2$	92 (88)	96
4	**3d**; $CH_3(CH_2)_4CH_2$	77 (72)	97
5	**3e**; $CH_3(CH_2)_8CH_2$	75 (72)	95
6	**3f**; $CH_2=CHCH_2$	>99 (98)	96
7	**3g**; $(CH_3)_2CH$	77 (71)	97
8	**3h**; C_6H_{11}	65 (60)	98
9	**3i**; C_6H_5	>99 (92)	97
10	**3j**; $4-FC_6H_4$	92 (85)	96
11	**3k**; $C_6H_5CH_2$	>99 (92)	97
12	**3l**; $4-ClC_6H_4CH_2$	>99 (94)	98

[a] *Reaction conditions:* 0.09 mmol L-Phe, 150 mg Lap pre-milled at 18 Hz, 20 min followed by the addition of 0.9 mmol **2a-2l**, 3.6 mmol **1**; the reaction was milled at 18 Hz, 60 min using 42 pcs Ø 5 mm ZrO_2 balls.
[b] Yield of the product purified by column chromatography.

Conclusion

In summary, we have developed a sustainable heterogeneous organocatalytic method to carry out the asymmetric Michael addition of an aldehyde to several *N*-substituted maleimides by using mechanochemistry. The reactions lead to chiral succinimide derivatives that are of huge importance as building blocks in pharmaceuticals. We examined two inorganic oxides

(Bentolite H and Laponite RD) as carriers for the chiral L-Phe catalyst. After studying the impact of different parameters on the reaction, Laponite RD proved to be more efficient as an additive. XRD measurements showed that the amino acid, apart from being adsorbed on the surface, also intercalates into the interlamellar space and no crystalline L-Phe was detected. We managed to reach high conversions of several *N*-substituted maleimides with great enantioselectivities under significantly reduced reaction times compared to conventional batch systems and under solvent-free conditions. Maleimides with short aliphatic substituents and *N*-benzyl or *N*-phenyl derivatives afforded almost complete conversions with high yields and enantiomeric excess. Our study is a significant step in the field of sustainable industrial synthesis of optically pure building blocks needed as intermediates to prepare active pharmaceuticals.

Acknowledgements

References
[1] T. Akiyama, I. Ojima (Eds.), Catalytic Asymmetric Synthesis, John Wiley & Sons, Hoboken, New Jersey, 2022.
[2] Z. Zhao, J. Yue, X. Ji, M. Nian, K. Kang, H. Qiao, X. Zheng, Bioorg. Chem. 108 (2021) 104557.
[3] T. C. Nugent, A. Sadiq, A. Bibi, T. Heine, L. L. Zeonjuk, N. Vankova, B. S. Bassil, Chem. Eur. J. 18 (2012) 4088.
[4] C. G. Kokotos, Org. Lett. 15 (2013) 2406.
[5] A. Schiza, N. Spiliopoulou, A. Shahu, C. G. Kokotos, New J. Chem. 42 (2018) 18844.
[6] A. Sadiq, T. C. Nugent, ChemistrySelect 5 (2020) 11934.
[7] C. E. Grünenfelder, J. K. Kisunzu, H. Wennemers, Angew. Chem. Int. Ed. 55 (2016) 8571.
[8] V. Kozma, Gy. Szőllősi, Catal. Sci. Technol. 12 (2022) 4709.
[9] E. Veverková, V. Poláčková, L. Liptáková, E. Kázmerová, M. Mečiarová, Š. Toma, R. Šebesta, ChemCatChem 4 (2012) 1013.
[10] Y.-F. Wang, R.-X. Chen, K. Wang, B.-B. Zhang, Z.-B. Li, D.-Q. Xu, Green Chem. 14 (2012) 893.
[11] V. J. Kolcsár, Gy. Szőllősi, Molecules 27 (2022) 5671.
[12] C. G. Avila-Ortiz, M. Pérez-Venegas, J. Vargas-Caporali, E. Juaristi, Tetrahedron Lett. 60 (2019) 1749.

TOPOLOGY INDICES AS PREDICTORS OF RETENTION BEHAVIOR OF NEWLY SYNTHESIZED ANDROSTANE 3-OXIMES IN RP-UHPLC: ARTIFICIAL INTELLIGENCE APPROACH

Strahinja Kovačević[1], Milica Karadžić Banjac[1], Jasmina Anojčić[2], Jovana Ajduković[2], Sanja Podunavac-Kuzmanović[1]

[1]Department of Applied and Engineering Chemistry, Faculty of Technology Novi Sad, University of Novi Sad, Bulevar cara Lazara 1, 21000 Novi Sad, Serbia
[2] Department of Chemistry, Biochemistry and Environmental Protection, Faculty of Sciences, University of Novi Sad, Trg Dositeja Obradovića 3, 21000 Novi Sad, Serbia
e-mail: strahko@uns.ac.rs

Abstract
The present study describes the application of artificial neural networks (ANNs), as artificial intelligence approach, as a tool in prediction of retention behavior of a series of newly synthesized series of androstane 3-oximes by using several molecular topology descriptors. The retention behavior of the studied androstane derivatives was determined by using reversed-phase ultra high performance liquid chromatography (RP-UHPLC) with C18 column, as stationary phase, and methanol/water mobile phase. The retention behavior was determined in the form of logarithm of capacity factor (*logk*). The ANN modeling was performed applying Broyden-Fletcher-Goldfarb-Shanno (BFGS) algorithm and multi-layer perceptron (MLP) feedforward networks. The obtained model successfully correlates hyper Wiener index (HWI), Szeged index (SZG) and Wiener index (WI) with *logk* values. The model was validated by internal validation and based on various statistical parameters. The model can be used for the prediction of retention behavior of the compounds structurally similar to those used in the modeling.

Introduction
Topology molecular descriptors (TMD) are very important in molecular modeling [1]. They rely on representing the molecule as a graph. TMD are actually a numerical measure of molecular topology that can be sensitive to various structural features of the molecule (shape, size, branching, symmetry, etc). TMD are obtained from application of algebraic operators to matrices that represent molecular graphs with values that do not depend on vertex numbering or labeling.
Chromatographic behavior of different compounds in various chromatographic systems can be predicted based on TMD by using quantitative structure-retention relationship (QSRR) approach [2]. The QSRR approach provides an insight into the retention behavior of molecules based on their structure and physico-chemical properties usually presented in the form of molecular descriptors. The QSRR models can be linear or non-linear. Univariate and multiple linear regression, principal component regression and partial least squares regression are the examples of linear methods, while the ANNs are the example of non-linear modeling based on artificial intelligence [3].
The present study is based on the application of ANNs for prediction of retention behavior of novel androstane 3-oximes, which have significant anticancer activity [4, 5], in reversed-phase ultra high performance liquid chromatography system with C18 stationary phase and methanol/water mobile phase. The influence of Wiener index (HWI), Szeged index (SZG) and Wiener index (WI), as TMD, was studied so these TMD served as input variables in the ANN

modeling, whilst the capacity factor (*logk*) determined in RP-UHPLC system was used as output variable.

Experimental

The studied compounds were synthesized at Department of Chemistry, Biochemistry and Environmental Protection, Faculty of Sciences, University of Novi Sad, according to the procedure described earlier [4]. The molecular structures of the analyzed compounds are presented din Figure 1. The RP-UHPLC analysis under isocratic conditions was carried out on UHPLC Agilent 1290 Infinity LC System with Diode Array Detector The applied column was ZORBAX Eclipse C18, 95Å, 2.1 × 50 mm, 1.8 µm (1200 bar pressure limit, LC Platform, Low Dispersion UHPLC). The column temperature was maintained at 25 °C. The mobile phase used was methanol/water mixture (90/10 v/v) with the flow of 0.2 ml/min. The injection volume was 10 µL. The peaks were detected at λ = 210 nm. The topology descriptors, including hyper Wiener index (HWI), Szeged index (SZG) and Wiener index (WI), were calculated by using Marvin Sketch v.14 program based on 2D molecular structures.
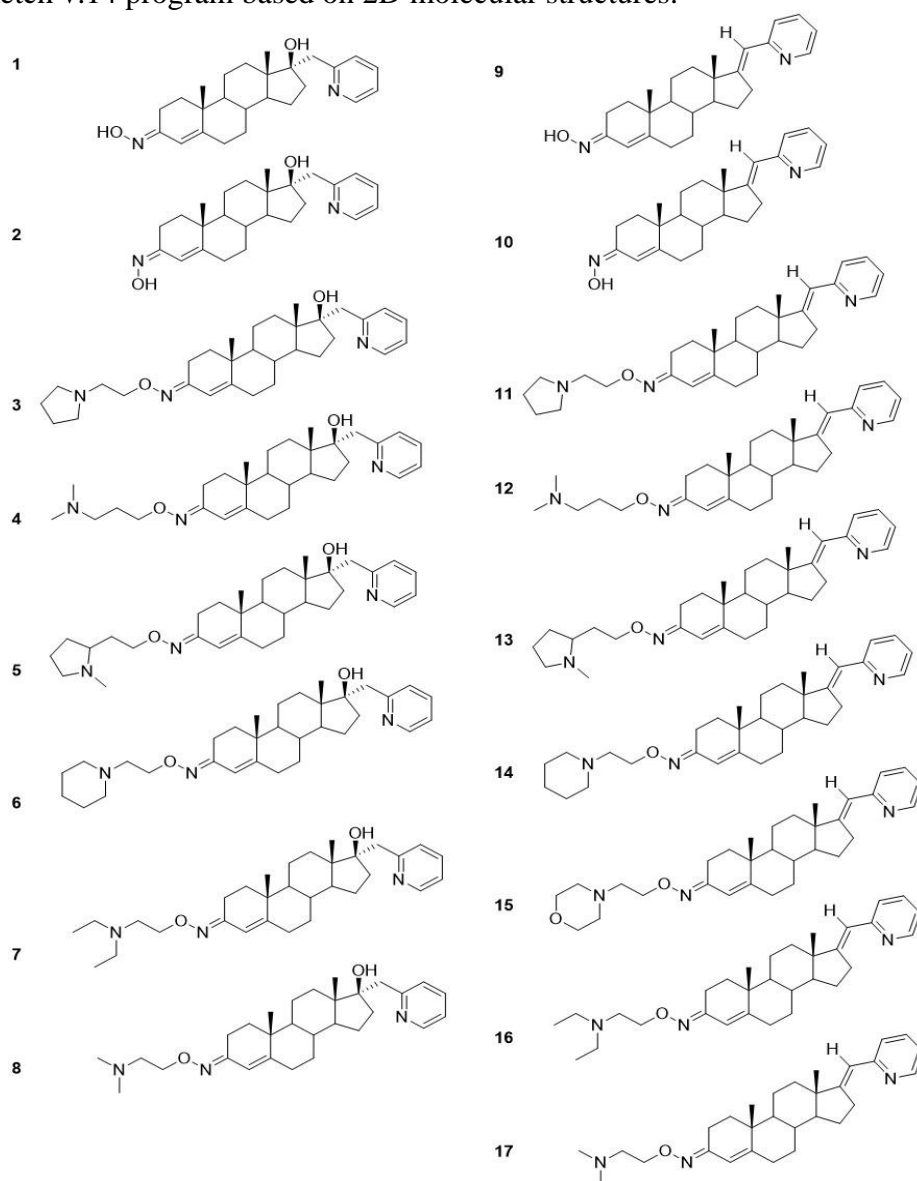
Figure 1. The molecular structures of the studied androstane derivatives

The ANN modeling was carried out using Statistica v.12 software. The modeling was performed applying Broyden-Fletcher-Goldfarb-Shanno (BFGS) algorithm and multi-layer perceptron (MLP) feedforward networks. The statistical parameters were calculated in the software NCSS 2023.

Results and discussion

The ANN modeling resulted in several ANNs among which the best one was chosen for further analysis based on statistical performance. The structure of the selected networks was 3-5-1 (3 input variables, 5 hidden neurons, 1 output variable). This network was established after 25 training cycles. The training of the networks was performed based on 13 compounds, whilst 2 compounds were used in test set, and 2 in the validation set. In Table 1, the target values represent the experimentally determined capacity factors and predicted *logk* values are obtained by using MLP 3-5-1 neural network. The residuals represent the differences between the target and predicted *logk* values. The modeling was performed without data normalization since in this case the data normalization resulted in ANNs of low statistical quality.

Table 1. The input and output (target) variables and the results of ANN modeling

Compound	Set	HWI	SZG	WI	*logk* - Target	*logk* - Predicted	*logk* - Residuals
1	Train	8533	4062	2120	-0.218	-0.228	0.010
2	Train	8533	4062	2120	-0.236	-0.228	-0.008
3	Train	24410	7794	4441	0.252	0.265	-0.014
4	Train	21965	7182	4088	0.216	0.378	-0.162
5	Train	27244	8377	4830	0.362	0.545	-0.183
6	Train	27656	8646	4862	0.453	0.441	0.012
7	Test	24425	7732	4446	0.393	0.345	0.047
8	Train	18765	6576	3674	0.167	0.102	0.065
9	Test	8008	3808	1977	0.539	0.549	-0.010
10	Train	8008	3808	1977	0.527	0.549	-0.022
11	Train	23099	7367	4197	0.714	0.652	0.063
12	Train	20774	6782	3859	0.749	0.874	-0.125
13	Train	25797	7924	4570	0.738	0.774	-0.035
14	Train	26192	8185	4601	0.858	0.632	0.225
15	Validation	26192	8185	4601	0.538	0.632	-0.094
16	Train	23114	7307	4202	0.877	0.738	0.139
17	Validation	17726	6203	3462	0.564	0.651	-0.087

The graphical comparison of target and predicted *logk* values is presented in Figure 2. The presented graph indicates a very good concurrence between the data. The slope of this linear relationship is very close to 1 and the intercept is quite close to zero. Also, the compounds from validation and test sets fits in the data from the training set which favors the good predictive ability of the model. The determination coefficient (R^2 = 0.9075) indicates the strong relationship between the experimental and predicted data.
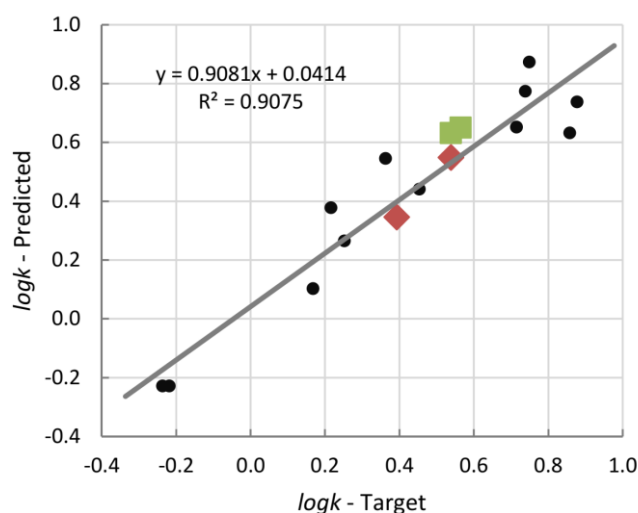
Figure 2. Linear relationship between target and predicted *logk* values
(● - training set, ■ - validation set, ◆ - test set)

In order to gain an overview of the presence of unbiased predictions and consistent variance, the residuals were plotted versus target *logk* values (Figure 3). The presented graph indicates the random distribution of the residuals as well as low amplitude of residuals, therefore unbiased predictions and consistent variance in the model were confirmed.
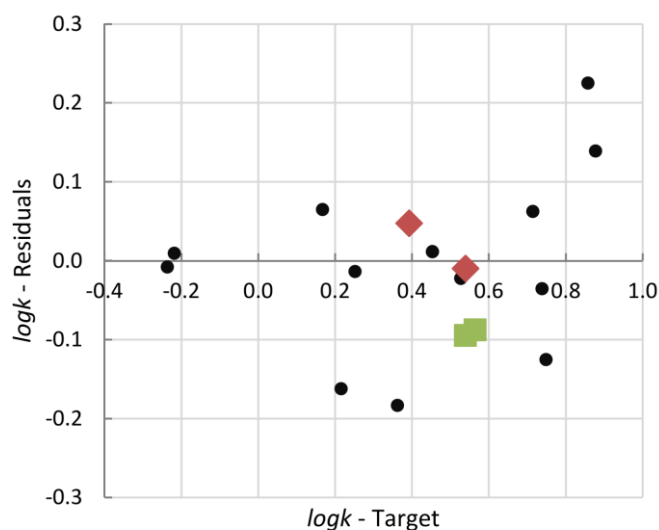
Figure 3. The distribution of the residuals vs. target *logk* values
(● - training set, ■ - validation set, ◆ - test set)

In order to estimate the influence of each input variable on network's characteristics, the global sensitivity analysis (GSA) was carried out. For each input variable, the GSA coefficient was calculated:
-   GSA (HWI) = 39922.8;
-   GSA (WI) = 2009.3;
-   GSA (SZG) = 1268.2.

Considering the fact that each variable is characterized by the GSA > 1, this means that all the variables have significant influence on network's performance and should be kept in the model.

Another conformation of the statistical quality of the established ANN model are the calculated statistical parameters presented in Table 2. Determination coefficient (R^2) of all data (test, validation and training), adjusted determination coefficient (R^2_{adj}), leave-one-out cross-validation determination coefficent (R^2_{CV}) indicate the good correlation between experimental and predicted data. High value of the *F-test* indicates the good fitting of the data, whilst the *RMSE* values show significantly low prediction errors.

Table 2. The statistical parameters of the ANN model

Statistical parameter	Value
R^2	0.9003
R^2_{adj}	0.8937
R^2_{CV}	0.8688
F-test	135.5
Training error (*RMSE*)	0.006
Test error (*RMSE*)	0.006
Validation error (*RMSE*)	0.004

Conclusion

The presented results indicate that the obtained ANN model successfully correlates topology descriptors hyper Wiener index (HWI), Szeged index (SZG) and Wiener index (WI) with retention behavior expressed as *logk* values of a series of newly synthesized androstane 3-oximes. The ANN model was validated by internal validation and tested by using validation and test sets. The concurrence between the experimental and predicted *logk* values confirmed the predictive power of the obtained model. The applicability domain of the model covers the compounds structurally similar to the analyzed ones as well as the compounds whose topology descriptors falls into the range of the topology descriptors used in the modeling.

References

[1] H. Wang, Q. Wang, X. Liao, R. Sun, M. Xie, React. Funct. Polym. 202 (2024) 105995.

[2] T. Liapikos, C. Zisi, D. Kodra, K. Kademoglou, D. Diamantidou, O. Begou, A. Pappa-Louisi, G. Theodoridis, J. Chromatogr. B. 1191 (2022) 123132.

[3] S. Z. Kovačević, S. O. Podunavac-Kuzmanović, L. R. Jevrić, E. A. Djurendić, J. J. Ajduković, Eur. J. Pharm. Sci. 62 (2014) 258-266.

[4] J. J. Ajduković, D. S. Jakimov, L. Rárová, M. Strnad, Y. U. Dzichenka, S. Usanov, D. Đ. Škorić, S. S. Jovanović-Šanta, M. N. Sakač, RSC Adv. 11 (2021) 37449.

[5] S. Kovačević, M. Karadžić Banjac, S. Podunavac-Kuzmanović, J. Ajduković, B. Salaković, L. Rárová, M. Đorđević, M. Ivanov, J. Mol. Struct. 1283 (2023) 135272.

CO-OPERATION FOR FOOD: LONG STORY OF METHANOGENIC ARCHEA AND ANAEROBIC FUNGI

Etelka Kovács[1, 3], Annabella Juhász-Erdélyi [1], Csilla Szűcs[1, 3], Zoltán Bagi[1, 2], Róbert Veprik[4], Tamás Papp[1], Kornél L. Kovács[1, 3]

[1]Department of Biotechnology and Microbiology, Faculty of Science and Informatics, University of Szeged;
[2]Institute of Biophysics, Biological Research Centre, Eötvös Loránd Research Network;
[3]Institute of Plant Biology, BRC, Eötvös Loránd Research Network;
[4]Szeged Zoo, Szeged, Hungary
e-mail: kovacset@bio.u-szeged.hu

Degradation of lignocellulose-rich material into biogas is an attractive strategy to face growing energy demands and moderate greenhouse gas emissions from the exploitation of fossil energy resources. Lignocellulosic residues (e.g. crop residues, green waste, mill waste) are highly frequent (1), they are easily accessible, cheap and do not require additional land to grow on in this way do not trigger "food or fuel" conflicts. This biomass is composed of interwoven cellulose and hemicellulose, coated by anaerobically almost undegradable lignin (2). This is the explanation why bacteria and archaea in the biogas reactor are not efficient in disintegration of the lignin, leaving a considerable portion of the more easily convertible sugars untouched. Microbial pre-treatment utilizing the fibre degrading potentials of aerobic fungi may be a much cheaper alternative but there are some drawbacks e.g. loss of carbohydrates by respiration and biomass build-up and the requirement of long pretreatment periods (3). Anaerobic fungi (AF) from the phylum Neocallimastigomycota living in the rumen are of particular importance in the nutrition of herbivorous animals (4), as they are able to break down lignocellulose with high efficiency. The AF attach to the plant material and crack the fibres mechanically by growth and expansion of their rhizoids or bulbous holdfasts (5). To exploit this feature, we need to understand what the ideal conditions are for them and which microbes are their "favorite" partners. During our study, we isolated anaerobic fungi and their methanogenic partners from anoa, elephant and mouflon. In our experiments, we monitored the degradation efficiency using pure anaerobic fungal culture and anaerobic fungal - methanogenic co-cultures.

In this study, treatment with anaerobic fungi cultures (14-day) increased the total biomethane yield during the experimental period of 20 days. Pretreatment with anaerobic fungi significantly improved the degradability of substrates. The results for AF biomethane yields correlated well with the organic acid concentrations measured by HPLC and with the enzyme activities. From these it can be concluded that the anaerobic fungi degraded the substrate efficiently during the 14-day long treatment.

Based on these results AF isolates were effective in enhancing cellulose degradation and successfully increased biogas production.

References
1 Williams, L., Gallagher, J., Bryant, D., Ravella, S.R. 2016. Anaerobic digestion and the use of pre-treatments on lignocellulosic feedstocks to improve biogas production and process economics. Advances in biofeedstocks and biofuels, Volume One: Biofeedstocks and their processing, pp. 121.
2 Rodriguez, C., A. Alaswad, K.Y. Benyounis, A.G. Olabi 2017. Pretreatment techniques used in biogas production from grass. Renew. Sust. Energy Rev., 68 (Part 2) (2017), pp. 1193-1204.

3 Isroi, M., Ria, Syamsiah, S., Niklasson, C., Cahyanto, M.N., Ludquist, K., Taherzadeh, M.J., 2011. Biological pretreatment of lignocelluloses with white-rot fungi and its applications: a review. BioResources 6(4), 5224-5259.

4 Liggenstoffer, A.S., Youssef, N.H., Couger, M.B., Elshahed, M.S. 2010.Phylogenetic diversity and community structure of anaerobic gut fungi (phylum Neocallimastigomycota) in ruminant and non-ruminant herbivores. ISME J., 4 (10) (2010), pp. 1225-1235

5 Akin, D.E., Borneman, W.S. 1990. Role of rumen fungi in fiber degradation. J. Dairy Sci., 73 (10) (1990), pp. 3023-3032

R7-SUBSTITUTED 8-HYDROXYQUINOLINES WITH MULTIDRUG RESISTANCE SELECTIVITY: SOLUTION CHEMISTRY AND METAL COMPLEXATION

Hilda Kovács[1], Bálint Hajdu[1], Nóra V. May[2], Norbert Lihi[3], István Szatmári[4], Gergely Szakács[5], Éva A. Enyedy[1]

[1]*Department of Molecular and Analytical Chemistry, Interdisciplinary Excellence Centre, University of Szeged, Dóm tér 7-8, H-6720 Szeged, Hungary*
[2]*Centre for Structural Science, Research Centre for Natural Sciences, Hungarian Research Network (HUN-REN), Magyar tudósok körútja 2, H-1117 Budapest, Hungary*
[3]*Department of Inorganic and Analytical Chemistry, University of Debrecen, Egyetem tér 1., H-4032 Debrecen, Hungary*
[4]*Institute of Pharmaceutical Chemistry and Stereochemistry Research Group, Eötvös Loránd Research Network, University of Szeged, Eötvös u. 6, H-6720 Szeged, Hungary*
[5]*Center for Cancer Research, Medical University of Vienna, Borschkegasse 8a, A-1090 Vienna, Austria*
e-mail: kovacs.hilda@chem.u-szeged.hu

8-hydroxyquinoline (8HQ) derivatives have a wide range of biological properties, including anticancer activity [1]. 8HQ-based Mannich bases with a methylamine subunit at position 7 (R7) are reported to have notable cytotoxicity, especially against multidrug resistant (MDR) cancer cell lines [2,3]. The biological activity of 8-hydroxyquinolines is often linked to complexation with the endogenous metal ions. The increased cytotoxicity of certain 8HQs on MDR cells is thought to result from either iron deprivation or the formation of redox-active copper(II) complexes [4].

Herein, studies on the interaction of five selected MDR-selective Mannich base HQ derivatives with Fe(II), Fe(III) and Cu(II) ions are presented in terms of solution speciation and redox properties of the forming complexes. The stoichiometry and formation constants of the complexes were determined via UV-visible spectrophotometric titrations. In the case of Cu(II) complexes, circular dichroism and electron paramagnetic resonance spectroscopy were also applied to confirm the coordination modes. To explore the redox properties of the iron and copper complexes cyclic voltammetric and spectroelectrochemical measurements were performed. The properties of the studied complexes are compared with those of non-MDR-selective 8HQs in order to identify differences in their solution chemical behavior.

References
[1] Y. Song, H. Xu, W. Chen, P. Zhan, X. Liu, Med. Chem.Commun. 6 (2015) 61–74.
[2] T. Pivarcsik, O. Dömötör, J. P. Mészáros, N. V. May, G. Spengler, O. Csuvik, I. Szatmári, É. A. Enyedy, Int. J. Mol. Sci. 22 (2021) 11281.
[3] V. F.S. Pape, A. Gaál, I. Szatmári, N. Kucsma, N. Szoboszlai, C. Streli, F. Fülöp, É. A. Enyedy, G. Szakács, Cancers 13 (2021) 154.
[4] V. F. S. Pape, R. Palkó, S. Tóth, M. J. Szabó, J. Sessler, G. Dormán, É. A. Enyedy, T. Soós, I. Szatmári, G. Szakács, J. Med. Chem. 65 (2022) 7729–7745.

BORON DOPED CARBON QUANTUM DOTS: PREPARATION, CHARACTERIZATION AND POTENTIAL APPLICATION

Nataša Tot[1, 2], Bojana Vasiljević[3], Vesna Despotović[1], <u>Jelena Kozić[3*]</u>, Duška Kleut[3], Jovana Prekodravac[3]

[1]*University of Novi Sad Faculty of Sciences, Department of Chemistry, Biochemistry and Environmental Protection, Trg Dositeja Obradovića 3, 21000 Novi Sad, Serbia,*
[2]*Technical College of Applied Sciences in Zrenjanin, Đorđa Stratimirovića 23, 23000 Zrenjanin, Serbia[3]*
Vinca Institute of Nuclear Sciences-National Institute of the Republic of Serbia, Universitz of Belgrade, Mike Petrovića Alasa 12-14, 11000 Belgrade, Serbia
*e-mail: jelena.kozic@vin.bg.ac.rs

Abstract

When thinking about adding dopants to carbon quantum dots, the element boron, which has a similar atomic radius to carbon, is a rather natural candidate. However, the carbon quantum dots surface can drastically alter the electrical properties and, as a result, the optical behaviour of hetero-atoms with more electrons than carbon. Despite the fact that boron is a heteroatom with less electrons than carbon, the majority of research publications on boron addition that have been published focus on boron/nitrogen co-doping, and there is very little work that specifically discusses boron doping. The presented research illustrates a straightforward, environmentally friendly method for creating boron doped carbon quantum dots. This is the first report on boron doped carbon quantum dots microwave synthesis under specific reaction circumstances that we are aware of in the literature. Prepared boron doped carbon quantum dots showed high photo-catalytic activity towards the model organic dye Rose Bengal chosen for this purpose, with 84% of the Rose Bengal dye removed.

Introduction

Carbon quantum dots (CQD) physical-chemical properties and ability to change them through doping by different hetero-atoms, gained research attention over the years [1], [2]. Nevertheless, finding the appropriate method for their preparation is a challenging task due to several issues such as high temperature, log hours and green medium for CQD synthesis. A variety of top-down and bottom-up techniques for CQD production have been developed over the years. The top-down method indicates the breaking of macro-molecules into small-sized CQD by physicochemical means, whereas the bottom-up method generally refers to the polymerization and carbonization of simple molecules into CQD through a chemical reaction. Because of its efficacy in synthesis and exploitation, the microwave (MW) pyrolysis process is one of the bottom-up methodologies that has attracted public attention [3]–[5]. This basic method of making CQD rich in oxygen-containing groups allows for quicker reactions, decreased energy usage, greater reaction yields, and increased particle size homogeneity while being environmentally friendly.

Despite the addition of both metal and non-metal (hetero-atom) dopants to the CQD matrix, the non-metal-based doping showed exceptional promise by enhancing their photo-luminescence powers. By substituting some carbon atoms with hetero-atoms like N, B, P, and S, one can modify the surface chemistry and electronic properties of CQD, which improves the structures' catalytic activity [6]. A wide range of possible uses for this material are made possible by the introduction of B dopant, which alters the surface chemistry and morphology of CQD. Carbon dots with boron doped could be used, among other things, for photo-catalytic destruction of

dangerous organics, Fe^{3+} detection, and radiometric intracellular pH monitoring in cancer cell lines [7]–[9].

Determination of the physical, chemical and optical properties is of greate significance in finding the right and full range of the potential applications for the selected materials. Therefore, the presented pear focus on the green synthesis of B-CQD using MW method and investigation on the morphological, elemental and optical properties with final application of prepared B-CQD in photo-catalytic reaction.

Experimental

Two precursors were used in the B-CQD synthesis process. Boric acid (0.02 g ml⁻¹) and glucose water solution (0.1 g ml⁻¹) were mixed for 30 minutes at 600 rpm on a magnetic stirrer. The reaction mixture was then heated for 5 minutes at a fixed temperature (170 °C) in a microwave reactor (Anton Paar Monowave 300), and then cooled to room temperature. The effective synthesis of B-CQD was demonstrated by the color change from translucent to light yellow that was seen. Dialysis (3.5 kDa) and filtration employing filters with various pore sizes were used to clean the sample.

Photocatalysis was carried out under constant conditions of reaction time of 300 minutes, medium pH of 7, B-CQD catalyst concentration of 0.2 mg ml⁻¹, and rose bengal (RB) dye as chosen pollutant in concentration of 0.03 mM. For the photocatalytic testing the home made photoreactor with six LEDs operating at 370 nm wavelength was used.

Results and discussion

The elemental composition of the prepared B-CQD was investigated using XPS and FTIR analysis methods (Figure 1).
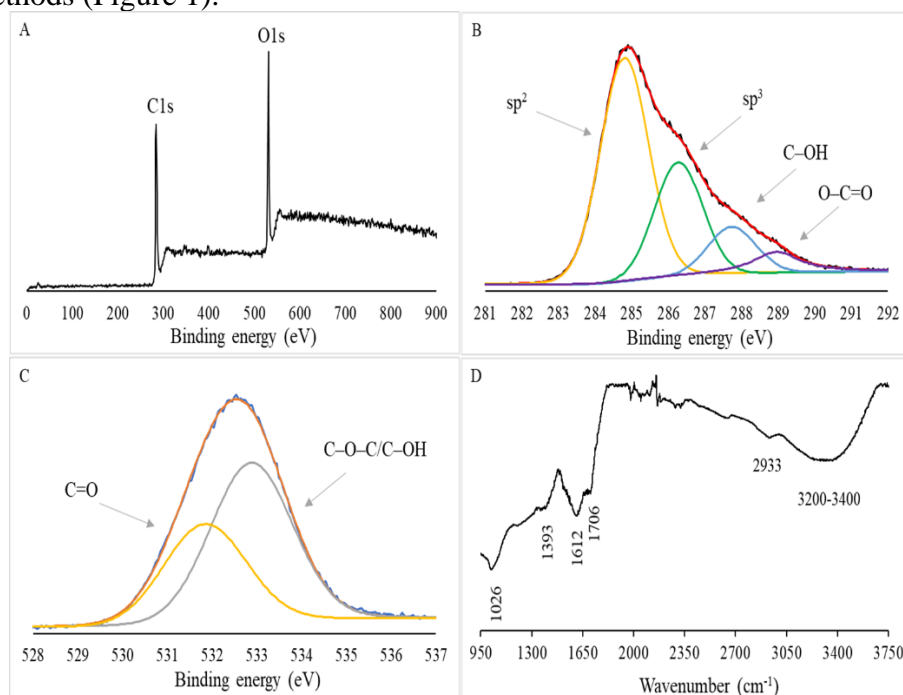
Figure 1. The B-CQD sample analysis showing the XPS full scan spectra (A), the C1s (B) and O1s (C), and FTIR (D).

From the obtained XPS results (Figure 1 A-C), the presence of carbon as sp² and sp³, and oxygen as C-OH and O-C=O, was confirmed after material preparation and purification. The presence of B dopant was not registered after XPS characterization due to the methods limit of detection which is below 0.3 at%. This was confirmed by performing additional

characterizations using ICP-OES analysis. The solid B-CQD nanomaterial contained 0.506 mg g^{-1} of B, which corresponds to a very low percentage of 0.051 B.

The FTIR study (Figure 1D) revealed peaks at 3200-3400 cm-1 and 2933 cm-1, respectively, resulting from the stretching vibrations of the O-H and C-H groups. The B-CQD surface had a lot of hydroxyl groups, which have a favourable hydrophilicity. Peaks also appear at 1706 cm-1 and 1612 cm-1, respectively, as a result of the stretching of the C=O and C=C bonds. The production of carboxylic acid groups on the surface of B-CQD nanoparticles was successfully demonstrated by the stretching of the hydroxyl and carboxyl groups as well as the symmetrical carbonyl stretching at 1706 cm-1. The formation of unsaturated C=C bonds in the carbon cores was shown by the occurrence of the 1612 cm-1 signal. Signals were also found at 1393 cm-1 and 1026 cm-1, which correlate to the stretching of B-O and B-C.

The investigation of the morphological features of synthesized B-CQD was obtained through AFM and TEM characterization (Figure 2). The AFM analysis (Figure 2A) showed monodispersing particles with a nearly spherical form with particle sizes ranging from 5 to 20 nm and average height between 1 and 5 nm. The obtained results were in correlation with TEM (Figure 2B) results were observed particles were between 7.5 nm and 17.5 nm in diameter.
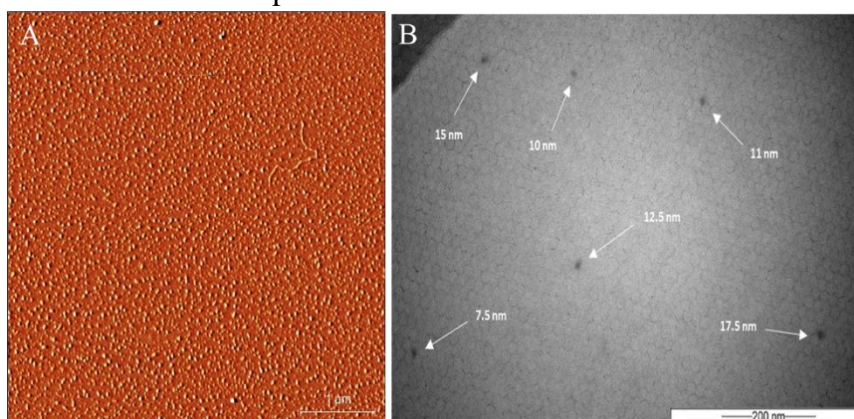
Figure 2. The B-CQD sample morphological analysis showing the AFM (A) and the TEM (B) images.

The optical properties of prepared B-CQD were examined by UV absorbance and PL (Figure 3). The absorbance at 268 and 356 nm, which corresponds to the existence of π- π* transitions of aromatic sp^2 domains (C=C) and n-π* transitions of C=O bonds, was discovered by UV-vis spectroscopy (Figure 3A).
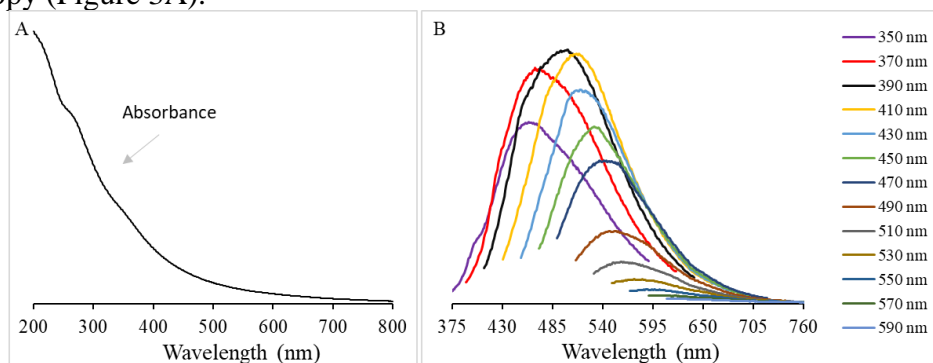
Figure 3. The B-CQD sample optical properties analysis showing the UV-vis absorbance (A) and the PL (B) spectrum.

The PL characteristics of carbon nanoparticles are caused by two different factors. Both intrinsic emission and emission from the defect state or trap state, which derives from various

surface functional groups connected to the carbon core, are related to particle size in one case. The emission of B-CQD in the 350-590 nm range displayed excitation dependence (Figure 3B). The maximum peak fluorescence emission was observed at 496 and 511 nm, respectively, after excitation at 390 and 410 nm, suggesting the blue-green emission spectrum. In this particular case, the Quantum Confinement Effect (QCE) model method is more likely to be the PL mechanism than emission from the defect state or trap state.

Prior to the photocatalytic activity investigation of B-CQD towards the RB organic dye degradation, the experiments of photolysis were performd in dark condditions and upon illumination (Figure 4). The obtained results suggested the RB dye self decomposition at 370 nm irradiation under 300 min of exposure up to 61%. However, in the presence of B-CQD nanomaterial, the adsorption in dark condditions was observed, where approximately 11% of the RB dye was adsorbed to the surface of the B-CQD photocatalyst. Under irradiation, the results obtained in the presence of a photocatalyst were coparable to the photolysis experiments i the first 90 minutes of irradiation. However, by prolongating the irradiation time up to 300 minutes, and obvious degradation effect and photoactivity of B-CQD nanomaterial was pronaunced. The final result showed the high B-CQD nanomaterial potential in RB organic dye removal efficiency of 84% under 300 min of irradiation.
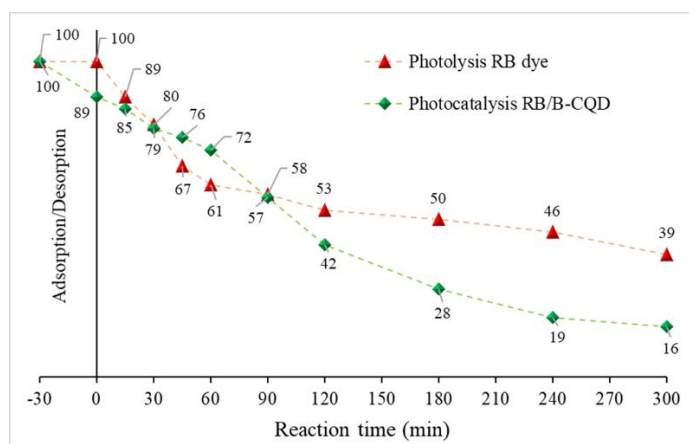
Figure 4. The B-CQD sample photocatalytic acivity in the presence of RB organic dye.

Conclusion

According to the study, it is possible to create boron-doped carbon quantum dots (B-CQD) using only glucose and boric acid and a microwave in under four minutes. The resulting B-CQD had an average diameter of 12 nm and were composed of negatively charged spheres. The hydroxyl, carbonyl, and carboxyl groups on B-CQD's surface are responsible for its excellent water dispersion capabilities. The rose Bengal (RB) dye was broken down by the B-CQD to 16%, respectively, within 300 minutes, demonstrating its excellent photocatalytic efficacy. The B-CQD produced in this work is shown to be an attractive option for the degradation of organic pollutants and ecological sustainability when considering its excellent photocatalytic activity and the ease with which it can be made using a microwave-assisted approach, without the need for time-consuming synthesis and purification.

Acknowledgements

References

[1] S. Jovanović, Z. Marković, M. Budimir, J. Prekodravac, D. Zmejkoski, D. Kepić, A. Bonasera, B. Todorović Marković, J. Pharm. 15 (2023) 1170.

[2] J. Prekodravac, Z. Marković, S. Jovanović, I. Holclajtner Antunović, D. Kepić, M. Budimir, B. Todorović Marković, Mater Res. Bull. 88 (2017) 114.

[3] Y. Wang, Q. Zhuang, Y. Ni, Chem. Eur. J. 21 (2015) 13004.

[4] K. K. Chan, C. Yang, Y. H. Chien, N. Panwar, K. T. Yong, New J. Chem. 43 (2019) 4734.

[5] S. F. El-Malla, E. A. Elshenawy, S. F. Hammad, F. R. Mansour, Anal. Chim. Acta. 1197 (2022) 339491

[6] Q. Xu, T. Kuang, Y. Liu, L. Cai, X. Peng, T. S. Sreeprasad, P. Zhao, Z. Yu, N. Li. J. Mater. Chem. B. 4 (2016) 7204.

[7] Y. Zhang, H. Qin, Y. Huang, F. Zhang, H. Liu, H. Liu, Z. J. Wang, R. Li. J. Mater. Chem. B. 9 (2021) 4654.

[8] L. Largitte, N. A. Travlou, M. Florent, J. Secor, T. J. Bandosz, J. Photochem. Photobiol. A. Chem. 405 (2021) 112903.

[9] A. Pal, K. Ahmad, D. Dutta, A. Chattopadhyay, Chem. Phys. Chem. 20 (2019) 1018.

SUSTAINABLE DYEING OF THE FABRICS BY USING AZO PYRIDONE DYES WITH IMPROVED WATER SOLUBILITY

Jelena Lađarević[1], Anita Lazić[2], Marija Dimitrijević[1], Aleksandra Mašulović[2], Luka Matović[2], Dušan Mijin[1], Aleksandra Ivanovska[2]

[1]*Faculty of Technology and Metallurgy, University of Belgrade, Karnegijeva 4, 11000 Belgrade, Serbia*
[2] *Innovation Center of the Faculty of Technology and Metallurgy, University of Belgrade, Karnegijeva 4, 11000 Belgrade, Serbia*
e-mail: jmirkovic@tmf.bg.ac.rs

Abstract
Colored effluents from the textile industry contribute significantly to water pollution, posing a serious environmental challenge. Reducing water pollution is a key focus in the EU's goal of achieving climate neutrality by 2050. In line with this, the idea of reusing the same dyebath for multiple dyeing cycles in textile industry is suggested. Therefore, in this study, two azo pyridone dyes with enhanced water solubility are synthesized, fully characterized and used for dyeing fabrics of different chemical compositions. Firstly, the affinity of dyes towards different fabrics is screened by using multifiber fabric, and thereafter individual fabrics are dyed following the principles of sustainable dyeing. The fabrics dyed in each cycle are further analyzed for color strength. The results demonstrate the feasibility of reusing the same dyebath up to four times, significantly reducing the concentration of synthetic dye in the final wastewater.

Introduction
The practices of the textile industry have led to numerous environmental and social challenges [1]. Among them, the disposal of colored effluents into natural ecosystems has become a global concern. Textile production is estimated to account for about 20% of global clean water pollution [2], largely due to the inefficiencies in the dyeing and finishing processes, where a large proportion of unfixed dyes are washed out. To address this, strategies aimed at improving dye fixation and reducing concentration of dyes in wastewater should be developed focusing on the development of dyes with improved properties, optimization of the dyeing process, and adoption of sustainable practices.

Although much effort has been made into developing eco-friendly natural dyes, synthetic dyes still outperform them due to their superior dyeing abilities and imparting excellent color fastness properties to fabrics. Also, synthetic dyes are convenient structures that can be modified by molecular design to finely tune their properties for different applications. In such a way, they can be tailored to be more soluble and/or to exhibit higher affinity towards the fabrics, ensuring better dye uptake and reducing the concentration of dyes in wastewater.

Among synthetic dyes, azo pyridone dyes have become widely used in the textile industry for their ease of production, imparting excellent color fastness properties to fabrics, vibrant color strength, and stability under heat and light [3]. Traditionally, these dyes are used as disperse dyes, which have low water solubility and are well-suited for dyeing hydrophobic fibers. However, a recent study showed that introducing a pyridinium ring into the pyridone structure increases the water solubility of the dyes and enhances their compatibility with a range of fibers, especially wool and cellulose diacetate [4].

Taking into account the above stated, this work aims to develop azo pyridone dyes with higher water solubility by introducing carboxylic (dye **1**) and sulpho (dye **2**) groups into phenyl ring

(Figure 1). They were further applied in the dyeing of fabrics of different chemical compositions. In order to tackle the environmental challenges caused by the textile industry, the fabric dyeing will be performed in an eco-friendly manner (no additional adjustment of dyebath pH value, lower temperature than recommended for similar dyeing procedures) while reducing the waste by using the same dyebath multiple times. In such a way, the amount of water and concentration of dyes in wastewater are reduced. The obtained fabrics will be characterized by K/S values.
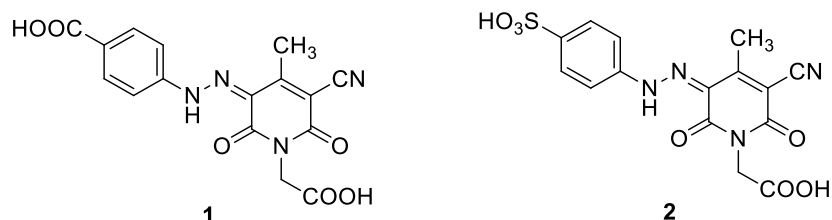
Figure 1.The structure of the azo pyridone dyes.

Experimental
Synthesis and characterization of pyridone dyes
Two pyridone dyes were synthesized according to the procedure previously reported [3]. Compound **1** has been already reported and characterized in the literature [3], while compound **2** is new and characterized by their melting points, elemental analysis, ATR-FTIR, UV–Vis, ^{1}H and ^{13}C NMR spectra.

5-(4-sulphophenylazo)-1-carboxymethyl-3-cyano-6-hydroxy-4-methyl-2-pyridone (**2**). Orange powder; yield: 48%; m.p. > 300 °C; ATR-FTIR (v/cm^{-1}): 3340 (OH substituent), 2225 (CN), 1731 (COOH), 1668, 1628 (C=O); ^{1}H NMR (200 MHz, DMSO-d_6, δ/ppm): 14.68 (1H, s, NH hydrazone), 7.95 (2H, d, J = 8.0 Hz, Ar–H), 7.69 (2H, d, J = 8.0 Hz, Ar–H), 4.54 (2H, s, CH$_2$COOH), 2.54 (3H, s, CH$_3$); ^{13}C NMR (50 MHz, DMSO-d_6, δ/ppm): 169.1 (COOH), 160.5 (Py), 160.1 (Py), 159.7 (Py), 127.3 (Ar), 123.0 (Py), 117.7 (Ar), 117.6 (Ar), 115.4 (CN), 115.3 (Ar), 99.4 (Py), 34.6 (CH$_2$COOH), 16.9 (CH$_3$); UV-Vis (EtOH) (λ_{max}/nm (log ε /mol^{-1}dm^{3}cm^{-1})): 431.5 (4.22).

Fabric dyeing and characterization
To assess the efficacy of synthesized dyes for dyeing fabrics of different chemical compositions, screening experiments were conducted utilizing a Multifiber Adjacent Fabric Style 49 (James Heal, England). This fabric consisted of 1.2 cm wide bands of diacetate (CA), bleached cotton (CO), spun polyamide 6.6 (PA), spun polyester (PES), spun polyacrylonitrile (PAN), silk (SILK), spun viscose (CV) and wool (WO). The dyeing procedure adhered to specific experimental parameters: a fabric-to-liquid ratio of 1:50, 0.34% o.w.f. (on the weight of fabric), 60 °C for 60 min with continuous shaking in a water bath (Memmert, WNE 14). The dyebath was prepared by dissolving 6.4 mg of dye in a solution comprising 10 ml of methanol and 85 ml of distilled water without pH adjustment (pH 4.4 for dye **1** and pH 4.3 for dye **2**). After dyeing, the fabrics underwent sequential washing cycles with warm and cold distilled water for 5 min, followed by air-drying at ambient temperature.

Screening experiments conducted on Multifiber Adjacent Fabric Style 49 revealed that the studied dyes demonstrated significant affinity towards dyeing PA and WO fabrics, with dye **1** additionally exhibiting affinity for dyeing CA fabric. Therefore, fabrics composed entirely of PA, WO, and CA in a plain weave were selected for simultaneous dyeing and functionalization experiments, maintaining the previously delineated experimental parameters.

Results and discussion

Azo pyridone dyes are well-known as structures exhibiting azo-hydrazone tautomerism (Figure 2). Tautomerism is significant not only for chemists but also for dye manufacturers, as the different tautomers can vary in color, tinctorial strength, and properties related to the dyed material such as wash fastness, light fastness, sublimation, and perspiration resistance. Thus, the determination of the tautomeric form of azo pyridone dyes is crucial since it can determine their suitability for different applications. According to spectral data, it is concluded that these dyes exist in hydrazone tautomeric form in the solid state and DMSO-d_6. Furthermore, UV-Vis spectra show that these dyes exist solely in hydrazone form in most of the solvents, while in the solvents of high basicity and permittivity (*N,N*-dimethylformamide, dimethylsulfoxide and *N,N*-dimethylacetamide), deprotonation of hydrazone form occurs leading to the acid-base equilibrium.
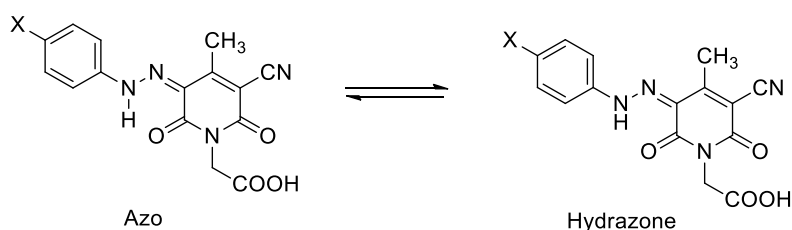
Figure 2. Azo-hydrazone tautomerism of the investigated dyes.

The introduction of the acidic groups (carboxy (**1**) and sulpho (**2**)) into azo pyridone dye architecture ensures higher water solubility when compared to traditional disperse pyridone dyes. The screening of the dyeing ability of the characterized dyes was performed using multifiber fabric (Figure 3). According to Figure 3, it can be observed that good dyeing performance is achieved for CA, PA and WO for dye **1**, while PA and WO exhibited the highest affinity towards dye **2**.
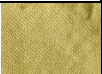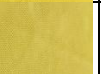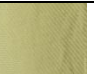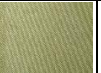
Figure 3. Multifiber fabrics' appearance after dyeing with **1** and **2** dye.

For further experiments, fabrics composed entirely of PA, WO, and CA were used for the dyeing process. The dyeing process that eliminates the need for harmful chemicals for dyebath pH adjustment, and is performed under mild acidic conditions at lower temperatures than recommended marks a significant advancement in the dyeing of CA, WO and PA. Furthermore, the concentration used for dyeing (0.34%) is significantly lower than the commonly used (> 1%), contributing to minimizing the environmental impact of the textile industry.

The dye exhaustion was tested by using the same dyebaths multiple times. The dyeing experiments showed that the same dyebath could be efficiently used for dyeing all fabrics up to 4 times, regardless of the used dye. Dyed fabrics are characterized by reflectance spectra that were further used for the calculation of the color strength (*K/S*), Table 1. The results in Table 1 show the expected decrease of the *K/S* values with the higher number of dyeing cycles. Even though the decline of color strength is evident, *K/S* values after the fourth dyeing cycle of WO

(for both dyes) and PA (for dye **1**) are still satisfactory (> 1). For dye **1**, the highest K/S value is obtained for PA while the lowest is observed for WO. On the contrary, for dye **2**, higher K/S values are obtained for WO indicating different governing forces responsible for the adhesion of two dyes onto fibers. Considering dyes, it should be pointed out that higher color strength is obtained for carboxy-substituted dye **1** for each dyeing cycle indicating better adhesion of this dye to WO and PA.

Table 1. K/S values and visual appearance of dyed fabrics for different dyeing cycles

	Dye **1**					Dye **2**		
	WO		PA		CA		WO	PA
I cycle	2.06		5.71		3.76		1.75	1.14
II cycle	1.67		3.55		3.01		1.33	0.95
III cycle	1.57		2.75		1.25		1.11	0.58
IV cycle	1.19		2.01		0.62		1.08	0.33

Conclusion

In this study, two azo pyridone dyes with improved water solubility are synthesized and characterized. The dyes are proven to exist in hydrazone form in solid state and most of the solvents. After detailed characterization, their dyeing ability was tested against multifiber fabric. Screening revealed that the best dyeing performance for carboxy-substituted dyes is achieved for WO, PA and CA, while sulpho-substituted dye exhibited good affinity towards WO and PA. The results demonstrate the feasibility of reusing the same dyebath for the dyeing of individual fabrics, significantly reducing the concentration of dye in the final wastewater. Good color strength values (K/S >1) are observed for WO for both dyes and for PA for carboxy-substituted dye after the fourth cycle. Additionally, the use of low dye concentrations, moderate dyebath temperatures and no need for harmful chemicals enhances energy efficiency and reduces pollution, making this dyeing procedure suitable for large-scale and commercial applications.

Acknowledgements

References

[1] S.L.H. Naqvi, M. Nadeem, F. Ayub, A. Yasar, S.H.Z. Naqvi, R. Tanveer, Social and Environmental Impacts in Textile Production. In: Singh, P. (eds) Dye Pollution from Textile Industry. Springer, Singapore, 2024, pp. 423-453.
[2] https://www.europarl.europa.eu/topics/en/article/20201208STO93327/the-impact-of-textile-production-and-waste-on-the-environment-infographics
[3] J. Lađarević, B. Božić, L. Matović, B. Božić Nedeljković, D. Mijin, Dyes Pigments 162 (2019) 562.
[4] A.D. Mašulović, J.M. Lađarević, A.M. Ivanovska, S.Lj. Stupar, M.M. Vukčević, M.M. Kostić, D.Ž. Mijin, Dyes Pigments 195 (2021) 109741.

MICROWAVE SYNTHESIS OF DISUBSTITUTED PYRROLIDINE-2,5-DIONE DERIVATIVES

Marija Dimitrijević[1], Kristina Gak Simić[2], Aleksandra Mašulović[2], Luka Matović[2], Jelena Lađarević[1], Nebojša Banjac[3], Nemanja Trišović[1], <u>Anita Lazić[2]</u>

[1]Faculty of Technology and Metallurgy , University of Belgrade, Karnegijeva 4, Belgrade, Serbia;
[2]Innovation Centre of the Faculty of Technology and Metallurgy, Karnegijeva 4, Belgrade, Serbia
[3]Faculty of Agriculture, University of Belgrade, Nemanjina street 6, Belgrade, Serbia
e-mail: alazic@tmf.bg.ac.rs

Abstract

Succinimide (pyrrolidine-2,5-dione) derivatives are organic compounds with a broad spectrum of pharmacological activities. Analogs of this cyclic ureide are well-known and comercially available anticonvulsants (ethosuccinimide, metosuccinimide and fensuccinimide), antipsychotics, sedatives, anticancer and antiviral agents. In this paper, using a modified microwave procedure, three succinimide derivatives were synthetized and completely structurally characterized by determination of melting points, as well as FT-IR/ATR, ^{1}H NMR, ^{13}C NMR and elemental analysis. The influence of chemical structure on the pharmacological activity of succinimide derivatives was evaluated using the pioneering "rule of five", Veber, Egan, and Ghose's empirical criteria, as well as using different *in silico* methods. Obtained values of molecular descriptors were compared with the characteristic values for reference drugs such as methosuccinimide and ethosuccinimide. Calculated molecular descriptors suggest that the investigated compounds fulfill necessary empirical criteria which qualify them as interesting drug candidates. The obtained descriptors indicate a high degree of gastrointestinal absorption (98%) of the synthesized succinimide derivatives. They are expected to successfully pass through the blood-brain barrier due to the adequate lipophilicity.

Introduction

During the last few decades, heterocyclic compounds have gained a lot of attention because of their numerous significant medical and biological uses. Research interest on heterocyclic compounds is rapidly increasing due to the extensive synthetic study and functional utility. They are found in more than 90% of novel drugs, and span the gap between biology and chemistry, where so much scientific discovery and application occurs. Heterocycles also play a role in different fields, such as agrochemicals and veterinary medicine [1]. Many heterocyclic scaffolds can be considered as privilege structures. According to literature, more than 85% of all pharmacologically-active compounds contain a heterocycle as a main structural motif. This fact reflects the central role of heterocycles in modern drug design. The application of heterocycles provides a useful tool for modification of solubility, lipophilicity, polarity, and hydrogen bonding capacity of pharmacologically active compounds, which results in the optimization of the ADME/Tox properties of drugs or drug candidates. Most frequently, nitrogen heterocycles or various positional combinations of nitrogen atoms, in five- or six-membered rings can be found [2]. Succinimide derivatives are mainly used in medicine as anticonvulsant drugs, under the names zarontin, milontin and celontin. In addition, numerous 2-arylsuccinimides such as 3-phenyl-2,3-dimethylsuccinimide and its *N*-methyl

derivative exhibit anticonvulsant properties and are generally used in the treatment of milder forms of epilepsy because they do not induce sedation. Disubstituted analogs such as *N*-methyl-2-phenyl-2-ethyl- and *N*-methyl-2-phenyl-3-methylsuccinimides are examples of non-toxic antiepileptics suitable for minor forms of seizures. Derivatives of this cyclic core are used in the treatment of various disorders of the central and peripheral nervous system, primarily tremors, partial tremors associated with Parkinson's disease and multiple sclerosis [3]. In more than 30 years of microwave chemistry, many green protocols in organic synthesis have been reported, showing significant advantages compared to the conventional heating. Selective, volumetric dielectric heating has resulted in time and energy savings, enabled the deployment of safer solvents or solvent-free processes, selective catalysis in fewer steps, and generally attaining higher selectivity and yields [4]. The technique offers simple, clean, fast, efficient, and economic features for the synthesis of a large number of organic compounds [5]. Guided by these facts, in order to establish quantitative correlation between chemical structure and pharmacological activity, we synthesized three disubstituted pyrrolidine-2,5-diones (Figure 1). All these compounds were synthesized in good yields taking advantage of the microwave process, and were completely structurally characterized by different spectroscopic techniques. The assessment of the pharmacokinetic profile was performed by predicting their ADMET (Absorption, Distribution, Metabolism, Excretion and Toxicity) properties, i.e bioavailability, using various empirical rules and software packages.
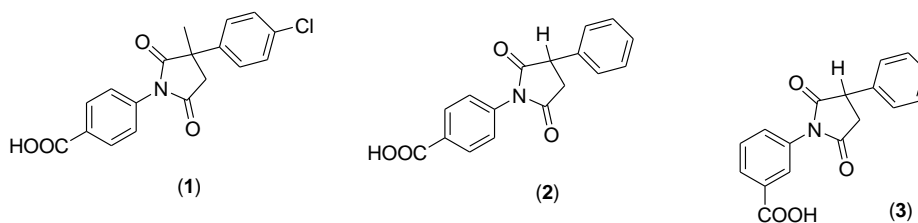
Figure 1. The chemical structure of the investigated compounds (**1**–**3**).

Experimental

General procedure for the synthesis of disubstituted pyrrolidine-2,5- diones (**1**–**3**)

Disubstituted pyrrolidine-2,5-dione derivatives were synthesized according to a modified method from the (Scheme 1) [6]. The disubstituted succinic acid (1 mol) was mixed with 3- or 4-substituted benzylamine (1.16 mol) in a microwave reactor and then the resulting reaction mixture was heated at 180 °C for 15 minutes. After cooling to room temperature, the product formed is purified by recrystallization from ethanol.

R_1	R_2	X		Compound	R_1	R_2	X
CH₃	4-Cl-C₆H₄-	4-CO₂H		1	CH₃	4-Cl-C₆H₄-	4-CO₂H
H	C₆H₅⁻	4-CO₂H		2	H	C₆H₅⁻	4-CO₂H
H	C₆H₅⁻	3-CO₂H		3	H	C₆H₅⁻	3-CO₂H
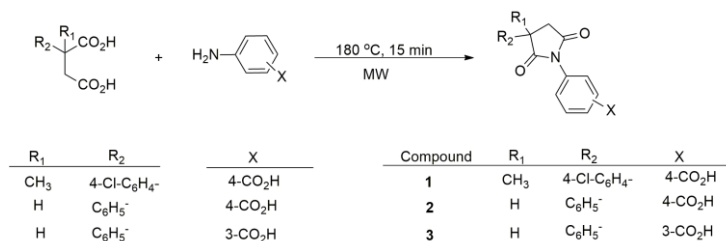
Scheme 1. Synthesis of the investigated compounds (**1**–**3**).

4-(3-(4-Chlorophenyl)-3-methyl-2,5-dioxopyrrolidin-1-yl)benzoic acid (1): White crystalline solid; Yield: 88%; m.p. = 163−172°C, FTIR/ATR (ν/ cm–1): 1696, 1681, 1674,

1661, 1635, 1625, 1622, 1595, 1574, 1557, 1525, 1519, 1511, 1495, 1453, 1439, 1422, 1384, 1343, 1309, 1285, 1281, 1233, 1169, 1127, 1002, 964, 864, 841, 821, 768, 694, 533, 527, 519, 504, 472, 460, 451; ^{1}H NMR (400 MHz, DMSO-d_6, δ/ppm): 11.0 (s, 1H, COOH), 8.07 (d, 2H, J = 8.4 Hz, C$_6$H$_4$), 7.51 (d, 2H, J = 10.0 Hz, C$_6$H$_4$), 7.37 (d, 2H, J = 8.4 Hz, C$_6$H$_4$), 7.27 (d, 2H, J = 8.4 Hz, C$_6$H$_4$), 3.59 (s, 1H, -CH-), 3.09–2.92 (m, 2H, -CH$_2$-), 1.78 (s, 3H,-CH$_3$-); ^{13}C NMR (100 MHz, DMSO-d_6, δ/ppm): 175.8, 174.9, 169.3, 137.1, 134.1, 133.2, 131.0, 130.5, 129.3, 124.3, 45.6, 24.5; Elementary analysis: Calculated for: C$_{18}$H$_{14}$ClNO$_4$ (343.76): C, 62.89; H, 4.10; N, 4.07; Found (%):C, 62.86; H, 4.13; N, 4.07.

4-(3-methyl-2,5-dioxo-3-pheylpyrrolidin-1-yl)benzoic acid (2): White crystalline solid; Yield: 72%; m.p. = 172−175°C, FTIR/ATR (ν/ cm–1): 1705, 1682, 1604, 1585, 1492, 1422, 1383, 1366, 1310, 1271, 1197, 1184, 1169, 1125, 1094, 927, 829, 792, 766, 768, 719, 703, 669, 646, 631, 540, 515, 503, 435; ^{1}H NMR (400 MHz, DMSO-d_6, δ/ppm): 11.0 (s, 1H, COOH), 8.04 (d, 2H, J = 8.4 Hz, -C$_6$H$_4$), 7.46 (d, 2H, J = 8.4 Hz, -C$_6$H$_4$-), 7.40–7.27 (m, 5H, -C$_6$H$_5$-), 4.01 (s, 1H, -CH-), 3.15–2.90 (m, 2H, -CH$_2$-); ^{13}C NMR (100 MHz, DMSO-d_6, δ/ppm): 176.5, 170.7, 169.6, 136.3, 130.5, 129.6, 129.2, 128.5, 127.6, 124.3, 38.0, 32.9; Elementary analysis: Calculated for: C$_{17}$H$_{13}$NO$_4$ (295.29): C, 69.15; H, 4.44; N, 4.74; Found (%):C, 69.18; H, 4.41; N, 4.74.

3-(3-methyl-2,5-dioxo-3-pheylpyrrolidin-1-yl)benzoic acid (3): White crystalline solid; Yield: 76%; m.p. = 193−196°C, FTIR/ATR (ν/ cm–1): 1700, 1682, 1653, 1603, 1587, 1497, 1425, 1387, 1310, 1280, 1234, 1190, 1178, 1167, 1127, 1101, 1076, 1017, 950, 928, 865, 767, 749, 696, 645, 638, 655, 519, 502, 489, 474, 465; ^{1}H NMR (400 MHz, DMSO-d_6, δ/ppm): 11.0 (s, 1H, COOH), 8.45 (s, 1H, -C$_6$H$_4$-), 7.95 (s, 1H, -C$_6$H$_4$-), 7.77 (s, 1H, -C$_6$H$_4$-), 7.64 (s, 1H, -C$_6$H$_4$-), 7.49–7.31 (m, 5H, -C$_6$H$_5$-), 3.56 (s, 1H, -CH-), 2.75–2.50 (m, 2H, -CH$_2$-); ^{13}C NMR (100 MHz, DMSO-d_6, δ/ppm): 176.5, 170.7, 166.3, 136.3, 135.2, 133.3, 133.1, 129.6, 129.2, 128.3, 127.6, 38.0, 32.9; Elementary analysis: Calculated for: C$_{17}$H$_{13}$NO$_4$ (295.29): C, 69.15; H, 4.44; N, 4.74; Found (%):C, 69.13; H, 4.46; N, 4.74.

Results and discussion

Generally speaking, oral bioavailability can be defined as the balance between different molecular descriptors that significantly affect the values of pharmacokinetic/pharmacodynamic parameters of potentially pharmacologically active compounds associated with its ADMET (Absorption-Distribution-Metabolism- Elimination-Toxicity) properties. Bimolecular characteristics, such as cell membrane permeability and bioavailability, are closely related to basic molecular descriptors such as the partition coefficient, molecular weight, topological polar surface of molecules and the number of hydrogen donor/acceptor atoms [7]. Traditional methods for evaluating oral bioavailability are based on the application of classical empirical rules, among which the most famous is the "rule of number five", i.e. the rule of Lipinski [8]. In accordance with this "pioneering rule", good oral absorption can be expected for compounds whose set of physicochemical parameters is in the following ranges: partition coefficient logP <5, number of hydrogen donor atoms <5, number of hydrogen acceptor atoms <10, and relative molecular weight <500. Compounds that are presumed to have characteristics similar to those of commercial drugs must not show more than one deviation from Lipinski's rules. According to Veber's criterion, adequate oral bioavailability is achieved with compounds that have less than ten rotating bonds and a topological polar surface (TPSA) less than 140 Å^2 [9], which significantly limits their flexibility. According to the modified versions of these two concepts, for compounds whose physico-chemical parameters meet the following ranges: 160 ≤ molecular weight (MW) ≤ 480; –0.4 ≤ WlogP ≤ 5.6; 40 ≤ molar refractivity (MR) ≤ 130; 20 ≤

number of atoms (NA) ≤ 70 (Ghose's criterion) and WlogP ≤ 5.88; TPSA ≤ 131.6 Å2 (Egan's criterion) there is a high probability of therapeutic effects.

Table 1. Physico-chemical properties of the investigated compounds [10,11].

Compound	MW, g/mol	NA	nrb	HBD	HBA	MR	TPSA, Å^2
1	343.76	24	3	1	4	92.63	74.68
2	295.29	22	3	1	4	82.93	74.68
3	295.29	22	3	1	4	82.93	74.68
methosuccinimide	203.24	15	1	0	2	60.42	37.38
ethosuccinimide	141.17	10	1	1	2	40.51	46.17

Table 2. Values of the partition coefficient of the studied compounds [11].

Compound	logP$_{o/w}$ (XLOGP3)	logP$_{o/w}$ (WLOGP)	logP$_{o/w}$ (MLOGP)	Gastrointestinal absorption %
1	2.91	2.88	3.28	97.45
2	1.93	2.05	2.54	98.78
3	1.93	2.05	2.54	99.18
methosuccinimide	1.20	0.95	1.91	95.89
ethosuccinimide	0.38	0.07	0.65	93.49

Based on the values of molecular descriptors covered by the mentioned empirical rules (Tables 1 and 2), it can be concluded that the studied succinimide analogs meet all the above criteria, i.e. fulfilling the theoretical precondition for adequate bioavailability in the organism, and thus possess the appropriate pharmacological potential. Compared with standard anticonvulsant drugs that are chemically and structurally derivatives of succinimides such as metosuccinimide and ethosuccinimide, the introduction of substituents at succinimide ring results in an increase in molecular weight. Based on the calculated value of the polar surface of the molecules (Table 1), it is expected that in *in vivo* conditions, the tested succinimide derivatives will show better intestinal absorption and passage through the blood-brain barrier. A moderate number of rotatable bonds also contribute to the optimal passage of the studied molecules through the blood-brain barrier.

The data illustrated in Table 2, demonstrate that diverse values of the partition coefficient were obtained for the same compound, which is a consequence of a different mathematical algorithm for calculating this parameter within the software packages used. The optimal values of log*Po/w* allow these molecules to pass more successfully through the blood-brain barrier to passive diffusion as well as more successful binding to active sites at appropriate receptors, which is especially important for achieving the optimal concentration of drugs that act on the central nervous system. In addition to the optimal values of physicochemical parameters, it is necessary that the potential pharmacologically active compound also has optimal pharmacokinetic parameters. Using relevant software packages [10, 11, 12], the evaluation of the pharmacokinetic characteristics of succinimide derivatives was performed by determining more important descriptor-gastrointestinal absorption. The data from Table 2 indicate that the analyzed succinimide derivatives show a high degree of gastrointestinal absorption (approximately 98%), as well as that they successfully pass through the blood-brain barrier due to their optimal lipophilicity.

Conclusion

In order to create new potentially pharmcologicaly active compounds, three succinimide derivatives were prepared in good yields using ecofriendly microwave assisted synthesis. All compounds were obtained in good yields due to all advantages of the microwave irradiation. The chemical structure of the synthesized compounds was confirmed by determining the melting point, FT-IR/ATR, ^{1}H NMR, ^{13}C NMR and elemental analysis. The influence of the chemical structure on the pharmacological potential of succinimide derivatives was assessed by applying the "rule of five", Veber, Egan, and Ghose's empirical criteria, as well as by applying various *in silico* methods. Compared to the reference comercially available drugs such as, metosuccinimide and ethosuccinimide, all synthesized compounds have good intestinal absorption (approximately 98%) and represent good starting point for the synthesis of some new potentially pharmacologically active compounds.

Acknowledgements

References

[1] E. Kabir, M. Uzzaman, Results Chem. 4 (2022) 100606.

[2] J. Jampilek, Molecules 24 (2019) 3839.

[3] N. Banjac, N. Trišović, N. Valentić, G. Ušćumlić, S. Petrović, Hem. Ind. 65 (2011) 439.

[4] K. Martina, G. Cravotto, R. S. Varma, J. Org. Chem. 86 (2021) 13857.

[5] S. Nain, R. Singh, S. Ravichandran, Adv. J. Che. A. 2 (2019) 94.

[6] J. Petković-Cvetković. B. Božić, N. Banjac, J. Petrović, M. Soković, V. Vitnik, Ž. Vitnik, G. Ušćumlić, V. Valentić, J. Mol. Struct. 1181 (2019) 148.

[7] S.K. Dhanda, D. Singla, A. Mondal, G. Raghava, Biol. Direct. 8 (2013) 1.

[8] C. Lipinski, F. Lombardo, B. Dominy, P. Feeney, Adv. Drug Deliv. Rev. 64 (2012) 4.

[9] D. Veber, S. Jojnson, H. Cheng, B. Smith, K. Ward, K. Kopple, J. Med. Chem. 45 (2002) 2615.

[10] https://www.molinspiration.com/cgi-bin/properties. Accessed September 10, 2024.

[11] http://www.swissadme.ch/. Accessed September 10, 2024.

[12] https://preadmet.bmdrc.kr/. Accessed September 10, 2024.

COMPARATIVE ANALYSIS OF MEADS MADE FROM DIFFERENT HONEYS

Csenge Mónika Pintér[1], Tiborné Bakos[1], Zoltán Péter Jákói[2], Balázs Lemmer[1], <u>József Mihalkó[1,3]</u>

[1]Department of Food Engineering, Faculty of Engineering, University of Szeged, H-6725 Szeged, Moszkvai krt. 5-7., Hungary
[2]Department of Biosystems Engineering, Faculty of Engineering, University of Szeged, H-6725 Szeged, Moszkvai krt. 9., Hungary
[3]Institute of Pharmaceutical Chemistry, University of Szeged, H-6720 Szeged, Eötvös u. 6, Hungary Doctoral School of Food Sciences, Hungarian University of Agricultural and Life Sciences, H-1118 Budapest, Villányi út 29-43., Hungary
e-mail: mihalko@mk.u-szeged.hu

Abstract

The topic is the production of mead, a less well-known honey-based alcoholic drink. The aim of our research is to compare the internal parameters of different types of honey produced by different producers and to study the meads made from them. Four different varieties of honey were selected as the basic material, which were acacia, milkweed, flower and hawthorn honey. The honey samples were measured for parameters important for brewing, including acidity and pH, water and dry matter content, invert and total sugars, D-glucose to D-fructose ratio, color and antioxidant content.

After testing the raw materials, the mead was produced. 2-2 kg per honey variety were used and mixed with 5 liters of drinking water pre-boiled and cooled to 20 °C. To each beer, 4-4 g of Mangrove Jack's Mead M05 yeast was added. And 1.6 grams of the yeast nutrient, consisting of diammonium phosphate and thiamine, was added on day zero, followed by 0.8 grams on days one, two and three. Fermentation was then stopped after 12 days due to the unchanged relative density values.

Subsequently, the finished products were also tested by measuring the color, the dielectric conductivity (dielectric constant (ε') and loss factor (ε'')), the alcohol content according to the standard, the final relative density and, of course, the organoleptic evaluation of the samples.

Overall, it is concluded that there are differences (e.g. final alcoholic strength, dielectric properties, color, etc.) between the honeys used in our tests and the meads made from them, most of which are of the same origin as the raw material. Considering organoleptic judgements, the most suitable raw materials to produce mead include mixed flower honey, acacia honey and silk grass honey. In the future, we would like to investigate honey blends to see if this has a positive or negative effect on our product.

Acknowledgements

A NEUROHYPOPHYSIS AND ADENOHYPOPHYSIS MODEL FOR THE INVESTIGATION OF DEPONATED CHEMICAL ENVIRONMENTAL LOADS

Zsolt Molnár[1], Péter Sándor Kiss[1], Miklós Mózes[1,2], Marianna Radács[1], Péter Hausinger[2], Krisztián Sepp[3], Márta Gálfi[1]

[1]*Department of Environmental Biology and Education, Institute of Applied Health Sciences and Environmental Education, Juhász Gyula Faculty of Education, University of Szeged, H-6720 Szeged, Boldogasszonys sgt. 6, Hungary*
[2]*Department of Neurosurgery, Albert Szent-Györgyi Medical School, University of Szeged, H-6725, Semmelweis u. Hungary*
[3]*Department of Internal Medicine; Albert Szent-Györgyi Medical School; University of Szeged, H-6725, Kálvária sgt. 57, Hungary*
e-mail: molnar.zsolt.02@szte.hu

Abstract

Persistent organic pollutants, chemicals with high chemical stability and low degradability, widely used in industry and/or agriculture. A heterogeneous group of these compounds include chlorobenzenes (ClB), which are deposited in the lipophilic phases of living organisms and induce dose-dependent toxic effects in the cells of affected tissues. The aim of this study was to monitor the effects of different doses of ClB treatments on changes in energy transfer (Mg^{2+}-ATPase) and protein production of neurohypophysis and adenohypophysis. Male Wistar rats were treated with ClB (1:1 mixture of hexachlorobenzene and 1,2,4-trichlorobenzene) in a dose of 1.0 and 10.0 µg /b.w. kg through a gastric tube. Rats were exposed to ClB for 30, 60, and 90 days. The results showed that ClB exposures significantly increased energy transfer and protein production in cell cultures.

Introduction

In higher order biological systems, the biological mechanisms regulated by the immune-neuro-endocrine system appear dominantly, showing a network connection with the properties of thes essential system [1]. The hypothalamic-pituitary axis shows a network connection with other subsystems [2], which can be studied separately, but must be treated as a complex unit with a homeostatic function. Due to its antidiuretic role, arginine-vasopressin (AVP), released from neurohypophysis (NH), is essential in osmoregulation, volume control, and plays a key role in behaviour, learning, and memory functions [1, 3]. In addition to the contractile and reproductive role of smooth muscle, oxytocin (OT) is also known as an effector neuropeptide of human social behaviour (e.g., attachment, trust, cognitive functions, empathogenic properties), a mediating element that strengthens the memory trace that can be linked to memory in learning processes [1]. In central regulation, the hormones secreted by the adenohypophysis (AdH) also coordinate important physiological mechanisms, such as e.g., growth hormone, prolactin, and adrenocorticotrophic hormone. The ectodermal cells (NH and AdH) mentioned above the key to discrete energy transfer is the Mg^{2+}-dependent ATPase [2], which can be used to detect environmental alterations. Chemicalization and its consequences - which initially served short-term needs of the society effectively, however, highly chemically stable substances as xenobiotics synthesized during chemicalization - have already changed the accommodation patterns of biological organisms, which is why such models are necessary with which even discrete changes can be easily tracked. The chemicals that burden the environment are chlorobenzenes (ClB) with massive chemical stability, which are deposited in the lipophilic phases of living organisms (e.g., brain and endocrine tissues) [4].

Aim

The purpose of this study was to monitor the effects of different doses of ClB treatments on changes in energy transfer (Mg^{2+}-ATPase) and protein production of NH and AdH.

Experimental

In vivo **protocol**

Male Wistar rats (Charles River, Isaszeg, Hungary, medically certified) from different litters (weighing 120-250 g, aged 4-6 weeks at the beginning of the research) were used for cell culture model systems. Animal care and research protocols were in full accordance with the guidelines of University of Szeged, Hungary. During the research period, rats were kept under controlled relative air humidity of 55-65% and $22\pm2°C$ ambient temperature. Experimental animals lived under automated diurnal conditions (12 h dark and 12 h light systems) in groups of 10 animals for the end of the research period. Standard pellet food (CRLT/N, Charles River, Magyarország) and tap water were available *ad libitum.* Male Wistar rats were treated with combined ClB (1:1 mixture of 1,2,4- trichlorobenzene /CAS number: CAS number: 2199-72-6, Sigma Aldrich, USA, St. Louis) and hexachlorobenzene / CAS number: 93952-14-8, Sigma Aldrich, USA, St. Louis), in 1 mL of 0.015% ethanol in distilled water was administered daily) in a dose of 1.0 and 10.0 µg/b.w. kg via a gastric tube. Rats were exposed to ClB for 30 (n=5), 60 (n=5) and 90 (n=5) days. Control (untreated) groups were set up [5].

In vitro **protocol**

After anesthesia with pentobarbital (4.5 mg/kg, Nembutal, Abott, USA), treated and untreated experimental animals were decapitated, and AdH and NH tissues were separated under a dissecting microscope. The tissues were prepared with enzymatical (trypsin: 0.2 % / Sigma Aldrich, USA, St. Louis / for 30 min; collagenase / Sigma Aldrich, USA, St. Louis /: 30 µg/mL for 40 minutes; dispase / Sigma Aldrich, USA, St. Louis /: 50 µg/mL for 40 min in phosphate buffer (PBS-A) at a temperature 37 °C), mechanical dissociation (using 48 µm pore diameter nylon-blutex filters). After checking cell viability ($\geq$ 95% based on trypan blue staining / Sigma Aldrich, USA, St. Louis/), the cell density was set to $2x10^5$/mL, then suspended cells were washed with Dulbecco's Modified Essential Medium (DMEM, Sigma Aldrich, USA, St. Louis) + 20% Fetal Calf Serum (FCS, Sigma Aldrich, USA, St. Louis) + 1.0 µg/mL Penicillin+Streptomycin (Sigma Aldrich, USA, St. Louis) nutrient solution, then placed in 24-well plastic culture dishes (Nunclon, Germany) and cultures were incubated (T= 37°C, pCO_2: 5%). Cell proliferation induction was performed on separate reference systems treated with 1 mg/mL benz[c]-acridine (BcA) for 168 h *in vitro*. *In vivo* pretreated with ClBs were treated with exposure to ClBs (0.1 and 10.0 µg/mL) for 168 h.

Protein and Mg^{2+}-ATPase activity determination

The protein content of the samples was determined using a modified Lowry method, and Pierce BCA Protein Assay Kit (Thermo Fisher Scientific Inc., Rockford, USA).

The Mg^{2+-}dependent ATPase activity after ClB treatment was measured using the modified method of Martin and Dotty to follow the discrete changes in energy transfer of cells. ATPase activity is expressed as control %.

Statistical analysis

To compare the means of different treatment doses (1.0 and 10.0 µg/b.w. kg) to the controls during 30, 60 and 90 days long pretreatments (n=5 in) two-way ANOVA were performed.

Results and discussion

III.1. Number of tumour clones as a result of ClB treatments

	NH	AdH
AC	0	0
BcA	33.5±3.1*	42.6±4.0*

Table 1. The number of tumour clones in response to the reference control and benz[c]-acridine (BcA) treatment (number of cells±s.e.m., *:p<0.001)

From the data in Table 1, BcA significantly induced tumour clones in the model system, confirming that the experimental setup is suitable for the numerical detection of tumour cells.

ClB treatment	NH			AdH		
	30 days	60 days	90 days	30 days	60 days	90 days
ClB 10.0 µg/bw. kg	0	0.91±0.03*	1.2±0.04*	0	1.1±0.06*	1.5±0.07*
ClB 1.0 µg/bw. kg	0	0	0.92±0.02*	0	0	1.38±0.03*

Table 2. The number of tumour clones in the different cell populations as a result of each ClB pretreatment (number of cells±s.e.m., *:p<0.001)

Table 2 shows that the number of tumorous clones increased significantly depending on dose and time.

III.2. Protein production and Mg^{2+}-dependent ATP activity after ClB treatments
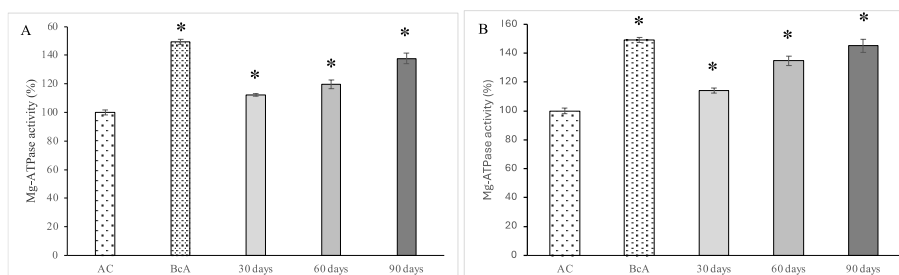
Figure 1. Effect of different exposures to ClB mix on Mg^{2+}-dependent ATPase activity in NH cell cultures (A: 1.0 µg/bw. kg, C: 10.0 µg/bw. kg, *:p< 0.001, n=5)

From the data in Figure 1, the Mg^{2+}-dependent ATPase activity increased compared to the AC group, this increase depending on time was stronger on day 60 (116.4±1.8%) and day 90 (116.4±4.2%). More intense activity was observed in the case of 10.0 µg/bw kg ClB treatment (114.2±1.7, 134.7±3.2, 145.2±4.5%).
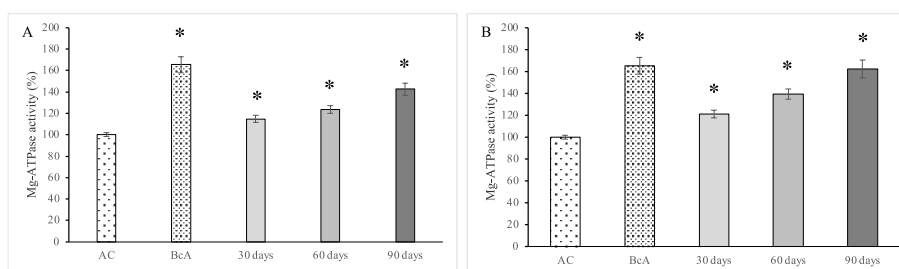
Figure 2. Effect of different exposures to ClB mix on Mg^{2+}-dependent ATPase activity in AdH cell cultures (A: 1.0 µg/bw. kg, B: 10.0 µg/bw. kg doses, *:p< 0.001, n=5)

If we examine the changes in the Mg^{2+}-dependent activity of AdH cell cultures as a function of exposure to ClB and duration, it can be observed that higher doses ClB exposures generated activity modulations similar to benz-(c)-acridine treatment.
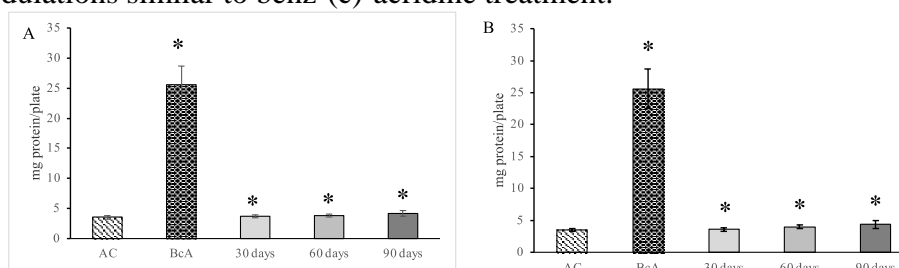
Figure 3. The effect of different ClB exposures on protein production in NH cell cultures (A: 1.0 µg/bw. kg, B: 10.0 µg/bw. kg doses, *:p<0.001, n= 5)

After 90 days, the 1.0 µg/bw. kg dose (4.17±0.51 mg protein/plate), and the 10.0 µg/bw. kg dose (4.36±0.62 mg protein/plate) ClB treatments also significantly increased NH protein production.
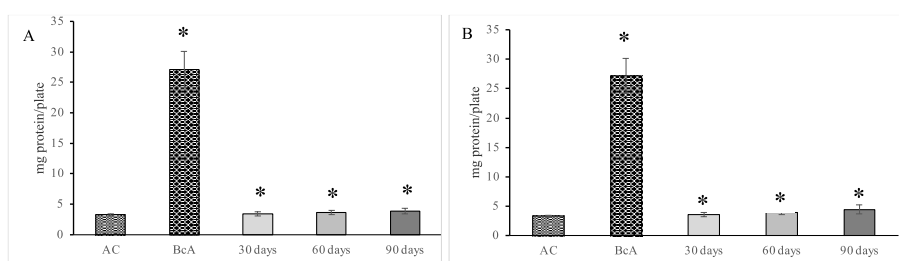
Figure 4. The effect of different ClB exposures on protein production in AdH cell cultures (A: 1.0 µg/bw. kg, B: 10.0 µg/bw. kg doses, *:p<0.001, n= 5)

In the case of AdH as well, we detected a significant increase in protein production as a function of dose and time compared to the values of the AC group.

ClBs can also be classified as artificial compounds created during chemical reactions that can generate changes in many physiological processes. Living systems are affected by complex environmental exposures *in vivo*, however, if these exposures are very low (subtoxic concentrations), they can exert their effects in a latent manner for a long time. As a result, it is necessary to develop a model that is suitable the evaluation and detection of the effects of subtoxic *in vivo* exposures in a complex manner. The hormones expressed and released by the hypothalamo-pituitary axis play a very important biological role in higher organisms, but their role in psychological functions has also been proven, such as OT, AVP, prolactin, adrenocortocotropic hormone [6].

Conclusion

As a result of treatment with a higher dose of ClB, tumour clone formation was generated in all primary cell cultures that we examined after only 60 days. The initiation effect of ClB was expressed less in the central regulatory elements. The relationship between Mg^{2+}-dependent ATPase enzyme protein production shows that the energy from the splitting of ATP is connected to the cell's own energy supply, and this is also manifested in increased protein production. Tumour cells can be characterized by increased cell proliferation activity and increased protein production [7]. This means that the ClB included in the model study influence both the initiation and the promotion.

Acknowledgements

References

[1] Z. Valkusz, G. Nagyéri, M. Radács, T. Ocskó, P. Hausinger, M. László, F.A. László, A. Juhász, J. Julesz, R. Pálföldi, Further analysis of behavioral and endocrine consequences of chronic exposure of male Wistar rats to subtoxic doses of endocrine disruptor chlorobenzenes. Physiol Behav. (2011) 103: 421-430.

[2] K.A. Cironi, T. Decater, J. Iwanaga, A.S. Dumont, R.S. Tubbs, Arterial Supply to the Pituitary Gland: A Comprehensive Review. World Neurosurg. (2020) 142: 206-211.

[3] B. Alescio-Lautier, B. Soumireu-Mourat, Role of vasopressin in learning and memory in the hippocampus. Prog. Brain. Res. (1998) 119: 501-521.

[4] P. Charisiadis, X.D. Andrianou, T.P. van der Meer, W.F.A. den Dunnen, D.F. Swaab, B.H.R. Wolffenbuttel, K.C. Makris, J.V. van Vliet-Ostaptchouk, Possible Obesogenic Effects of Bisphenols Accumulation in the Human Brain. Sci Rep. (2018) 8(1): 8186.

[5] K. Sepp, A. László, M. Gálfi, M. Radács, M. Mózes, P. Hausinger, R. Pálföldi, M. Veszelka, Z. Valkusz, Z. Molnár, Study of endocrine disruptor effects in AVP and OT mediated behavioral and reproductive processes in female rat models. Physiol Behav. (2024) 283: 114597

[6] G.P. Chrousos The role of stress and the hypothalamic-pituitary-adrenal axis in the pathogenesis of the metabolic syndrome: neuro-endocrine and target tissue-related causes. Int J Obes Relat Metab Disord. (2000) 2: S50-5.

[7] Z. Zhang, Y. Zhang, S. Xia, Q. Kong, S. Li, X. Liu, C. Junqueira, K.F. Meza-Sosa, T.M.Y. Mok, J. Ansara, S. Sengupta, Y. Yao, H. Wu, J. Lieberman, Gasdermin E suppresses tumour growth by activating anti-tumour immunity. Nature. (2020) 579(7799): 415-420.

COMPARISON OF TOTAL POLYPHENOL CONTENT AND ANTIOXIDANT CAPACITIES OF FRUIT AND VEGETABLE JUICE CONCENTRATES MEASURED BY DIFFERENT METHODS

Anna Maria Nagy[1,3], Éva Stefanovits-Bányai[2], Mónika Máté[3]

[1]Holi-Medic Ltd., *H-5600 Békéscsaba, Munkácsy Street 17, Hungary,*
[2]MATE Institute of Food Science and Technology, Department of Food Chemistry and Analytics, H-*1118 Budapest, Villány Street 29-43, Hungary,*
[3]MATE Institute of Food Science and Technology, Department of Fruit and Vegetables Processing Technology*, H-1118 Budapest, Villány Street 29-43, Hungary,*
Email: *holimedic@gmail.com*

Abstract

In our research, the total polyphenol content and antioxidant capacity of 6 types of 65% fruit juice concentrates (rosehip, sour cherry, sea buckthorn, beetroot, jerusalem artichoke, papaya) were measured and compared with TEAC and FRAP methods. Despite the fact that the highest TPC value was measured for sour cherries and the second highest for rosehips, the highest antioxidant capacity was measured not for sour cherries but for rosehips, using both (FRAP and TEAC) antioxidant capacity measurement methods. The antioxidant capacity of sour cherries ranks second after rosehips in the case of the TEAC measurement method, while in the FRAP method, it ranks only third in the order of the 6 samples examined. The third highest TPC value was measured in sea buckthorn, whose antioxidant capacity measured by the TEAC method - similarly - is also in third place, but measured by the FRAP method, ahead of cherries, it ranks second. The values of beetroot, Jerusalem artichoke and papaya juice concentrates were in exactly the same (4-5-6th) position in all three measurements (TPC, TEAC, FRAP). Based on our results, it can be stated that the results measured with different antioxidant capacity methods are not comparable with each other, only the values measured by the same method can be compared. Rather, we can interpret the results obtained in different methods as complementary, which point out the different nutritional properties of each plant and their unique complexity.

Introduction

More and more publications worldwide confirm the health-damaging effects of free radicals and the health-protecting effects of antioxidants, therefore there is an increasing demand for more and more accurate determination of the antioxidant capacity of various foods in order to consume the required amount of antioxidants [1] regularly. Several studies have confirmed the excellent health-protecting effects of rosehip [2], sour cherry[3], sea buckthorn [4], beetroot [5], jerusalem artichoke [6], papaya [7], which are due to their outstanding but significantly different nutritional values.

Antioxidant capacity can be defined as the combined effect of all antioxidant compounds in the examined sample. Over a hundred methods have been developed in recent decades to measure antioxidant capacity [8], but every examination method has advantages and disadvantages. Neither method is suitable for accurately modelling the biochemical processes taking place in the body on its own, so it is of paramount importance to formulate a conclusion about the sample based on the combined results of several test methods.

The measurement methods developed so far can be divided into 2 main groups [9]: hydrogen atom transition (HAT: Hydrogen Atom Transfer) and electron transition (ET: Electron Transfer). HAT methods are primarily based on reaction kinetics: they measure how

effective the sample is against a given free radical and determine its free radical scavenging capacity [10]. In the case of ET methods, antioxidant capacity can be inferred from the degree of colour change during the reaction [11]. The antioxidant capacity results determined by the HAT and ET methods are not necessarily correlated since the reducing capacity of a sample is not necessarily related to its radical scavenging capacity [11]. The most commonly used methods worldwide mainly belong to the ET group due to their simplicity, speed and low cost. The TPC, FRAP, and TEAC methods used in our present studies also belong to the ET group.

Materials

In our experiment, 4 types of fruit juice concentrate with a dry matter content of 65% (belonging to botanically different families) were used: rosehip (*Rosa canina),* sour cherry (*Prunus cerasus),* sea buckthorn (*Hippophae rhamnoides),* Papaya *(Carica papaya)* and 2 types of root-vegetable juice concentrates beetroot (*Beta vulgaris*) and jerusalem artichoke (*Helianthus tuberosus).* All juice concentrates were in accordance with food safety rules, strictly controlled, produced under the HACCP quality assurance system, stored and distributed in an aseptic manner (distributed by Intercooperation Ltd.). The chemicals used were purchased from Sigma-Aldrich.

Analytical methods

Determination of total polyphenol content (TPC) by Folin-Ciocalteu method: The Folin-Ciocalteu spectrophotometric method by Singleton and Rossi [12], at 760 nm is an electron transfer based on assay and shows the reducing capacity, which is expressed as phenolic content. Gallic acid (GA) was used to prepare the standard curve. The results were expressed as μM GA/g of dry matter (DM).

Determination of antioxidant capacities by FRAP (Ferric Reducing Antioxidant Power) method: Measurement of ferric reducing antioxidant power of the juice concentrates was carried out based on Benzie and Strain's procedure [13], at 593 nm. Ascorbic acid (AA) was used as a standard to prepare the calibration solutions. Results were expressed as μMAA/g DM.

Determination of antioxidant capacities by TEAC (Trolox-equivalent antioxidant capacity) method: The total antioxidant capacity was measured with Trolox-equivalent antioxidant capacity (TEAC) method described by Miller et al. at 734 nm [14]. The method is based on ABTS+ free radical scavenging by antioxidants measured with a spectrophotometer. For the calibration Trolox (the hydrophilic analogue of vitamin E) was used, and results were expressed in μMtrolox equivalent/g DM.

Results and discussion

I.) Results of total polyphenol content (TPC) by Folin-Ciocalteu method

The results of the measurements of the 6 types of concentrated juice showed that the total polyphenolic content of sour cherry juice concentrate was the highest (76,2 μMGS/g), and papaya was the lowest (14,9 μMGS/g). Sour cherries are followed by rosehips (69 μMGS/g), sea buckthorn (58.5 μMGS/g) and beetroot (57.3 μMGS/g), the latter two with only a slight difference. It should be noted that the first 4 TPC values are in similar ranges, with a maximum difference of only 18.9 μMGS/g. But Jerusalem artichoke (20,9 μMGS/g) and papaya (14,9 μMGS/g), which have a much lower TPC value, are significantly separated from the first 4 types of samples (Fig. 1).
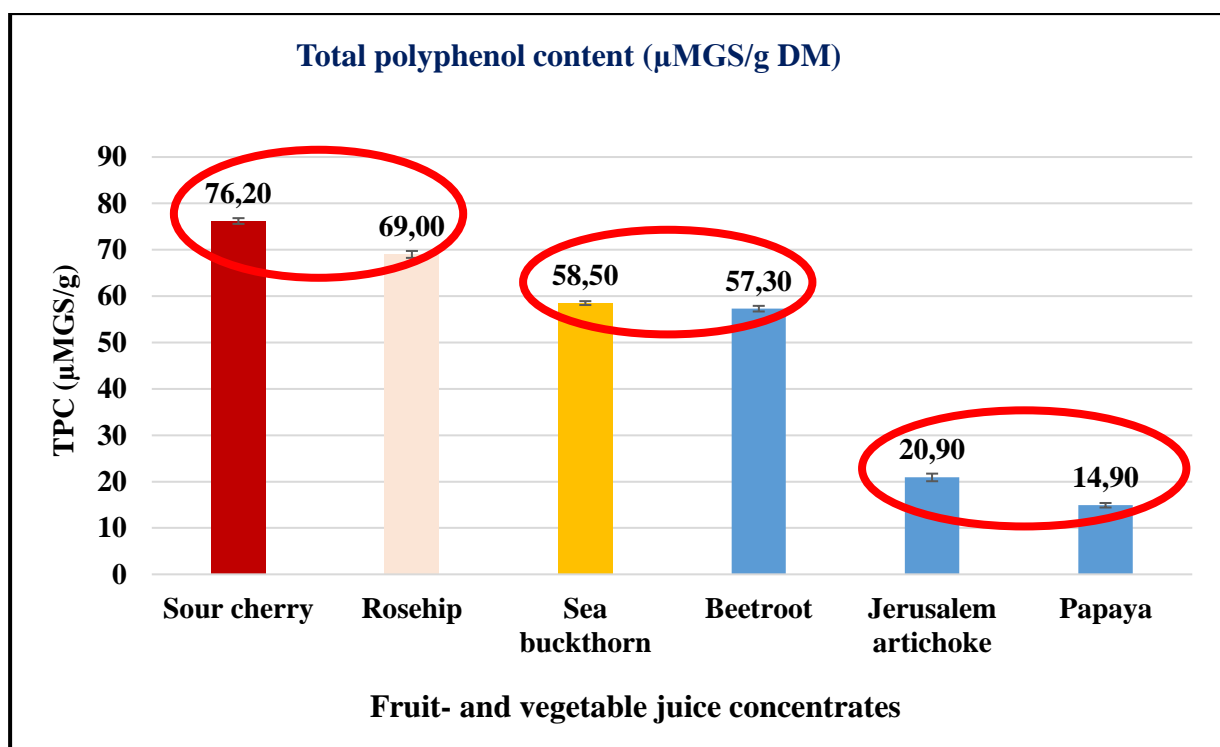
Fig. 1. Total phenolic content of different juice concentrates (μMGA/g DM)

II.) Antioxidant capacity measurement results using TEAC and FRAP methods

In our research, we investigated the antioxidant capacity of 6 types of 65% juice concentrates using the TEAC method based on free radical scavenging capacity (Fig.2.) and the FRAP method based on iron-reducing ability (Fig. 3). Our results were as follows:

1.) For both measurement methods (FRAP, TEAC), outstanding antioxidant capacity values were measured in the rosehip juice concentrate. The antioxidant capacity of the other 5 types of juice concentrate was so significantly separated from rosehip in both methods that a separate (smaller) figure had to be made within the large figure for better illustration (Fig.2-3).

2.) With the TEAC measurement method, the sour cherry (188.59 μMtrolox/g) is in second place, followed by the sea buckthorn (160.56 μMtrolox/g) in third place by a small margin.

3.) At the same time, in the FRAP measurement method, the order of the same 2 concentrates is reversed, and it should be emphasized that here they are not in the same range (as in the case of TEAC), but the sea buckthorn (481.78 μMAS/g) shows a significant difference, more than 10 times higher FRAP value than sour cherries (43.37 μMAS/g).

4.) The order of beetroot, Jerusalem artichoke, and papaya is the same for TPC, TEAC and FRAP measurements, so these have been marked with the same (blue) colour.

5.) In TEAC measurement, Jerusalem artichoke (20.57 μMtrolox/g) and papaya (19.53 μMtrolox/g) show almost similar values, from which beetroot is separated by a significant margin, more than 5 times higher (108.94 μMtrolox/g).

6.) In contrast, in the FRAP measurement method, beetroot (37.8 μMAS/g) and sour cherries (43.37 μMAS/g) show similar antioxidant capacity values, compared to which Jerusalem artichoke (10.17 μMAS/g) and papaya (4.85 μMAS/g) are almost 4 times lower.
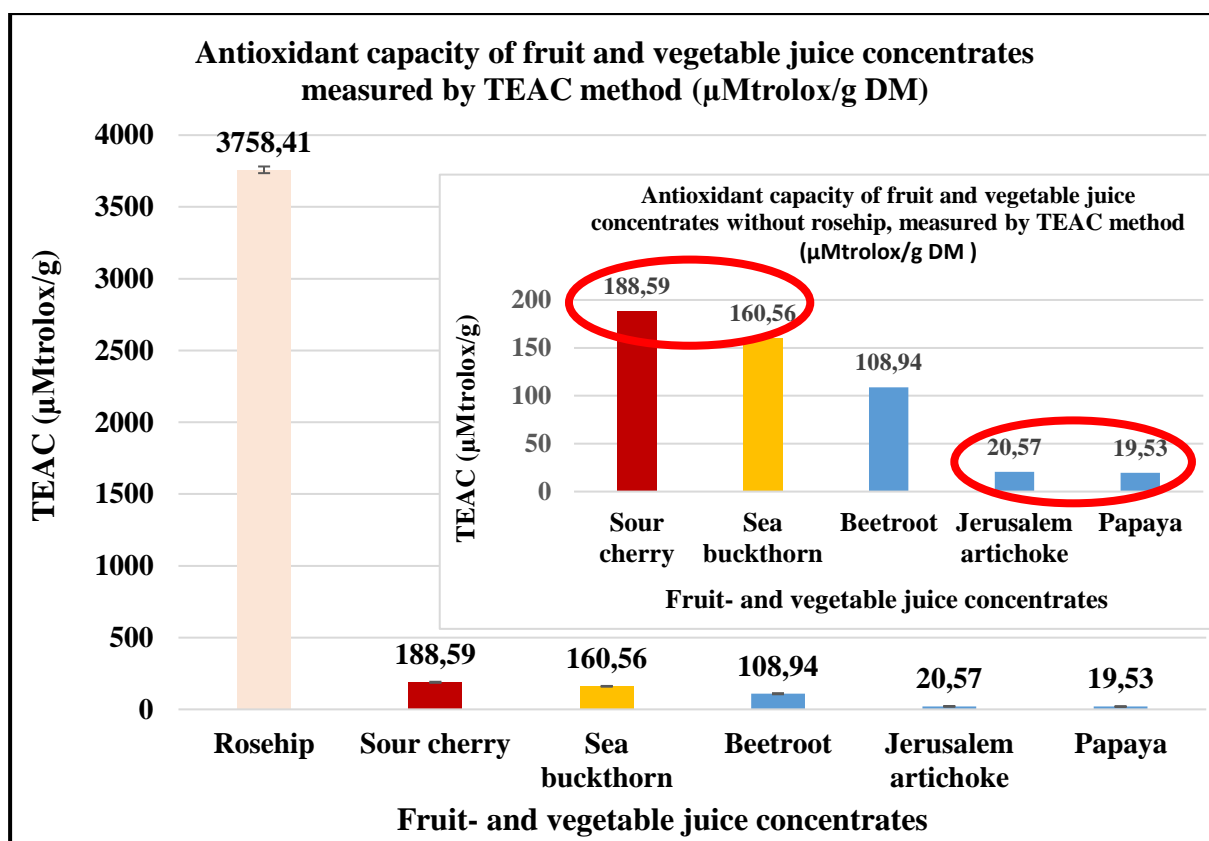
Figure 2. Antioxidant capacity of 6 types of fruit and vegetable juice concentrates measured by TEAC method (µMtrolox/g DM)
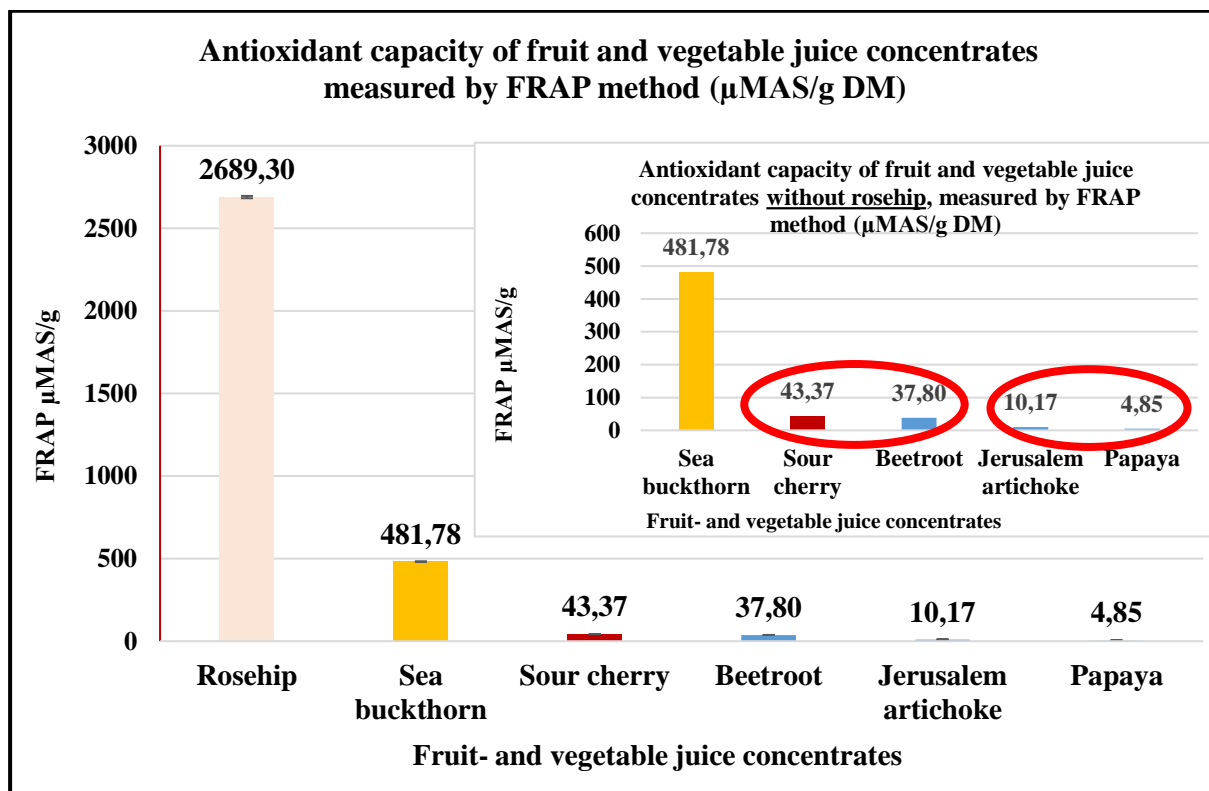
Figure-3. Antioxidant capacity of fruit and vegetable juice concentrates measured by FRAP method (µMAS/g DM)

III.) Sequences due to differences in methods and relationship between total polyphenol content and antioxidant capacity values measured by 2 different methods (FRAP, TEAC)

Despite the fact that the highest TPC value was measured for sour cherries and the second highest for rosehips, the highest antioxidant capacity was measured not for sour cherries but for rosehips using both (FRAP and TEAC) antioxidant capacity measurement methods. Sour cherries came second with TEAC measurement, while FRAP only came third (Table 1). The TPC value of sea buckthorn came in third, yet a higher antioxidant capacity was measured with the FRAP method than with cherries with the best TPC value.

Table-1. The order of the 6 types of concentrated juice in the results of TPC, TEAC, FRAP tests

Methods	Sequence					
	1	2	3	4	5	6
TPC	Sour cherry	Rosehip	Sea buckthorn	Beetroot	Jerusalem artichoke	papaya
FRAP	Rosehip	Sea buckthorn	Sour cherry	Beetroot	Jerusalem artichoke	papaya
TEAC	Rosehip	Sour cherry	Sea buckthorn	Beetroot	Jerusalem artichoke	papaya

Conclusion

Our results draw attention to the fact that there may be very significant differences between different antioxidant capacity measurement methods; therefore, it is not possible to draw far-reaching conclusions based on the test results of individual vegetables, fruits and their juice concentrates using only a few measurement methods.

In the case of 3 concentrates (beetroot, jerusalem artichoke, papaya), we saw a correlation between TPC and antioxidant capacity measured by 2 methods. At the same time, the antioxidant capacity values of the 2 fruits with the highest total polyphenol content (sour cherry and rosehip) were not correlated with their TPC values and their order.

These results suggest that, in addition to TPC, several other biologically active components may play a significant role in the antioxidant capacity of fruits and vegetables (such as the significant vitamin C content in rosehip), which requires further research.

References
[1] C.G.Fraga, P.I.Oteiza, M.C. Litterio et al, Acta Hort. (ISHS) 939 (2012), 63-67.
[2] S. Patel, Trends in Food Science & Technology, Volume 63 (2017) P 29-38,
[3] F.M. Yılmaz et al., Critical Reviews in Food Science and Nutr., 59 (2018) 3549-3563
[4] Z. Wang, F. Zhao, P. Wei et al., Frontiers in Nutrition, 9 (2022) 6406–6420
[5] L. Chen, Y. Zhu, Z. Hu, S et al., Food Science & Nutrition, 9 (2021) 6406–6420
[6] A.Méndez-Yáñez, P.Ramos, L. Morales-Quintana, Horticulturae (2022). n.page
[7] G.V.Anjana et al., Asian J. of Pharmaceutical and Clin.Research (2018): n. pag.
[8] U. Cornetti, Clinics in Dermatology 27 (2009) 175-194.
[9] E.N. Frankel, A.S. Meyer, J. of the Science of Food and Agricult. 80 (2000) 1925-1941.
[10] A. Ghiselli, M.Serafini et al., Free Radical Biol. and Med. 29 (2000) 1106-1114.
[11] R. Apak, K. Guclu et al., Molecules 12 (2007) 1496-1547.
[12] V.L. Singleton, J.A. Rossi, Am. J. of Enol. and Viticult. 16 (1965) 144-158.
[13] I.F.F. Benzie, J.J. Strain, Biochem. 239(1) (1996) 70–76.
[14] N.J. Miller, C. Rice-Evans, M.J. Davies et al, Clinic.Sci. 84 (1993) 407-412.

INTENSIFICATION AND MONITORING OF ANAEROBIC FERMENTATION OF SEWAGE SLUDGE FROM THE MEAT INDUSTRY

Zsófia Gréta Sánta[1,2], Balázs Lemmer[2], Zoltán Péter Jákói[1], Sándor Beszédes[1]

[1]*Department of Biosystems Engineering, Faculty of Engineering, University of Szeged, Moszkvai krt. 9, H-6725 Szeged, Hungary*
[2]*Department of Food Engineering, Faculty of Engineering, University of Szeged, Moszkvai krt. 5-7, H-6725 Szeged, Hungary*
e-mail: zsofiasanta71@gmail.com

Abstract
My goal was to investigate the effect of different pretreatments on the quantity and methane content of biogas produced during anaerobic digestion of sewage sludge from meat processing plants. Both the accumulation of waste and the depletion of non-renewable energy resources are major problems of modern times, and the use of sewage sludge as a feedstock for biogas production may be a promising solution. Anaerobic digestion is a complex process, and the right quality of feedstock is essential for its proper completion. Although, meat industry wastewater is not ideal feedstock for biogas production, its properties can be improved by pre-treatments. In my chosen pre-treatments, we added magnetite nanoparticles to the sludge and then irradiated it with microwaves at different power levels. Monitoring the fermentation is crucial, especially in industrial practice. We monitored the progress by measuring the dielectric properties of the sludge samples.
Our results show that dielectric measurements are a promising alternative for monitoring the anaerobic fermentation because there is a clear correlation between the changes in the value of the dielectric constant and the progression of the fermentation. Our results also clearly support the positive effect of the chosen pretreatments on the amount of biogas produced during fermentation. While the amount of gas increased, the methane content of the biogas produced did not change as verified by gas analysis.

Introduction
In the past decade, rapidly increasing industrial production and the growth of the Earth's population have led to two major problems: the accumulation of waste and the depletion of non-renewable energy sources. As with other types of waste, the amount of wastewater produced by humanity has increased significantly. The extreme volumes of wastewater make it inevitable that more efficient methods of wastewater treatment and recovery must be developed.
One such modern processing method uses sewage sludge as a feedstock in biogas production. The huge advantage of this method is that not only is the biogas produced as a final product is a suitable energy source, but the process often kills pathogenic microbes that were present in the original wastewater and stabilizes the sludge. [1] So the material left over after fermentation can be usually safely used for soil improvement.
However, not all wastewater is equally suitable as feedstock for biogas production. The meat industry requires large quantities of clean water and, depending on the specific plant, the technology used and the efficiency of the water management in the plant, a large proportion of the water used is heavily contaminated. The most common and most abundant contaminants are blood, fat, bone fragments, meat scraps, hair, feathers, feces, as well as salt from marinades and chemicals used for disinfection and cleaning to meet strict hygiene requirements [2].
Therefore, the meat industry could provide a significant amount of sewage sludge as feedstock for biogas production, but this sludge in itself is more than often not optimal. In the biogas

production process, microbial bacteria and specific archaea degrade the organic matter in the feedstock under anaerobic conditions, producing an energy-rich gas mixture which has many applications.

The quality of the feedstock is essential to ensure the optimal fermentation process and the quality of the produced biogas. [3] Most of the nutrients important for microbial growth are found in flocks and consequently, has relatively low bioavailability. Furthermore, residual disinfectants and detergents can inhibit the proper activity of the gas-producing microbes. Due to these properties, it is advisable to pre-treat meat industry sludge before using them as feedstock for biogas production to improve their properties and to be able to extract biogas with higher yields and better quality.

Due to their high water-content, sewage sludges effectively absorb microwave radiation, which is absorbed and transfers its energy to the material, causing a rapid and gradual temperature rise and deterioration, which aids sludge degradation. [4] Although microwave pre-treatment cannot change the chemical composition of the sludge, it improves the bioavailability of the required nutrients by bringing the useful components into solution. However, in case of dense, thickened sludge samples the material homogeneity is usually low, and due to the microwave's selective heating ability these samples cannot be heated uniformly. To reduce temperature inhomogeneity, small-scale microwave absorbers should be mixed homogeneously with the material, such as silicon carbide, carbon nano tubes or metal nanoparticles.

The aim of my work was to investigate the effect of microwave pre-treatment of meat industry wastewater in the presence of magnetite nanoparticles on the amount and CH_4 content of biogas produced.

Experimental

The sludge used in the experiments came from a local meat processing plant. We used a Labotron 500 laboratory microwave unit operating at 2450 MHz frequency for the pre-treatments. The pre-treatments were performed at two different power levels: 250 W and 500 W. In order to keep the energy irradiated constant regardless of the power, the irradiation time was adjusting accordingly: 1.5 min at 500 W and 3 min at 250 W. For the combined pre-treatments, 15 mL of magnetite nanoparticle suspension was added to the wastewater to be fermented before microwave pre-treatment to promote uniform heating. The concentration of the suspension was 0.71 g/100 mL, while the average particle size was 110 nm. After the different treatments, inoculum sludge was added to the sludge samples to ensure the proper microbial composition. To monitor the dielectric properties of the samples, an open-ended dielectric sensor (DAK 3.5, SPEAG, Switzerland) connected to a vector network analyzer (Rhode & Schwarz, Germany) with a coaxial cable was used in the frequency range of 200-2400 MHz. During the anaerobic digestion, the amount of the produced biogas was measured with pressure sensors, and the quality (methane content) of the samples were determined with an OPTIMA7 biogas analyzer, equipped with a pair of NDIR sensors to detect CH_4 and CO_2.

Results and discussion

Our results demonstrate (Figure 1) that the chosen pretreatments had a clearly positive effect on gas production, as the control sample produced less biogas than any of the pretreated ones. The most effective pre-treatment was the one combined with magnetite particles at 250 W for 3 minutes, which produced more than three times as much gas as the control sample.

We can also see that the two pre-treatments together were more effective than either microwave treatment (at any power level tested) or nanoparticle treatment alone. This suggests that the effects of the two pre-treatments are additive, meaning that they enhance each other. One form of this is likely to be that the magnetite nanoparticles act as hotspots during heating and

successfully eliminate the temperature inhomogeneities. Regardless, the presence of metal nanoparticles stimulated gas production even without microwave heating, suggesting that the presence of iron plays a role in microbial metabolism.

Not only did the treatments have a beneficial effect on the volume of gas produced, but they also catalyzed the initiation of gas production: gas production started several days earlier in treated samples than in untreated ones.
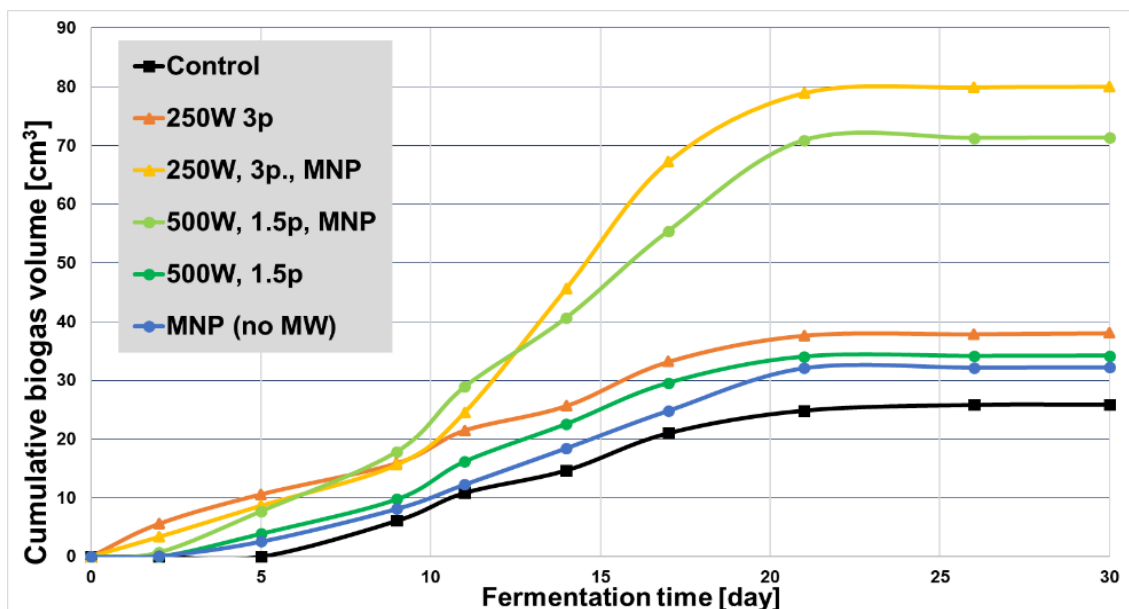

Figure 1. Changes in the total amount of biogas produced as the fermentation time progresses
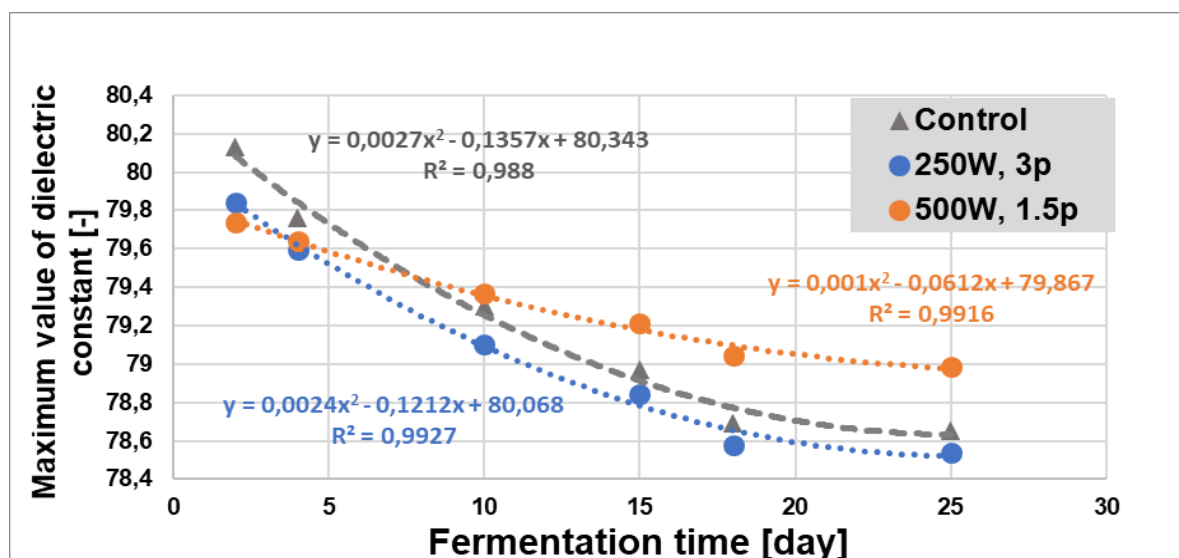
Figure 2. Changing of the maximum dielectric constant of sewage sludge during fermentation

Another focus of our research was to monitor the dielectric constant of sewage sludge samples as fermentation progressed. We measured the dielectric constant values in the frequency range 200-2400 MHz. As can be seen in Figure 2, the maximum dielectric constant of the sewage sludge decreases in a second-order trend for all samples. This suggests that the molecular

changes that take place during the different stages of the anaerobic fermentation is also reflected in the change of the system's dielectric behavior. This means that the method based on the measurement of dielectric properties can be used to monitor the fermentation process regardless of the type of pre-treatment used.

The CH_4-CO_2 ratio determined across all samples averaged 83%±2.7% in favor of methane, so there was no significant difference between the gas quality of the treated samples and the control. In other words, the applied pretreatments increased the volume of gas produced without having a negative effect on its methane content, so the amount of CH_4 produced increased notably as a result of these treatments.

Conclusion

Our results show that microwave treatment with the addition of magnetite particles increases the amount of biogas produced during anaerobic fermentation without reducing its quality. The pre-treatment at 250 W combined with magnetite nanoparticles proved to be the best. The effectiveness of the 250 W treatment is not necessarily a result of the lower power, it is possible that the longer treatment time allowed the microwave treatment to have a more uniform beneficial effects. In the future, we plan to investigate the treatment time as an influencing parameter. The earlier start of gas production is probably due to the shorter lag phase. Thus, the bacteria of the fermentation culture adapt more quickly to the new conditions and reach the state necessary for division and intensive metabolic processes. On a larger scale, such as in industrial applications, this can lead to significant cost savings. If the microbes start their metabolic processes more quickly, the required temperature and mixing levels have to be maintained for a shorter period, reducing energy and operational costs.

It can also be seen from the results that the maximum value of the dielectric constant decreases steadily as the fermentation proceeds. This decrease is present regardless of the pre-treatment and follows a second order trend. This means that we can consider the measurement of dielectric properties. a non-destructive and real-time monitoring method for sewage sludge fermentation monitoring.

Acknowledgements

References

[1] Demirbas, A., Taylan, O., & Kaya, D. (2016). Biogas production from municipal sewage sludge (MSS). Energy Sources, Part A: Recovery, Utilization, and Environmental Effects, 38(20), 3027–3033.
[2] Cserhalmi, Zs., Éliás, I., Tóthné Szita, K. (1998). Hús- és Baromfiipar környezeti hatásai, Stratégiai kutatások a Magyar Tudományos Akadémián. 54-74.
[3] Xue, S., Wang, Y., Lyu, X., Zhao, N., Song, J., Wang, X., & Yang, G. (2020). Interactive effects of carbohydrate, lipid, protein composition and carbon/nitrogen ratio on biogas production of different food wastes. Bioresource Technology, 312, 123566.
[4] Leonelli, C., & Mason, T. J. (2010). Microwave and ultrasonic processing: Now a realistic option for industry. Chemical Engineering and Processing: Process Intensification, 49(9), 885-900.

ADSORPTION OF OIL ON SELECTED SYNTHETIC ZEOLITES

Marjana Simonič

Faculty of Chemistry and Chemical Engineering, University of Maribor, Smetanova 17, 2000 Maribor, Slovenia
email: marjana.simonic@um.si

Abstract
The aim of the study was to test the chosen zeolites for oil removal from wastewater. Two types of synthetic granular zeolites (ZAG-MFI and ZAG-4A) were chosen as adsorbents. The focus was on characterisation of zeolites and oils as well as oil adsorption performance onto zeolites. Characterisation was performed using Fourier transform infrared spectroscopy (FTIR). The water content in oil was determined.

Introduction
Wastewater contains various pollutants such as hydrocarbons, oils, fats, phenols, sulphides and many other organic compounds. In recent decades, many studies have been conducted to remove these compounds, but it is still a challenge to find an efficient and sustainable wastewater treatment, focusing on the removal of oil from wastewater. **Hiba! A hivatkozási forrás nem található.**.

Natural and modified zeolites are used to remove ammonia and metal ions. Modified zeolites are used to remove viruses, bacteria and other organic compounds. [2] The main advantage of using zeolites is the low cost and the associated rapid removal efficiency. Zeolite based composite materials are promising adsorbents for removal of toxic compounds from water [3]. Zeolites are porous aluminosilicate materials. Due to the uniform distribution of pores, they are also known as molecular sieves.[4,5] The large specific surface and the multiple strong adsorption sites in the porous structure of zeolite, which are obtained with thermal treatment, mean that products display excelent adsorption properties. Granulates zeolites exhibit great regeneartion properties.

The main objective of the work presented here was to test granulated zeolites (ZAG) for oil removal from wastewater. Two types of zeolites were chosen: ZAG-MFI and ZAG-4A. Both were characterised by Fourier transform infrared spectroscopy (FTIR), while titrimetric water content analyses in oils were performed.

Experimental
Two types of sythetic zeolite were chosen based on producer recommendations. Producer is Silkem, Kidričevo, Slovenia a widely recognised manufacturer of special materials in the fields of zeolites, silicates and other types of alumina.

Zeolite (Z1) ZAG-MFI (Fig. 1a), is activated granulate with SiO_2, no alumina. Specific weight was $720 – 820$ kg/m^3 and pH between 7 and 11. Water content should be $2 \pm 1{,}5$ %. Density $0{,}77 \pm 0{,}05$ g/cm^3 and size of granule $0{,}5 – 2{,}5$ mm [4].

Zeolite (Z2) ZAG-4A (Fig. 1b), is activated granulate, non-fibrous, silica rich (80 ± 3 %). Specific weight was $610 – 800$ kg/m^3. Water content should be 2 ± 1 %. Density $0{,}73 \pm 0{,}07$ g/cm^3 and size of granule $2{,}5 – 5{,}0$ mm [5].

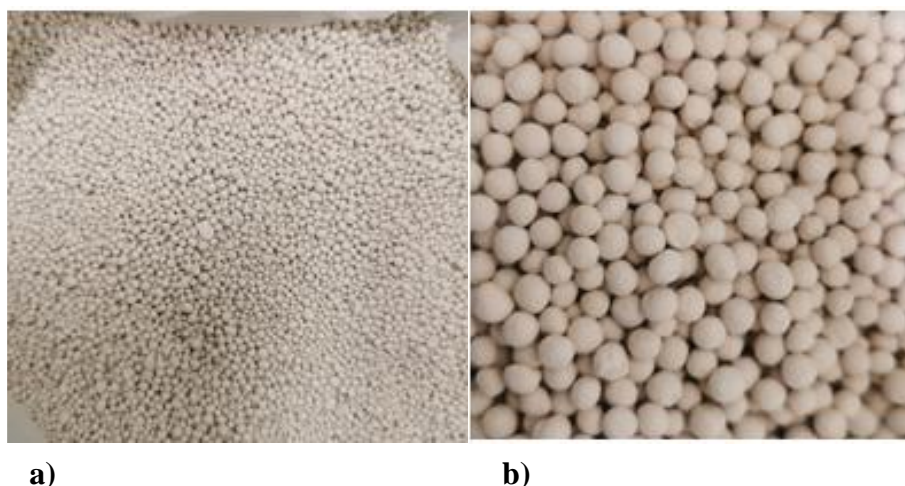a)   b)

Figure1. Zeolit 1 (a) Zeolite ZAG-MFI and b) Zeolite ZAG-4A.

Sunflower refined oil was chosen as reference oil (Zvijezda, Croatia). Chemically it is ranked among refined cooking oil. The share of saturated fatty acids is 12 %.

Standard Test Method for Sorbent Performance of Adsorbents, following ASTM F726-12 was performed [6]. Tests were performed in two time interavals of 15 min ± 20 s and 24 h ± 30 min, respectively. The material before and after adsortion was weighted and the mass percentage of adsorbed material (% m/m) was calculated.

Characterisation
Karl Fisher titration procedure is an analytical method used to determine the quantity of water in different fluids. The water content in oil was measured by equipment T50 Titrator, Mettler Toledo (Figure 2). This equipment is completely automated, requiring only add the sample to be analyzed. The solution used for measurements was a Karl Fisher Hydranal Composite 5 solution and a toluene/methanol solvent (1:1). The test was performed according to the ASTM D6304-07 standard method.

Figure 2. Mettler Toledo titrator T50.

FTIR was used for characterisation. Samples were dried at 60 °C, cooled to room temperature and FTIR was performed. The samples were analyzed with the spectrometer ATR FTIR Perkin Elmer SpectrumGX (Ljubljana, Slovenia). A total of 16 scans were taken of each sample for

signal accumulation with a resolution of 4 cm^{-1}. All spectra were recorded at ambient temperature over a wavenumber range between 4000 cm^{-1} and 450 cm^{-1}.

Results and discussion
Water Content
The water content in reference oil was determined at 0.34 % H_2O and in waste oil 17.5 % H_2O. The water content in oil is low and represent noo risk to form emulsions that could modify rheological behavior of the oil. However, the water content in waste oil is quite high and might form emulsions.

FTIR analyses
From the FTIR spectra of Zeolite1, the peaks at 1057 cm^{-1} and 793 cm^{-1} typical asymetric vibration of Si–O bonds are evident. At 1217 cm^{-1} and 793 cm^{-1} there are bonds of quartz or amorphous SiO_2 vibrations, and at 1217 cm^{-1} and 538 cm^{-1} characteristic peaks of crystalline zeolites with asymetric vibrations of Si–O–Si were observed. Signal at 1631 cm^{-1} corresponds to O–H or H–OH on zeolite surface.

From the FTIR spectra of Zeolite2, the peak at 976 cm^{-1} represent the asymetric Si–OH group. The peaks at 975 cm^{-1} and 554 cm^{-1} correspond to asymetric Si–O–Si bond. The band at 485 cm^{-1} represent symetric stretch of T-O-T (T = Si or Al).
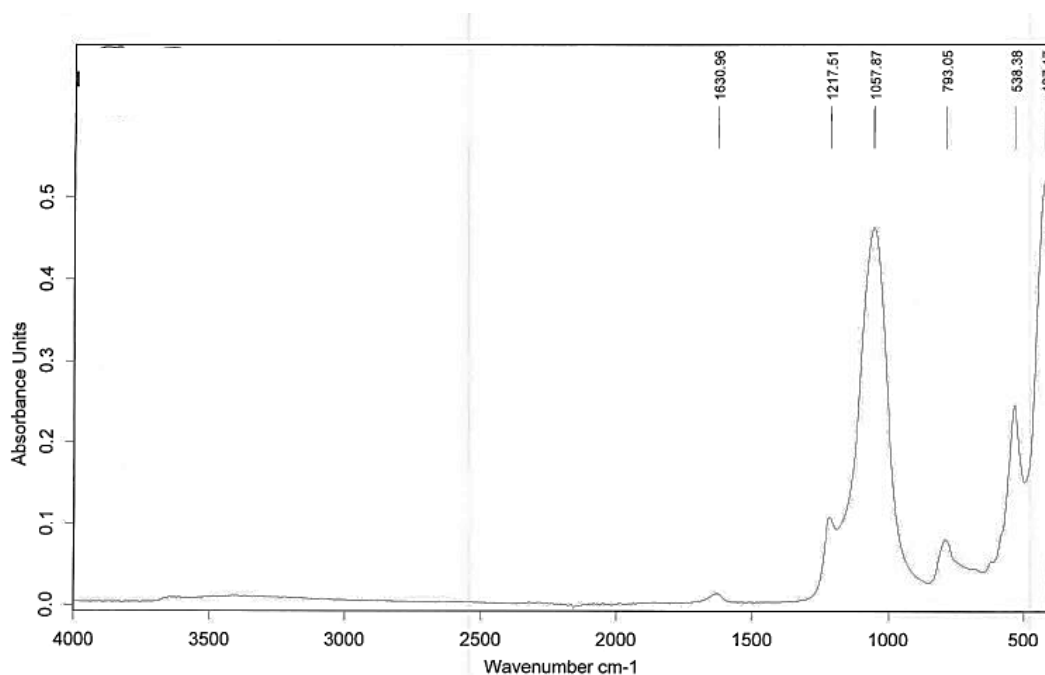
Figure 3. FTIR spectra of Zeolite Z1
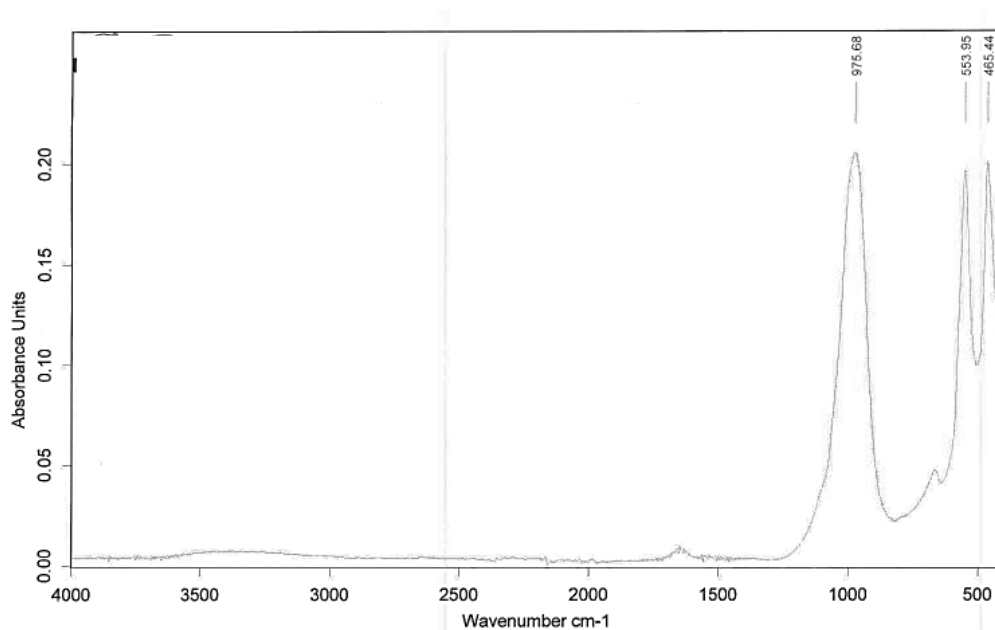
Figure 4. FTIR spectra of Zeolite Z2

Adsorption study

Figure 6 represents the results of adsorption kinetics on both zeolites Z1 and Z2. The major part of oils is adsorbed in less then 15 min. After 60 min the capacity increased for 4.0 ± 0.5 %(m/m) and 8.0 ± 0.5 %(m/m) for Zeolite Z1 and Z2, respectively. The results showed that the capacity of Zeolite Z2 was higher in both tests. Zeolite Z2 adsorbed 10.0 ± 0.5 %(m/m) more oils after 15 min and 17.0 ± 0.5 %(m/m) after 24 h compared with Zeolite 1. The reason could be in different SiO_2/Al_2O_3 molar ratio of both zeolites [7]. It could be also connected to the observation that a distinct portion of the zeolite's pore volume discriminatively accommodates hydrophobic compounds, such as oils.[8]
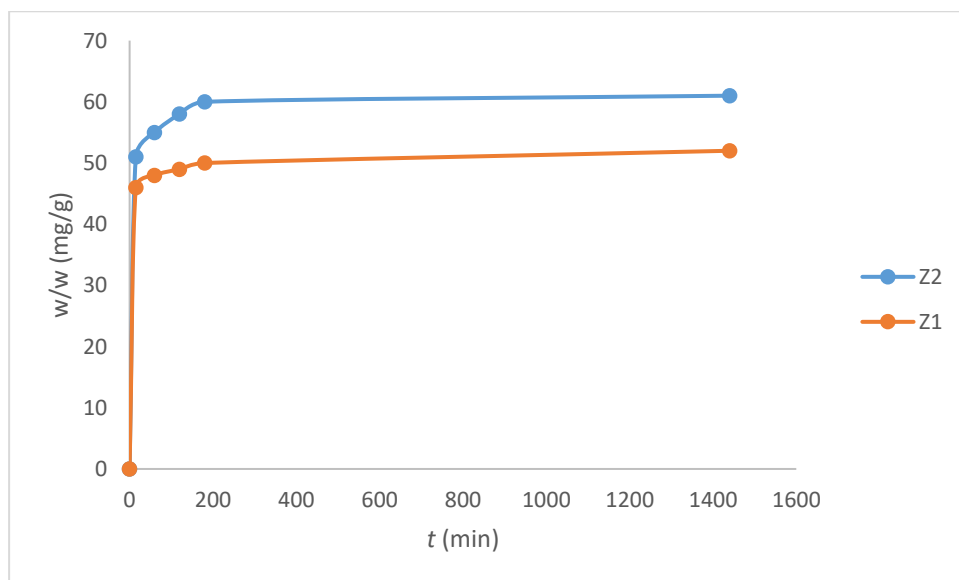
Figure 6. Adsorption kinetic curves of oil adsorption on both Zeolites Z1 and Z2

Conclusion

The zeolites were tested for oil adsorption. The FTIR analysis confirmed the hypothesis that the zeolites are uniform. The efficiencies of adsorbed oils onto ZAG-MFI and ZAG-4A were up to 21 %(m/m) and 25 %(m/m), respectively.

Acknowledgement

References

[1]   Y. Rabbani, M. Dhariaty-Niassar, S. A. Seyyed Ebrahimi, The effect of superhydrophobicity of prickly shape carbonyl iron particles on the oil-water adsorption, Ceramics International, 47 (20) (2021) 28400 – 28410.

[2]   X. Jin et al., Biomimetic and flexible 3D carbon nanofiber networks with fire-resistance and high oil-sorption capabilities, Chemical Engineering Journal, 412 (2021) 128635.

[3]   L. R. Rad, M. Anbia, Zeolite-based composites from the adsorption of toxic matters from water: A review, Journal of Environmental Chemical Engineering, 9 (5) (2021) 106088.

[4]   Safety data sheet according to Regulation (EC) 1907/2006, Asorbio® ZAG-4A, 2020, Accessed (1/8/2023): https://my.chemius.net/p/V14I24/en/gh/en

[5]   Safety data sheet according to Regulation (EC) 1907/2006, Asorbio® ZAG-MFI, 2017, Accessed (1/8/2023): https://my.chemius.net/p/icfkr1/en/gh/en

[6]   Standard Test Method for Sorbent Performance of Adsorbents, ASTM F726-17, ASTM International, 2017. Accessed (1/8/2023): https://www.astm.org/Standards/F726.htm

[7]   T. Fakin, A. Ristić, V. Mavrodinova, N.Z. Logar, Hyghly crystalline binder-free ZSM-5 granules preparation, Microporous and Mesoporous Materials, 213 (2015) 108-117.

[8]   S.Y. Mirsalami, M. Mirsalami, Investigation of oil biodegradation using expanded zeolite infused with oil-consuming microorganisms, Environmental Advances, 16 (2024) 100551.

YIELD, MORPHOLOGICAL AND PHYSIOLOGICAL PARAMETERS OF ORGANIC *AVENA SATIVA* L. PLANT AS AFFECTED BY MINERAL, ORGANO-MINERAL AND STEEL SLAG AMENDMENTS TO ACID SOIL

Aleksandra Stanojković-Sebić[1], Dobrivoj Poštić[2], Marina Jovković[1], Radmila Pivić[1]

[1]Institute of Soil Science, T. Drajzera 7, 11000 Belgrade, Serbia
[2]Institute for Plant Protection and Environment, T. Drajzera 9, 11000 Belgrade, Serbia
e-mail: astanojkovic@yahoo.com

Abstract
Oat (*Avena sativa* L.) is one of the most important self-fertilizing field plant belonging to the Poaceae family, with multiple purposes as a fodder plant and in human nutrition. Of all the cereals, it tolerates heavy and wet soils the best, but with a very good reaction to fertilization [1]. The current study evaluated the effects of solely application of mineral (NPK) and organo-mineral (OM) fertilizers, and their individual combination with steel slag (SS), on the certain measured morphological parameters (mean number of leaves per plant - MNLP; minimum leaf length per plant - MinLL, in cm; maximum leaf length per plant - MaxLL, in cm; number of ears per plant - NEP), physiological parameters [content of: chlorophyll - Chl, flavonoids - Flv, anthocyanins - Ant, nitrogen balance index (Chl/Flav Ratio) - NBI], and the yield, in oat crops, between the treatments and in relation to the control. The experiment was performed in semi-controlled greenhouse conditions, in pots, from the 4th decade of March to the 4th decade of June, in 2024, using organic oat seeds, with Eutric Cambisol [2]. The soil is characterized as a light clay with an acid reaction. Steel slag was taken from the steel factory different deposition sites and characterized to have very alkaline reaction, Ca and Mg contents mainly in their oxide forms, and high total Fe and Mn content (but with lower amounts in their soluble forms) [3]. NBI and the contents of Chl, Flv, Ant, were measured using portable Dualex optical leafclip sensor (FORCE-A, Orsay, France). The obtained results showed that the MNLP, MinLL, MaxLL, NEP, the contents of Chl, Flv, Ant and NB index, in organic oats, significantly differed between the treatments applied and in relation to control. The effect of treatments on obtained oat yield insignificantly differed between the treatments, but significantly in relation to the control. The best results were obtained with the use of OM+SS, whereby good results were obtained with the NPK+SS use. Concluding, applied steel slag, in combination with mineral and organo-mineral fertilizer, respectively, showed the positive effects on the morphological and physiological parameters in organic oat and its yield, grown on acid type of soil. Regarding this research, in such combinations steel slag showed high potential in usage toward improvement of tested soil fertility without adverse effects.

References
[1] Dj.Glamočlija, Field Production - Grains and Grain Legumes, Faculty of Agriculture, Zemun - Belgrade, Serbia, 2012, pp. 87. (in Serbian)
[2] IUSS Working Group WRB, World Reference Base for Soil Resources, 4th ed., Vienna, Austria, 2022.
[3] R.Pivić, A.Stanojković, S.Maksimović, D.Stevanović, Fresenius Env. Bull. 20 (2011) 875.

THE ELECTRICAL PROPERTIES OF THE $Sb_xAs_{37-x}S_{48}I_{15}$ GLASS SYSTEM IMPORTANT FOR EFFICIENT ENERGY USAGE

Goran Štrbac[1], Ondrej Bošák[2], <u>Dragana Štrbac</u>[3], Marian Kubliha[2]

[1]*University of Novi Sad, Faculty of Sciences, Trg Dositeja Obradovića 4, Novi Sad, Serbia*
[2]*Faculty of Materials Science and Technology, Slovak University of Technology, Bottova 25, 91724 Trnava, Slovakia*
[3]*University of Novi Sad, Faculty of Technical Sciences, Trg Dositeja Obradovića 6, Novi Sad, Serbia*
e-mail: draganastrbac@uns.ac.rs

Abstract
This work presents the results of measuring the electrical conductivity parameters of glasses from the $Sb_xAs_{37-x}S_{48}I_{15}$ system, carried out in both DC and AC regimes. Measurements were performed on both amorphous and annealed samples, in which the crystallization of SbSI and Sb_2S_3 structural units was induced. It was shown that the conductivity of the annealed samples is several tens of times higher compared to the amorphous samples. The temperature dependence of conductivity follows Arrhenius behavior. The values of the activation energy ΔE_{DC} obtained by fitting the DC component of the conductivity as a function of temperature and the decreasing character of this quantity with an increase in the proportion of antimony was determined. The results of the conductivity tests as a function of frequency showed that conductivity increases with rising temperature, antimony proportion, and frequency. Measurements were made in the frequency range of 0 to 10^5 Hz and the temperature range from room temperature to 398 K. ΔE_{AC} values at 100 Hz and 1000 Hz were determined. In this regime, the activation energies showed complex relaxation mechanisms. Impedance spectra were analyzed using an equivalent-circuit model, through relaxation time values and the activation energies of the relaxation process were determined. The presence of a temperature-dependent electrical relaxation phenomenon of the non-Debye type was confirmed. Additionally, effect of frequency and temperature on the loss factor (ε'') within the measured frequency range was analyzed.

EFFECT OF MICROWAVE TREATMENT AND TRADITIONAL PASTEURIZATION ON THE PROPERTIES OF FRUIT JUICES

Beatrix Szabó-Nótin, Anett Sebe, Mónika Máté

Department of Fruit and Vegetable Processing Technology
Institute of Food Science and Technology, Hungarian University of Agriculture and Life Sciences
H-1118, Budapest, Villányi street 29-43. Hungary
e-mail: szabo-notin.beatrix@uni-mate.hu

Abstract

During our research work, the main goal was to investigate the effects of microwave and traditional heat treatment, which was performed on fresh pressed apple and orange juice. Commercially available fruit-based drinks are always subjected to heat treatment for preservation purposes, but this process usually causes a loss of the valuable, heat-sensitive components of the fruit juice.

In addition to samples heat-treated at 80 and 90 °C, apple and orange juice samples treated at 700 W for 3 minutes were prepared, and their pH, refraction, colour, density, viscosity and total polyphenol content were examined during 6-month storage. Accordingly, to the results, the use of microwave (MW) treatment may be proposed as an alternative to traditional heat treatment in order to preserve the fruit juice quality.

Introduction

Apple and orange juice is one of the most popular beverages in Iraq as well as in the worldwide. During storage of these juices colour changes and gradually turns brown. However, it has been shown that the browning occurred in acidic fruit juices during storage was attributed mainly to nonenzymatic reactions [1; 2]. Commercial fruit juices have been traditionally heat-processed to destroy spoiling microorganisms and inactivate enzymes [3] Heat treatment often induces undesirable changes in the colour, flavour and nutritional value of the fruit juices [4] Furthermore, heat treatment can reduce organoleptic quality [5]. Researchers have emphasised the importance of optimising time/temperature profiles in order to minimise the exposure of food to heat. In order to mitigate the detrimental effects of heat treatments on food products, the food industry is calling for the development of alternative technologies capable of reducing the deteriorating impact at temperatures below those typically employed during thermal processing [6]. Consequently, non-thermal food treatment techniques are attracting significant interest due to their potential to reduce or even eliminate heat exposure. Fresh pressed fruit juices have emerged as a prominent candidate for non-thermal processing due to the degradation of its fresh flavour characteristics by the thermal processes currently employed for ready-to-drink products, such as pasteurisation. Electromagnetic heating, on the other hand, has been successfully used for the efficient pasteurization of fruit juices in the recent years [7; 8]. A number of studies have been conducted into the MW pasteurisation of fruit juices, which has been demonstrated to preserve the natural organoleptic characteristics of the juice while reducing the time of exposure to energy, thereby lowering the risk of losing essential thermolabile nutrients [7].

The aim of the present study is to examine the effect of MW treatment on the preservation of fresh pressed apple and orange juice in comparison with 80 and 90°C heat treatment.

Experimental

Apple (variety 'Idared') and orange (variety 'Valencia') were purchased from the local market. Juice was pressed using a laboratory pressing machine. Samples were then heat-treated in 200

ml bottles at 80 and 90 °C for 0.002-0.004 sterilization equivalents and microwaved at 700 watts (2450 Hz) for 3 minutes.

Determination of pH
Measurements were made with a TESTO 206-pH2 digital pH meter for each sample with three repetitions.

Water-soluble dry matter content (refraction) measurement
Determination of water soluable dry material content of the juices was performed by using a ATAGO DBX-55 refractometer, with three repetitions.

Colour measurements
Colour is a determining factor in the definition of the quality of any food. The colour of the samples were also measured with 3 parallels using a Konica Minolta CR400 chromameter. Results were expressed as L*, a*, and b* values. L* is a measure of the brightness from black (0) to white (100), while a* describes the redgreen color (a*> 0 indicates redness, a* < 0 indicates greenness), and b* describes yellow-blue color (b*> 0 indicates yellowness, b* < 0 indicates blueness). To determine the total color difference between two samples using all the three coordinates, the following formula was used: $\Delta E^* = \sqrt{(\Delta L^*)^2 + (\Delta a^*)^2 + (\Delta b^*)^2}$

Density measurements
Density measurements were carried out by using DENDI-2 density meter.

Viscosity measurements
Measurements were performed with Physica MCR 51 (Anton Paar) rotary and oscillating viscometer with CC27 probe. RheoPlus software was used to record and evaluate the measurement results. The measurement profile was recorded by the software to increase the deformation rate from 500 1/s to 1200 1/s during the 90 second measurement time, while taking the measurement points every 5 seconds. Samples were tested at 20° C. From the flow curve, viscosity values (Pas) were determined.

Determination of total polyphenol content
Total phenolics were determined using the Folin–Ciocalteu colorimetric method as described by Singleton and Rossi (1965) [9]. The results were expressed in gallic acid equivalents (GAE, mg L^{-1} juice).

Results and discussion
The average water-soluble solid content of the tested juices is shown in Figure 1. The refraction % of orange juice in all three samples treated shows an increasing trend. The highest increase in water soluble solids was observed in the microwave-treated orange juice, from 11,07 % to 11,97 %. This sample had the highest refraction %, already at time 0. While the dry matter content of the other two samples decreased or stagnated, the microwaved sample was higher than the raw sample. At the end of the storage experiment, was measured the same for orange juice treated at 80 and 90 °C, 11 %. The refraction results of the apple juice samples also show that there was an increase in all cases compared to measurement time 0. As with the oranges, the microwaved apple juice had the highest dry matter content.
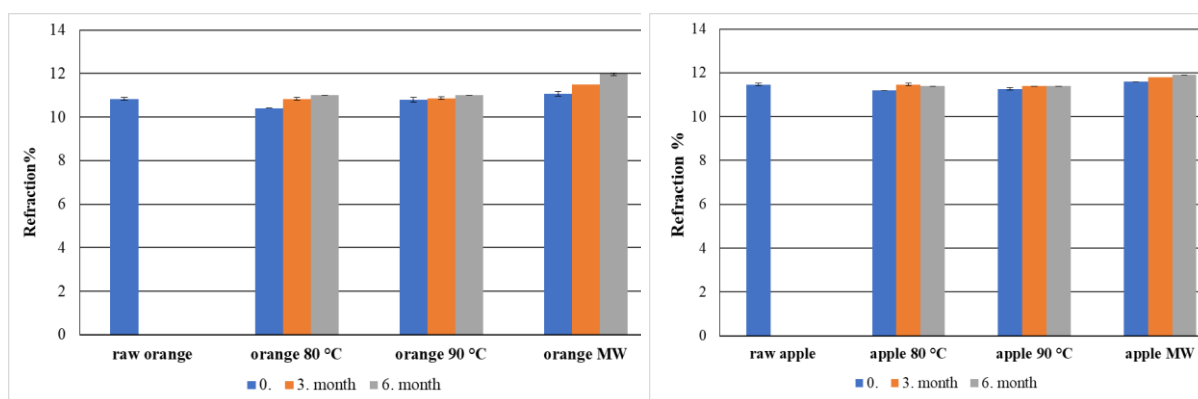
Figure 1. Water soluble dry matter content of orange and apple juices

The ΔE* values of the samples are shown in Figure 2. On the 0. day the samples were compare to the raw apple and orange juice, and after during the storage 3-month samples and 6 moths stored samples were compare to the 0. day (freshly produced) samples.

In case of orange juice, the smallest colour difference was shown by 80°C heat treated sample, and the largest by orange MW 6-month stored compared to the 0. day MW.

In case of apple juice, the smallest colour difference was shown by MW treated sample, and the largest by apple 80°heat treated compared to the 0. day raw apple juice.

The colour stimulus difference shows the extent of the visible difference between the colours of two tested samples: below 0.5 it is not noticeable; between 0.5 and 1.5 slightly noticeable; noticeable between 1.5 and 3.0; 3.0 to 6.0 clearly visible and in the case of a value above 6.0, we are talking about a great visibility [9].
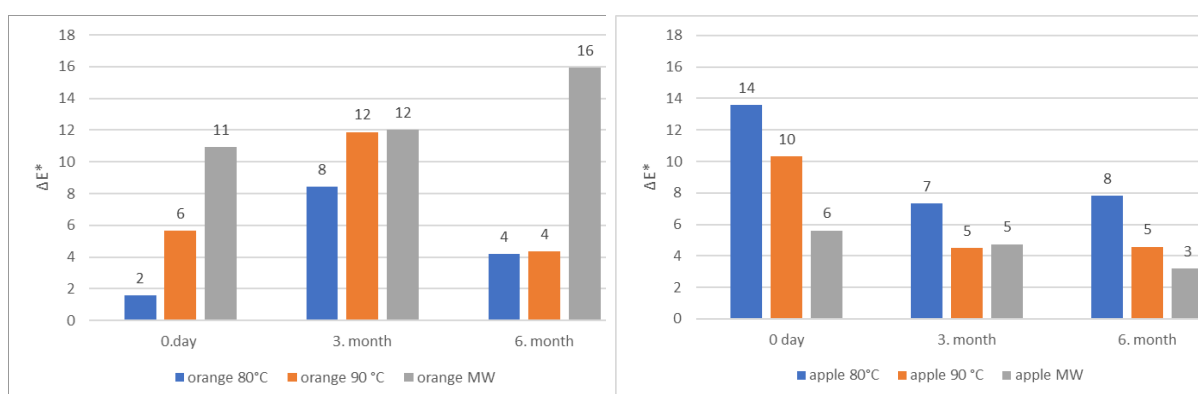
Figure 2. Inger color difference between the orange and apple juices

Rheology studies of pressed fruit juice samples were performed at 20° C. In each case, from the flow curves viscosity values were determined and the results are shown is Table 1.

	Viscosity values (Pas)		
	0. day	3. month	6. month
raw orange juice	0,01	-	-
orange 80 °C	0.0107	0.0087	0.009
orange 90 °C	0.0103	0.0085	0.0087
orange MW	0.0104	0.0098	0.0092
raw apple juice	0.0083	-	-
apple 80°C	0.0089	0.0088	0.0085
apple 90 °C	0.0087	0.0085	0.0081
apple MW	0.0087	0.0086	0.0082

It can be seen, that at the 0. day, after the treatments, there were not differences between the samples, but during the storage, viscosities were decreasing a little bit.

The polyphenol content of the samples is shown in Figure 3. It can be seen, that after the treatments, and during the storage polyphenol content were decreasing continuously, especially in case of the apple juice. Unfortunately, in case of apple juice, microwave treatment had a negative effect, because the microwave-treated samples showed the greatest reduction in polyphenol content. Total polyphenol values in case of orange were between 151 mg GSE L^{-1} g and 198 mg GSE L^{-1} The lowest total polyphenol content was in case of the 6 month stored apple juices (56-63 mg GSE L^{-1}), which is significantly ($P<0.05$) difference compared to the other samples. In the case of apple juice,
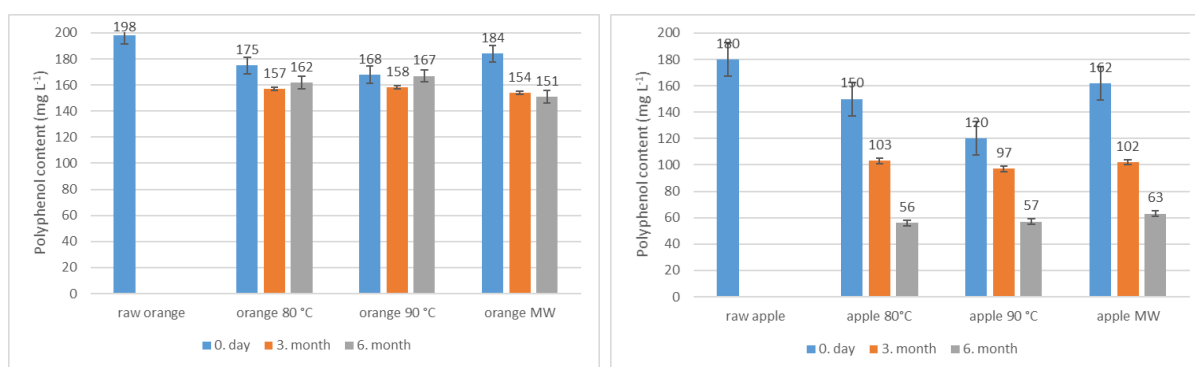
Figure 3. Total polyphenol content of the orange and apple juices

Conclusions
In all cases, heat preservation causes a loss of valuable materials, and it is important to choose the right temperature and treatment time to reduce this. This is why next to the microwave treatment, pasteurised samples at 80 and 90 °C were also prepared. The measured characteristics were compared with the raw sample without heat treatment and the juices subjected to the different methods were also compared with each other in terms of the characteristics tested. Based on the work, can be stated, that the microwave treatment showed very similar results, compare to the heat treatment in case of orange juice. Using MW process shas shown promising results for improving product quality and, particularly for shortening the treatment times.

References

[1] H. S. Burdurlu, F. F. Karadeniz (2003). Food Chem. 80: 91-97.

[2] T. A Khalil, M. I. Al-Zubaidy (2010). Kinetics of nonenzymatic browning reaction in citrus juice concentrates during storage. 4th International Conference, "Innovative in Food Science and Nutrition: Future Challenges", NRC, Cairo, 27-29 Sep. 2010

[3] R. J. Braddock (1999). Handbook of Citrus By-products and Treatment Technology. Wiley, New York

[4] J. Giner,; V. Gimeno; M. Palom´es ; G. V Barbosa-Canovas, O. Martın (2003). Eur. Food Res. Technol. 217:43–48.

[5] L. F.; F. A. N. Damasceno, M. M. A Fernandes, and E. S. Brito (2008). Brazilian Journal of Chemical Engineering 25 (2): 313-320.

[6] M. F.; R. D. Kozempel, O. J Cook Scullen ,B. A. Annous (2000).
Journal of Food Process and Preservation 24: 287–301.

[7] J. A Canumir, J. E Celis, J. de Bruijn & L. V. Vidal (2002). *Lebensmittel-Wissenschaft und -Technologie- Food Sci. and Technol*, 35(5), 389–392. https://doi.org/10.1006/fstl.2001.0865

[8] S. Tajchakavit, H.S Ramaswamy. (1995). J. of Microwave Power and Electromagn. En., 30:3, 141-148, DOI: 10.1080/08327823.1995.11688270

[9] V.L., Singleton, J.A., Rossi, (1965) Am. J. of Enol. and Vitic., 16, pp.144–158.

[10] K., Wenzl-Gerőfy (2014): A CIE L*a*b* színrendszer. 128. ISBN: 978-963-313-202-9

INNOVATIVE USAGE OF INFRARED REMOTE SENSING: EXAMINATION OF THE SLAB INSULATION OF RESIDENTIAL BUILDINGS AT MUNICIPAL LEVEL

Hajnalka Dürgő[1], Szalma Elemér Imre[2]

[1]*Department of Technology, University of Szeged, H-6720 Szeged, Boldogasszony sgt 6, Hungary*
[2]*PlantaDrone Ltd., Hungary*
*e-mail: szalma.elemer@gmail.com*

Abstract
Due to the social, and environmental processes taking place in our wider environment, the issue of residential energy use and energy saving has become increasingly important in recent years. Taking a closer look at the issue, on the one hand, this sector is obviously undergoing major changes in terms of the source of the energy used, and on the other hand, everyone is trying to reduce the amount of energy used by their household for environmental-, or even more so for financial reasons. In residential properties, up to 40% heating/cooling energy savings can be achieved with proper insulation and the installation of high-quality windows and doors. In terms of insulation, preventing heat radiation from the slab would be the first and most important step. In our study, we took a closer look at the slab insulation of residential properties in a small rural town using a new method, optimizing the drone aerial remote sensing parameters with an infrared and multispectral camera in such a way as to obtain as much analytical data as possible regarding the slab insulation in the shortest possible flight time. Our results clearly illustrate the building and energy status of rural settlements, and even the structure of the settlement emerges from the results. The method can be used effectively when the relative infrared radiation ratios of larger areas need to be done quickly.

Introduction
Currently the greatest challenge of humanity is the increase of the concentration of greenhouse gases in the athmosphere, which is the main cause of the global warming (climate change) of the World's atmosphere (greenhouse effect). According to our experiences and forecasts, global warming and weather anomalies will change the current thermal conditions in different parts of the world differently. In 2024, the concentration of the athospheric CO_2 is 426 ppm [1]. The main cause of greenhouse gas emission is the usage of fossil fuels. The primary energy usage of Hungary was 1157.2 PJ in 2020 [2], and the residential fraction was 33.9%, meaning a significant amount of saveable energy consumption is concentrated in the hands of the homeowners, mainly in the field of heating and cooling the houses/flats, and making warm water [3]. As relevated in the study of NEGAJOULE2020 we could save up to 40% of energy (and the money spent on it) with appropriate and thoughtful energetical building renovations, resulting a lower amount of greenhouse gas emission into the atmosphere. In our study we investigated the energy efficiency of residential buildings in an average Hungarian village with a new point of view and method: examination of the slab insulation with infrared and multispectral drone records. The heat transfer of the roof can inform us about the insulation of the slab. The multispectral results can help us to find the best sampling point of a roof's thermal infrared data. The infrared (IR) part of the light starts from the red end of the visible light (750 nm-1000 μm wavelength range), the thermal infrared is from 3 μm[4].

Experimental

It is important to note at this point that this test method does not produce a raster file withexact temperature values. This method produces a relative grayscale heatmap, which data comes from the heat emission of the slabs. We used the pixel values behind the grayscale colors to represent the heat radiation of the individual buildings. Based on these values**,** the properties of the village were divided into 10 categories from „no heat transfer was detected through the slab" to „Extreme heat transfer through the slab". A village with 3-4000 inhabitants was selected for this examination and a drone with a1280x1024 radiometric thermal pixel resolution was used for the infrared recording of the settlement. The height and the other key flying parameters were set up regarding the desired field resolution (GSD). We had to record in the early morning hours at winter time so the heat escaping from the slab could be precisely detected, without the disturbing signals of daytime heat radiation, and reflection. The day before the flight was cloudy, so the heating effect of the sun also did not affect the measurement. There was no snow coverage at the time of the inspection. The temperature was slightly below zero (-2°C). We did another recording with a multispectral drone in the afternoon of the same day. The captured recordings were processed with a photogrammetric software (Figure 1). The LCI (Leaf Chlorophyll Index) of the plants on the roof was calculated from the reflectance data captured by the multispectral drone, using theformula below: (NIR-RedEdge) / (NIR+Red).
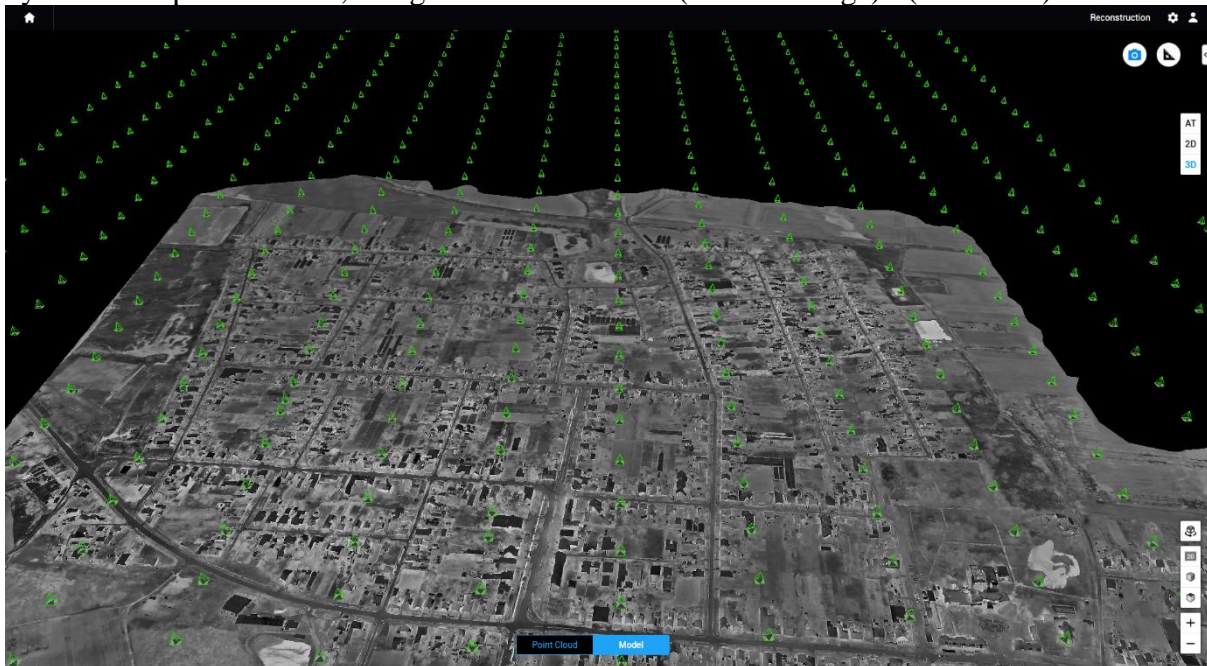
1.   Figure 1. Photogrammetrical-bounded 3D heatmapmodel of the investigated settlement

We had to examine all three available parameters (for every property) during the evaluation: Infrared, LCI, and RGB results. The examination, comparison and evaluation of the data was done by a GIS application (ArcMap 10.8.2.). We realised that the objects/artifacts and the moss or crush on the roof affects the obtained IR results, this is why we needed the multispectral, and visible survey beside the Infrared. Layering the collected data we had to find an appropriate 1 meter radius „clean/indicative" part on every roof that is usable for evaluation and comparison. The number of investigated, inhabited properties were 1462.

Results and discussion

The range of the obtained grayscale pixel values from the infrared orthomosaic was between 23,82 and 159,21. This range was divided into 10 equal parts, of which we created ten slab-

insulation categories (Figure 2). The standard deviation of the results, projected on every building, can be seen in the table below (Table 1).
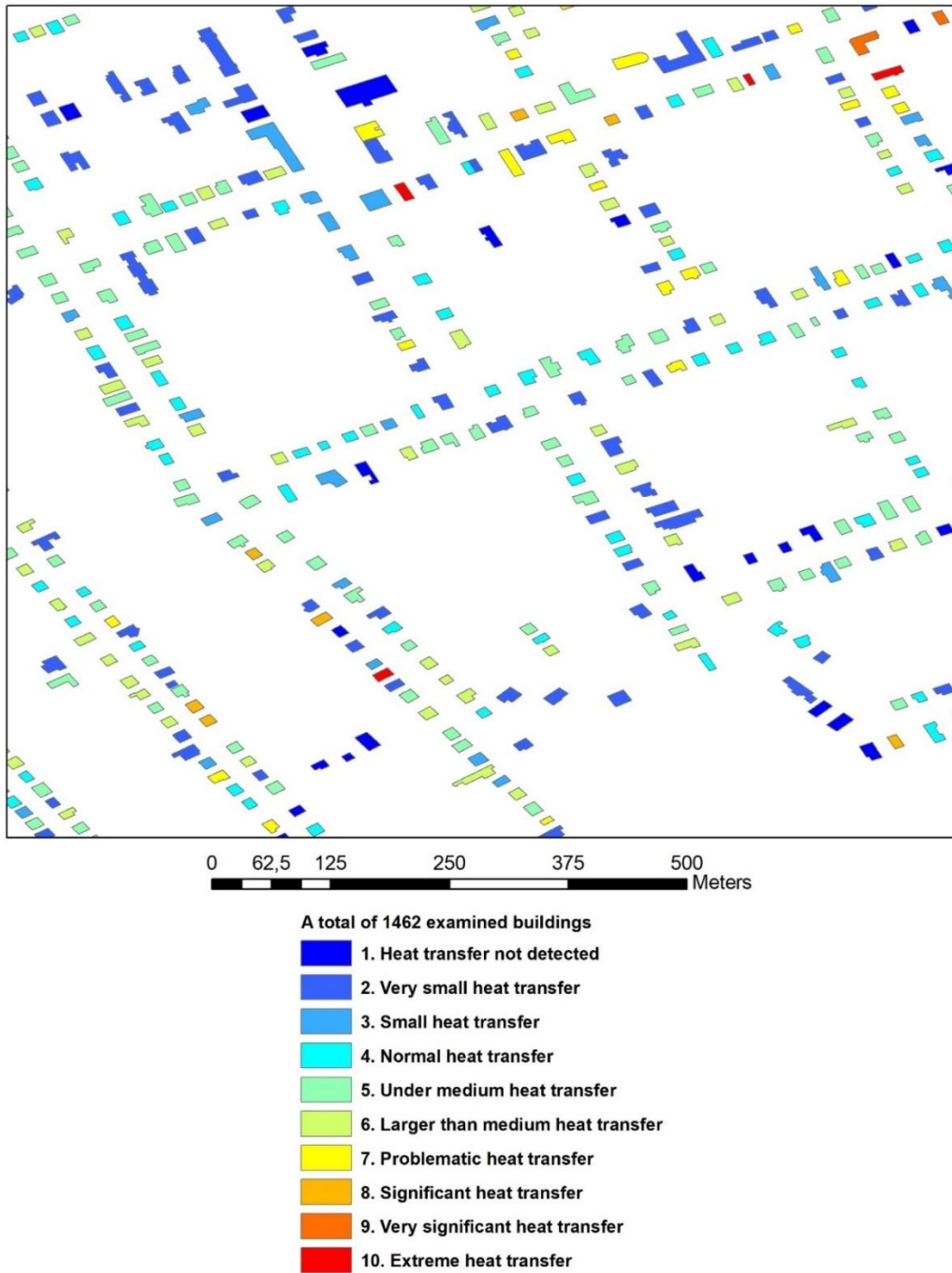

Figure 2. The color code of the 10 categories

categories	Number of the properties in the categories	%	Heat transfer through the slab
1.	91	6,22	no/not detected
2.	268	18,33	very small heat transfer
3.	228	15,6	small heat transfer
4.	240	16,41	normal heat transfer
5.	307	21	under medium heat transfer
6.	215	14,7	larger than medium heat transfer
7.	74	5,06	problematic heat transfer
8.	27	1,85	significant heat transfer
9.	7	0,48	very significant heat transfer
10.	5	0,34	extreme heat transfer

Table 1. Distribution of residental properties according to slab heat transfer per category

The properties with extreme heat emission were personally visited, and the important data of these bulidings were recorded. Based on these data we found that the age of the residental properties of the rural part of Hungary are 40-50 years. Most of these buildings are „Kádár-cubes", which is a special type of Hungarian construction from the socialist years (1960-1979). We found a very interesting Kádár-cube, where the left half of the house was in original conditions with no insulations and with old windows, but the right half was insulated and renovated. We couldn't even ask for a better representation of the urgent need, and obvious advantages of a properly insulated house (Figure 3).

Figure 3. RGB, LCI, IR and cathegorized IR-records of the semi-modernized Kádár-cube

Conclusion

For a significant part (about 75%) of the residential properties of rural Hungary, the boundary walls are insulated, the doors and windows are modernized, but the insulation of the slabs are old or missing in many cases. The lack of adequate insulation could be of financial, as well as marketing reasons. There are no advertisements about the importance of the slab insulation, most likely because it does not require special knowledge or professional work, so the effect of this for the national economy is relatively small. Our results clearly illustrate the buildings'average energy status in rural settlements, and even the structure of the settlement emerges from the results. The method can be used effectively when the relative infrared radiation ratios of larger areas are needed to be done quickly. Our task to be solved is the development of the automation of post-production.

Acknowledgements

References

[1]https://www.statista.com/statistics/1091999/atmospheric-concentration-of-co2-historic/ (letöltés dátuma: 2024.09.14.)

[2] https://www.ksh.hu/stadat_files/ene/hu/ene0006.html (letöltésdátuma: 2023.04.17.)

[3] https://energiaklub.hu/projekt/negajoule-2020-magyarorszag-lakoepulet-allomanyanak-energiahatekonysagi-potencialvizsgalata-2817 (letöltésdátuma: 2023.04.17.)

[4] Mucsi, L.: Műholdastávérzékelés.Libelluskiadó, Szeged, 2004.

[5] Szatmári J. et al.: Légi távérzékeléses módszerrel támogatott hőtérképezés Szegeden pp. 321-328. Konferenciakötet. https://giskonferencia.unideb.hu/arch/GIS_Konf_kotet_2010.pdf (letöltés dátuma: 2024.09.19.)

[6] Nagy I. et al.: Műszaki diagnosztika II. Termográfia, Delta-3N Kft. 7. fejezet pp. 103-118. 2007 https://docplayer.hu/6462025-Muszaki-diagnosztika-ii-termografia.html (letöltés dátuma: 2024.09.19.)

COMPARISON OF DIFFERENT QUINCE (*CYDONIA OBLONGA* MILL.) VARIETIES BASED ON THEIR PHYSICAL AND CHEMICAL PROPERTIES

<u>Lilla Szalóki-Dorkó</u>, Anita Márta Rikker, Mónika Máté

Department of Fruit and Vegetable Processing Technology, Institute of Food Science and Technology, Hungarian University of Agriculture and Life Science,, H-1118 Budapest, Villányi út 29-43, Hungary
e-mail: szaloki-dorko.lilla@uni-mate.hu

Abstract
Quince (*Cydonia oblonga* Mill.) is a worldwide fruit, which is not consumed as a raw fruit because of its tart taste and hard texture, but it has become favourite by processing it into juice, jam, brandy, or even quince cheese. During our work, five different varieties of quince ('Bereczki', 'Bereczki bőtermő', 'Leskovaci', 'Vranja', 'Cydora robusta') were examined in terms of the total dry matter content, water soluble solids, antioxidant capacity (FRAP) and total polyphenol content (TPC) of the raw fruit. Based on the results, 'Leskovaci' had the highest total dry matter content (22.23%) and water-soluble dry matter content (16.77%), which is more preferable in quince cheese production. However, 'Bereczki' contained the highest TPC (241.53 mg GSE/ 100 g) and FRAP (428.39 mg ASE/ 100 g) values. These two varieties can be promising for processing, but more examinations are needed.

Introduction
Quince fruit (*Cydonia oblonga)* that belongs to the Rosacea family and native to the Mediterranean region has been studied for decades for its unique importance in food and medicine. Quince is not suitable for direct consumption due to hardness, bitterness and astringency [1,2] so fruit is used to process to jam, <u>marmalades</u>, fresh fruit compote, jellies, dried slices and wines in the food industry and at home [3,4]. Quince contains high health promoting compound content such as polyphenols and varied functional molecules [5,6]. Its nutritional value is given by its vitamin C content (30 mg/100 g), its sugar content is 7.5–13.2 %, its acid content is 0.5–2.4 %, and its pectin content is high [7]. Based on FoodData, the water content of quince per 100 grams is 83.8 g, the energy content is 57 kcal/238 kJ, the protein content is 0.4 g, the vitamin C content is 15 mg, the vitamin B1 (thiamine) content is 0.02 mg, B 2 vitamin (riboflavin) content 0.03 mg, vitamin B6 content 0.04 mg [8]. The pectin content of quince is 0.7–1.8%, the vitamin content is higher than that of apples and pears [9].
The aim of this study to compare five different quince varieties ('Bereczki', 'Bereczki bőtermő', 'Leskovaci', 'Vranja', 'Cydora robusta') and evaluate them based on their physical and chemical properties and in aspect from processing.

Experimental
Materials
Five quince varieties, namely 'Bereczki', 'Bereczki bőtermő', 'Leskovaci', 'Vranja', 'Cydora robusta' (Figure 1.) were involved in this study to examine some different physical and chemical properties. The fruits were harvested from Kecel (County of Bács-Kiskun) and Harc (County of Tolna), Hungary in the year of 2023.
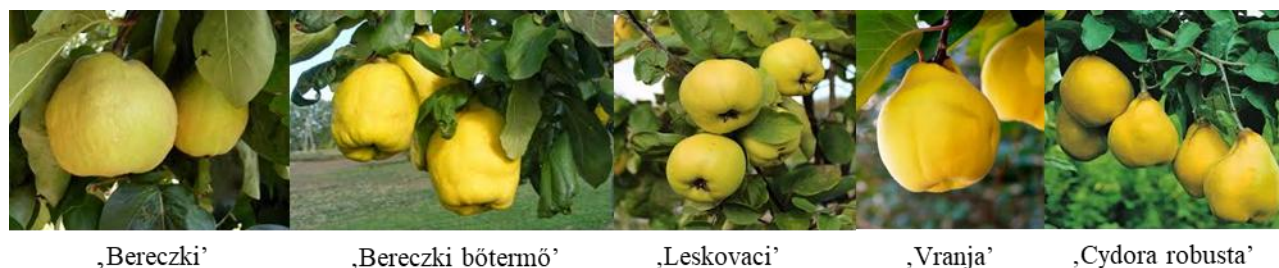
,Bereczki'   ,Bereczki bőtermő'   ,Leskovaci'   ,Vranja'   ,Cydora robusta'

Figure 1. Quince varieties in the study

Methods
Total dry matter content
The samples were dried in an oven at 105±2 °C for three hours until the weight was constant. After cooling, the dried samples were reweighed and calculated the total dry matter content of the samples in %.

W*ater soluble solids*
The *determination* of *water soluble solids was carried out with digital refractometer. The unit of the values was given in Brix%.*

Extraction method for the spectrophotometric measurement
Using solid-liquid extraction, the extractant was: 50% methanol, 50% distilled water. The mixture of quince crushed (approx. 0.5 g) and the extractant (40 ml) was added and standing for 10 minutes. Then it was placed in an ultrasound bath for 10 minutes, and centrifuged at 4000 rpm for 5 minutes to separate the solid part from the liquid. The supernatant was examined further.

Total antioxidant capacity (FRAP)
The FRAP value (Ferric Reducing Ability of Plasma) was determined based on the Benzie and Strain [10] method at $\lambda=593$ nm with Hitachi U-2900 spectrophotometer. The results were given in mg ascorbic acid equivalents (AAE)/100 g units. The equation of the calibration line used for calculation ($y = 0.2541x + 0.0042$, $R^2 = 0.9961$).

Total polyphenol content (TPC)
The amount of total phenolic components were measured by method of Singleton and Rossi [11] at $\lambda=760$ nm with Hitachi U-2900 spectrophotometer. The results were given in mg gallic acid equivalents (GAE)/100 g units. The equation of the calibration line used for calculation ($y = 0.0106x + 0.0013$, $R^2 = 0.9958$).

Statistical analysis
T-test was used for the analysis of the effect of varieties on total dry matter content, water solube solid content, total antioxidant capacity and total polyphenol concentration. Significant differences between the varieties were considered when P value was <0.05.

Results and discussion
Total dry matter content
The average total dry matter content of the five types of quince varied between 17.29 % and 22.12 % (Figure 2. A). The lowest total dry matter content was measured in 'Vranja' quince variety (17.29 %), while the 'Leskovaci' sample contained the highest value (22.23 %).

According to Nyéki [12] the general total dry matter content of quince can be between 14.4-18.6%, which is similar that we measured in all varieties.
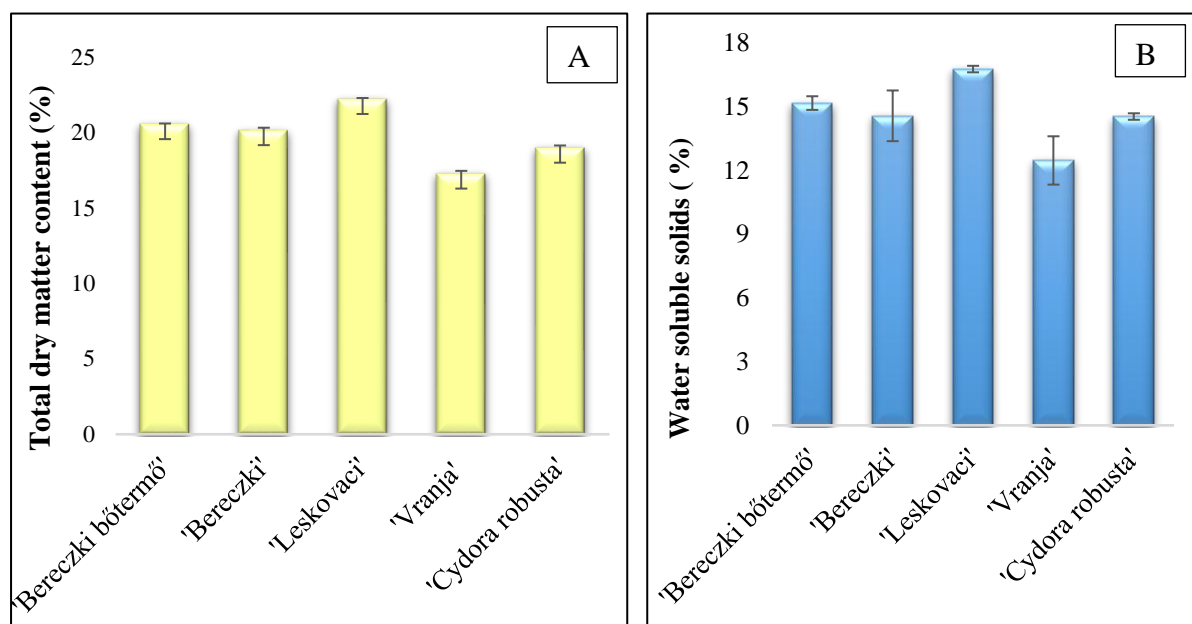

Figure 2. Total dry matter content (A) and water soluble solid content (B) of the examined quince varieties.

Water soluble solid content

The average water soluble solid content of the tested quince samples is shown in Figure 2. B. The highest water-soluble solids was measured for the variety 'Leskovaci' (16.77 %), while the lowest was for the variety 'Cydora robusta' (14.53%). There is no significant differences ($p > 0.05$) between the samples. According to the provisions of Directive No. 2-601 of the Hungarian Food Code (Codex Alimentarius Hungaricus), the water-soluble solid content should be at least 7% in case of quince cheese production. Based on this, all examined samples were suitable for this, if the ratio of the quince is at least 50%, since the water soluble solid values were between 14.53% and 16.77%.

Total antioxidant capacity (FRAP) and total polyphenol content (TPC)

Among the tested quince varieties, the 'Bereczki' variety had the significantly ($P < 0.05$) highest antioxidant capacity (428.39 mg ASE/ 100 g), followed by the 'Leskovaci' variety (74.8 mg ASE/ 100 g), then the 'Cydora robusta' (74.53 mg ASE/ 100 g) and the 'Bereczki bőtermő variety (60.1 mg ASE/ 100 g), while the 'Vranja' variety had the lowest FRAP value (39.54 mg ASE/ 100 g) (Figure 4. A).

Total polyphenol values (Figure 4. B) were between 66.28 mg GSE/ 100 g and 241.53 mg GSE/ 100 g. The lowest total polyphenol content was in case of 'Vranja' quince variety (66.28 mg GSE/ 100 g), while 'Bereczki' quince variety had the highest data (241.53 mg GSE/ 100 g), which is significantly ($P < 0.05$) difference compared to the other samples. The values of the other three quince varieties were as follows: for the 'Bereczki bőtermő variety 80.95 mg GSE/ 100 g, 'Leskovaci ' variety had 103.12 mg GSE/100 g, and 'Cydora robusta' had 85.98 mg GSE/100 g. These values are below that Najman et al. [13] measured in quince harvested from Poland. The tendency between the varieties were the same in case of FRAP and TPC values.
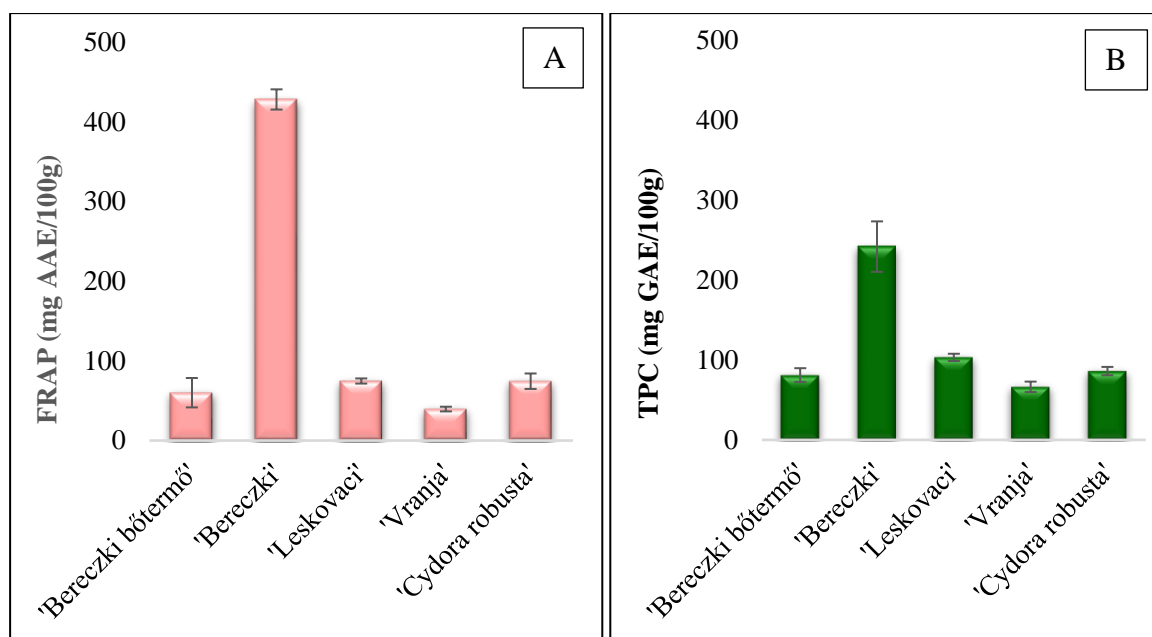
Figure 4. FRAP (A) and TPC (B) values of the examined quince varieties

Conclusion

Five quince varieties were compared in this study based on different physical and chemical properties. Generally, the quince is consumed in processed form (jam, fruit cheese etc.), parameters of the raw fruit can be influenced the characteristic of the final product. As regard the total dry matter and water soluble solid content, 'Leskovaci' variety had the highest values while the lowest data was measured in case of 'Vranja'. 'Bereczki' sample contained significantly higher FRAP and TPC values compared to the other varieties, however 'Vranja' variety had the lowest values in this case as well. So based on this one-year experiment 'Leskovaci' and 'Bereczki' can be promising for processing, but more examinations are needed because the differences in the results can be a variety dependent characteristic or a vintage-effect.

References

[1] B.M. Silva, P.B. Andrade, R.C. Martins, P. Valentao, F. Ferreres, R.M Seabra et al., J. Agric. Food Chem. 53 (2005) 111–122.

[2] E. Hanan, V. Sharma, F.J. Ahmad, Int. J. Food Process. Technol. 11 (2020) 831.

[3] L. Laureiro, J. Gim´enez, A. Balatti, MSc. thesis (2009)

[4] I. Al-Zughbi, M. Krayem, Food Chem. 393 (2022) 133362.

[5] C. Oliveira, I.B. Valentim, M.O.F. Goulart, C.A. Silva, E.J.H. Bechara, M.T.S. Trevisan. New Chem. 32 (2009) 689–702.

[6] A.S.B.M. Magalhães, J.A. Pereira, P.B. Andrade, P. Valentão, M. Carvalho, Food Chem. Toxicol. 47 (2009) 1372–1377.

[7] A. Keszei, Gyümölcstermesztés. Mezőgazdasági Szaktudás Kiadó, Budapest, 1999, pp. 135–137.

[8] USDA, Quinces. 2009. letöltés dátuma:2024.09.08. forrás: https://fdc.nal.usda.gov/fdc-app.html#/food-details/168163/nutrients

[9] H.M. Takácsné, 2021. Zöldségek és gyümölcsök szerepe a táplálkozásban, Debrecen: Debreceni Egyetemi Kiadó. Letöltés dátuma: 2014.04.08. forrás:

https://dea.lib.unideb.hu/server/api/core/bitstreams/57acab8b-f74c-4166-9aaa-8a6605c30204/content

[10] I.F.F. Benzie, J.J. Strain, Anal. Biochem. 239 (1996) 70–76.

[11] V.L. Singleton, J.A. Rossi, AJEV 16 (1965) 144–158.

[12] J. Nyéki J. Birs. In: J. Papp (Eds.), A gyümölcsök termesztése. Budapest, Mezőgazda Kiadó, 2004, pp. 151–168.

[13] K. Najman, S. Adrian, A. Sadowska, K. Świąder, E. Hallmann, K. Buczak, B. Waszkiewicz-Robak, A. Szterk, *Molecules* 28 (2023) 3066.

IDENTIFICATION OF FOULING MECHANISM IN ULTRAFILTRATION USING A 3D PRINTED TURBULENCE PROMOTER

Nikolett Sz.Gulyás[1], Cecilia Hodúr[2], Szabolcs Kertész[2]

[1]*Institute of Environmental Science and Technology, University of Szeged, H-6725 Szeged, Tisza Lajos krt. 103., Hungary*
[2]*Department of Biosystems Engineering, Faculty of Engineering University of Szeged, H-6725 Szeged, Moszkvai krt. 9., Hungary*
e-mail: gulyasn@mk.u-szeged.hu

Abstract
Membrane filtration processes (such as ultrafiltration, UF or nanofiltration, NF) seem to be promising methods for the treatment of dairy industrial wastewater, which has several advantages compared with other conventional methods. Unavoidably, membrane fouling always hinders the membrane performance. Fouling decreases permeate flux severely and thus increases filtration processing time, which is not economically effective. The characterization of membrane fouling mechanism is highly important especially during the ultrafiltration process. In order to produce higher permeate flux and greater solute rejections, a clear understanding on membrane fouling mechanism is essential.
In this study, we compared the ultrafiltration of model dairy wastewater without and with turbulence promoter. We used a 3D printed turbulence promoter, which was designed based on our previous work. The comparison included the examination of the reduction of fluxes at different pressure values (0.1, 0.2 and 0.3 MPa), different mixing speeds (100, 200, 300 and 400 rpm) and the different fouling models. With the resistance-in series model, the Hermia model and the Makardij model, we investigated how the membrane fouling changes with the use of the promoter.

FLUORESCENCE-BASED DETERMINATION OF CARBAMAZEPINE PHARMACEUTICAL ACTIVE INGREDIENT

Eszter Takács[1], Borbála Gémes[1], Augustine Siakwa[1,2], Szandra Klátyik[1], Fanni Szendrei[3], András Székács[1]

[1]*Institute of Environmental Sciences, Hungarian University of Agriculture and Life Sciences, H-2100 Gödöllő, Páter Károly u. 1., Hungary*
[2]*Doctoral School of Environmental Sciences, Hungarian University of Agriculture and Life Sciences, H-2100 Gödöllő, Páter Károly u. 1., Hungary*
[3]*Institute of Isotopes Co. Ltd., H-1121 Budapest, Konkoly-Thege Miklós út 29-33, Hungary*
e-mail: takacs.eszter84@uni-mate.hu

Pharmaceutical active ingredient carbamazepine (CBZ) is a tricyclic compound, that consists of a fused dibenzazapine ring system and an aminocarbonyl group on the azepine nitrogen atom. CBZ is widely marketed and used to treat neural conditions (epilepsy, nerve pain, trigeminal neuralgia, and acute manic and mixed episodes in bipolar disorder), and consequently it emerged as a contaminant in aquatic environments like rivers, ponds, and lakes. CBZ and its metabolites were frequently detected in raw waters at average concentration of 13 ng/L and 54 ng/L, respectively [1]. It has also been reported as one of the most detected persistent pharmaceuticals that is frequently detected in wastewater effluent-impacted surface water and groundwater [2]. As a persistent water pollutant, CBZ bioaccumulates in aquatic organism thorough food contamination, and can affect the community of different aquatic organisms through alteration of primary production and dissolved nutrients [3–5]. In Hungary, CBZ was recently detected in the Lake Balaton at the maximum concentration of 77.5 ng/L [6]. The aim of the present study was to develop an enzyme-linked fluorescent immunoassay (ELFIA) for the quantification and monitoring of the water contaminant, pharmaceutical active ingredient CBZ.

The prototype of a novel instrumentation has been developed in our collaborative project Aquafluosense (NVKP_16-1-2016-0049) to detect environmental pollutants and water quality parameters using induced fluorescence signals [7–10]. The immunofluorescence module of this prototype was applied in this study to develop indirect competitive ELFIAs. CBZ calibration curves were obtained in assay buffer and fitted by the Rodbard equation in the range of 0–50 ng/mL. CBZ standards were determined by both visual and fluorescent signals. Absorbance (optical density) and fluorescence were measured at 576 nm and at 593 nm wavelengths, respectively. Figure 1. demonstrates the two calibration curves and represents that determination by fluorescence provides a wider and steeper dynamic range for quantification of CBZ.
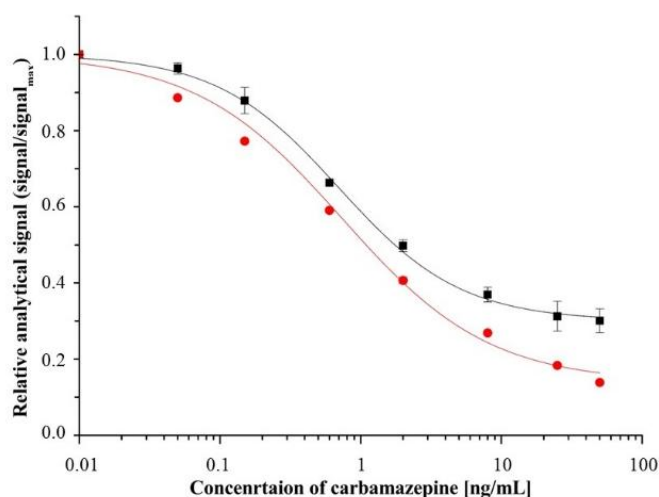
Figure 1. Competitive indirect calibration curves for carbamazepine determined by absorbance (black) and fluorescence (red)

References
[1] M. Huerta-Fontela, M.T. Galceran, F. Ventura, F. Water Research, 45 (2007) 1432-1442.
[2] N. Gottschall, E. Topp, C. Metcalfe, M. Edwards, M. Payne, S. Kleywegt, D.R. Lapen, Chemosphere, 87 (2012) 194-203.
[3] G. Vernouillet, P. Eullaffroy, A. Lajeunesse, C. Blaise, F. Gagné, P. Juneau. Chemosphere, 80 (2010) 1062-1068.
[4] G.R. Garcia, P.D. Noyes, R.L. Tanguay. Pharmacol Ther, 161 (2016) 11-21.
[5] A.L. Jarvis, M.J. Bernot, R.J. Bernot. Sci Total Environ, 496 (2014) 461-470.
[6] Zs. Pirger, É. Molnár, J. Győri, A. Farkas. Ökotoxikológia, 3 (2021) 26-31.
[7] The Aquafluosense Project. Available online: http://aquafluosense.hu. (accessed on 25 September 2024).
[8] E. Takács, D. Lázár, A. Siakwa, Sz. Klátyik, M. Mörtl, L. Kocsányi, A. Barócsi, S. Lenk, E. Lengyel, A. Székács. Toxics, 12 (2024) 238.
[9] E. Takács, B. Gémes, F. Szendrei, C. Keszei, A. Barócsi, S. Lenk, L. Domján, M. Mörtl, A. Székács, Molecules, 27 (2022) 6514.
[10] B. Gémes, E. Takács, P. Gádoros, A. Barócsi, L. Kocsányi, S. Lenk, A. Csákányi, Sz. Kautny, L. Domján, G. Szarvas, N. Adányi, A. Nabok, M. Mörtl, A. Székács. Toxins, 13 (2021) 182.

ANALYTICAL POSSIBILITIES OF LAYER STRUCTURED CARBON NANOTUBE BUCKYPAPERS DOPED BY HYDROPHILIC 1D NANOMATERIALS

I. Y. Tóth

Department of Applied and Environmental Chemistry, University of Szeged, Interdisciplinary Excellence Centre, H-6720, Szeged, Rerrich Béla tér 1, Hungary
e-mail: ildiko.toth@chem.u-szeged.hu

Abstract

The evaporation of liquids from porous films is a very complex phenomenon, which can be followed by simultaneous weight monitoring, electric resistance measurement, infrared imaging and contact angel measurement. The appropriate evaluation of these measurement results can carry both quantitative and qualitative analytical information. The aim of our recent work is to demonstrate this opportunity through the example of the evaporation of simple solvents from layer structured porous buckypapers prepared from non-functionalized carbon nanotubes (*nf*-CNT) doped by hydrophilic 1D nanomaterials.

Introduction

Recent developments in nanotechnology have highlighted the importance of the classical topics of wetting, droplet spreading and evaporation due to their pronounced effect in technological applications (*e.g.,* air/fuel premixing, micro-fluidics, oil recovery, etc.) [1,2]. Multiple phenomena take place simultaneously when a liquid droplet contacts a porous surface: wetting, spreading, capillary filling, gravity induced convective flow, adsorption, evaporation from the surface, evaporation from the pores, etc. The evaporation of a sessile droplet can be studied by several experimental methods: transmission electron microscopy, environmental scanning electron microscopy, contact angle measurement, high speed camera recordings, thermal imaging, just to name a few. The evaporation of sessile droplets can be followed by an equipment assembled at the Department of Applied and Environmental Chemistry, University of Szeged: this equipment can guide simultaneous weight monitoring, electric resistance measurement and infrared imaging at a controlled temperature (typically at 50 °C). There are several experimental results characteristic for the evaporation process, the most important ones being the total evaporation time, time of evaporation only from the surface, full width at half maximum of the time-dependent mass and resistance curves, evaporation rate, initial area of the droplet, and the wetted area at the moment of total evaporation from the surface, etc. [3-5]. The main goal of this work was to demonstrate the analytical possibilities of the mass and resistivity measurements and IR videos through the example of sessile droplet evaporation (acetone, methanol, ethanol, water) from layer structured porous buckypapers (BP) prepared from *nf*-CNT and doped by prepared from non-functionalized carbon nanotubes (*nf*-CNT) doped by hydrophilic 1D nanomaterials.

Experimental

The multiwall **carbon nanotubes** were synthesized by 2 h of catalytic chemical vapor deposition from a C_2H_4:N_2 (30:300 cm^3/min) gas mixture at 650 °C over Fe,Co/Al_2O_3 catalyst (metal loading: 2.5-2.5 m/m%). The synthesized materials were purified by repeating 4 h of refluxing in 10 mol/dm^3 aqueous NaOH, then 4 h in cc. HCl solution four times. The **goethite** nanomaterials were prepared by oxidation-precipitation method from water based solution of $FeCl_2$, precipitated by NaOH solution and oxidized by $NaNO_3$. The synthesis was performed at room temperature and under normal atmosphere. The yellow product was purified by

centrifugation. The **imogolite** nanomaterials were produced by purification from a natural mineral collected in Japan. The *nf*-CNTs were converted into **buckypaper** (BP) by filtering 100 cm^3 of their 0.1 g/dm^3 suspensions through a 0.45 µm nominal pore diameter Whatmann nylon membrane filter. The *nf*-CNTs were suspended by ultrasonication in N,N-dimethylformamide [3,4]. After the samples had dried (20 hours, 80°C), the aqueous suspensions of imogolite and goethite were filtered onto the pure *nf-CNT* BPs in a similar way to the previous one. After drying, layer structured samples were obtained.

Electrophoretic mobilities of the CNTs and goethite nanomaterials were measured in a Nano ZS (Malvern) apparatus with a 4 mW He−Ne laser source (λ = 633 nm) using disposable zeta cells (DTS 1070) at 25 ± 0.1 °C. The zeta-standard of Malvern (−55 ± 5 mV) was used for calibration and the samples were diluted to give an optimal intensity. To get comparable data, the dispersions were homogenized in an ultrasonic bath for 10 s, after which 2 min relaxation was allowed. The effect of pH variation were studied at 10 mM NaCl. The Smoluchowski equation was applied to convert electrophoretic mobilities to electrokinetic potential values. The accuracy of the measurements was ±5 mV.

Liquid droplet evaporation (acetone, methanol, ethanol, water) was studied from the buckypaper film. The droplets (5 µL, 50 °C) were instilled with an Eppendorf Xplorer electronic pipette on the surface of the porous films. The temperature, the electric resistance and weight variations could be simultaneously monitored by the equipment assembled at the Department of Applied and Environmental Chemistry, University of Szeged. Buckypaper was placed onto a purpose-built sample holder and kept in place by a top piece that had a 1.4 cm diameter circular opening in it for placing the liquid droplet. The setup included a type K thermocouple in contact with the non-wetted part of the BP. The distance between the porous film and the heater was 1 cm. Data from the thermocouple was fed back to the temperature controller that maintained a base BP temperature of 50 ± 0.5 °C by continuously adjusting the heater power using fuzzy logic control. The sample holder was placed on a Sartorius Cubis microbalance with 0.01 mg readability and the weigh variation during droplet evaporation was recorded. For thermal imaging a FLIR A655sc infrared (IR) camera was used. This unit has a thermal sensitivity of 30 mK, an accuracy of ±2 °C for temperatures up to 650 °C at 640x480 resolution. Its uncooled microbolometer detector has a spectral range of 7.5-14.0 µm. The IR camera is equipped with a 2.9x (50 µm) IR close-up lens, with 32x24 mm field of view and 50 µm spatial resolution. The recorded images are transferred to a PC with FLIR ResearchIR Max software. Sessile droplet evaporation movies were acquired at maximum resolution with 50 Hz frame rate. Each CNT film's emissivity (ε_{film}) was determined by calibration at the initial film temperature (25 °C) with a black electrical tape (ε = 0.95). During liquid surface evaporation the temperature was determined by taking into account the emissivity of the liquid (ε_L = 0.95); after surface evaporation, the emissivity of the wetted film was calculated as the average between the emissivities of the studied liquid and the porous film. The sample holder plastic plate with the 0.7 cm radius gap in the center was equipped with two copper electrical connections at the opposite edges of the gap on the bottom of the sheet. The BP was fixed to the bottom of the plastic section with magnetic clips. The copper electrodes were contacted to the source meter by 0.3 mm diameter copper wires. The rigidity of these wires did not affect the balance because of the large inertia of the whole assembly mounted on the balance plate. This was confirmed by independent experiments before the evaporation profile (electrical resistance variation as a function of time) measurements. The computer recorded the electrical resistance of the buckypaper as measured by a Keithley 2612A Source Meter. Before the measurements, the BP film was mounted in the assembly and heating at initial temperature was applied until the electrical resistance and the sample weight both stabilized. Then all three recordings (resistivity, IR imaging and sample weight) were started a few seconds before

dropping. The evaporation was studied by dropping a single droplet of a selected solvent to the center of the BP film and simultaneously recording the IR video, the mass and electrical resistance until they returned to their original values. The schematic of the equipment is presented in Fig. 1. The ambient air temperature and the relative humidity of the ambient atmosphere were kept constant (at 25 °C and 55 RH%, respectively) [3-5].
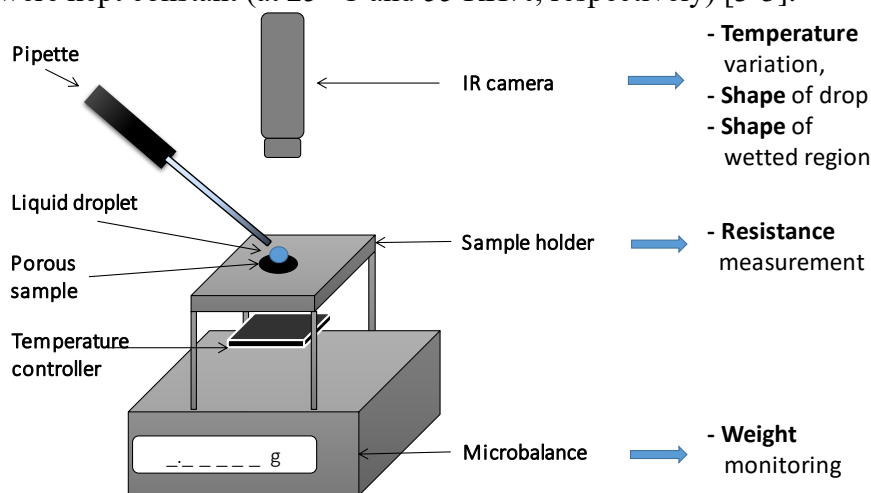

Figure 1. Evaporation monitoring equipment schematic.

Results and discussion

Based on the zeta potential measurements of the pure nanomaterilas, the isoelectric point (IEP, at which the net charge of CNT is zero) is at pH~3 for *nf*-CNT, at pH~4.5 for goethite and at pH~10 for imogolite. The values of zeta potential shift to negative region with increasing pH.

In general at the moment we drop the liquid on the buckypaper film (t_0), the liquid starts to diffuse immediately into the pores of the BP, but a part of it remains spread on the surface of the film. The evaporation of this liquid from the surface takes place together with the diffusion. Once all liquid evaporates from the surface, namely the primary surface evaporation is complete (t_s), liquid is left only in the pores. The solvent gradually evaporates from the pores as well. The complete evaporation of the solvent (t_t) was confirmed by the fact that the mass and the resistivity of the buckypaper returned to the baseline.

One typical mass variation is illustrated in Fig. 2., where t_0 marks the time when the drop was instilled. The mass of the BP increased as soon as the solvent was dropped to the film and this is followed by a quasi-linear weight decrease. Once the primary surface evaporation is complete (t_s), the mass of the buckypaper decreases as linear (within experimental error) functions of time due to the continuous evaporation of the solvent. The total evaporation time (t_t) was at the moment when the mass of the BP returned to the baseline. At the linear weight decreasing ranges, the rate of evaporation (-dm/dt) is constant. The change of -dm/dt value suggests the change of the dominant evaporation process, *e.g.*, evaporation of the droplet sitting on the surface of the BP, evaporation of the condensed water from the porous system or the evaporation of the adsorbed water from the microscopical surface of the porous system (see the linear ranges in Fig. 4.). From this measurement, the typical experimentally determined data are the shape of the curve: m_{max}, area, FWHM; t_s and t_t, evaporation rate -dm/dt and its change. These are characteristic for the measured system and can be used to identify them [3-5].
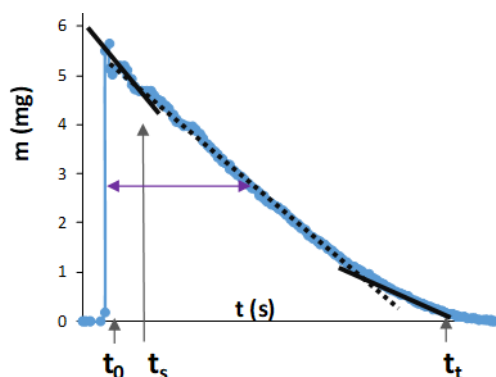
Figure 2. Weight variation of a BP as a functions of time during the evaporation process.

The IR videos were evaluated at selected representative moments, such a typical series of images is shown in Fig. 3. It is possible to determine the spot area and average temperature of the drop (S_d, T_d) and of the wetted region (S_w, T_w) as a function of time. Some data extracted from weight and resistivity variation and from infrared videos are characteristic for the evaporation of the selected liquid/solid system: surface evaporation time (t_s), total evaporation time (t_t), evaporation rate ($-dm/dt$) and its change, FWHM values of the curves, initial area of the drops ($S_{d(t0)}$), area of the wetted region at t_s ($S_{w(ts)}$), etc.
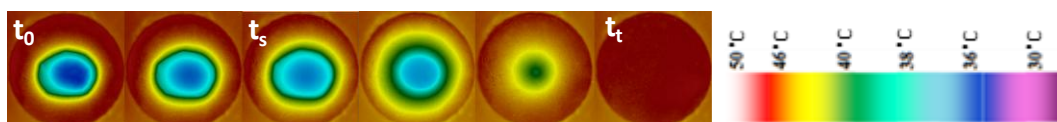

Figure 3. Images exported pro rata from the IR video correspond to t_0, t_s, t_t and several representative intermediate times (5 µL EtOH, 50°C).

Conclusion

The weight monitoring of the evaporation of liquids from porous films can provide information about the mechanism of wetting and vaporization which is a significant area of the basic researches. Furthermore, it can be proved by using appropriate statistical methods (*e.g.,* matrix of Pearson correlation coefficients, hierarchical cluster analysis, functional analysis, etc.), that the experimentally determined characteristic values are specific for the physical properties of the solvents, and they are also dependent on the quality of the solid materials, therefore, they can be used for qualitative chemical analysis via the estimation of physical properties. The results allow us to presume the possibility of this experimental setup and theoretical approach for a potential future application in the field of analytics.

Acknowledgements

References

[1] D. Bonn, et al., Mod. Phys. 81(2) (2009) 739−804.
[2] H.Y. Erbil, Adv. Colloid Interface Sci. 170(1-2) (2012) 67−86.
[3] G. Schuszter, et al., Mic. Mes. Mat. 209 (2015) 105–112.
[4] E.S. Bogya, et al., Carbon 100 (2016) 27–35.
[5] I.Y. Tóth, et al., J. Mol. Liquids 305 (2020) 112826

ANALYSIS OF XANTHAN PRODUCED ON CRUDE GLYCEROL: PROLONGED EMULSIFICATION TEST WITH HYDROCARBONS AND OILS

Ida Zahović, Jelena Dodić, Zorana Trivunović

University of Novi Sad, Faculty of Technology Novi Sad, Department of Biotechnology,
Bulevar cara Lazara 1, 21102 Novi Sad, Serbia
e-mail: ida.zahovic@uns.ac.rs

Abstract

Xanthan is known as one of the commercially most important microbial polysaccharide. Exceptional rheological characteristics, biocompatibility, biodegradability, and non-toxicity enable its extensive application in food, cosmetics, pharmaceutical, paper, textile, and other industries. It is widely used as a stabilizer, thickener, and emulsifier because of its high viscosity at low concentrations, stability over a broad range of temperature and pH value, and excellent solubility in hot and cold water, among other. Industrial-scale xanthan production is generally performed by aerobic submerged batch cultivation of the reference strain *Xanthomonas campestris* ATCC 13951 on a medium containing glucose or sucrose under optimal conditions [1]. Taking into account that the cost of substrate is an important factor for commercial xanthan production and that an actual rise in prices of aforementioned sugars is present, it is necessary to exploit more economical carbon sources in order to reduce the overall production costs. Specific characteristics and low price of crude glycerol indicate that this effluent may be a suitable substrate for biotechnological xanthan production [2].

The aim of this study was to examine the emulsifying properties of xanthan, produced by the reference strain *X. campestris* ATCC 13951 on crude glycerol-based medium, after 240 h of rest.

Xanthan synthesized by reference strain *X. campestris* ATCC 13951 on medium containing crude glycerol from biodiesel production in a factory located in the Republic of Serbia under previously reported conditions [2], was used in this study. The emulsifying properties of separated xanthan were tested by measuring the emulsification index using the method described by Cooper and Goldenberg (1987) [3]. Hydrocarbon (n-hexane, toluene, liquid paraffin, and chloroform) or oil (sunflower, soybean, and olive oil) was added to the aqueous phase containing xanthan (0.1% w/v) at a ratio of 3:2 (v/v) and agitated vigorously for 2 min on a vortex mixer (VIBROMIX 10 Vortex Mixer, Domel, Železniki, Slovenia) at 2850 rpm. After 240 h of rest at 25 °C, the emulsified layer height and total height of the liquid layer were measured and used for calculation of emulsification index, as proposed by the applied method and previous study [4].

The results of the emulsification test show that the formation of xanthan emulsions with soybean, sunflower, and olive oils is reflected by higher values of the emulsification index comparing to hydrocarbons. The highest emulsification index of approximately 61% was obtained when the emulsifying activity of xanthan was examined with soybean oil, while somewhat lower values, i.e. 57% and 59% were achieved when using sunflower and olive oil, respectively. These values are in agreement with the results of a previous study in which the emulsifying activity of xanthan in the same oils was examined for 24 h, and values higher than 50% were reported [4]. The obtained results indicate that there is no drastic change in the emulsifying properties of xanthan with prolongation of the resting time when oils are used. However, a much lower emulsification index was noted when prolonged emulsification test was conducted with hydrocarbons. The emulsification index was approximately 20% for liquid

paraffin and less than 10% for toluene and chloroform. The lowest emulsification index of approximately 3.6 % was achieved when the emulsifying activity was examined with n-hexane. According to the results obtained in this study, xanthan produced on a crude glycerol-based medium can be used as an emulsion-forming and stabilizing agent between aqueous solutions and hydrocarbons or oils, but an increase in resting time has a negative effect on the xanthan emulsification index when using hydrocarbons. The findings of this study provide valuable information that can be used in future research related to the examination of potential xanthan applications.

Acknowledgements

References
[1] I.M. Bhat, S.M. Wani, S.A. Mir, F.A. Masoodi, Biocatal. Agric. Biotechnol. 42 (2022) 102328.
[2] I. Zahović, J. Dodić, J. Grahovac, A. Ranitović, M. Grahovac, I. Pajčin, Z.Trivunović, Period. Polytech. Chem. Eng. 66(4) (2022) 641–649.
[3]D.G. Cooper, B.G. Goldenberg, Appl. Environ. Microbiol. 53 (1987) 224–229.
[4] A. Bilić, S.J. Armaković, M.M. Savanović, I. Zahović, J. Dodić, Z. Trivunović, I. Savić, T. Gajo, S. Armaković, Catal. Commun. 186 (2024) 106821.

SQUALENOYLATED NANOPARTICLE PRODRUGS

Hiba Zeini[1], Erzsébet Mernyák[1], Máté Vágvölgyi[1], Gábor Girst[1], Róbert Berkecz[2], Attila Hunyadi[1,3]

[1]Institute of Pharmacognosy, University of Szeged, H-6720 Szeged, Hungary
[2]Institute of Pharmaceutical Analysis, University of Szeged, 4, 6720 Szeged, Hungary
[3]HUN-REN-SZTE Biologically Active Natural Products Research Group, Eötvös u. 6, H-6720 Szeged, Hungary
*e-mail: hibazeini92@gmail.com*

Abstract

Self-assembling drug conjugates offer a promising strategy in cancer therapy by forming pro-drugs through hydrolysable conjugation with inducers like squalene. In this study, self-assembling squalenoylated conjugates were prepared aimed at improving bioavailability and anti-tumor efficacy. The newly synthesized compounds were purified by HPLC to over 95% and their structures were confirmed by NMR and HRMS. The squalenoylated compounds will be used for the synthesis of self-assembling nanoparticles, which will be subjected to investigation of their antiproliferative activity. This approach may enhance the stability and biological activity of the lead compound, advancing its therapeutic potential.

Introduction

Self-assembling drug conjugates have gained attention as an effective cancer treatment strategy, especially for improving bioavailability and reducing negative side effects [1]. This approach leverages hydrolysable conjugation with biocompatible compounds like squalene, a triterpene known for its compatibility and inertness [2]. Its conjugated nanoparticles don't remain free when they enter the bloodstream. Instead, they dissolve into low-density lipoprotein LDL [3]. In this study, we aimed to synthesize self-assembling conjugates of our lead compounds (LCs).

Results and Discussion

Concerning that phenolic esters tend to be unstable, here we performed certain modifications to LCs (**1**) aimed at improving stability and efficacy by replacing the ester bond with a more stable ether bond, resulting in compound **2**. Then basic hydrolysis of compound **2** resulted in carboxylic acid derivative **3** (Scheme 1). This acid was then esterified with squalene alcohol, yielding compound **4**. Flash chromatography, supercritical fluid chromatography (SFC), and HPLC were used for the separation and purification of the compounds. All newly synthesized compounds (**1**–**4**) achieved a purity level greater than 95%, as confirmed by NMR and HRMS analysis. Compounds **4** will be further developed into self-assembling nanoparticles to evaluate their physical properties, stability and anti-cancer potential. This method holds promise for improving the stability and biological function of LCs, increasing their effectiveness for cancer treatment.
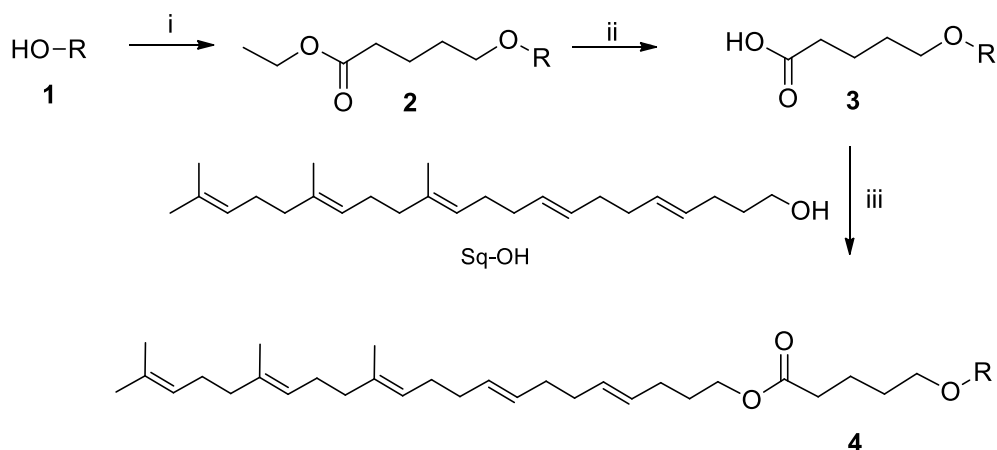
Scheme 1 Synthesis of squalenoylated LCs (4). Reagents and conditions: (i) Br-(CH$_2$)$_4$-COOEt, DBU, DMF 70 °C, 3 h; (ii) 1. NaOH, THF,MeOH, 2. HCl; (iii) DMAP, EDC·HCl , rt, Ar atmosphere, 3 h.

Conclusions

We elaborated efficient procedures for the syntheses of new squalene-conjugated LCs (**4**) with high purity, confirmed by NMR and HRMS analysis. The conjugates will be subjected to the formation of nanoparticles, followed by determination of their antiproliferative properties against certain cancer cell lines. Our results can make a promising contribution to an advanced cancer treatment by improving bioavailability and therapeutic effectiveness of LCs.

Acknowledgements

References

[1] Kim, J., Lee, S., Kim, Y., Choi, M., Lee, I., Kim, E., Yoon, C.G., Pu, K., Kang, H. and Kim, J.S., 2023. In situ self-assembly for cancer therapy and imaging. Nature Reviews Materials, 8(11), pp.710-725.

[2] Markovic, M., Deodhar, S., Machhi, J., Yeapuri, P., Saleh, M., J. Edagwa, B., Mosley, R.L. and Gendelman, H.E., 2022. Prodrug therapies for infectious and neurodegenerative diseases. Pharmaceutics, 14(3), p.518.

[3] Vágvölgyi, M., Bélteky, P., Bogdán, D., Nové, M., Spengler, G., Latif, A.D., Zupkó, I., Gáti, T., Tóth, G., Kónya, Z. and Hunyadi, A., 2020. Squalenoylated nanoparticle pro-drugs of adjuvant antitumor 11α-hydroxyecdysteroid 2, 3-acetonides act as cytoprotective agents against doxorubicin and paclitaxel. *Frontiers in Pharmacology*, *11*, p.552088.